DESIGN OF MECHANICALLY AGITATED CONTACTORS OR REACTORS WITH "ATTITUDE"

A thesis submitted to The University of Manchester for the degree of

Doctor of Philosophy

in the Faculty of Engineering and Physical Sciences

2005

Mike Cooke

SCHOOL OF CHEMICAL ENGINEERING AND ANALYTICAL SCIENCE

ProQuest LLC.
789 East Eisenhower Parkway
P.O. Box 1346
Ann Arbor, MI 48106 – 1346

THE UNIVERSITY OF MANCHESTER

ABSTRACT OF THESIS submitted by M Cooke for the degree of Doctor of Philosophy and entitled **Design of Mechanically Agitated Contactors or Reactors with "Attitude"** August 2005.

This study is concerned with the design of reactors with "Attitude" addressing questions as how to experimentally study "real reactors" using real fluids or good analogues at appropriate specific energy dissipation rates (up to 10W/kg) and superficial gas velocities (up to 0.25m/s). The experiments were carried out in single, two-phase and three-phase systems in a range of fully baffled agitated vessels of diameters ranging from 0.08 to 1.79 m in order to test and study scale-up relationships

Techniques are developed to measure shaft torque, mixing, gas-liquid mass transfer, and local phase fractions, overall phase fractions, bubble measurement techniques and ERT (Electrical Resistance Tomography). Model fluids are used to mimic the behaviour of real systems. The bubble measurement techniques developed are used to study bubble behaviour in industrially important fluids at elevated temperature and pressure.
Single and multi-phase systems are studied for vessels agitated by a large range of agitator types and sizes and for single and multiple agitators. Shaft power is measured for a range of agitators under single and multiphase conditions. An equation is proposed for the effect of scale and blade geometry on the power number of concave hollow blade agitators. Liquid phase mixing studies are undertaken for a range of agitator and tank geometries along with complementary flow visualisation work. Scale-up relations relationships are developed and discussed. Gas-liquid mass transfer, gas-hold-up and hydrodynamics are studied and correlations proposed. These are compared with literature correlations. The "flooding-loading" transition is studied for a number of types of hollow blade agitators. A simple method, resulting from these studies, is proposed to avoid "flooding" for radial turbines, including the hollow-blade types. Rules for avoiding foam out at high phase fractions are developed. Solid suspension with novel agitators for two and three phase systems are tested and relationships developed. Compared at equal diameters, the curved hollow blade agitator is shown to be more energetically efficient for solid suspension than most common alternatives, especially under gassed conditions.

Foaming is studied and a method of controlling foam based on an inverted hollow cone rotating on the agitator shaft above the normal aerated liquid level is developed. This is tested successfully on industrial fermenters.

TABLE OF CONTENTS

Dedications xx
Chapter 1 Introduction 1
Chapter 2 Literature Reviews 1
2.1 Scope 1
2.2 Outline 2
2.2.1 Introduction to the Dimensionless Groups 2
2.2.1.1 Agitator Reynolds Number, Re. 3
2.2.1.2 Agitator Power Number, Po. 4
2.2.1.3 Agitator Flow Number, N_Q 4
2.2.1.4 Gas Flow Number, Fl_G 6
2.2.1.5 Froude Number, Fr 6
2.2.1.6 Weber Number, We 6
2.2.2 Agitation 7
2.2.2.1 Radial Flow Agitators 10
2.2.2.2 Axial Flow Impellers 12
2.2.2.3 Mixed Flow Impellers 13
2.2.2.4 Multiple Impellers 13
2.2.2.4.1 Down-pumping Axial or Mixed Flow Agitators 13
2.2.2.4.2 Up-pumping Axial Agitators 15
2.2.2.5 Selection of Agitators 16
2.2.2.5.1 Selection of Radial Flow Agitators 17
2.2.2.5.2 Selection of Axial Flow Impellers 20
2.2.3 Agitator Power Prediction 23
2.2.3.1 Ungassed Agitator Power Prediction 23
2.2.3.2 Prediction of the Power of Gassed Agitators 25
2.2.3.3 Power Draw in a Boiling and Near Boiling Reactor. 27
2.2.4 Agitator Pumping Rates 28
2.2.4.1 Effect of D/T on Agitator Pumping Rates and Shear Rates 33
2.2.4.2 Effect of Gas-phase and /or Solid-phase on Agitator Pumping Rates 38
2.3 Hydrodynamics 41
2.3.1 Agitator Hydrodynamics under Gassed Conditions 41
2.3.2 Bubble Hydrodynamics 54
2.4 Turbulence 58
2.4.1 The Kolmogorov Theory of Local Homogeneous Isotropic Turbulence: The Eddy Spectrum 60
2.5 Mixing 65
2.5.1 Diffusion 66
2.5.2 Convection 66
2.5.3 Bulk Movement 67
2.5.4 Macro-scale and Micro-scale Mixing. 67
2.5.5 Mixing Times 70

2.5.5.1 Decolourisation Techniques 71
2.5.5.2 Conductivity Techniques 72
2.5.5.3 Degree of Mixing 73
2.5.5.4 Comparisons of Mixing Results with Different Methods 75
2.5.5.5 Mixing Time Constant 76
2.5.5.6 Effect of Agitator Type (standard tank H=T) on Mixing 77
2.5.5.7 Effect of Impeller Diameter on Mixing 78
2.5.5.8 Effect of Aspect Ratio H/T on Mixing 79
2.5.5.9 Effect of Viscosity on Mixing 80
2.5.5.10 Effect of Gas and Solid Phases on Mixing 82
2.5.5.11 Effect of Tracer Properties (Volume, Density and Viscosity) on Mixing 82
2.6 Rheology 83
2.6.1 Newtonian Fluids 83
2.6.2 Non-Newtonian Fluids. 84
2.6.2.1 Pseudoplastic Fluids. 85
2.6.2.2 Plastic Fluids. 86
2.6.2.3 Cavern Formation 86
2.6.2.4 Effect of Solids on Fluid Flow Properties 88
2.7 Solid Suspension 89
2.7.1 Scale-up for Solid Suspension 90
2.7.2 Effect of Multiple Impellers on Solid-liquid Suspension 94
2.7.3 Effect of Gas on Solid-liquid Suspension 95
2.8 Mass and Heat Transfer 99
2.8.1 Analogies 99
2.8.1.1 Heat Transfer and j Factors 100
2.8.1.2 Mass Transfer and j Factors 101
2.8.2 Heat Transfer in Agitated Vessels by Means of Jackets and Coils Containing a Heat Transfer Fluid 103
2.8.2.1 Forced Convective Heat Transfer in Agitated Vessels 105
2.8.2.2 Heat Transfer in Jacketed Vessels and Vessels Fitted with Coils 106
2.8.3 Mass Transfer in Agitated Vessels 110
2.8.3.1 Gas-liquid Mass Transfer and Interfacial Area in Agitated Vessels 111
2.8.3.2 Methods of Measuring Gas-liquid Mass Transfer and Interfacial Area: A Critical Review 117
2.8.3.3 Transient Gas-liquid Mass Transfer Measurements 118
2.8.3.3.1 Liquid Film Control 122
2.8.3.3.2 Henry's Law 124
2.8.3.3.3 Liquid Mixing 124
2.8.3.3.4 Probe Lag 125
2.8.3.3.5 Gas-phase Composition 126
2.8.3.3.6 Dynamic k_La Measurements in Live Fermentation Cultures. 130
2.8.3.3.7 Undesirable Effect of a Two-component System, Using Transient Methods to Estimate k_La in Aerated Systems 131
2.8.3.3.8 Conclusions Regarding the Dynamic Methods of measuring k_La in Aerated Systems 132

2.8.3.4 Steady-state or Pseudo Steady-state Gas-liquid Mass Transfer Measurements 133
2.8.3.4.1 Respiring Yeast for Steady-state Gas-liquid Mass Transfer Measurements 139
2.8.3.4.2 The Peroxide Technique for Pseudo Steady-state Gas-liquid Mass Transfer Measurements 140
2.8.3.5 Solid-liquid Mass Transfer in Agitated Vessels 142
2.8.3.6 Gas-liquid-solid Mass Transfer in Agitated Vessels 143
2.8.4. Literature Gas-liquid Mass Transfer Results and Correlations 145
2.8.4.1 Effect of Temperature on k_La 151
2.8.4.2 Effect of Viscosity on k_La 152
2.8.4.3 Effect of Solids on k_La 154
2.8.5 Gas-liquid Hold-up Correlations 155
2.9 Reaction Kinetics 158
2.10 Scale-up or Scale-down. 161
2.10.1 Other Aspects of Scale 163
2.10.2 Choice of Equipment for Gas-liquid Contacting 164
2.11 Concluding Remarks about the Literature Review. 165
Chapter 3 Experimental Equipment and Techniques 166
3.1 Equipment 166
3.2 Techniques 171
3.2.1 Flow Visualisation 171
3.2.2 Shaft Power Measurement 172
3.2.3 Overall Gas-Liquid Hold-up 172
3.2.4 Local Gas-Liquid Hold-up 173
3.2.5 Overall Liquid Mixing Times 175
3.2.6 Electrical Resistance Tomography (ERT) System 176
3.3.7 Gas-Liquid Mass Transfer k_La 178
3.2.8 Viscosity Measurements 180
Chapter 4 : Model Fluids 181
4.1 Modelling of Filamentous Fermentations 181
4.2 Modelling of Paint 181
4.3 Modelling Non-coalescing Liquids 184
4.4 Modelling Boiling Aerated Reactors 185
Chapter 5 Bubble Studies using the Buchi Rig 186
5.1: Background and Summary of Buchi work 186
5.2 Introduction 186
5.3 Literature And Theory 189
5.4 Equipment and Conditions 195
5.5 Buchi Rig Agitator Hydrodynamics 199
5.6 Experimental Details 201
5.6.1 Dynamic Gas Disengagement Experiments 201
5.6.1.1 Problems Encountered With the Dynamic Gas Disengagement Method 204
5.6.2 Bubble Measurements and Counting Experiments. 205
5.6.2.1 Manual Counting 205

5.6.2.1.1 Possible Sources of Error with Manual Counting....206
5.6.2.2 Semi-Automatic Counting....207
5.7 Results Summary....208
5.8 Presentation of Results, Discussion and Conclusions....213
5.8.1 Bubble Pictures....213
5.8.2 Heterogeneous Bubble Behaviour in a Mechanically Agitated Contactor....220
5.8.3 Bubble Rise Velocities from DGD Analysis....224
5.8.5 Effect of Agitation on Bubble Size....225
5.8.6 Effect of Superficial Gas Velocity on Bubble Size....231
5.8.7 Gas Hold-up....237
5.7.9 Test of Equation (5.2) $v_S = \left(\frac{dh}{dt}\right)_I$ 239
5.7.10 Effect of Solids on the Small Bubble Fraction....240
Chapter 6 : Single Phase Hydrodynamics....243
: Covering the Effects of Geometry and Scale on Flow, Mixing and Agitator Power In Mechanically Agitated Vessels under Fully Turbulent Conditions....243
6.1 Summary....243
6.2 Aims of the Study....245
6.3 Background to these Mixing Studies....246
6.4 Details of Tests and Geometries....251
6.4.1 Comparative Mixing Tests....252
6.4.2 Notes on Flow Visualisation....253
6.4.3 Geometries of the Vessels and Agitators....253
6.5 Results....255
6.5.1 Results for Comparative Tests on the 0.286 m Vessel....255
6.5.1.1 Agitator Power Numbers in Fully Turbulent Flow....255
6.5.1.2 Flow Visualisation for Various Agitator Configurations in Fully Turbulent Flow....257
6.5.1.3 Mixing Times in Fully Turbulent Flow....262
6.5.1.3.1 Mixing Times in Fully Turbulent Flow for $H = T$ aspect ratio....264
6.5.1.3.1.1 Effect of Specific Power Input on Mixing....264
6.5.1.3.1.2 Effect of D/T on the Rate of Mixing....265
6.5.1.3.1.3 Comparisons with Earlier Work for $H=T$ Geometries....266
6.5.1.3.2 Mixing Times in Fully Turbulent Flow for all Aspect Ratios in the 0.286 m Diameter Vessel....268
6.5.2 Results of Comparative Tests on the 0.61m Diameter Vessel....272
6.5.2.1 Discussion of the Results of the Mixing Tests from the 0.61 m Vessel....275
6.5.3 Mixing Studies using the ERT Tomography Sensors in the 0.61m Diameter Vessel....276
6.6 Power Numbers for Hollow Blade Turbines....279
Chapter 7 Multi-phase Hydrodynamics....285
7.1 Scope....286

7.2 Gas-Liquid Power and Hydrodynamics 286
7.2.1 Cavity Structure of Radial Turbines under Aerated Conditions 288
7.2.2 Hydrodynamics of Radial Turbines – Literature and Discussion 292
7.2.2.2.1 Literature studies on Flooding of Rushton turbines 295
7.2.2.2 Flooding of Hollow Blade Turbines 300
7.2.3 Experimental Studies of the "Flooding-Loading" and "Loading-Compete Dispersion" Transitions with Rushton and Hollow Blade Turbines. 302
7.2.3.1 Experimental Studies using Rushton Turbines 303
7.2.3.2 Experimental Studies on the Flooding of Hollow Blade Turbines. 305
7.3 Recommendations for the Design of Radial Turbines for Dispersion. 315
7.3.1 Consideration of H/T, D/T, Impeller Clearance and Multiple Impellers for Gas Dispersion 315
7.4 Conclusions Regarding F-L with HBT agitators 316
7.5 Gassed Power 316
7.6 Gas Hold-up 321
7.6.1 Overall Gas Hold-up 323
7.6.2 Local Gas Hold-up 325
7.6.3 Foam 329
7.7 Gas-liquid Mass Transfer 331
7.7.1 Experimental Gas-liquid Mass Transfer Measurements 331
7.7.2 Performance Equations for Mass Transfer Operations 335
7.8 Solid Suspension 338
7.8.1 Experimental Measurements of N_{JS} for Various Agitators 339
7.8.2 Affect of Increasing the Liquid Level at Constant Solids for Various Agitators 342
7.8.3 Experimental Determination of the Effect of Gas on Solid Suspension for Hollow Blade and Up-pumping LIGHTNIN A345 Agitators 345
7.9 Multi-phase Mixing 349
Chapter 8 : Spinning Cones as Pumps and Degassers. 351
8.1 Summary 351
8.2 Introduction 352
8.3 Literature Review 353
8.4 Experimental Details 361
8.4.1 The Stirred Tank Rigs 361
8.4.2 The Spinning Cone Rig to Measure Pumping Rates 363
8.4.3 Scouting Experiments on Reactor 2 Geometry (Table 8-2) 365
8.4.3.1 Effect of Cone Angle - Tests with a 15° Cone 366
8.4.4 Cone Pumping Rate Measurements 366
8.4.5 Experiments with Cones with an Half Angle of 30° 367
8.4.6 Effects of Cone Angle, Geometry and Physical Properties 368
8.4.7 Test of Literature Equation 371
8.4.8 Optimum Cone Angle 372
8.4.9 Effect of Aeration on Pumping 372

8.4.10 Contribution of the Internal and External Cone Surfaces to Pumping....374
8.4.11 Stirred Tank Experiments....374
8.4.12 Scale-up....376
8.4.12.1 Studies with the 0.61 m Vessel....378
8.4.12.2 Studies with the 0.914 m vessel....381
8.5 Conclusions....382
8.6 Power Draw for Spinning Cones....385
8.7 Further Work....385
8.7.1 Pilot Fermenter Work....385
8.7.2 Further Work at UMIST....388
Chapter 9 : An Electrical Resistance Tomography (ERT) System as a Diagnostic Tool....389
9.1 Aims of the Study....389
9.2 Summary of the Work....389
9.3 Part 1: Demonstration of a Novel Retrofit Tomography Baffle Cage, for Gas-liquid Mixing Studies under Intense Operating Conditions....391
9.3.1 Background to ERT Retrofit....391
9.3.2 Electrical Resistance Tomography System....392
9.3.4 Experimental Details....393
9.3.4.1 Retrofit of the 0.61 m Stirred Tank Facility to Include an ERT Capability....393
9.3.4.2 Geometric Details....395
9.3.5 Commissioning Trials....396
9.3.5.1 Tribulations....396
9.3.5.2 The Fix....397
9.3.6 Demonstration Trials....397
9.3.7 Results....398
9.3.8 Conclusions and Further Work....402
9.4: Determination of the Radial Sensitivity and 3*D* Effect in an 8-plane ERT Sensor Arrangement Fitted to a Stirred Tank....404
9.4.1 Introduction....404
9.4.2 Experimental Equipment....405
9.4.3 Procedure....407
9 .4.4 Results....409
9.4.4.1: 76 mm Diameter Stainless Steel Ball....409
9.4.4.2: 25 mm Diameter Stainless Steel Ball....414
9.4.4.3: 42.7 mm Diameter Golf Ball....417
Chapter 10 : Summary, Main Conclusions and Suggestions for Further Work..422
10.1: Summary....422
10.2: Some Successes....425
10.3 General Conclusions and Design Recommendations....426
10.4: Comments on the Experiments and Suggestions for Further Work. ..429
10.4.1: The Hard Bits....429
10.4.2: Comments on the Buchi Rig Work and Suggestions for Further Work....431

10.4.2.1: Effect of solids on the gas bubble distribution. 432
10.4.2.2 : Implication of Equation (5.2) $v_S = \left(\frac{dh}{dt}\right)_l$ 433
10.4.3: Regarding Chapter 6: Single Phase Hydrodynamics 433
10.4.3.1: Effect of clearance on mixing 433
10.4.3.2: Effect of Agitator Choice on Mixing in Tall Vessels. 434
10.4.3.3: The Effect of Scale-up on Mixing. 435
10.4.3.4: Regarding Chapter 7: Multi Phase Hydrodynamics 435
10.4.5: Inverted Hollow Spinning Cones 436
10.4.6 Tomography 436
Appendices 1
Appendix 1: Shaft Torque and Power. 1
A1.1 Calibration of Strain Gauges 2
Appendix 2: Overall Gas Hold-up 5
A2.1 Overall Gas Hold-up by Video 5
A2.2 Overall Gas Hold-up by Ultra Sonic Level Probe 5
Appendix 3: Local Gas Hold-up 13
Appendix 5: An Example $k_L a$ Calculation Using the Peroxide Method 13
Appendix 6: Measurement of Viscosity. 15
Appendix 7: Analysis of Dynamic Gas Disengagement Curves 15
Appendix 8: Examples of Frequency Counts from Bubble Size Measurements 18
Appendix 9: List of Folders in Accompanying CD 18
Bibliography 1

LIST OF FIGURES

Number *Page*

Figure 0-1 xx
Figure 0-2 xxi
Figure 2-1: Discharge flow from a Rushton turbine. From Nienow (1998) .....
Figure 2-2: Normalised velocity profiles, a) Rushton turbine, b) 6SRGT from Kovacs (2001). .....
Figure 2-3: Standard Rushton turbine agitated vessel .....
Figure 2-4: Main flow loops with a Rushton turbine 1
Figure 2-5: Main flow loops with an axial flow impeller 1
Figure 2-6: Possible flow combinations with combined radial below down-pumping impellers. 1
Figure 2-7: Stable flow with flow reinforcement at the interchange for a radial plus up-pumping agitator combination. 1
Figure 2-8: 4 blade-turbine 1
Figure 2-9: 6-blade Rushton-turbine 1
Figure 2-10: CHEMINEER CD-6 impeller 1
Figure 2-11: CHEMINEER BT-6 impeller 1
Figure 2-12: SCABA 6SRGT agitator 1
Figure 2-13: LIGHTNIN R500 (Sawtooth) agitator 1
Figure 2-14: ChemShear Impeller 1
Figure 2-15: 8-vaned disc agitator 1
Figure 2-16: PFAUDLER Glass-coated retreat curve impeller 1
Figure 2-17: Anchor 2
Figure 2-18: Single Flight Helical Ribbon with Screw 2
Figure 2-19: LIGHTNIN A310/510 Impeller 2
Figure 2-20: CHEMINEER HE-3 Impeller 2
Figure 2-21: LIGHTNIN A100 Propeller 2
Figure 2-22: LIGHTNIN A200 45° pitched blade impeller or 4MFD 2
Figure 2-23: CHEMINEER SC-3 Impeller 2
Figure 2-24: LIGHTNIN A315 2
Figure 2-25: CHEMINEER Maxflo W Impeller 2
Figure 2-26: LIGHTNIN A340 2
Figure 2-27: LIGHTNIN A345 impeller 2
Figure 2-28: APV B2-30U impeller. 2
Figure 2-29: Power curve for a Rushton turbine. Baffled curve (1) diverges from unbaffled curve (2) above Re = 300. Below Re =300, baffling does not effect Po. 2
Figure 2-30: Effect of dual impellers on power. From Gray (1966). Reference power P_1 is a flat blade turbine in each case 2
Figure 2-31: Gassing curves for a Rushton turbine in air-water. From Nienow (1998) 2

Figure 2-32: Drop-size data for silicon oil in water agitated with various diameters of Rushton turbines in two vessels. Data from Musgrove and Ruszkowski (2000) is shown against impeller speed. 34
Figure 2-33: Same data as for Figure 2.32, only this time correlated against tip speed....34
Figure 2-34: Data from Zhou and Cresta 1998 showing drop size correlates with tip speed for a given agitator type....35
Figure 2-35: The vortex structure and cavities behind the blades of Rushton turbines from van't Riet *et al.* (1976) 43
Figure 2-36: Change in the cavity regime with increasing air rate for a Rushton turbine in low viscosity fluids from Nienow (1985)....44
Figure 2-37: The flooding - loading – complete dispersion transitions for a Rushton turbine from Nienow *et al.* (1985) 44
Figure 2-38: Power curves at constant Q_G for a Rushton turbine from Nienow *et al.* (1985) 45
Figure 2-39: Calculation of coalescing recirculating gas flow. From van't Riet *et al.* (1976)....48
Figure 2-40: Flow maps for a gassed Rushton turbine, $D=T/3$, at two scales....51
Figure 2-41: Homogeneous a) and heterogeneous flow b), c) and d) in a gassed, stirred vessel. From Gezork *et al.* (2000)....55
Figure 2-42: Air-water bubbles in 0.91m diameter vessel, agitated with a Rushton turbine of diameter $D = T/3$ 57
Figure 2-43 Terminal velocity for air-bubbles in tap water as a function of bubble size, (Haberman and Morton, 1956)....57
Figure 2-44: Kolmogorov eddy size spectrum 61
Figure 2-45: Turbulent Energy Spectrum....61
Figure 2-46: (a) top Graphical mixing time, (b) Mixing index....76
Figure 2-47: Some typical flow curves (shear stress against shear rate) for different types of fluids, Harnby (1992). 85
Figure 2-48: Well agitated caverns in pseudoplastic fluids: Left agitated by a pitch blade turbine: Right agitated by a Rushton turbine. From Witchterle and Wein (1981). 87
Figure 2-49: showing the relationship between power per unit volume, particle concentration and scale, taken from Herringe (1979). Note that y is the power index in the solid suspension scale-up relationship: $P/V \propto D^y$. For geometric similarity this is the same as $P/V \propto T^y$. 92
Figure 2-50: Common heat-transfer surfaces, from Oldshue (1983)....105
Figure 2-51: Comparison of agitators at constant speed for heat transfer from jackets. The data is from Table 2-13. 109
Figure 2-52: Interfacial behaviour for physical absorption according to the two-film theory....111
Figure 2-53: Current plateau for a polarographic probe....120
Figure 2-54: Testing the well mixed liquid phase assumption for air-water. To be well mixed the ratio of the time constant for mass transfer ($\tau(k_La) = 1/k_La$) should be ≥ three times the time constant for mixing (τ_{mix}).

Assuming first order mixing $\tau_{mix} = t_{90}/\ln(10)$. The calculations were done assuming an $H=T$ baffled cylindrical vessel containing a single $D=T/2$, Scaba 6SRGT impeller at a clearance of $T/4$. 13
Figure 2-55: Resistances to oxygen absorption by cells in an aerobic fermenter....14
Figure 2-56: Scale-up maintaining geometric similarity. Important geometric ratios are kept constant. 16
Figure 3-1: The 0.286 m diameter stirred tank rig 16
Figure 3-2: Rotameter feeds to 0.286 m and 0.61 m diameter vessels....16
Figure 3-3: The 0.61 m vessel fitted with dual LIGHTNIN A345 agitators....16
Figure 3-4: An overview of the 0.914 m diameter stirred tank equipment....16
Figure 3-5: A close-up of the 0.914 m diameter vessel showing the curved blade agitator (6HBT) with shaft strain gauges above and details of bottom bearing fitted with a Teflon sleeve. 17
Figure 3-6: Picture of Local Hold-up Probe....17
Figure 3-7: Khang and Levenspeil (1976) mixing probes used in tests 17
Figure 3-8: Picture of Tomography baffle cage in the 0.61 m vessel. 17
Figure 3-9: Views of the ELECTRSENSE DOT Probes. Thread on outside of the body is ¾ inch BSP to fit our standard analysis ports. 18
Figure 4-1: Experimentally determined consistency factors for various concentrations of CMC Hercules Powder grade 7H4C fitted to a 5th order polynomial. 18
Figure 4-2: Experimentally determined power law indices for various concentrations of CMC Hercules Powder grade 7H4C fitted to a linear relationship to the reciprocal of the indices. 18
Figure 4-3: Effect of temperature on gas hold-up in 20-ppm PPG solution in a 0.61 m diameter bubble column, H/T = 1.3, superficial gas velocity =0.21m/s....18
Figure 5-1: Disengagement trace for boiling, nitrogen sparged, acetic acid in the Buchi rig (coalescing system) 19
Figure 5-2: Disengagement trace for cold air-sparged PPG solution in the 0.61 m diameter vessel. (non-coalescing) 19
Figure 5-3: Disengagement illustrations from Schumpe and Grund (1986)....19
Figure 5-4: The Buchi 1 set-up. Top is assembled rig. Bottom shows agitator and sparge assembly 19
Figure 5-5:Line diagram of Buchi rig as set up for the 10 barg pressure work. 19
Figure 5-6: Drag coefficient as a function of Reynolds number from Hill(1998)....20
Figure 5-7: Buchi agitator and photo region details....20
Figure 5-8: Nitrogen bubbles in cold acetic acid....21
Figure 5-9: Gas bubbles in nitrogen sparged boiling acetic acid....21
Figure 5-10: Nitrogen bubbles in cold water 21
Figure 5-11: Water vapour bubbles in boiling water 21
Figure 5-12: Gas bubbles in hot water sparged with ethylene at 10 barg....21
Figure 5-13: Gas bubbles in hot water sparged with nitrogen at 10 barg....21
Figure 5-14: Nitrogen gas bubbles in cold aniline....21
Figure 5-15: Gas bubbles in boiling aniline sparged with nitrogen 21

Figure 5-16: Nitrogen gas bubbles in a cold 20-ppm PPG solution 218
Figure 5-17: Nitrogen gas bubbles in a cold 0.2 molar sodium sulphate solution 219
Figure 5-18: Gas bubbles in hot methanol sparged with ethylene at 10 barg 219
Figure 5-19: Gas bubbles in hot methanol sparged with nitrogen at 10 barg 220
Figure 5-20: Gas hold-up by DGD analysis for a 0.2 molar sodium sulphate solution in the 2ft vessel R1 geometry at 280 rpm: Operation is in the heterogeneous regime 221
Figure 5-21: 2ft vessel R1 Gas hold-up by DGD at constant rpm for a 20-ppm PPG solution at 280 rpm. Operation is in the heterogeneous regime. 221
Figure 5-22: Gas hold-up by DGD in the 2 ft vessel R3 geometry at constant 300 rpm for a 20 ppm PPG solution. Operation in the heterogeneous regime 222
Figure 5-23: 2 ft vessel, R3 geometry. Gas hold-up at v_S = 0.033 m/s by DGD for 20 ppm PPG 222
Figure 5-24: 2 ft vessel, R3 geometry. Gas hold-up at v_S = 0.074 m/s by DGD for a 20 ppm PPG solution 223
Figure 5-25: 2 ft vessel, R3 geometry. Gas hold-up at v_S =0.13m/s by DGD for a 20 ppm PPG solution. 223
Figure 5-26: Bubble rise velocities versus superficial gas velocities measured by the dynamic gas disengagement technique in the 2 ft vessel, R1 geometry at 280 rpm, for a 0.2 molar sodium sulphate solution,. 224
Figure 5-27: Bubble rise velocities versus superficial gas velocities measured by the dynamic gas disengagement technique in the 2 ft vessel, R1 geometry at 280 rpm, for a 20 ppm PPG solution. 225
Figure 5-28: Boiling acetic acid d_{10} and d_{32} from photographic analysis in Buchi R1 geometry 226
Figure 5-29: Boiling acetic acid large and small bubbles from DGD analysis in the Buchi R1 geometry. 227
Figure 5-30: Boiling aniline d_{10} and d_{32} from photographic analysis at an inlet v_S of 0.0066m/s in Buchi R1 reactor geometry. 227
Figure 5-31: Boiling aniline small bubbles sizes from DGD analysis at an inlet v_S of 0.0066m/s in Buchi R1 reactor geometry. 228
Figure 5-32: 20 ppm PPG solution; d_{10} and d_{32} from photographic analysis on two sizes of equipment; the Buchi R1 and the 0.61 m vessel R1 geometries 228
Figure 5-33: Bubbles sizes in 20 ppm PPG from DGD analysis on two sizes of equipment; the Buchi R1 and the 0.61 m vessel R1 geometries. 229
Figure 5-34: Bubble sizes in the Buchi 1 geometry for 0.2 molar sodium sulphate solution d_{10} and d_{32} are from photographic analysis 229
Figure 5-35: Buchi R1 geometry. 0.2 molar sodium sulphate solution large and small bubbles sizes from DGD analysis. 230
Figure 5-36: Buchi R1 mean bubble sizes. Cold, hot and boiling water at 1 and 10 atmospheres pressure at various v_S showing d_{10} and d_{32} from photographic analysis 230

Figure 5-37: Buchi R1 geometry. Cold and boiling water, small bubbles sizes from DGD analysis at various v_S 23
Figure 5-38: Buchi R1 geometry. 0.2 molar sodium sulphate solution d_{10} and d_{32} from photographic analysis at fixed rpm and various superficial gas velocities. 23
Figure 5-39: Buchi R1 geometry. 0.2 molar sodium sulphate solution large and small bubbles sizes from DGD analysis at fixed rpm and various superficial gas velocities. 23
Figure 5-40: Mean bubble sizes in the Buchi R1 reactor geometry. Cold demineralised water, d_{10} and d_{32} from photographic analysis at fixed rpm and various superficial gas velocities 23
Figure 5-41: Buchi R1 geometry. Cold demineralised water, mean small bubbles sizes from DGD analysis at fixed rpm and various superficial gas velocities. 23
Figure 5-42: Buchi R1 geometry. Boiling demineralised water, mean d_{10} and d_{32} from photographic analysis at fixed rpm and various superficial gas velocities 23
Figure 5-43: Buchi R1 geometry. Boiling demineralised water, small bubbles sizes from DGD analysis at fixed rpm and various superficial gas velocities. 23
Figure 5-44: Buchi R1 geometry. Cold aniline, d_{10} and d_{32} from photographic analysis at a fixed 1300 rpm and various superficial gas velocities 23
Figure 5-45: Buchi R1 geometry. Cold aniline, small bubbles sizes from DGD analysis at 1300 rpm and various superficial gas velocities. 23
Figure 5-46: Buchi R1 geometry. Boiling aniline, d_{10} and d_{32} from photographic analysis at 1300 rpm and various superficial gas velocities. 23
Figure 5-47: Buchi R1 geometry. Boiling aniline, small bubbles sizes from DGD analysis at 1300 rpm and various superficial gas velocities. 23
Figure 5-48: Gas hold-up for cold water in Buchi 1 geometry: P/V varied. Operation in homogeneous and heterogeneous regime/ 23
Figure 5-49: Total gas hold-up for cold and boiling demineralised water in Buchi 1 as a function of superficial gas velocity 23
Figure 5-50: Gas hold-up for boiling aniline in Buchi 1 geometry. Operation is in the homogeneous regime. P/V varied. 23
Figure 5-51: Gas hold-up for boiling acetic acid in the Buchi 1 geometry: Operation in homogeneous and heterogeneous regime. P/V varied. 23
Figure 5-52: Test of equation (5.2) $(dh/dt)_{(t)} = v_S$ at steady state 24
Figure 5-53: Effect of 205 micron glass ballotini solids on the dense phase gas hold-up. Data from the 0.61m vessel R2 geometry. Superficial gas velocity is constant at 0.07 m/s. 24
Figure 6-1: Types of agitators used in the mixing studies. Note A315 –up rotates in anti-clockwise direction. The remaining agitators are rotated clockwise. 24
Figure 6-2: Power numbers for the Rushton turbines used in the mixing work on the 0.286 m diameter tank. 25

Figure 6-3: Power numbers for the D = T/2, SCABA 6SRGT obtained in water in the 0.286 m diameter tank 256
Figure 6-4: Power numbers for the 0.15 m diameter LIGHTNIN A310 agitator in water in the 0.286 m diameter tank for H=T. 256
Figure 6-5: Power numbers for the 0.145 m diameter 4MFD agitator in water in the 0.286 m diameter tank 257
Figure 6-6: Power numbers for the 4MFU agitator in water in the 0.286 m diameter tank 257
Figure 6-7: Flow patterns for single agitators at a clearance of $T/4$, illustrating the effects of agitator choice and H/T on the flow patterns. 259
Figure 6-8: Flow patterns for multiple agitators: Effect of agitator separation and the clearance of top agitator on the flow patterns. 260
Figure 6-9: Dual A345 agitators. Caustic injected into the bottom zone: 261
Figure 6-10: A 6HBT below a 6MFU as per Figure 6-7(c). The 6MFU is one agitator diameter from the free surface. Video clip from a colour change experiment obtained by adding caustic at the side of the bottom 6HBT. 261
Figure 6-11: Effect of specific power input on mixing to 90% in water for various agitators in the 0.286 m vessel. Note that in all cases the D/T on the figure is approximate. For example the actual D of the A310 is 0.524T. The actual D/T is used in all calculations. See Table 6-4 for precise D/T information. 265
Figure 6-12: Effect of specific power input on mixing to 95% in water for various agitators in the 0.286 m vessel. 265
Figure 6-13: Determination of the effect of agitator diameter on mixing for Rushton turbines in water in the 0.286 m diameter tank. Power law fit. 266
Figure 6-14: Data for $H = T$ geometries plotted against the Cooke *et al.* (1988) correlation (equation 2.54). 268
Figure 6-15: Data for $H = T$ geometries against the Ruszkowski (1994) correlation (equation 2.55). 268
Figure 6-16: The effect of H/T on the mixing power number ($Nt_{95}Po^{1/3}$) for single agitators at $c = T/4$ in the 0.286 m diameter vessel. 269
Figure 6-17: The effect of the liquid height on the mixing power number ($Nt_{95}Po^{1/3}$) for single agitators at $c = T/4$ in the 0.286 m diameter vessel. 270
Figure 6-18: Comparisons of mixing constants at different aspect ratios (H/T) for single agitators in 0.286 m diameter vessel with the Cooke *et al.* (1988) prediction given by equation (6.2) 272
Figure 6-19: dual agitators, a parabolic blade 6HBT below a 6MFU-45°. 273
Figure 6-20: Typical average 4-pixel conductivity-time history. From the measurement file the injection first appeared at frame 21 and 150 data points were collected in 33.0 s. From this data 90% mixing is achieved at frame 65. Thus: t_{90} = (65-21) x 33/150 = 9.68 s 278
Figure 6-21: Typical mutual bulk resistance time history. P1 to P8 are the tomography plane numbers, with 16 electrodes in each plane 278

Figure 6-22: Various hollow blade shapes and mountings. Shown as clockwise rotation so concave to flow direction. 28
Figure 6-23: Concave hollow blade details referred to in Table 6-8. 28
Figure 6-24: Fitting the normalized Power numbers of hollow 6-blade turbines to the aspect ratio of the impeller; (a) - best fit for disc type hollow blade turbines; below – (b) fit for all types of concave hollow blade turbin 28
Figure 7-1: Selection of hollow blade agitators 28
Figure 7-2: Pictures of flow from a $D = T/2$ SCABA 6SRGT in aerated 0.4% CMC, viewed from below. T = 0.286 m. Agitator clearance was $T/3$. For flow conditions see Table 7-1. 29
Figure 7-3: Same as Figure 7.1 but viewed from the side. Agitation rate is 480 RPM. Still (a) is as the gas is introduced. Subsequent pictures are shown in real time as shown on the video clock. Flow conditions are given in Table 7-1 29
Figure 7-4: From Wisdom (1973), depicting the effect of agitation and air rate on gas distribution using a Rushton Agitator under "flooded" conditions 29
Figure 7-5: Showing the transition between "flooding" and "loading" (N_F) and "loading" to "complete dispersion" (N_{CD}) for radial turbines 29
Figure 7-6: Refit of for D/T in equation 7.5 from Nienow *et al.* (1985) 30
Figure 7-7: Data of Saito *et al.* (1992) relating Gas flow number and Froude number for D=T/3 Rushton and 6SRGT turbines in air-water. 30
Figure 7-8: Observed "flooding-loading" and "loading-complete dispersion" transition: comparison with theory of Nienow *et al.* (1985). Top (a) is for the 0.9144 m vessel and bottom (b) is for the 1.79 m diameter vessel 30
Figure 7-9: Type A: Gassing factors versus agitation speed for the 0.149 m diameter 6SRGT agitator in the 0.286 m diameter vessel for air-water. (Note that in these figures the gassing rates are given at outlet conditions) 30
Figure 7-10: Type B: Gassing factors versus agitation speed for the 0.248 m diameter parabolic 6HBDT agitator in the 0.61 m diameter vessel for air-water. 30
Figure 7-11: Type C: Gassing factors versus agitation speed for the 0.145 m diameter parabolic 6HBT agitator in the 0.286 m diameter vessel for air-water. 30
Figure 7-12: Type D: Gassing factors versus agitation speed for the 0.4148 m diameter parabolic 6HBT agitator in the 0.914 m diameter vessel for air-water. 30
Figure 7-13: Type B: Gassing factors versus specific shaft power for the 0.248 m diameter parabolic 6HBDT agitator in the 0.61 m diameter vessel for air-water. 30
Figure 7-14: An expanded view of the "flooding- loading" transition for data from Figure 7-8 - Type B: Gassing factors versus agitation speed for

the 0.248 m diameter parabolic 6HBDT agitator in the 0.61 m diameter vessel for air-water. 310
Figure 7-15: Comparison of the specific gas buoyancy power with the specific shaft power at the "flooding-loading" transition for the various hollow blade agitators described in Table 7-4. The dotted line represents equal gas and shaft power at the transition. Data for both graphically and visually determined transitions are included. 312
Figure 7-16: Gassing factors as a function of gas flow number for various agitator types and scales at an ungassed specific power input of approximately 0.5W/kg in air -water 319
Figure 7-17: Gassing factors as a function of gas flow number for various agitator types and scales at an ungassed specific power input of approximately 3 W/kg in air –water 320
Figure 7-18: The effect of adding surfactant to the water on the gassing factor for the same hollow blade turbine (6HBT), at a specific energy input of approximately 3W/kg 320
Figure 7-19: Gassed power data for Rushton turbines on two scales plotted against the superficial gas velocity, at an ungassed specific power input of approximately 3 W/kg. 321
Figure 7-20: Illustrating the fit of the air-water hold-up data for various agitators and vessel geometries to eq. (7.13). 325
Figure 7-21: Comparison of overall gas hold-up with local axial values for a 0.61 m diameter bubble column. Local hold-up probe is 9.5 cm from the vessel wall. Fluids are air-20 ppm PPG. Superficial gas velocity is 0.06 m/s 328
Figure 7-22: Comparison of overall gas hold-up with local axial values in the 0.61 m diameter vessel agitated with three LIGHTNIN A345 up-pumping agitators at 274 RPM and a superficial gas velocity of 0.05 m/s in aerated 20 ppm PPG solution. Axial profile is taken 7 cm from the vessel wall, midway between the baffles. 328
Figure 7-23: Comparison of overall gas hold-up with local axial values in the 0.61 m diameter vessel agitated with a 6HBT below a 6MFU agitator at 300 RPM and a v_S of 0.07 m/s in aerated 20 ppm PPG solution. Axial profile is taken 7 cm from the vessel wall, midway between the baffles. 329
Figure 7-24: Comparison of mean $k_l a$ values in the 0.61 m diameter vessel, in aerated 20 ppm PPG solution, for three different agitator configuration at various agitation and gas rates. 333
Figure 7-25: Agitators tested *for* solid suspension on the 0.286 m vessel 339
Figure 7-26: A 0.15 m diameter 6HBDT agitator in the 0.286 m diameter tank for a 0.54 wt fraction of glass ballotini in water. Illustrating progression of solids pick-up, from the vessel base, with increasing agitation speed up to N_{JS} 343
Figure 7-27: The above pictures are of the 0.286 m vessel containing 0.54 wt fraction of 206 micron glass ballotini beads. Agitation is by the 0.15 m diameter 6HBDT. They illustrate the progressive expansion of solids

bed as agitation speed is increased. For glass Ballotini solids it requires approximately twice the just suspension speed to obtain a bed expansion to the surface, when no gas is introduced.....34
Figure 7-28: Illustration of the increase in power factor below N_{JS} for hollow blade agitators suspending 206 micron glass ballotini in water, in the 0.286 m tank.....34
Figure 8-1: Schematic of the stirred tank rigs using a spinning cone with three LIGHTNIN A345 agitators.....36
Figure 8-2: Cone pumping-rate measuring rig.....36
Figure 8-3: Cones used in scouting experiments in the 0.61m diameter vessel.....36
Figure 8-4: Cone pumping considerations.....36
Figure 8-5: Data fit for 30^0cones to: $Q = 21.8" g_r" r^{1.37} (l/\min)$.....36
Figure 8-6: Data fit for all cones to:.....37
Figure 8-7: Pumping rate data fit to: $Q = 2\pi r^2 \sqrt{\frac{\omega\mu \sin\phi_C}{\rho}}$.....37
Figure 8-8: Optimum cone angle for pumping with fixed cone inlet and outlet diameters. Predicted using equation (8.18) for water with conditions N = 600 RPM, r_o = 7.5 cm and r_i = 2.5 cm. Indicates a maxima at around 40°.....37
Figure 8-9: Affect of aeration and surfactants on the pumping rates of cones, for 30° plastic cones. Gas hold-up approximately 20% under aerated conditions.....37
Figure 8-10: Showing the effect of blocking-up the inside of a 30° cone on pumping. Flow rate is approximately halved Solid line is prediction from equation (8.17).....37
Figure 8-11: Reduction in gas hold-up using a 30° cone on reactor geometry 2. System is air-water with 20-ppm polypropylene glycol added as a surfactant.....37
Figure 8-12: Foam out on the 0.61 m vessel due to aerated 10 ppm soap.....37
Figure 8-13: Dual A345 agitators with a 30°cone in the 0.61 m diameter vessel.....37
Figure 8-14:. 0.61 m vessel. Cone flooded, agitator switched on to bring foam under control for a 10 ppm soap solution.....37
Figure 8-15: Level coming under control in the 0.61 m vessel at 274 rpm for a 10 ppm soap solution.....38
Figure 8-16: Level completely under control for the 0.61 m vessel at 274 rpm for a 10 ppm soap solution.....38
Figure 8-17: The cone is flooded in the 0.61m diameter vessel at 274 rpm for a soap solution increased to 16 ppm.....38
Figure 8-18: picture of cone used in the 0.914m vessel work.....38
Figure 8-19: The reduction of the foam at 180 rpm after complete foam-out at 40 rpm in the 0.914 m tank for a 10 ppm soap solution.....38
Figure 8-20: Equilibrium foam at 180 rpm in the 0.914 m tank for a 10 ppm soap solution.....38

Figure 8-21: Stable operation at 150 rpm in the 914 m tank for a 10 ppm soap solution. 384
Figure 8-22: Just coping with foam at 140 rpm in the 0.914 m tank for a 10 ppm soap solution. 384
Figure 8-23: Cone used in the Novozymes fermenter tests 387
Figure 8-24: Comparison of pilot plant runs with and without the spinning cone. 388
Figure 9-1: View looking inside the vessel at the tomography cage 394
Figure 9-2: Agitator used in tests 395
Figure 9-3: Gas sparging with no agitation 399
Figure 9-4: Sequence of two measurement sets following the addition of a high conductivity trace near the lower impeller (time interval approximately 0.5 s) 400
Figure 9-5: Tomographical images of (left) liquid and (right) gas-liquid mixing at 300 rpm. Overall gas-liquid hold-up for the gas-liquid case was 23.4%. Operation was in the bubble regime 400
Figure 9-6: Tomographic images for mixing at 360 rpm. Overall gas hold-up 50%. $v_S = 0.1\text{m/s}$ 401
Figure 9-7: Sequential mixing of tracer in the bottom plane. Addition is top left. There is a 0.33 s time interval between images. 402
Figure 9-8: Mean conductivity values at each measurement following addition of high conductivity pulse (top) addition near impeller, (bottom) on liquid surface 403
Figure 9-9: Large ball suspended in vessel 406
Figure 9-10: Balls used in test 406
Figure 9-11: Experimental Set Up 407
Figure 9-12: Schematic of electrode strip 408
Figure 9-13: Radial positions of object within sensor 408
Figure-9-14: Time series of tomographic images from plane 5 as the 3 inch stainless steel ball is moved across the measurement plane 410
Figure 9-15: Maximum pixel conductivities with 76 mm stainless steel sphere suspended in measurement plane 5 for (a) all measurement planes and (b) measurement planes 4, 5 & 6 412
Figure 9-16: Maximum pixel conductivities with 76 mm stainless steel sphere suspended between measurement planes 4 & 5 for (a) all measurement planes and (b) measurement planes 4 & 5 413
Figure 9-17: 3-*D* images of the sensor showing the ball in the first six positions 414
Figure 9-18: Maximum pixel conductivities with 25 mm stainless steel sphere suspended in measurement plane 5 for (a) all measurement planes and (b) measurement planes 4, 5 & 6 416
Figure 9-19: Maximum pixel conductivities with 25 mm stainless steel sphere suspended between measurement planes 4 & 5 for (a) all measurement planes and (b) measurement planes 4 & 5 417

Figure 9-20: Minimum pixel conductivities with golf ball suspended in measurement plane 5 for (a) all measurement planes and (b) measurement planes 4, 5 & 6 41
Figure 9-21: Minimum pixel conductivities with golf ball suspended between measurement planes 4 & 5 for (a) all measurement planes and (b) measurement planes 4 & 5 41

ACKNOWLEDGMENTS

The author wishes to sincerely thank professor Peter Heggs for his help, support and guidance throughout this project.

Thank you to the engineers from Dupont Polyesters particularly, Martin Davis, Duncan Housley, Finbar McDonnell and Eric Hindmarsh who have provided support and many interesting problems. Likewise Huntsman polyurethane's; in particular, Don Jones and Archie Eaglesham.

Grateful thanks to Richard Halliwell and Denis Corrigan, from SOG at Runcorn Heath, for their invaluable help with designs and for the project work which helped to support this work.

Thank you to ICI Technology Group for the research grant, the assistance in setting up the equipment and also to Hamish Rankin who made my transfer to UMIST possible. Also, David Southgate from ICI Paints for his interesting problems.

All the past students I have worked with who enlivened the workplace and gave me valuable assistance.

I also to thank my co-workers Alvin Nienow, John Middleton, Waldek Bujalski, Colin Chapman, Larry Gibilaro, Steve Davies, Gary Bolton, Ken Primrose, Peter Lynch and Klaus Gezork. I also like to thank the support and workshop staff at UMIST, in particular Stewart Grace, Bob Clegg, Andy Evans, Tony Diggle, Craig Shore and Brian Handcock.

Dedications

This thesis is dedicated to my wife Maria and my children Paul, Liz, Patrick and Anthony without whose support I would never have attempted this project.

GLOSSARY

a	Acceleration	$m\ s^{-2}$
a	Interfacial area	$m^2\ m^{-3}$
A_e	Heat transfer area	m^2
B	Baffles	
B_d	Agitator blade depth	m
c	Clearance from centreline of agitator to bottom of vessel	m
c_S	Clearance of sparger from bottom of tank	m
C	Concentration	$kmol\ m^{-3}$
C^*	Equilibrium concentration	$kmol\ m^{-3}$
C_A	Concentration of component A	$kmol\ m^{-3}$
C_B	Concentration of component B etc	$kmol\ m^{-3}$
C_{od}	Drag coefficient	
d_p	Diameter of particle	m
d_{10}	Number mean bubble size	m
d_{32}	Sauter mean bubble size	$m^3\ m^{-2}$
d_b	Diameter of bubble	m
D	Dimension, Impeller diameter	m
D_C	Diameter of cavern or cone	m
D_S	Diameter of sparger	m
Da	Damkohler number = τ_D/τ_R	
D_L	Diffusion coefficient of gas in liquid	$m^2\ s^{-1}$
E_G	Volume fraction of gas	
E_T	Total energy input by agitator and gas	W
F	Fouling factor	
Fl_G	Agitator gas flow number = Q_G/ND^3	
Fr	Froude number = N^2D/g	
g	Gravitational constant	$m\ s^{-2}$
"g"	Ratio of centrifugal force to gravitational force = $D\omega^2/2g$	
H	Height	m
H_L	Liquid height	m
H_p	Pumping head	m
Ha	Hatta number = $\sqrt{\tau_D/\tau_R}$	
H_C	Height of cavern	m

h	Height of cone above the liquid level	m
h_O	Process side heat transfer film coefficient	$W\ m^{-2}K^{-1}$
I	Specific intensity of turbulence	
K	Consistency factor	Pa s
k	Wave number	
k_h	Constant in eq (2.13)	
k_1 *and* k_2	Reaction rate constants	
k_m	Proportionality factor for mixing equations	
k_r	Ratio of tangential fluid velocity to impeller tip velocity	
k_S	Agitator shear rate constant	
k_L	Liquid side mass transfer coefficient	$m\ s^{-1}$
k_G	Gas film mass transfer coefficient	$m\ s^{-1}$
k_La	Liquid side mass transfer factor	s^{-1}
K_L	Overall liquid side mass transfer coefficient	$m\ s^{-1}$
K_G	Overall gas side mass transfer coefficient	$m\ s^{-1}$
He	Henry's law partition coefficient (consistent units)	
M	Torque	N m
M	Mixing index = $1-\sqrt{\sigma_C^2}$	
N	Agitation speed	s^{-1}
N_C	Agitation speed for complete suspension of solids	s^{-1}
N_Q	Agitator liquid flow number = Q_l/ND^3	
N_{JS}	Agitator just suspension speed for solids	s^{-1}
N_{SS}	Agitation speed for the onset of sedimentation	s^{-1}
P	Power	W
P_Q	Power input by gas	W
P_S	Shaft Power	W
P_t	Theoretical cone power	W
P_G	Shaft power under gassed conditions	W
p_i	Partial pressure of transferring species at the interface	Atm
p_G	Partial oxygen pressure	Atm
Po	Agitator power number = $P/(\rho N^3D^5)$	
Q	Volumetric flow-rate	$m^3\ s^{-1}$
Q'	Volumetric flow-rate of recirculating gas	$m^3\ s^{-1}$
Q_S	Volumetric flow-rate of sparged gas	$m^3\ s^{-1}$
$Q_{H_2O_2}$	Molar feed rate of hydrogen peroxide	$mol\ s^{-1}$
Q_H	Rate of heat transfer	$W\ s^{-1}$

Q	Stoichiometric ratio	
Re	Agitator Reynolds number = $ND^2\rho/\mu$	
Re_d	Drop Reynolds number = $vd_p\rho/\mu$	
r_A	Rate of reaction of A	mol s^{-1}
R	Radius	m
R	Gas constant	J mol^{-1} K^{-1}
Ri	Richardson Number = Static head/dynamic head.	
s	Shape factor in Zwietering equation	
S	Agitator separation	m
S	Surface area of bubbles	m^2
Tay	Cone Reynolds number = $\rho\omega r^2/\mu$	
t	Time	s
t_C	Circulation time	s
t_m	Colorimetric based mixing time	s
t_{90}	90% mixing time	s
t_{95}	95% mixing time	s
T	Temperature	°C
ΔT	Temperature difference	°C or K
T	Tank diameter	m
U	Velocity	m s^{-1}
u_t	Terminal rise velocity of a bubble in an infinite medium	m s^{-1}
U_o	Overall heat transfer coefficient	W $m^{-2}K^{-1}$
V	Volume	m^3
v	Velocity	m s^{-1}
Va	Tracer volume	m^3
VVM	Volume of gas per volume of liquid per minute	min^{-1}
v_S	Superficial gas velocity	m s^{-1}
v_s	Velocity of material leaving the cone = $2\pi Nr_o$	m s^{-1}
v_t	Agitator tip velocity	m s^{-1}
W	Power	Watts
We	Weber number = $\rho N^2D^3/\sigma$	
X	Weight of solids per weight of liquid	
X_d	Agitator disc thickness	m
w	Agitator blade width (height for radial type)	m
	Greek letters	
α	Distribution coefficient between fresh and recirculating gas	

δ	Film thickness	m
σ	Surface tension	N m
σ_C	Standard deviation on concentration fluctuations	
ϕ	Angle to the vertical	°
ρ	Density	kg/m^3
κ	Thermal conductivity	$W\ m^{-1}K^{-1}$
λ	1/He	
Σ	Conductivity	$mS\ cm^{-1}$
λ_k	Kolmogorov length scale	m
τ	Shear stress	$N\ m^{-2}$
τ_y	Yield stress	$N\ m^{-2}$
τ_c	Time constant = 1/rate constant	s
τ_D	Characteristic diffusion time constant	s
τ_R	Characteristic reaction time constant	s
τ_p	Time constant of DOT probe	s
μ	Viscosity	Pa s
μ_a	Apparent viscosity of non-Newtonian fluid	Pa s
θ	Specified degree of mixing	
ϑ_t	Exposure time	s
ω	Angular velocity	radians s^{-1}
$\varepsilon_G, \varepsilon_L, \varepsilon_S$	Volume fraction of dispersed phase	
ε_T	Energy dissipation rate	$W\ kg^{-1}$
ν	Kinematic viscosity	$m^2\ s^{-1}$
γ	Shear rate	s^{-1}
$\dot{\gamma}$	Average shear rate	s^{-1}
	Subscripts	
G	Gas	
D	Dynamic	
B or b	Bubble	
HB	Herschel-Bulkley:	
JS	Just suspended	
L	Liquid	
NN	Non Newtonian	
r	Applies to submerged radius (cones work)	
S	Solid or specific	
tb	Tiny bubbles	

I	Inside or inlet conditions	
O	Outside or outlet conditions	
U	Ungassed	
w	Water	
	Abbreviations	
A345	LIGHTNIN high solidity up-pumping hydrofoil	
6CDT	6 Curved blade Disc Turbine (van't Riet or Smith type)	
6HBT	6 Hollow Blade Turbine	
6HBDT	6 Hollow Blade Disc Turbine (includes Smith type)	
CCD	Charged Couple Devices	
CFD	Computational Fluid Dynamics	
CD	Complete Dispersion	
CSTR	Continuous Stirred Tank Reactor	
CMC	Sodium Carboxyl-methyl-Cellulose	
DGD	Dynamic Gas Disengagement	
ERT	Electrical Resistive Tomography	
F	Flooding	
L	Loading	
LDA	Laser Doppler Anemometry	
LIF	Laser Induced Fluorescence	
PBT	Pitched Blade Turbine	
6PBTD	6 Pitched Blade Turbine Down pumping	
6T	Six blade Turbine	
MFD	Mixed Flow Down	
OUR	Oxygen Uptake Rate	kmol $m^{-3} s^{-1}$
OTR	Oxygen Transfer Rate	kmol $m^{-3} s^{-1}$
MFU	Mixed Flow Up	
PBT	Pitched Blade Turbine	
PVC	Poly Vinyl Chloride	
PPG	Poly Propylene Glycol	
PIV	Particle Image Velocimetry	
RT	Rushton Turbine	
RPD	Relative Power Demand	
rms	Root Mean Square	
rpm	Revolutions per Minute	
www	World Wide Web	

Chapter 1 Introduction

In 24 years working as an experimental fluid mechanic in the ICI Mixing and Reactions Team it always seemed as I was working on the mixer or reactor design with "Attitude". When I first started it was in a "blue sky" team called "The Process Intensification Group" with objectives of finding new ways of doing things, developing new processes; intensifying old processes, preferably using "gizmos" – cyclones, tee jet mixers and static mixers. Latterly, as manager of The Experimental Fluid Dynamics Laboratory at ICI Widnes Experimental Centre, it was boiling reactors with high gas phase fractions (up to 60%), high solids concentrations, (up to 30%), high stirring intensities (up to 10 kW/kg), high superficial gas velocities (typically 0.25 m/s) giving foaming and carry-over problems, high temperature, high pressure, corrosive, explosive, toxic (all of which make flow visualisation of reaction brews very difficult); or it was high viscosity, non-Newtonian fluids as found in fermenters or paint mixers. Mixing was also a big issue when scaling up reactors where competing reactions were mixing sensitive. In that period, the mixing literature seemed to be concentrating very much on air-water systems at low power inputs with specific energy dissipation rates, (ε_T) up to ~2 W/kg and gas flow rates of up to ~2 *VVM* or superficial gas velocity, v_S, of <~0.01 m/s and was not always a useful guide to dealing with the problems. At high gas hold-ups even prediction of shaft power is difficult as operation is way outside published correlations.

This PhD is therefore dedicated to the study of the design of reactors with "Attitude" and addresses questions such as how to experimentally study "real reactors" using real fluids or good analogues at appropriate specific energy dissipation rates (up to 10 W/kg) and superficial gas velocities up to 0.25 m/s. Chapter 2 gives a critical literature review on topics, general to multi-phase mixing and reactor design with mechanical agitation, with more specific reviews in the following chapters as appropriate.

Introduction

The general experimental equipment is described in Chapter 3. These are the 1 ft (0.29 m diameter), 2 ft (0.61 m diameter) and 3 ft (0.91 m in diameter) mixing rigs, with the shaft torque measuring systems and techniques developed to measure shaft torque, mixing, gas-liquid mass transfer, local phase fractions, overall phase fractions, bubble measurement techniques and Electrical Resistive Tomography (ERT).

Model fluids are described in Chapter 4 along with scale-up and scale down techniques.

The Buchi rig is described in Chapter 5 along with its use in obtaining data on "real fluids" with the effect of boiling and pressure on bubble size and phase fraction. The effect of solids on the gas phase fractions is also investigated. Data for cold and boiling water, aniline, acetic acid and methanol are included. Two techniques are developed and discussed to estimate bubble sizes and phase fractions (photographic and dynamic disengagement).

Chapter 6 describes power, mixing and hydrodynamics for single-phase fluids using novel agitators or agitator combinations with comparisons against conventional agitators such as the Rushton turbine.

Multi-phase work is presented in Chapter 7. This covers high gas fractions, high superficial gas velocities and specific agitator power inputs from zero (bubble column) up to ~10 W/kg. Mixing, gas-liquid mass transfer, gas-hold-up and hydrodynamics are studied. Rules for avoiding foam out at high phase fractions are developed. Solid suspension with novel agitators for two and three phase systems are tested and relationships developed.

Chapter 8 describes and characterizes a novel device (spinning cone) for controlling foam and its level. The literature is also studied.

In Chapter 9, ERT is studied as a diagnostic tool. The literature is examined and the retrofit of an 8 plane x 16 elements ERT into the 0.61 m diameter stirred tank rig is described. Teething problems are discussed and eliminated. The use of ERT to study mixing and phase distribution in high phase

fractions at high specific energy dissipation rates is demonstrated and some interesting results presented and discussed.

In Chapter 10 an overview of the work and the main conclusions are given along with recommendations for further work.

Appendices containing data, calculations and addition information follow Chapter 10.

Chapter 2 Literature Reviews

2.1 Scope

The multi-phase stirred tank literature is very extensive; hence the following review concentrates on the aspects considered most pertinent to this study as defined in Chapter 1. This study is therefore confined to the hydrodynamic understanding and the design of mechanically agitated contactors and reactors for single (liquid) and multi-phase (liquid-solid-gas) systems. Typical industrial important examples of gas-liquid reactions carried out in mechanically stirred contactors are organic oxidations, carbonations, hydrogenations, fermentations, nitrations and chlorinations. Many of these involve a boiling solvent that contributes to the vapour loading and many also include solids either as a reactant, catalyst or a product.

The purpose of gas-liquid contacting in mechanically agitated vessels is to cause mass transfer between the phases. In purely physical absorption or stripping processes, mass transfer rates will often determine the equipment size needed for a given duty. Where the transferred species has to undergo a chemical or biochemical reaction the mass transfer rate is often the limiting step. Break-up of bubbles to provide the interfacial area is thus an important consideration. The understanding the hydrodynamics of the bubble break-up – coalescence and mixing processes and how these are affected by the vessel and agitator design is paramount to good design and reliable scale-up.

This chapter presents a critical review of the literature on mechanically agitated gas-liquid and gas-liquid-solid contacting with special attention to the purpose of mechanical agitation, agitator choice, design, hydrodynamics and scale-up and also the tools available to experimentally study these systems. Liquid-liquid is recognized as an important branch of multi-phase contacting but is not covered in any detail by this study, as the breadth would become too wide.

Literature Reviews

Over the years many reviews have been published in the gas-liquid mixing area. Examples include Sideman *et al.* (1966) and van't Riet (1979) who published critical reviews of mass transfer in gas-liquid contacting systems. General reviews have been published by Joshi *et al.* (1982), Midoux and Charpentier (1984) and more recently Nienow (1998) published an excellent review of the hydrodynamics of stirred bioreactors.

The general consensus is that an optimum design and scale-up of a reactor depends on an understanding of the underlying hydrodynamic principles and their interaction with the agitation, the dependence on the fluid properties and reaction kinetics where a reaction is involved.

Mathematical studies are increasingly popular because of the low cost of computation, due to the recent staggering increase in computational power and speed. The physics and chemistry can be linked together into a single package. Computational fluid dynamics (CFD) is one such tool that is an increasingly popular method for studying the hydrodynamics of single and multi-phase systems. Whilst recognizing the increasing importance of these tools, especially when dealing with complex systems, this study is more concerned with physical experimentation.

2.2 Outline

Factors considered important for multi-phase contacting and reactor design include (in alphabetical order), agitation, agitator power prediction, baffles, bubble behaviour, heat and mass transfer, hydrodynamics, kinetics, mixing, phases, physical properties, rheology, scale, time scales, turbulence and vessel design. These are considered in the following sections. Firstly, however, the dimensionless numbers used in the text are introduced and defined.

2.2.1 Introduction to the Dimensionless Groups

Dimensionless groups are commonly used in the mixing literature to correlate data in terms of physical properties, scalar quantities and time. These are described in the following sub-sections.

Commonly accepted nomenclature used in these groups are shown in Table2.1

a	Interfacial area	$m^2 m^{-3}$
c	Impeller clearance from bottom of base to impeller centreline	m
D	Dimension, Impeller diameter	m
g	Gravitational constant	$m s^{-2}$
k_S	Metzner and Otto (1957) shear rate constant	
Q	Volumetric flow-rate	$m^3 s^{-1}$
N	Agitation speed	s^{-1}
t	Time	s
T	Tank diameter	m
U	Velocity	$m s^{-1}$
V	Volume	m^3
w	Agitator blade width	m
ξ	Axial coordinate	m
σ	Surface tension	N m
ρ	Density	$kg m^{-3}$
μ	Viscosity	Pa s
ω	Angular velocity	$rads s^{-1}$
γ	Shear rate	s^{-1}

Table 2-1: Nomenclature used in the dimensionless groups used in hydrodynamic studies

2.2.1.1 Agitator Reynolds Number, Re.

In mixing the Reynolds number is an important group. It is the ratio of inertial to viscous forces. For an agitator the Reynolds number is defined as:

$$\mathrm{Re} = \frac{ND^2\rho}{\mu} \qquad (2.1)$$

Three agitation regimes are described by the agitator Reynolds number,

- Laminar, $\mathrm{Re} \leq 10$
- Transitional $10 > \mathrm{Re} < 10^4$
- Fully turbulent $\mathrm{Re} \geq 10^4$

Literature Reviews

The impellor Reynolds number in a non-Newtonian fluid uses an apparent viscosity μ_a calculated using the Metzner and Otto (1957) approach. They proposed that for the laminar regime, the average shear rate ($\dot{\gamma}$) was related to the agitator speed according to:

$$\dot{\gamma} = k_S N \tag{2.2}$$

where k_S is an agitator specific constant.

2.2.1.2 Agitator Power Number, Po.

The agitator power number Po is analogous to the friction factor in pipe flow. It represents the ratio of the pressure differences producing flow to inertial forces and takes the form:

$$\mathrm{Po} = \frac{P}{\rho N^3 D^5} \tag{2.3}$$

2.2.1.3 Agitator Flow Number, N_Q.

The flow number is a discharge coefficient used to define the liquid volumetric flow (Q_L) from the impeller blades in dimensionless terms:

$$\mathrm{N_Q} = \frac{Q_L}{ND^3} \tag{2.4}$$

where for a radial turbine

$$Q_L = \pi D \int_{-w/2}^{+w/2} U_r dz \tag{2.5}$$

i.e., the integral of the velocity over the blade height through the area swept by the blade tips. Revill (1982) reviewed the data for Rushton turbines (see Figure 2-9) and recommended that $N_Q = 0.75 \pm 0.15$ should be used for design for Re $\geq 10^4$ for $0.2 \leq D/T \leq 0.5$ and for $0.3 \leq c/T \leq 0.5$.

The velocity profile is bell shaped as depicted in Figure 2-1, with a maximum velocity around 0.8 of the tip speed, Oldhue (1983). The entrained flow is up to 2.5 times this flow.

For a SCABA 6SRGT (see Figure 2-12) the velocity profile is much more focused giving a pronounced peak, Kovács (2001) as shown in Figure 2-2, where it is compared to his Rushton turbine profile. From this work the maximum discharge velocity for the 6SRGT was 0.79 of the tip velocity.

For axial impellers the flow is defined through the swept circle immediately below the lower edge of the impeller for down pumping (opposite for up-pumping). Again the entrained flow is much greater than the directly pumped flow. Typical discharge coefficients for high solidity axial impellers are around 0.7 to 0.8 and are similar to the Rushton turbine. For $Re < 10^3$ the discharge coefficient falls. In laminar flow ($Re \leq 10$) the discharge coefficient can be an order of magnitude lower.

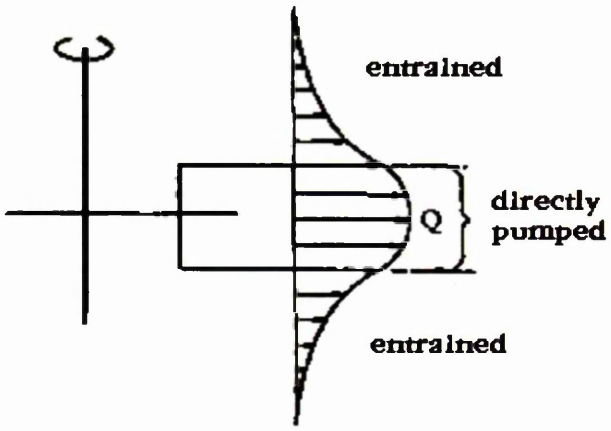

Figure 2-1: Discharge flow from a Rushton turbine. From Nienow (1998)

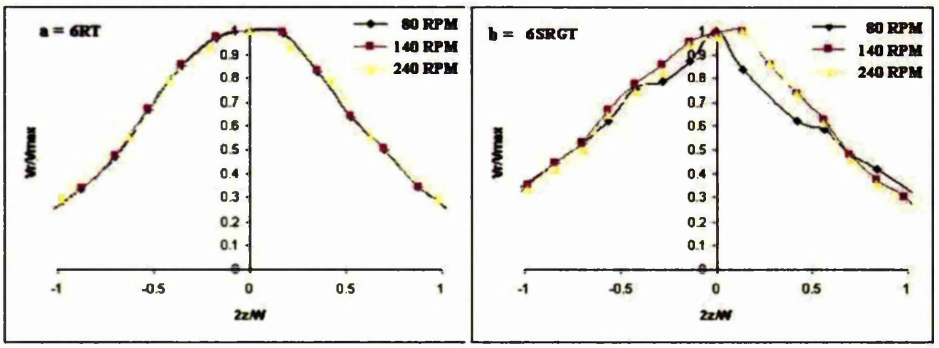

Figure 2-2: Normalised velocity profiles, a) Rushton turbine, b) 6SRGT from Kovacs (2001).

2.2.1.4 Gas Flow Number, Fl_G.

The gas flow number Fl_G (sometimes called aeration number) is the ratio of gas flow-rate Q_G to the agitator pumping rate

$$Fl_G = \frac{Q_G}{ND^3} \tag{2.6}$$

2.2.1.5 Froude Number, Fr

The Froude Number (Fr) is the ratio of inertial to gravitational forces:

$$Fr = \frac{N^2 D}{g} \tag{2.7}$$

Another way of expressing this ratio is in terms of "g" forces

$$"g" = \frac{(2\pi N)^2 D}{2g} = \frac{\omega^2 D}{2g} \tag{2.8}$$

where "g" is the ratio of the actual centripetal force at the agitator tip to the gravitational force. This is useful when deciding whether agitation effects or gravity will dominate in for example a gassed system. If "g" is < 1 then it is obvious that gravity will dominate. When "g" is >1 then the agitator will dominate. This effect is not always obvious from consideration of a Froude number. By comparison of equations (2.7) and (2.8), 19.74 "g" = Fr and therefore 1.0 "g" ≅ 0.05 Fr.

2.2.1.6 Weber Number, We

The Weber Number represents the ratio of applied to surface tension forces and is used to correlate particle, drop and bubble size.

$$We = \frac{\rho N^2 D^3}{\sigma} \tag{2.9}$$

2.2.2 Agitation

Agitated vessels come in many shapes and sizes and this has implications for all facets of mixing. Much of the literature work has been done on "standard vessels" so this standard has to be defined, as deviations will obviously effect the literature conclusions

The "standard" tank shown in Figure 2-3 has a centrally mounted vertical shaft to mount the impellers. In low viscosity fluids, baffles are used in to eliminate a central vortex, to make full use of the agitator power and as a means of converting rotary motion into vertical turnover patterns. Many baffling arrangements are possible. The standard used here (designed to apply full agitator power) is four vertical flat baffles of width $T/10$, 90^0 apart and set off the wall by a distance $T/60$. The amount of baffling will obviously effect the power. Many vessels are supplied with a baffle width of $T/12$ and here the power will be reduced by about 10% (Uhl and Gray, 1966). For agitator power prediction any deviations from standard have to be allowed for. Bujalski *et al.* (1987) found an effect of scale on Rushton turbines to $T^{0.067}$, also a strong dependency of power number on the disc thickness X_d.

For viscous mixing (Re ≤ 300) baffling is probably unnecessary. Here, the absence of baffling will have little effect on power as apparent from power curves of Po versus Re. See later, for example

Figure 2-29.

Mechanical agitation and the choice of agitators are obviously very important since it impacts directly on the operation and influences many of the factors listed above. The role of the agitation is to create turbulence and flow for bubble break-up, transport of material, heat and mass transfer, bulk mixing and homogenisation (minimisation of concentration and temperature

differences) of the phases. The choice of agitators depends on the duty required.

Tank diameter	T	1 m
Baffles	B	4
Baffle width	W_b	$T/10$
Baffle clearance from wall	S_b	$T/60$
Tank bottom		$T/4$ Dish
Impeller diameter	D	$T/3$
Blade length	L	$D/4$
Blade width	W	$D/5$
Blade thickness	X	
Disc thickness	X_d	
Disc diameter	D_d	$3D/4$
Impeller clearance	C	$T/3$
Submergence	S	$2T/3$

Table 2-2: Dimensions of the standard tank configuration

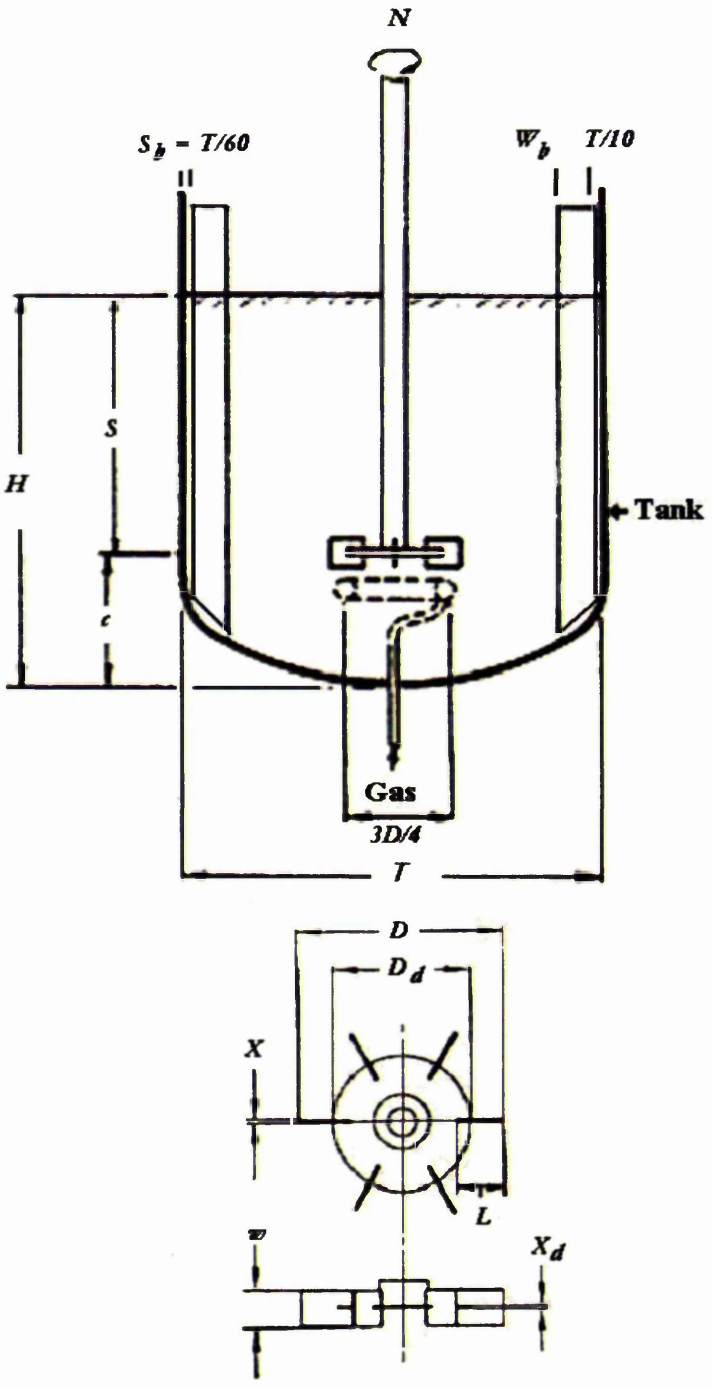

Figure 2-3: Standard Rushton turbine agitated vessel

Agitators can be broadly classed into three types, those producing radial flow, axial flow and mixed flow.

2.2.2.1 Radial Flow Agitators

Refer to pages 17 to 20.

Typical radial agitators are disc turbines and paddles. In cylindrical vessels at a clearance c above the base $\geq 1/5$ of the vessel diameter T, these agitators give two main circulation loops above and below the centre-line of the impeller as shown in Figure 2-4.

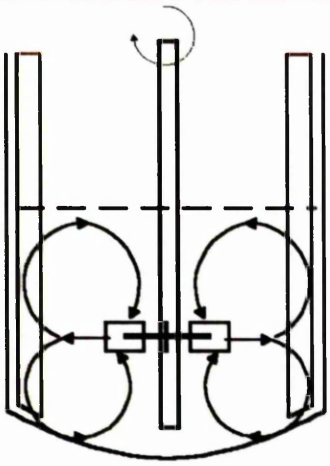

Figure 2-4: Main flow loops with a Rushton turbine

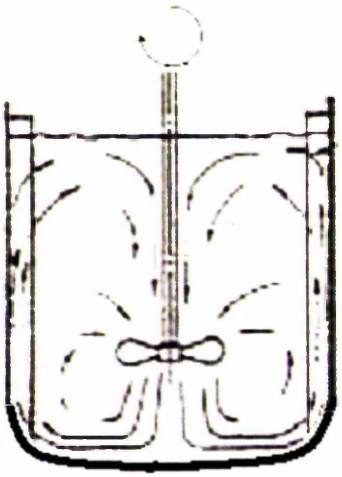

Figure 2-5: Main flow loops with an axial flow impeller

For gas-liquid duties, the radial Rushton turbine (see Figure 2-9) has traditionally been a popular choice. However, this has the disadvantage that the gas adversely affects the performance. Under gassed conditions, the

agitation power falls due to gas cavities that attach to the low-pressure region behind the blades. These cavities are described in detail by Warmoeskerken and Smith (1985) and Nienow *et al.* (1985).

Many workers have linked mass transfer coefficients to agitation power, for example, van't Riet (1979), Whitton and Nienow, (1993) and Gezork *et al.* (2001). With radial agitators mixing is also adversely affected by this loss in power as shown by Cooke *et al.* (1988) and Cronin *et al.* (1994). There may be some exceptions to this case for operation in the flooding regime (see later text on agitator hydrodynamic regimes) as with high gassing rates the recirculation caused by the rising plume of gas can actually improve the mixing, Cronin *et al.* (1994). As noted however by Nienow (1998), operation in the flooding regime is not a desirable design. At high gas rates the energy imparted by the gas can also be significant and if the gas and liquid flows are harmonized (act in the same direction) then mixing can be improved on gassing.

The blade profile is usually flat, though other profiles have been used to improve the performance. Examples are the arrowhead disperser and the curved blade impellers investigated by Rushton *et al.* (1950). The power characteristics of these are similar to the flat blade equivalents. In recent years a number of new radial agitators have come on to the market designed to prevent power loss on gassing and these are claimed to handle more gas than a Rushton turbine before flooding. Amongst these is the concave design attributable to van't Riet (1975a), now marketed as the CHEMINEER CD-6 (Figure 2-10), and the more streamlined versions such as the SCABA 6RGT (Figure 2-12) which Nienow (1998) claims will handle approximately 3-times as much gas as the same size Rushton turbine before flooding. A new asymmetric design has recently by introduced by CHEMINEER and marketed as the BT-6 (Figure 2-11). The manufacturers claim this to have nearly six times the gas handling capability of the Rushton impeller and to unload less than the CD-6. They also claim that the unloading (lowering of the gassing factor) is nearly all due to the change in effective density of the gassed

liquid. However, in this work, with similar agitators, gassing factors as high as 0.8 have been measured in systems with 50% gas hold-up, therefore the explanation for the fall in power on gassing is not as simple as that. This is discussed in greater detail in the section on agitator hydrodynamics. They also claim that the mass transfer capability of the BT-6 is on the order of 10% better than the CD-6 and that, unlike many other gas-dispersing impellers, the BT-6 is relatively insensitive to viscosity.

2.2.2.2 Axial Flow Impellers

Refer to pages 20 to 23.

Axial impellers pump axially and hence are intended to produce a single circulation loop throughout the vessel as shown in Figure 2-5. Hence top to bottom mixing is better than with radial flow impellers especially when multiple agitators are used. Typical axial flow impellers are marine propellers and the proprietary hydrofoil equivalents such as the LIGHTNIN "A" series (for example Figure 2-19), the CHEMINEER HE3 and the SCABA SHP impellers. The power curves for these agitators tend to be steeper in the transitional regime and thus are not as flexible as radial impellers over a viscosity range. Propellers are not often used on a large scale and independent literature power data for propriety agitators is scarce and rudimentary, leading to undue reliance on manufacturers' recommendations. There is a lack of reliable comparative data for such agitators. In general however, because of the flow patterns produced, lower velocities close to the wall are expected in comparison with radial flow impellers, hence wall shear will be lower which may have important implications for heat transfer. The power numbers for axial flow impellers are considerably lower than for radial flow impellers reducing torque requirements.

2.2.2.3 Mixed Flow Impellers

Pitched blade turbines are typical of this classification. They offer a compromise, producing components of axial and radial flow. It should be noted however that even the so called axial flow impellers will produce some radial flow and many of the propriety agitators such as the LIGHTNIN A310 should be classed as mixed flow agitators. The impeller-jetting angle becomes shallower as the viscosity increases. This may explain why the shape of the transitional regime is steeper, in that the power number will increase as the component of radial flow increases. The term mixed flow impeller has also been used by Mann (1983) to describe the double acting impellers such as the EKATO MIG and INTER MIG impellers. These all reverse the direction of the pitch at the tips to give a reverse pumping action at the outer edge. The net effect will be to promote better top to bottom mixing by reinforcing the axial flow streams.

2.2.2.4 Multiple Impellers

In vessels with high aspect ratios, operating height H / vessel diameter $T > 1$, multiple agitators are often desirable. The use of multiple radial agitators results in compartmentalization and long overall mixing times according to Cooke *et al.* (1988) and Cronin *et al.* (1994). Overall mixing times can be reduced by using axial agitators or axial/radial combinations, as shown for example by Cooke *et al.* (1988) and Hari-Prajitno (1999).

2.2.2.4.1 Down-pumping Axial or Mixed Flow Agitators

A popular combination has traditionally been down-pumping axial agitators above a radial disperser. For single phase operation the impeller size and spacing is an important consideration if improved bulk blending is to be

achieved as incorrect combinations are inherently unstable because many flow scenarios are possible, see Figure 2-6 (a), (b) and (c).

Figure 2-6(a) illustrates ideal flow from a bulk mixing point of view, which my own experience suggests, is rarely achieved and requires the D/T of the axial flow agitators to be greater than the D/T of the radial flow agitators and impeller spacing of $0.5D$ to $1D$. Also as viscosity increases, the radial component of flow decreases and makes the ideal more difficult to achieve.

Figure 2-6(b) depicts compartmentalized flow and in Figure 2-6(c) there are unstable flows, which are in opposition to each other.

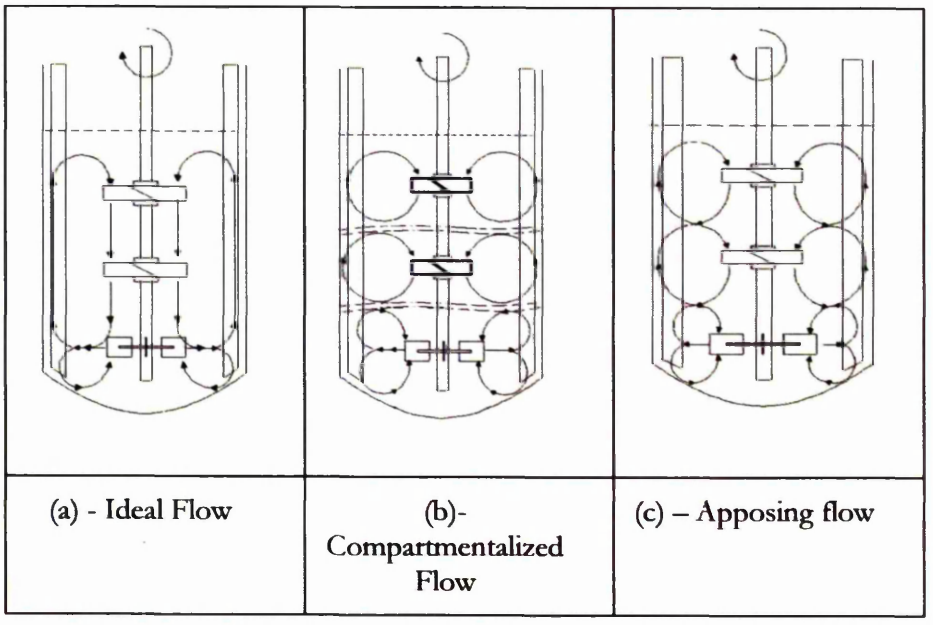

Figure 2-6: Possible flow combinations with combined radial below down-pumping impellers.

When gassing occurs the situation is worsened by gravitational affects as the rising plume of gas is acted on by down-flow of liquid from the agitator. If the gas flow number is very small and the liquid viscosity is low then the agitator will dominate. However as gas flow numbers increase the gas will coalesce in the down-flow forming large bubbles which periodically break-through causing instabilities and the risk of mechanical damage. Frijlink *et al.* (1984) described a similar mechanism as the switching from direct to indirect loading.

Literature Reviews

For gassed work with down-pumping impellors, the agitator choice is a critical factor. The agitator solidity (the ratio of the projected area of the blades to the swept area), Oldshue (1989), is also important. To maximise the gas handling capabilities a high solidity impeller should be chosen. A high solidity is also preferred for agitating viscous material. The choice of the gas input is important. MacFarlane *et al.* (1996) recommend a sparger of diameter $D_S = 0.8D$ with a clearance of $c_S/c = 0.6$, when used with a MAXFLO T of $D/T = 0.45$, for optimum gas handling. This sort of information can be most reliably obtained by physical modelling, though even this is fraught with uncertainties unless an exact process fluid analogue is used.

If solids require suspending in a three-phase system, the gas can severely affect the suspension, Chapman *et al.* (1983). Thus the chose of an agitation system where gas flows and liquid flows are in opposition appears to be nonsensical.

If the gas can be introduced into the up-flow, the gravitational problems associated with directly loading an up-flow agitator can be avoided, though some loss of gas dispersion could result.

2.2.2.4.2 Up-pumping Axial Agitators

A much more rational solution to multiple agitators is to use up-flow agitators for axial mixing in gassed duties. Radial / axial combinations can be configured to give positive flow reinforcement at the interchanges (shown in Figure 2-7) which is important for bulk mixing. For axial/axial up-pumping configurations the gas and liquid flows work in unison encouraging good top to bottom flow. In ICI Technology the concept of positive reinforcement of flows has been used for a number of years for in-house designs and there is now plenty of literature support for this approach. Examples are Chapman *et al.* (1983) who showed that solid suspension was more efficient with up pumping than with down-pumping turbines under gassed conditions. Bujalski *et al.* (1990) found that up-pumping turbines gave

equal gas hold-up and $k_L a$ to Rushton turbines when compared at the same specific power inputs and gassing rates.

Axial up-flow/down-flow combinations which results in a stable figure-of-eight flow loop, with positive flow reinforcement at the interchange, have also been recommended, Nienow (1998).

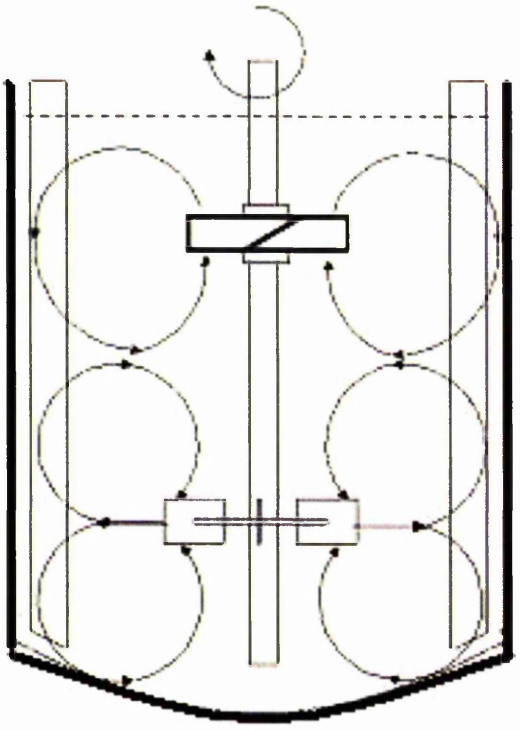

Figure 2-7: Stable flow with flow reinforcement at the interchange for a radial plus up-pumping agitator combination.

2.2.2.5 Selection of Agitators

For a given agitation duty there will be invariably many ways of achieving the desired aim. Therefore the choice of agitators should be on practical and economic grounds. Practical considerations may be in relationship with the vendor trust, reliability, and the availability of spares, back up and inter-changeability (e.g. if a motor or gearbox is common to a number of items of

equipment then it decreases the need to carry spares). Economic considerations should address running costs as well as installation costs.

There are a bewildering number of agitators available on the market. A selection of these from our own collection and from the WEB sites of LIGHTNIN, CHEMINEER and SCABA are shown in Figures 2-8 to 2-28. Where a proprietary agitator is shown the description of the suitable agitation duty is taken from the manufacturers sales material without comment and is marked with an * CHEMINEER and ** LIGHTNIN. It should be noted that not all claims have been tested in the open literature

2.2.2.5.1 Selection of Radial Flow Agitators

Paddles or flat blade turbines are the simplest designs of radial flow agitators and have the benefits of being cheap and non-propriety. They are often preferred for batch duties. Simple 2-blade designs are used in paint mixers at low transitional Reynolds numbers and have the benefit of being easy to clean. A 4-blade version from CHEMINEER is shown in Figure 2-8.

	**S-4 or Straight Blade Impeller** **Favourable Applications: *** A cost effective impeller for operation very near the floor of a tank for agitating the heel in solids suspension applications. Also an effective impeller in laminar flow applications, especially when impeller Reynolds numbers drop below 50

Figure 2-8: 4 blade-turbine

	**D-6 or Rushton Impeller** **Favourable Applications: *** Good cost effective impeller for low concentrations of immiscible liquid or gas. Two very strong trailing vortices are shed from each blade. These areas of high shear are responsible for breaking the larger droplets to smaller droplets. Maximum aeration numbers should be limited to 0.1.

Figure 2-9: 6-blade Rushton-turbine

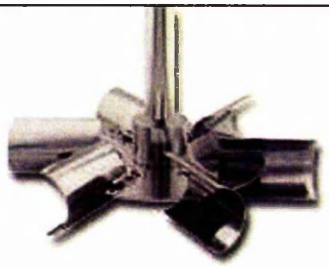

CD-6 Impeller
Favourable Applications: *

The CD-6 is a second-generation gas and immiscible liquid dispersion impeller. The CD-6 can handle about 2.4 times the maximum gas capacity of the D-6 impeller. The CD-6 is similar to the Smith impeller, but there are substantial power and gas dispersion capability differences available. This impeller has been used at aeration numbers as high as 2.1.

Figure 2-10: CHEMINEER CD-6 impeller

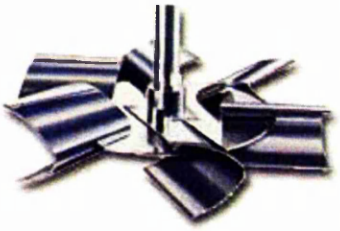

BT-6 Impeller
Favourable Applications: *

Highest gas dispersing capability available. Can disperse nearly six times the gas handling capability of the D-6 or Rushton impeller. Unloads less than the CD-6. In fact, the unloading is nearly all due to the change in effective density of the gassed liquid. The mass transfer capability is on the order of 10% better than the CD-6. Unlike many other gas dispersing impellers, the BT-6 is relatively insensitive to viscosity.

Figure 2-11: CHEMINEER BT-6 impeller

POWER, GAS DISPERSION AND HOMOGENISATION CHARACTERISTICS OF SCABA SRGT AND RUSHTON TURBINE IMPELLERS

SAITO *et al.* (1992)

SCABA 6SRGT Impeller

The Scaba SRGT agitator with six blades when gassed draws between 1 and 0.8 times the ungassed power in fluids of low and moderate viscosity respectively. Under similar conditions, the gassed Rushton turbine draws 0.5 to 0.4 times the ungassed power. In addition, some three times more gas can be handled at the same ungassed power by this SRGT before flooding occurs. The increased hold-up achieved by the 6SRGT is commensurate with the increased power input and it is argued that the potentially extra power available should be able to give a similarly enhanced k_La. The 6SRGT agitator also gives an equivalent homogenisation performance to a standard Rushton turbine agitator of the same size at the same gassed power input. When gassed reactors are fitted with motors of sufficient power to be capable of running at full speed when ungassed, This agitator offers simple retrofitting possibilities potentially leading to considerably enhanced performance.

Figure 2-12: SCABA 6SRGT agitator

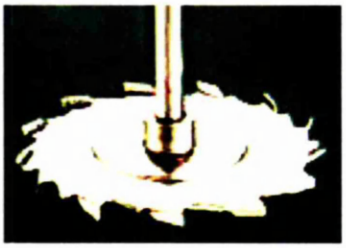

R500 SAWTOOTH
Recommended for: High-shear applications with elements that are difficult to disperse **

Provides the highest shear of all LIGHTNIN impeller designs Excellent for high-shear, solid-liquid and liquid-liquid applications. These are typically used with difficult-to-dispense pigments

Figure 2-13: LIGHTNIN R500 (Sawtooth) agitator

ChemShear Impeller
Favourable Applications: *

ChemShear Impellers are made in 4 different styles. Style 1 has the widest blades and style 4 the narrowest blades. Various processes require different ratios of shear and pumping. The wider blades pump more, and the narrower blades have the higher level of shear. They work well in applications which require moderately high shear but also some level of pumping. Many high shear devices are very low in pumping capability and require an auxiliary impeller to provide turnover. ChemShear impellers often overcome the need for an auxiliary pumping impeller. ChemShear impellers have been used in microencapsulation processes producing particles in the 2-micron range.

Figure 2-14: ChemShear Impeller

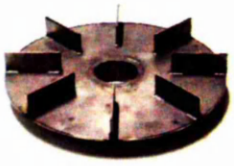

Vaned disc impeller

Vaned disc agitator viewed from below. Disc prevents recirculation from above. Used in gas-liquid duties where recirculation of the gas is deemed undesirable. Can be used as shown as a reflux slinger to distribute reflux to the walls.

Figure 2-15: 8-vaned disc agitator

PFAUDLER Glass-coated retreat curve impeller

Recommended by vendors for blending and heat transfer, gas dispersion and suspension, especially useful for suspension of friable particles. Glass lining enables use in hostile environments.

Figure 2-16: PFAUDLER Glass-coated retreat curve impeller

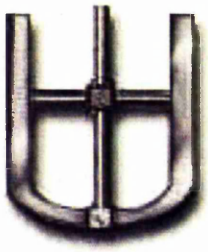

Anchor Impeller
Relative Impeller Size: Of the order of 95% of the Tank Diameter
Favourable Applications: *

The anchor impeller is the most economical laminar flow impeller. It is most effective in squat batches where vertical pumping is not as important as in tall batches. Blend times are somewhat longer than helical ribbon type impellers. It is the easiest high viscosity impeller onto which scrapers can be mounted for very difficult heat transfer applications.

Figure 2-17: Anchor

2.2.2.5.2 Selection of Axial Flow Impellers

Single Flight Helical Ribbon with Screw
Relative Impeller Size: Approx. 95% of the Tank Diameter
Favourable Applications: **

A reasonably efficient high viscosity, laminar flow impeller. Blend times are about the same to somewhat longer than the double flight helical ribbon impeller. The central screw can effectively pull down solids and liquids from the surface when the helical ribbon is pumping up. Generally used for applications where viscosities are ordinarily greater than 30,000 MPa. Heat transfer coefficients are only slightly less than the double helical ribbon impeller.

Figure 2-18: Single Flight Helical Ribbon with Screw

A310/A510 (Low Solidity Ratio)

Recommended for low-viscosity flow-controlled applications **

Varying angle options optimise processes by changing the impeller diameter/tank ratio Maximizes flow with ability to add shear options. Standard on the LIGHTNIN LFD Flocculator

Figure 2-19: LIGHTNIN A310/510 Impeller

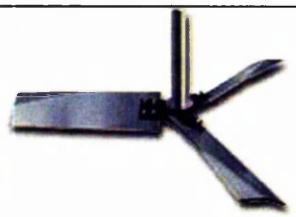

HE-3 Impeller (low Solidity Ratio)
Favourable Applications: *

An extremely efficient turbulent flow impeller for blending, heat transfer and solids suspension. Most effective for Reynolds numbers over 50. Developed to minimize the creation of trailing vortices and incorporating the otherwise wasted energy into macro-flow.

Figure 2-20: CHEMINEER HE-3 Impeller

A100 Propeller
Recommended for applications requiring moderate pumping action and powder-wetting capabilities**

Super-pitch design
1.5 pitch ratio for greater mixing capabilities
Standard axial flow
Optional ring guard prevents damage from dip tubes, temperature probes and other in-tank devices

Figure 2-21: LIGHTNIN A100 Propeller

A200 or 4MFD
Recommended for low- to medium-viscosity, flow-controlled applications **

Classic 45° pitched blade design. Produces a desirable balance of flow and shear. The impeller of choice in many standard applications including solid suspension.

Note these are also produced in six blade versions - 6MFD and in up-pumping versions denoted as 4MFU and 6MFU, dependent on the number of blades...

Figure 2-22: LIGHTNIN A200 45° pitched blade impeller or 4MFD

CHEMINEER SC-3 Impeller
Favourable Applications: *

The new Chemineer SC-3 Impeller features an advanced design engineered for deep tanks. It produces flow characteristics of much larger impellers, without the added weight, or the resulting loss in pumping efficiency. The highly efficient SC-3 Impeller's reduced weight allows for the use of longer shaft extensions for deeper tanks, and resolves associated critical speed limitations. The use of an SC-3 impeller can produce an overall agitator cost savings as much as 33%.

Figure 2-23: CHEMINEER SC-3 Impeller

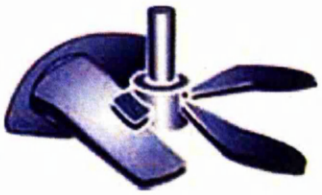

LIGHTNIN A315 (High solidity)
Recommended for gas-liquid dispersion and mass transfer-controlled applications**

Can improve mass transfer by 30% compared with Rushton turbines. Decreases shear rates up to 75%. Can reduce energy costs up to 45%. Improves yields in shear-sensitive processes.

Figure 2-24: LIGHTNIN A315

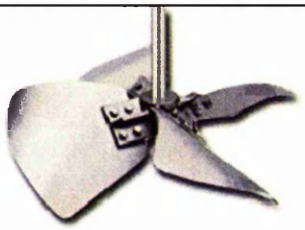

CHEMINEER Maxflo W Impeller (High solidity)
Favourable Applications: *

The Maxflo W impeller, with about 10% more effectiveness in pumping efficiency, is an improved version and full replacement impeller for the Maxflo T. Excellent in abrasive solids suspension, solids suspension in the presence of small amounts of gas introduced or generated in-situ, and in boiling or near boiling applications

Figure 2-25: CHEMINEER Maxflo W Impeller

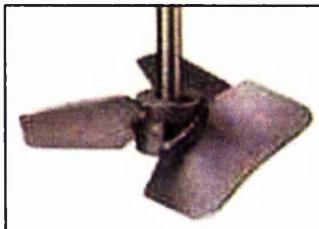

LIGHTNIN A340
Recommended for up-pumping applications **

Ideal for multi-phase applications, such as fermentation, polymerisation and hydrogenation High gas induction from surface.

Controls foaming

Figure 2-26: LIGHTNIN A340

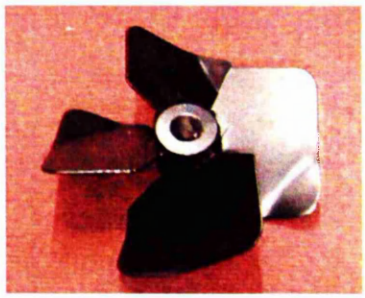

LIGHTNIN A345 (High solidity)

Recommended for up-pumping applications

4-bladed version of A340. More stable for high gassing operations

Figure 2-27: LIGHTNIN A345 impeller

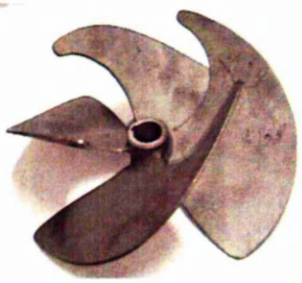

APV-B2-30U (High solidity)

Recommended for up-pumping applications

APV version of LIGHTNIN A345. Claimed improved stability, high gassing factor and low torque fluctuation.

Figure 2-28: APV B2-30U impeller.

2.2.3 Agitator Power Prediction

The engineer needs to be able to predict agitator power and torque in order to ensure the desired mechanical energy levels are achieved and for installation of the motor, gearbox and shaft.

2.2.3.1 Ungassed Agitator Power Prediction

This is based on the approach developed by Rushton *et al.* (1950). They used dimensional analysis techniques to show that the agitator power characteristics in geometrically similar vessels can be expressed as:

$$\mathrm{Po} = \frac{P}{\rho N^3 D^5} = \text{constant} \times \mathrm{Re}^a \times \mathrm{Fr}^b \qquad (2.10)$$

The work of Rushton *et al.* was extended by Bates *et al.* (1963). Extensive data in the form of plots of Po versus Re are available in the literature, examples are Uhl and Gray (1966) and Oldshue (1983). These cover a wide range of agitators in baffled and unbaffled vessels.

In fully baffled vessels the influence of the Froude number on the ungassed power number is negligible and the index (b) in equation (2.10) approaches 0. The Po is constant for homogeneous fluids in fully turbulent flow ($\mathrm{Re} \geq 10^4$). This means that the indices (a) and (b) in equation (2.10) are zero. Hence in the turbulent regime, the agitator shaft power P_S is given by:

$$P_s = \mathrm{Po}\,\rho N^3 D^5 = 2\pi NM \qquad \textbf{(2.11)}$$

where M is the shaft torque.

In the laminar regime (Re ≤ 10) the index (a) in equation (2.10) is –1, whilst (b) =0. For the transitional regime (10 >Re <10^4) index (a) varies and the curve is usually fitted to a polynomial.

A typical power curve for a Rushton turbine is shown in Figure 2-29

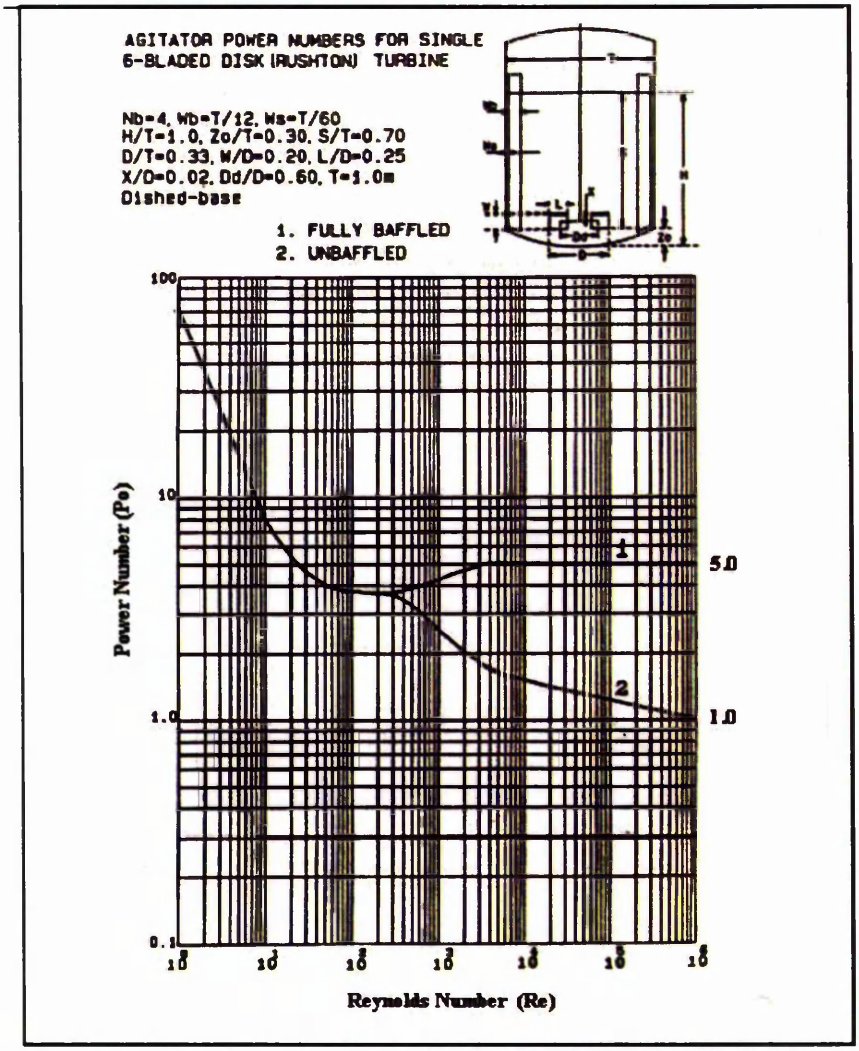

Figure 2-29: Power curve for a Rushton turbine. Baffled curve (1) diverges from unbaffled curve (2) above Re = 300. Below Re =300, baffling does not effect Po.

For multiple impellers the power depends on the agitator spacing S. When S/D *is* ≥ 1 then the total ungassed Po is generally constant, though not necessarily equal to the sum of individual power numbers defined for a "standard" tank. For axial impellers the combined power is usually less than the sum of the individual power numbers up to $S/D = 4$. When radial impellers are set too close together $S/D \leq 1$, the total power number can exceed the sum due to the two impellers acting as one with a combined radial flow. This is shown in Figure 2-30 reproduced from Bates *et al.* (1963) and taken from Uhl and Gray (1966). Here P_2 is the dual agitator power and P_1 is the single agitator power for a flat blade turbine in each case. This figure also illustrates dual pitched blade turbines draw less power than a single flat blade turbine.

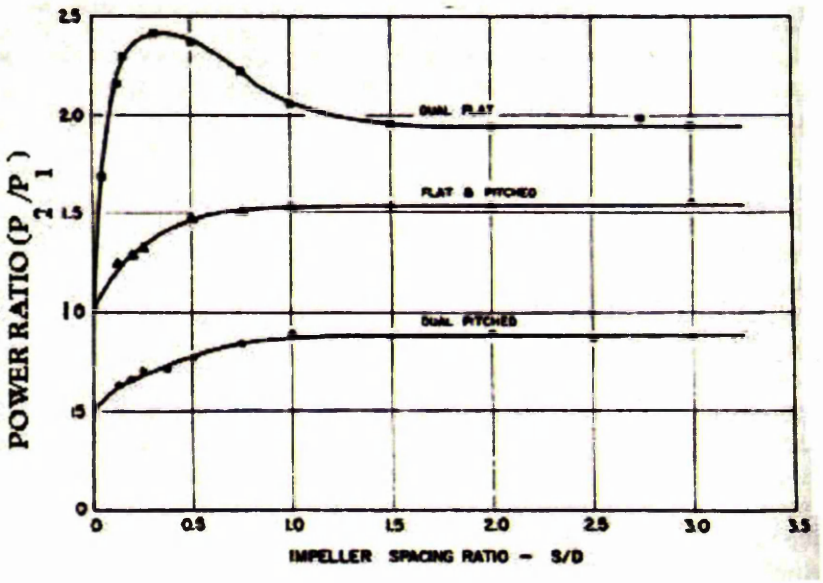

Figure 2-30: Effect of dual impellers on power. From Gray (1966). Reference power P_1 is a flat blade turbine in each case

2.2.3.2 Prediction of the Power of Gassed Agitators

The prediction of the power for gassed systems is only possible when the agitator and the process hydrodynamics are understood and predictable.

Literature Reviews

Although much work has been done to understand the agitator hydrodynamics (see Page 41), most of this work has been done on a relatively small scale in air-water systems. The data are generally expressed as plots of relative power demand (RPD), or ratios of gassed to un-gassed power (PG /PU) versus the Gas Flow Number. Typical plots for a Rushton turbine are shown in Figure 2-31.

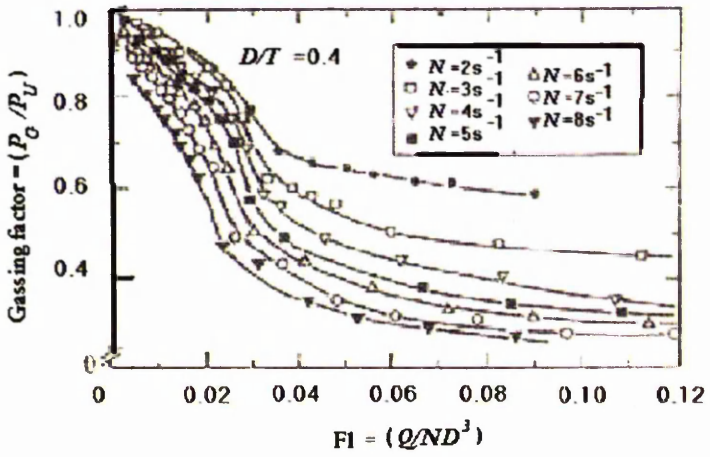

Figure 2-31: Gassing curves for a Rushton turbine in air-water. From Nienow (1998).

These curves at constant N illustrate that gas flow number alone will not correlate the gas power data. The family of curves shown are due to gas recirculation through the impeller region at higher N as demonstrated by Bruijn *et al.* (1974). By using a large vessel with a small impeller (effectively eliminating recirculation through the impeller) they discovered that a single gassing curve plotted against Fl is obtained for a wide range of N.

For Rushton turbines, the empirical correlation of Michel and Miller (1962) is often quoted for estimation of the gassed power in turbulent systems. This correlation is,

$$P_G = 0.72\left(\frac{P_U^2 ND}{Q_G^{0.56}}\right)^{0.45} \qquad (2.12)$$

However, Nienow (1998) shows that the apparent success of this correlation is in fact an artefact of the data treatment and is NOT recommended. Quoting directly, *"such an approach can be used to "correlate" any set of P_G/P_U against gas flow rate, Q_G m^3/s, data, no matter how different they are, from any impeller configuration; or even if random numbers are used for P_G/P_U and Q_G".*

2.2.3.3 Power Draw in a Boiling and Near Boiling Reactor.

Smith (1994) investigated agitator power draw in boiling, boiling sparged and hot sparged reactors. He found that mechanical agitation of boiling liquids is controlled by cavitation rather than the mechanisms of gas dispersion. The relative power demand, (*RPD*), is higher than would be associated with a cold gas sparged at a similar volumetric throughout. The work was done on a 0.44 m fully baffled vessel agitated by a 0.18 m diameter Rushton turbine. For boiling water, with this system, he correlated his results as:

$$RPD = \frac{P_G}{P_U} = k_b \left[\frac{2gS}{v_t^2} \right]^b \qquad (2.13)$$

where S is the agitator submergence and v_t is the agitator tip speed. The term in brackets is defined as a simplified form of the cavitation number. For this system it was determined that the value of constant $k_b = 0.74$ with the exponent $b = 0.4$. The value of the critical cavitation number (above which the power = P_U) for this agitator is therefore 2.12. Note that equation (2.13) has no effect of boiling rate. With a purely boiling system the gas boils where the system pressure is lowest which is close to the liquid surface and in the low pressure regions behind the agitator blades (cavitation).

When an inert gas is sparged into a boiling liquid, it lowers the temperature of vapour generation and also shifts the relative power demand characteristic towards gassed flooding conditions. This is due to vapourisation into the inert gas bubbles. The temperature drop occurs due to the reduction in the vapour

pressure in accordance with Dalton's law of partial pressures. Liquid temperature measurement of the boiling sparged system can therefore be used to estimate the total gas phase loading of the impeller.

Hot (non boiling) gas sparged water systems behave like cold sparged systems and the power level for the agitation of sparged hot water correlates directly with the total volumetric flow rate of gas saturated with vapour at the bulk liquid temperature.

In an earlier paper, Smith and Smit (1988) claim that when turbine impellers operate in boiling or nearly boiling liquids the blades develop cavities similar to those in sparged gas-liquid systems.

2.2.4 Agitator Pumping Rates

Much work has been done on the theory and measurement of impeller pumping. The derivation of Gray (Uhl and Gray, Chapter 4) (1967) is included here because of its generality to agitator types and because it links directly the torque on the blades to the pumping rate and head. Gray used the following basic principles to obtain a relationship between impeller speed and the flow rate of fluid:

1) The rate of change of angular momentum of the fluid passing through an impeller is equal to the torque required to rotate the impeller
2) The theoretical fluid head induced by an impeller is equal to the static head plus the kinetic head of the fluid at the exit of the impeller

Assuming the angular momentum of the fluid entering the impeller is equal to zero then the rate of change of angular momentum with time of fluid passing through the impeller equals the torque (M) applied to the fluid by the impeller blades. That is,

$$M = Q\rho\omega k_t r^2 \qquad (2.14)$$

where ω is the impeller angular velocity = $2\pi N$ and k_r is the ratio of the tangential fluid velocity leaving the impeller to the tip velocity. Therefore combining these with equations (2.10) and (2.11) results in,

$$M = \frac{\mathrm{Po}\,\rho N^3 D^5}{2\pi N} = \frac{Q\rho\pi k_r N D^2}{2} \tag{2.15}$$

In this case,

$$\frac{\mathrm{Po}}{k_r \pi^2} = \frac{Q}{ND^3} \tag{2.16}$$

Combining equation (2.13) with (2.4) gives

$$k_r = \frac{\mathrm{Po}}{\pi^2 N_Q} \tag{2.17}$$

The ratio $\mathrm{Po}/\mathrm{N_Q}$ was used to define a pumping efficiency by Nagata *et al.* (1958). This reduces to,

$$\frac{\mathrm{Po}}{\mathrm{N_Q}} = \frac{P}{\rho N^3 D^5} \cdot \frac{ND^3}{Q} = \frac{P}{\rho N^2 D^2 Q} \tag{2.18}$$

Thus, the ratio is proportional to the power required per unit flow rate of fluid through the agitator when ρ, N and D are the same for all impellers. Although this statement quoted from Gray (1966) is undoubtedly correct, it does not truly represent the picture. Consideration of the literature data for Po and $\mathrm{N_Q}$, shown in Table 2-3, enables for example a comparison of the Kovács (2001) data for the Rushton turbine and radial SCABA 6SRGT. $\mathrm{Po}/\mathrm{N_Q}$ is > 2 times higher for the Rushton implying it takes more than twice the power per unit to produce unit flow of fluid than the 6SRGT. This is because the comparison is at the same N and D. However at the same tip speed the Rushton is drawing more than three times the power as the 6SRGT. Kovács (2001) states that the Rushton turbine pumps about 20% less fluid than the 6SRGT at the same power. This is only true because the diameter of the Rushton turbine was smaller than the 6SRGT in his experiments. It has already been shown that reducing D reduces pumping at the same power input.

A fairer comparison is at equal D and equal power. This reduces the speed of the Rushton in the ratio of $(Po_{(Scaba)}/Po_{(Rushton)})^{1/3} = 0.67$ from equation (2.10). If you do that you find the pumping rates are almost identical, see Table 2-4. However, even though the pumping rate is the same, the velocity is ≈ 40% higher for the 6SRGT, because of the higher tip velocity. This is due to the more concentrated jet (see earlier, Figure 2-2) produced by the 6SRGT. This means the jet is more energetic and therefore should be more suitable for suspending solids than the Rushton turbine. For three-phase duties, where it is required to disperse gas and to suspend solids, this makes the concave agitator a much better choice as the main disperser than the conventional Rushton turbine.

Impeller	Po	N_Q	Po/ N_Q	k_r	Reference
Rushton Turbine	5.2	0.75	6.93	0.70	A
Rushton Turbine	5	0.74	6.76	0.68	B
Rushton Turbine	6	0.81	7.41	0.75	C
Rushton Turbine	5.2	0.72	7.22	0.73	D
Rushton Turbine	5.5	0.75	7.33	0.74	E
SCABA 6SRGT	1.84	0.52	3.54	0.36	C
4 blade 45^0 PBT	1.27	0.79	1.61	0.16	D
4 blade 45^0 PBT	1.25	0.7	1.79	0.18	E
6 blade 45^0 PBT	1.7	0.73	2.33	0.24	B
LIGHTNIN A315	0.75	0.73	1.03	0.10	D
LIGHTNIN A310	0.3	0.56	0.54	0.05	D
CHEMINEER HE-3	0.3	0.41	0.73	0.07	B
CHEMINEER HE-3	0.3	0.46	0.65	0.07	F
CHEMINEER HE-3	0.27	0.5	0.54	0.05	E*

Table 2-3: Power Numbers and Flow Numbers for various agitators at Re ≥ 10^4.

References: A = Revill (1982), B= Nienow (1998). C= Kovacs (2001), D = Weetman and Oldshue (1988). E = Myers *et al.* (1996) - Chemineer data, * agrees with reference F if D/T of 0.2 is chosen. F= Fascano *et al.* (1994) - Chemineer data for $D=T/2$ HE-3

In Table 2-4, the discharge rates and velocities are compared at equal D and equal agitation power. The comparison is on an arbitrary scale applied by

setting the Revill (1982) Rushton turbine data for pumping and velocity at unity and comparing all other results with it. It makes an interesting comparison for it shows that the same agitator diameter and specific power inputs produces a wide range of pumping rates and velocities, dependent upon the agitator type. Thus the agitator can be tailored to the process requirement.

Impeller	Po	N_Q	Qp/Qp_1	$Vtip/Vtip_1$	Hp/Hp_1	Refs
Rushton Turbine	5.2	0.75	1.00	1.00	1.00	A
Rushton Turbine	5	0.74	1.00	1.01	1.00	B
Rushton Turbine	6	0.81	1.03	0.95	0.97	C
Rushton Turbine	5.2	0.72	0.96	1.00	1.04	D
Rushton Turbine	5.5	0.75	0.98	0.98	1.02	E
SCABA 6SRGT	1.84	0.52	0.98	1.41	1.02	C
4 blade 45^0 PBT	1.27	0.79	1.69	1.60	0.59	D
4 blade 45^0 PBT	1.25	0.7	1.50	1.61	0.67	E
6 blade 45^0 PBT	1.7	0.73	1.41	1.45	0.71	B
LIGHTNIN A315	0.75	0.73	1.86	1.91	0.54	D
LIGHTNIN A310	0.3	0.56	1.93	2.59	0.52	D
CHEMINEER HE-3	0.3	0.41	1.41	2.59	0.71	B
CHEMINEER HE-3	0.3	0.46	1.59	2.59	0.63	F
CHEMINEER HE-3	0.27	0.5	1.79	2.68	0.56	E*

Table 2-4: Relative pumping rates (Qp/Qp_1), velocities ($Vtip/Vtip_1$) and theoretical pumping heads (Hp/Hp_1) at constant fluid properties, constant power and D for Re ≥ 10^4. References as for Table 2-3.

Note that at constant fluid properties, constant power and D for Re≥10^4 from equation (2) with base case N_1 and Po_1 for disc turbine

$$NPo = N_1Po_1$$

$$N = \left(\frac{Po_1}{Po}\right)^{1/3} N_1$$

$$\text{Relative liquid pumping rates} = \frac{Q_P}{Q_{P1}} = \frac{N_Q N}{N_{Q1} N_1} = \frac{N_Q}{N_{Q1}}\left(\frac{Po_1}{Po}\right)^{1/3}$$

Agitator speed tip speed = πND

Relative tip velocity = $$\frac{Vtip}{Vtip_1} = \frac{\pi ND}{\pi N_1 D} = \frac{N}{N_1} = \left(\frac{\mathrm{Po}_1}{\mathrm{Po}}\right)^{1/3}$$

From Table 2-4, it might be reasonably concluded that for turbulent blending duties the low solidity impellers (such as the A10 or HE3) are the most efficient, as these give the highest pumping rates compared at equal P/V. The circulation theory of Khang and Levenspiel (1975) claims that mixing is effectively complete after 5 circulation loops. However, in practice a whole range of equal D/T impellers in $H=T$ aspect ratio vessels give similar mixing times at equal P/V (see page 77). It appears that turbulent mixing occurs in the universal equilibrium regime of the stirred tank energy spectrum, which is independent of agitator type. (See section 2.4.1 The Kolmogorov Theory of Local Homogeneous Isotropic Turbulence: The Eddy Spectrum)

Gray (1966) related the power draw from an agitator to the theoretical velocity head (H) according to,

$$P = Q\rho gH \tag{2.19}$$

Equation (2.19) is substituted in (2.18) to obtain:

$$\frac{\mathrm{Po}}{\mathrm{N_Q}} = \frac{Q\rho gH}{\rho N^2 D^2 Q} = \frac{gH}{N^2 D^2} \tag{2.20}$$

Therefore, the ratio is also proportional to the theoretical velocity head of the fluid discharged if the tip speed (πND) is kept constant. However, in these comparisons, the agitator power number is not constant. Comparisons of the relative theoretical velocity heads are also given in Table 2-4. This shows that compared at equal power, D and fluid properties the SCABA 6SRGT and the Rushton turbines are identical. The axial impellers all produce a lower head.

2.2.4.1 Effect of D/T on Agitator Pumping Rates and Shear Rates

In the section above, the comparisons were with constant D/T. What happens when this is changed?

Equation (2.2) shows us that for a given impeller type, the average shear rate $\dot{\gamma}$ depends only on N and not on D.

Oldshue (1983) however, claims that the maximum shear rate at the agitator tip depends upon the tip velocity and is proportional to ND. His maximum shear diagram is for shear close to the tip.

Van't Riet (1975a) found that the maximum shear rate (of the order 90N for a Rushton turbine in the fully turbulent regime) occurs in the vortices behind the blades and his data, which fits his proposed model, have been made dimensionless by dividing the shear rate by N and the radius by D, which infers that the maximum shear-rate is independent of D and depends only on N. It is noted however, that the author did his measurements on a single agitator hence D was not varied. Also the liquid-liquid dispersion literature shows that as D is decreased at constant N the drop-size increases as shown by Musgrove and Ruszkowski (2000) who used a silicon-oil in water dispersion. Their data are reproduced for Rushton turbines in two vessels at different D/T ratios as Figure 2-32. However, a good correlation of the same data can be obtained by re-plotting it against tip speed where all the data approximate to the same line, see Figure 2-33. The data of Zhou and Cresta (1998) also illustrate (in Figure 2-34) that drop sizes can be correlated with tip speed, for a given type of agitator.

A reasonable assumption is that the equilibrium drop-size is a function of the maximum shear-rate, therefore these data suggest that the maximum shear rates do increase with tip speed as claimed by Oldshue (1983), contrary to the

argument that the maximum shear-rates are independent of D and dependent only on N.

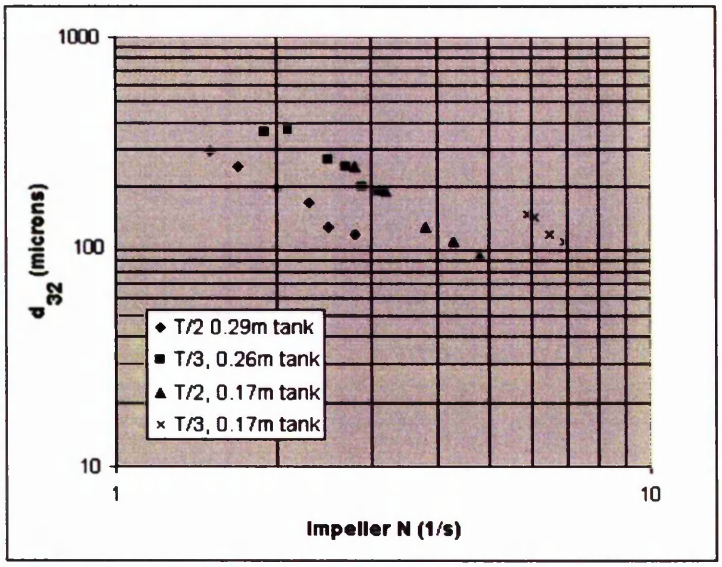

Figure 2-32: Drop-size data for silicon oil in water agitated with various diameters of Rushton turbines in two vessels. Data from Musgrove and Ruszkowski (2000) is shown against impeller speed.

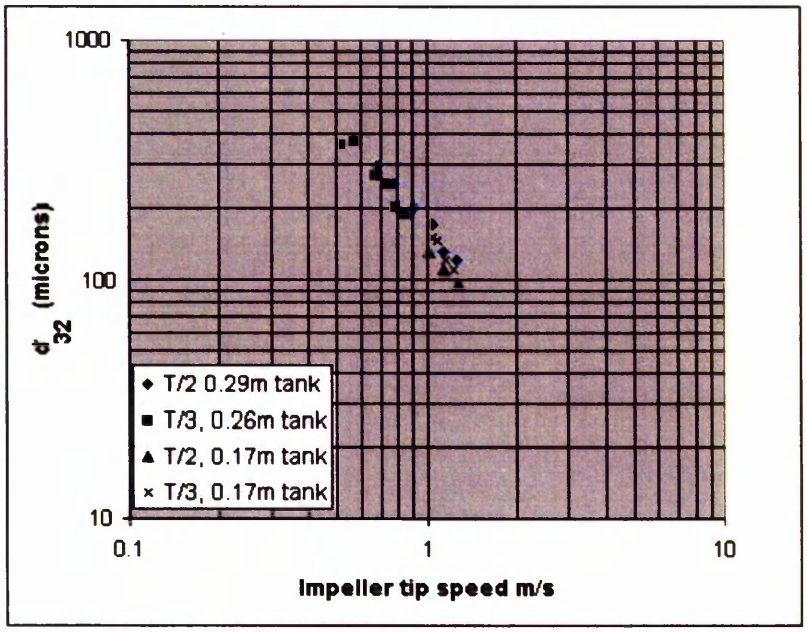

Figure 2-33: Same data as for Figure 2.32, only this time correlated against tip speed

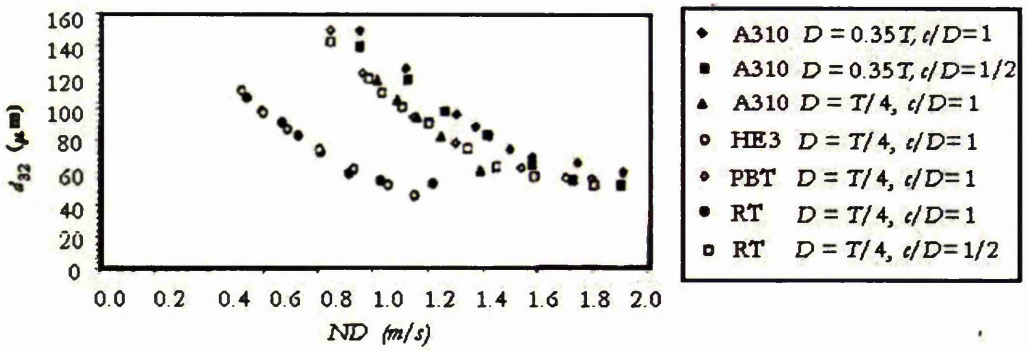

Figure 2-34: Data from Zhou and Cresta 1998 showing drop size correlates with tip speed for a given agitator type.

If Oldshue (1983) is right by saying that the shear-rate at the tip increases with diameter at constant N and van't Riet (1975a) is right to assume that the maximum shear-rate in the vortex is about $90N$ and depends only on N, what happens on scale up at constant geometry and constant P/V? N decreases so maximum shear-rate in the vortex decreases but ND increases so the maximum shear-rate at the tip increases. This suggests that the tip shear-rate exceeds the vortex shear-rate at a certain scale?

Is it possible to resolve this paradox by considering the turbulence at the Kolmogorov length scale (see Section 2.4) which are independent of scale? The shear rate is related to energy dissipation rates and for water at an energy dissipation rate of 1 W/kg, the shear rates are 1000 s^{-1} at this scale (using the equations given in section 2.4). This is much higher than the shear rates proposed by Oldshue (1983) or Van't Riet (1973). So in essence, for scale-up at geometric similarity and equal power per unit volume the shear rates responsible for break-up mechanisms should remain constant. However, a further study of the liquid-liquid literature indicates that average energy dissipation rates do not correlate drop sizes either between agitators or scales. In fact, scale up a geometric similarity and equal average energy dissipation per unit mass results in decreased drop sizes on scale-up as found by Colenbrander (2000) and by Musgrove and Ruszkowski (2000). Even more

remarkable, they found the so called low shear impellers such as the LIGHTNIN A310 produce smaller drops than the supposedly high shear Rushton turbines when compared at equal mean enetgy dissipation rates. A better correlation is found when the maximum energy dissipation rate in the agitator region is used. However, this does not altogether correlate different types of impellers as shown by Musgrove and Ruszkowski (2000). In order to obtain a good correlation these authors found that a local per-blade dissipation rate had to be used. The smaller drop-size for the 3-blade hydrofoils was explained in terms of the energy dissipation per blade, which was higher for these impellers, because they had fewer blades.

It would appear logical then that changing D/T at constant power changes both the average shear and the maximum shear in the vessel. The maximum shear-rate however, also depends on the head, which from equation (2.19) is proportional to P/Q. Thus for given power a small impeller will produce a comparatively high shear (low Q), whilst a large impeller will give more flow but less shear. The pumping to the velocity head can be related by linking equations (2.3), (2.4) and (2.19)

For a given agitator type in a given fluid:

$$P \propto N^3D^5 \propto QH \propto ND^3H$$

$$N^2D^2 \propto H$$

$$QN/D \propto H$$

$$\text{Thus, } \frac{Q}{H} \propto \frac{D}{N} \qquad (2.21)$$

Q/H is also proportional to $(D/T)^{8/3}$ at constant power. Therefore, for example, halving the D/T for the same power results in the ratio Q/H decreasing by a factor of $0.5^{8/3} = 0.157$. This means that altering either D/T for a given agitator or alternatively changing the agitator type can adjust the ratio of pumping to fluid shear rate. On scale up at geometric similarity and

constant power per volume, D increases and N decreases therefore Q/H must increase.

In order to choose the best option of impeller type, impeller speed and diameter for a given duty it is necessary to focus on the duty. Lots of applications, such as blending and suspension, can be argued to rely mainly on flow. Thus agitators producing high flow with a low head would be most efficient for this duty.

Applications relying on shear for particle drop or bubble size reduction, require high shear. Providing the total contacting time is sufficiently large, and there is no agglomeration or coalescence involved, then the highest shear is the optimum requirement as eventually all the material will pass through the high shear region. When break-up and coalescence are involved, then an optimum may exist between maximum shear and circulation time (flow).

For gas-liquid mass transfer using the sulphite oxidation method (where salts will inhibit coalescence) Oldshue Chapter 13 (1983) claims that the optimum D/T for the most energy efficient transfer depended on the specific energy input and the gas-liquid hydrodynamics. According to these data, low energy inputs and large gassing rates (gas dominated) are favoured by large D/T agitators. This is because in this case flow is the most important factor. This seems highly sensible. As agitator energy inputs are increased and we move to agitator-dominated conditions the k_La is increasingly favoured by the higher shear from the smaller D/T agitators. At very high P/V there is so much energy it is irrelevant how it is supplied and all D/T ratios are equally efficient. This all looks very plausible. However, this literature search has not revealed any other credible claims that D/T is important to gas-liquid mass transfer in low viscosity fluids. Most experimenters claim that it is P/V that counts, not the agitator, provided the gas is fully dispersed.

If the system had been highly coalescing a different pattern may have emerged as the time spent outside the high shear area would then have a larger

significance and the optimum balance between break-up and coalescence requires an optimum balance between circulation and shear.

The biggest cost driver in the selection of agitation equipment is torque. High torque means thicker shafts and large gearboxes. Therefore, given a choice, the agitator manufacturers will invariably offer to supply the lowest torque equipment for a given duty in order to be competitive, even if the option uses more power. However, for gas-liquid-solid duties flow is very important and remembering agitator flow/unit volume decreases with scale-up then larger *D/T's* are often a much safer option. When considering options, the cost of any extra power over a reasonable life span of the equipment should also be considered.

For many design applications, equivalence between shear rate and the time in the high shear zone is assumed. For processes where both shear and circulation are important it would be useful to quantify whether a shorter time in a high shear zone is as beneficial as a longer time in a lower shear zone for a given total energy input.

Comparing a single impeller type at different options of *D*/T and agitation speed is relatively easy. However, when a different agitator type is involved it becomes more difficult as the power number needs to be taken into account and a suitable basis of comparison needs to be defined. Oldshue, Chapter 8, (1983) suggests that the best evaluation would be to compare torque, power, flow, flow/power etcetera on the bases of maintaining say flow and agitation speed (or any other parameter) constant. He produced a useful table showing the functional relationship of variables for a range of bases in his Table 8-4 and this is a useful reference when considering options.

2.2.4.2 Effect of Gas-phase and /or Solid-phase on Agitator Pumping Rates

Techniques successfully used to measure the mean and fluctuating velocities close to the impellers and in the bulk of the vessel are shown in Table 2-5.

Literature Reviews

Laser Doppler Anemometry (LDA) is now the most widely used tool. Other techniques such as Particle Image Velocimetry (PIV) and Laser Induced Fluorescence (LIV) are becoming increasingly common. None of these techniques lend themselves readily to evaluations at high phase fractions of gas or/and solids. Therefore data to evaluate the effect of the 2nd phase on pumping are scarce and limited to low phase fractions.

Technique	Literature examples
Streak photography	Sachs and Rushton (1954) Cutter (1966)
Neutrally buoyant flow followers to measure circulation times; Example: radio pill	Bryant *et al.* (1979) Middleton (1979) by Nikiforaki *et al.* (1999)
Hot Wire Anemometry (HWA)	Bowers (1965)
3-D Pitot tubes and Hot Film Anemometry (HFA)	Nagata *et al.* (1975) Fort and Mala (1982)
Laser Doppler Anemometry (LDA)	Van der Molan and van Maanen (1975), Dyster *et al.* (1993) Jaworski and Nienow, (1994)
Particle Image Velocimetry (PIV)	Wittmer *et al.* (1997)
Laser Induced Fluorescence (LIV)	Distelhoff and Marquis (1999)

Table 2-5: Techniques successfully used to measure the mean and fluctuating velocities close to the impellers and in the bulk of the vessel

Many workers have suggested that the effect of gas on the pumping rate is proportional to the decrease in power. Tragardh (1988) and Bakker *et al.* (1991) assumed, $Q_G/Q = P_G/P_U$. This seems unlikely since velocity profiles are normalized using tip speed and since power is proportional to N^3 then Q is proportional $P^{1/3}$ and you therefore would expect a more reasonable estimate to be,

$$\frac{Q_G}{Q} = \left(\frac{P_G}{P_U}\right)^{1/3} \tag{2.22}$$

Patterson (1991) reported some experimental results for a Rushton turbine at very low gassing rates, Fl_G= 0.015, where only a small effect was seen on the impeller power number and also found only a small effect of the gas on the radial discharge velocities. However, he did find a greater effect on velocities away from the agitator, particularly above the agitator near the tank wall.

Rousar and van den Akker (1994), following Tragardh (1988) and Bakker *et al.* (1991), suggested that that the liquid flow rate with gas is kinematically similar to that without gas and can be related at any point in the vessel to the relative decrease in power due to gassing according to,

$$\frac{u_{ig}}{u_i} = \left(\frac{P_G}{P_U}\right)^{\beta} \tag{2.23}$$

where u_{ig} and u_i denote local velocity components under gassed and ungassed conditions. From their LDA results they found that at the impeller tip:

$$\frac{ur_{\max}}{u_{tip}} = 0.747\left(\frac{P_G}{P_U}\right)^{0.34} \tag{2.24}$$

where ur_{max} is the maximum radial velocity. The exponent on equation (2.24) agrees with what was predicted by equation (2.22). They further found that the mean and rms velocity profiles at the impeller tip all fall on one curve for all single and multiple impellers providing that the relative power draw of each impeller is considered. In the bulk, close to the impeller, similarities of liquid velocity profiles were observed and the velocity profiles, at various agitation and gas-rates, can be compressed into a single curve with the scaling factor $(P_G/P_U)^{1/3}$. In regions far from the impeller, the bubble swarm was found to drastically affect the liquid flow patterns.

Warmoeskerken *et al.* (1984b) studied the effect of solids on the Rushton turbine hydrodynamics, using a strain gauge vane sensor close to the agitator.

Using sand, in the range 0.1 to 5% by mass, of size range 80% between 100 – 160 μm, they report no measurable effect on the formation of gassed filled cavities on the gassed power demand.

In the heterogeneous regime, solid particles supplant small gas bubbles in the dense phase (see Section 2.3.2). This must affect the agitation power.

Harrop *et al.* (1997), found that solids can increase the liquid mixing time by a factor of 6 for a LIGHTNIN A315 impeller, when operation is below N_{JS}, at sand concentrations between 10 and 20% by mass. This is due to a zoning effect when a solid-liquid interface is present.

Pantula (1997), found that the increase in speed required to re-suspend solids when gas was introduced was related to the torque. It is claimed that the agitator torque required to suspend the solids is independent of the gassing rates for radial turbines and up-pumping pitch blade turbines. This did not work with down-pumping turbines, presumably because the liquid and gas flows are in opposition. Chapman *et al.* (1983) found that down pumping pitch blade turbines were unstable when gassed from below and inefficient at suspending solids under these conditions.

2.3 Hydrodynamics

Both the agitator and bubble hydrodynamics are considered.

2.3.1 Agitator Hydrodynamics under Gassed Conditions

Until recently, radial flow disc turbine agitators were generally recommended for gas-liquid operations. It is therefore not surprising that most of the literature data for the effect of gassing concerns the Rushton turbine. The introduction of gas into a Rushton turbine agitated system is accompanied by

a large reduction in the power drawn by the agitator, as illustrated earlier in Figure 2-31.

Until the early 1970's it was believed that this power reduction was due mainly to a reduction in bulk density of the fluid. Indeed, many agitation manufacturers still design agitators on that premise. Valentine (1967) and Rennie and Valentin (1968) produced photographs of attached gas bubbles behind the moving turbine blades and described the twin trailing vortices. The modern conception of the flow around turbine blades has resulted from the detailed studies by a number of workers, notably; van't Riet and Smith (1973), van't Riet *et al.* (1975a and b), Smith (1985 and 1988) Warmeoskerken *et al.* (1984 and 1985) and Nienow and his co-workers (1978 and 1985). As a result of this work the importance of the trailing roll vortexes formed behind the blades of the rotating turbine is now fully appreciated. These vortexes are shown schematically in Figure 2-35.

In turbulent flow high shear rates (up to 90 N) are found within these vortices, van't Riet (1975a). This is an order of magnitude greater than the average shear rate in the vessel. When gas is introduced into the system, the centrifugal forces cause it to migrate to the low-pressure area inside the vortices. It then travels along the vortex core until it is expelled at the end as small bubbles as shown in Figure 2-35. Thus, provided the centrifugal forces are sufficient to overcome buoyancy effects, a gas filled cavity is formed. The minimum Froude number at which stable cavities can form, was found by Smith and Warmeoskerken (1985) to be 0.045. A number of distinct cavity regimes have been identified as shown in Figure 2-35 and Figure 2-36.

These are claimed to coincide with different identifiable hydrodynamic regimes.

Three hydrodynamic regimes are of particular importance and these are shown in Figure 2-37. These are:

Flooded, loaded and complete dispersion.

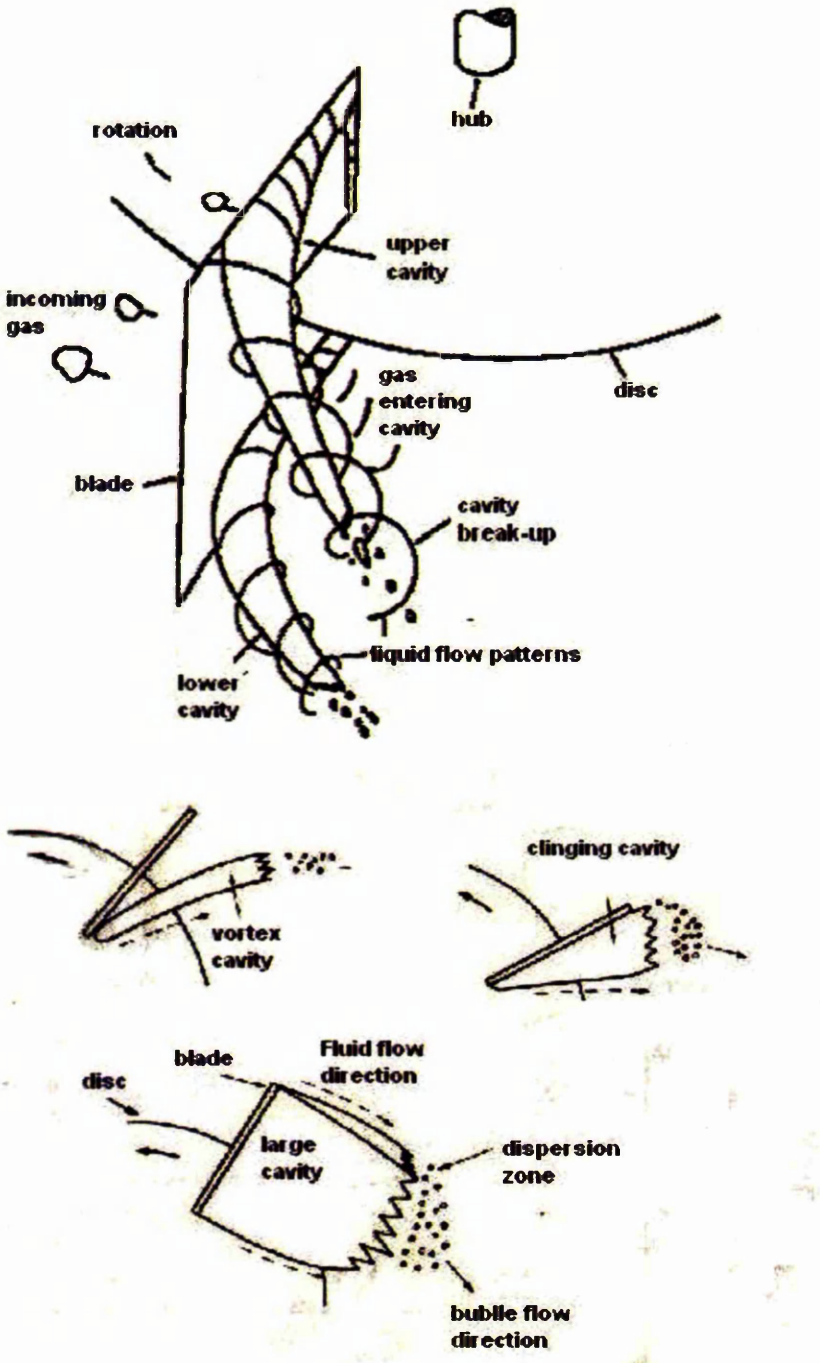

Figure 2-35: The vortex structure and cavities behind the blades of Rushton turbines from van't Riet *et al.* (1976)

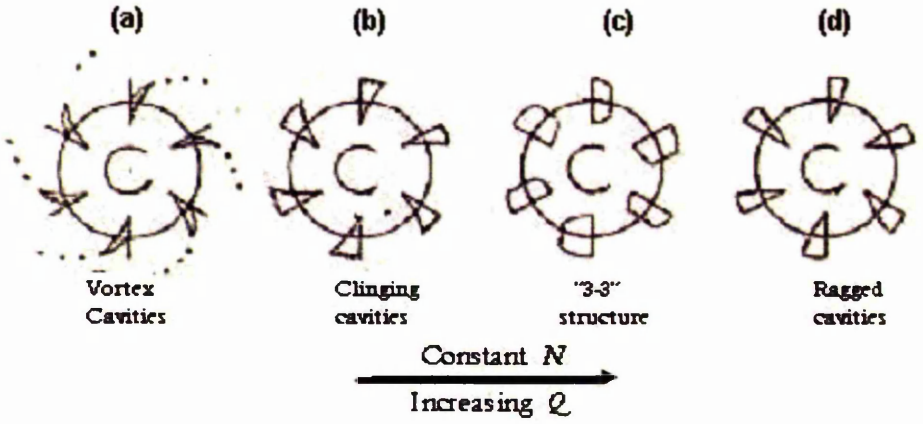

Figure 2-36: Change in the cavity regime with increasing air rate for a Rushton turbine in low viscosity fluids from Nienow (1985).

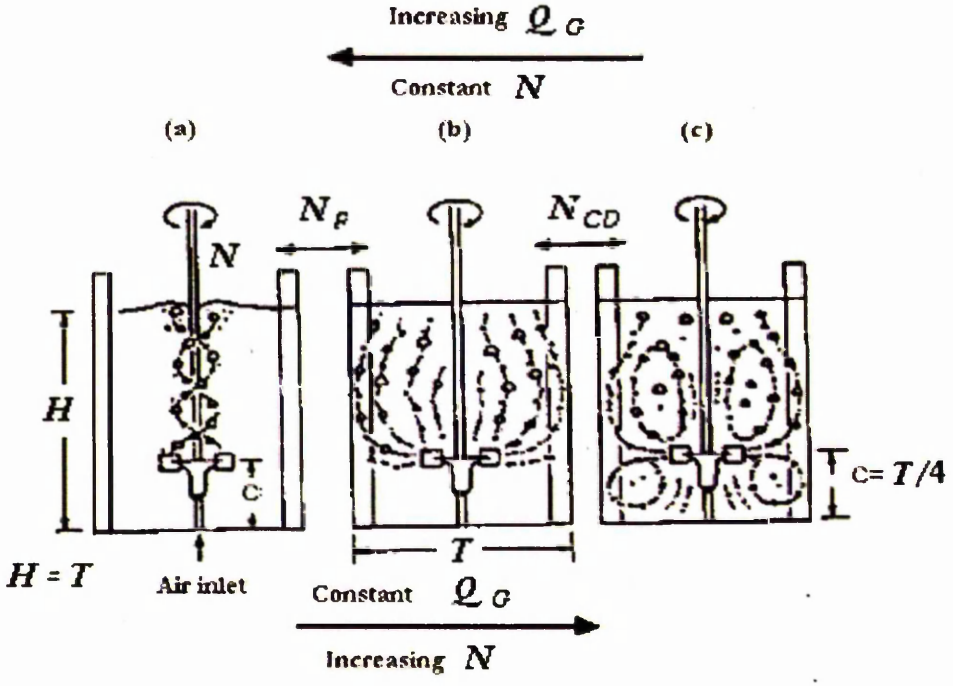

Figure 2-37: The flooding - loading – complete dispersion transitions for a Rushton turbine from Nienow *et al.* (1985)

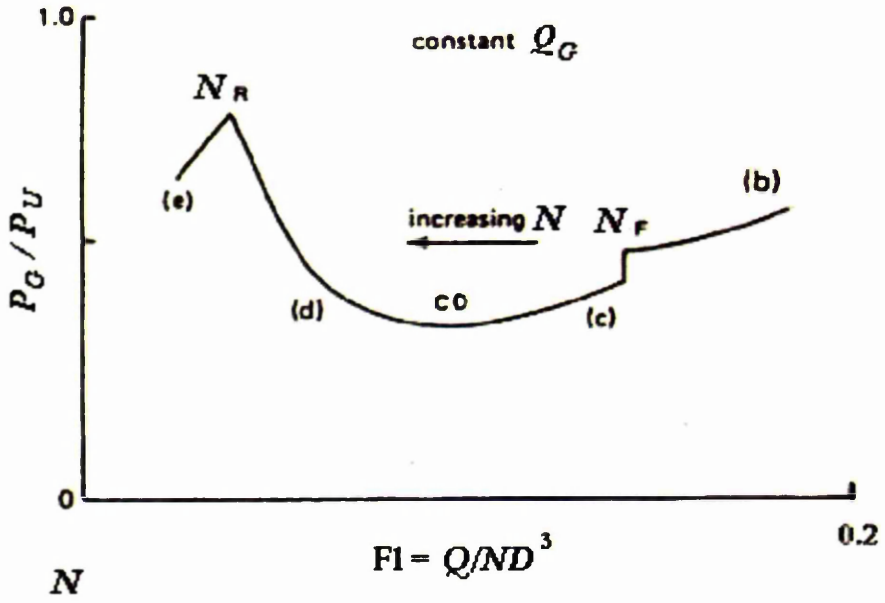

Figure 2-38: Power curves at constant Q_G for a Rushton turbine from Nienow *et al.* (1985)

The flooded regime (Figure 2-37a) corresponds to the operating region in which a large part of the gas bypasses the agitator and breaks through the surface as large bubbles around the impeller shaft. This regime is gas flow dominated and should obviously be avoided. It can result from increasing the gas rate (Q_G) at constant stirrer speed (N) or decreasing N at constant Q_G. In this regime ragged cavities are formed. At high superficial gas velocities the flow patterns are not as shown in Figure 2-37a as the energy input from the gas is considerable and hence the gas may be recirculated throughout the vessel, as shown in Figure 2-37c. However the regime can still be recognized as flooded, since observation of the surface indicates bypass with gas spouting up near the centre.

Loaded regime (Figure 2-37b): Increasing N, or decreasing Q_G, causes more of the gas to be distributed outwards. The loading point is defined as the point at which all the gas is just distributed, flowing out horizontally to the walls before rising in bubble column type behavior. This region is agitator

dominated. Note there is no circulation of the gas into the bottom loop at this stage. Nienow *et al.* (1985) found that the increase in gassing rate, which caused a transition from loading to flooding, is accompanied by a change from 3 large plus three small clinging cavities to 6 ragged cavities for D/T of ≤ 0.4. At this transition there is a step increase in the power drawn. When $D/T = 0.5$ the transition is from clinging to ragged cavities, accompanied by a step decrease in the power drawn. The flooding-loading (*F-L*) transition was found to occur at,

$$\mathrm{Fl_F} = 30\left(\frac{D}{T}\right)^{3.5} \mathrm{Fr_F} \qquad (2.25)$$

"It is likely that this transition is dominated by the Froude number and will be approximately the same for all fluids" Nienow (1998). However, very tiny bubbles will be dispersed at very low agitation rates and when these are present the "flooding-loading" transition is not easy to define. Note that for constant Q_G and T it is easily shown that $N_{(F\text{-}L)} \propto D^{-2.5}$ so, since power is $\propto N^3D^5$, then substituting $D^{2.5}$ for N gives that power to overcome flooding as $\propto D^{-7.5}\,D^5$, which is also $\propto$ to $D^{-2.5}$. Thus a small (D/T) agitator will require more power to overcome flooding than one with a large (D/T). A similar analysis shows that scale-up at geometric similarity and constant P/V means a greater likelihood of operation in the flooding region, i.e. more power is required to avoid flooding on a larger scale.

Complete Dispersion N_{CD} (Figure 2-37c): After loading, further increases in N will eventually result in circulation of gas throughout the region below the impeller and recirculation of gas through the impeller. The point at which gas is distributed to the base of the vessel is called the complete dispersion point

(N_{CD}). This transition depends largely upon the mean bubble size and one would not expect it to be generally correlated by a simple Froude number relationship. For very tiny bubbles the complete dispersion point can coincide with the loading point whilst for large bubbles the speed will have to be increased considerably above N_{F-L} to obtain complete dispersion.

Nienow *et al.* (1985) for Rushton turbines in air-water found that,

$$\mathrm{Fl}_{CD} = 0.2(D/T)^{0.5}\,\mathrm{Fr}^{0.5} \qquad (2.26)$$

Equation (2.26) was analysed in order to judge the effect of D/T. This analysis gives $N_{CD} \propto D^{-2}$ and power for compete dispersion is $\propto D^{-1}$. This means that it requires less energy to obtain complete dispersion with a larger impeller at a given scale. Combining equations 2.11 and 2.26 also shows that more specific energy is required to achieve complete dispersion on a geometrically similar larger scale.

The cavity formation maps at two scales in Figure 2-40, illustrate the effect of scale on the flooding-loading and the loading-complete dispersion transition.

Gross recirculation of gas N_R (Figure 2-38): Further increases in N above CD, at a fixed gas rate, results in an increasing amount of gas recirculating through the impeller and a corresponding rise in power draw. This rise in power peaks at N_R (see Figure 2-38). The power then starts to fall again as gross recirculation occurs giving a well mixed gas phase. The peak N_R has been defined as the onset of recirculation by Nienow *et al.* (1978) and for standard vessels containing Rushton turbines in air-water systems as,

$$\mathrm{Fl}_R = 13(\mathrm{Fr})_R^2 (D/T)^5 \qquad (2.27)$$

Analysis of this equation for constant Q_G and T gives $N_R \propto 1/D^2$ and $P \propto D^1$, which means that you need more power to achieve N_R with a smaller agitator. Scale-up at constant geometry and VVM results in $Q_G \propto D^3$ and gives;

$N_R \propto D^{-0.4}$. As power per unit volume, with geometric similarity, is proportional to N^3D^2 then substituting for N_R results in $P/V \propto (D^{-0.4})^3 \times D^2 = D^{0.8}$ which implies that more power is required to achieve recirculation on scale up.

Van't Riet *et al.* (1976) compared gassing curves with and without recirculation to estimate the ratio of gas recirculation. See Figure 2-39.

They defined an external distribution coefficient (alpha) as

$$\alpha = \frac{Q^1}{Q} \tag{2.28}$$

where Q^1 is the recirculating gas volume and Q is the sparged gas volume.

They estimated alpha for a number of different agitators on 2 scales. They reported alpha factors up to 3, i.e. three times as much "old" gas as fresh gas recirculating through the impeller.

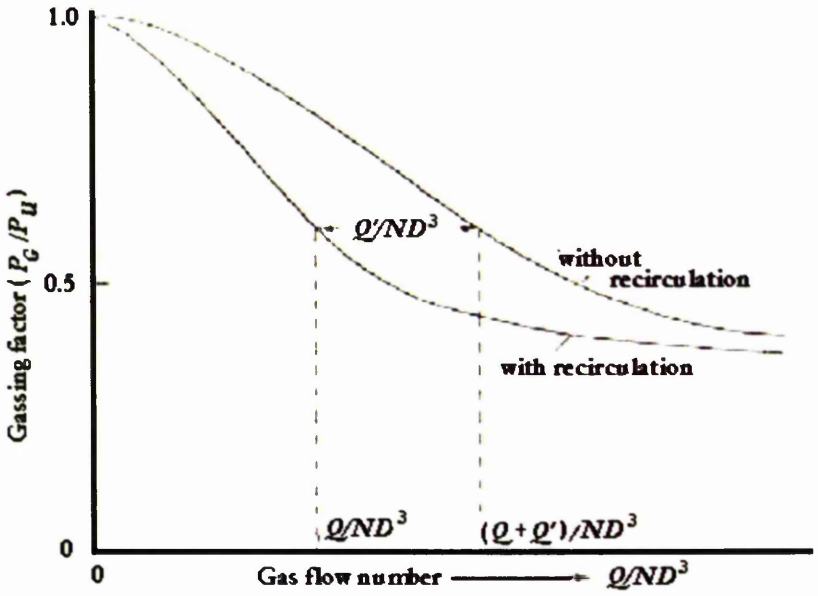

Figure 2-39: Calculation of coalescing recirculating gas flow. From van't Riet *et al.* (1976)

Literature Reviews

Nienow *et al.* (1979) used a tracer technique to estimate alpha factors for a standard disc turbine agitated vessel and found that the volumetric flow of recirculating gas through the impeller can be > 3 times the sparged gas flow. This has implications for gas-liquid mass transfer driving force when inerts are present and the outlet concentration of the "reactant" gas species is significantly below the inlet concentration.

Smith and Smit (1988) acknowledge that the distinctions between some of the cavity regimes are not as clear-cut as earlier work suggested. They identify 4 regimes of importance described by the following equations,

a) Minimum Froude number for the retention of stable cavities.

$$Fr = 0.045 \qquad (2.29)$$

Note from equation (2.8) this is equivalent to 0.9 "g" so this makes some sort of sense. Until the "g" force approaches unity, you would expect gravity to dominate. Note also that this defines a minimum gas loading point for any agitator, because until the agitator "g" force approaches unity gravity will dominate and under these circumstances the agitator must be flooded.

b) The maximum gas flow at which clinging-vortex cavities can be maintained

This is the 3:3 cavity – clinging vortex cavity transition line and is given by,

$$Fl_{3,3} = 0.0038(Re^2/Fr)^{0.067}(T/D)^{0.5} \qquad (2.30)$$

c) The maximum gas rate that can be recirculated through the vessel

This defines the loading-complete recirculation transition and is described by equation (2.26).

d) The Maximum gas flow that can be handled without flooding the impeller

This is the flooding-loading transition and is given by equation (2.25).

These ventilated cavities can give rise fluctuating forces on the shaft. Shedding of cavities from the agitator blades can also lead to large torque fluctuations

and mechanical vibration, which in some cases can be severe, Chapman *et al.* (1983), Cooke (1989) and Nienow *et al.* (1994).

Pearce and Thomas (1990) have observed the structure of these shedding cavities and measured the force transients. By fitting a drag force transducer to a Rushton turbine blade they identified large amplitude bursts in the time record. They used these bursts to trigger flash photographs that showed that they were caused by the rupture of large bubbles attached to the blade.

Nienow *et al.* (1985) and Warmoeskerken and Smith (1985) used dimensionless flow maps based on the equations given above to show the operating regime. Flow maps are constructed using equations 2.25, 2.26, 2.29 and 2.30 in Figure 2-40 for $D=T/3$ Rushton turbines on two scales. Note how the scale up at equal P/V and VVM moves the curves upwards, so that the transitions occur at a higher specific power on the larger scale. This illustrates the increasing likelihood of operating under flooded conditions on scale-up.

The gassing (P_G/P_U) depends upon the type of gas cavities formed hence prediction of these aids gassed power prediction. As far as satisfactory operation is concerned the most important transition is the flooding-loading transition as operation under flooded conditions is not desirable. The equations used to construct the flow maps are claimed to be scale independent, though there is no evidence to suggest they have been tested at scales above 1.83 m vessel diameter.

The data used to derive equation 2.25 from Nienow *et al.* (1985) is reconsidered here. These authors found that the flooding-loading transition for a given Rushton turbine D/T could be described by the equation:

$Fl_{F\text{-}L}$ = a constant x $Fr_{F\text{-}L,}$ where the constant depended upon D/T only.

A plot of these constants versus D/T on log: log axes produced an approximately straight-line graph, which was interpretated as equation 2.25. The data that constituted this analysis is represented here as Table 2-6. The fit of equation 2.25 to the data is poor in some cases. For a D/T of 0.5 the

experimental constant was 4.7, whilst equation 2.25 predicts a constant of 2.65.

Of the form given by equation 2.25, the overall constant taking an arithmetic mean is 33 (10% higher than that given) with a standard deviation of 12. In fact a power law fit of the experimental constants versus D/T produces a much better fit to $(D/T)^4$ rather than $(D/T)^{3.5}$. These discrepancies are discussed in greater detail in chapter 7.

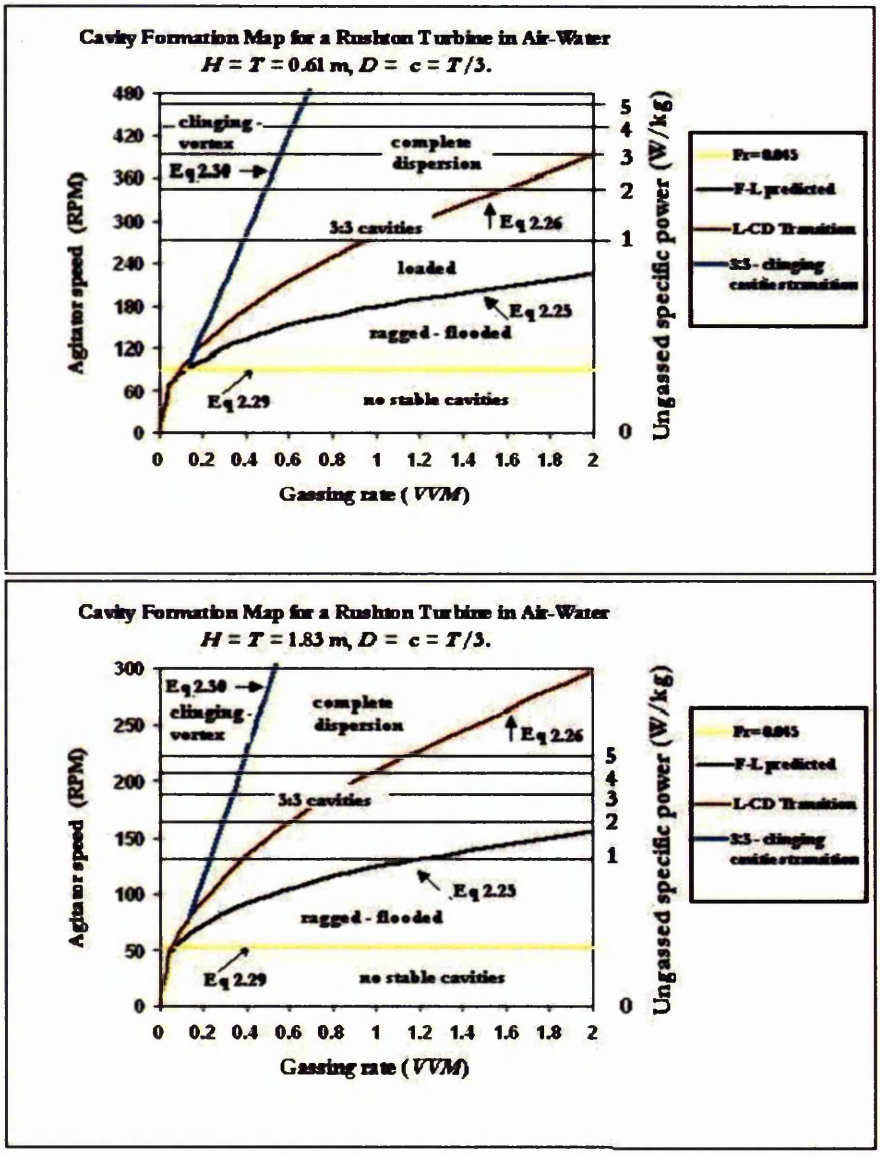

Figure 2-40: Flow maps for a gassed Rushton turbine, $D=T/3$, at two scales

D/T	$Fl_{F\text{-}L}$ = constant x $Fr_{F\text{-}L}$ constant from Nienow *et al* (1985)	Constant predicted by Eq 2.35	constant/$(D/T)^{3.5}$
0.220	0.13	0.15	26.03
0.220	0.17	0.15	34.04
0.333	0.48	0.64	22.46
0.400	1.20	1.21	29.65
0.500	4.70	2.65	53.17
		Average	33.07
		Stdev	12.03

Table 2-6: Analysis of flooding-loading data from Nienow *et al.* (1985)

The Rushton turbine has been used as an example in this section to show the complications of dispersed flow around agitators. Similar literature is available illustrating cavity structure and flow around other agitators and selections of such references are shown in Table 2-7.

Reference source	Agitators	Key Measurements
Bujalski *et al.* (1988)	45⁰ PBT up-pumping and down-pumping	For 3-phase Just suspension speed Flow patterns Hydrodynamics N_F and N_{CD} Power numbers Up-pumping recommended for gassed solid suspension
Bujalski *et al.* (1990)	45⁰ up-pumping PBT	k_La similar to Rushton at same power and gas.
Cooke *et al* (1988)	Various including ICI Gasfoil, non-Newtonian Model fluids	Mixing, Power, k_La Gasfoil k_La and mixing similar to RT when compared at the same size and power.
Saito *et al* (1992)	Four and six blade SCABA SRGT compared with a Rushton turbine	Flow, Power Numbers Gassing factors F-L characteristics Scaba has higher gassing factor and handles 3 times the gas before flooding than RT 4-blade SRGT suffers from flow instabilities.
Dawson, M.K., (1991)	Rushton turbine and Intermig comparisons in non-Newtonian liquid	Fluid dynamics and k_La Higher k_La with Intermig at same Power and gas due to lower apparent viscosity
Hari-Prajitno (1997),	Single and dual hydrofoil impellers pumping up and down. APV B2-30 and B2-45 compared to LIGHTNIN A315	Power characteristics and mixing time. Found that dual APV gave lower relative power fluctuations than the A315 and Rushton turbine and also gave a shorter mixing time.
Gezork *et al* (2001)	Mass Transfer and hold-up characteristics in a gassed, stirred vessel at intensified operating conditions	k_La, Gas-liquid hold-up, in homogeneous and heterogeneous regime

Table 2-7: Some literature comparisons of agitators

2.3.2 Bubble Hydrodynamics

Gas-liquid systems are generally classed as coalescing or non-coalescing. Low viscosity pure fluids liquids are generally coalescing system and as such the bubbles created in the agitator region coalesce as they move to less energetic regions away from the agitator, decreasing surface area. Coalescence requires bubbles to come into close proximity; hence coalescence rates increase with increasing gas-liquid hold-up. This means that coalescence is enhanced in regions where gas hold-up is highest, for example in a recirculating flow due to gravitational effects. In the first instance the rate of coalescence is dependent upon liquid surface properties. Aerated surfactant solutions or salt solutions have a highly polarised gas-liquid interface; therefore two approaching bubbles have to overcome a higher energy level before coalescence can occur. When a solute is present at the interface, stretching of the film as it thins may set up interfacial tension gradients sufficient to prevent any further stretching (Lee and Meyrick (1970) thereby inhibiting coalescence.

In dispersed gas-liquid flow two regimes are possible, the homogeneous or bubble regime and the churn-turbulent or heterogeneous flow regime. In a bubble column the transition from bubble flow to heterogeneous flow occurs when the superficial gas velocity exceeds the rise velocity of the bubbles in the bubble regime. At this stage local gas concentrations are so high that the excess gas coalesces into larger bubbles to satisfy the material balance. The literature on this subject is considered in more detail in Chapter 5.

Krishna and Ellenberger (1995) and De Swart and Krisna (1995), studying bubble columns confirmed the transition criteria and found that for the:

- ***Bubble regime*** the bubble sizes are small and controlled by the physical properties of the liquid and gas.

- ***Heterogeneous regime***, the fractional hold-up of small bubbles (dense phase) is fixed and increasing the superficial gas velocity only increases the fraction of large bubbles.
- In the ***heterogeneous regime***, solid particles supplant gas in the dense phase on a volume fraction basis. Hence, the total volumetric hold-up of solid plus gas remains constant in the dense phase.

Gezork *et al.* (2000) showed similar behaviour in mechanically agitated gas-liquid dispersions. For a mechanically agitated vessel the transition to the heterogeneous regime may occur before the superficial velocity (v_S) equals the dense phase rise velocity due to gas recirculation. They found the transition for the 6RT and 6SRGT impeller, when operated at almost complete dispersed gas conditions, to be largely dependent on the solution used. Transitional gas velocities of v_{trans}~0.03 m/s for the non-coalescing 0.2 M Na_2SO_4 and v_{trans}~0.04 m/s for the coalescing water were found. This compares with typical values of v_{trans}~0.07 m/s for air-water, shown by Krishna *et al.* (1995). A schematic of the transition process is shown in Figure 2-41.

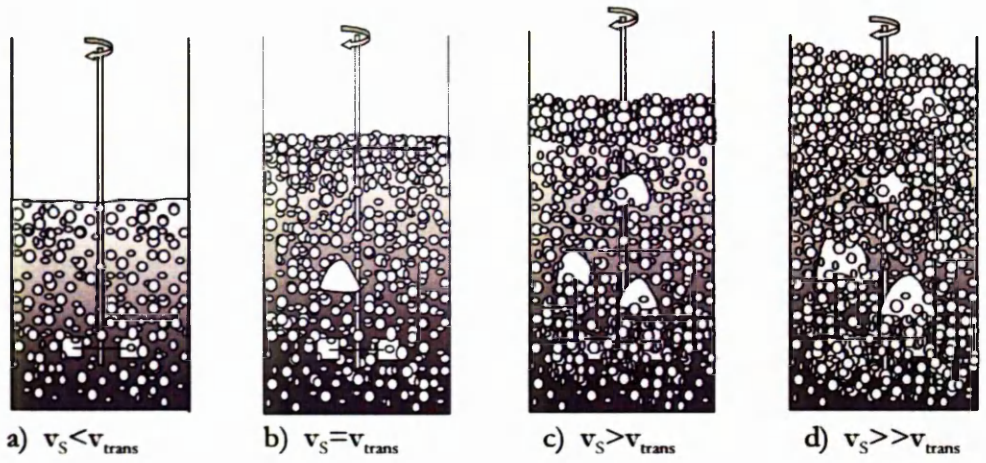

Figure 2-41: Homogeneous a) and heterogeneous flow b), c) and d) in a gassed, stirred vessel. From Gezork *et al.* (2000)

Gas-liquid hold-up is controlled by bubble size, bubble rise velocity and bubble recirculation. Only very small bubbles of diameter ≤ 1 mm are spherical. The relationship between bubble size and shape is given in Table 2-8. The equivalent diameter of irregular shaped bubbles is defined in terms of the volume:

$$d_b = \left(\frac{6V_b}{\pi}\right)^{1/3} \tag{2.31}$$

Equivalent diameter (mm)	Shape
≤ 1	Spherical
> 1 ≤ 6	Oblate spheroids
> 6 ≤ 17	Irregular ellipsoidal
>17	Spherical cap

Table 2-8: Bubble shape versus size in free rise. From Valentin (1967)

Pictures of air bubbles in tap water are shown in Figure 2-42 that illustrate the non-spherical nature of the bubbles.

The change in shape with size has implications for the bubble drag coefficients and free-rise velocities. Experimental data for terminal free rise velocities of air in water are shown in Figure 2-43.

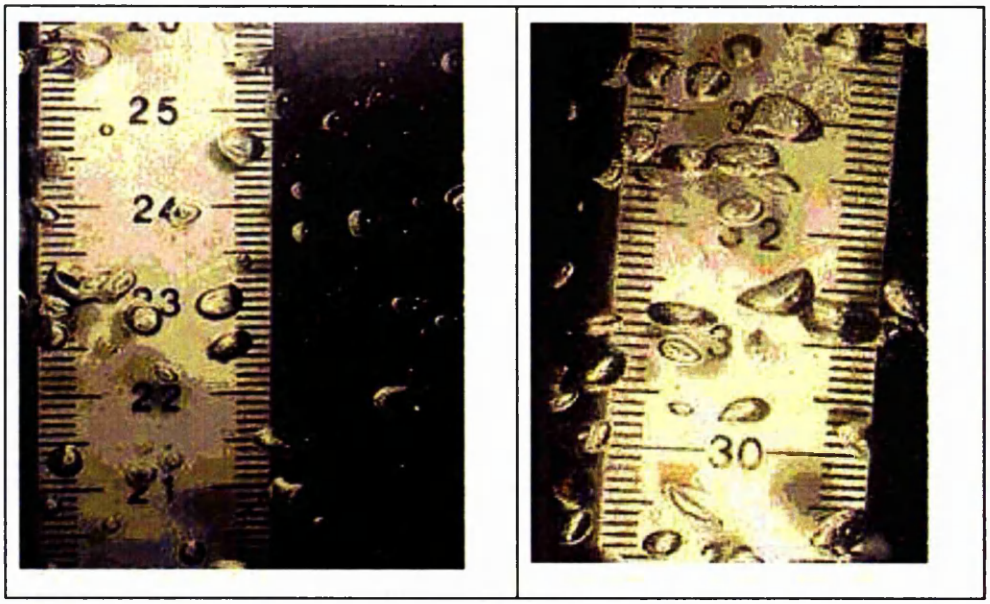

Figure 2-42: Air-water bubbles in 0.91m diameter vessel, agitated with a Rushton turbine of diameter $D = T/3$

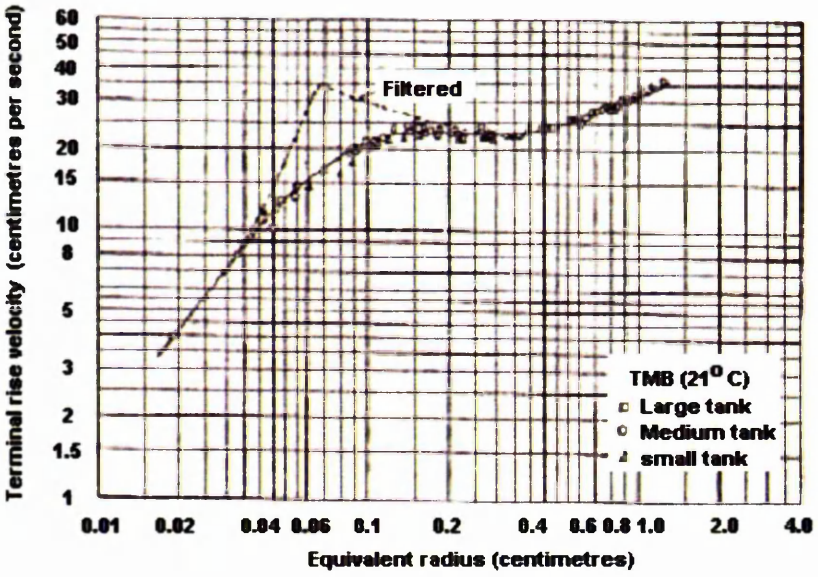

Figure 2-43 Terminal velocity for air-bubbles in tap water as a function of bubble size, (Haberman and Morton, 1956)

2.4 Turbulence

Anyone who has flown has almost certainly experienced turbulence. Nevertheless, it is a difficult thing to define. A quote by Lewis Richardson, erstwhile professor of mathematics: [summarising his paper "The supply of energy from and to atmospheric eddies" 1920] sums it up poetically,

Big whorls have little whorls,

That feed on their velocity;

And little whorls have lesser whorls,

And so on to viscosity.

To understand turbulence its properties need to be considered.

- Turbulence is a property of flow at large Reynolds numbers.
- The random nature of turbulence makes it necessary to describe it in statistical terms.
- Turbulence is rotational and three-dimensional. Deformation occurs by the utilisation of turbulent kinetic energy through viscous shear stresses and requires a supply of energy to be maintained.
- Turbulent diffusion enhances rates of heat, mass and momentum transfer.
- Turbulence is described by the equations of fluid dynamics.

Turbulence in fluids is characterized by three-dimensional random fluctuations in velocity as observed at a single point (whether fixed in space or moving with the fluid). It is usually measured using LDA or HFA techniques (as described in section 2.2.4.2).

From Nienow (1998), for a statistical description, the motion is commonly described in terms of its deviation from the time average values, so that,

$$u_i = u + u' \tag{2.32}$$

where

$$u = \frac{1}{t}\int_0^t u_i dt \tag{2.33}$$

in which t is large, with similar expressions for v and w in the y and z direction.

Homogeneous turbulence is when, at all points in the system, the same time averaged fluctuations occur at all points.

Isotropic turbulence at a point is when deviations are similar in all directions, averaged in time and using a root mean square for the averaging.

The specific intensity of turbulence, I, is defined in terms of these variations such that, for the case when the mean flow u is in a defined direction, then

$$I = \frac{\sqrt{\frac{1}{3}(\overline{u'^2} + \overline{v'^2} + \overline{w'^2})}}{u} \tag{2.34}$$

For isotropic turbulence, the deviations are direction independent such that

$$\overline{u'^2} = \overline{v'^2} = \overline{w'^2}$$

and

$$I = \frac{\sqrt{(\overline{u'^2})}}{u} = \frac{u_{rms}}{u} \tag{2.35}$$

Turbulent flow also gives rise to turbulent Reynolds shear stresses due to the interaction between velocity fluctuations in different directions, that is, $-\rho\overline{u'v'}$. This product relates to the transfer of momentum due to turbulence, just as viscosity transfers momentum due to velocity gradients in laminar flow. There are two other turbulent shear stresses $-\rho\overline{u'w'}$ and $-\rho\overline{v'w'}$ and three normal stresses, $\rho\overline{u'^2}$ $\rho\overline{v'^2}$ and $\rho\overline{w'^2}$.

By suitable treatment of the data from a hot film or laser Doppler anemometer, micro and macro scales of turbulence as well as local energy dissipation rates can be obtained.

2.4.1 The Kolmogorov Theory of Local Homogeneous Isotropic Turbulence: The Eddy Spectrum

The complexity of the turbulent flow in stirred makes analysis difficult. However, Nienow (1998) states that provided the Reynolds number of the main flow is high enough, the Kolmogorov (1941) theory of local homogeneous isotropic turbulence can be used to give some insight into its structure, and has therefore been used extensively for the analysis of stirred reactor problems. Turbulent motion can be considered as a superposition of a spectrum of velocity fluctuations and eddy sizes on an overall mean flow. The large primary eddies have large velocity fluctuations of low frequency and are of a size comparable with the physical dimension of the system, for example, the impeller diameter D (see Figure 2-44). These eddies are non-isotropic and contain the bulk of the kinetic energy. Interaction of the large eddies with slow-moving streams, produces smaller eddies of high frequency that further disintegrate until finally they are dissipated into heat by viscous forces. There is a transfer of kinetic energy down the scale from larger eddies to smaller eddies, the directional elements of the main flow being progressively lost in the process.

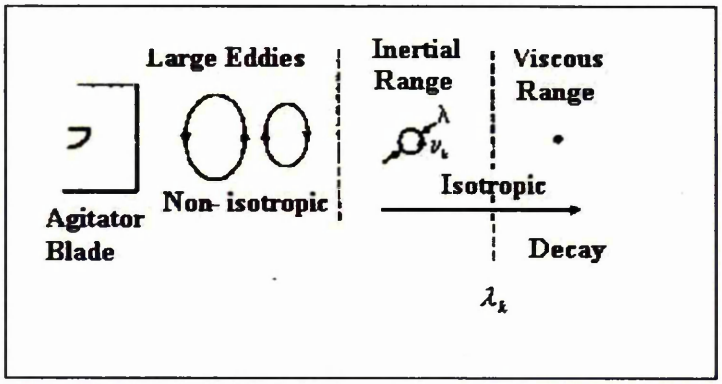

Figure 2-44: Kolmogorov eddy size spectrum

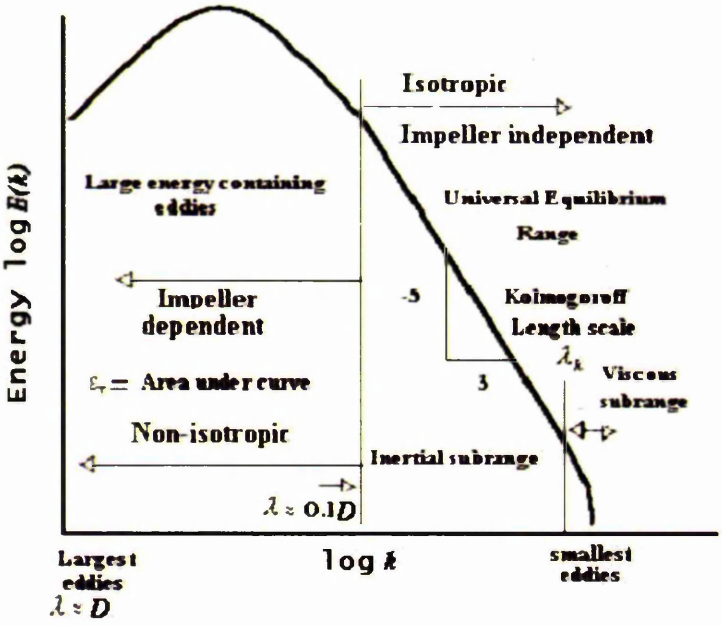

Figure 2-45: Turbulent Energy Spectrum

Kolmogorov's first hypothesis was that, for large Reynolds numbers in any flow system, there is a range of wave numbers (k) where all statistical quantities are functions of the energy dissipation rate /unit mass, ε_T, and the kinematic viscosity (ν) only. This range is known as the viscous subrange. The eddies are independent of the bulk motion and are locally homogeneous and isotropic in the viscous subrange.

The Kolmogorov length scale λ_k occurs where inertial and viscous forces are

in balance, that is, the eddy Reynolds number (Re_k) for the Kolmogorov length scale is unity,

$$Re_k = \lambda_k v_k / \nu = 1 \tag{2.36}$$

The condition $\lambda \leq \lambda_k$ is the viscous subrange.

Kolmogorov's second hypothesis was that, when the Reynolds number is very high, there is another range of wave numbers above λ_k where the eddies are still small enough so that locally the turbulence remains homogeneous and isotropic. However, these eddies are still too large to dissipate energy by viscous forces. This range is known as the inertial subrange. Together with the viscous subrange these make up the universal equilibrium range. Eddies in the inertial subrange receive energy from the larger eddies and then pass this energy to the small eddies in the viscous subrange where it is dissipated as heat. Figure 2-45 shows this structure.

From dimensional reasoning, Kolmogorov proposed the following velocity, length and time scales,

$$v_k = (\nu \varepsilon_T)^{1/4} \tag{2.37}$$

$$\lambda_k = (\nu^3 / \varepsilon_T)^{1/4} \tag{2.38}$$

$$\tau_k = (\nu / \varepsilon_T)^{1/2} \tag{2.39}$$

and the shear rate is,

$$\gamma_k = v_k / \lambda_k = (\varepsilon_T / \nu)^{1/2} \tag{2.40}$$

For an energy dissipation rate of 1.0 W/kg in water, equation (2.38) gives:

$\lambda_k = (10^{-18}/1)^{1/4} = 32$ microns with a shear rate of $(1/10^{-6})^{0.5} = 1000\ s^{-1}$ at the Kolmogorov length scale.

For the inertial sub-range, $\lambda > \lambda_k$ the energy is a function only of the wave-number and the energy dissipation rate and is independent of viscosity, so

again from dimensional reasoning,

$$v_k = f(\varepsilon_T \lambda) = (\varepsilon_T \lambda)^{1/3} \tag{2.41}$$

and the shear rate is,

$$\gamma_k = v_k / \lambda_k = f(\varepsilon_T \lambda) = (\varepsilon_T / \lambda^2)^{1/3} \tag{2.42}$$

Kolmogorov also postulated the following spectrum law for the inertial subrange

$$E(k) = \text{constant}.\varepsilon^{2/3} k^{-5/3}, (k << 1/\lambda_k) \tag{2.43}$$

For the viscous subrange, $\lambda_k > \lambda$,

$$v_\lambda = f(\varepsilon_T \nu \lambda) = \lambda(\varepsilon_T / \nu)^{1/2} \tag{2.44}$$

and the shear rate is,

$$\gamma_k = (\varepsilon_T \lambda^2 / \nu^2) \tag{2.45}$$

By implication, Nienow (1998) points out that processes which are particularity dependent on turbulent eddies and their associated forces are likely to be well correlated by energy dissipation rate. Gas-liquid mass transfer rates, liquid-liquid drop sizes and gas-liquid hold-up fall into that category. However, processes which are dependent on the non-isotropic main flows and for which the non-homogeneous nature of stirred tanks turbulence is significant, for example, the flow rate of air that an impeller can disperse, are not well correlated that way.

Komogorov (1949) and Hinze (1955) applied the theory of isotropic turbulence to the prediction of the maximum drop-size in non-coalescing liquid-liquid dispersions, for drops of low viscosity, whose diameters fall within the inertial subrange of turbulence. This expression is,

$$d^o_{\max} = C_x \sigma^{0.6} \varepsilon_T^{\ 0.4} \rho_C^{\ -0.6} \tag{2.46}$$

or expressed as a Weber number this gives,

$$\frac{d_{\max}^{a}}{D} = C_y \, \mathrm{We}^{-0.6} \tag{2.47}$$

where C_x and C_y are constants and $\mathrm{We} = \frac{\rho N^2 D^3}{\sigma}$.

It was however found that this equation does not scale as predicted. Podgorska and Baldyga (2001) argue this is due to the phenomenon known as "fine-scale intermittency" or the multi-fractal theory of turbulence based on scaling invariance of the Navier Stokes equation as developed by Frish and Parisi (1985). The effect of intermittency on the break-up rate was deduced by Baldyga and Podgorska (1998). They used their model to predict the effect of scale-up for 4 different scale-up criteria:

- Equal power per unit mass and geometric similarity.
- Equal circulation time and geometric similarity.
- Equal power per unit mass and equal circulation time
- Equal tip speed and geometric similarity.

They did this for two cases, fast and slow coalescence.

Their predictions would indicate it is better to scale up at equal power per unit mass, though the drop size is predicted to increase slightly with scale up by this method, even for the equal circulation time case. Equal circulation time and equal tip speed both predicted very different drop-sizes on scale-up.

How do these predictions match with experiments?

Colenbrander (2000) and Musgrove and Ruszkowski (2000) both report drop sizes decrease on scale-up at constant power per unit mass. Also equal tip speed scales well for a single agitator type. See Figure 2-33 and the data of Zhou and Cresta (1998) that was reproduced in Figure 2-34. In fact in order to correlate drop-size with energy dissipation rates for a range of agitator types, Musgrove and Ruszkowski (2000) found they had to consider the maximum

energy dissipation rate per agitator blade. From this it is concluded that although the intermittency theory helps explain the shortcomings of the Komogorov (1949) approach to drop size prediction, it is insufficiently developed at present to predict accurately the effect of scale and agitator selection on drop-size distribution.

Podgorska and Baldyga (2001) have used the intermittency theory to predict the transient drop size distributions by solving the population balance equation for a single-circulation-loop model of agitated tank. When used with fitted constants for the break-up and coalescence parameters, the transient predictions were in good agreement with the reported data of Konno and Saito (1988). Similarly Baldyga *et al.* (2001) show that they can fit their data on two scales to the intermittency model. This is encouraging but apparently not yet fully predictive.

2.5 Mixing

The term mixing describes processes by which non-uniformities of composition, properties or temperature of materials are reduced in the bulk of the fluid. Mechanical agitation provides the deformation and flow required for the mixing to occur, due to the mechanisms of diffusion, convection and bulk movement.

For co-mixed fluids, mixing quality is described in terms of scale and intensity. Uhl and Gray (1966) define scale as the average difference between centres of maximum differences in properties. In turbulent mixing scale corresponds to the size of the turbulent eddies and is reduced by eddy break-up. In laminar mixing, scale is reduced by thinning layers, stretching threads of the components and flattening lumps. Intensity is defined in terms of the variance or range of properties existing in a mixture. When fluids of different compositions are initially brought together, the difference in properties or

spread is at its maximum. In practical terms, intensity does not decrease until the scale of the non-uniformity becomes smaller than the sample size.

2.5.1 Diffusion

If two materials are brought together in a container then, in time, the molecules will intermingle, as a result of concentration gradients and random molecular motion, to form a uniform mixture on the sub-micron scale. This is called molecular diffusion. This process can take a very long time. Imposing velocity gradients can considerably enhance diffusion rates as high velocity streams entrain low velocity streams.

In turbulent flow, the transfer of fluid is greatly enhanced by the random nature of the velocity fluctuations. Thus, eddy diffusion effects can be used to greatly enhance the mixing process by generating turbulence.

2.5.2 Convection

Convection is the motions imparted to the fluid by inertial forces. An agitator causes motion in a vessel at some distance from the stirrer due to convective forces and the inertial effects of the agitator. Viscosity has a big effect on convection. High viscosity damps down inertial forces so it is more difficult to move fluid to all parts of the vessel. This can lead to dead zones or in extreme cases "cavern" formation as shown in Figure 2-48. It is important therefore to design mixers to avoid stagnation regions, as this leads to inefficient mixing. Increasing agitator D/T and using high solidity agitators is the best way to avoid stagnation regions.

2.5.3 Bulk Movement

Mixing of fluids by bulk movement results from the intermingling of fluids by cutting, dividing and recombining. This happens in all mechanically agitated processes but in fluids of very high viscosity, where turbulence generation would be energetically prohibitive, this becomes the main mode of mixing. For example, a kneading motion using a process of separation and recombination is used for thick dough mixing.

2.5.4 Macro-scale and Micro-scale Mixing.

Macro-scale mixing is mixing in the bulk of the vessel brought about by turbulent diffusion and back mixing. For most blending operations and for mixing involving relatively slow reactions where homogenisation down to the molecular scale (micro mixing) takes place before any significant reaction occurs, this is all that is required. For two fluids to react they must be brought together at a molecular scale through molecular diffusion. If there is only one product then, providing the contact time is longer than the sum of the residence time, calculated from the reactions kinetics, plus the mixing time required for bulk mixing to occur (macro-mixing), then the reaction will proceed normally.

However, in some cases competition between reaction and mixing results an undesirable product spectrum and in these cases micro mixing is extremely important. Bourne *et al.* (1981) and Bourne (1982) used fast, competing consecutive reactions schemes with a stoichiometry,

$A + B \rightarrow R,$

$R + B \rightarrow S,$

with a product distribution X_S given as,

$X_S = 2C_S/(C_R-2C_S)$

$r_R = k_1[A][B] \approx 7.3 \times 10^3\ m^3 mol^{-1} s^{-1}$

$r_S = k_2[R][B] \approx 3.5\ m^3 mol^{-1} s^{-1}$,

The above constants for the diazo-coupling reaction (used by Bourne to study micro mixing) are given by Middleton *et al.* (1986). The maximum yield of the intermediate R is obtained when species A and B can be brought together at the molecular scale before significant reaction has occurred. When however, the reaction is instantaneous compared to mixing, the reaction goes to completion and the yield of R approaches zero. This would happen for example if A were added slowly to B. If B is added to A, then the ratio of the products will depend on the relative rates of the two reactions.

Consider a concentrated volume of B being added to a reactor containing a well mixed volume of A. Molecular diffusion will transfer some B into A and some A into B. The B that moves into A will reaction to form R while the A that moves into B will form S as B will be in excess. Initially the surface area will be small so not much reaction will occur. However, as turbulent diffusion and bulk flow breaks the clumps up, the surface area will increase and become smeared out by molecular diffusion until mixing is complete. For a fast reaction, the reaction will occur at the interface of A and B and the product distribution will depend on the balance between reaction and diffusion and the ratio of the reaction rate constants k_1/k_2.

The process of turbulent diffusive mixing is continuously being interrupted because eddies have a finite lifetime. It is important to note that the reaction cannot occur until the clumps have been ground down to a scale of the order of the distance the reactants can diffuse in the lifetime of an eddy. Therefore, the important parameter is the ratio of the reaction time to the time taken for material to diffuse through the thickness of an eddy. The ratio, sometimes called the Damkohler number (Da) is,

$$\mathrm{Da} = \frac{\tau_D}{\tau_R} \tag{2.48}$$

Bourne (1997) takes the characteristic reaction time as the half-life of the limiting component *B*, after which half of *B* has been consumed by reaction, assuming this is not mixing limited. Therefore, when $k_1 >> k_2$ and the stoichiometric ratio of reactants ≅ 1, it follows that,

$$\tau_R = (k_1 C_O)^{-1} \tag{2.49}$$

where C_O is the concentration of *A* and *B* in the bulk after mixing, assuming no reaction.

The characteristic diffusion time depends on the lifetime of a typical eddy diffusion, which depends on the kinematic viscosity, the rate of energy dissipation and the diffusion coefficient and has been described as follows,

$$\tau_D = (\nu / \varepsilon_T)^{1/2} (\nu / D_L) \tag{2.50}$$

D_L is the diffusion coefficient and ν / D_L is the Schmidt number.

The theory of this approach with detailed modelling is given by Bourne (1997) and the references therein.

A major conclusion from the above is that where micro mixing is important then addition points and mixing energy becomes a critical design parameter. Specific Power input needs to be high. Feed addition should be at the main agitator where ε_T is at its maximum and multiple feeds should be considered.

More recently Buchmann (2000) described a rather clever tomographical dual wavelength photometry technique to study simultaneous macro and micro mixing, measured at a multitude of points, inside a stirred reactor. A mixture of an inert and a reacting dye are injected into the vessel. The inert dye serves as a tracer for the macro mixing, whereas the vanishing of the reacting dye shows the micro mixing. The concentration fields of the dyes are measured simultaneously by trans-illuminating the vessel from three directions with superimposed laser beams of different wavelengths. The light absorption by

the dyes is measured with CCD-cameras and these projections are used for the tomographical reconstruction of the concentration fields. Low Reynolds' number measurements with a Rushton turbine showed better macro and micro mixing for a dye injection closer to the stirrer shaft compared to a position closer to the main vortex. They claim CFD predictions compared well with the experimental results after implementing a new model to describe the deformation of small fluid elements and the molecular exchange between these elements and the surrounding liquid. This model is implemented through two transport equations into the CFD software and yields the local mixing quality at a multitude of points through the vessel. This was necessary as the CFD software does not resolve below the finite volume size of the grid and this is larger than the molecular scale.

2.5.5 Mixing Times

This thesis is limited to the blending of miscible liquids, which may be complicated by the effects of density and / or viscosity differences, viscosity and the presence of gas and / or solid phases.

The mixing time t_m is a function of the liquid properties and the geometry of the mixing vessel. In the dimensionless form the mixing time constant Nt_m is a function of Re, Fr, ε_T and geometrical parameters such as D/T, H/T and c/T. In fully baffled vessels for the turbulent regime where no density differences exist the mixing time constant is independent of Reynolds and Froude and depends solely on energy input and geometric parameters.

Bulk mixing (macro mixing) has been studied in different ways. Examples are:

Colorimetric methods:

- By dye addition, Example – Mann *et al.* (1987).
- By pH shift using an indicator, or decolourisation of a starch iodine solution by sodium thiosulphate, Examples, Cronin *et al.* (1994) and Hari-Prajitno (1997)

Literature Reviews

Conductivity:

- By addition of a conductivity pulse monitored by conductivity probe(s)/meter(s). Examples, Khang and Levenspiel, (1976), Cooke *et al.* (1988) and Ruszkowski (1994).

Transient pH shifts:

- Example, Singh *et al.* (1986)

Temperature transients:

- Using thermocouples for example, Shiue and Wong (1984)
- Liquid crystal thermography as reported by Lee and Yianneskis. (1997)

Tomographic, for examples:

- Dual wavelength photometry, Buchmann (2000)
- ERT (electrical resistance tomography) Cooke *et al.* (2001).

Flow followers to measure circulation times, Example:

- Bryant and Sadeghzadeh (1979).

2.5.5.1 Decolourisation Techniques

The decolourisations methods are very useful for looking at inter zone mixing and for determining stagnation regions. However, some doubts must exist about the precise level of mixing that is being measured by colouration /decolourisation techniques. The total decolourisation point is subject to operator bias and depends upon stoichiometry. If for example the decolourisation agent is 10% in excess, then it follows that the vessel will be

totally decoloured when the vessel is 90% mixed. Hence to make any meaningful comparisons the excess needs to be precisely known.

The technique is also useful when a second phase is present which will affect conductivity probes. However, it is still necessary to ascertain what effect the second phase has on the reacting species. For example a common decolourisation technique is to use glacial acetic acid to decolourise a weak solution of sodium hydroxide containing phenolphthalein indicator. In an aerated system the air will strip acetic acid from the system; hence carefully planned stoichiometric ratios can be easily thwarted.

2.5.5.2 Conductivity Techniques

Earlier work (Cooke *et al.* 1988), standardised on the conductivity technique, using conductivity probes based an **a** design used by Khang and Levenspiel (1976) because,

- The measuring volume is small and known.
- The probes have a very fast response time.
- The response of the probes is linear over a wide range of liquid conductivities
- The conductivity probes are stable over long time intervals.
- The probes give a continuous time history of the concentration fluctuations at the sample points. These concentration-time histories can readily be analysed to obtain mixing tines for a specific degree of mixing.

However, this was combined with decolourisation techniques to look at zoning effects and to identify stagnation regions.

2.5.5.3 Degree of Mixing

The degree of mixing is not always given in the literature results. For analysis of responses from step changes in the input a specified degree of mixing is the time taken from the pulse injection until the concentrations fluctuations are just within specified limits of the final step change. Thus, for example, a 90% mixing time t_{90} is the time taken from injection until the first point that all values are within ± 10% of the equilibrium step change.

As mixing is a chaotic process and the mixing time is dependent, amongst other factors, on the precise flow conditions at the time of the tracer addition then it follows that mixing times are not repeatable. The experimenter has to average a number of runs (usually a minimum of 6 but preferably 10) to obtain an average mixing time. When the data is collected electronically, it is convenient to analyse the data statistically, using identical criteria, to obtain reproducible self-consistent data.

Khang and Levenspiel (1975) used four probes connected in a ring around the impeller to measure the mixing time that they fitted to a decay constant using RTD theory.

The Cooke *et al.* (1988) triple agitator data was obtained using 3 probes sited at the walls opposite the agitators. The tracer was added to the surface. The responses were analysed graphically to obtain a 90% mixing time for each probe and a vessel average was obtained from the 3 probe results. The mixing time for a particular operating condition was the average of several repeats. For $H = T$ work a single probe sited at the wall opposite the agitator was used. Additions were of concentrated potassium chloride solution, with the addition size weighted to give a 0.05 g/l step change in concentration. Several additive additions were made before the solution was changed. Solutions changes were dictated by "noise" increase as the solution became more concentrated. Some of this "noise" can be attributed to air bubbles in the system. The higher the

background conductivity, the greater the effects of low conductivity contaminants such as air.

Ruszkowski (1994) used similar probes to the above to determine mixing times from the average of 8 runs. Three probes were used in a baffled $H=T$ geometry vessel, one in the impeller stream, one close to a baffle and a third in the middle of the tank at different heights, radial positions from the shaft and at different sides of the vessel in order to sample as representatively as possible. The tracer was added at the impeller. The data was normalized and the root mean square of the conductivity of all three probes was calculated from,

$$C_i rms = \sqrt{1/3(C_{i1}^2 + C_{i2}^2 + C_{i3}^3} \qquad (2.51)$$

Using three probes provides a more representative view of the tank concentration variance and is probably essential to obtain a vessel representative mixing time when addition is at the impeller. One would expect the mean mixing time from such an analysis to be weighted towards the longest mixing time. The effect of averaging 3 probes reduces the variance and increases the sample volume. This enables one to measure more repeatedly a higher degree of mixing. It should provide a better picture of the overall concentration variance in the vessel. If however, you take this to the extreme of an infinite number of probes of infinitely small volume you finish up measuring the sample input time rather than the mixing time as once the pulse has been injected the average vessel concentration does not change.

A mixing index was calculated from the variance calculated from a 8 point moving average taken over time steps that are very much smaller than the mixing time,

$$\sigma_c^2(n) = \frac{1}{8}\sum_{j=n}^{j=n+7}(c_j - c(\infty))^2 \qquad (2.52)$$

where,

$\sigma_c^2(n)$ is nth value of σ_c^2

C_J is the concentration at the *Jth* data point

$C(\infty)$ is the final average concentration = 1 for a perfectly mixed system.

For the above, the variance is time-averaged over 8 points and space-averaged over 3 points giving a total variance over 24 data points.

A mixing index was then calculated from,

$$M = 1-\sqrt{\sigma_C^2} \qquad (2.53)$$

assuming that $C(\infty) = 1$ for a perfectly mixed system.

They found that variance decays exponentially with time, allowing a first order time constant to be determined which can be related to any degree of mixing.

2.5.5.4 Comparisons of Mixing Results with Different Methods

Although the method of Ruszkowski (1994) looks very different from the graphical method of Cooke (1988), in practice it yields very similar results. For a single probe 8 data points are not enough to calculate the variance, hence the sample frequency is increased and the variance is calculated over a 32 point moving average with the sample frequency chosen so that the time averaging step is << shorter than the mixing time.

Figure 2-46 compares a single probe mixing trace as a plot of normalized concentration versus time for a 32 point moving average with the same data plotted as the mixing index calculated according to equation (2.52). Quite clearly the 90% mixing time and the mixing index of 0.9 are reached at the same time when the same averaging process is used. Note that these results were obtained with a surface addition and measurement by a single probe in the base to measure an overall mixing time. Had, for instance, the tracer been added at the impeller there would have been a big overshoot on the graphical output. However, from experience, the 90% time and the M =0.9 point would still be coincident.

2.5.5.5 Mixing Time Constant

It is generally found that for geometrically similar vessels, in the turbulent regime, Nt_{90} (or $N\theta$) is a constant, where θ is a specified degree of mixing. The exception to this is when the mixing vessel is compartmentalized, either due to a significant poorly agitated region, or to a poor interchange between numbers of well-mixed regions. In these cases there can exist a different relationship between the agitation speeds for interchange rates compared with mixing times in the well-mixed zones and then $N\theta \neq$ constant.

Kipke (1983) reviewed scale-up anomalies and noted that the expression $N\theta$ = constant, for geometrically similar vessels, does not necessarily scale-up. He argued that this was because the macro-scale of turbulence scales with impeller size. Thus larger eddies are found in large vessels that result in larger variations and therefore the final state of mixing is achieved later in larger vessels.

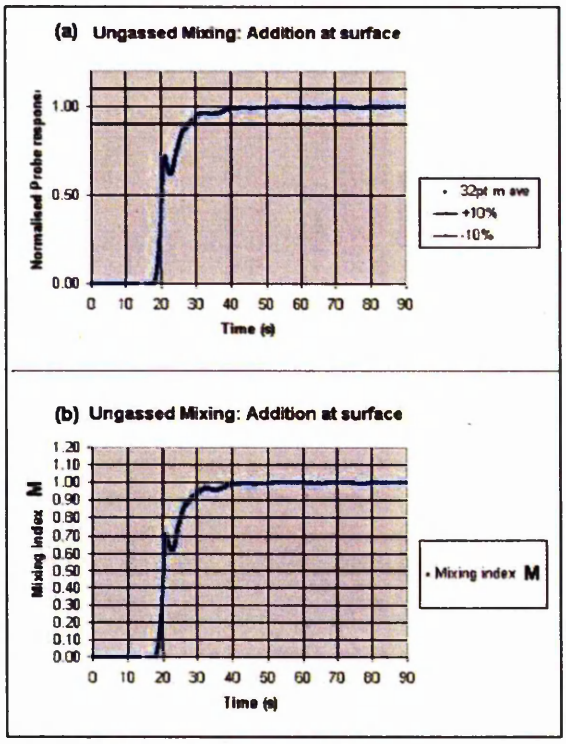

Figure 2-46: (a) top Graphical mixing time, (b) Mixing index

2.5.5.6 Effect of Agitator Type (standard tank H=T) on Mixing

Compared at equal P/V and D/T there appears to be very little to choose between different impellers. Our own data, Cooke *et al.* (1988), found little difference between a Gasfoil and a Rushton turbine under turbulent conditions:
The results could all be described by,

$$Nt_{90}Po^{1/3}(D/T)^{2.2} = 3.9 \qquad (2.54)$$

where Po represented the power number both in ungassed and gassed conditions.

Ruszkowski (1994) comparing 4 and 6 blade pitched turbines, Rushton turbines and propeller agitator, claimed that all his results could be correlated by a single equation for single phase turbulent mixing such that:

$$N\theta Po^{1/3}(D/T)^{2} = 5.3 \qquad (2.55)$$

where θ represent a mixing index M = 0.95.
Note that equations (2.54) and (2.55) are very similar. Assuming first order mixing, then 95% mixing is 1.301 times longer than 90% mixing. Hence, compared at the same degree of mixing, the constant in equation (2.54) becomes 5.07.

Comparing the 95% mixing time for a D=T/2 Rushton turbine, of Po = 5.5, at 2 revs per second, gives,
From Cooke *et al.* (1988), $\theta = 5.07/ (2*5.5^{1/3}*0.5^{2.2}) = 6.6$ s

And Ruszkowski (1994), $\theta = 5.3/ (2*5.5^{1/3}*0.5^{2}) = 6.0$ s

Thus the Ruszkowski (1994) equation predicts a similar but slightly shorter mixing time to Cooke *et al.* (1988). This could be due to data smoothing and

averaging the three probes, or may be due to differences in scale.

Nienow (1998) shows a comparison of the data of Hass and Nienow (1989) comparing an equal diameter, Prochem Maxflo T impeller with a Rushton turbine and also the Saito *et al.* data of 1992, comparing a Rushton turbine with a equal diameter Scaba 6SRGT. The mixing data, which was measured by the decolourisation technique, in gassed and ungassed conditions, showed good agreement with the Ruszkowski (1994) equation (2.55).

Note that not all workers agree that all impellers are equally energetically efficient. For example the correlations of Khang and Levenspiel (1976) (that are similar to the Ruszkowsi correlation, but do not contain a power number terms and is based on circulation time theory) implies that the propeller is more energy efficient for mixing than a disc turbine by a factor of around 4. However, when compared at the same degree of mixing the Cooke *et al.* (1988) and the Ruszkowski (1994) do predict very similar mixing times. The main conclusion from the above is that, in turbulent conditions, it is power rather than the agitator type that is the most important parameter for mixing. This is in agreement with turbulence theory (Section 2.4).

2.5.5.7 Effect of Impeller Diameter on Mixing

Most workers agree that at Re > 10^4, Nθ = constant x $(T/D)^{2\pm A}$ where A takes values of 0 to 0.3.

Khang and Levenspiel (1976) found the exponent A = 0 for propellers and 0.3 for turbines
Cooke *et al.* (1988) found A = 0.2 for turbines,
Ruszkowski (1994) found A = 0 for a range of agitators

Equations (2.54) and (2.55) can be rewritten as,

$$\theta = k\left(\frac{1}{N}\right)\left(\frac{1}{\mathrm{Po}}\right)^{\frac{1}{3}}\left(\frac{D}{T}\right)^{-\beta} \tag{2.56}$$

$$\text{where, } \frac{1}{\mathrm{Po}} = \frac{\rho N^3 D^5}{P} \tag{2.57}$$

For $H=T$ and a flat base

$$P = \frac{\varepsilon_T \rho \pi T^3}{4} \tag{2.58}$$

Substitute equations (2.57) and (2.58) in (2.56),

$$\theta = k\left(\frac{4}{\pi}\right)^{1/3} \varepsilon_T^{-1/3}\left(\frac{D}{T}\right)^{5/3}\left(\frac{D}{T}\right)^{-\beta} \tag{2.59}$$

Thus, if $\beta = 5/3$, there would be no effect of D/T ratio at constant P/V. For $\beta = 2$, then $\theta \propto (D/T)^{-1/3}$ and for $\beta = 2.2$, then $\theta \propto (D/T)^{-0.533}$.

The above implies that a larger diameter agitator mixes more efficiently than a smaller one. Most workers have only tested these relationships up to $D = 0.5T$.

Also from equation (2.59) at constant P/V and geometric similarity,

$$\theta \propto T^{2/3} \tag{2.60}$$

2.5.5.8 Effect of Aspect Ratio *H/T* on Mixing

This is the most uncertain area. There has not been a lot of work done. Cooke *et al.* (1988) compared 1:1 with 3: 1 aspect ratio tanks, fitted with disc turbines or ICI Gasfoils and found that Nt_{90} increases dramatically with increasing H, due to compartmentalization effects according to.

$$\mathrm{Nt}_{90} = 3.3\left(\frac{1}{\mathrm{Po}}\right)_{total}^{1/3}\left(\frac{H}{D}\right)^{2.43} \tag{2.61}$$

Thus when the aspect ratio is changed from 1:1 to 3:1 the mixing time increases by a factor of approximately 10. When the top two disc turbines were replaced by 6MFD agitators t_{90} decreased by a factor of 2 at the same power input. Other workers have reported similar staging effects using multiple radial impellers for example Cronin *et al.* (1994) for Rushton turbines. The reduction in the overall mixing time by about 50%, obtained by replacing the two upper turbine agitators with axial flow agitators, has been confirmed by Manikowski *et al.* (1994) and Otomo *et al.* (1995) according to Nienow (1998).

The dramatic increase in overall mixing times for the turbine multiple agitators in high aspect ratio vessels, are due to compartmentalization. Where this can be avoided, then from circulation time theory, the increase in mixing time with height might be expected to be directly proportional to operating height at constant P/V. This hypothesis is worth testing. However, even if this is true, the overall mixing time will increase with an increase in batch height. For processes that rely on mixing to supply vital reagents or nutrients to all parts of the vessel the effect of H/T on mixing could therefore be a vital factor. Aerobic fermentation processes could well fall into that category.

Oldshue (1983) shows that for laminar mixing ($Re \leq 50$) with a continuous ribbon agitator (see Figure 2-18) the mixing time is directly proportional to (H/D).

2.5.5.9 Effect of Viscosity on Mixing

Below the transition point mixing times increase dramatically and $\theta = f(Re)$. For Newtonian fluids Khang and Levenspiel (1976) show a transition at around $Re \approx 3300$ for turbines and $Re \approx 10^4$ for propellers. Cooke *et al.* (1988)

found for Rushton turbines in non-Newtonian systems the constant in equation (2.61) was $1174Re^{-0.7}$ with the transition at Re = 4400.

In the laminar regime it is difficult to get good top to bottom mixing. Nagata (1975) proposed the helical ribbon as the most efficient method of mixing such fluids. A popular geometry is the twin bladed ribbon pumping upwards with a double central down pumping screw. Oldshue (1983) gives the following preferred geometry for these agitators:

Double helix (up-pumping) ($w = D/6$), and $D = 0.92T$ and double inner screw ($Di = D/3$) down pumping with pitch = h/D = 1.0 and H/D =1.0, where:

- h = height of helix for 1 revolution,
- D = helix swept diameter
- Di = screw swept diameter
- w = width of outer ribbon
- H =liquid height

Then,

$$\mathrm{PoRe} = 255 \tag{2.62}$$

$$\mathrm{Nt_m} = 30 \tag{2.63}$$

$$\mathrm{Nt_m} \approx 30\left(\frac{H}{D}\right) \tag{2.64}$$

Oldshue (1983) indicates that there are approximately three fluid turnovers (circulations) per mixing time. That is,

$$\mathrm{Nt_m} \approx 3\,\mathrm{Nt_c} \tag{2.65}$$

where t_C is circulation time and t_m is a colorimetric based mixing time.

$$\mathrm{Nt}_C = 10 \tag{2.66}$$

2.5.5.10 Effect of Gas and Solid Phases on Mixing

See also section 2.2.4.2.

Cooke *et al.* (1988) found that the same equation correlated the data for liquid and gassed liquid mixing (2.54) providing the operation is in the agitator-dominated region.

Harrop *et al.* (1997) found that solids can increase the liquid mixing time by a factor of 6 for a LIGHTNIN A315 impeller when operation is below N_{JS} at sand concentrations between 10 and 20% by mass, due to a zoning effect when a solid-liquid interface is present.

Takenaka *et al.* (2001) studied a 3-phase liquid-gas-solid system at solids concentrations up to 40% by weight and gas flow rates up to 2 *VVM*. They used two different radial flow impellers, a Scaba 6SRGT and a Rushton turbine plus a six-bladed mixed flow impeller with pitch angle of 45° that was operated in both downward and upward pumping modes. They confirmed the Harrop *et al.* (1997) trend of increased mixing time for the solid-liquid case compared with the liquid only case. However, for the three-phase case the increase in mixing time was relatively small, especially with the SCABA and 6MFU impellers. It appears the gas-phase prevents a stable solid-liquid forming.

2.5.5.11 Effect of Tracer Properties (Volume, Density and Viscosity) on Mixing

The effects of tracer properties (volume, density and viscosity) on mixing were recently studied by Pandit *et al.* (2000). They used tracer viscosity (μ_a) to the bulk fluid viscosity ((μ_b) ratios ($\mu_a/(\mu_b$) up to 150 and tracer density to bulk density ratios [$(\rho_a - \rho_b)/\rho_b$] up to 0.145. They varied the tracer volume (Va)

ratio from $Va/V = 0.005$ to 0.075. They found no effect of viscosity ratio on mixing, but did find an effect of the tracer volume and density difference due to buoyancy effects. They correlated these effects into a modified Richardson number (Ri), which is the ratio of static head of liquid to dynamic head of flowing liquid. Since the buoyancy of the tracer also depends on its volume, the modification they proposed was to multiply the Richardson number by the factor Va/V to give the following modified Richardson number Ri_O,

$$Ri_O = \frac{\Delta\rho g H}{\rho N^2 D^3} \cdot \frac{Va}{V} \tag{2.67}$$

For an agitators tested they found critical Richardson numbers above which the effect of the tracer volume and density increased the mixing time and they proposed a generalised correlation to account for these effects. The degree of mixing was not given in this paper. This prevents easy comparison with other published data so this generalised correlation is not reproduced here.

2.6 Rheology

Below the flow transition point, $Re < 10^4$, the fluid rheological properties need to be considered as they can drastically affect the mixing and dispersion process.

2.6.1 Newtonian Fluids

Newton defined fluid viscosity as

$$\mu = \frac{\tau}{\gamma} \tag{2.68}$$

where τ is the shear stress and γ is the shear rate.

For Newtonian fluids (shear stress/shear rate) is a constant and hence the viscosity is independent of agitator type or agitation rate.

Agitator Reynolds numbers ($\rho ND^2/\mu$) however depend on N and D and on scale up the D^2 term dominates. Hence, for scale-down at constant viscosity, Reynolds numbers decrease. This is an important consideration if the fluid is viscous and scale down decreases the Reynolds number below the transition.

2.6.2 Non-Newtonian Fluids.

Non-Newtonian fluids do not obey Newton's law of viscous flow. The viscosity is dependent on shear-rate and therefore depends on agitator type and agitation speed.

For non-Newtonian fluids

$$\mu_a = \frac{\tau}{\dot{\gamma}} \tag{2.69}$$

where μ_a is an apparent viscosity and $\dot{\gamma}$ is an average shear rate.

The dependency of the average shear-rate ($\dot{\gamma}$) on N was given by equation (2.2) as $\dot{\gamma} = k_S N$, where k_S is an agitator specific constant which is 10 ± 3 for a range of commonly used agitators. Exceptions from this rule include Intermigs ($k_S \approx 17$) according to Nienow (1998) and Dawson *et al.* (1993).

Some typical rheological models are illustrated in Figure 2-47.

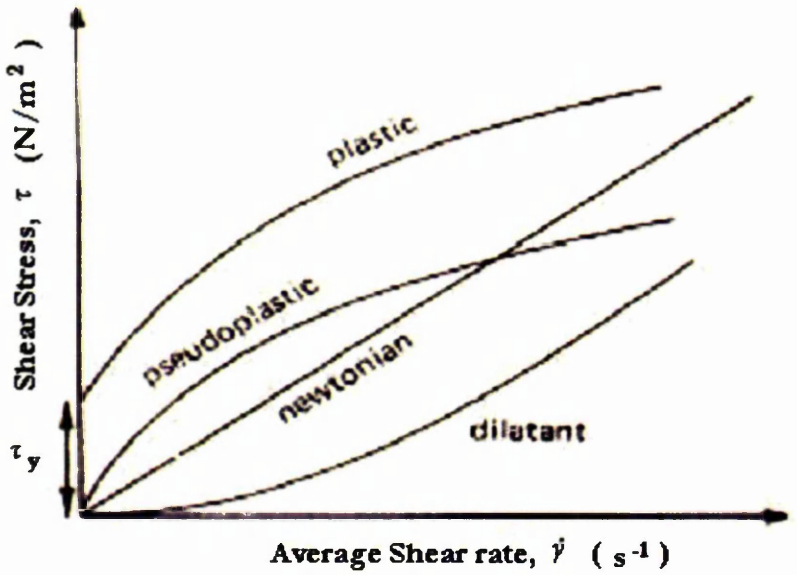

Figure 2-47: Some typical flow curves (shear stress against shear rate) for different types of fluids, Harnby (1992).

2.6.2.1 Pseudoplastic Fluids.

Many non-Newtonian fluids can be fitted to a power law, at least over the shear rates typically experienced in a mechanically stirred vessel. Shear thinning power-law fluids are called pseudoplastics and can be fitted by the relationship,

$$\tau = K\dot{\gamma}^n \qquad (2.70)$$

Combining with equation (2.69) gives

$$\mu_a = K\dot{\gamma}^{n-1} \qquad (2.71)$$

This apparent viscosity can be used in the Reynolds number equation.

2.6.2.2 Plastic Fluids.

These are fluids exhibiting a yield stress, which means an initial level of shear is required before flow occurs. A Bingham plastic is like a Newtonian fluid once flow occurs and is described by

$$\tau = \tau_y + K_B \dot{\gamma} \tag{2.72}$$

where τ_y is the yield stress and K_B is a constant. $1/K_B$ is often referred to as the mobility of the plastic.

Another equation often used to describe plastic fluids is the Herschel-Bulkley model as follows,

$$\tau = \tau_y + K_{HB} \dot{\gamma}^n \tag{2.73}$$

Equation (2.73) is similar to a power law fluid but includes a yield stress.

2.6.2.3 Cavern Formation

With plastic and pseudoplastic fluids there is a tendency for the agitator to "cut a hole" in the fluid, producing a "well agitated cavern" with little or poor movement of fluid outside. With pseudoplastic fluids, the mechanism for this is the shear thinning nature of the fluid that results in a much lower viscosity near the impeller where the shear rate is highest. This gives a turbulent region close to the impeller. Away from the impeller the apparent viscosity increases as the shear rates decrease giving laminar flow and stagnant regions where shear rates are low. Wichterle and Wein (1981) experimented with pseudoplastic and plastic fluids and described the well-agitated region as a cavern (see Figure 2-48). They argued the threshold of mixing occurred when the well-agitated cavern just filled the fluid volume, i.e., no stagnation. They defined a non Newtonian Reynolds number and related it to the threshold of mixing point via an experimental determined empirical model:

$$\mathrm{Re}_{NN} = \frac{\rho N^{2-n} D^2}{K} = \left(\frac{D_c}{\alpha D}\right)^2 \tag{2.74}$$

where K is the consistency index, n = power law index, D_c = cavern size = vessel diameter for threshold of mixing and α is a proportionality constant = 0.6 for a propeller-type agitator and 0.3 for a turbine type.

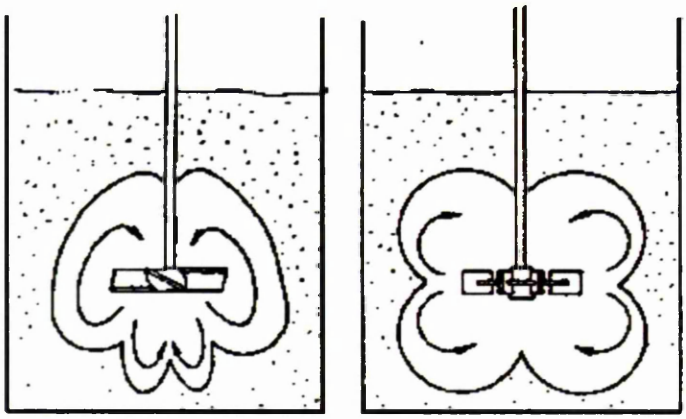

Figure 2-48: Well agitated caverns in pseudoplastic fluids: Left agitated by a pitch blade turbine: Right agitated by a Rushton turbine. From Witchterle and Wein (1981).

With plastic fluids, in regions away from the impeller, the shear stress has to be greater than the yield stress to avoid stagnation. The boundary of the cavern can be defined as the surface where the yield stress and the shear stress are equal. Using this definition and assuming that tangential flow dominates in a cavern, Elson *et al.* (1986) defined the cavern as a right circular cylinder of height H_c and diameter D_c centred on the impeller using the expression,

$$\left(\frac{D_c}{D}\right)^3 = \left(\frac{\mathrm{Po}\,\rho N^2 D^2}{\tau_Y}\right)\left(\frac{1}{(H_c/D_c + 1/3)\pi^2}\right) \tag{2.75}$$

Nienow (1998) gives typical values of H_c/D_c of 0.4 for Rushton turbines and SCABA 6SRGT with 0.75 for a propeller and 0.6 for a LIGHTNIN A315. Once the cavern reaches the wall the height increases with N for Rushton and pitched blade turbines, but is proportionate to $N^{0.5}$ for SCABA 6SRGT and LIGHTNIN A315 agitators.

Numerical analysis show that both equations (2.74) and (2.75) infer larger agitators should be used to avoid cavern formation. For radial turbines Po is ≈ constant at Re ≥ 30 (see earlier Figure 2-29). Therefore for a given scale, larger slow speed agitators require less power to overcome cavern formation. At constant power and assuming a typical power law n of 0.5, then according to equation (2.74), D_c is proportional to $D^{11/12}$

Whilst from equation (2.75) D_c is proportional to $D^{5/9}$

2.6.2.4 Effect of Solids on Fluid Flow Properties

The effect of solids on the dense phase gas hold-up is discussed in Chapter 2, section 2.3.2. The effects of solids on mixing are discussed in Chapter 2 section 2.5.5.1. Very high solids concentrations exhibit plastic behaviour. The high solids concentration can occur for a number of reasons:

- "Sanding in" after an agitator trip. If the overall concentration of solids is high enough, the settled solids partially or wholly cover the agitator. If this is likely to occur, then the agitator system needs to be designed to overcome the resulting high starting torque.
- Operation below $N_{JS,}$ giving a very bottom heavy suspension. Hence, locally the fluid may exhibit non-Newtonian, plastic behaviour. This can happen for a number of reasons, by design or due to other factors such as undesirable air entrainment (Ditl *et al.* 1997).
- Poor design of solids off-take. If control is based on the off-take solid concentration, then a poorly designed off-take system may require

operation in the vessel at much higher concentrations then the off-take. (Buurman *et al.* 1985)

MacTaggart *et al.* (1991) discusses problems with solids sampling. The local solids concentration from a slurry-mixing tank was measured by the withdrawal of samples from the vessel. It was shown that the sample tube design (shape, diameter and tip angle) and sampling technique (withdrawal velocity and location in the mixing tank) could significantly affect the solids concentration and the particle size distribution of the sample withdrawn. It proved practically impossible to obtain reliable measurements of local solids concentration by sample withdrawal from a mixing tank. Turned on its head "the off-take from a solid-liquid mixture in an agitated mixing vessel is not representative of the solids in the vessel". The authors show that sampling errors can be minimized with the use of fine solids and by sampling at high velocities.

2.7 Solid Suspension

The suspensions of solids heavier than the liquid are considered in this thesis. There are two mechanisms to consider, the lifting of settled solids from the base of the vessel and the prevention of settling. It is generally considered that it requires more energy to lift settled solids than to prevent settlement, Seichter *et al.* (1997). Baldi *et al.* considered the lifting of the settled solids from the vessel base as due mainly to turbulent eddies of size comparable to the particle size. When considering the suspension of solids the Zwietering "just suspension" (N_{JS}) criteria is usually used, Zwietering, (1958), Nienow, (1968) Chapman *et al.* (1983), Bujalski, (1986), Frijlink *et al.* (1990), Mak *et al.* (1997).

Zwietering defined the just suspension criterion, from observations through a transparent base, as the point when no particles remain stationary on the bottom of the vessel for longer than 1 second. This is defined as off-bottom

suspension and is not necessarily a homogeneous suspension. The homogeneity of the suspension at N_{JS} depends upon particle size (settling velocity) and whether the vessel agitation system is designed to ensure primary circulation to all parts of the vessel. For a high aspect ratio vessel with a single agitator set close to the bottom this may well not be the case even for small particles with settling velocities around 1 to 2 cm/s.

From dimensional analysis Zwietering (1958) proposed the following empirical correlation to fit his extensive experimental data:

$$N_{JS} = \frac{s d_P^{0.2} X^{0.13} \mu_L^{0.1} [g(\rho_S - \rho_L)]^{0.45}}{\rho_L^{0.55} D^{0.85}} \qquad (2.76)$$

where s is an agitator dependent shape factor, which also depends on the geometric ratios c/T and D/T, d_p is the mean particle diameter and X is the percentage weight of solids per weight of liquid. A great deal of work on solid suspension has been done since Zwietering. However, the general consensus from the references quoted at the beginning of this section is that Zwietering got it just about right and the Zwietering equation is widely used with appropriate "s" factors to design for solid suspension.

2.7.1 Scale-up for Solid Suspension

If geometric similarity is maintained then Equation (2.76) suggests that for a given fluid-particle system, then (assuming Po is independent of scale) at N_{JS}, the P/V decreases with scale up according to the relationship,

$$P/V = \text{constant} \times T^{-0.55} \qquad (2.77)$$

However, Zweitering only tested scaling rules on vessels between 0.15 to 0.6 m in diameter with particles in size range 125 to 850 micron and two solid

densities 2160 and 2600 kg/m^3, so some doubt must exist about the universal generality of the equation. Oldshue (1983) cautions that his literature review of power per unit volume for solid suspension scale-up yields almost as many conclusions as investigators.

Herringe (1979) showed a relationship between power/unit volume, particle concentration and scale and concluded that on scale-up power per unit volume either increases or decreases depending on particle size (see Figure 2-49). According to these relationships, small particles require lower power per unit volume on scale-up, particles around 600 micron scale-up at constant power per unit volume whilst particles of diameter ≥ 800 microns require an increase in power per unit volume on scale-up. The decrease in power per unit volume on scale-up for small particles was also found to be a function of particle concentration.

Chapman *et al.* (1983), using 1% sand particles in water, with a mean particle size of 470 microns and scales from 0.3 to 1.8 m diameter, found power per unit varied on scale-up proportional to $D^{-0.28}$. This is in general agreement with the trend showed by Herringe (1979).

Rieger and Ditl (2000) follow the Herringe (1979) view that the scale-up of solid suspension should be based on particle size. They proposed a procedure for designing mixing devices for particle suspension based on experimental results involving plots of the energetic dimensionless criterion (π_5). This expresses impeller efficiency on the ratio d_p/T, which they found are almost identical for many axial impellers, within the relative vessel to impeller diameter ratio T/D range from *2.5* to *4*. This was confirmed experimentally for pitched three, four and six-blade turbines operating in flat and dished-bottom cylindrical baffled vessels, for particle concentration of 2.5 and 10% by volume respectively.

Bourman *et al.* (1986) investigated scaling rules on two geometrically similar vessels of diameters 0.48m and 4.3 m diameter respectively. They used sand of mean diameter 157 microns, at concentrations up to 15% by volume. From

their results, for similar degrees of homogeneity on the two scales, they recommended scale-up at constant power per unit volume according to the scaling rule:

$$N_C = \text{constant} \times D^{-2/3} \tag{2.78}$$

where N_C is the agitation speed for complete off-bottom suspension (which is not necessarily homogeneous). By comparison to equation (2.78), the scaling rule of constant P/V and geometric similarity, means no effect of D or T on the P/V required for solid suspension.

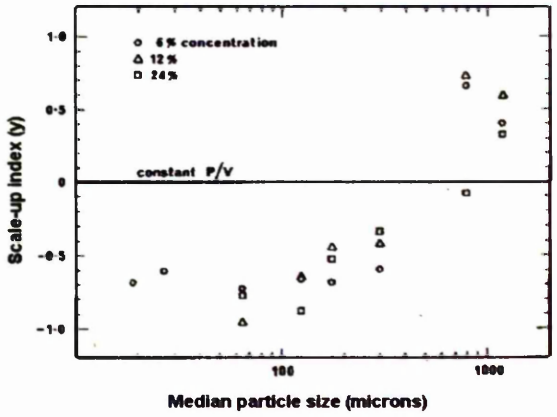

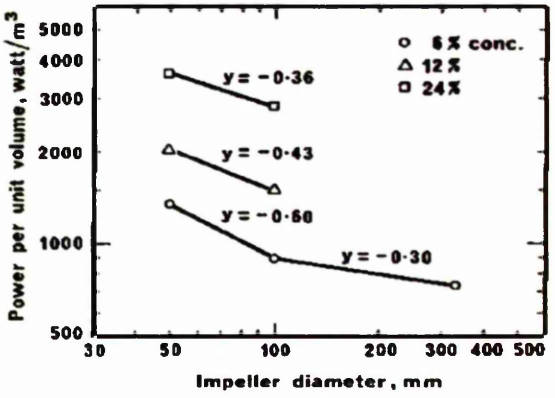

Figure 2-49: showing the relationship between power per unit volume, particle concentration and scale, taken from Herringe (1979). Note that *y* is the power index in the solid suspension scale-up relationship $P/V \propto D^y$. For geometric similarity this is the same as $P/V \propto T^y$.

More recently Mak *et al.* (1997) carried out CFD and experimental studies of solid-liquid suspensions in stirred tanks of diameter 0.30 to 2.67 m, to investigate the effect of scale using a pitched blade turbine. Their results for the just suspension condition were in agreement with the Zwietering empirical correlation. They also confirmed that constant power per unit volume appeared to be the appropriate scale-up criterion to obtain the same degree of homogeneity at different scales (which is a different criterion than N_{JS}). They found good agreement for concentration profiles determined by CFD simulations and from experimental results.

Seichter *et al.* (1997) found different scaling rules for concentrated slurries of fine particles of micro-milled limestone and precipitated gypsum, using slurry concentrations up to 60%. The differences in scaling rules were attributed to the rheological complexities of the suspensions. However, the ratio of impeller speeds for the onset of sedimentation (N_{SS}) and the start of re-suspension (N_{JS}) was found to be constant and was expressed as,

$$N_{SS} = 0.8N_{JS} \tag{2.79}$$

Considering all of the above review, scale-up of a solid suspension system should be satisfied conservatively, for most cases, by geometrical similarity and constant power per unit volume.

Where surface aeration is problematic on scale-up, as described for example by Ditl *et al.* (1997), then tip speed needs to be minimized. Scale-up at conditions of geometric similarity and constant power per unit results in an increase in impeller tip speed with scale-up that can result in surface aeration on scale-up. These authors showed that surface aeration scales at almost constant tip speed. Surface aeration can affect the quality of the solid suspension by increasing the just suspension speed and can effect pumping, especially for small solids, which can form a stable emulsion with entrained gas. Under such conditions it is worthwhile exploring whether the solids can

be adequately suspended at a lower power per unit volume on the larger scale following Herringe (1979) or Rieger and Ditl (2000).

2.7.2 Effect of Multiple Impellers on Solid-liquid Suspension.

Very little work has been reported on multiple impeller systems for solid suspension. Armenante *et al.* (1992) and Armenante and Li (1993), studied the effect of multiple flat-blade turbines on the minimum agitation speed to just suspend solid particles in agitated vessel. The agitation system consisted of a stirred tank provided with one, two, or three impellers, and in which glass particles, 110 μm in diameter were suspended in water. It was found that the N_{JS} for a given impeller diameter was nearly independent of the number of impellers used. In all cases, the value of N_{JS} measured when multiple impellers were used was either, nearly the same as that for the single impeller case or higher. The corresponding power consumption was always higher than for single impellers. They concluded that the lower impeller plays the major role in the off-bottom suspension of the solids, and the presence of additional flat-blade turbines either does not affect the suspension process or actually interferes with it. The presence of more than one flat-blade turbine is either unnecessary for, or actually detrimental to, the achievement of the solid suspension state. Therefore, their use is not justified if off-bottom solid suspension is the sole mixing requirement.

Later work by Armenante and Uehara-Nagamine (1997) studied the effect of the off-bottom impeller clearance on the minimum impeller speed for solid suspension (N_{JS}) in single- and double-impeller systems using three different impeller types; 6 blade Rushton turbines, 6 flat blade turbines and down pumping 6 pitched blade turbines (PBT). It was found that N_{JS} increased or decreased when a second impeller was added, depending on the type of impeller. The effect of the clearance of the lower impeller, on the flow pattern produced by the lower impeller was also investigated for the case in which the position of the upper impeller was kept constant. They reported that when radial impellers were used in a flat-based vessel at low off-bottom clearances,

which caused the loss of the lower circulation loop, the addition of a second impeller increased N_{JS}. For a PTB at low clearance the addition of a second PTB above decreased N_{JS}.

The conditions under which these conditions were achieved were at clearances where the pumping action was restricted by the low clearances. This flow pattern change was observed for:

- Disc turbines which change from only upper circulation loops to upper and lower circulation loops at $0.16 < c/T < 0.20$
- Flat blade turbines that change from only upper circulation loops to upper and lower circulation loops at $0.23 < c/T < 0.24$
- For the down-pumping 6 blade PBT no change in flow patterns were observed down to $C_b/T = 1/48$.

where C_b is the clearance from the bottom of the vessel to the lowest point of the impeller.

2.7.3 Effect of Gas on Solid-liquid Suspension

Gas may be introduced into a liquid solid suspension by direct addition, surface entrainment or vaporization. The introduction of gas affects the liquid flow and can cause a large reduction in agitation power and requires an increase in agitation speed to maintain solids suspension, (Nienow (1994). Extensive studies of the hydrodynamics of 3-phase single impeller systems have been reported by Wiedmann *et al.* (1980), Chapman *et al.* (1983), Bujalski *et al.* (1988), Frijlink *et al.* (1990) and Patula and Ahmed (1997).

Chapman *et al.* (1983) compared a large number of single impellers in solid-liquid, gas-liquid and gas-liquid-solid systems in flat-bottomed vessels of diameters from 0.29 m to 1.8 m. They argued that many three-phase systems required both good gas dispersion, as well as maintaining suspension. Hence, conditions both for N_{CD} and N_{JS} have to be satisfied. Except for very small density differences it was found that the agitation speed for N_{CD} occurred

before N_{JS}, hence the design requirement is usually to satisfy N_{JS}. Down-pumping agitators were found to require the least power to suspend solids in solid-liquid systems but were only suitable for handling very low gas flows. As gassing rates are increased, down-pumping agitators become unstable due to gas and liquid flows in opposition. At high gassing rates they become energetically inefficient for solids suspension compared to disc turbines and up-pumping agitators. Upward pumping impellers do not suffer from flow instabilities and are hardly affected by gassing and are recommended by Chapman *et al.* (1983), and Bujalski *et al.* (1988). However, Frijlink *et al.* (1990) report that up-pumping pitched blade turbines show insufficient suspension performance with high concentrations of dense solids. All the above workers recommend disc turbines for three phase dispersions at an off bottom clearance of $T/4$ as combining good stable operation with energetically efficient solid suspension at high gas rates.

The use of a dished bottom to improve suspension performance is recommended by Frijlink *et al.* (1990) for both liquid-solid and gas-liquid-solid systems.

In practice, scale-up of gas requirements is generally at constant volumetric flow rate of gas per volume of liquid. This is expressed as VVM (volume gas/volume of liquid/minute); hence the effect of gas on solid suspension is often considered in these terms. The literature correlations for the effect of gas on solid suspension performance for single impeller systems are listed in Table 2-9. For a number of impellers (excluding down-pumping types) both Frijlink *et al.* (1990) and Patula and Ahmed (1997) report that,

$$\frac{\mathrm{Po}^{*}_{\mathrm{JSG}}}{\mathrm{Po}^{*}_{\mathrm{JSU}}} = \left(\frac{N_{JSG}}{N_{JSU}}\right)^{-2} \qquad (2.80)$$

where Po^{*} is an apparent power number which takes in the effects of density changes, due to solids and gassing, resulting from the following assumption:

$$P = 2\pi NM = \mathrm{Po}^{*}\,\rho_l N^3 D^5 \tag{2.81}$$

Patula and Ahmed (1997) argue that if the torque is equal at both gassed and ungassed conditions for the just suspension case therefore, using the apparent power number concept,

$$M = Po^{*}_{JSU}\rho_l N^3_{JSU} D^5 = Po^{*}_{JSG}\rho_l N^3_{JSG} D^5 \tag{2.82}$$

Equation (2.82) reduces to equation (2.81) implying the experimental relationship derived by these workers reduces to equal torque for the gassed and ungassed case.

The constant torque rule to account for gassing was found to be not applicable to the down-pumping case. This is possibly due to the unstable flow noted for this case on gassing.

Figure 19 of Frijlink *et al.* (1990) suggests the Smith type curved blade agitator is the most energetically efficient for solid suspension at high gassing rates. It would be interesting to obtain some results for high efficiency curved blade designs such as the SCABA 6SRGT or the CHEMINEER BT-6.

Literature source	Agitator Type	T (m)	VVM	D/T	c/T	Correlation
Chapman *et al.* (1983)	6 RT	0.29 -1.8 flat base	0 to 1	0.5	0.25	$N_{JSG} = N_{JS} + 0.94VVM$
Bujal;ski *et al.* (1988)	6 RT 6PBTD 6PBTU	0.3-1.8 0.3-1.8 0.3-1.8 all flat base	0 to 3.5 0.28 to 3.5	0.5 0.5 0.5	0.25 0.25 0.25	$N_{JSG} = N_{JS} + 0.65VVM$ $N_{JSG} = N_{JS}(0.83 + 0.31VVM)$ $N_{JSG} = (1 + 0.31VVM)^{0.11}$
Frijlink *et al.* (1990)	6RT 6CDT 6T 6PBTU 4PDTD 6PBTD 4PBTD	0.44-1.2 flat and dished bases	?	0.4	0.17, 0.25 and 0.4	$\frac{Po^*_{JSG}}{Po^*_{JSU}} = \left(\frac{N_{JSG}}{N_{JSU}}\right)^{-2}$ $\frac{Po^*_{JSG}}{Po^*_{JSU}} = \left(\frac{N_{JSG}}{N_{JSU}}\right)^{-1.1}$
Patula and Ahmed (1997)	6RT 6CDT PBTU PBTD	0.4 flat and dished bases	0 to 1	0.5, 0.33 0.33 0.5 0.5	0.25	$\frac{Po^*_{JSG}}{Po^*_{JSU}} = \left(\frac{N_{JSG}}{N_{JSU}}\right)^{-2}$ $\frac{Po^*_{JSG}}{Po^*_{JSU}} = \left(\frac{N_{JSG}}{N_{JSU}}\right)^{-1.3}$

Table 2-9: Effect of gassing on the speed required to suspend particles in agitated vessels from various studies. Note that Frijlink *et al.* (1990) tested pitch blade turbines (PBT) of pitch 30°, 45° and 60°. The other authors report results for 45° only. The 6CDT impeller is the Smith curved blade disc turbine of the van't Riet (1975a) design. U and B refer to pumping up or down.

2.8 Mass and Heat Transfer

2.8.1 Analogies

Mass heat and momentum transfer are analogous, as shown for example by Treybal (1968) by analysis of laminar flow past a solid surface. Thus for analogous situations, with temperature and concentration profiles in dimensionless form, the heat and mass transfer coefficients in the form of dimensionless groups are given by the same functions and are interchangeable. The analogies can be used to convert equations or data correlations from heat to mass transfer or visa versa by replacing the dimensionless groups of the former with the corresponding groups of the latter, providing:

- The flow conditions and geometry are the same.
- There is of no net mass transfer.
- The boundary conditions are also analogous.

The theory was developed from consideration of the elementary physics of simple gases and from this theory there emerge two dimensionless groups,

$\frac{C_p \mu}{\kappa}$ = Pr = Prantl group and,

$\frac{\mu}{\rho D_{AB}}$ = Sc = Schmidt group.

For the theory to be applicable both Sc and Pr must be close to unity. In practice for gases, Pr lies between 0.65 and 0.90 whilst Sc is between 0.67 and 0.83. The values for liquids are very much higher and consequently none of the theory strictly applies to liquids.

Reynolds restricted his analogy to gases alone and stated simply Reynolds analogy is:

$$\frac{\text{Momentum lost to surface represented by skin friction}}{\text{momentum lost if all of the fluid was at the surface velocity}} =$$

$$\frac{\text{Heat actually supplied to the fluid}}{\text{Heat required to bring all of the fluid to the surface temperature}} =$$

$$\frac{\text{Mass transferred from the fluid}}{\text{The total mass that could be transferred}}$$

The expansion and derivations of all these equations can be found in the many textbooks on the subject for example Treybal (1968).

The Reynolds analogy assumed turbulence everywhere, except at the actual boundary layer. Prandtl and Taylor modified this by considering a turbulent zone, a laminar layer and finally a boundary layer. Later theories include a transition regime in the analysis.

2.8.1.1 Heat Transfer and j Factors

Among early standard recommended equations for flow in pipes are

Sieder and Tate (1936),

$$Nu = 0.027\,Re^{0.8}\,Pr^{0.33}\left(\frac{\mu}{\mu_s}\right) \qquad (2.83)$$

and Chilton and Colburn,

$$Nu = 0.023\,Re^{0.8}\,Pr^{0.33} \qquad (2.84)$$

In eq (2.84) the physical properties are taken at the mean film temperature,

$$\frac{\text{temperature at the wall} + \text{temperature of bulk}}{2}$$

These equations have the same structure and if they are divided by RePr a basic equation is derived. For example using eq (2.84)

$$\frac{Nu}{RePr} = St = \frac{h}{u\rho Cp} = 0.023\,Re^{-0.2}\,Pr^{-2/3} \qquad (2.85)$$

Note the inclusion of the Prandtl number that allows for the different physical properties of liquids.

Chilton and Coburn then defined for flow in pipes,

$$j_h = 0.023\,Re^{-0.2} = St\,Pr^{2/3} \qquad (2.86)$$

where j_h can be thought of as the Stanton number for heat transfer , corrected for liquids by the inclusion of the Pr group. A plot of j_h versus Re gives virtually the same shape as the friction factor chart.

2.8.1.2 Mass Transfer and j Factors

The mass transfer equations are presented in a similar form to the heat transfer equations and this led to an assumption that could be checked experimentally,

$$j_m = St_m Sc^{2/3} = j_h = St_h\,Pr^{2/3} \qquad (2.87)$$

From experiments in wind tunnels, in open air and on wetted walls, in a variety of geometries and in the three flow regimes a number of correlations have been presented which have firmly established the analogy of heat and mass transfer.

A list of corresponding dimensionless groups of mass and heat transfer applicable to agitated vessels is listed in Table 2-10.

Treybal (1968) gives examples of the use of these analogies to extend the very extensive existing heat transfer information to produce corresponding mass transfer data. Also, where local mass transfer characteristics can be easily measured for example by sublimation or dissolution of solids, these can be converted to the analogous heat transfer coefficients that are difficult to measure.

Heat transfer	Mass transfer
Driving force (dimensionless) $\frac{t - t_1}{t_2 - t_1}$	Driving force (dimensionless) $\frac{C_A - C_{A1}}{C_{A2} - C_{A1}}$
Reynolds Number $\mathrm{Re} = \frac{D^2 N \rho}{\mu}$	Reynolds Number $\mathrm{Re} = \frac{D^2 N \rho}{\mu}$
Prandtl Number $\mathrm{Pr} = \frac{C_p \mu}{\kappa}$	Schmidt Number $\mathrm{Sc} = \frac{\mu}{\rho D_{AB}}$
Nusselt number $\mathrm{Nu} = \frac{h_O T}{\kappa}$	Sherwood Number* $\mathrm{Sh} = \frac{k_L T}{D_{AB}}$ *Sherwood number can take a number of forms dependent on mass transfer.
Peclet Number $\mathrm{Pe} = \mathrm{Re}\,\mathrm{Pr} = \frac{D^2 N \rho C_p}{\kappa}$	Peclet Number $\mathrm{Pe} = \mathrm{Re}\,\mathrm{Sc} = \frac{D^2 N}{D_{AB}}$
Stanton Number $\mathrm{St_h} = \frac{\mathrm{Nu}}{\mathrm{Pe}} = \frac{h_O T}{D^2 N \rho C_p}$	Stanton Number $\mathrm{St_m} = \frac{\mathrm{Sh}}{\mathrm{Pe}} = \frac{k_L T}{D^2 N}$
$j_h = \mathrm{St_h}\,\mathrm{Pr}^{2/3}$; $j_h \cong j_m = (1.09 j_m)$	$j_m = \mathrm{St_m}\mathrm{Sc}^{2/3}$

Table 2-10: Equivalent heat and mass transfer dimensionless groups applicable to agitated vessels.

2.8.2 Heat Transfer in Agitated Vessels by Means of Jackets and Coils Containing a Heat Transfer Fluid

The heat transfer literature is very extensive and many excellent standard texts are available for heat transfer in agitated vessels. For example, Heggs and Hill (1998) cover the design of heat exchangers for batch reactors.

Heat transfer in an agitated vessel is dependent upon a temperature difference *(ΔT)* between the heat transfer fluid and process fluid, the heat transfer area *(A)* and the overall heat transfer coefficient *(U)* such that the rate of heat transfer (Q_h) is:

$$Q_h = UA\Delta T = \frac{\text{Driving force}}{\text{Resistance}} = \frac{\Delta T}{R}\frac{(K)}{(K/W)} \qquad (2.88)$$

If the liquid phase mixing is good so that neither the temperature of the process fluid or the associated heat transfer coefficients vary significantly throughout the bulk a change in heat transfer rate can be calculated due to the result of changing any of the three parameters in equation (2.88).

For tubes and cylindrical vessels the heat transfer surface is curved and hence the area over which the heat transfer coefficient relates must be defined.

The overall heat transfer coefficient (*U*) is governed by the sum of several heat transfer resistances,

$$\frac{1}{UA} = \sum_{i=1}^{n} R_i = \frac{1}{(hA)_O} + \frac{F_O}{A_O} + R_w + \frac{F_i}{A_i} + \frac{1}{(hA)_i} \qquad (2.89)$$

where subscript (*o*) refers to the outside the heat transfer fluid or to the process fluid and (*i*) refers to adjacent to the heat transfer fluid (or inside). *F* is a fouling factor and R_w is the wall resistance due to the wall thickness and material over a defined area *(t/κA)*. The designer or experimenter defines the relevant area (*A*.) For tubular heat exchanger the heat transfer coefficient is always defined on the outside area and all other resistances are corrected to that value.

Literature Reviews

Mechanical agitation affects only the outside coefficient and possibly the process-side fouling factor. Oldshue (1983) claims that many heat transfer applications are limited by the process side heat transfer coefficient and hence the effect of agitation on the overall heat transfer coefficient will usually be significant.

The film coefficient represents the conductivity of thin layer of fluid next to the heat transfer surface. This film is often represented as stationary for analysis purposes. The basis of the analysis is Prandtl's boundary layer theory.

Prandtl stated that any viscous fluid in motion could be broken down into two basic flow fields. The field close to the stationary surface (the boundary layer) constituted an area where viscous forces are important and need to be included in the analysis, whereas the field beyond the boundary layer could be considered as an ideal fluid where viscous effects are minimal; and can be ignored. For heat transfer purposes the properties of the boundary layer is very important and its characteristics will determine the film coefficient.

Heat transfer through the boundary layer is mainly by molecular conduction; therefore the thickness of the boundary layer is of paramount importance. This is affected by the physical nature of the mainstream fluid, such as velocity and viscosity and whether it turbulent or laminar. In heat transfer this is further complicated by temperature gradients in the boundary layer which leads to viscosity gradients, the direction of which depend on whether the duty is heating or cooling. Thus the benefits of mechanical agitation for heat transfer can be summarized as to eliminate gross temperature gradients in the process fluid in order to maximize the temperature driving force ΔT across the resisting film whilst minimizing the film thickness by maintaining high velocities close to the heat transfer surface.

In order to predict heat transfer rates in agitated vessels, the process side heat transfer coefficient needs to be estimated as discussed in the following section.

2.8.2.1 Forced Convective Heat Transfer in Agitated Vessels

Forced convective heating or cooling in agitated vessels is achieved in most cases using jackets or limpet coils. Internal coils are primarily used to supplement the heat transfer area of jacketed vessels or for cases where heat transfer through the walls is impractical, for example in plastic tanks or rubber lined vessels. Internal coils are often preferred for corrosive duty as greater corrosion allowance can be allowed more cost effectively in coils than vessels and they are easier and cheaper to replace. When the heating duty is large, extra area can be found using baffles for heat transfer area, or even the agitators as described for example Nagata *et al.* (1972) as heat transfer surfaces. External heat exchangers are also used. The most common heat transfer arrangements are shown in Figure 2-50.

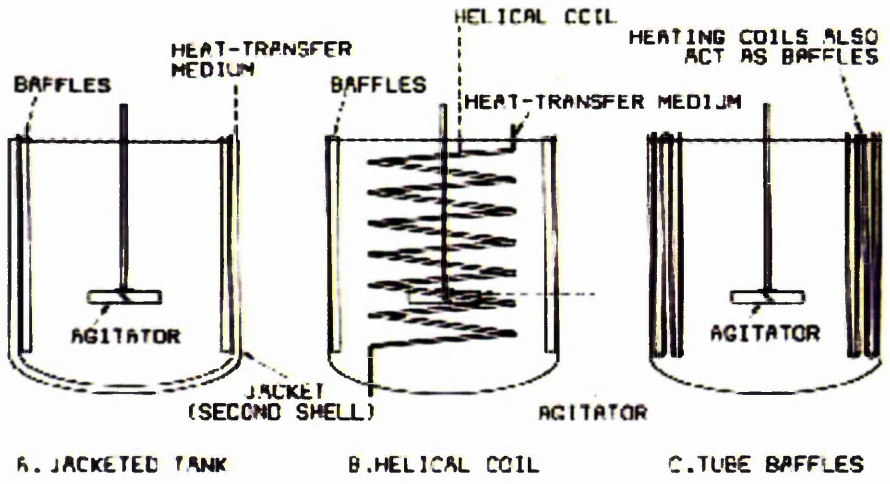

Figure 2-50: Common heat-transfer surfaces, from Oldshue (1983)

In order to predict heat transfer in a stirred vessel the process side heat transfer coefficient h_O must be estimated. Using dimensional analysis of heat flow and energy balance equations the heat transfer coefficient can be

expressed in the Nusselt number as a function of the Reynolds and Prandtl numbers as follows:

$$\mathrm{Nu} = h_O T / \kappa = f(\mathrm{Re}\,\mathrm{Pr}) \tag{2.90}$$

This equation has been expanded to fit experimental data in a form similar to the classical forced convection empirical equation for liquid flow through tubes, as derived by Seider and Tate (1936), which is expressed as:

$$\mathrm{Nu} = k_1\,\mathrm{Re}^a\,\mathrm{Pr}^b\left(\frac{\mu}{\mu_S}\right)^c f(\textit{geometry}) \tag{2.91}$$

The function of geometry can contain many dimensionless constants to account for vessel, agitator or coil geometry such as D/T, H/T, c/T, and so on. The multiplicity factor k_1 depends on the type of impeller and the heat transfer surface. μ Is the viscosity of the bulk fluid and μ_S is the viscosity at the wall surface temperature.

2.8.2.2 Heat Transfer in Jacketed Vessels and Vessels Fitted with Coils

Uhl (1966) shows that over a wide range of impellers and Reynolds numbers (300 to 6 x 10^5), the exponents a and b are most usually found to be 2/3 and 1/3 respectively. The exponent c is most generally taken as 0.14, although higher values have been reported. From Uhl's (1966), literature review for common cases where:

$$\frac{h_O T}{\kappa} = k_1\left(\frac{D^2 N\rho}{\mu}\right)^{2/3}\left(\frac{C_P\mu}{\kappa}\right)^{1/3}\left(\frac{\mu}{\mu_S}\right)^{0.14} \tag{2.92}$$

In eq (2.92), the multiplicity factor k_1 varies from 0.36 to 0.6 for paddles, 0.6 for twin curved blade turbines, 0.54 for a disc turbine in an unbaffled vessel and 0.74 for the same disc turbine in a baffled vessel. Values of k_1 from various studies at H/T= 1 fitted to equation (2.92) are also listed in Table 2-11.

Literature Reviews

The exponent of 2/3 on Reynolds number is shown by Dunlap and Rushton (1953) to be due to forced convection. Forced convection is the result of bulk mixing by the agitator with turbulent flow at the heat transfer surface. Under poor agitation conditions due in insufficient agitation or highly viscous fluids, natural convection dominates which results in a lower exponent on the Reynolds number. At very high agitation rates the fluid becomes so turbulent that further increases in agitation has little further effect and the exponent on Reynolds decreases again. Hence design conditions should preferably be in the range where forced convection dominates.

Agitator	No blades	No baffles	Re	T (m)	D (m)	D/T	Po	c/T	k_1	Ref
Disc turbine	6	0	40-$3x10^5$	0.51	0.152	0.3	?	0.33	0.54	1
Disc turbine	6	1,2,4	300-$3x10^5$	0.51	0.152	0.3	?	0.33	0.74	1
Disc turbine	6	4	10^4-$4x10^4$	0.45	0.15	0.33	5.5	0.33	0.74	2
Disc turbine	6	4	10^4-$4x10^4$	0.45	0.15	0.33	5.8	0.33	0.73	3
Convex disc turbine	8	4	10^4-$4x10^4$	0.45	0.189	0.42	3.5	0.42	0.68	2
Concave disc turbine	8	4	10^4-$4x10^4$	0.45	0.189	0.42	2.8	0.42	0.62	2
Flat blade turbine w/D=0.2	6	4	10^4-$4x10^4$	0.45	0.15	0.33	4.4	0.33	0.57	3
Pitch blade turbine 45° w/D=0.2	6	4	10^4-$4x10^4$	0.45	0.15	0.33	1.46	0.33	0.43	3
Propeller	3	4	10^4-$4x10^4$	0.45	0.15	0.33	0.33	0.33	0.29	3

Table 2-11: Values for the constant k_1 in equation (2.92), for non-proximity agitators in Newtonian fluids: References cited ate from;

Brooks and Su (1959) – taken from Uhl and Gray, vol. I (1966)

Karcz and Kaminska-Brzoska (1994)

Strek and Karcz (1997)

Similar relationships to equation (2.92) have been used successfully to correlate experimental data for helical or vertical coils. The viscosity is taken either at the surface temperature (μ_s) or at the mean film temperature (μ_f). When the viscosity ratio refers to the mean film temperature, the exponent on the viscosity increases. Shrek and Karcz (1997) compared geometrically similar agitators in turbulent vessels heated with, (a) jacket and (b) with a vertical tubular baffle. They found that the heat transfer was very similar for the two heating arrangements and obtained nearly identical multiplicity factors when the data were fitted to equation (2.92) as shown in Table 2-12.

T (m)	0.45			0.60		
Heat transfer surface	Jacket			Vertical tubular heating baffles		
Stirrer	D/T	Po	k_1	D/T	Po	k_1
Disc turbine	0.33	5.75	0.73	0.33	5.49	0.74
Flat blade turbine	0.33	4.35	0.57	0.33	4.42	0.58
Pitch blade turbine	0.33	1.46	0.43	0.33	1.58	0.47
Propeller	0.33	0.33	0.29	0.33	0.23	0.28

Table 2-12: Comparison of the factor k_1 in equation (2.92), for two types of heating for four agitator types in a turbulent Newtonian fluid from Strek and Karcz (1997).

Since in turbulent flow, for a given agitator and constant fluid properties, agitation power is proportional to N^3, it follows from equation (2.92) that the effect of changing speed on the agitation power P, for a given agitator type and diameter on the heat transfer is given by,

$$h_O \propto P^{2/9} \tag{2.93}$$

The effect of changing agitator type can be examined from the data for $D=T/3$ agitators given in Table 2-11. At constant speed, and for a given system, the heat transfer factor is proportional to k_1 whereas the power is

proportional to the power number Po. A review the data, normalized to unity for the propeller case (see Table 2-13), reveals that the paddle has twice the heat transfer as that of the propeller but draws 13.3 times as much power. The relationship between heat transfer coefficient and power from this data is approximately:

$$h_o \propto P^{0.3} \tag{2.94}$$

These data are presented graphically in Figure 2-51.

Agitator	Normalized h_o	Normalized power
Propeller	1.00	1.00
6MFD	1.48	4.42
Paddle	1.97	13.33
6DT	2.52	17.58
6DT	2.55	16.67

Table 2-13: Comparison of process side heat transfer coefficients with power for various $D=T/3$ agitators.

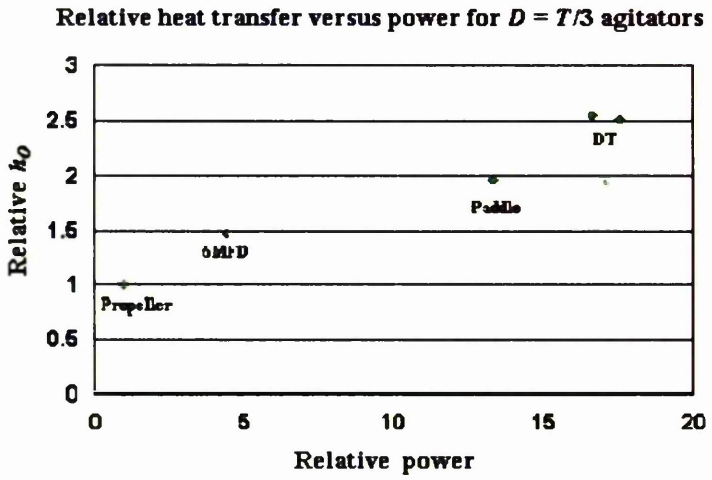

Figure 2-51: Comparison of agitators at constant speed for heat transfer from jackets. The data is from Table 2-13.

Thus increasing the power input does not have a great effect on heat transfer in stirred vessels.

Literature Reviews

The general consensus seems to be that under turbulent bulk flow conditions baffling improves heat transfer as shown for example by the work of Brooks and Su (1959).

The effect of gassing on heat transfer is not clear. Some workers claim it improves heat transfer, others that it hinders heat transfer and there are those that say it has little effect. The answer probably lies in the effect the gas has on the liquid flow patterns, fluid mixing and velocities close to the heat transfer surfaces. If the gas is introduced in a way that reinforces the liquid circulation it is likely to be beneficial to heat transfer. If the gas opposes the agitator bulk flows it is likely to reduce heat transfer.

For laminar flow conditions, close clearance agitators (anchors or helical screws) are often used especially for heat transfer involving non-Newtonian plastic or pseudo-plastic fluids where cavern formation (described in section 2.6.2.3) is likely with small high-speed agitators. Low speed, close clearance agitators, promotes liquid movement close to the heat transfer surfaces, which is beneficial to heat transfer. Edwards and Wilkinson (1972) describe the addition of surface scrapers to enhance heat transfer and prevent surface build-up. These authors also review the design equations from a large number of experimenters covering a range of heat transfer surfaces and agitators.

Because surface area to volume decreases with scale-up maintaining geometric similarity, heat transfer can be quickly become limiting with increasing scale. Extra heat transfer area can be obtained using finned tubes and plates as described for example by Heggs (1999) and Sunden and Heggs (2000). A novel way of inputting large amounts of heat into a mixing vessel is by use of induction heating, Heggs and Linn (1988) and Linn (1989).

2.8.3 Mass Transfer in Agitated Vessels

Gas-liquid mass transfer, solid-liquid mass and gas-liquid solid mass transfer is considered in the following sections.

2.8.3.1 Gas-liquid Mass Transfer and Interfacial Area in Agitated Vessels

Mass transfer can be considered like heat transfer in terms of a film theory with molecular diffusion controlling transfer through a laminar film whose thickness depends on conditions in the bulk fluid. See Figure 2-52.

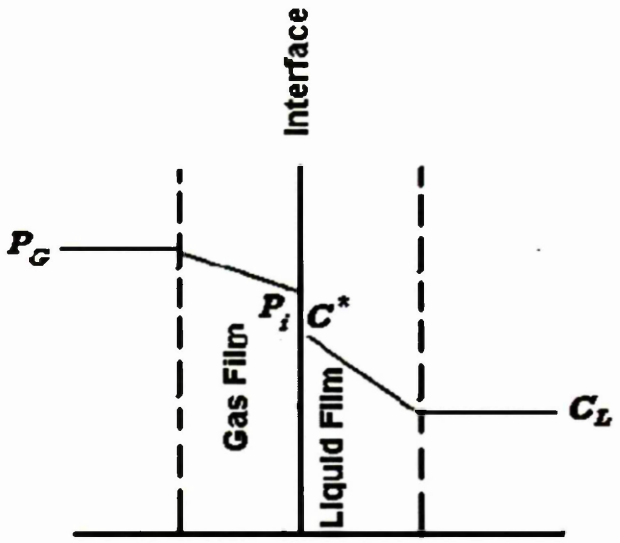

Figure 2-52: Interfacial behaviour for physical absorption according to the two-film theory

It is assumed that a laminar film exists each side of the interface from which transfer is by molecular diffusion alone. The concentration gradient is therefore considered linear in these layers and zero outside. The rate equation (r_A) for transfer across a contact area of A for this process is written as,

$$r_A = k_G(p_G - p_i) = k_L(C_i - C_L) \text{ (mol m}^{-2}\text{s}^{-1}\text{)} \qquad (2.95)$$

where k_G and k_L are the gas and liquid mass transfer coefficients (m/s)

For purely physical absorption the interfacial concentrations are assumed to be equilibrium such that C_i is the solubility of the transferring species at its

partial pressure. For a sparingly soluble species such as oxygen a linear partition coefficient exists between the solubility of the dissolved gas and its partial pressure. This is known as Henry's law. The gas and liquid are considered to be at equilibrium at the interface such that,

$$p_i = HeC_i \tag{2.96}$$

where He is the Henry's Law partition coefficient. p_i and Ci can be eliminated from equation (2.95) to give,

$$r_A = \frac{(p_G - HeC_L)}{\frac{1}{k_G} + \frac{He}{k_L}} = \frac{(\frac{p_G}{He} - C_L)}{\frac{1}{k_L} + \frac{1}{Hek_G}} \tag{2.97}$$

or

$$r_A = K_G(p_G - HeC_L) = K_L(\frac{p_G}{He} - C_L) \tag{2.98}$$

where,

$$\frac{I}{K_G} = \frac{1}{k_G} + \frac{He}{k_L} \tag{2.99}$$

and,

$$\frac{I}{K_L} = \frac{1}{k_L} + \frac{1}{Hek_G} \tag{2.100}$$

where K_L and K_G are the overall liquid and gas mass transfer coefficients.

For a sparingly soluble gas the gas film resistance is negligible and as $k_G > k_L$, then $1/k_L >> 1/(Hek_G)$ therefore,

$$k_L \cong K_L \tag{2.101}$$

If the gas phase resistance dominates then agitation of the liquid-phase should not make much difference to the mass transfer process. Therefore, in this

thesis only mass transfer where the liquid phase resistance dominates is considered.

According to the film theory there is a direct dependency of k_L on diffusivity,

$$k_L = \frac{D_L}{\delta} \tag{2.102}$$

where δ is the thickness of the liquid film.

Modifications of the film theory, such as the penetration theory or the surface renewal or surface engulfment theory are also used in order to explain experimental mass transfer results and build predictive models. These show a different dependency of k_L on diffusivity. For instance the surface renewal theory predicts (Danckwerts (1970)),

$$k_L = 2\sqrt{\frac{D_L}{\pi \vartheta_t}} \tag{2.103}$$

where ϑ_t is the exposure time, which depends upon the hydrodynamics of the system.

The film theory is normally considered adequate to describe the process by which mass transfer occurs and is often preferred due to its simplicity. Danckwerts (1970) showed that predictions based on this theory are normally quantitatively very similar to those resulting from the more complicated models.

Like heat transfer the process of rate of mass transfer is controlled by the products of a mass transfer coefficient an area and a concentration driving force,

$$J = k_L a \Delta C \tag{2.104}$$

where J is in molar rate of transfer per second per m^3 of liquid, k_L is the liquid film mass transfer coefficient (m/s), "a" is the specific gas-liquid interfacial area (m^2/m^3) and ΔC is the concentration driving force (mol/m^3).

The volumetric rate of transfer per unit volume of liquid (r) is,

$$r = k_L a \Delta C V_L \text{ (mol/s)} \tag{2.105}$$

where V_L is the liquid volume

For gas liquid mass transfer in stirred vessels, the mass transfer coefficient cannot be easily separated from the interfacial area. The gas hold-up is related to the interfacial area from:

$$a = \frac{6\varepsilon_G}{d_b} \tag{2.106}$$

where ε_G is the hold-up fraction (m^3 gas per m^3 dispersion) and d_b is the mean bubble size (m). Thus it is common to use a lumped parameter approach and quote the mass transfer factor as $k_L a$ since this is what is often measured.

These $k_L a$ data are often correlated in a simple form in terms of energy dissipation rates and gassing rates expressed in terms of the superficial gas velocity such as that proposed recently by Gezork *et al.* (2001), who found their data for a very wide of specific power inputs and gassing rates could all be correlated by the following empirical equation:

$$k_L a = 0.0059(P/V)^{0.61} v_s^{0.36} \tag{2.107}$$

where units of $k_L a$ are s^{-1}, (P/V) in W/m^3 liquid and v_S in m/s.

Hence to achieve a higher mass transfer factor requires an increase in the specific power input and /or the gassing rate. This however also imparts on the driving force ΔC and the liquid volume V_L, which may well decrease as a consequence and thus reduce the overall benefit.

The data can be correlated in dimensionless groups relating heat and mass transfer, for example by Calderbank and Moo-Young (1961) who obtained the following correlations applicable to aerated mixing vessels:

For rigid spheres the correlating equation is,

$$k_L \, \mathrm{Sc}^{2/3} = \frac{h_C}{C p \rho_C} (\mathrm{Pr})^{2/3} = 0.31 \left(\frac{\Delta \rho \mu_C g}{\rho_C^2} \right)^{1/3} \tag{2.108}$$

For bubbles >2.5 mm that do not behave like rigid spheres they found,

$$k_L \, \mathrm{Sc}^{1/2} = 0.42\left(\frac{\Delta\rho\mu_C g}{\rho_C^2}\right)^{1/3} \tag{2.109}$$

where the subscript $_C$ refers to the continuous phase. These equations, which were obtained for a range of solutes, with a large range of physical properties, suggest that the mass transfer coefficient is independent of the specific power input and agitator size, and depends solely on the physical properties of the fluid. This is possible for a highly turbulent system. This in turn suggests that, as far as gas-liquid mass transfer is concerned, the sole purpose of mechanical agitation is to generate interfacial area for the mass transfer process.

Calderbank (1958) had earlier studied gas-liquid hold-up and interfacial area using a pressure technique for gas hold-up and a light scattering technique to estimate the interfacial area. He combined the results to estimate bubble sizes using equation (2.106). He quotes his bubble sizes in terms of the Sauter mean bubble size, d_{32} which relates the volume to the surface area for transfer according to,

$$d_{32} = \sum_{i=1}^{N} d_{b.i}^3 \Big/ \sum_{i=1}^{N} d_{b.i}^2 \tag{2.110}$$

The bubble size estimates were confirmed using a photographic technique. He found that gas bubbles in pure fluids (coalescing) bubbles sizes have Sauter mean diameters in the range 2 – 5 mm in agitated vessels that rise with a constant velocity (v_t) of 0.27 m/s. The interfacial area (a) is given by:

$$a = 1.44\left[\frac{(P_G / V_L)^{0.4}\rho_c^{0.2}}{\sigma^{0.6}}\right]\left(\frac{v_S}{u_t}\right)^{0.5} \tag{2.111}$$

where the expression in square brackets was derived by consideration of a force balance between surface tension forces and those due to turbulent fluctuations, that is by using the Kolmogorov theory of local homogeneous

isotropic turbulence. P_G is the mechanical power input to the gas-liquid dispersion.

Sridhar and Potter (1980) also used the light attenuation technique to measure interfacial area and extended the above correlation for higher superficial gas velocities (up to 5 cm s^{-1}) and increased pressures, with gas density up to 18 kg/m^3 and higher specific power inputs (P_G/V) up to ≅ 10 W/kg) and obtained the following modified correlation:

$$a = 1.44\left[\frac{(P_G/V)^{0.4}\rho_c^{0.2}}{\sigma^{0.6}}\right]\left(\frac{v_S}{u_t}\right)^{0.5}\left(\frac{E_T}{P_G}\right)\left(\frac{\rho_G}{\rho_{air}}\right)^{0.16} \qquad (2.112)$$

where E_T is the sum of the mechanical energy input P_G and the gas energy input P_Q. The gas energy input is given by the following:

$$P_Q = Q_G(\rho_L - \rho_G)g(H_L - c_S) \qquad (2.113)$$

where c_S is the height of the sparger from the bottom of the tank.

Thus the increase in interfacial area is due directly to the increase in energy input by the gas at higher superficial gas velocity and is also due to the increased gas density. The 15 times increase in gas density used in this work is predicted by equation (2.112) to produce a 54% increase in interfacial area.

The effect of the pressure or gas density on the interfacial area appears to be linked also to the superficial gas velocity. From bubble column studies Wilkinson *et al.* (1990) and (1992) explained that this occurred due the increased gas density delaying the transition from homogeneous to heterogeneous flow. These authors found a relationship between gas-liquid hold-up, interfacial area and gas density with a proportionality of:

Increase in area or hold-up is proportional to $(\rho_G/\rho_{atm})^{0.11}$.

This is not too dissimilar to what Sridhar and Potter (1980) proposed for mechanically stirred vessels. Other workers have confirmed this effect in bubble columns; for example Stegeman *et al.* (1996), who likewise confirmed no effect of pressure on interfacial area in the homogeneous regime. In an

earlier paper Stegeman *et al.* (1995) claimed no effect of pressure on hold-up and interfacial area in agitated stirred vessels "except at extreme values of gas inlet velocity". In this work in a 0.156 m diameter vessel the maximum superficial gas velocity was 0.02 m/s. Except at very high agitation rates this is almost certainly operation in the homogeneous regime. Note however that scale-up at constant *VVM* would quickly raise the superficial gas velocity to values above the transition. Most large-scale gas-liquid contactors operate in the heterogeneous regime where the effect of pressure on interfacial area will be significant.

Oyevaar (1991) measured interfacial area, using the chemical absorption of CO_2 into aqueous diethanalamine (DEA). They reported a relative increase of up to 200 % in interfacial area in a stirred tank contactor when the pressure was raised from 0.15 to 8 mPa, dependent on specific power input and gassing rate. This is consistent with a coalescence hindering theory for delaying the transition to heterogeneous flow. They also claimed a distributor effect.

2.8.3.2 Methods of Measuring Gas-liquid Mass Transfer and Interfacial Area: A Critical Review

No subject in the stirred tank hydrodynamic literature seems to have courted as much controversy as gas-liquid mass transfer coefficient measurements. Gas-liquid mass transfer measurements can broadly be classified into two main groups: transient methods and steady-state (or pseudo steady-state) methods. These are considered separately looking at the methods, the underlying assumptions, any shortcomings and assessing their suitability and applicability. Reviews of measuring methods for k_La have been covered amongst others by van't Riet (1979), Keitel and Onken (1981), Linek and Benes (1982), Sobotka *et al.* (1982), Linek *et al.* (1989), (1991), Nicontini (1990) and Linek and Sinkule, (1993).

2.8.3.3 Transient Gas-liquid Mass Transfer Measurements

These measurements are generally made using a dissolved oxygen tension (DOT) probe to follow the transient of oxygen transferred to or from the liquid following a step change in the inlet conditions due to a step change in either the inlet gas phase composition or the pressure.

DOT probes obtained commercially are of two general types: galvanic or polarographic.

Oxygen sensitive electrodes consist usually of two metal electrodes in contact with an electrolyte and separated from the test medium by an oxygen permeable membrane.

The galvanic types are simple electro-chemical cells in which oxygen is reduced at an inert cathode according to the equation,

$$\frac{1}{2}O_2 + H_2O + 2e^- \rightarrow 2OH^-$$

with an accompanying anodic reaction of,

$$M^{++} + 2OH^- \rightarrow M(OH)_2 + 2e^-$$

where (M^{++}) is a metal ion.

The current produced by the galvanic reaction is limited by the rate of oxygen diffusion across the membrane, which is proportional to the oxygen concentration in the test medium.

With the polarographic type electrodes a polarizing voltage is applied across the electrodes and current flows in the presence of oxygen, which is proportion to the partial pressure of oxygen in the test medium. For example a polarographic probe with a silver anode, a platinum cathode and a potassium chloride solution electrolyte causes oxygen to be reduced at the Platinum cathode according to,

$$\frac{1}{2}O_2 + H_2O + 2e^- \rightarrow 2OH^-$$

whilst at the anode silver is oxidised,

$$2Ag \rightarrow 2Ag^+ + 2e^-$$

then

$$Ag^+ + Cl^- \rightarrow AgCl$$

The overall cell reaction is thus,

$$\frac{1}{2}O_2 + H_2O + 2Ag + 2Cl^- \rightarrow 2OH^- + 2AgCl \qquad (2.114)$$

The cell reaction sets up a current flow due to the conduction of electrons from anode to cathode. The hydroxyl ions in the cell are entirely from oxygen transported across the membrane since this is designed to be impermeable to these ions.

The value of the applied voltages is such that that the current passed by the cell in the presence of oxygen lies on the plateau (BC) (sketched in Figure 2-53) where (A) represents the decomposition voltage for a specific reaction.

(BC) lies between 0.5 and 0.9 V for the cell reaction shown in equation (2.114) and for such an applied voltage the current passed is proportional to the rate of oxygen diffusion across the membrane and hence to the oxygen concentration in the test medium

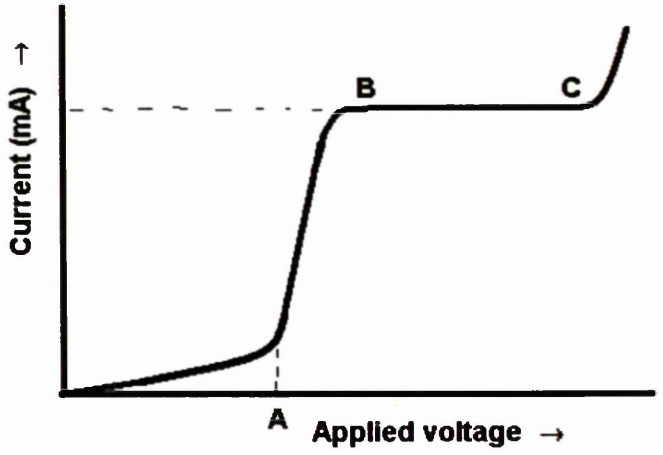

Figure 2-53: Current plateau for a polarographic probe

Some points to note that affect the analysis of the output from these probes are given below:

- The probes have a lag time. The probe dynamics are complicated and depend upon the design of the probe (Spriet and Botterman (1984). The dynamics have been variously modelled as a first order lag for "rapid response probes" for examples Wisdom (1973), Davies *et al.* (1985) or for slower probes, a second order lag consisting of a first order diffusion film lag in series with a first order membrane lag as proposed by Dang *et al.* (1977). For second order behaviour, this diffusion lag also depends on the local hydrodynamics and van't Riet (1979) recommends positioning these types of probe in the impeller stream, if these effects are to be neglected. Other methods suggested include using an auxiliary disc rotating in a direction parallel to the probe membrane, Kipke (1977). However, this method has been claimed to cause additional gas dispersion and affect the local

hydrodynamics, thus artificially enhancing the measured k_La value according to König *et al.* (1979).

- The probes consume oxygen. This means that if the fluid turnover at the membrane is not sufficiently fast then local oxygen depletion will occur. This means that the probe position is important. Also the faster the probe response is, generally, the more oxygen they consume and the more they are sensitive to the local hydrodynamics.

- They measure a local concentration. This concentration may only be representative of the whole vessel if the liquid phase mixing is fast compared to the mass transfer. In earlier work, Cooke *et al.* (1988) showed that the mixing had to be approximately three times faster than the mass transfer in order for the "well-mixed" liquid with respect to the mass transfer assumption to be realistic.

- The probe reading is proportional to the partial pressure of oxygen which is required to produce the equilibrium oxygen concentration in the solution, regardless of its solubility in the solution at a given temperature. Hence, if the solubility changes, due changes in composition of the solute, the equilibrium reading will not change. This is important in systems like fermentations where changes in glucose concentrations with time can have a marked effect on oxygen solubility with a consequent change in calibration.

- Following from the above, they do not differentiate between the oxygen partial pressure in the liquid and the oxygen partial pressure in the gas. They measure both without distinction. Votruba and Sobota (1976) showed that ignoring the influence of the gas-phase contribution to the probe readings could lead to an overestimation of the overall mass transfer factor k_La. Votruba *et al.* (1977 and 1978) suggested a method of correcting for the effect of local hold-up on the probe. To minimise the effect of gas bubbles "seen" by the probe membrane the probe needs to be orientated so that the probe

membrane receives a positive liquid flow (high pressure at the membrane), so that it "sees" predominantly liquid and not gas at the membrane.

- The readings are temperature sensitive so temperature should be controlled or compensated for.

Dynamic response analysis using DOT probes consists of analysing the response of probes to a step change in either the inlet gas phase composition or the pressure.

Some methods by which the step change in oxygen concentration has been achieved are included in Table 2-14.

Although the dynamic method quickly gained considerable popularity it was soon realised that under many conditions considerable errors resulted from its use.

It can be seen how these errors arrive by consideration of the assumptions behind the modelling.

2.8.3.3.1 Liquid Film Control

It is assumed that the transfer of gas to and from the liquid film is controlled by diffusion of oxygen across the film at the surface of the bubble. This is a reasonable assumption for a sparingly soluble gas.

Method of Achieving Oxygen step change:	Reference example	Comments
1/ Stripping with nitrogen gas with instantaneous switching to air at constant gassing and stirring rates. Can be operated in reverse direction switching from air to nitrogen. In some variants the outlet gas-phase concentration with time is also measured.	Chapman (1981) Chapman *et al.* (1982) Gibilaro *et al.* (1985)	The way the nitrogen gas leaves the vessel depends upon gas-phase mixing. The gas-phase oxygen concentration changes markedly with time. Simultaneous dissolution and devolution is occurring
2/ Stripping with nitrogen gas. Nitrogen and agitation switched off to allow bubbles to escape then simultaneously switching on air and agitation at the desired gassing rate.	Yagi and Yoshida (1975)	Both P/V and the gas hold-up vary with time during the initial period after the gas and agitation is switched on.
3/ Stripping with nitrogen gas. Switching off nitrogen to allow bubbles to escape with agitator on, then suddenly switching to air at the desired gassing rate.	Smith *et al.* (1977)	Both P/V and the gas hold-up vary with time after the gas is switched on.
4/ Similar to the above but stripping by vacuum desorption and then switching to oxygen	Linek *et al.* (1982)	Start-up time has to be modelled but the gas-phase composition does not change with time. Not suitable to large scale tests.
5/ Continuous air input. Oxygen stripped chemically using a small amount of sodium sulphite with cobalt catalyst. When the sulphite is used up the transient begins.	Wisdom (1973)	System has to be dosed with salts to prevent change in ionic concentration effecting coalescence, hence only suitable for "non-coalescing" "tests.
6/ Fermentation at steady-state oxygen. Switch off air and measure oxygen uptake rate by fall in oxygen concentration. Then when air is switched back on k_La can be estimated from absorption curve, as the oxygen uptake rate is then known.	Williams (1961)	Problems associated with other variants of the dynamic method still exist
7/ Over-pressure used. At time zero a sudden change in pressure from steady-state condition results in a transient oxygen concentration change.	Linek *et al.* (1991) and (1994).	Gas volume and power input changes initially until the new equilibrium is established. For pressure reduction, bubble nucleation occurs Linek *et al.* (1994). Gas-phase composition is constant

Table 2-14: Some dynamic k_La methods

2.8.3.3.2 Henry's Law

The oxygen concentration of the liquid at the gas-liquid interface is assumed to be always in equilibrium with the gas phase as defined by Henry's Law. This implies that the rate at which oxygen is transferred across a single bubble of surface (S) is given by:

$$k_L \int_S (\lambda C_G - C_L) dS \tag{2.115}$$

where λ is $1/He$ and He is the Henry's law factor. Subscripts G and L refer to the gas and liquid phase respectively. Note that Henry's constant changes with changes in composition and temperature. With transient methods the equilibrium value is measured at the end of the transient, hence calibration can be achieved by normalizing with C^* noting that at equilibrium $C^* = \lambda C_G$.

2.8.3.3.3 Liquid Mixing

As stated by Bailey and Ollis (1986) the local oxygen transfer rate often varies with position in the reactor. For the output of a single probe to represent the whole of the vessel requires an assumption that the liquid is perfectly backed mixed. That is that the measured value of C_L is independent of position. This means that the liquid mixing must be faster than the mass transfer. Cooke *et al.* (1988) showed that the liquid mixing needed to be three times faster than the mass transfer for this assumption to be approximately valid. If the liquid is well mixed with regards to the mass transfer then,

$$V_L \frac{dC_L}{dt} = k_L \int_S \lambda C_G dS - V_L k_L a C_L \tag{2.116}$$

where S is the surface area of the bubbles, $\lambda C_G = C^*$ and:

$$k_L a = \frac{k_L \int_S dS}{V_L} \tag{2.117}$$

Usage of a number of probes in different positions still requires an assumption that locally the liquid is well mixed and the imposition of a volume over which the ideal liquid phase mixing is applied. For multiple agitated vessels this could be the volume agitated by each agitator. In a recent paper by Lu *et al.* (2002), the authors estimated k_La using a small DOT probe in many numerous places in a multiple agitation system and reported variations not only between agitation zones but also within them? The authors show control volumes over which they have assumed the liquid is locally well mixed. This approach certainly demonstrated that the bulk liquid is not well mixed in this case, but whether the k_La values estimated have any real meaning in this case is debatable, although one could argue a global average of all the results is likely to be more representative of the vessel than a single value, when a global well-mixed liquid is clearly not applicable.

2.8.3.3.4 Probe Lag

Wisdom (1973) outlined a method whereby the response of the probe and measuring system to a step change at the sensor could be tested for first order response behaviour by plotting a graph of the logarithm of the concentration deficit (C^*-C) against time where a resulting straight line confirmed a reasonable fit to first order behaviour. Rapid response probes with time constants (τ_p) of ≤ 3 seconds can usually be adequately modelled as a first order lag and this can be then be used to de-convolute the measured concentrations in either the gas or liquid phase according to,

$$\frac{dC_M}{dt} = \frac{(C - C_M)}{\tau_p} \qquad (2.118)$$

Van't Riet (1979) reports that the probe lag can be neglected when $\tau_p \leq 1/5\ k_La$ as this produces an error in k_La of < 3%.

2.8.3.3.5 Gas-phase Composition

For method 4 (or method 5 used with pure oxygen) listed in Table 2-14, for all times greater than $t = 0$, the gas phase consists of a single component gas hence the oxygen concentration of the gas-phase does not change and providing any start-up period can be reasonably modelled (as described for instance by Linek *et al.* 1982), the method should give a good approximation of a global $k_L a$ when the liquid-phase can be considered well-mixed.

For cases involving oxygen transport from air then in order to solve equation (2.116) the corresponding gas-phase concentration need to be estimated. For a single probe representing a well-mixed liquid vessel this needs to be a global estimate and this has variously been represented as no depletion, ideally back mixed, ideal plug flow, non-ideally mixed using a dispersion model or by measuring the outlet concentration with time (double response) analysis as discussed below.

No depletion or simple model: The oxygen concentration is assumed to the same everywhere and equal to the inlet. The justification for this approach is that oxygen is only sparingly soluble in aqueous systems. Therefore, providing $k_L a$ is low and the gas phase residence time (τ_G) is very much shorter than the time constant for $k_L a$, this approach has been shown to give very similar results to more robust measurement techniques in air-water. The attraction of the technique is that it is quick and simple to apply. The mass balance gives:

$$\frac{dC_L}{dt} = k_L a(\lambda C_{Gi} - C_L) \qquad (2.119)$$

where $\lambda C_{Gi} = C_L^* =$ the equilibrium liquid-phase oxygen concentration.

Integration of equation (2.119) yields:

$$k_L a = \frac{\ln\left(\frac{C_L^* - C_{L(t_1)}}{C_L^* - C_{L(t_2)}}\right)}{(t_2 - t_1)} \qquad (2.120)$$

This model has been variously used with methods 1 to 5 in Table 2-14.

In methods 1 to 4 it is usual to start at time t_1 about one third up the response curve to allow either all the residual nitrogen gas to have escaped from the vessel or to establish the hold-up from the start-up time. Method 5 can be used from $t = 0$ = start of transient but note in this case the presence of salts means that the system is ionic and it will seen later that this poses its own problems with dynamic measurements. The usual test for consistency of this modelling is that $\ln\{(C_L^*-C_{L(0)})/(C_L^*-C_L)\}$ versus t should fit a straight line with an R^2 correlation coefficient of ≥ 0.999.

This method only gives acceptable results if $\tau_G << 1/k_L a$.

Van't Riet (1979) showed that $\tau_G = \varepsilon_G H_L / v_S$ and that as ε_G scales with v_S at constant (P/V) then it follows that τ_G increases with scale. Therefore, the method is only suitable for small vessels where τ_G is truly $<< 1/k_L a$. If methods 1 to 4, from Table 2-14, are applied by fitting equation (2.119) from $t = 0$ and $C_L = 0$, then it cannot be justified as the effect of the start-up period on either the gas-phase hold-up and energy dissipation rates or the effect of residual nitrogen gas for quick change-over methods, leads to errors in fitting the beginning of the response curve. This leads to an underestimation of $k_L a$ even for values apparently $< 0.04 s^{-1}$ by this method as shown by Chapman (1981) and again by Davies (1986).

In spite of the drawbacks and bad press; examples Dunn and Einsele (1975), Dang *et al.* (1977) Davies (1986) Linek *et al.* (1989), (1991), Nicontini (1990) and Linek and Sinkule, (1993); the above method is still being used. A recent example was Lu *et al.* (2002) using method 1 from Table 2-14 fitted to equation (2.119), and ignoring the probe lag time. In this case it was probably

justified as the work was done in air-water and for the conditions they used both $\tau_p \leq 1/5k_La$ and $\tau_G \leq 1/5k_La$.

Well-mixed gas and liquid-phase model: Dunn and Einsele (1975) pointed out the danger of ignoring the probe and gas-phase dynamics and proposed a model with a well-mixed gas and liquid-phase where the probe lag was also included. In order to apply this model, for example for method 1 in Table 2-14, requires some more generalising assumptions. It is assumed that at any time t the gas concentration is equal everywhere but in this case equal to the outlet concentration, which is not necessarily the same as the inlet. Ignoring nitrogen devolution from the liquid then from the perfect liquid mixing assumption:

$$\frac{dC_L}{dt} = k_L a(\lambda C_G - C_L) \tag{2.121}$$

A gas-phase oxygen balance shows oxygen supplied with the sparge stream and lost by gas leaving the reactor plus oxygen lost to the liquid stream by transfer thus:

$$V_G \frac{dC_G}{dt} = Q(C_{Gi} - C_G) - V_L k_L a(\lambda C_G - C_L) \tag{2.122}$$

with boundary conditions $C_G = C_L = 0$ at time $t = 0$.

Davies (1986), showed that this model (applied to method 1) consistently overestimates k_La as it underestimates the oxygen driving force. It can only be applicable in cases of very high gas recirculation rates.

Plug-flow gas phase model: A physically more realistic model of the gas-phase, especially for larger vessels with higher superficial gas velocities, is ideal plug flow. In this case the unsteady-state gas balance allows the gas-phase to

change with position as well as time. A mass balance to describe method 1 in Table 2-14 was given by Davies (1986):

Non-ideal (double response) gas-phase model:

Chapman *et al.* (1982) argued that by simultaneously measuring the liquid concentration and the outlet gas concentration the gas-phase mixing term could be eliminated. Initially, at time zero there is no oxygen in the system. At some time later the amount of oxygen retained in the system is the difference between the oxygen sparged in and that in the outlet gas. The authors assumed a mono-sized gas dispersion and negligible change in gas volume (or that the amount of oxygen transfer from the gas phase to the liquid equals the amount of nitrogen devolved). The gas and liquid concentrations were normalized by dividing gas and liquid concentrations by the final steady-state values to obtain the following mass balance:

$$k_L a = \frac{\frac{dC_L^*}{dt}}{\frac{Q}{V_G}\int_0 (1-C_o^*)dt - C_L^*\left(\frac{\lambda V_L}{V_G}+1\right)} \qquad (2.123)$$

The off-gas was collected in an inverted funnel arrangement and measured using an oxygen probe. The data were de-convoluted for probe lags using equation (2.118). The lag in the sampling system needs to be modelled. In my own experience of the use of this method, this was modelled as a distance-time lag assuming plug flow followed by a first order probe lag. The distance-time lag was a fitted value as the flow was not easy to determine. It was noted that for a large vessel, the "fitted" value was much longer than physics would suggest from a lag from the free liquid surface to the probe, and would seem to include the gas residence time from the liquid probe to the free surface. Nevertheless this method proved to be reasonably robust for air-water and in agreement with steady-state methods of measuring $k_L a$ in the same system. In the comparisons made by Davies (1986) the double response method gave

results that were higher though close to the ideal plug flow gas phase model. By comparison the simple no-depletion model seriously underestimated k_La under some conditions, whilst under the same conditions the fully back-mixed gas-phase model seriously overestimated k_La and these effects were both non-linear meaning that the methods were not even viable for comparative tests.

2.8.3.3.6 Dynamic k_La Measurements in Live Fermentation Cultures.

This is method 6 in Table 2-14

$$\frac{dC_L}{dt} = k_L a\left(C_L{}^* - C_L\right) - a_{O_2} X \tag{2.124}$$

X is cell constant and a_{O_2} is the specific oxygen uptake rate. Other terms have their usual meaning. When air is switched off, the first term is zero:

$$\begin{aligned} &\frac{dC}{dt} = -a_{O_2} X \rightarrow \int_{C_o}^{C} dC = -\int_{t=0}^{t=t} a_{O_2} X dt \\ &C - C_o = -a_{O_2} Xt \\ &C = -a_{O_2} Xt + C_o \end{aligned} \tag{2.125}$$

The group $a_{O_2} X$. can be evaluated by Plotting "C" against time.

When the air is switched on,

$$\frac{dC}{dt} + a_{O_2} X = k_L a\left(C^* - C\right) \tag{2.126}$$

As the group $a_{O_2} X$ is known, this expression can be evaluated to yield k_La.

2.8.3.3.7 Undesirable Effect of a Two-component System, Using Transient Methods to Estimate k_La in Aerated Systems

For air-liquid systems other than pure water, experimenters using transient methods compared to steady-state evaluations have reported some large differences in estimated k_La values. Examples include Cooke *et al.* (1991) where it is found that for water containing either 20-ppm polypropylene glycol (PPG) or 0.4% sodium carboxyl-methyl-cellulose (CMC), the transient k_La is around 20% of the steady-state values at the same conditions. Likewise Linek *et al.* (1991) reported transient k_La by the gassing out technique as low as 15% of values determined from the pressure swing technique in fermentation medium.

Heijnen *et al.* (1980) identified the influence of the tiny gas bubbles in transient two-component gas systems as the cause of these discrepancies. When subjected to a transient change in the gas-phase composition these bubbles have such a small gas-liquid equilibrium time compared to their residence time that they act as a pseudo-liquid with the oxygen change in these tiny bubbles mirroring the liquid-phase composition. However as oxygen at equilibrium is approximately 30 times as concentrated in the gas phase as the liquid phase a small volume percentage of these bubbles makes a large difference to the oxygen up-take rate. The authors proposed a correction method for dynamic k_La according to the following relationship:

$$k_La = k_La_D(1 + He\varepsilon_{tb}) \tag{2.126}$$

where k_La_D is the dynamic mass transfer factor and ε_{tb} $(= V_{tb}/V_L)$ is the volume fraction of tiny (two-component) bubbles. Taking a typical value of He as 30 for air-water, then a 3% hold-up of tiny bubbles is predicted to decrease the "dynamic" value k_La to 53% of the real "steady-state" value.

2.8.3.3.8 Conclusions Regarding the Dynamic Methods of measuring k_La in Aerated Systems

The transient method of k_La measurement in air-water systems is only suitable for pure coalescing liquids except by the positive pressure swing method. For fluids containing electrolytes or surfactants or whose properties give rise to a fraction of tiny bubbles with a residence time >> equilibrium time, the transient method will give an artificially "low" value and considerable errors.

When used the method has include a "realistic" description of the gas-phase dynamics as described above.

Method 4 from Table 2-14 is sound but is only suitable for small-scale work where large quantities of oxygen are not demanded. Hence it cannot be used to investigate scale effects.

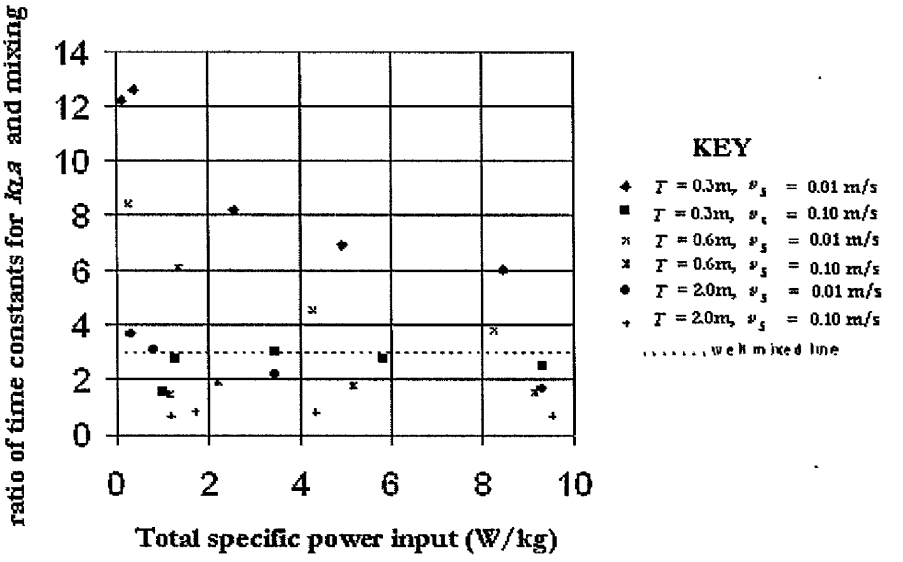

Figure 2-54: Testing the well mixed liquid phase assumption for air-water. To be well mixed the ratio of the time constant for mass transfer ($\tau(k_La) = 1/k_La$) should be ≥ three times the time constant for mixing (τ_{mix}). Assuming first order mixing $\tau_{mix} = t_{90}/\ln(10)$. The calculations were done assuming an $H=T$ baffled cylindrical vessel containing a single $D=T/2$, Scaba 6SRGT impeller at a clearance of $T/4$.

All methods (including steady-state methods) use a well-mixed liquid phase assumption. It can be shown that this is only justified globally for modest power inputs, scales and gassing rates. An examination of equations (2.54) (mixing) and equation (2.107) (mass-transfer) shows that on a given scale mixing times are proportional to $P^{1/3}$ whereas k_La is proportional to $P^{0.61}$. Thus as P/V increases it becomes less likely that the well-mixed liquid assumption applies. With higher H/T and multiple agitators the mixing gets worse overall but not the mass transfer. As scale increases the mixing gets worse. For a 2 m diameter vessel, calculations show that at almost all practical operating conditions in air-water the well-mixed assumption is not justified even for a single agitator in an $H = T$ geometry. This is illustrated in Figure 2-54, by data points below the "well-mixed line". Even a small vessel of T = 0.3 m is not well mixed with respect to mass transfer at a superficial gas velocity of 0.1 m/s. On the 2 m vessel all k_La values above 0.07 s^{-1} (a common fermentation value) cannot be assumed to satisfy a well-mixed liquid phase assumption.

2.8.3.4 Steady-state or Pseudo Steady-state Gas-liquid Mass Transfer Measurements

Steady-state methods have the advantage that they are not as dependent on the gas-phase hydrodynamics when two component gas-phase systems are used, since they involve sparingly soluble gases and in most cases the differences between the inlet and outlet gas phase composition is small.

König *et al.* (1979) used a purely physical steady-state method feeding nitrogen stripped liquid from a bubble column to a temperature controlled aerated stirred tank reactor. The liquid was continuously removed from the reactor and fed back via a degasser to the bubble column where it the oxygen was removed. The oxygen in the feed C_{Li} and the oxygen in the stirred tank C_L were continuously measured. k_La is calculated from an overall oxygen balance. For the gas-phase,

In = out - transfer

$$Q_{Gi}C_{Gi} = Q_{GO} + V_L k_L a(\lambda C_G - C_L)$$

For the liquid phase,

In = out + transfer

$$Q_{Li}C_{Li} = Q_{LO} - V_L k_L a(\lambda C_G - C_L)$$

where Q is a volumetric flow rate and subscripts G, L, i and o refer to gas, liquid, inlet and outlet respectively and λC_G is the equilibrium oxygen at the interface = C_L*.

At steady-state, since oxygen is only sparingly soluble in water,

$Q_G = Q_{Gi} = Q_{GO}$ and $Q_L = Q_{Li} = Q_{LO}$

Assuming a well-mixed liquid, then $C_L = C_{LO}$. Therefore:

$$V_L k_L a(C_L^* - C_L) = Q_G(C_{Gi} - C_{GO}) = Q_L(C_L - C_{Li}) \quad (2.128)$$

Thus $k_L a$ can be found by rearranging the above equation to give,

$$k_L a = \frac{Q_G(C_{Gi} - C_{GO})}{V_L(C_L^* - C_L)} \quad (2.129)$$

The unknown C_{GO} can be found from equation (2.123)

$$C_{GO} = C_{Gi} - \frac{Q_L}{Q_G}(C_L - C_{Li}) \quad (2.130)$$

which substituted back into equation (2.124) results in,

$$k_L a = \frac{Q_L(C_L - C_{Li})}{V_L(C_L^* - C_L)} \quad (2.131)$$

Note that Q_L/V_L is the liquid residence time τ_L.

The oxygen driving force $(C_L^* - C_L)$ can be estimated for the following cases:

No oxygen Depletion: $(C_L^* - C_L) = (\lambda C_{Gi} - C_L)$

Well mixed gas-phase: $(C_L^* - C_L) = (\lambda C_{GO} - C_L)$

Plug flow gas-phase: $(C_L^* - C_L) = \dfrac{(C_{Li}^* - C_L) - (C_{LO}^* - C_L)}{\ln\left(\dfrac{C_{Li}^* - C_L}{C_{LO}^* - C_L}\right)} = \dfrac{\lambda(C_{Gi} - C_{GO})}{\ln\left(\dfrac{C_{Li}^* - C_L}{C_{LO}^* - C_L}\right)}$

This looks an elegant technique. In practice however, it is found that in order to minimise errors C_L needs to be well below the saturation value as shown for example by Keitel and Onken (1981). This requires high liquid flows, which limits the applications to small scale and may effect the well-mixed liquid assumption as well as the local hydrodynamics.

Note also that here the "well mixed" assumption infers C^* and C_L are independent of position and time. Bailey and Ollis (1986) teach us that in practice these quantities vary with position and should be considered the summation or integration of point values within the system. Therefore the oxygen probe should be used in a number of positions or multiple probes should be used.

Chemical methods can be used to yield simultaneously the liquid side mass transfer coefficient "k_L" and the interfacial area "a", according to the theory given by Danckwerts (1970). This is based on the film theory, although it is shown that other theories result in almost identical predictions. The treatment revolves around the relative rates of gas-liquid mass transfer and reaction. The reaction rate controls the overall rate if it is very slow. If it is fast the overall rate is controlled by the mass transfer rate. Very fast reactions influence the diffusion process, causing enhancement of mass transfer above the purely physical case; this enhancement depends upon the reaction rate. In the "instantaneous" reaction regime, mass transfer again controls the overall rate of the process.

Literature Reviews

According to Danckwerts (1970), the use of a chemical reaction to simultaneously measure "k_L" and "a" is dependent on a general pseudo-order reaction scheme of the type:

$$nA + mB \rightarrow products \tag{2.132}$$

of order n in dissolving gas component A and m in liquid phase component B, and where $n/m = q$.

If C_A and C_B represent the molar concentrations of A and B respectively in the liquid, then the rate of reaction of A is given by,

$$r_A = k_{nm} C_A^n C_B^m \text{ moles/s/unit vol. of liquid.} \tag{2.133}$$

A reaction time (τ_R) is defined as,

$$\tau_R = \left(\frac{n+1}{2k_{nm} C_A^{(n-1)} C_B^m} \right) \tag{2.134}$$

The mass transfer of A into the liquid is described by,

$$r_A = k_L a(C_A^* - C_A) \text{ moles/s/unit vol. of liquid} \tag{2.135}$$

where k_L is the mass transfer coefficient, "a" is the interfacial area per unit volume of reactor and C^* is the interface concentration of A.

A mass transfer diffusion time is defined as,

$$\tau_D = \frac{D_L}{k_L^{\,2}} \tag{2.136}$$

where D_L is the diffusivity of the transferring species A in the liquid. If a "fast" reaction is occurring within the diffusion film near the interface it will enhance the reaction and equation (2.135) becomes,

$$r_A = k_L * a(C_A^* - C_A) \tag{2.137}$$

where

$$k_L^* = \sqrt{\frac{2D_L k_{nm}\left(C_A^* - C_A\right)^{n-1}\left(C_B^0\right)^m}{n+1}} \tag{2.133}$$

It is noted that k_L^* depends on the reaction rates not the hydrodynamics conditions. Also for fast reactions C_A is zero as the gas reacts as soon as it is transferred. The ratio of diffusion to reaction near the gas-liquid interface is expressed as the Hatta number (Ha) that is expressed as,

$$\mathrm{Ha} = \sqrt{\tau_D/\tau_R} \tag{2.136}$$

The Hatta number determines the extent to which diffusion controls the liquid phase reaction rate.

Diffusion control: For a pseudo m^{th} order reaction where the concentration of B in the film is approximately constant the following condition given by Sharma and Danckwerts (1970) holds,

$$Ha = \frac{1}{k_L}\sqrt{\left(\frac{2D_L k_{nm}\left(C_A^*\right)^{n-1}\left(C_B^0\right)^m}{n+1}\right)} << \frac{C_B^0}{qC_A^*} \tag{2.140}$$

For a pseudo first order reaction (first order in A and B with $B >> A$), which is moderately fast so that,

$$0.02 < \sqrt{\frac{\tau_D}{\tau_R}} < 2 \tag{2.141}$$

then in this region,

$$r_{1'} = aC_A^*\sqrt{D_L k_2 C_B^0 + k_L^{\ 2}} \tag{2.142}$$

Therefore, if C_B^0 is varied, a plot of $(r_{1'})^2$ versus $k_2 C_B^0$ has a slope of $D_L(aC_A^*)^2$ and an intercept of $(k_L C_A^*)^2$. Thus, k_L and a can be determined simultaneously. This is known as a Danckwerts plot.

If the rate of reaction is sufficiently fast such that the Hatta number (Ha) > 3, in which,

$$Ha = \frac{1}{k_L}\sqrt{\left(\frac{2D_L k_{nm}\left(C_A^*\right)^{n-1}\left(C_B^0\right)^m}{n+1}\right)} > 3 \qquad (2.143)$$

Then the reaction occurs in the film near the liquid interface (no liquid film resistance) and the rate of absorption of gas per unit volume of dispersion for a pseudo first order reaction is given by,

$$r_{1'} = aC_A^*\sqrt{D_L k C_B^0} \qquad (2.144)$$

In this regime the interfacial area "a" can be determined.

The oxidation of sodium sulphite catalysed by small amounts of Cu^{2+} or Co^{2+} ions in an aqueous phase has classically been used for mass transfer and interfacial area determinations. However the presence of sulphite and sulphate ions means that solution is non-coalescing and hence is not suitable for studying non-coalescing systems. The chemical kinetics of the reaction must be accurately known (difficult when small quantities are involved) for reliable measurements to be made. As the oxygen concentration in the liquid phase tends to zero, the rate of absorption of oxygen is monitored by titration of the unreacted sulphite with time.

Danckwerts (10-3, 1970) and Van't Riet (1979) have reviewed the problems with the chemical technique using the sodium sulphite oxidation scheme that includes complicated kinetics, which are affected by ions, concentrations, pH and impurities and these and other unfavourable reviews have led to the decrease in the use of this technique for interfacial area and $k_L a$ measurements.

Sridharan and Sharma (1976) give a comprehensive list of systems that have been developed for the measurement of the "effective" interfacial area by the chemical method, which allow the use of a wide range of hydrocarbon solvents using the reaction between carbon dioxide and amines.

The term "effective" surface area for interfacial area derived by chemical techniques arises from the fact that considerable differences in interfacial area

determined by the chemical technique compared to physical techniques such as light scattering have been reported by, for example, Sridar and Potter (1978). The interfacial area determined by the chemical method is less than that found by physical methods. This was considered to be due to variations in mass transfer regimes in different regions of the vessel due to spatial variations in energy dissipation rates. It may also be due to incorrect kinetics being applied.

2.8.3.4.1 Respiring Yeast for Steady-state Gas-liquid Mass Transfer Measurements

Biological systems containing living organisms can be used to estimate $k_L a$ under steady-state conditions by measuring the dissolved oxygen concentration and the oxygen uptake rate (*OUR*), *which* is determined by a mass balance on oxygen. At equilibrium,

$$OUR = Q_G(C_{Gi} - C_{Go})K'/V_L = k_l a(C^* - C_L) \qquad (2.145)$$

where Q_G is the volumetric gas flow and the constant K' is determined from the ideal gas laws, $K' = \frac{p_i}{RT}$.

Note p_i is the inlet pressure = (atmospheric + head + over-pressure).

However, as pointed out in section 2.8.3.3.2, the solubility of oxygen in fermentation medium depends on composition, which is difficult to keep constant. This makes determination of the correct Henry's law constant to use at any given time in the fermentation process somewhat problematic.

Hickman (1985) overcame this problem by using respiring yeast in a model fluid to estimate mass transfer coefficients in model fermentation broths. Yeast has little or no effect on Henry's constant and is equally happy under aerobic and anaerobic conditions producing alcohol under the latter conditions. By use of a limiting glucose supply he was able achieve steady-state dissolved oxygen levels using the respiring yeast, coupled with constant

low glucose concentrations in the liquid (constant Henry's law constant). He was concerned with the effect of the rheological properties on the mass transfer properties which he altered using CMC additions. The liquid side mass transfer factor was determined from equation (2.145).

2.8.3.4.2 The Peroxide Technique for Pseudo Steady-state Gas-liquid Mass Transfer Measurements

This method was originally proposed by Hickman (1988) and investigated by Cooke *et al.* (1991). In its original formulation 30% hydrogen peroxide is continuously added to the liquid phase at a molar feed rate $Q_{H_2O_2}$ where it broken down by the enzyme Catalase (BDH Ltd or Sigma Chemicals Ltd, bovine liver extract, 2 x 10^5 enzyme units (EU) per ml. The reaction scheme is as follows,

$$2H_2O_2 \xrightarrow{Cat} 2H_20 + O_2 \qquad (2.146)$$

with a rate of,

$$r = \text{constant} \times [H_2O_2]^A [cat]^B \qquad (2.147)$$

Muller and Davidson, (1992) and Martin *et al.* (1994) used activated manganese dioxide as an alternative catalyst. Vasconcelos *et al.* (1997) showed that the same reaction kinetics could be applied for both methods of catalysis (obtaining comparable results both methods), which are first order with respect to hydrogen peroxide and independent of the catalyst concentration over a wide range. That is, A=1 and B=0.

Oxygen is continuously produced in the liquid and stripped by the continuous flow of air. Initially hydrogen peroxide and oxygen accumulate in the liquid until a steady state is reached where the reaction rate is balanced by the peroxide addition rate and the rate of oxygen production is equal to the

oxygen transfer rate (*OTR*) from the liquid phase to the gas phase. For this condition,

$$r = \frac{Q_{H_2O_2}}{V_L} \tag{2.148}$$

and from the stoichiometry,

$$\frac{r}{2} = OTR = k_L a(C_L - \frac{C_G}{He}) \tag{2.149}$$

The outlet gas concentration C_{Go} can be measured or may be calculated by mass balance, once the outlet gas flow Q_{Go} is known. Assuming the ideal gas law applies this is as follows,

$$Q_{Go} = \left(Q_{Gi} + \frac{OTR.V_L RT}{p_i} \right) \frac{p_i}{p_0} \tag{2.150}$$

giving,

$$C_{Go} = \frac{(Cgi + OTR.V_L)}{Q_{Go}} \tag{2.151}$$

Hickman (1988) claims the calculated outlet gas concentration is in good agreement with the measured value.

Then assuming a well-mixed liquid phase, C_L is constant and the driving force (C_L-C_G/He) can be calculated according to,

For a well-mixed gas phase,

$$C_G = C_{GO} \tag{2.152}$$

For a plug flow gas-phase,

$$(C_L - C_G^*) = \frac{(C_{Go}^* - C_{Gi}^*)}{\ln\left(\frac{C_L - C_{Gi}^*}{C_L - C_{Go}^*} \right)} \tag{2.153}$$

Under the experimental conditions used, there is little difference between the inlet and outlet gas concentrations and differences in $k_L a$ values between the

two gas-phase models are generally < 5%. The difference in gas flow rates between the inlet and outlet is also small, generally about 0.5%.

The liquid-phase mixing could be important as pointed out by Hickman (1988); "*If liquid mixing were poor, then the reaction kinetics are such that it would be possible to have point to point variations of peroxide concentration and reaction rate. Consequently there would be point to point variations of dissolved oxygen concentration which would prevent the measurement of accurate k_La values*". In extreme cases, very viscous, or large vessels where the liquid mixing is very poor he recommends the use of multi-point addition of hydrogen peroxide.

Catalase is quickly deactivated in strong electrolyte solutions containing salts so manganese dioxide is preferred in this case. The latter is also much more stable.

The restrictions to the use of manganese dioxide are when a dissolved species may be absorbed by manganese dioxide and therefore more easily degraded by oxidation. For example carbohydrates or polyhydroxy compounds such as polypropylene glycol (PPG) as reported by Martin *et al.* (1994) and Vasconcelos *et al.* (1997). Martin reports the effect of the MnO_2 catalyst on PPG solutions is to rapidly reduce the coalescence retardation properties of the solution.

The hydrogen peroxide method with the choice of catalyst to suit the solution is rapidly becoming "the standard" technique for mass transfer measurements in gas-liquid systems.

2.8.3.5 Solid-liquid Mass Transfer in Agitated Vessels

For solid-liquid mass transfer, off-bottom suspension is usually all that is required. Nienow and Miles (1978) found that the mass transfer coefficient at the just suspension condition is almost independent of mixer type, size and specific power input for a baffled vessel and a given solid-liquid system. Hence

agitator configurations that are particularly efficient for particle suspension require less mechanical power to achieve a given mass transfer duty.

Unbaffled vessels which utilise swirl to achieve just suspension conditions at lower power inputs than baffled tank have been shown to have higher values of particle-fluid mass transfer coefficients at the same power consumption as baffled vessels for example by Grisafi *et al.* (1994).

It is concluded that for a batch system off-bottom suspension is generally all that is required for particle-liquid mass transfer. However, in a continuous system a bottom heavy suspension could result in a shorter residence time for the solid phase, which would result in poorer mass transfer. Hence for a continuous system the residence time distribution of the phases needs to be considered for mass transfer purposes.

2.8.3.6 Gas-liquid-solid Mass Transfer in Agitated Vessels

A typical example of gas-liquid-solid mass transfer is an aerobic fermentation where oxygen from the gas-phase must reach the surface of the growing cells that are suspended in the liquid. The resistance diagram for this is shown in Figure 2-55 from Levenspiel (1972 - Chapter 13, Fluid-Fluid Reactions).

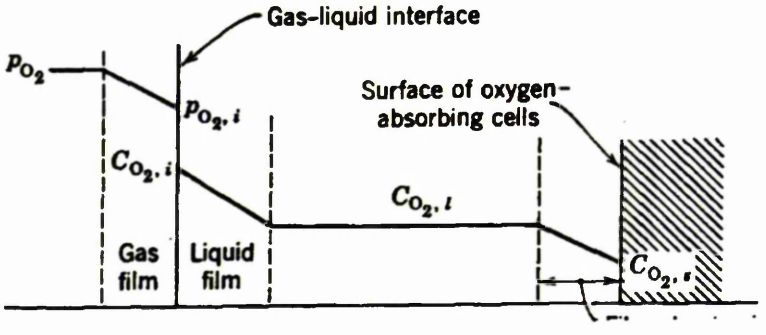

Figure 2-55: Resistances to oxygen absorption by cells in an aerobic fermenter

It is obviously important for a designer to decide whether the major mass transfer limitation lies at gas-liquid or solid-liquid interfaces and this can be ascertained by independently changing the gas-liquid interfacial area and the amount or size of the solid.

A strategy using a semi-technical reactor could for example be:

Under isothermal conditions and with reactant gas at a rate where the reacting gas leaves the reactor and with slurry concentration and particle size distribution fixed:

Alter the pressure to alter the equilibrium concentration(C^*). Unless reaction is instantaneous, this should affect the rate.

Alter the agitation rate at fixed temperature, pressure and gassing rate. This alters k_L, k_G and "a". No effect would suggest a slow reaction rate or major mass transfer barrier at the liquid solid interface. If there was no effect, change the temperature to determine whether it is diffusion at solid surface or surface reaction that controls.

Alter the gassing rate. This changes k_La, superficial gas velocity, gas-liquid hold-up and power.

Alter the gas dilution (blend with nitrogen) but change total pressure so that the partial pressure of reacting gas is constant. If this affects rates that could indicate a gas-phase diffusion control mechanism.

Change the specific surface area of particles or volume of particles at fixed size. An effect means that particle-liquid mass transfer is controlling.

Change the temperature to find out whether it is solid-liquid reaction rates or pore diffusion rates control.

2.8.4. Literature Gas-liquid Mass Transfer Results and Correlations

Using dimensional analysis Sideman *et al.* (1966) proposed a general form for the gas-mass transfer equation in terms of a modified Sherwood number Sh' as,

$$\mathrm{Sh}' = \frac{k_L a D^2}{D_L} = k(\mathrm{Re})^a (\mathrm{Sc})^b \left(\frac{\mu v_S}{\sigma}\right)^c \left(\frac{\mu_G}{\mu_L}\right)^d \qquad (2.154)$$

where Re and Sc are defined in Table 2-10, the group $(\frac{\mu v_S}{\sigma})$ is a gas flow number in terms the liquid phase viscosity, superficial gas velocity and interfacial tension and μ_G, μ_L are the gas and liquid phase viscosities respectively.

Unfortunately the physical properties do not always reflect the mass transfer behaviour and small quantities of impurities can have a marked effect on gas-liquid mass transfer, interfacial area and gas-liquid hold-up as shown by the examples below.

The addition of small quantities of salts (around 0.1 molar concentration, dependent on the ions) markedly hinders coalescence, decreases the mean bubble size and increases gas-liquid hold-up and $k_L a$. The mechanisms for this are discussed by Lee and Meyrick (1970) and Lessard and Zieminski (1971). The mass transfer factor ($k_L a$) approximately doubles when potassium chloride is added to water in an aerated stirred vessel at 0.1 molar concentration as reported for example by Cooke *et al.* (1991) and Van't Riet (1979). Martin *et al.* (1994), report an increase in $k_L a$ with increasing concentration of sulphate ions. Machon *et al.* (1997) reported that regardless of surface tension, the bubble sizes in solutions of electrolytes were approximately the same and much less than water. Machon and Linek (1974)

investigated the effect of salts on the rate of mass transfer across a plane interface between a gas and a mechanically agitated aqueous solution of inorganic electrolytes. They reported that the liquid mass transfer coefficient k_L decreases with increasing salt concentration. They attributed this to the surface film properties of the electrolyte solutions. The decrease in k_L however, is more than offset by the increase in interfacial area.

Antifoams also have a marked effect on coalescence at very low concentrations, albeit by a different mechanism from salts [Lee and Meyrick (1970)] due to adsorption at the gas-liquid interface. Silicone antifoams reduce interfacial area and have been found to adversely affect k_La.

Plichon *et al.* (1976) reports the addition of the anti-foam, silicon "Rhodorsil" during fermentation provokes an important diminution of the dissolved oxygen rate and an interruption of bacterial growth. Warmoeskerken and Smith (1978) reported that when small amounts of silicone oil were added to otherwise pure distilled water, which was absorbing oxygen from dispersed air, the gas-liquid mass-transfer rate decreased even for microscopic quantities of added oil. It was also established that several hours are needed before the effects reach their maximum.

Van de Donk *et al.* (1979) reported that traces of silicone oil decreased k_La by approximately 20% in a plunging jet contactor.

Polypropylene glycol (PPG) is also used as an antifoam agent. This produces a very large increase in surface area. Cooke *et al.* (1988) reported that it enhanced gas-liquid mass transfer in simulated fermentation brews but showed a lower mass transfer when added to pure water Cooke *et al.* (1991). Martin *et al.* (1994) reported that addition of traces of PPG to water gave similar mass transfer coefficients to water but caused foaming and a large increase in gas hold-up and interfacial area.

Bruining *et al.* (1986), examined the effect of small amounts. (0.5-1 vol. %) of a dispersed organic phase, for example (hexadecane, decane, decanol, cyclohexane), on the rate of gas-liquid mass transfer, using the sulphite

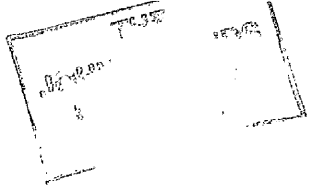

oxidation technique, in a stirred cell. They reported that the mass-transfer rate was enhanced by the presence of these materials when the drop diameter was ≤ the film thickness and the oxygen solubility in the organic phase was larger than that in water. They proposed a model that they claim predicts their experimental enhancement factors with reasonable accuracy.

For constant fluid properties in mechanically stirred vessels equation (2.154) reduces to the form,

$$k_L a = \text{constant} \times (P/V)^a v_S^{\ b} \qquad (2.155)$$

This is generally used for comparative data.

In this form it is generally reported, for constant fluid properties and operation in the agitator-dominated regime, that the proportionality constant and power law indices are independent of agitator type. Using this form, Cooke *et al.* (1988) reported no effect of agitator type for 6 agitator types. Bujalski *et al.* (1990) found that up-pumping turbines gave equal $k_L a$ to Rushton turbines when compared at the same specific power inputs and gassing rates. Martin *et al.* (1994) at constant gas rate, shows very little difference in the mass transfer performance of a Rushton turbine and a Prochem Maxflo when the data is plotted against the energy dissipation rate (P/V). John *et al.* (1997) also showed no effect of impeller choice and Whitton and Nienow (1993) reported that the relationship was independent of scale.

The specific power input is sometimes quoted as total power, which includes the specific gas power: The relationship between specific gas power ($P_Q / \rho_L V_L = Q_G(\rho_L - \rho_G)g(H_L - c_S)/\rho_L V_L$) and superficial gas velocity ($v_S = 4Q_G/\pi T^2$) is apparent. For a standard vessel ($V_L = \pi T^2 H_L/4$), therefore (where the gas density (ρ_G) can be ignored and providing $c_S = 0$, that is gas sparged in at the bottom of the base),

$$\frac{P_Q}{\rho V_L} = g v_S \qquad (2.156)$$

Units of specific power input should be W/kg, although they are sometimes quoted as W/m^3. Some literature data on the basis of equation (2.155) are shown in Table 2-15. Where necessary, the literature proportionality constant has been adjusted to show the correlation in terms of *W/kg*. In each case a "std" k_La has been computed for a mechanical P/V of 1 W/kg and a superficial gas velocity of 0.05 m/s; noting from equation (2.156) that specific gas power in *W/kg* is gv_S.

The standard (std) comparison for air-water shows a large variability range with predictions of 0.074 s^{-1} to 0.159 s^{-1}. This is an average of 0.108 s^{-1} ± 47%.

The peroxide technique seems to give much higher results than the so-called "good" transient results of Cooke *et al.* (1988) and Linek *et al.* (1987). It makes one wonder whether there is some change in physical properties with pure water for this system. The reaction is exothermic so perhaps there is a change in the interfacial properties? Catalase is dissolved in methanol so this may affect interfacial properties. Finely divided manganese dioxide catalyst could also be present at the interface causing a change in interfacial gradients. It has been reported that small quantities of active carbon significantly enhance k_L by for example Kars *et al.* (1979) and Alper *et al.* (1980) and active MnO_2 could act in the same way.

On the other hand the predictions for electrolyte are much more consistent. Ignoring the van't Riet (1979) correlation that appears to give too low a value, all the other data predicts (std) values between 0.231 s^{-1} and 0.280 s^{-1}, with an average of 0.253 s^{-1} ± 10%. These are approximately double those for air-water.

It is noted that the range of power law indices is quite remarkable, suggesting that these types of correlations are only useful for comparative purposes. The variations in these constants and indices, found by different experimenters, are perhaps not too surprising considering they cover a range of agitator and

bubble hydrodynamic regimes. Davies (1986), following Smith *et al.* (1985), found different constants and indices for operation between the vortex and the 3:3 cavity regimes for disc turbines, although the data could be correlated together almost as well.

Lopes de Figueiredo and Calderbank, (1979) using a transient, fully back-mixed gas-phase model on two scales claimed a scale effect. Their scale-up equation for air-water was,

$$\frac{k_L a V_L}{T} = 1x10^{-3} P^{0.58} v_S^{0.75} \qquad (2.157)$$

However, as shown earlier a fully back-mixed gas-phase model is inappropriate in most cases.

Equation type: $k_L a = k(P/V)^a v_s^b$ .Where agitation power alone has been used for P/V in the correlation the data reference source is marked with a *.							
Reference source /Method	Scale (m) /Aspect ratio	Agitator types	Fluids	*k*	*a*	*b*	Compare "std" $k_L a$ (s^{-1})
Smith *et al.* 1977 Transient-No depletion	*T* (m) = 0.61-1.83 *H/T* = 1:1	6RT *D=T/3* *D=T/2*	Air-water	0.111	0.69	0.23	0.074
Van't Riet (1979)* Various	2 – 2600 l 2-4400 l	?	Air-water Air-electrolyte	0.412 0.252	0.4 0.7	0.5 0.2	0.092 0.138
Linek *et al.* (1987)* Transient using 0 - pure O_2	*T* = 0.29 m 1:1	6RT *D=T/3*	Air-water Air-electrolyte	0.298 0.930	0.593 0.946	0.4 0.4	0.090 0.280
Hickman (1988)* Peroxide	0.6 m, 2.0 m *H/T* = 1:1	6RT *D=T/3*	Air-water	1.18	0.47	0.67	0.159
Cooke *et al.* (1988) Transient 2-probe	*T* = 0.29 m *H/T* = 3:1	3x6RT 6GF+ 2x4PHF *D=T/2*	Air-water	0.2	0.7	0.3	0.108
Cooke *et al.* (1991) Transient 2-probe Peroxide	*T* = 0.29 m *H/T* = 1:1	6RT *D=T/2*	Air-0.1M KCl	0.69	0.6	0.42	0.249
Vasconcelos *et al.* (1997)*	*T* = 0.61 m *H/T* =1:1	APV-B2	Air-water	0.353	0.66	0.34	0.128
Gerzork *et al.*(2001)* Peroxide	*T* = 0.29 m *H/T* =1:1	6RT 6SRGT dual 6RT	Air-water Air-0.2m Na_2SO_4	0.391 0.656	0.607 0.790	0.360 0.349	0.133 0.231

Table 2-15: Compilation of $k_L a$ correlations for oxygen transfer to water and electrolyte solutions.

2.8.4.1 Effect of Temperature on k_La

Temperature has been found to affect the mass transfer factor k_La. The correction equations from various reference sources are in Table 2-16.

Reference Source	System	Correction equation
Bewtra *et al.* (1970)	Air-water in aeration tank at various aeration rates 10°-30°C in 2.5°C steps	$k_La = (k_La)_{20}1.0192^{(T-20)}$
Smith *et al.* (1977)	0.178m³ stirred tank agitated by D=T/3 Rushton turbine. Two speeds and two gassing rates. Temperature range 8°-36°C in approx. 1°C increments.	
	General – for low viscosity fluids	$\frac{k_La\mu}{(T+273)} = const.$
	Air-water	$(k_La)_{20} = \frac{100(k_La)_\theta}{100+2.665(T-20)}$
	Air electrolytes	$(k_La)_{20} = \frac{100(k_La)_\theta}{100+2.609(T-20)}$
Jackson and Shen (1978)	Various air rates in 1.8m vessel at depth of 13m. No mechanical agitation.	$k_La = (k_La)_{20}1.020^{(T-20)}$

Table 2-16: Effect of temperature on k_La for low viscosity fluids, where T is temperature in degrees Celsius.

For the general (low viscosity fluid) correlation of Smith *et al.* (1977), note the similarity to the effect of temperature on diffusion for low viscosity fluids given by the Stokes-Einstien relationship for molecular diffusivity (Perry, 5th edit. 3-234),

$$\frac{D_L\mu}{(T+273)} = \text{constant} \qquad (2.158)$$

As for a pure fluid, "a" is not likely to be effected much by a small change in temperature, so this suggests that k_L is proportional to D_L as predicted by the film theory. Note that this relationship may not hold when surfactants are used. For instance with PPG there is a large effect of temperature on the gas-liquid hold-up and interfacial area, which increases as temperature is reduced. Therefore, dropping the temperature decreases k_L but increases "a" so the total effect is unpredictable.

The equation of Jackson and Shen (1978) reportedly fits the Stokes-Einstien relationship in conjunction with the surface renewal model. Jackson and Shen used both a transient method and the sulphite oxidation method for k_La estimation but do not make it clear which was used for the temperature work. They cite Eckenfelder and Ford (1968) as giving, $k_La = (k_La)_{20}\vartheta^{(T-20)}$ with the value of the temperature coefficient ϑ, for an impeller-sparger combination, varying from 1.016 to 1.037.

2.8.4.2 Effect of Viscosity on k_La

The effect of viscosity on gas-liquid mass transfer is complex as it alters both the liquid-side mass transfer coefficient k_L and the interfacial area. Increasing viscosity generally lowers the mass transfer rate, although initially it has been found to increase k_La, probably due to coalescence suppression, Hickman (1985). It has been found that the k_La data can be correlated for viscosity by adding a liquid viscosity term as shown below,

$$k_La = k(P/V)^a v_S^{\ b} \mu^c \qquad (2.159)$$

Some literature values the viscosity power law indices "c" are given in Table 2-17. These indices range from –0.43 to –1.17

*Reference Source	Method	System	Index on viscosity
Cooke *et al.*(1988)	Transient 2-probe, Steady-state Peroxide.	T=0.29m and 1.83m $H=T$, single (various type) agitators. $H=3T$, in 0.29m vessel, various triple agitator combinations. Paper fibre suspensions, fermentation culture and CMC.	-1.0
Hickman (1988)	Peroxide, pseudo-steady-state	T=0.6m, $H=T$, 6RT. CMC solutions	-0.6
Nocentini *et al.* (1993)	Transient	Multiple 6RT (3 and 4). Water-glycerol	-1.17
John (1997)	Steady-state	0.75m vessel, $H=2T$ with 2- independently driven impellers, either dual 6RT or lower 6RT with upper Scaba 3SHP1. Fluids air-A. Niger fermentation broth	-0.43

Table 2-17: A selection of literature indices for viscosity found in the fitted equation, $k_L a = k(P/V)^a v_S^{\ b} \mu^c$

Cooke *et al.* (1988) reasoned that for shear thinning fluids, a viscosity index of (-1) implied an effect of agitator power number, agitator D/T and scale on $k_L a$, assuming similar proportionality constants (k_S) in the Metzner and Otto (1957) relationship. This suggests at a given D, and specific energy input, low power number agitators would give higher $k_L a$ providing that cavern formation does not occur. They also noted that $k_L a$ halved at equal (P/V) and v_S on scale-up from a 0.29 m to a 1.83 m vessel at geometric similarity in 0.4% CMC solution. This was in agreement with prediction. Buckland *et al.* (1988)

confirms an improvement in k_La in mycelia fermentation after retrofitting to larger, lower power number Prochem agitators.

2.8.4.3 Effect of Solids on k_La

There are three mechanisms by which solids are claimed to effect gas-liquid mass transfer;

I. A viscosity effect – due to turbulence damping by the solids

II. In the heterogeneous regime, solids supplant small bubbles in the dense-phase. This must affect gas-liquid mass transfer.

III. An interface effect for very tiny active particles acting at the interface to enhance k_L.

Joosten *et al.* (1977) examined the effect of particles size and concentration on the relative viscosity of the dispersion and the gas-liquid mass transfer k_La. Measurements were made using a dynamic method by stripping helium from kerosene with nitrogen gas. The measurement technique used a Cathrometer coupled to a fast response recorder to measure the transient helium concentration of the off-gas from a small mechanically stirred tank.

The data are presented for constant P/V (1.5 kW/m^3) and superficial gas velocity (2.5 cm/s) as plots of k_La versus relative viscosity and k_La versus volume % solids for a range of solids and particle size fractions. The k_La remained steady (at approximately 0.2 s^{-1}) until a relative viscosity of 4 or a solids concentration of 20% by volume, from which point it fell rapidly with increasing solids concentration or relative viscosity. The fall off was quicker with decreasing solids density and particle size. The mass transfer factor for the smallest and lightest particles (polypropylene, size range 53 to105 microns) dropped by an order of magnitude (to a value of 0.02 s^{-1}) at a relative viscosity around 30 and a solids concentration around 36%. It was noted that at high solids concentration, gas holdup is low, with large gas bubbles.

The effects noted do not seem to tally with either relative viscosity or solids concentration as being the primary variable as neither accounts for size and density variations It is likely from remarks about gas-liquid hold-up that mechanism II is the principal driver.

Chapman *et al.*, Part IV (1983) report similar effect of solids on air-water, gas-liquid mass transfer. They report no effect up to 3% by weight solids and a considerable effect at 20% by weight glass ballotini in air-water (considerably less by volume). The effect shown depends on P/V and gassing rate, increasing with an increase of either of these parameters. The authors suggest this may be due to turbulence damping but again, in consideration of the fact that it is P/V and v_S sensitive, the major effect probably occurs when the total volume fraction of gas and solids saturates the dense phase and the solids start to displace gas from this phase. That is mechanism II above.

Very small quantities of tiny surface-active solids (such as activated carbon black) have been reported to enhance mass transfer due to interface effects. These effects have been reported for example by Kars *et al.* (1979) and by Alper *et al.* (1980).

2.8.5 Gas-liquid Hold-up Correlations

It is common to correlate gas-liquid hold-up in a similar way to mass transfer, that is,

$$\varepsilon_G = \text{constant} \times \left(\frac{P}{V_L} \right)^a v_S^b \tag{2.160}$$

where,

$$\varepsilon_G = \left(\frac{V_L}{V_L + V_G} \right) \tag{2.161}$$

The above type of correlation is sensitive to agitator hydrodynamic regimes (see section 2.3.1) and also bubble regimes (see section 2.3.2). As with mass transfer some workers have included the gas expansion power in P, either using the isothermal gas expansion expression,

$$P_Q = \frac{Q_G RT}{(RMM)\ln(p_S / p_O)} \tag{2.161}$$

where RMM is the relative molecular mass and p_S and p_O are the pressure at the sparger and outlet respectively or alternatively as the gas potential energy given by equation (2.113). Both these methods yield very similar values of P_Q. It is important to determine whether this has been done before comparing correlations.

One might expect the hold-up behaviour to be different under flooded, loaded and completely dispersed conditions. It would also be foolish to apply a correlation of this type across the transition from the homogeneous to the heterogeneous regime, as the hold-up trends are totally different in the two regimes (section 2.3.2).

Most of the literature results have been measured on a small scale at superficial gas velocities that relate to the bubble or homogeneous regime. Scale-up may well involve operation in the heterogeneous regime as scale-up at geometric similarity and constant volumetric gas demand inevitably results in higher superficial gas velocities. These means that correlations need to be treated with caution to ensure they apply to the design conditions. The electrolyte correlation line of Smith *et al* (1978) clearly shows a marked deviation from linearity at high gas hold-up indicating the transition to heterogeneous flow behaviour.

Section 2.8.3.1 discussed how increased pressure effected interfacial area and gas-hold-up by increasing the critical superficial gas velocity for the transition to heterogeneous flow thereby increasing the dense phase hold-up.

Some literature correlations on the bases of equation (2.160) for air-water are shown in Table 2-18. These references were tested against as standard (std)

case (within the confines of the original correlation) and the agreement is sufficiently good for first approximation design applications and to establish possible trends.

Literature Source	System	Constant in eq (2.160)	a	b	Predict ε_G std*
Smith *et al.* (1978)	RT v_S 0.005 to 0.05 m/s ε_T 1 to 5 W/kg T=0.91m and 1.83 m	0.559**	0.48	0.4	0.104
Chapman (1981)	MFU, MFD, RT D=T/4 and D=T/2 v_S up to 0.019 m/s ε_T 0.2 to 2 W/kg T = 0.56 m	1.79	0.31	0.67	0.107
Bujalski *et al.* (1988)	MFU, MFD, RT v_S up to 0.048 m/s ε_T 0.2 to 3 W/kg T = 0.29, 0.45, 0.61 and 1.83 m	2.11	0.326	0.776	0.081

Table 2-18: Some air-water literature correlations for gas-liquid hold-up in stirred tanks.

Notes: Fractional gas hold-up with P/V as specific gassed shaft power in W/kg. The std* comparisons are made at ε_T = 1 W/kg and v_S = 0.015 m/s (that is within bounds of all the correlations used). ** The constant is estimated from Figure 11 of that reference.

The change in the fluid can have a big effect on hold-up as will viscosity. Smith *et al.* (1978) report the same values for the constants a, b in electrolytes but a much higher proportionality constant. When a viscosity term is added the indices on viscosity varies from -0.17 for Rushton turbines in CMC solution by Dawson (1992) to -0.42 for a range of agitators in paper fibre suspensions, fermentation culture and CMC solution according Cooke *et al.* (1988).

2.9 Reaction Kinetics

Knowledge of the rate processes are important in order to make a sensible choice of equipment for the process and enable processes to run at an optimum rate (ideally to allow the chemistry to operate at its natural rate).

In some instances the rate processes and the chemical kinetics are not fully understood and the first step is to try to determine the appropriate rate data.

Some aspects of gas-liquid kinetics were discussed in earlier sections. In section 2.5.4 the importance of micro mixing on product distribution for competing reactions was discussed and the Damkohler number (the ratio of the time constants for diffusion/reaction) for assessing whether micro mixing will influence the process was introduced.

In section 2.8.3.4 the theory of gas-liquid reactions was introduced. The Hatta number (ratio of the time constants for diffusion/reaction)$^{1/2}$ can be used to determine the interfacial conditions, whether reaction dominated with very slow reactions (or high $k_L a$); mass transfer dominated with reaction in the bulk; enhanced mass transfer with reaction in the film or, for very fast reactions, at the interface.

Middleton, Chapter 15, in Harnby *et al.* (1997) gives a useful table showing the various regimes for isothermal reactions. This is reproduced as Table 2-19.

Middleton (1997) points out some of the salient features of this table:

Regime I: "a" is unimportant providing it is adequate but high gas-liquid hold-up is desirable so a bubble column reactor is suggested.

Regimes II, IV or V; need high "a" and k_L so a stirred tank reactor may well be appropriate if a more intense device cannot better match the chemical rate process due to other limitations such as heat transfer or off-gas handling.

Regime III; In this regime all the liquid should ideally be in the film suggesting a thin film device such as a packed column should be used. Enhancement of k_L in this regime may also make the gas side resistance significant and this needs to be checked.

Exothermic reactions that occur in the film or interface can make a big difference to the enhancement factor. The rise in temperature near the film, affect the gas solubility (decreasing the reaction rate) whilst increasing the reaction rate due the Arrhenius effect. The combination of these two effects can lead to a multiplicity of steady-states as illustrated by Mann *et al.* (1977) for SO_3 reacting with dodecylbenzene. Boiling and exothermic reactions also increase the risk of foaming.

Middleton (1997) highlights that the ideal design arises from measurement of chemical kinetics unhindered by mixing or mass transfer effects. That is operation in regime I. For gas-liquid reactions this is not possible unless the gas can be provided pre-dissolved in a liquid solvent (under high pressure). Then there are rapid mixers that will allow us to measure kinetics of reaction rates above 10 milliseconds.

A small continuous stirred tank reactor *CSTR* can be used to measure reaction rates of 10s or longer without mass transfer effects operating within regime I. For faster reactions, provided the reaction scheme can be simplified to one of known order, the small *CSTR* can be used to infer reaction rate constants for fast reactions by utilization of regime III and IV rate expressions in Table 2-18. Middleton (1997) suggests this may be done as follows:

Change C_A^* by altering pressure or solvent concentration to distinguish between the regime unless $n = 1$. If $n = 1$, the agitator speed should be changed. If this has no effect then operation in regime I is indicated. If agitation has no effect, the temperature should be increased by say *10°C*. If the rate increases by a factor around *1.2* to *1.3* regime II is indicated but if it increases by *2* to *5* times, regime III is indicated. Middleton suggests that this experiment decides whether the effect of agitator speed was only on "*a*" *or* $k_L a$.

A very small temperature effect may indicate gas-side resistance dominating especially if the gas solubility is high or the gas is dilute.

This sort of information can be used for scale-up.

	REGIME	CONDITIONS	IMPORTANT VARIABLES	CONCENTRATION PROFILES
I	*Kinetic control* Slow reaction	$\sqrt{\frac{t_D}{t_R}} < 0.02$	Rate α ϵ_L α k_{nm} α $(C^\circ_{AL})^n$ α $(C_{BL})^m$ Independent of a (if a adequate) Independent of k_L	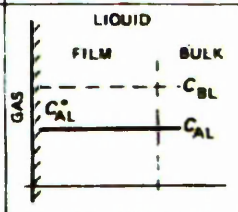
II	*Diffusion control* Moderately fast reaction in bulk of liquid $C_{AL} \simeq 0$	$0.02 < \sqrt{\frac{t_D}{t_R}} < 2$ Design so that $\frac{\epsilon_L}{a} > 100\,\frac{D_{AL}}{k_L}$	Rate α a α k_L α C°_{AL} Independent of k_{nm} Independent of ϵ_L (if ϵ_L adequate)	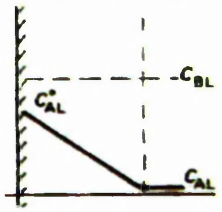
III	*Fast reaction* Reaction in film $C_{AL} \simeq 0$ (pseudo first order in A)	$2 < \sqrt{\frac{t_D}{t_R}} < \frac{C_{BL}}{q\,C^\circ_{AL}}$ $C_{BL} \gg C^\circ_{AL}$	Rate α a α $\sqrt{k_{nm}}^{(n+1)/2}$ α $\left(C^\circ_{AL}\right)$ Independent of k_L Independent of ϵ_L	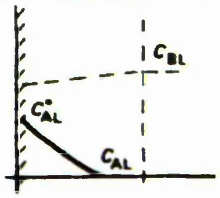
IV	*Very fast reaction* General case of III	$2 < \sqrt{\frac{t_D}{t_R}}$ $C_{BL} \sim C^\circ_{AL}$	Rate α a depends on $k_L, k_{nm}, C^\circ_{AL}, C_{BL}$ Independent of ϵ_L	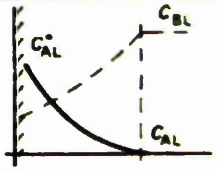
V	*Instantaneous reaction* Reaction 'at interface'. Controlled by transfer of B to interface from bulk. $J \alpha k_L a$	$\sqrt{\frac{t_D}{t_R}} \gg \frac{C_{BL}}{q\,C^\circ_{AL}}$	Rate α a α k_L Independent of C°_{AL} Independent of k_{nm} Independent of ϵ_L	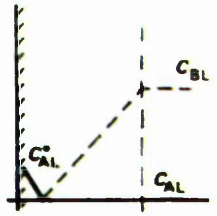

Table 2-19: Various gas-liquid mass transfer regimes with isothermal reaction. Reproduced from Middleton (1997).

2.10 Scale-up or Scale-down.

Principles of similarities are used. These are dynamic, geometric and kinematic.

Dynamic similarity requires that on two different scales, all relevant forces ratios must have a common ratio. For a stirred vessel the most important force is that input by the mixer, which is an inertial force. Three apposing forces; viscosity, gravity and surface tension resist this. For scale up with the same fluid at the same conditions then density and surface tension remain constant with scale-up so it is apparent the only two of these force ratios can be equal on scale up.

Geometric similarity is maintained when all relevant dimensions are similar and have a common ratio. Geometric ratios should ideally be kept constant on scale-up as illustrated in Figure 2-56.

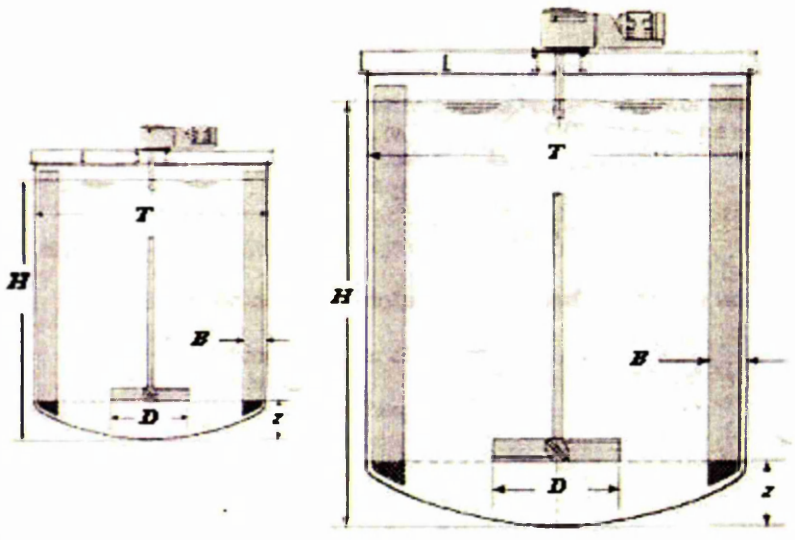

Figure 2-56: Scale-up maintaining geometric similarity. Important geometric ratios are kept constant.

This is the easiest to achieve but in practice is not always adhered to because of process limitations. For instance heat transfer limitations may require a higher aspect ratio *(H/T)* in order to satisfy heat transfer area requirements since scale-up at geometric ratio decreases the surface area to volume ratio. All techniques of scale-up will require some correction if geometric similarity is not maintained.

Kinematic similarity is satisfied when on two scales all velocities at equal locations have a common ratio. Many experimenters have shown that for a given agitator, the hydrodynamics of a given impeller is independent of scale, diameter and speed when normalized with either tip speed (example Costes and Couderc (1982)), or the maximum mean velocity, Cooper and Wolf (1968) and Kovács (2001). Thus kinematic similarity is maintained for scale-up at constant tip speed whilst maintaining geometric similarity.

Concepts of geometric and dynamic similarity lead us naturally to the dimensionless groups defined in section 2.2.1.

Common scale-up relations that have been recommended in the literature are:

- Scale-up at constant power per unit volume.
- Scale-up at constant tip speed.
- Scale-up at constant torque per unit volume.
- Scale-up using dimensionless numbers.

These scaling rules when used with appropriate scaling factors defined from experimentation allow reliable scale-up in most instances.

Some comments on the above scaling rules are:

When the design data is in the form of dimensionless number correlation then the use of dimensionless numbers for scaling is suggested.

Power per unit volume is often recommended for drop size maintenance, gas-liquid mass-transfer or particle size reduction.

Scale-up at constant torque per unit volume is the same as constant tip speed if geometric similarity is maintained. It gives an extra degree of flexibility to

constant tip speed when D/T is varied. Some agitator manufacturers favour this method, as torque is a major cost driver.

Smit (1994) suggests that the general method of scaling up stirred vessels, by use of a one-dimensional approach, fails in the case of complex mixing processes, where multiple mixing-demands are present. He gave an example of a fast coalescing liquid-liquid dispersion which needed a two dimensional approach to successfully scale down the process so that it could be studied on the small scale. Scale-down of the process at geometric similarity and constant power per unit volume did not exhibit the same coalescence behaviour of the full-scale plant. This was because the circulation time was too short for coalescence to occur. In order to make the circulation time and the P/V equal on both scales he had to alter D/T giving equal tip speed as well as equal P/V on both scales. This gave a successful scale-down with similar behaviour on the two scales.

2.10.1 Other Aspects of Scale

Some aspects of scale include:

The average shear rate in an agitated vessel depends on N and not D. See equation (2.2). Scale up at constant ε_T and geometric similarity, reduces N on scale-up and hence the average shear. This could reduce $k_L a$ in shear thinning fluids (Cooke *et al.* (1988)). It has been suggested that scale-up or down can be achieved by altering D/T to obtain the same relationship between flow and shear on the two scales.

For particle size reduction or drop size maintenance, it is probably the maximum shear rate that is important. According to van't Riet (1975) this occurs is the impeller vortex region and is proportional to N. This leads, for scale-up at constant ε_T and geometric similarity, to maximum shear is proportional to $T^{-0.76}$ according to Middleton (1997). However as discussed in section 2.2.4.1, Oldshue (1983) claims the maximum shear rate scales with tip

speed and the experimental data on reduction in drop size found in the literature for scale-up at constant ε_T and geometric similarity would seem to support this point of view.

Heat transfer area reduces on scale-up at geometric similarity.

It is unlikely that liquid mixing can be maintained on scale-up as this requires constant N at geometric similarity and this would be prohibitive on power.

Agitator Reynolds is proportional to D^2 therefore Reynolds number increases with scale-up. Scale-down is particularly important for viscous fluids since this may result in operating in a different hydrodynamic regime, for example from fully turbulent to transitional. Conversely problems experienced on the small scale due to viscous effects may disappear on full scale because the fluid becomes turbulent.

Gas residence time and residence time distribution are likely to alter with scale. For scale-up at constant VVM (most usual) then v_s scales directly with T. However ε_G increases with v_s so the gas residence time increases. The gas phase is likely to be more plug flow on scale-up.

Many other aspects of scale are commented on in the body of this review.

2.10.2 Choice of Equipment for Gas-liquid Contacting

Although a mechanically stirred vessel may be the right choice at a small scale it is not always the case at large scale, since as previously discussed the superficial gas velocity increases with scale-up at constant P/V and geometric similarity. The relationship between specific gas power ($P_Q / \rho_L V_L = Q_G \rho_L g(H_L - c_S)/\rho_L V_L$) and superficial gas velocity ($v_S = 4Q_G/\pi T^2$) is apparent. For a standard vessel ($V_L = \pi T^2 H_L/4$), therefore (providing $c_S = 0$, that is gas sparged in at the bottom of the base),

$$\frac{P_Q}{\rho V_L} = gv_S \tag{2.161}$$

This means that if the superficial gas velocity is say 0.25 m/s (a not uncommon value on a large scale) then approximately 2.5 W/kg is input by the gas. This is often more than the impellor power. Hence, on this scale a bubble column may well be a more sensible choice.

2.11 Concluding Remarks about the Literature Review.

The literature review is by no means exhaustive. However, it does attempt to cover the criteria set out in the introduction. There are several standard texts that cover some aspects in more detail. For mixing Uhl and Gray, parts I and II, (1966) and 1967), Nagata, (1975), Oldshue, (1983), Tatterson, (1991) and Harnby *et al.* (1997) are recommended, who all bring their own perspective to the subject.

Where possible and in the great majority of cases I have quoted from the original reference. With some of the older references my knowledge is second-hand. For instance I have not read Kolmogov, (1941) and (1949) and owe much of my understanding of turbulence theory to standard textbooks and Nienow (1998). I confess also I have not read Stokes, (1880) though it seemed a shame not to include the reference and one day may be I will get to read it. Similarly the poem by Lewis Richardson (1920) is second hand from Middleton (2002) via the www.

Where equations have been involved, I have tried to assess their applicability and implications for design or scale-up. Where there was a conflict in the literature, for example whether the maximum shear rate scales with N or ND I have tried to bring in independent literature to make a judgement on which is more likely. There is a lot of conflicting literature and I have not cited all I have read since other sources have already subjected them to critical review.

Chapter 3 Experimental Equipment and Techniques

3.1 Equipment

The stirred tank equipment consists of three state of the art mixing rigs made from Perspex with dimensions as detailed in Table 3-1. Pictures of these rigs are shown in Figure 3-1 to Figure 3-4.

Diameter of cylindrical section	Height of cylindrical section
28.6 cm (nominal 1ft)	61 cm (2ft) and 122 cm (4ft)
61.0 cm (2ft)	152 cm (5ft)
91.4 cm (3ft)	137 cm (4.5ft)

Table 3-1: Tank dimensions

The cylindrical sections are fitted inside square jackets through which water can be circulated for temperature control. The vessels are constructed from Perspex and the square jackets provide distortion free viewing windows for flow visualization.

Variable speed motors drive the shafts with accurate speed control over a very wide range. Shaft rotational speeds are monitored using ferro-magnetic proximity sensors coupled to COMPACT MICRO 48 tachometers. Shaft powers are measured using torque strain gauges bonded to the shafts. These strain gauges are wired to ASTECH strain gauge bridges fitted with telemetry readout connected to a LABVIEW data acquisition unit.

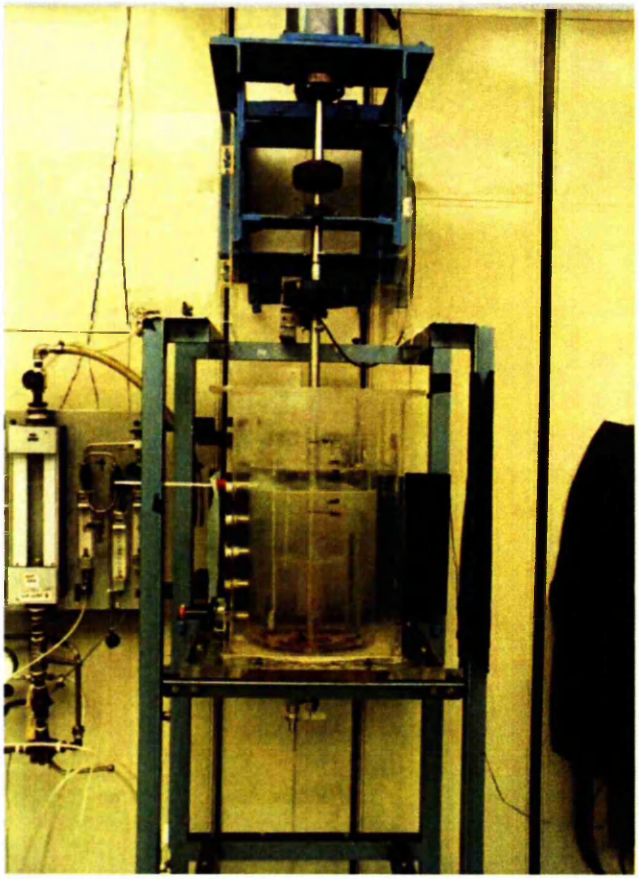

Figure 3-1: The 0.286 m diameter stirred tank rig

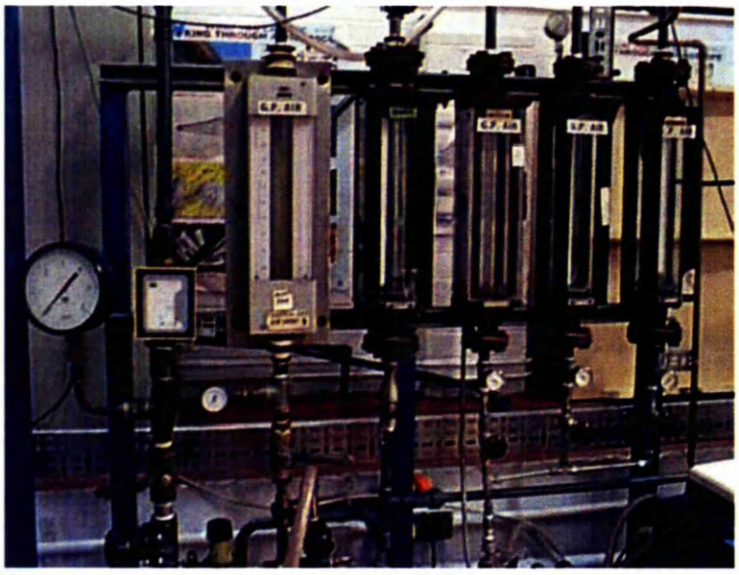

Figure 3-2: Rotameter feeds to 0.286 m and 0.61 m diameter vessels

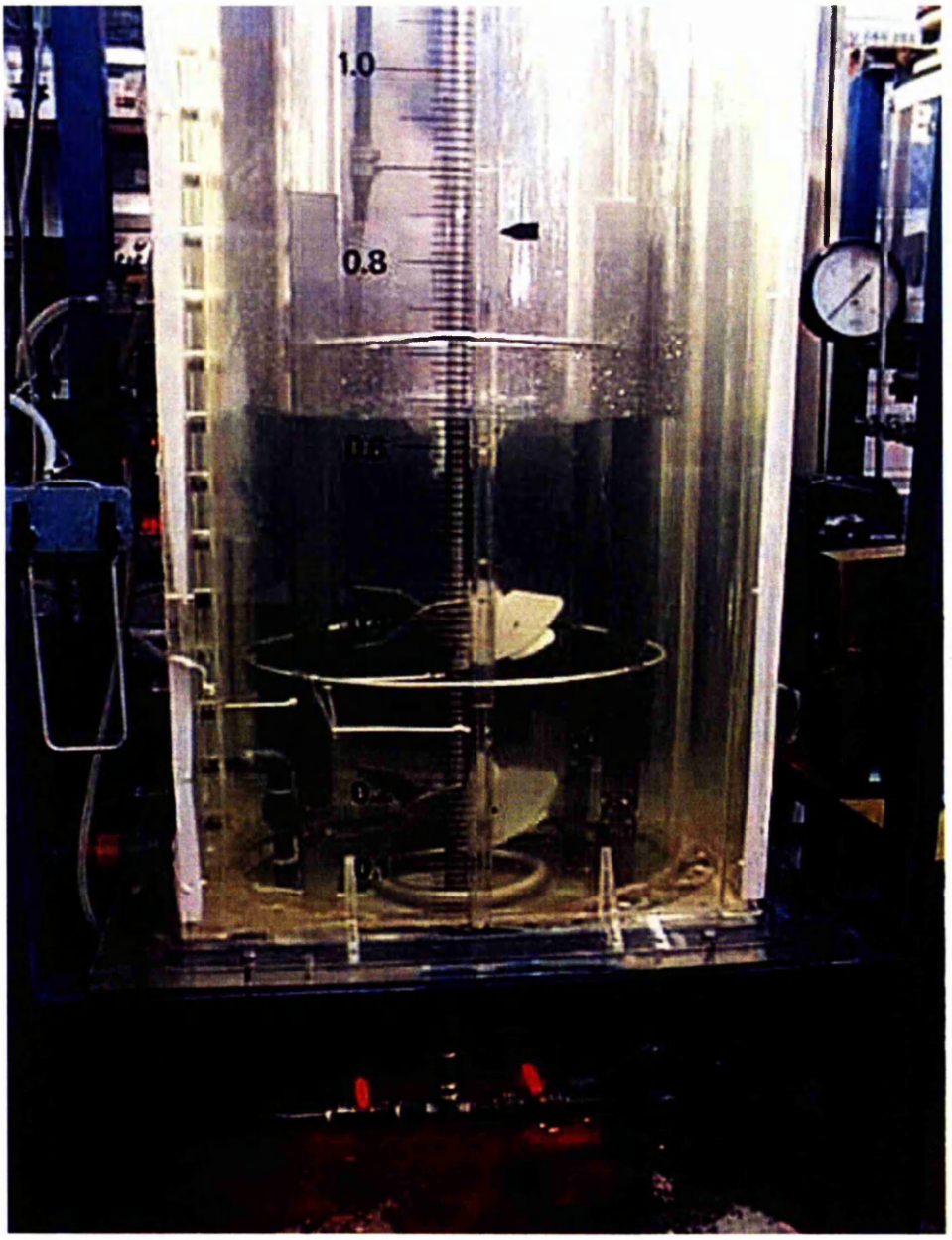

Figure 3-3: The 0.61 m vessel fitted with dual LIGHTNIN A345 agitators

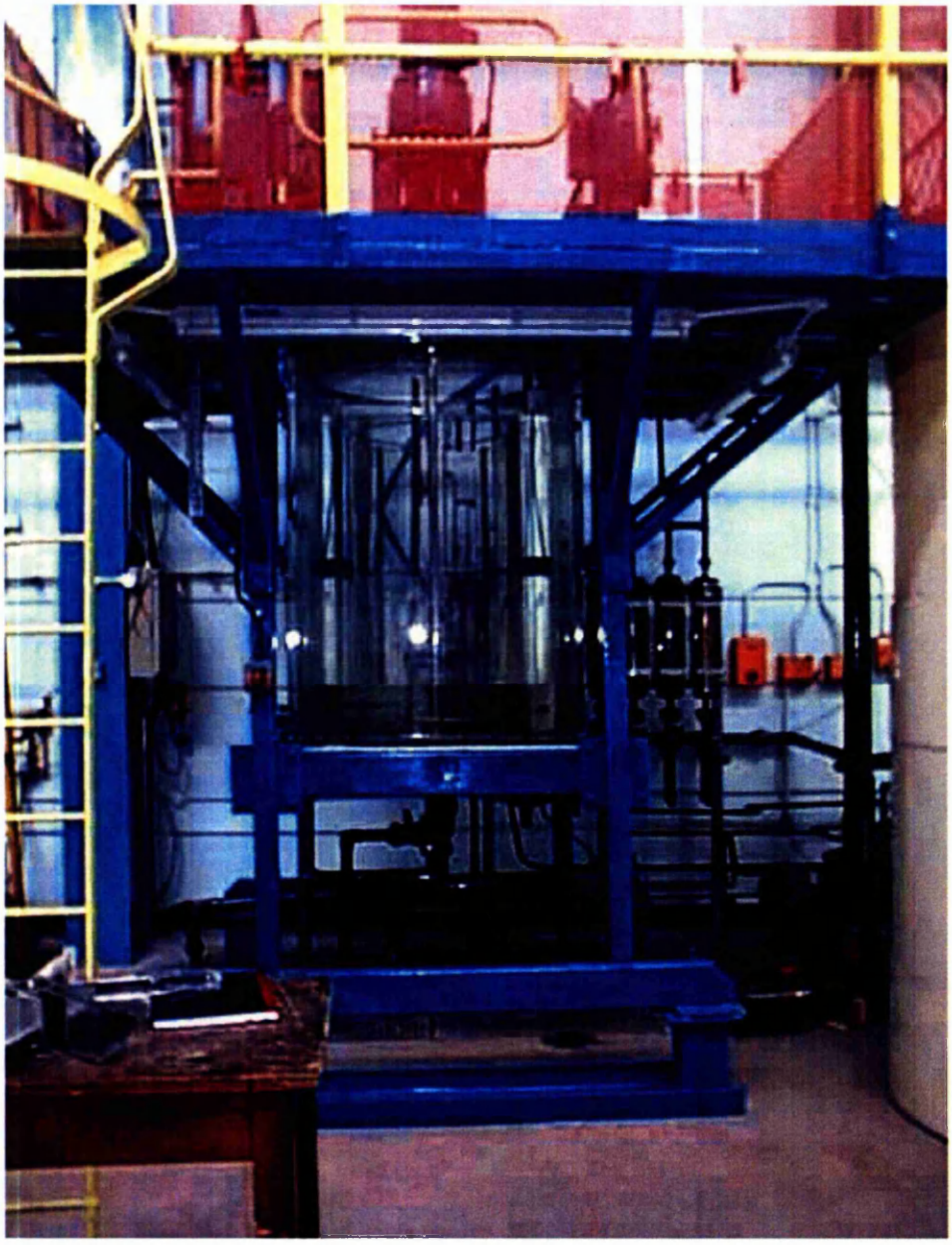

Figure 3-4: An overview of the 0.914 m diameter stirred tank equipment

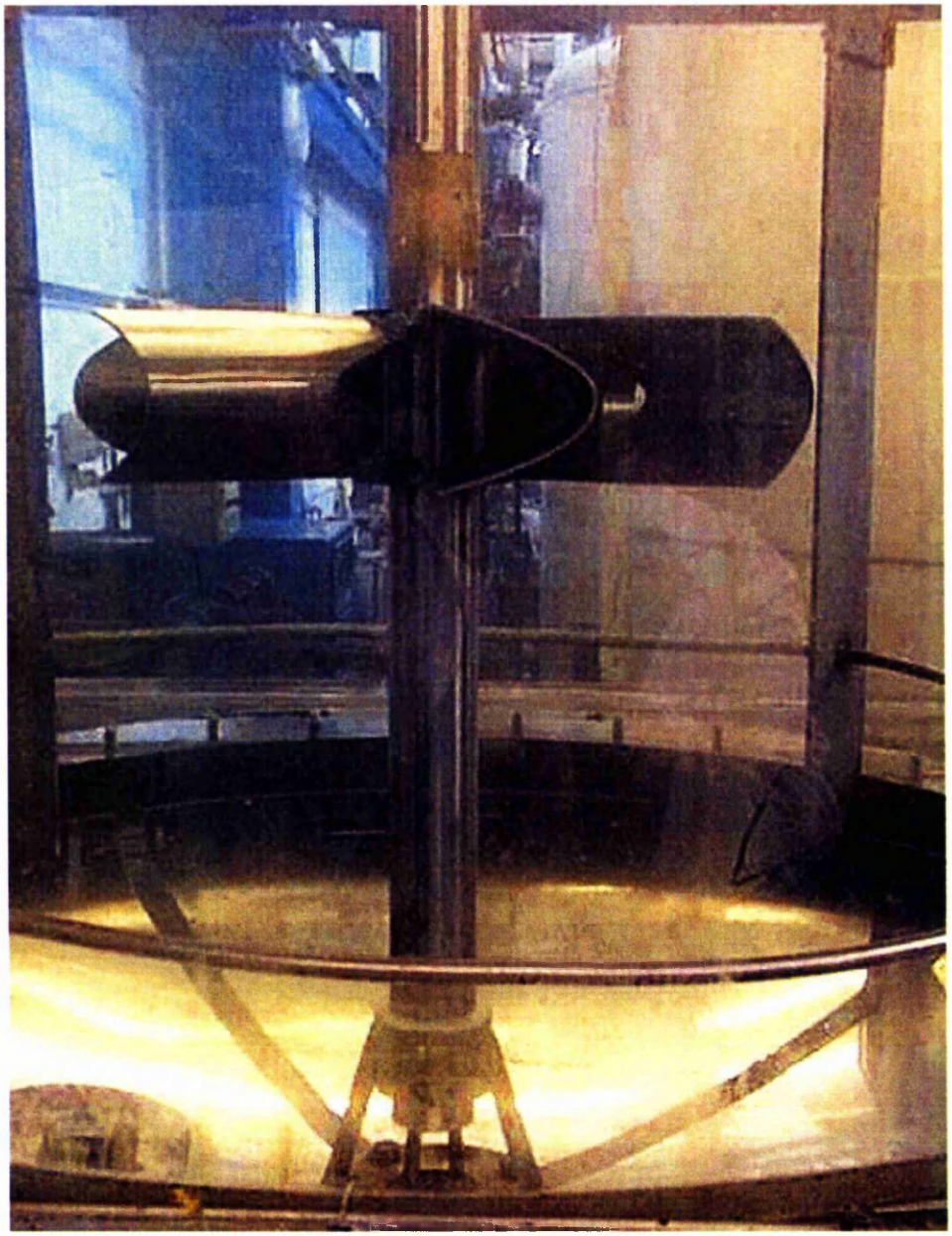

Figure 3-5: A close-up of the 0.914 m diameter vessel showing the curved blade agitator (6HBT) with shaft strain gauges above and details of bottom bearing fitted with a Teflon sleeve.

The vessels contents temperatures can be monitored using thermocouples inserted through the analysis blocks.

The analysis blocks allow other probes to be inserted for example:

Experimental Equipment and Techniques:

- Conductivity measurements (for mixing and local phase fraction measurements)
- Dissolved oxygen probes for oxygen concentration measurements that are used for gas–liquid (k_La) measurements
- Sampling probes
- Local hold-up probes

Electrical Resistance Tomography (ERT) measurements are made using specially constructed sensor baffle cages and the ITS 2000 data analyser (see Chapter 9).

The vessels are fitted with removable bases and baffles. There are choices of base types – flat, dished, hemispherical and conical.

There is a wide range of agitators. Multiple agitators on the shaft can be tested for aspect ratios (dispersion height/tank diameter) of up to 3 to 1.

Slit lighting and/or flow followers can be used to aid flow visualisation.

3.2 Techniques

Several techniques are used and these are described in the following sections:

3.2.1 Flow Visualisation

The colour change tests were done using glacial acetic acid and sodium hydroxide solution with phenolphthalein (pp) indicator to effect a colour change induced by a pH shift with a 10% stoichiometric excess of acid or base (determined by titration) added to the vessel. The method was scaled to the vessel size. For example, for 150 litres of water in the 0.61 m vessel, 10 ml of indicator and 2 ml of glacial acetic acid were used to acidify the vessel. This gave a clear water solution at around pH 4.0. The amount of sodium

hydroxide solution required to provide 10% excess was calculated. This was then either injected at the feed location via an injection loop or added the surface dependent on whether it was feed mixing or bulk mixing that was being evaluated. When fully mixed this turned the contents pink with a pH of around 10. Injecting approximately 2.4 ml of glacial acetic acid to turn the solution clear then reversed the process. The colour changes were recorded on video.

3.2.2 Shaft Power Measurement

Shaft torque (M) was measured using the shaft strain gauges coupled to the ASTECH radio telemetry system. Data acquisition is at one-second intervals using the LABVIEW data acquisition package. At least 60 data points are used to evaluate each point. Details of the data treatment and strain gauge calibration are given in Appendix 1. Shaft power (P_S) was calculated from:

$$P_S = 2\pi NM \tag{3.1}$$

Agitator Power numbers (P_O) were calculated from:

$$P_O = \frac{P_S}{\rho N^3 D^5} \tag{3.2}$$

3.2.3 Overall Gas-Liquid Hold-up

This was estimated by the level rise when gas was injected. The gas-liquid hold-up was determined by measuring the heights of aerated and unaerated levels. Levels were estimated from either time averaged calibrated video records or using an ultrasonic hold-up probe. Details of calibrations are given in Appendix 2. Volumes are calculated ignoring the volume of the internals

(shaft, agitators and baffles). Thus the percentage gas hold-up is calculated from the calculated volumes estimated from the levels according to:

$$\varepsilon_G = 100 \times \left(\frac{V_G}{V_D} \right) \tag{3.3}$$

where V_G and V_D are the gas and dispersion volumes respectively.

3.2.4 Local Gas-Liquid Hold-up

Local hold-up fractions are measured using a hold up probe. This measures local hold-ups of non-conducting particles in a conducting fluid. These can be gaseous or solid. This is a rod type conductivity probe, consisting of two 1.5 mm copper rods; 15 mm long with centres 15 mm apart. These rods are imbedded in a non-conducting block and attached to a hollow stainless steel support rod through which the connecting wires are fed. This is attached to a 2 m stainless extension tube, which is fed down the vessel allowing an axial scan to be done. A picture of the gas hold-up probe is shown in Figure 3-6.

This dimensionless conductivity output of this type of probe was found to be nearly linear with volumetric hold-up between air (0%) and tap water (100%). Assuming a linear relationship slightly overestimates the volume fraction of the non-conducting phase. When corrected using the Maxwell (1881) equation, simplified using the assumption that the dispersed phase is non-conducting, there is excellent agreement between the integration of the local gas hold-up values measured by the probe and the overall hold-up measured by the total volume increase. The simplified Maxwell equation is:

$$\frac{\Sigma_D}{\Sigma_L} = \frac{2\varepsilon_L}{3 - \varepsilon_L} \tag{3.4}$$

where Σ is conductivity and subscripts D and L refer to the mean conductivity of the dispersion and the pure liquid respectively. ε_L is the liquid volume

fraction. In practice dimensionless conductance is used. This is the conductance of the dispersion over the conductance of the liquid alone. The Bruggeman (1935) equation was also tested but discarded as it overcorrects at high dispersed phase fractions. It is noted that the original theories were developed assuming volume fractions of dispersed phase up to about 20% and homogeneous conditions. In this work the local values are averaged over time to approach a homogeneous value.

This technique will not work with demineralised water. Where this was being used, local hold-ups were measured after the mixing experiments (salt additions) to ensure the water was conductive.

The probe is constructed so that it can be used in an L mode to scan under the agitators as well as in a down pointing axial mode.

The data are collected on a LABVIEW data acquisition package at a rate of 1/s for around 300 seconds for each point. The time-averaged data are then entered into a spreadsheet to evaluate the actual percentage hold-up. Graphs are drawn to show these profiles. An example of the data treatment is given in Appendix 3.

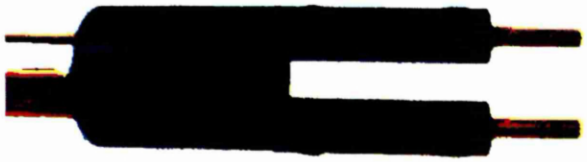

Figure 3-6: Picture of Local Hold-up Probe

3.2.5 Overall Liquid Mixing Times

The mixing time θ (where θ is a specified degree of mixing) is determined by conductivity measurements. The conductivity is linearly related to the concentration and so the measurement of the fluid conductivity gives a direct indication on the concentration of the tracer in the vessel contents, and thus indicates the amount of mixing achieved.

The mixing probes used in this work are of the Khang and Levenspiel (1976) type. A typical probe construction is shown in Figure 3-7.

These probes have several advantages: They are small in size so the sample volume is small. They have a fast response time, they are stable over a long time and they give a continuous time history of the conductivity fluctuations at the same point.

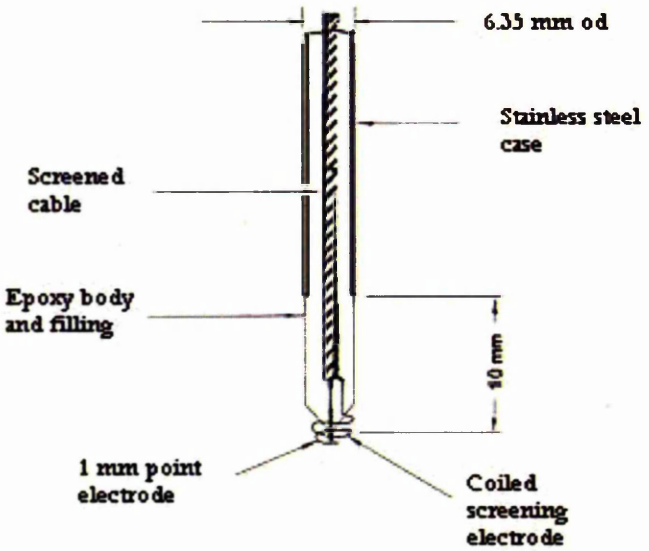

Figure 3-7: Khang and Levenspeil (1976) mixing probes used in tests

Experimental Equipment and Techniques:

The probes are used to measure the response to an addition of a conducting tracer solution (typically 25 ml of 200 g/l sodium chloride solution in 100 litre and dependent on the liquid volume to give a 0.05 g/l step change in the vessel). For overall mixing times the mixing probe is sited in the base and the tracer is added at the surface. The mixing time for a specified degree of mixing is measured from the time of addition. Up to ten mixing time experiments (a minimum of six) are carried out for each condition. These data are collected using a fast data collection routine in LABVIEW, which allows a sampling rate of up 100 times per second for up to 4 probes operated simultaneously.

The mixing data are analysed by the method described by Ruszkowski (1994), using the concept of a mixing index. A 90% mixing time is the time from addition until the last mixing index is ≥ 0.9. For this work the mixing index is the root mean square of the deviations on a 32-point moving average. The sampling rate and the total sampling time were adjusted to allow mixing index to be calculated from the variance calculated from a 32 point moving average taken over time steps that are $<<$ t (mixing), as described in section 2.5.5.3

A limited amount of data was collected for liquid mixing with tracer addition at the feed. This gave comparative data to that collected by ERT. For these runs the tracer addition was sodium hydroxide solution into a dilute acetic acid solution containing phenolphthalein indicator in order to give a simultaneous colour change experiment that was recorded on video. An example of the data analysis is given in Appendix 4.

3.2.6 Electrical Resistance Tomography (ERT) System

The ERT system used during this study was an Industrial Tomography Systems (www.itoms.com) P2000 instrument. The P2000 instrument is driven by a Microsoft Windows based software package that can be used for both measurement and data analysis. Image reconstruction was performed by linear back projection, making use of a sensitivity map. Further data and

statistical analysis features include pixel history which allows image pixels of specific interest to be monitored, for example, the region close to a feed point, bulk properties which clearly show when complete mixing has been achieved.

The ERT assembly consists of 8 rows of 16 stainless steel electrodes (128), each measuring 32 x 28 mm and terminating in 8 centronic connectors. On the 0.61 m vessel the rows are 8 cm apart designed to span an $H = T$ cylindrical section. An adjacent measurement protocol is used providing 104 individual measurements per plane and a total of 832 interrogative measures of the liquid volume using the 8 planes. Because of the special design of the model vessel, the tomography set-up needed to be an add-on unit that fitted inside the vessel with minimum interference with flow visualisation and with no interference to analysis ports and existing instrumentation. To achieve this, the tomography sensors were made to form an integral part of a specially designed baffle cage. All electrical connections were sealed internally and were made water and chemical proof. All exposed metal was minimised in order to minimise distortion of the electrical fields. In order to avoid stray emf's, caused by dissimilar metals, only stainless steel metal was used. The baffles and electrode-wire carriers were made from plastic. Three expansion rings held the baffle cage in position. Pictures of the tomography baffle cage are shown in Figure 3.9.

The P2000 instrument was obtained from ITS and I am grateful to their engineer (Gary Bolton) who provided able assistance sorting out teething problems and helped to process the data. More details are given in Chapter 9: An Electrical Resistance Tomography (ERT) System as a Diagnostic Tool.

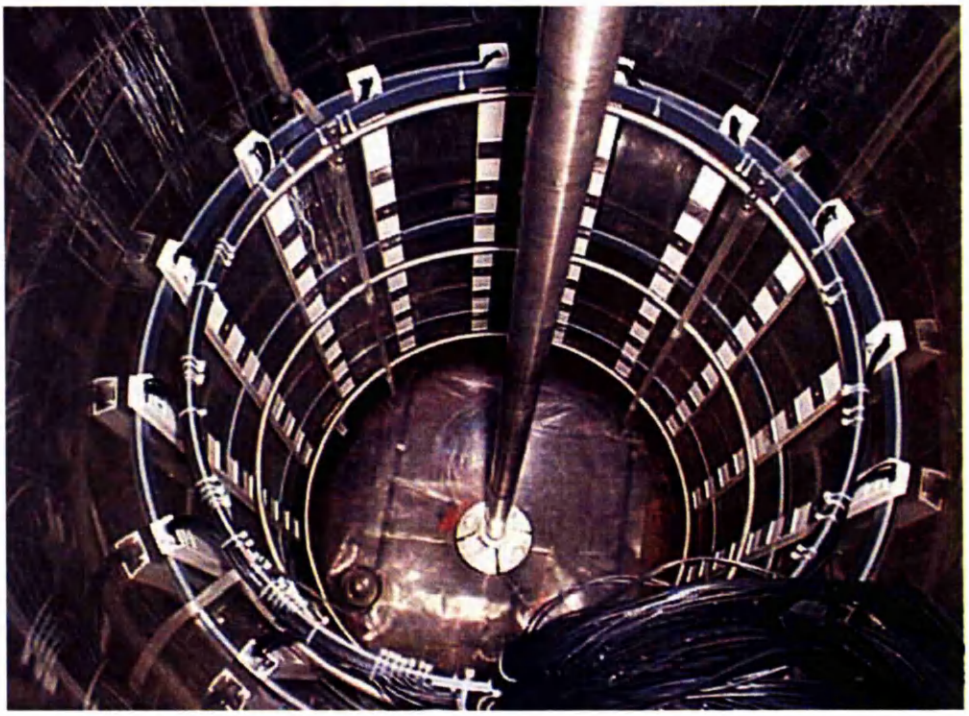

Figure 3-8: Picture of Tomography baffle cage in the 0.61 m vessel.

3.3.7 Gas-Liquid Mass Transfer k_La

The overall gas-liquid mass transfer factor k_La was estimated using the hydrogen peroxide steady-state technique described in detail by Hickman (1988), Cooke *et al.* (1991) and Vasconcelos *et al.* (1997). See also section 2.8.3.4.2 The Peroxide Technique for Pseudo Steady-state Gas-liquid Mass Transfer Measurements. ELECTROSENSE fast response polarographic dissolved oxygen tension probes (supplier Jim Young, Tel. Frodsham 09287 33800) are used to measure the liquid phase oxygen concentration. An exploded view of these is shown in Figure 3-9.

The technique briefly is as follows: As many as three DOT probes are sited flush with the inner tank wall. Normally at least two DOT probes are used, unless there is only a single agitator and separate tests had shown that the well-mixed liquid phase assumption was valid. These are zeroed and spanned in

the agitated vessel using sparged nitrogen and air for calibration. The air rate and agitation rate are set at the desired rates and the vessel contents allowed time to reach air equilibrium, as monitored by the DOT probes. The liquid is then dosed with the required amount of either CATALASE or finely divided, activated manganese dioxide catalyst dependent on the system (see section 2.8.3..4.2). A metering pump was used to feed a steady flow of hydrogen peroxide into the vessel where it is broken down by the catalyst to form oxygen and water. Placing the feed vessel onto an electronic balance and timing the addition of a measured weight with a stopwatch measures the peroxide flow. At first the oxygen accumulates in the liquid phase until it reaches a new equilibrium where the addition rate and the transfer rate to the gas phase are in balance. The new equilibrium is measured and the k_La estimated from a mass balance. When the peroxide is switched off it is checked that the air equilibrium is the same. The probes used are not automatically temperature calibrated. Hence they are calibrated for temperature and any temperature drift noted and compensated for.

When working with polypropylene glycol (PPG) systems it was found that the gas hold-up is very temperature sensitive and it is important to operate the experiments within tight temperature limits. Also PPG is oxidised by manganese dioxide so CATALASE is the best choice of catalyst for these solutions. An example k_La calculation is given in Appendix 5. The hydrogen peroxide used in these tests was BDH Ltd GPR 30% solution (assay 29% - 31%). The precise strength is determined by permanganate titration in accordance with Vogel (1961). Activated manganese dioxide was BDH Ltd precipitated Manganese (IV) oxide. Catalase was BDH Ltd , bovine liver extract, 2×10^5 units per ml.

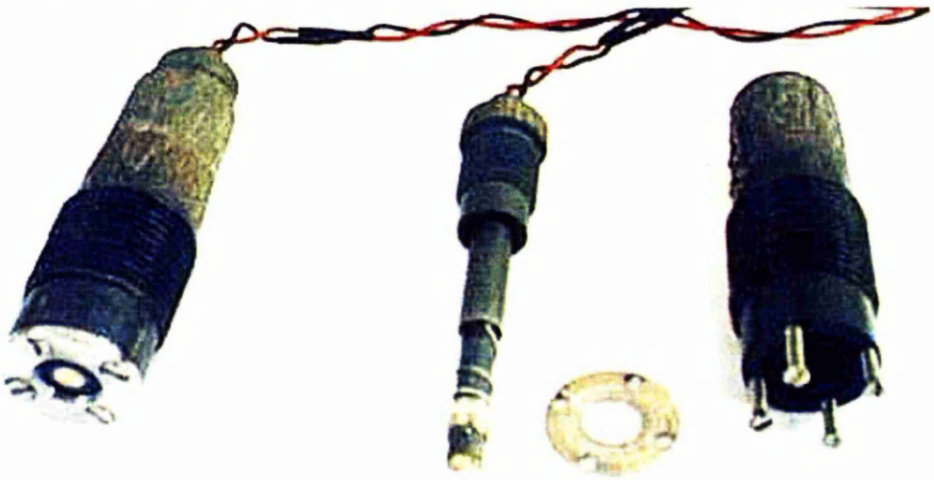

Figure 3-9: Views of the ELECTRSENSE DOT Probes. Thread on outside of the body is ¾ inch BSP to fit our standard analysis ports.

3.2.8 Viscosity Measurements

Viscosity is measured using the HAAKE Rotovisco RV3 viscometer as a function of shear rate. This is a dual range machine fitted with 50g and 500g heads. There is a range of sensors for this viscometer dependent on the application, including impeller sensors for materials containing coarse particles. Measurements and calibrations are in accordance with the manufacturers instructions. A typical calibration and result is described in Appendix 6.

Chapter 4 : Model Fluids

Apart from the studies on "real fluid" detailed in Chapter 5 most of the modelling was done with air-water. Additives were added to the water where necessary in order to mimic important properties of process fluids. Some examples are given in the following sections.

4.1 Modelling of Filamentous Fermentations

The work on modelling filamentous fermentations was reported earlier by Cooke *et al.* (1988). The filamentous fermentation culture material was found to have a yield stress with properties that were dependent on the biomass concentration. A paper fibre suspension consisting of short Celbi Eucalypt fibre (from PIRA Leatherhead) was found to be a reasonable analogue.

4.2 Modelling of Paint

Many modern paints are shear thinning and viscous. The Herschel-Bulkley model, as follows, usually describes non-drip paints:

$$\tau = \tau_y + K_{HB}\dot{\gamma}^n \qquad (4.1)$$

However, over the shear rates of interest, these (and most other paints) can be simplified to the power law model,

$$\tau = K\dot{\gamma}^n \qquad (4.2)$$

where τ is the shear stress, K is the consistency factor and $\dot{\gamma}$ is the average shear rate.

: Model Fluids:

Modelling these on a small scale using transparent analogues can be challenging, since in order to mimic the behaviour on the full-scale, the test scale should operate at the same power per unit volume, the same shear thinning behaviour and the same Reynolds number. CMC solutions made up from Hercules Powder Co, grade 7H4C, are shear thinning and a power law has been fitted for a range of concentrations of this material as listed in Table 4-1. The variation of the consistency factor K and power law indices n with CMC concentration was fitted. These fits are depicted in Figures 4-1 and 4.2 and allow us to predict these constants for any concentration of this CMC up to 1.4% by weight.

Assuming scale down at equal Reynolds number and geometric similarity give us equal power numbers on the plant and model scale then from equation (2.11) it follows that to scale at equal specific power input,

$$\frac{P}{V} \propto \rho N^3 D^2 \tag{4.3}$$

Thus for a plant mixer speed N_{PLANT} the model speed N_{MODEL} is given by,

$$N_{MODEL} = N_{PLANT}\left(\frac{\rho_{PLANT}}{\rho_{MODEL}}\right)^{1/3}\left(\frac{D_{PLANT}}{D_{MODEL}}\right)^{2/3} \tag{4.4}$$

The average shear rate of the plant mixer is estimated from the Metzner and Otto (1957) equation (2.2) $\dot{\gamma} = k_s N$. k_s are used to calculate the average plant shear rate at the plant operating speed. If a literature value for k_s is not available then for a first estimate it can be assumed it is 10 for the purpose of scale down. The plant apparent viscosity for a given power law fluid at the operational speed is then,

$$\mu_{a(PLANT)} = K(k_s N)^{n-1} \tag{4.5}$$

The plant Reynolds number is,

$$\mathrm{Re}_{a(PLANT)} = \left(\frac{\rho D^2 N}{\mu_a}\right)_{PLANT} \tag{4.6}$$

: Model Fluids:

The model apparent viscosity is then found from,

$$\mu_{a(MODEL)} = \frac{(\rho N^2 D)_{MODEL}}{\mathrm{Re}_{a(PLANT)}} \qquad (4.7)$$

Thus, knowing the required apparent viscosity, N_{MODEL} and k_s enables a match of a CMC solution that will give the required apparent viscosity at the scale conditions to meet the initial criteria of equal Reynolds number, P/V and similar power law behaviour. This approach can also be used for modelling fermentation broths.

7H4C CMC %	Measured *K*	Measured *n*	Predicted *K*	Predicted *n*
0.015	0.0031	0.92	0.0030	0.87
0.03	0.0067	0.84	0.0068	0.86
0.1	0.0249	0.83	0.0248	0.81
0.2	0.0789	0.78	0.0789	0.75
0.4	0.5	0.6	0.50	0.66
0.8	4.11	0.53	4.11	0.53
1.4	16.6	0.41	16.60	0.41

Table 4-1: Experimental data from HAAKE RV3 viscometer showing a fit to a power law

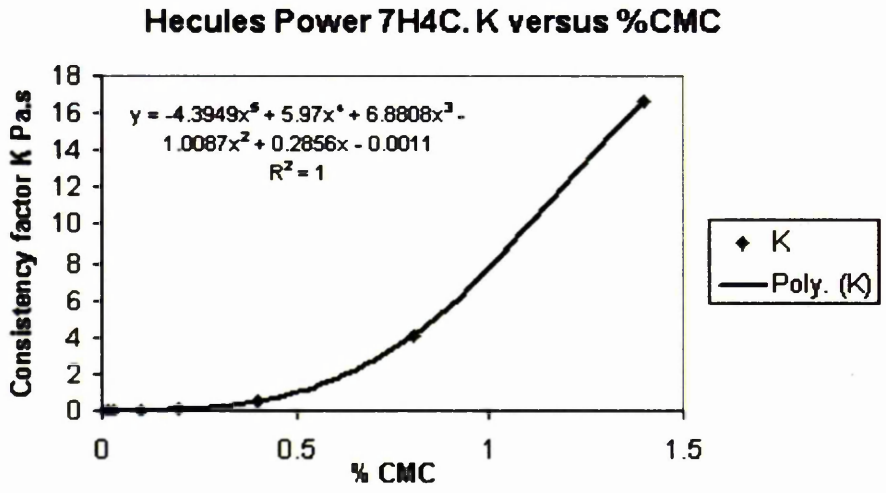

Figure 4-1: Experimentally determined consistency factors for various concentrations of CMC Hercules Powder grade 7H4C fitted to a 5th order polynomial.

: Model Fluids:

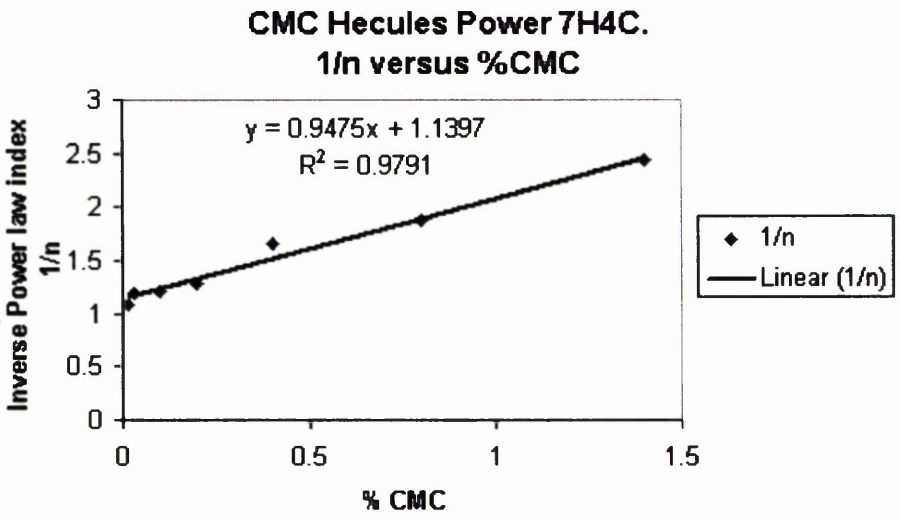

Figure 4-2: Experimentally determined power law indices for various concentrations of CMC Hercules Powder grade 7H4C fitted to a linear relationship to the reciprocal of the indices.

4.3 Modelling Non-coalescing Liquids

Water can be made non-coalescing by adding low concentrations of inorganic salts as described for example by Lee and Meyrick (1970) and Machon *et al.*(1997). Lessard, and Zieminski (1971) studied the coalescence behaviour of two touching bubbles in a stagnant pool. They found 100% of bubbles coalesced in pure water. With the addition of small quantities of salts coalescence rates decreased. They defined a critical coalescence when only 50% of the bubbles coalesced and found that the salt concentration to achieve this depended on the valency of the ions. This varies from 0.04 molar for high valency ion combinations for example 3-1, as in AlCl up to 0.2 molar for 1-1 combinations such as KCl. Thus, water containing low concentrations of salts can be used to mimic non-coalescing behaviour.

: Model Fluids:

4.4 Modelling Boiling Aerated Reactors

Boiling aerated reactors can operate at high volume fractions of gas, typically 50%. In order to study the effects of high gas volume fraction on for examples liquid phase mixing or agitation power using cold analogue fluid surfactants need to be added. Ideally it is required to study the system at the same gas flow number (Q/ND^3) to mimic the process agitator hydrodynamics and also the same process superficial gas velocity as this mimics the specific power input of the gas. It was found that a low concentration of poly propylene glycol (PPG) BDH Ltd, mol weight 2025, produce very high gas hold-ups, typically 50% gas hold-up at 20 parts per million concentrations in aerated water. This material has a density of 1000kg/m^3 and a viscosity of 0.4Pa.s at 20°C. The effect of this additive is temperature sensitive. Within the limits of 10 to 25°C it was found that the gas hold-up increases with decreasing temperature. Data for bubble column results are shown in Figure 4-3. Temperature control controlled to at least ± 1°C is essential if consistent hold-up data is required.

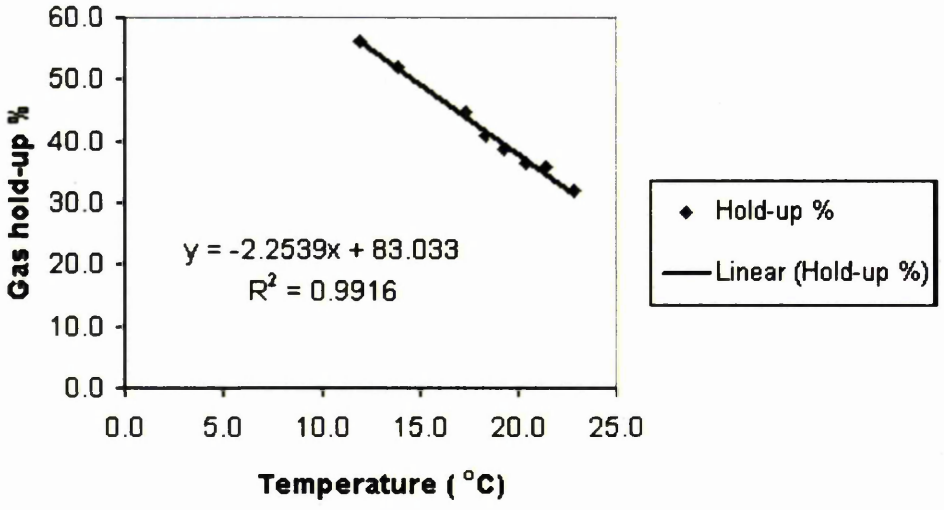

Figure 4-3: Effect of temperature on gas hold-up in 20-ppm PPG solution in a 0.61 m diameter bubble column, H/T = 1.3, superficial gas velocity =0.21m/s

Chapter 5 Bubble Studies using the Buchi Rig

5.1: Background and Summary of Buchi work

Gas-liquid mass transfer is an important unit operation carried out in bubble columns and stirred tank contactors. The transfer rate is strongly dependent on the gas-liquid interfacial area, which in turn depends on liquid flow patterns, bubble size distribution and bubble-rise velocity. This chapter describes two techniques, dynamic gas disengagement and photographic to determine gas hold-up, bubble sizes and bubble-rise velocities in model and industrial important fluids in bubble columns and mechanically stirred contactors. Operation is in the bubble and the heterogeneous regimes. Bimodal mean bubble size, gas-liquid hold-up fractions, of the dense and dilute phases, and bubble rise velocities are presented for cold sparged, boiling and boiling sparged fluids.

Results are represented from work on two scales: (i) A 0.08 m Buchi glass reactor, double-jacketed with wall heating using transparent silicon oil. This is operated from atmospheric up to 10 bar overpressure. (ii) The 0.61m diameter stirred vessel described in Chapter 3 is operated under "cold" atmospheric conditions. The dynamic disengagement experiments are recorded on video for analysis purposes.

The model fluids used are water and water with non-coalescing agents added. "Real" pure liquids fluids are methanol, aniline and acetic acid and gases are air, nitrogen and ethylene.

5.2 Introduction

Many industrial processes involve the introduction of gases into liquid or result in gaseous products through reaction, heat input or pressure reduction.

Bubble Studies using the Buchi Rig

Examples are oxidations, fermentations, carbonations, chlorinations and hydrogenations. Operation on an industrial scale very often results in large superficial gas velocities in the heterogeneous regime and high gas phase fractions. Very often there is very little information on the gas-liquid behaviour of these systems due to hostile environments, high temperature, pressure or the need to maintain aseptic conditions. The lack of "real data" presents a credibility gap for physical or mathematical modelling. In order to bridge this gap a glass Buchi has been used to study the gas-liquid behaviour of some industrially important fluids at elevated temperature and pressure. Measurements were also made using water based fluids at ambient temperature and pressure, which were repeated on a larger 0.61 m diameter vessel in order to test scale-up relationships.

A summary of the conditions used is given in Table 5-1 and Table 5-2.

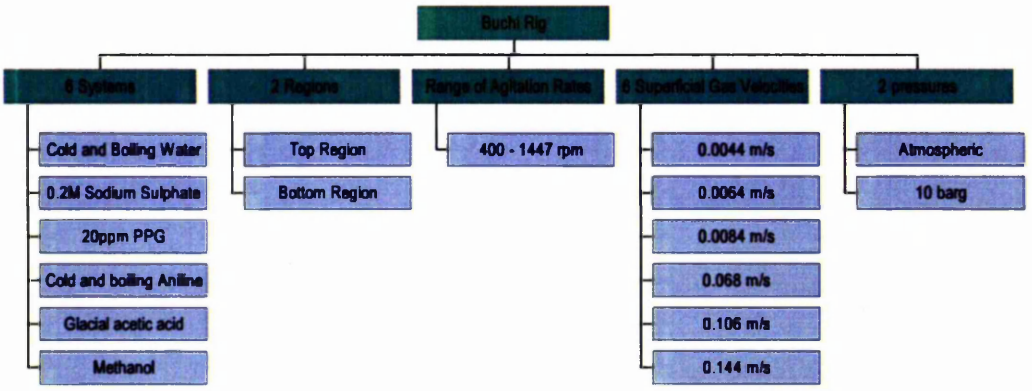

Table 5-1: Conditions used in the 0.08 m diameter Buchi reactor

Bubble Studies using the Buchi Rig

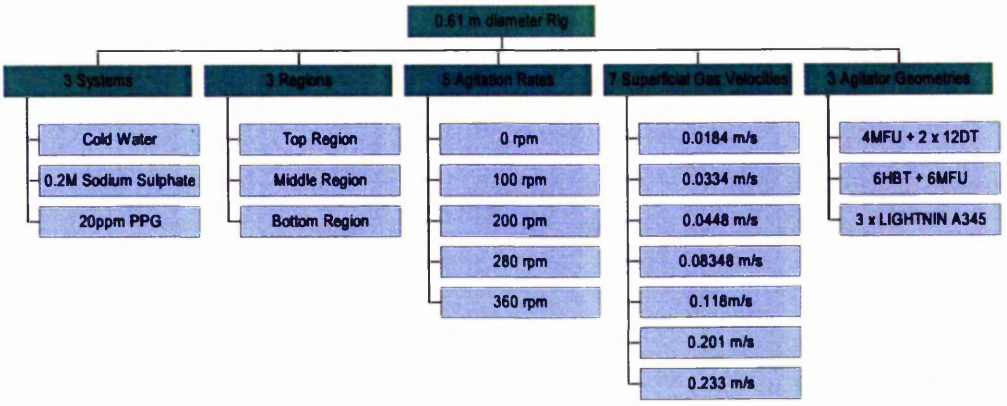

Table 5-2: Conditions tested in the 0.61 m diameter stirred tank.

The aim of this work is to determine how the operating parameters, fluids, agitation rates, temperature, pressure and gas-in rates affect bubble sizes in the vessels.

Two methods were used to estimate the average gas bubble size. The first involved taking photographs of the vessel under the required conditions and then measuring the size of those bubbles that were in focus. This was either done by hand or using a semi-automatic method. The bubble photographs of the systems tested were analysed to obtain the number average mean bubble size (d_{10}) (important for bubble rise velocities and gas retention time) and the Sauter mean bubble diameter (d_{32}) (required to estimate surface area for mass transfer). This approach, although relatively direct, is tedious and suffers from the limitation that only bubbles close to the vessel walls are measured. It was therefore necessary to use another method to obtain bubble size information that referred to the whole vessel, rather than just the near wall region. For this a dynamic gas disengagement technique was used. This relates the drop in gas hold-up with time (after simultaneously switching off the agitation and the gas) to the bubble rise velocity and allows average bubble diameter to be estimated.

5.3 Literature And Theory

De Swart *et al.* (1995) and Krishna and Ellenberger (1995), studying bubble columns, identified two basic hydrodynamic regimes:

The ***bubble regime or homogeneous regime,*** where the bubble size is small and controlled by the physical properties of the liquid and gas and:

The ***churn regime or heterogeneous regime***, where the fraction of small bubbles (dense phase) is fixed and increasing the superficial gas velocity only increases the fraction of large bubbles.

Wilkinson *et al.* (1990) gives the fraction of large bubbles as,

$$\varepsilon_{large} = (v_S - v_{tran})^{0.8}, v_S \geq v_{tran} \qquad \textbf{(5.1)}$$

where ε_{large} is the large bubble hold-up fraction, v_S the superficial gas velocity and v_{tran} the superficial gas velocity at which the transition from homogeneous to heterogeneous flow occurs.

Gezork *et al.* (2000) showed similar behaviour in mechanically agitated gas-liquid dispersions. For a mechanically agitated vessel the transition to the heterogeneous regime may occur before the superficial velocity equals the dense phase rise velocities due to gas recirculation or coalescence in agitator regions.

Wilkinson *et al.* (1990) showed that pressure increased gas hold-up by delaying the transition from homogeneous to heterogeneous flow. Their data were obtained for a range of gases from hydrogen to Freon 114 and at pressures from 0.1 to 2 MPa. They concluded that:

- The influence of both pressure and gas molecular weight on gas hold-up in a bubble column has the same cause.
- The effects of gas density are not due to any effects on bubble formation at the gas sparger but are due to a decrease in the bubble

stability with increasing density and these effects can be qualitatively explained with a Kelvin-Helmholz stability analysis.

- Larger gas densities increase bubble break rates whilst having little or no effect on coalescence. This results in increased gas hold-up for operation in the heterogeneous regime due to a higher dense phase fraction.

The significance of these results is not limited to water or bubble columns. The gas density is an important parameter in design of other gas-liquid contactors including mechanically stirred tanks.

Sriram and Mann (1977) first proposed the gas disengagement method to evaluate models of gas-liquid flow within a bubble column. The method can also yield bubble rise velocities and hold-up fractions. It can be extended to bubble size distributions since bubble rise velocity depends on bubble diameter and gas hold-up. The method depends upon measuring the profile of liquid level drop versus elapsed time following the fast shut off of the gas supply. Many other workers have used the technique in bubble columns and mechanically stirred vessels. Mann *et al.* (1981) used the method in an agitated vessel to study gas-liquid flow parameters. For these tests the agitator was left running because information was required regarding internal recirculation. Schumpe and Grund (1986) and Patel *et al.* (1989) used a version of the method in bubble columns to determine the transition from homogeneous to heterogeneous flow, bubble fractions for two bubble classes and their associated bubble rise velocities. In their analysis it is assumed that the bubble structure remains undisturbed by bubble interactions after cutting off the gas and that the gas is uniformly distributed. These simplistic approximations are justified by the consideration that the information required has been simplified to two distinct bubble classes. Gezork *et al.* (2000) extended the Schumpe and Grund (1986) method to estimate the transition from homogeneous to transitional flow and to estimate bubble rise velocities in mechanically agitated vessels by simultaneously shutting off the gas and agitator.

Bubble Studies using the Buchi Rig

Typical disengagement curves (following the liquid surface with time after simultaneously switching off the gas and agitator) are depicted in Figure 5-1 and Figure 5-2. These are typical illustrations of the heterogeneous regime; a bimodal distribution with larger bubbles escaping quickly and smaller bubbles taking longer. Within the distribution, the dense phase is saturated with small bubbles and any extra gas is coalesced into larger bubbles

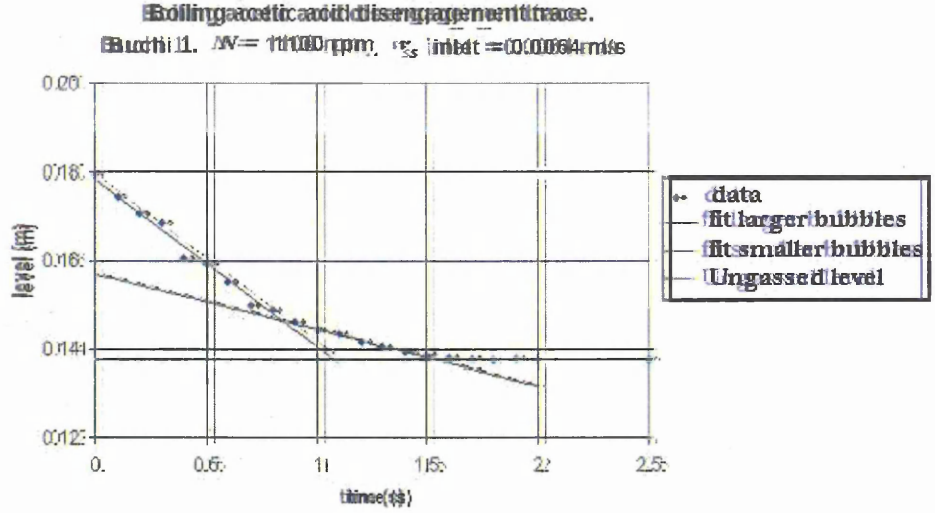

Figure 5-1: Disengagement trace for boiling, nitrogen sparged, acetic acid in the Buchi rig (coalescing system)

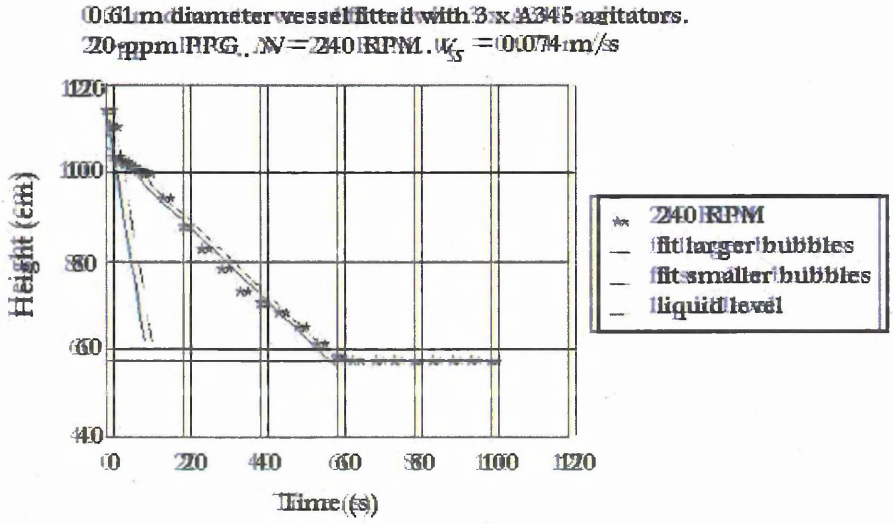

Figure 5-2: Disengagement trace for cold air-sparged PPG solution in the 0.61 m diameter vessel. (non-coalescing)

Bubble Studies using the Buchi Rig

In this work, for a bimodal bubble distribution, the analysis of Schumpe and Grund (1986) was used to yield the bubble size fractions and bubble rise velocities. Figure 5-3 illustrates what is happening,

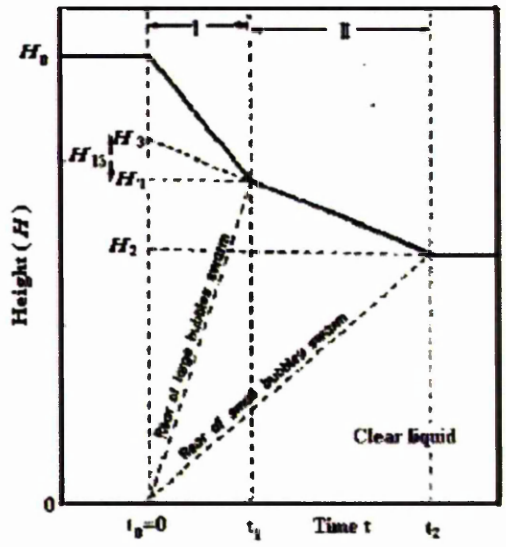

(a) Schematic description of the disengagement of two bubble classes

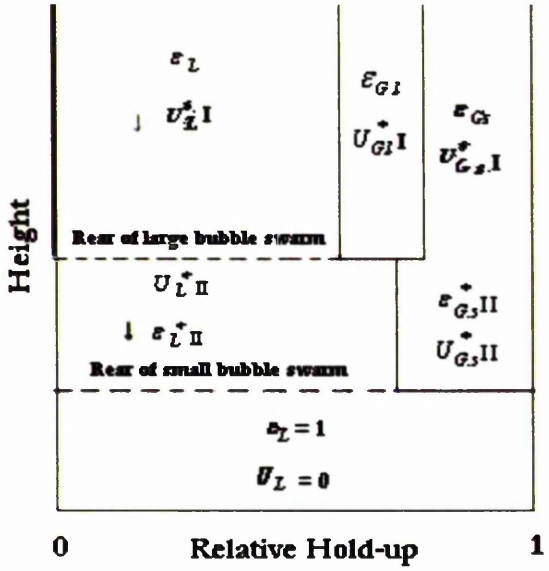

(b) The illustration of the local hold-up structure during period I

Figure 5-3: Disengagement illustrations from Schumpe and Grund (1986)

Bubble Studies using the Buchi Rig

Referring to (a) H_0 is the operating level of the system. At time = t_0, agitation and gas are simultaneously switched off.

The gas escapes in two periods. In time period *I*, all of the large bubbles and some of the small bubbles disengage. In time period *II*, the remaining small bubbles disengage (hence the slope is not as steep). When time = t_2, there is no gas left in the system. The liquid in the system is then at a height H_2 from the base. Figure 5-3(b) shows the distribution of hold-up between large bubbles, small bubbles and the liquid (ε_G, ε_{Gs} *and* ε_L) as the operating level of the system drops (during time periods *I, II* and the finishing level).

The Schumpe and Grund (1986) method of estimating bubble rise velocities and hold-up fractions from dynamic gas disengagement (DGD) traces is as follows:

The method assumes that at time = t_0 the bubbles rise at a constant slip velocity relative to the liquid, which enables the liquid backflow to be accounted for.

It is necessary to determine U_{Gs} and its contribution to the overall superficial gas velocity v_s. However this cannot be found directly from the superficial gas velocity in period *II* because the hold-up in period *II* differs from the initial hold-up. Therefore, U_{Gs} at steady-state operation must be found using the continuous operation hold-up. Calculating H_{13}, which is the initial level of the vessel excluding large bubbles, does this. Referring to Figure 5-3 (a), H_{13} lies somewhere between H_1 and H_3. The logic for this is that extrapolating the line in period *II* back *to* t = t_0 would assume that small bubble disengagement took place in the same way during period *I* as in period *II*, when in fact it must be slower due to the contribution of the large bubbles to the liquid backflow.

In the following explanations the parameters which differ from the steady-state conditions which existed up to t = t_0 are denoted with an asterisk (*).

- Indices *II and I* refers to time periods *II* and *I* respectively.
- Subscripts *L* and *G* refer to liquid and gas respectively.

Bubble Studies using the Buchi Rig

- Subscripts *s* and *l* refer to small bubbles and large bubbles respectively.
- ε refers to hold-up.
- During disengagement, the net down flow of liquid hinders bubble motion.
- During continuous operation, this is not the
- During disengagement, the local liquid superficial velocity equals gas flow in the opposite direction (i.e. $U^*_L = -U^*_G$). Hence the initial fall $(dh/dt)_I$ is equal to the superficial gas velocity at steady state (v_S).

According to Scumpe and Grund (1986) the relevant equations to solve the mass balance are:

Superficial gas velocity at steady state:

$$v_S = \left(\frac{dh}{dt}\right)_I \tag{5.2}$$

Hold-up fraction of large bubbles:

$$\varepsilon_{G.l} = (H_0 - H_{13})/H_0 \tag{5.3}$$

Hold-up fraction of small bubbles:

$$\varepsilon_{G.s} = (H_{13} - H_2)/H_0 \tag{5.4}$$

Superficial gas velocity of large bubbles:

$$U_{G.l} = U_G - U_{Gs} \tag{5.5}$$

Superficial gas velocity of small bubbles:

$$U_{G.s} = \left(\frac{dh}{dt}\right)_{I.s} = \left(\frac{dh}{dt}\right)_{II} \frac{(H_{13} - H_2)(H_1 - H_2 t_1/t_2)}{H_0(H_1 - H_2)} \tag{5.6}$$

Note that by definition,

$$H_{13} = H_1 - t_1\left(\frac{dh}{dt}\right)_{I.s} \text{ or } \left(\frac{dh}{dt}\right)_{I.s} = \frac{H_1 - H_{13}}{t_1} \tag{5.7}$$

Bubble Studies using the Buchi Rig

Thus combining equations (5.6) and (5.7), replacing $(dh/dt)_{L,}$ H_{13} can be expressed in terms of H_1, H_2, t_1 and t_2:

$$H_{13} = \frac{\frac{H_1}{t_1} + \left(\frac{H_2 - H_1}{t_2 - t_1}\right)\frac{H_2(H_1 - H_2 t_1/t_2)}{H_0(H_1 - H_2)}}{\frac{1}{t_1} + \left(\frac{H_2 - H_1}{t_2 - t_1}\right)\frac{(H_1 - H_2 t_1/t_2)}{H_0(H_1 - H_2)}} \qquad (5.8)$$

$$\left[\text{with}\left(\frac{dh}{dt}\right)_{11} = \frac{H_2 - H_1}{t_2 - t_1}\right]$$

Knowing H_{13}, allows $U_{G,}$ to be calculated in equation (5.6).

The Rise velocities of large and small bubbles are:

$$U_{B.l} = U_{G.l} / \varepsilon_{G.l} \qquad (5.9)$$

$$U_{B.s} = U_{G.s} / \varepsilon_{G.s} \qquad (5.10)$$

These are standard equations so the derivations have not been provided.

Note that the above analysis can be extended to more than two bubble classes using similar reasoning, however in view of the assumptions made this probably is not justified.

Single Bubble class case: For a single bubble class (i.e. operations take place in the homogeneous regime), then:

$$v_S = -(dh/dt) \qquad (5.11)$$

$$U_B = v_S / \varepsilon_G \qquad (5.12)$$

5.4 Equipment and Conditions

Two fully baffled vessels were used in this work.

Bubble Studies using the Buchi Rig

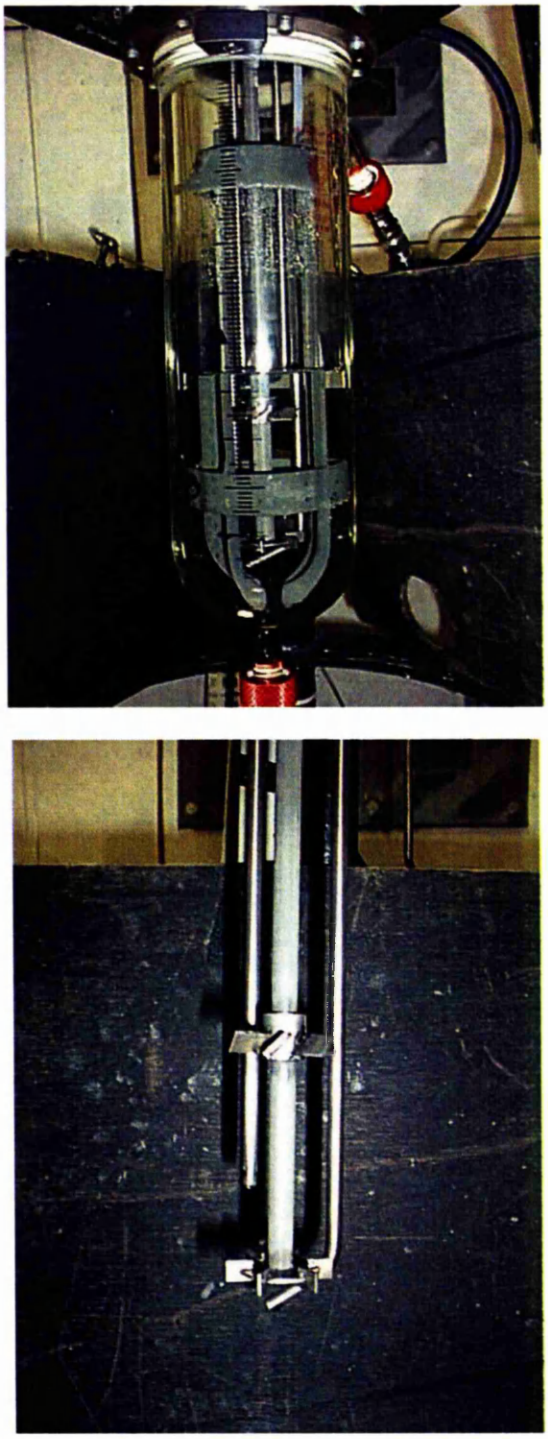

Figure 5-4: The Buchi 1 set-up. Top is assembled rig. Bottom shows agitator and sparge assembly

Bubble Studies using the Buchi Rig

The Buchi rig is a 0.08 m diameter cylindrical glass vessel with a hemispherical base as shown in Figure 5-4. Heating or cooling of the vessel contents is by clear silicon oil circulated through the glass jacket. The internals are titanium for most of the work, to cope with boiling acetic acid, but are changed to stainless steel for the methanol tests. The oil temperature is controlled using a Churchill oil heater with a water cooler. Pressure is controlled using an adjustable Gall valve. It can be operated up to 200°C and 12 barg. The larger stirred tank rig as described in Chapter 3 (see photograph in Figure 3-3) is a 0.61 m diameter Perspex cylindrical vessel with a shallow dished base.

Both vessels have a vertical scale up the vessel wall for the dynamic gas disengagement measurements. Graticules with 1 mm divisions are fixed on the inner wall of the vessels for bubble sizing by photographic techniques. Agitator details are listed in Table 5-3. Tachometers are used to measure the speeds of rotation of the shafts. Gas rates are measured using calibrated flow meters. Thermocouple probes accurate to ± 0.1C are used to measure the vessels liquid temperatures.

Gases used were nitrogen, ethylene and air. Liquids employed were methanol, acetic acid, aniline, 0.2 molar sodium sulphate solution, water and 20 ppm polypropylene glycol solution (PPG) [mol wt = 2025]. Tests were done at room temperature; hot sparged, boiling and boiling sparged conditions. Pressure was atmospheric apart from water and methanol, which were also tested at 10 barg.

The amount of fluid used in the rigs was chosen so that the gassed heights were approximately constant at around one agitator diameter above the top agitator to allow effective agitation of the vessel. For the Buchi rig this meant that the liquid volume was approximately 0.65 litres ungassed rising to around 0.79 litres under gassed conditions. For the 0.61 m diameter rig the liquid volumes were 200 to 400 litres.

Gas-in rates were chosen to give:

- Normal agitator gas loading.

Bubble Studies using the Buchi Rig

- A range of superficial gas velocities that encompass the transition from homogeneous to heterogeneous flow, with an overlap of superficial gas velocities on both scales.
- High gas hold-ups.

Agitation rates were chosen to give a range of specific power inputs up to 8 kW/m^3 of liquid on both scales.

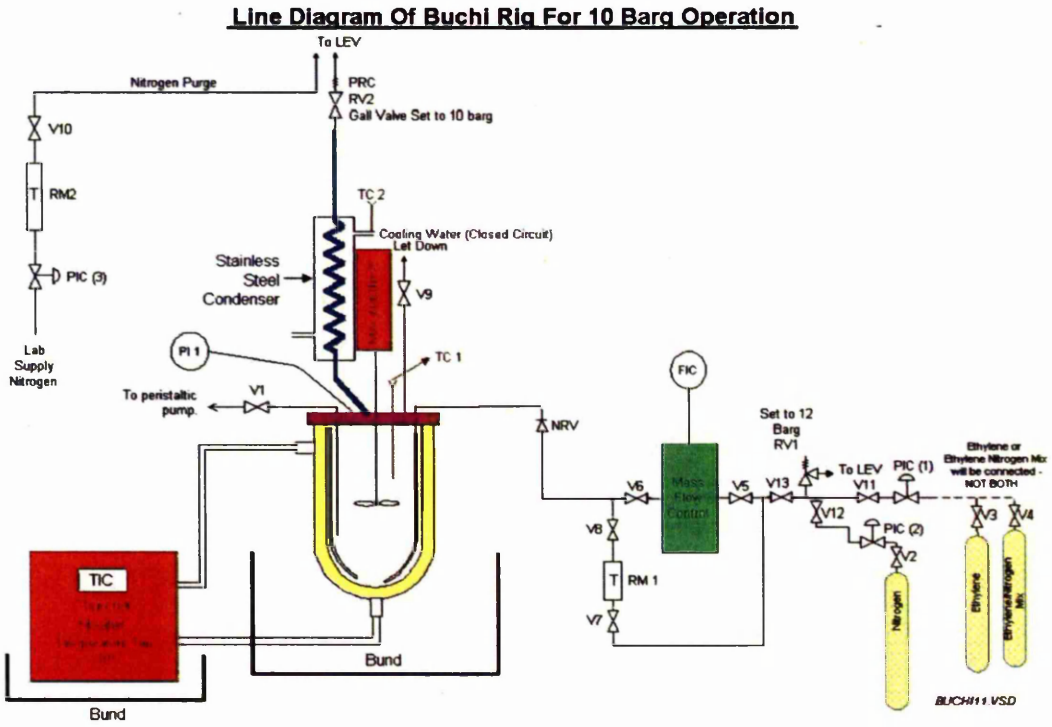

Figure 5-5:Line diagram of Buchi rig as set up for the 10 barg pressure work.

Vessel diameter	T (m)	0.08	0.08	0.61	0.61	0.61
Geometry key		Buchi 1	Buchi 2	2 ft R1	2 ft R2	2 ft R3
Operating levels	H (m)	0.17	0.08	0.95	1.38	1.43
Agitator type	Bottom	6RT	6RT	4MFU	6HBT	A345
	Mid			12DT		A345
	Top	6MFU		12DT	6MFU	A345
Agitator diameters	D (m)	0.04	0.027	0.33	0.311	0.344
	Bottom (m)			0.30		0.344
	Mid (m)			0.30	0.310	0.344
Agitator clearances	Bottom (m)	0.04	0.04	0.2	0.26	0.2
	Mid (m)			0.44		0.62
	Top (m)	0.125		0.680	0.83	1.04
Operating volume	V (m^3)	0.00079	0.00034	0.26	0.38	0.40

Table 5-3: Agitator geometries used in tests

5.5 Buchi Rig Agitator Hydrodynamics

In the introduction to this chapter the transition from homogeneous to heterogeneous bubble behaviour was discussed. It is important to separate this from the effects of agitator hydrodynamics discussed in Chapter 2, section 2.3.1.

For the flat 6-blade turbine, which has a low pressure region behind the blades where gas can collect to form cavities, Smith *et al.* (1988) identifies four main hydrodynamic transitions:

Minimum Froude number for the retention of stable cavities:

$$Fr = 0.045 \tag{5.13}$$

The maximum gas flow at which clinging-vortex cavities can be maintained

This is the 3:3 cavity – clinging vortex cavity transition line and is given by,

$$Fl_G = 0.0038\left(\frac{Re^2}{Fr}\right)^{0.067}\left(\frac{T}{D}\right)^{0.5} \tag{5.14}$$

Bubble Studies using the Buchi Rig

Maximum gas rate that can be recirculated through the vessel (defines the loading-complete recirculation transition):

$$Fl_{CD} = 13\,Fr^2\left(T/D\right)^{-5} \qquad (5.15)$$

The Maximum gas flow that can be handled without flooding the impeller

This is the flooding-loading transition and is given by

$$Fl_{F-L} = 30\,Fr\left(T/D\right)^{-3.5} \qquad (5.16)$$

For the conditions used in these tests:

All agitator conditions were above the minimum Froude number for stable cavities to form.

All agitator conditions were above the flooding-loading transition, meaning the agitator was not flooded.

All conditions were above the loading-complete recirculation transition, meaning the gas was recirculated through the vessel.

Most of the conditions were in the large stable cavity region. At the lowest gassing rate and with agitation speed of 1100 and above, the vessel went through the clinging-vortex to 3:3 large or large plus clinging cavity transition.

In summary, all of the conditions used were above the flooding point and most were in the same cavity region. This means that any transition between regimes was unlikely to have been caused by the agitator hydrodynamics.

The estimated specific power input used for the various experiments and the superficial gas velocity of the inerts is listed in Table 5-4 for the Buchi 1 geometry. For these calculations it was assumed that the total Po = 6, volume of liquid = 650 cm^3 with a liquid density of 1000kg/m^3 and:

Low gas is $\leq$ 1.34 litres /minute, $Pg/Pu = 0.6$.

Medium gas is $> 1.34 \leq 2.0$ litres/minute, $Pg/Pu = 0.5$

Boiling or High gas is > 2litres / minute gas, $Pg/Pu = 0.4$

Bubble Studies using the Buchi Rig

These figures are informed estimates only but considered fit for the purpose of comparison.

Agitation speed	Specific power input P/V (W/kg)		
(RPM)	Boiling or High gas	Medium gas	Low gas
400	0.11	0.14	0.17
8	0.90	1.12	1.34
897	1.26	1.58	1.90
1100	2.33	2.91	3.49
1277	3.65	4.56	5.47
1300	3.85	4.81	5.77
1447	5.30	6.63	7.96

Table 5-4: Estimates of Specific Power Inputs Used in the Buchi Work

5.6 Experimental Details

5.6.1 Dynamic Gas Disengagement Experiments

A Panasonic SVHS video camera is used to record the drop in level when the gas and agitation is simultaneously turned off. The disengagements are analysed using a Panasonic SVHS 4700 series, stop-frame video that allows each frame to be frozen and analysed. The tape is paused at the instant that the gas and agitation are turned off. This corresponds to time = 0 seconds (t_0). At each interval, the level seen by the video is noted. The camera is placed in set positions with respect to the vessels and the level "seen by the camera" is calibrated against the true level "seen by eye". Hold-up fractions and bubble rise velocities are estimated in a spreadsheet program, according to the theory developed by Schumpe and Grund (1986). The small bubbles rise velocities are affected by gas hold-up (ε_G). In this work, the relationship between small bubble rise velocity, relative to a stationary liquid, and terminal rise velocity of a small bubble in an infinite medium, proposed by Marrucci (1965) is used to correct for this effect This is given by,

$$u_t = \frac{U_{B,s}(1-\varepsilon_{G,s}^{5/3})}{(1-\varepsilon_{G,s})^2} \tag{5.17}$$

No corrections have been made for the rise velocity of larger bubbles. Krishna *et al.* (1999) claim that a large bubble swarm can rise faster than a single spherical cap bubble because of the interactions with the wake of the previous bubbles. From the corrected value of the rise velocity, the bubble diameters are calculated using one of two methods.

For Reynolds number (Re) ≤ 2, Stoke's law is used to estimate bubble diameters as follows,

$$d_{b,s} = \left(\frac{18\mu_l u_t}{g(\rho_l - \rho_g}\right)^{1/2} \tag{5.18}$$

where inertial terms (Re > 2) are important a drag coefficient is used to fit the experimental data. The following analysis is from Valentin (1967):

$$C_d = \frac{2R'}{\rho_L A_o U^2} \tag{5.19}$$

where R' = total fluid resisting force and A_o is cross-sectional area normal to the direction of rise and ρ_L is the liquid density. For constant velocity u_t

$$R' = V_b \Delta\rho g \tag{5.20}$$

where V_b is the volume of the rising bubble.

For spherical bubbles A_o and V_b are simple functions of diameter. For deformed bubbles A_o and V_b are expressed in terms of the equivalent diameter of a sphere equal in volume to the bubble as follows,

$$d_b = \left(\frac{6V_b}{\pi}\right)^{1/3} \tag{5.21}$$

which when substituted yields,

$$C_d = \frac{4}{3}\left(\frac{\rho_L - \rho_G}{\rho_L}\right)\left(\frac{d_b g}{u_t^2}\right) \tag{5.22}$$

where ρ_L is the liquid density, ρ_G is the bubble density, d_b is the bubble diameter, g is the acceleration due to gravity and u_t is the terminal bubble rise velocity.

Hill (1998) used two (empirical) curve fits to the drag coefficient versus Reynolds curve for pure water shown in
Figure 5-6 for the drag coefficient as a function of bubble Reynolds number. These are:

For ($Re_b < 450$),

$$\ln(C_d) = 2.699467 - 0.335816.\ln(Re_b) - 0.07135617.[\ln(Re_b)]^2 \tag{5.23}$$

and for ($Re_b > 450$),

$$\ln(C_d) = -51.77171 + 13.16707.\ln(Re_b) - 0.82356.[\ln(Re_b)]^2 \tag{5.24}$$

These equations are used in this work by applying the solution for a quadratic equation (see appendix 7) to yield bubble diameters from rise velocities.

Referring to Figure 2-43, it is apparent that for bubbles in a low viscosity fluid, a transition occurs at a bubble rise velocity of approximately 0.3 m/s. In the transition region the dynamic disengagement method is unsuitable for bubble size analysis. This applies for bubbles with diameters between approximately 1 and 30 mm as Figure 2-43 illustrates. In this region only bubble rise velocities and hold-up is estimated using the dynamic gas disengagement method.

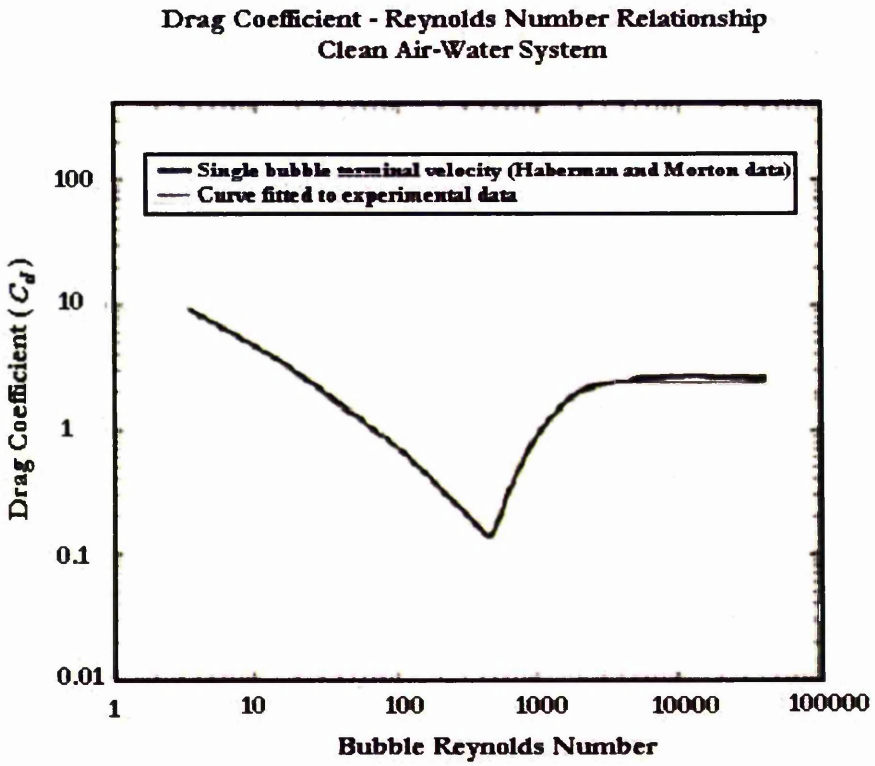

Figure 5-6: Drag coefficient as a function of Reynolds number from Hill(1998)

5.6.1.1 Problems Encountered With the Dynamic Gas Disengagement Method

Bubble retardation described by Gezork *et al.* (2000) sometimes occurs with very small bubbles queuing at the surface during the latter stages of the disengagement trace. This "queuing" produces high local gas hold-ups slowing the bubble escape process down. This applies particularly to the smaller bubbles as seen by a tail on the disengagement curve. To try to account for this, when plotting the lines of regression, only the initial part of the curve is used, before the 'queuing' begins. There is a judgement here since this "tail"

might have been due in part to another class of tinier bubbles which if ignored will not have been accounted for.

For the Buchi rig experiments at low hold-ups the surface bounce was significant with respect to the change in level and this produced very noisy traces on which only the initial part of the disengagement curve could be determined with any accuracy. Low hold-ups were avoided whenever possible, but to help cope with this problem the liquid level was noted for several seconds before the disengagement and an average value was used as the initial aerated level.

The single regression (an assumed homogeneous distribution) method was used in 2 cases:

I. Where there obviously only one line corresponding to small bubbles in the bubble regime.

II. If it was not possible to distinguish between the different regions because of "noise" or suspected "bubble retardation".

5.6.2 Bubble Measurements and Counting Experiments.

Bubble photographs were taken of selected areas of the vessel wall using a 1/50,000 of a second flash and a fast film. The areas photographed for the Buchi rig are shown in Figure 5-7.

5.6.2.1 Manual Counting

The photographs are printed to A3 size for bubble measuring and counting. The scale is evaluated from the graticule. For a meaningful bubble size distribution, at least 600 bubbles must be counted for each condition. To obtain a fair distribution, all the "in focus" bubbles on each photograph are counted. If the number counted in one photograph is less than 600, then all

the bubbles in the next photograph for that condition, are also counted. All bubbles are assumed spherical. For bubbles that were ellipsoidal an average diameter was taken from several chords. Only bubbles judged to be in focus are counted to minimize perspective errors.

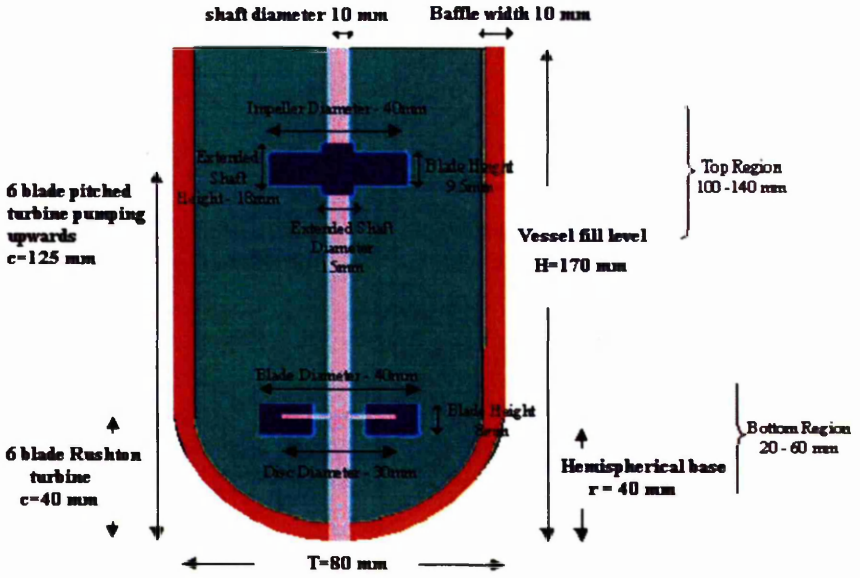

Figure 5-7: Buchi agitator and photo region details

From this data, the number mean bubble diameter (d_{10}) and the Sauter mean bubble diameter (d_{32}) can be calculated according to:

$$d_{10} = \sum_{i=1}^{N} d_{b,i} \Big/ N \tag{5.25}$$

$$d_{32} = \sum_{i=1}^{N} d_{b,i}^3 \Big/ \sum_{i=1}^{N} d_{b,i}^2 \tag{5.26}$$

where $d_{b,i}$ = diameter of each individual bubble and N = total number of bubbles counted

5.6.2.1.1 Possible Sources of Error with Manual Counting

Bubble Studies using the Buchi Rig

- Some bubbles are too small for the eye to detect amongst a bubble cloud.
- Some bubbles being so small that they look in focus when they are not. A large bubble that is slightly out of focus could be discarded when a small bubble that is a lot more out of focus is counted.
- Small bubbles are more difficult to measure accurately
- At the edge of the photograph, bubbles are generally less in focus because of the vessel curvature.
- Large bubbles are very visible but smaller ones are much harder to spot, especially at high gas hold-ups.
- Human error caused by judgements changing when bubbles are counted over a long period of time.
- Slight changes in the picture due to photocopying (assumed to be negligible).
- Non-spherical bubbles.

5.6.2.2 Semi-Automatic Counting

Some of the sets of photographs were sent to a specialist ICI Technology laboratory where the bubbles were counted and measured semi-automatically using a commercial software package. This was done from a scanned computer image of the photographs taken. It was assumed that this method of counting bubbles is generally more accurate. However, comparative tests reported in Table 5-5, show reasonable agreement between the two methods.

Bubbles are tallied according to size, with the bubbles from 0-400 microns recorded in classes of 100 microns, and bubbles > 400 microns are recorded in classes of 200 microns.

Fluid	Method	d_{10}	d_{32}
20 ppm PPG at 1277 rpm and 2.54 l/min gas	Hand Counted	166	625
	Semi-Automatic Counting	205	504
0.2 M Sodium Sulphate at 1277 rpm and 2.54 l/min gas	Hand Counted	275	1229
	Semi-Automatic Counting	275	1229

Table 5-5: Comparison of bubble sizes by hand counted and semi automatic counting methods.

5.7 Results Summary

Results for all fluids tested are summarized in Table 5-6 to Table 5-11. Note that nomenclature for these tables is as follows: DGD = dynamic gas disengagement; d_{10} is the number mean bubble size from photographic bubble size analysis; d_{32} is the Sauter mean bubble size from photographic bubble size analysis; v_S = superficial gas velocity based on inlet gas and vessel cross-section; U_{sb} and U_{lb} are rise velocities of small and large bubble swarms; N = agitation speed; ε_G, ε_S and ε_T refer to volumetric hold-ups of gas, solids and total (gas plus solid) respectively. Subscripts: s = smaller, l = larger, L = liquid, b = bubbles. R = region of vessel photographed. Solids are glass ballotini of mean size 205 microns. For details of vessel geometries see Table 5-3.

A typical dynamic gas disengagement worksheet is appended in appendix 7.

A frequency count from the bubble counting is appended as Appendix 6, which also contains a record of the video calibration.

Bubble Studies using the Buchi Rig

	R	N	v_S	d_{10}	d_{32}	DGD_S	DGD_L	ε_S	ε_{GS}	ε_{GL}	$\varepsilon_{GS}+\varepsilon_{GL}$	ε_T	P/V_L	U_{sb}	U_{lb}
Vessel		RPM	(m/s)	μm	μm	μm	μm	%	%	%	%	%	kW/	Cm/s	cm/s
Buchi 1	Bottom	897	0.0044	208	551	200	539	0	4.2	13.5	17.8	17.8	1.9	1.24	2.82
Nitrogen		897	0.0064			222	529	0	6.4	15.4	21.8	21.8	1.6	1.28	3.87
Gas		897	0.0084			135	403	0	4.6	23.6	28.2	28.2	1.9	0.58	3.53
		1100	0.0044			173	392	0	4	16.9	20.9	20.9	2.3	1.10	2.68
	Bottom	1100	0.0064	242	627	308	480	0	8.8	15.9	24.7	24.7	2.9	1.75	2.68
		1100	0.0084			258	504	0	4.8	28.3	33.1	33.1	3.5	1.20	2.44
		1277	0.0044			113	400	0	6.4	13.4	19.7	19.7	3.7	0.48	2.55
		1277	0.0064			125	464	0	6.2	24.3	30.5	30.5	4.6	0.48	3.17
	Bottom	1277	0.0084	184	564	131	481	0	3.6	34.2	37.8	37.8	5.8	0.45	2.88
2ft tank		0	0.0880			623	14915	0	2.79	58.15	60.94	60.9	0.43	2.24	142.9
R1		280	0.0337			341	821	0	33.3	11.9	45.3	45.3	4.73	1.67	12.6
4MFU +		280	0.0450			366	970	0	34.4	8.8	43.2	43.2	4.32	1.79	18.0
2 x 12DT		280	0.0585			359	814	0	33.9	10.9	44.8	44.8	4.17	1.76	12.4
Gas = air		280	0.0840			387	16485	0	36.3	12.3	48.7	48.7	3.93	1.85	38.2
.		280	0.1182			350	1260	0	35	14.1	49.1	49.1	3.90	1.67	34.3
		280	0.2019			333	17108	0	35.7	18.5	54.2	54.2	3.71	1.54	44.2
	Mid	280	0.0840	246	463	387	16485	0	36.3	12.3	48.7	48.7	3.93	1.85	38.2
		0.0	0.1355			397	16018	0.00	4.3	47.0	51.3	51.3	0.90	1.65	109.3
2ft tank		252.0	0.1353			402	17466	0.00	6.8	41.3	48.1	48.1	2.84	1.93	59.0
R2		252.0	0.0782			436	16205	0.00	4.7	41.7	46.4	46.4	2.56	2.11	36.5
GF+6MF		252.0	0.0342			479	17461	0.00	3.5	37.4	41.0	41.0	2.37	2.58	54.6
Gas = air		330.0	0.0770			337	17381	2.49	5.8	40.4	46.1	48.6	5.50	1.47	50.0
		252.0	0.0771			346	17448	2.56	4.9	41.7	46.6	49.1	3.02	1.45	53.3
		330.0	0.0768			348	17234	5.00	6.7	35.5	42.2	47.2	5.90	1.61	46.3
		330.0	0.0768			389	17159	7.71	7.6	32.8	40.4	48.2	6.77	1.84	45.0
		330.0	0.0771			362	17449	0.00	5.9	42.3	48.3	48.3	5.07	1.63	53.4
2ft tank		0	0.033			615		0.00	18.62	0.0	18.6	18.6	0.35	5.25	0.0
R3		0	0.074			566	14668	0.00	47.63	3.1	50.7	50.7	0.78	2.51	151.1
3 x A345		0	0.13			435	15051	0.00	46.7	7.1	53.8	53.8	1.37	1.73	138.5
Gas =air		0	0.202			434	14495	0.00	46.9	9.4	56.4	56.4	2.19	1.71	157.1
		0	0.28			380	14943	0.00	41.1	18.5	59.6	59.6	2.99	1.63	142.0
		120	0.033			705		0.00	27.9	0.0	27.9	27.9	0.64	5.57	0
		180	0.033			609		0.00	38.4	0.0	38.4	38.4	1.23	3.48	0.0
		240	0.033			516	15303	0.00	36.2	2.7	39.0	39.0	2.24	2.80	130.6
		300	0.033			411	16062	0.00	30.1	6.9	37.1	37.1	3.40	2.28	35.7
		360	0.033			455	17371	0.00	34.3	4.8	39.1	39.1	4.90	2.41	66.4
		120	0.074			575	17364	0.00	44.1	3.5	47.6	47.6	1.06	2.79	66.7
		180	0.074			515	17150	0.00	41.3	3.9	45.2	45.2	1.66	2.50	75.4
		240	0.074			428	17413	0.00	37.9	7.1	45.0	45.0	2.58	2.05	64.0
		300	0.074			416	17414	0.00	32.1	12.6	44.6	44.6	3.72	2.23	63.9
		360	0.074			385	17450	0.00	30.5	14.1	44.6	44.6	5.43	2.07	61.1
		120	0.130			497	14356	0.00	47.9	6.3	54.1	54.1	1.64	2.04	161.9
		180	0.130			428	17368	0.00	44.5	9.6	54.0	54.0	2.23	1.78	66.5
		240	0.130			356	17387	0.00	39.5	13.9	53.3	53.3	3.11	1.55	65.5
		300	0.130			319	17409	0.00	34.4	18.7	53.1	53.1	4.35	1.50	64.2
		360	0.130			302	17416	0.00	30.3	22.6	52.9	52.9	6.04	1.53	63.8

Table 5-6: Results from PPG experiments at 12 ± 1°C and atmospheric pressure

Bubble Studies using the Buchi Rig

Vessel	R	N	v_S	Pressure	d_{10}	d_{32}	DGD_S	DGD_L	$\varepsilon_{G,S}$	$\varepsilon_{G,I}$	$\varepsilon_{G,S}+\varepsilon_{G,I}$	P/V_L	U_{Sb}	U_{lb}
		RPM	(m/s)		µm	µm	µm	µm	%	%	%	kW/m³	cm/s	cm/s
Buchi 1	Bottom	897	0.0084	1atm	404	2222	748		9	0.0	9.0	1.3	8.9	
Ambient T		1100	0.0084		332	1441	843		9.6	0.0	9.6	2.3	11.1	
Nitrogen		1277	0.0044		371	2751	810		8.7	0.0	8.7	5.5	10.4	
Gas		1277	0.0064		394	2202	783		10.1	0.0	10.1	4.6	9.5	
		1277	0.0084		464	2016	822		9.6	0.0	9.6	3.7	10.6	
		1441	0.0681		233	1365	516	1055	8.9	11.2	20.1	5.3	4.7	17.64
		1444	0.1056		232	1375	450	769	5.4	14.0	19.3	5.2	4.1	8.54
		1444	0.1437		244	1585	568		12.7	11.2	23.9	5.1	5.4	32.51
	Top	897	0.0084	1atm	451	4242	748		9	0.0	9.0	1.3	8.9	
		1100	0.0084		299	4953	843		9.6	0.0	9.6	2.3	11.1	
		1277	0.0044		243	2277	810		8.7	0.0	8.7	5.5	10.4	
		1277	0.0064		262	3013	783		10.1	0.0	10.1	4.6	9.5	
		1277	0.0084		297	3364	822		9.6	0.0	9.6	3.7	10.6	
		1444	0.1437		236	1677	568		12.7	11.2	23.9	5.1	5.4	32.51
Buchi 1	Bottom	897	0	1atm			497		6.1	0.0	6.1	1.9	15.2	
Boiling		897	0.0084		461	2411			6	0.0	6.0	1.2	30.7	
Jacket		1100	0				535		5	0.0	5.0	3.5	18.8	
T =132°C		1100	0.0084		562	3963	533		8.3	0.0	8.3	2.2	15.5	
		1277	0		866	2888	527		5.9	0.0	5.9	5.4	17.7	
		1277	0.0044		280	3431	505		7.8	0.0	7.8	5.3	14.0	
		1277	0.0064		483	1574	543		8.9	0.0	8.9	4.4	16.1	
		1447	0.0084		449	1683	471		11.9	0.0	11.9	5.1	10.8	
	Top	1277	0.0044		1273	4478	505		7.8	0.0	7.8	5.3	14.0	
		1447	0.0084		856	3910	471		11.9	0.0	11.9	5.1	10.8	
Buchi 2														
T=69.7°C	Top	1082	0.00015	140 psig	645	2363			low			0.9		
2ft	Bottom	0	0.0858	1atm			1247		13.7	0.0	13.7	0.90		33.3
R1		100	0.0828				853	17449	3.1	9.9	13.0	0.82	12.8	53.4
T=12±1°C		200	0.0830				871	1157	4.3	15.0	19.3	2.01	13.1	27.3
Gas = air		280	0.0186				1082		16.2	0.0	16.2	4.68	17.1	
		280	0.0442				920	1147	8	14.1	22.1	4.16	13.7	26.7
		280	0.0832		1173	2694	1037	16777	14.6	14.3	28.9	3.66	15.9	40.5
		280	0.1157				1074	17332	16	13.3	29.3	3.65	16.8	48.5
		280	0.1991				1027	17421	15	19.1	34.1	3.95	15.4	51.7
		360	0.2321		1215	2265	1114	17456	22.1	21.6	43.7	6.63	17.5	54.1
	Mid	360	0.2321		1409	3542	1114	17456	22.1	21.6	43.7	6.63	17.5	54.1
	Top	360	0.2321		1350	2644	1114	17456	22.1	21.6	43.7	6.63	17.5	54.1

Table 5-7: Results from demineralised water experiments

Bubble Studies using the Buchi Rig

Vessel	R	N	v_S	Pressure	d_{10}	d_{32}	DGD	DGD	ε_{G1}	ε_{G2}	$\varepsilon_{G1}+\varepsilon_{G2}$	P/V_L	U_{sb}	U_{lb}
		RPM	(m/s)		µm	µm	µm	µm	%	%	%	kW/m³	Cm/s	cm/s
Buchi 1	Bottom	897	0.0044	1atm			329	611	3.1	6.9	10.0	1.9	2.50	6.09
@		897	0.0064		333	740	326	719	3.3	7.0	10.2	1.6	2.46	8.07
Ambient		897	0.0084		329	1274	335	686	3.3	6.6	9.9	1.3	2.56	7.47
Temp.		1100	0.0044		317	876	349	629	7.1	6.0	13.1	3.5	2.54	6.04
		1100	0.0064				352	675	5.5	7.6	13.1	2.9	2.57	6.83
		1100	0.0084		331	879	336	722	5	9.2	14.3	2.3	2.37	7.54
		1277	0.0044		288	453	636		21.6		21.6	5.5	5.24	
		1277	0.0064		294	903	651	1022	12.5	6.3	18.8	4.6	5.76	14.21
		1277	0.0084		275	1229	510	769	6.6	16.7	23.3	3.7	3.56	7.16
		1447	0.0681		326	933	317	828	5.7	17.7	23.4	5.2	2.59	9.22
			0.1056		246	750	339	797	6.9	18.3	25.2	5.1	2.75	8.45
			0.1441		216	1061	525	1071	14.7	15.9	30.6	5.0	4.38	16.75
		897	0.0084	1atm	254	1360	335	686	3.3	6.6	9.9	1.3	2.56	7.47
		1100	0.0084		249	732	336	722	5	9.2	14.3	2.3	2.37	7.54
		1277	0.0044		274	420	636				21.6	5.5	5.24	
		1277	0.0064		302	562	651	1022	12.5	6.3	18.8	4.6	5.76	14.21
		1277	0.0084		247	493	510	769	6.6	16.7	23.3	3.7	3.56	7.16
		1447	0.1441		273	1794	525	1071	14.7	15.9	30.6	5.0	4.38	16.75
2ft Tank	Bottom	0	0.0187	1atm			935		2.9	4.9	7.9	0.19	15.63	75.83
Bubble			0.0344				744		2.9	7.3	10.1	0.36	9.87	41.43
Column			0.0464				737		4.7	7.4	12.1	0.47	9.38	76.75
T=12 ± 1C			0.0597				602	1233	3.9	10.3	14.2	0.63	6.66	32.34
			0.0876				577		4.5	14.1	18.6	0.92	6.14	42.40
			0.1230				577		5.4	19.0	24.4	1.30	6.04	37.99
			0.2152				486	1176	7.0	28.6	35.6	2.24	4.49	28.49
2ft		280	0.0184	1 atm			457	913	8.4	15.4	23.8	4.49	4.00	15.72
R1			0.0334				447	960	8.8	19.6	28.3	3.95	3.84	17.54
T=12 ± 1C			0.0448				437	1032	8.6	20.8	29.4	4.11	3.73	20.69
			0.0586				451	1089	8.8	22.4	31.2	3.66	3.89	23.50
			0.0835		274	422	436	1215	8.4	24.6	33.0	3.81	3.74	31.05
			0.1175				435	1209	7.6	31.2	38.8	4.07	3.78	30.69
			0.2010				403	1198	7.8	34.5	42.3	3.94	3.39	29.96
			0.2263				402		8.1	35.2	43.3	4.02	3.36	36.77
		360	0.2330		268	501	313		15.0	38.9	53.9	5.02	2.14	44.80
	Mid	360	0.2330	1atm	271	798	313		15	38.9	53.9	5.02	2.14	44.80
	Top	360	0.2330	1atm	257	444	313		15	38.9	53.9	5.02	2.14	44.80

Table 5-8: Results from 0.2 molar sodium sulphate solution experiments

Bubble Studies using the Buchi Rig

Vessel	R	N	v_S	Pressure	d_{10}	d_{32}	DGD_S	DGD_L	ε_{GS}	ε_{GI}	$\varepsilon_{GS}+\varepsilon_{GI}$	P/V_L	U_{sb}	U_{lb}
		RPM	(m/s)		µm	µm	µm	µm	%	%	%	KW/m³	cm/s	cm/s
Buchi 1	Bottom	400	0.0066	1atm	590	3393	451		10.3		10.3	0.1	9.036	
Jacket at		800	0.0066		601	1901	477		18.4		18.4	0.8	9.098	
196°C		1100	0.0066		446	1477			29.2		29.2	2.2		
Boiling		1300	0.0066		473	1676	461		26.1		26.1	3.5	7.025	
		1300	0.0033		749	1939	492		25.2		25.2	3.4	8.009	
		1300	0.0000		733	3335	514		32.9		32.9	3.3	9.221	
		1300	0.0099		538	2401	561		26.5		26.5	3.4	10.26	
	Top	400	0.0066	1atm	628	1968	451		10.3		10.3	0.1	9.036	
		800	0.0066		429	1795	477		18.4		18.4	0.8	9.098	
		1100	0.0066		336	8071			29.2		29.2	2.2		
		1300	0.0066		313	2620	461		26.1		26.1	3.5	7.025	
		1300	0.0033		465	1582	492		25.2		25.2	3.4	8.009	
		1300	0.0000		568	2400	514		32.9		32.9	3.3	9.221	
		1300	0.0099		362	4727	561		26.5		26.5	3.4	10.26	
Buchi 1	Bottom	400	0.0066	1atm	339	1503	1553		2.6		2.6	0.1	9.7	
Jacket at		800	0.0066		416	777	978		7.7		7.7	1.1	4.6	
ambient		1100	0.0066		213	401	1058		10.7		10.7	3.0	4.81	
Temp.		1300	0.0066		197	360	1067		14.0		14.0	4.7	4.58	
		1300	0.0033		161	281	927		9.9		9.9	5.9	4.13	
		1300	0.0099		147	223	1194		16.5		16.5	3.7	5.08	
	Top	400	0.0066	1atm	232	482	1553		2.6		2.6	0.1	9.7	
		800	0.0066		214	378	978		7.7		7.7	1.1	4.6	
		1100	0.0066		187	388	1058		10.7		10.7	3.0	4.81	
		1300	0.0066		159	261	1067		14.0		14.0	4.7	4.58	

Table 5-9: Results from aniline experiments

Vessel	Region	N	v_S	Pressure	d_{10}	d_{32}	DGD_S	DGD_L	ε_{G1}	ε_{G2}	$\varepsilon_{G1}+\varepsilon_{G2}$	P/V_L	U_{sb}	U_{lb}
		RPM	(m/s)		µm	µm	µm	µm	%	%	%	kW/m³	cm/s	cm/s
Buchi 1	Bottom	1277	0.0084	1atm	414	1048	516		8.8	20.7	29.5	3.5	9.06	20.58
Jacket at		1277	0.0064				547	753	12.0	15.5	27.5	3.5	9.63	19.51
170C		1277	0.0044				534		9.2	17.7	26.8	3.5	9.66	20.22
boiling		1277	0.0000				603		17.8		17.8	3.5	10.74	
		1100	0.0084				487		9.1	17.6	25.2	2.2	8.02	23.15
		1100	0.0064		344	982	531	748	10.3	14.6	24.9	2.2	9.35	19.48
		1100	0.0044				658		25.2		25.2	2.2	11.47	
		1100	0				581		16.9		16.9	2.2	10.03	
		897	0.0084				496		6.5	19.3	25.8	1.2	8.71	21.15
		897	0.0064				510	760	9.7	13.5	23.2	1.2	8.71	20.81
		897	0.0044		351	1035	665		19.2		19.2	1.2	13.17	
		897	0.0000				598		13.7		13.7	1.2	11.36	

Table 5-10: Results from acetic acid experiments

Vessel	Region	N	v_S	Gas	Pressure	Temp	d_{10}	d_{32}	ε_G	P/V_L
		RPM	(m/s)			°C	mm	mm	%	KW/m³
Buchi 2	Top	1082	0.00015	Ethylene	142	70.1	756	1650	very low	0.9
Hot										
sparged		1082	0.00015	Nitrogen	142	69.9	426	1491	very low	0.9

Table 5-11: Results from methanol experiments

5.8 Presentation of Results, Discussion and Conclusions.

5.8.1 Bubble Pictures

Representative bubble pictures of all the fluids tested are displayed in Figure 5-8 to Figure 5-19. A study of these photographs reveals:

The division of bubbles into to a single class for the homogeneous regime and two classes for the heterogeneous regime is a gross over-simplification. The pictures of water with a Sauter mean bubble diameter around 3 mm show some bubbles as small as 100 microns or less.

Bubble Studies using the Buchi Rig

The liquid fluid makes a very large difference to the bubble size distribution. The salt solution and surfactant-laden solution have much smaller bubbles than coalescing fluids such as water, methanol and acetic acid.

Heating and elevated pressure make surprising little difference to the observed bubble size distribution, apart from aniline where the bubbles are noticeably larger for the boiling case.

Vapour bubbles from boiling fluids look very similar to cold sparged gas bubbles.

Changing the gas from nitrogen to ethylene did not produce any noticeably different bubbles.

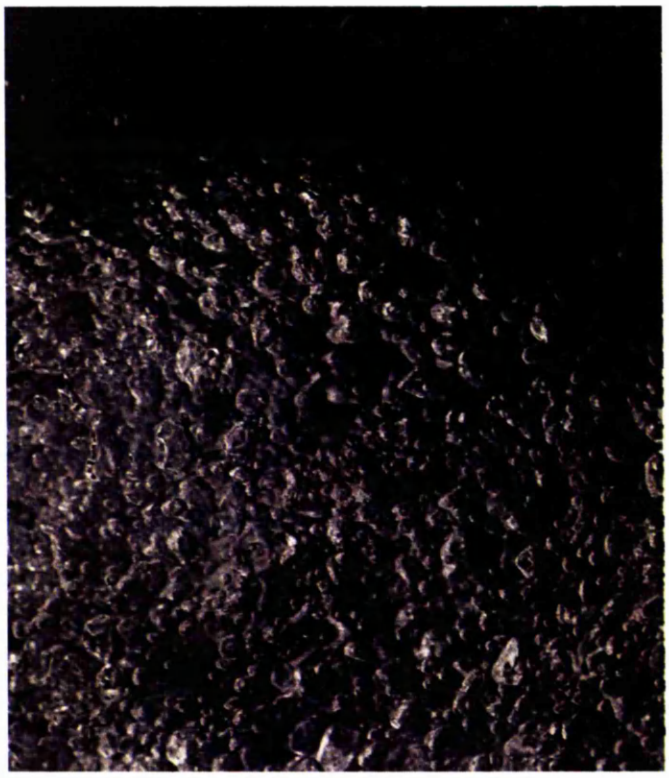

Figure 5-8: Nitrogen bubbles in cold acetic acid

Bubble Studies using the Buchi Rig

Figure 5-9: Gas bubbles in nitrogen sparged boiling acetic acid

Figure 5-10: Nitrogen bubbles in cold water

Bubble Studies using the Buchi Rig

Figure 5-11: Water vapour bubbles in boiling water

Figure 5-12: Gas bubbles in hot water sparged with ethylene at 10 barg

Bubble Studies using the Buchi Rig

Figure 5-13: Gas bubbles in hot water sparged with nitrogen at 10 barg

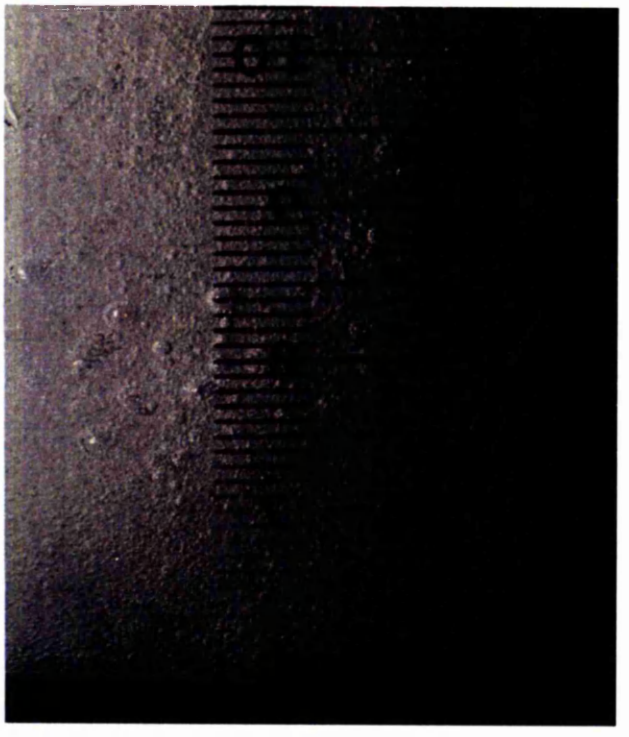

Figure 5-14: Nitrogen gas bubbles in cold aniline

Bubble Studies using the Buchi Rig

Figure 5-15: Gas bubbles in boiling aniline sparged with nitrogen

Figure 5-16: Nitrogen gas bubbles in a cold 20-ppm PPG solution

Bubble Studies using the Buchi Rig

Figure 5-17: Nitrogen gas bubbles in a cold 0.2 molar sodium sulphate solution

Figure 5-18: Gas bubbles in hot methanol sparged with ethylene at 10 barg

Bubble Studies using the Buchi Rig

Figure 5-19: Gas bubbles in hot methanol sparged with nitrogen at 10 barg

5.8.2 Heterogeneous Bubble Behaviour in a Mechanically Agitated Contactor

For bubble columns Krishna and Ellenberger (1995) describe the heterogeneous regime as two bubble classes, a dense phase of small bubbles which has a constant volume fraction with larger bubbles making up the rest of the distribution. Above the transitional superficial gas velocity required to trigger heterogeneous behaviour extra gas simply adds to the large bubble fraction. For operation at constant agitation rate, the same behaviour for mechanically stirred vessels is found, as illustrated by Figure 5-20 to Figure 5-22. The relative bubble fractions are very different for a 0.2 molar sodium sulphate solution compared to that for a 20 ppm polypropylene glycol solution in the same reactor geometry, but very similar for two 20 ppm PPG results in very different geometries. However when 20 ppm PPG solution results are compared at constant superficial gas velocity a large effect of

agitation on the fractions of large and small bubbles is found, as illustrated by Figure 5-23 to Figure 5-25. Greater agitation increases the fraction of large bubbles at the expense of small bubbles. This suggests coalescence rates increase faster than break-up rates with increasing agitation rates for this system.

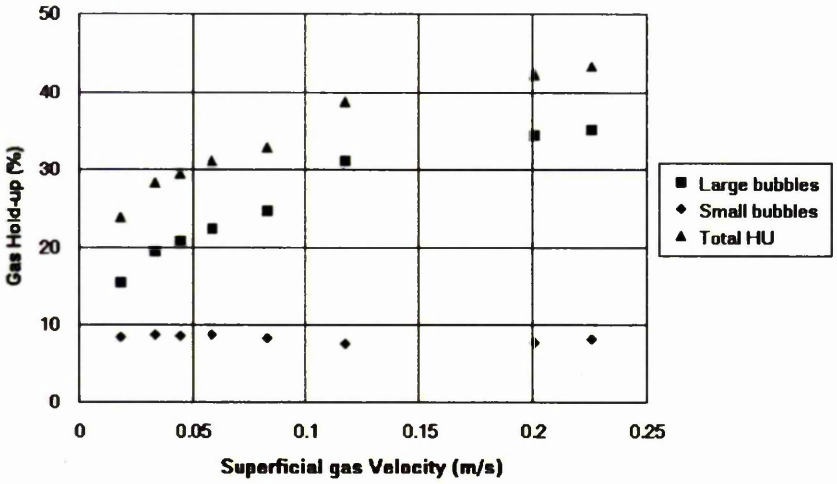

Figure 5-20: Gas hold-up by DGD analysis for a 0.2 molar sodium sulphate solution in the 2ft vessel R1 geometry at 280 rpm: Operation is in the heterogeneous regime

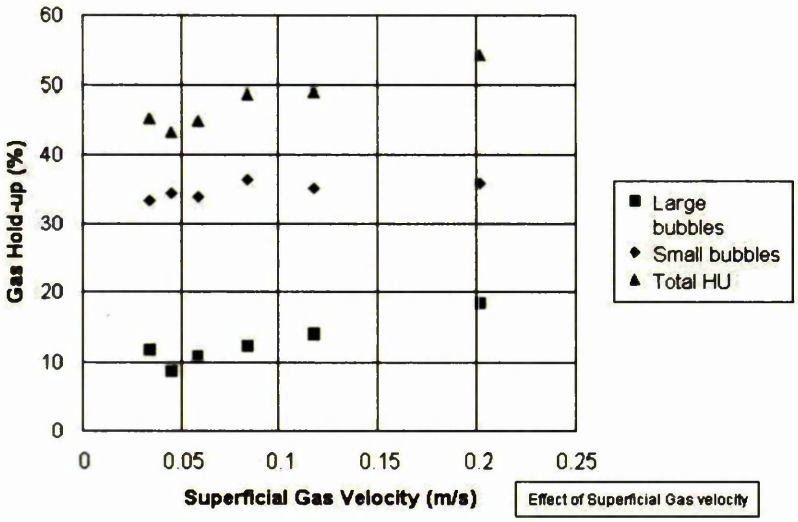

Figure 5-21: 2ft vessel R1 Gas hold-up by DGD at constant rpm for a 20-ppm PPG solution at 280 rpm. Operation is in the heterogeneous regime.

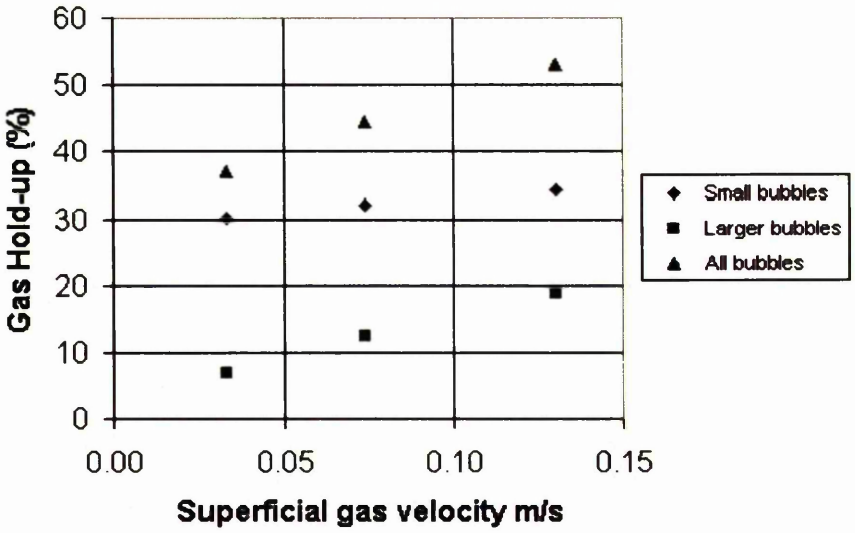

Figure 5-22: Gas hold-up by DGD in the 2 ft vessel R3 geometry at constant 300 rpm for a 20 ppm PPG solution. Operation in the heterogeneous regime

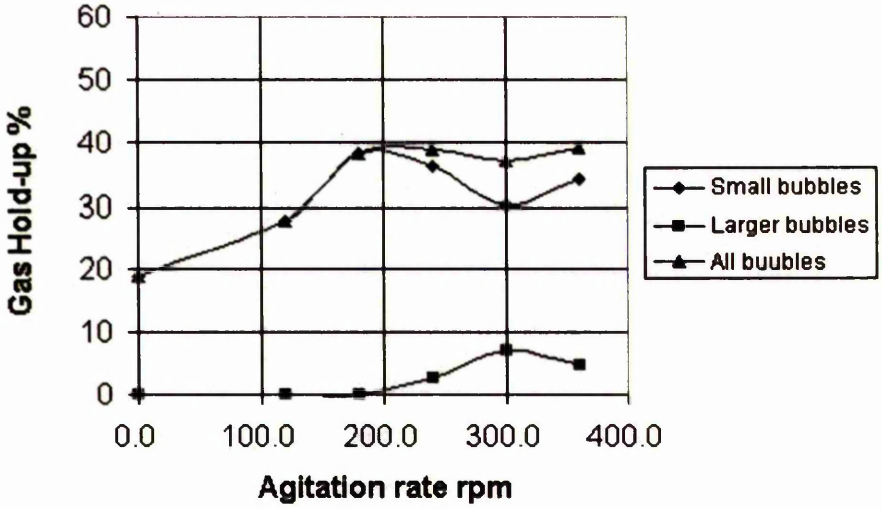

Figure 5-23: 2 ft vessel, R3 geometry. Gas hold-up at v_S = 0.033 m/s by DGD for 20 ppm PPG

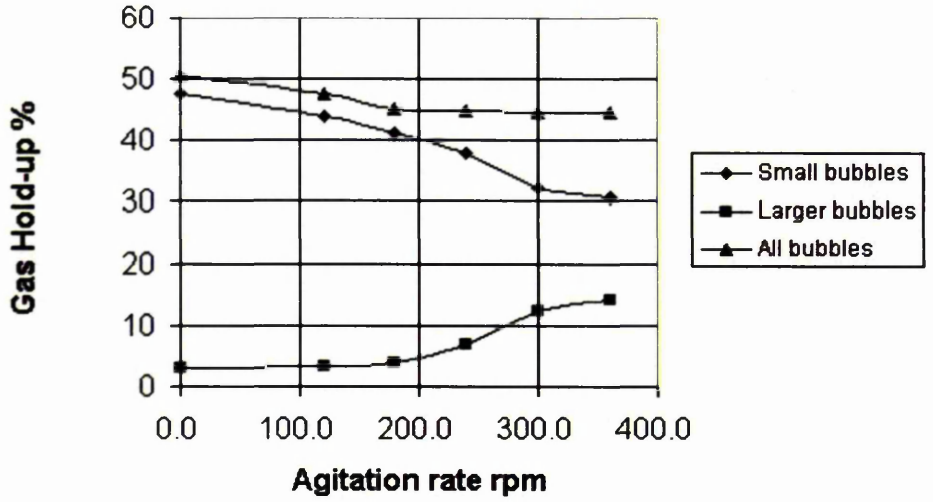

Figure 5-24: 2 ft vessel, R3 geometry. Gas hold-up at v_S= 0.074 m/s by DGD for a 20 ppm PPG solution

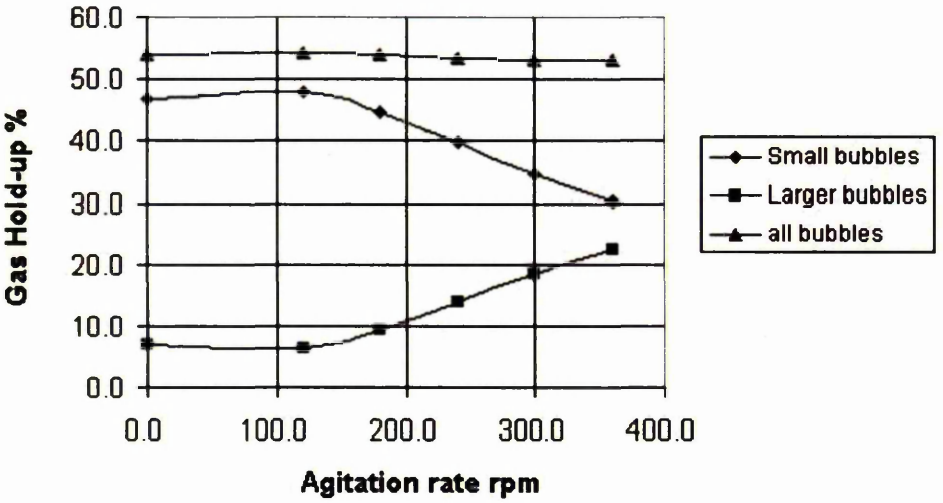

Figure 5-25: 2 ft vessel, R3 geometry. Gas hold-up at v_S =0.13m/s by DGD for a 20 ppm PPG solution.

5.8.3 Bubble Rise Velocities from DGD Analysis

Bubble rise velocities for a 0.2 M sodium sulphate solution and in a 20 ppm PPG solution at a fixed agitation rate are plotted against superficial gas velocities in Figures 5-26 and 5.27. These data were obtained on the 2 ft vessel R1 geometry for a fixed agitation speed. The data trend for the two systems is remarkably similar. Small bubble rise velocities are effectively constant for the range of gas rates suggesting a constant bubble size for the dense phase. The larger bubbles rise velocities increase with increasing gas rates. The shapes of the larger bubble curves are very similar to the classical curves of terminal velocity of air bubbles in low viscosity fluids as a function of bubble size (see Figure 2-43

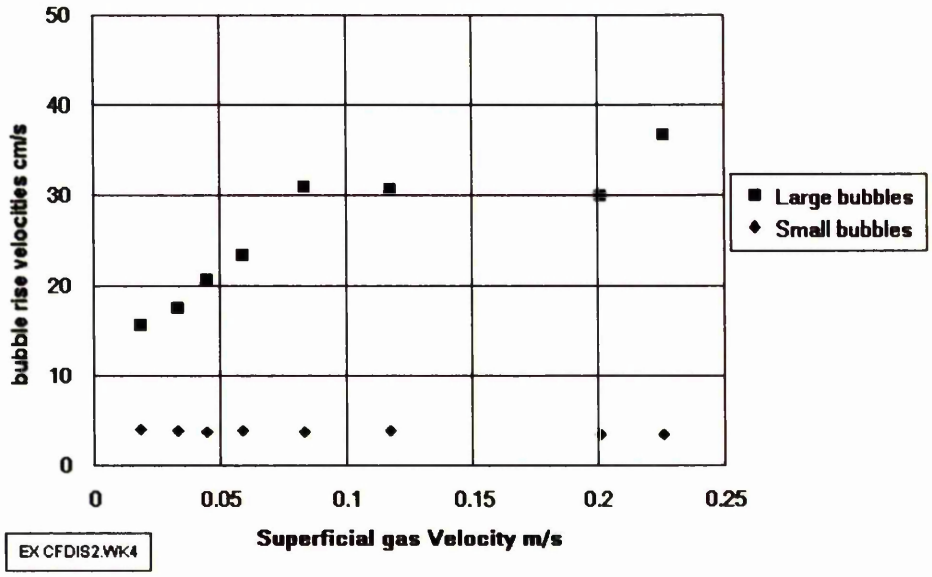

Figure 5-26: Bubble rise velocities versus superficial gas velocities measured by the dynamic gas disengagement technique in the 2 ft vessel, R1 geometry at 280 rpm, for a 0.2 molar sodium sulphate solution,.

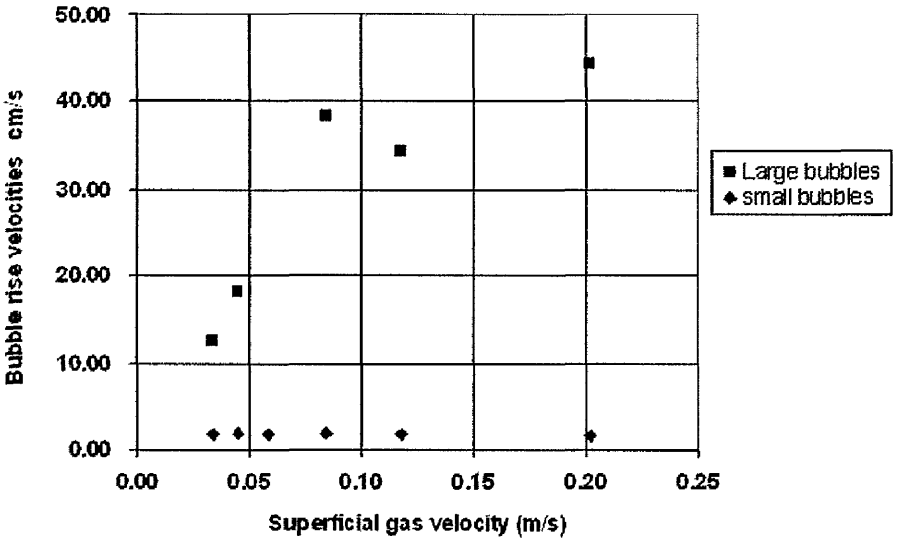

Figure 5-27: Bubble rise velocities versus superficial gas velocities measured by the dynamic gas disengagement technique in the 2 ft vessel, R1 geometry at 280 rpm, for a 20 ppm PPG solution.

5.8.5 Effect of Agitation on Bubble Size.

Agitation appears to have a surprising little effect on bubble size as illustrated by the series of graphs of bubble size versus agitation rate or agitation power in Figure 5-28 to Figure 5-37. What effect there is, mainly influences the Sauter mean bubble size rather than the number mean. The Sauter mean is weighted towards the larger bubbles. This suggests a shift in the distribution towards the smaller bubble sizes as agitation is increased, especially for operation in the homogeneous regime where this effect is more obvious.

A similar trend with the bubble sizes estimated from dynamic gas disengagement is noted. By this analysis the small bubble sizes estimated show reasonable agreement to the number mean determined from photographic analysis. By the DGD technique, the size of larger bubbles in the transitional regime (indicated by Figure 2-43) cannot be estimated.

Bubble Studies using the Buchi Rig

It appears that the sizes of the small bubbles are much more affected by the physical properties of the fluid than by the effects of agitation.

The bubble size graphs for water, determined by photographic analysis, confirm the impression given by the photographs that temperature and pressure do not have a dramatic effect on bubble size. However the dynamic gas disengagement technique does detect a difference between the cold and boiling water with cold water bubbles some 300 microns larger than boiling bubbles (see Figure 5-37).

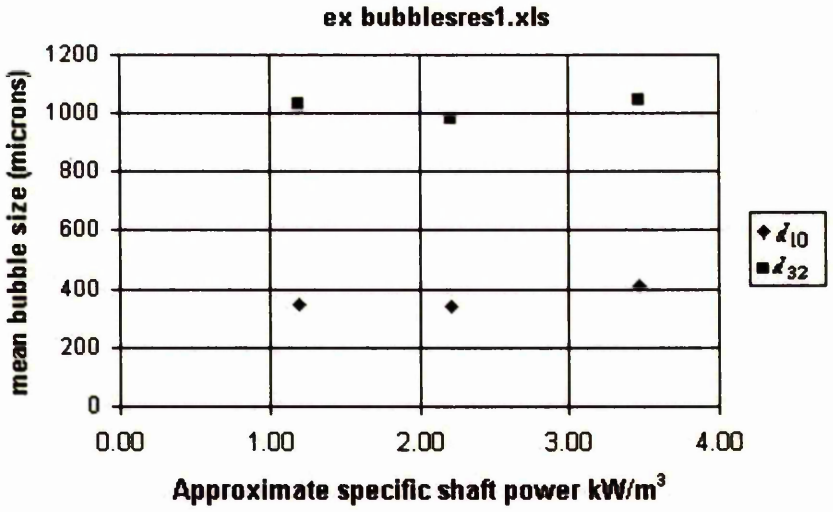

Figure 5-28: Boiling acetic acid d_{10} and d_{32} from photographic analysis in Buchi R1 geometry

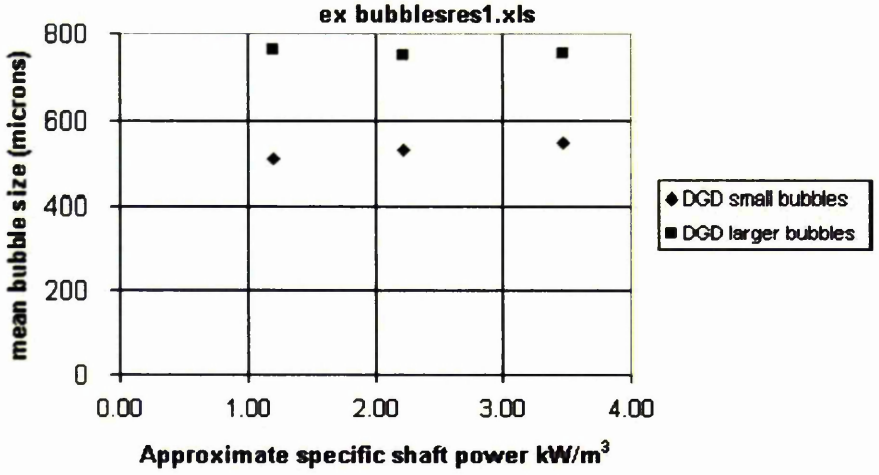

Figure 5-29: Boiling acetic acid large and small bubbles from DGD analysis in the Buchi R1 geometry.

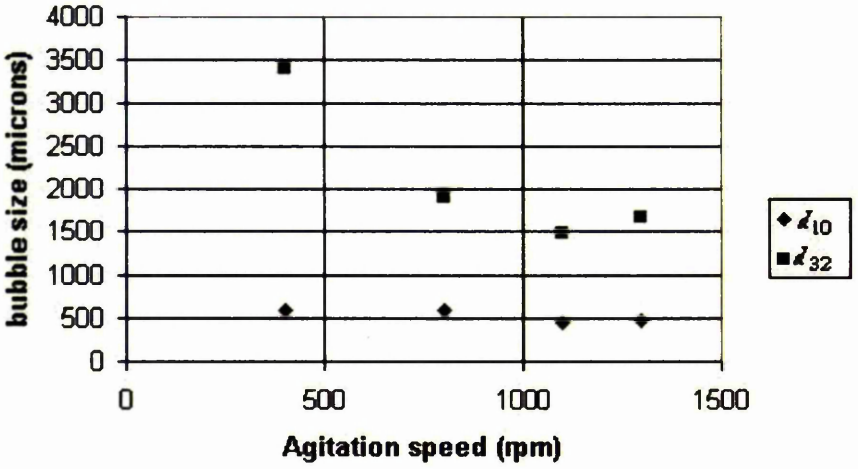

Figure 5-30: Boiling aniline d_{10} and d_{32} from photographic analysis at an inlet v_S of 0.0066m/s in Buchi R1 reactor geometry.

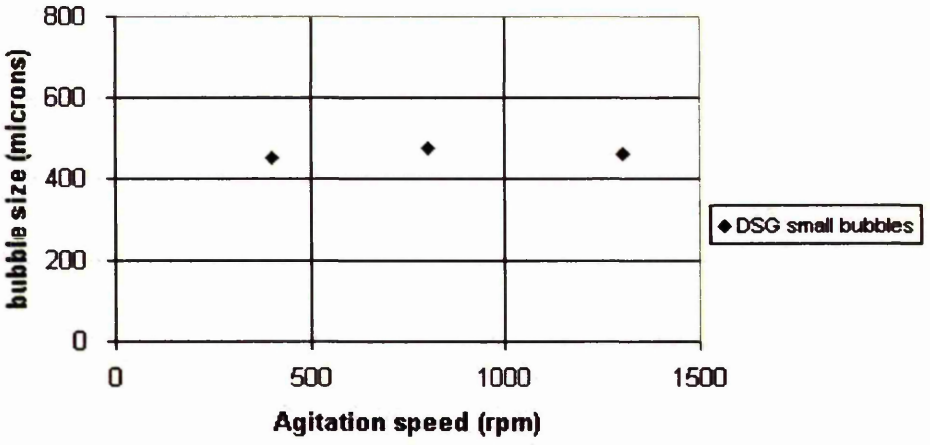

Figure 5-31: Boiling aniline small bubbles sizes from DGD analysis at an inlet v_S of 0.0066m/s in Buchi R1 reactor geometry.

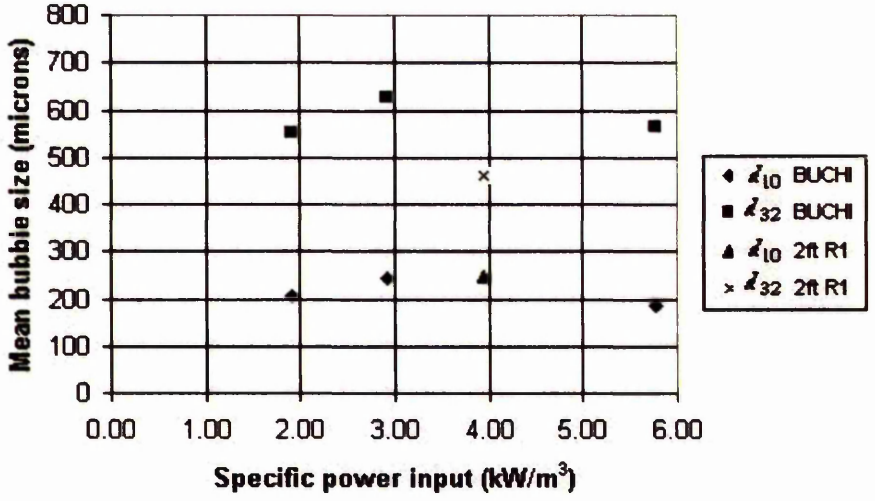

Figure 5-32: 20 ppm PPG solution; d_{10} and d_{32} from photographic analysis on two sizes of equipment; the Buchi R1 and the 0.61 m vessel R1 geometries.

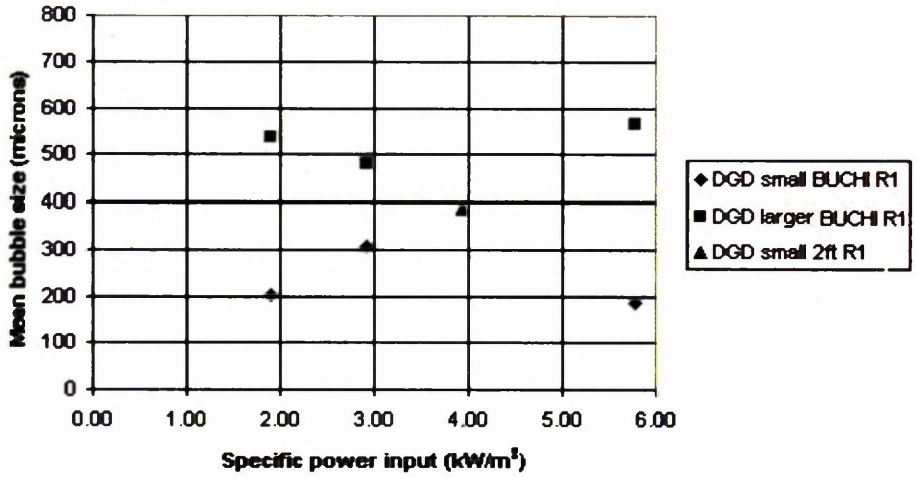

Figure 5-33: Bubbles sizes in 20 ppm PPG from DGD analysis on two sizes of equipment; the Buchi R1 and the 0.61 m vessel R1 geometries.

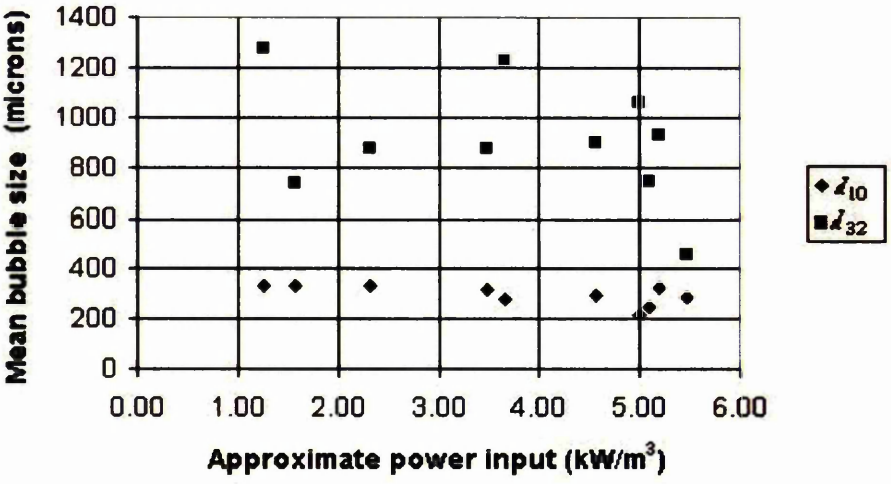

Figure 5-34: Bubble sizes in the Buchi 1 geometry for 0.2 molar sodium sulphate solution d_{10} and d_{32} are from photographic analysis

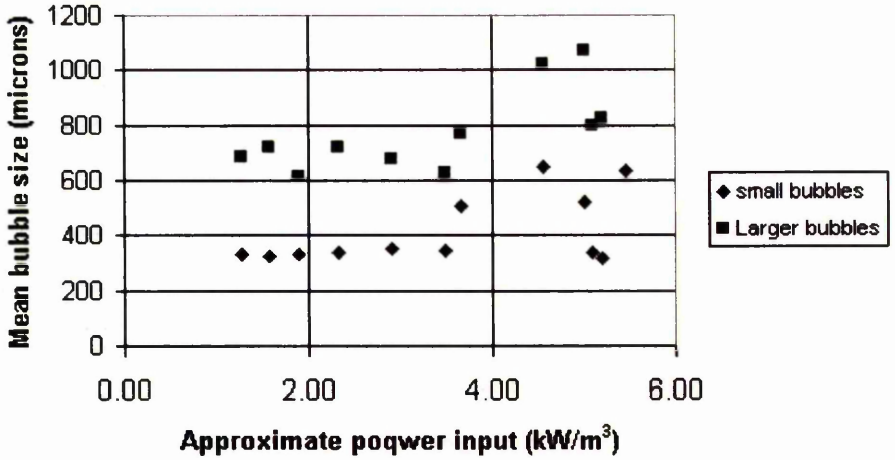

Figure 5-35: Buchi R1 geometry. 0.2 molar sodium sulphate solution large and small bubbles sizes from DGD analysis.

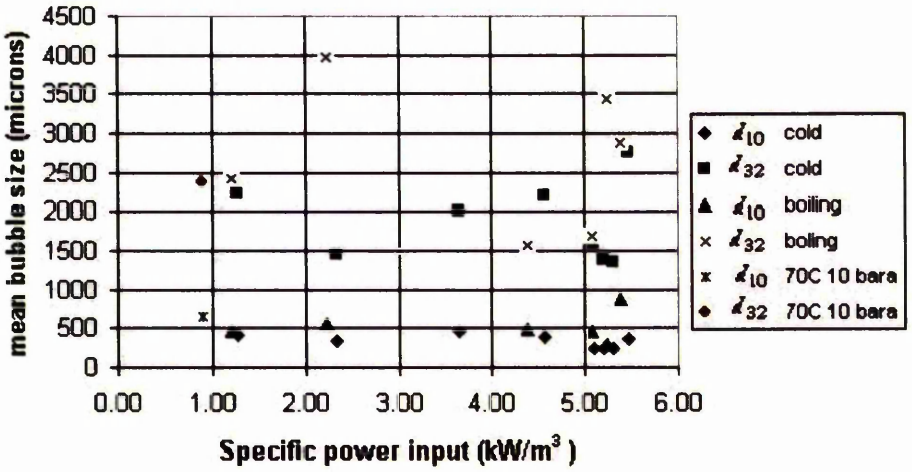

Figure 5-36: Buchi R1 mean bubble sizes. Cold, hot and boiling water at 1 and 10 atmospheres pressure at various v_S showing d_{10} and d_{32} from photographic analysis

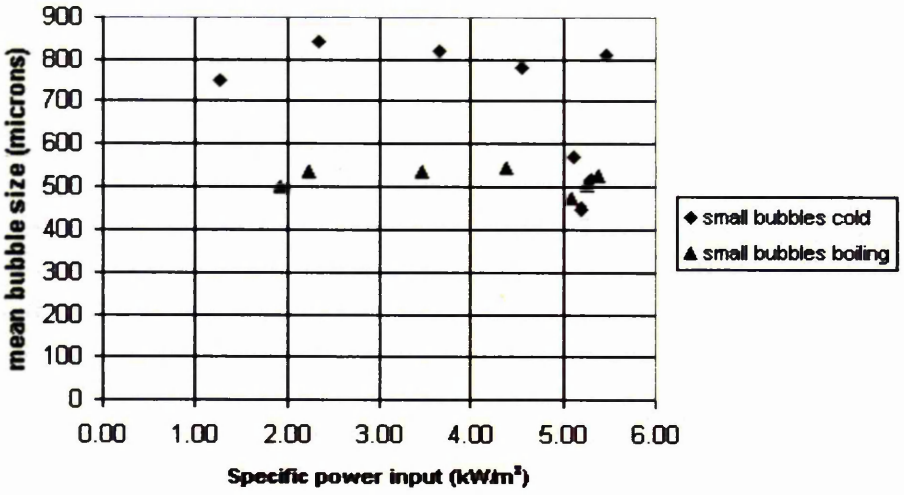

Figure 5-37: Buchi R1 geometry. Cold and boiling water, small bubbles sizes from DGD analysis at various v_S.

5.8.6 Effect of Superficial Gas Velocity on Bubble Size.

There is little effect of superficial gas velocity on the number mean bubble sizes (d_{10}) and the small bubble sizes determined by DGD analysis. This is illustrated by the series of graphs in Figure 5-38 to Figure 5-47. However, the effect of superficial gas velocity on the Sauter mean bubble size and on larger bubble sizes estimated by DGD analysis is not clear from this series of graphs.

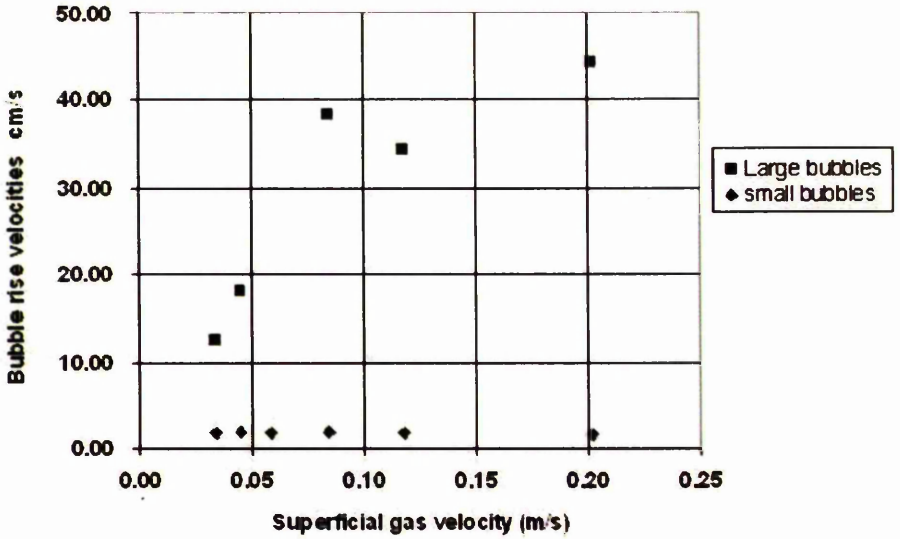

Figure 5-27 suggests that larger bubble sizes increase with greater superficial gas velocity in the heterogeneous regime.

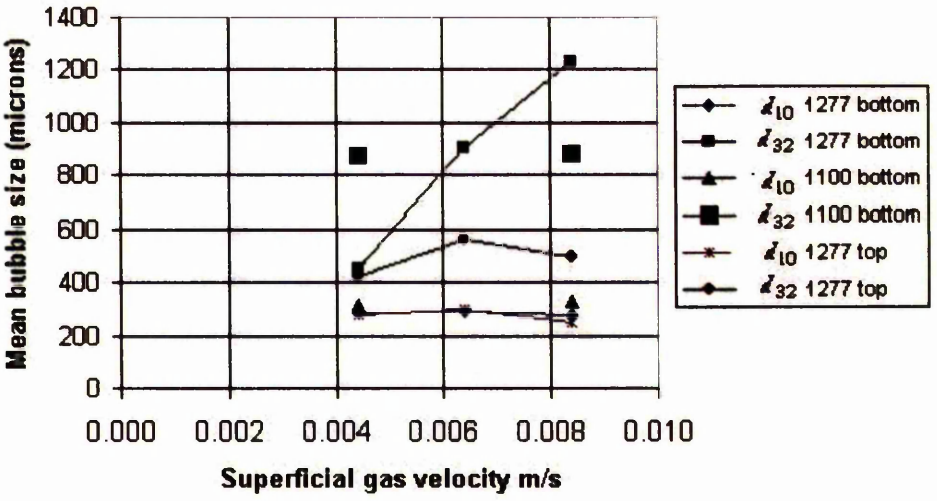

Figure 5-38: Buchi R1 geometry. 0.2 molar sodium sulphate solution d_{10} and d_{32} from photographic analysis at fixed rpm and various superficial gas velocities.

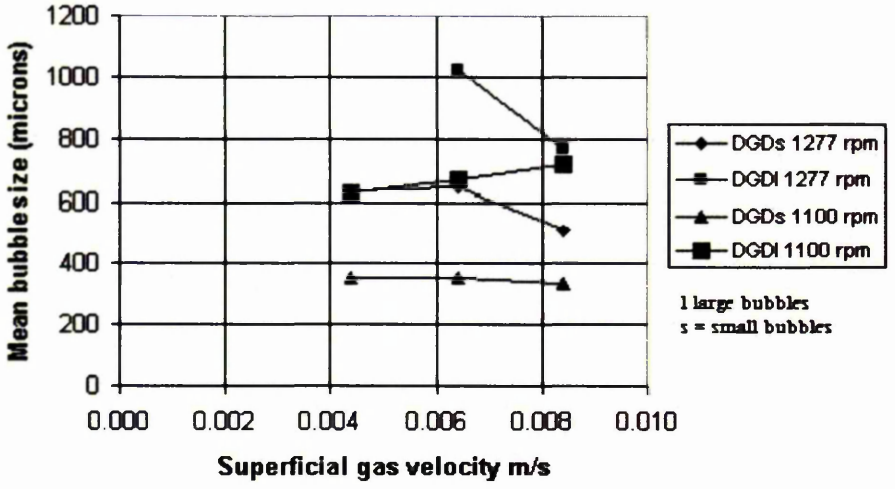

Figure 5-39: Buchi R1 geometry. 0.2 molar sodium sulphate solution large and small bubbles sizes from DGD analysis at fixed rpm and various superficial gas velocities.

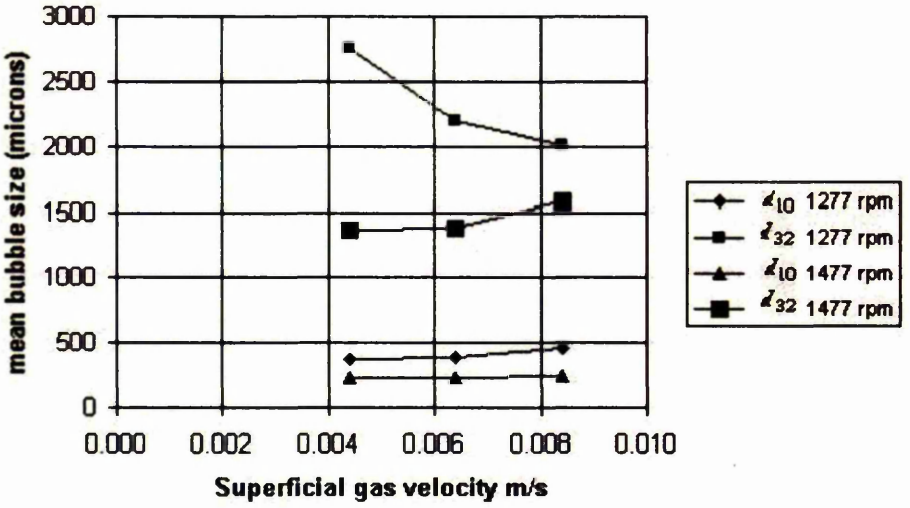

Figure 5-40: Mean bubble sizes in the Buchi R1 reactor geometry. Cold demineralised water, d_{10} and d_{32} from photographic analysis at fixed rpm and various superficial gas velocities

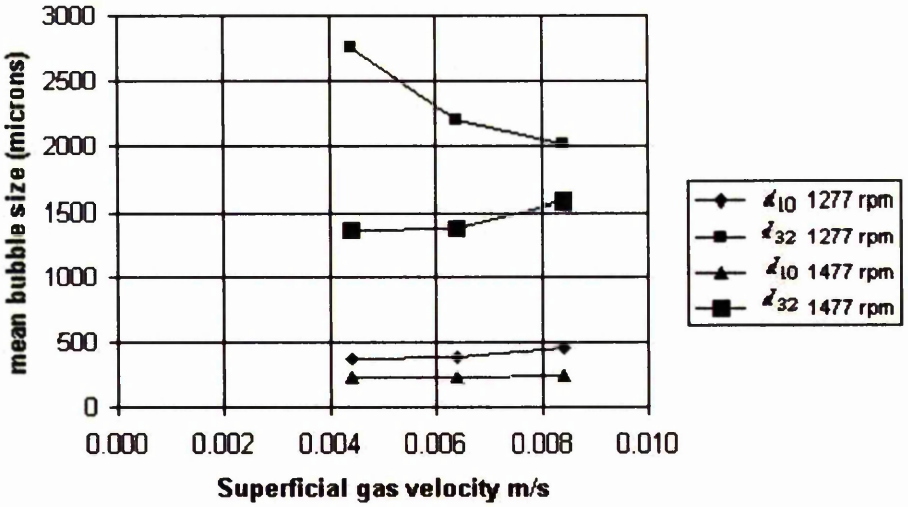

Figure 5-41: Buchi R1 geometry. Cold demineralised water, mean small bubbles sizes from DGD analysis at fixed rpm and various superficial gas velocities.

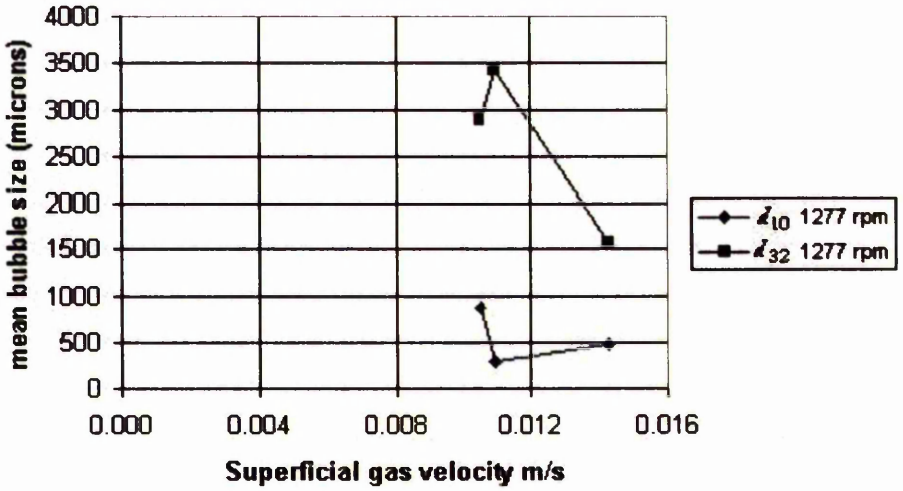

Figure 5-42: Buchi R1 geometry. Boiling demineralised water, mean d_{10} and d_{32} from photographic analysis at fixed rpm and various superficial gas velocities

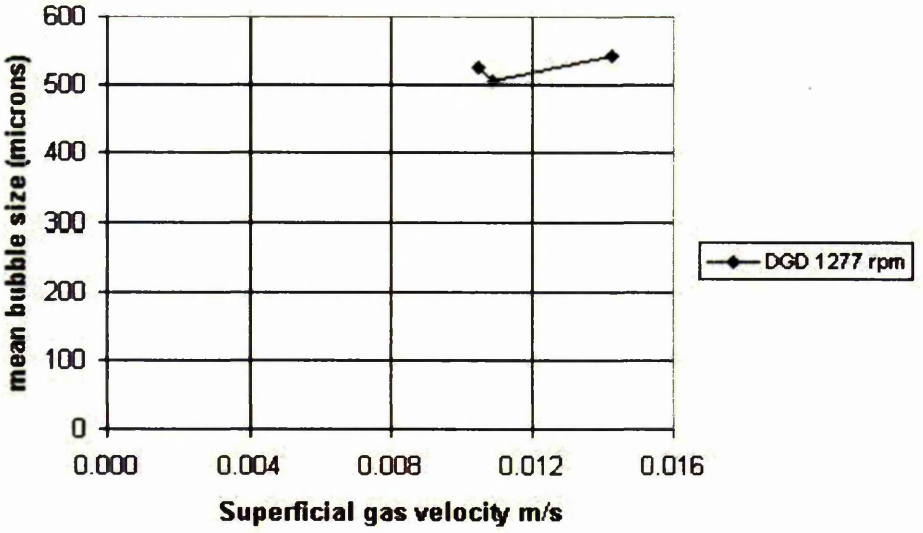

Figure 5-43: Buchi R1 geometry. Boiling demineralised water, small bubbles sizes from DGD analysis at fixed rpm and various superficial gas velocities.

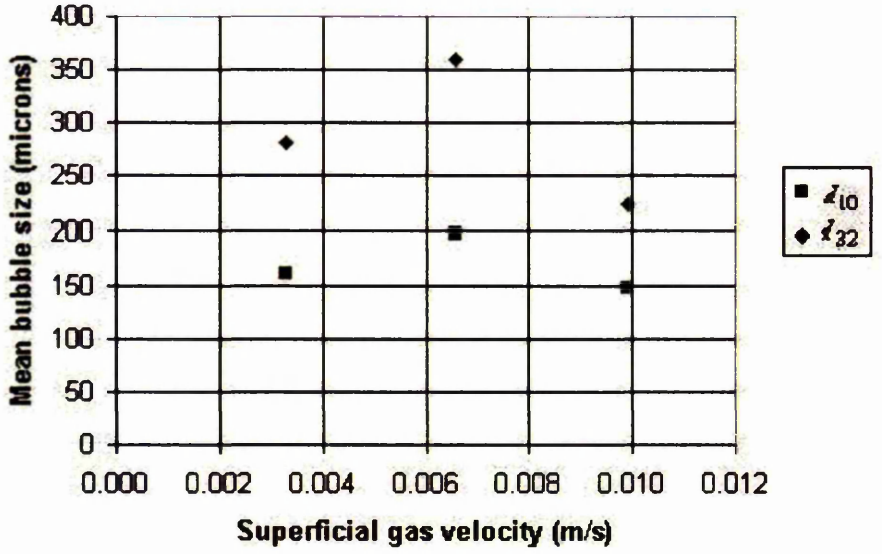

Figure 5-44: Buchi R1 geometry. Cold aniline, d_{10} and d_{32} from photographic analysis at a fixed 1300 rpm and various superficial gas velocities

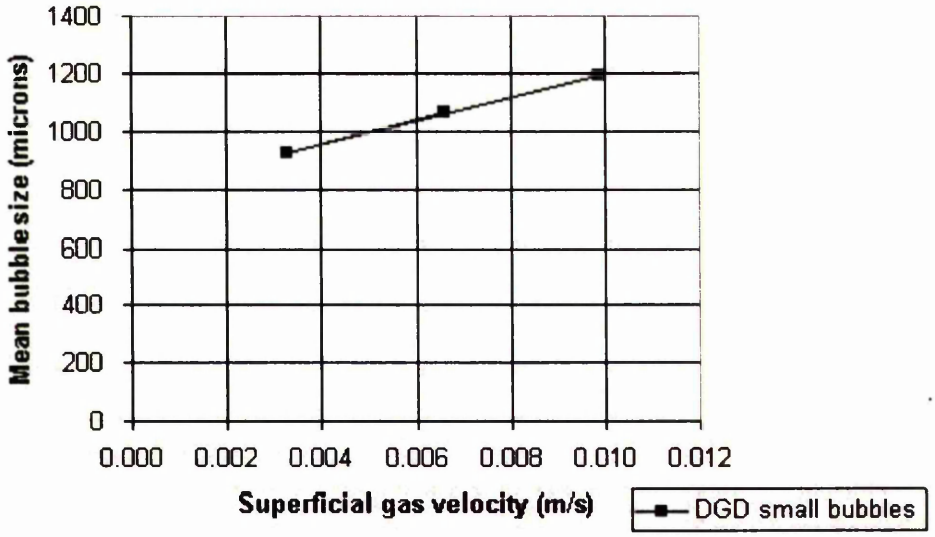

Figure 5-45: Buchi R1 geometry. Cold aniline, small bubbles sizes from DGD analysis at 1300 rpm and various superficial gas velocities.

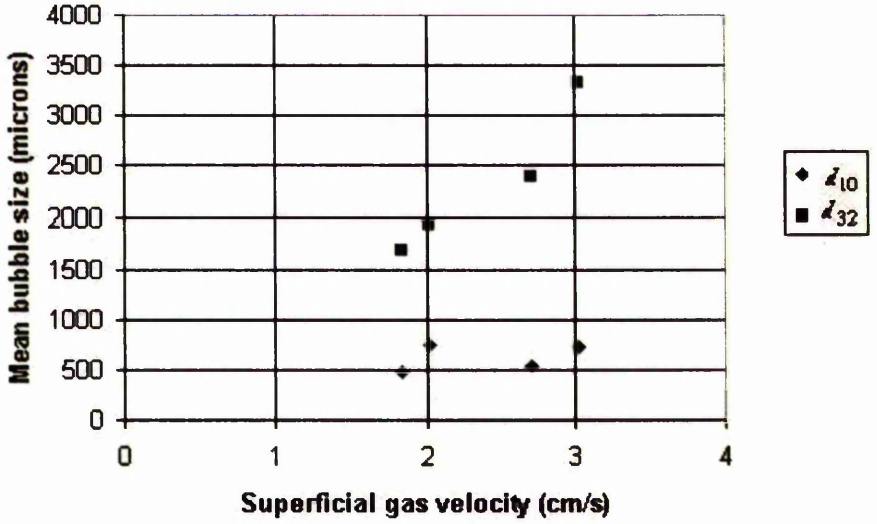

Figure 5-46: Buchi R1 geometry. Boiling aniline, d_{10} and d_{32} from photographic analysis at 1300 rpm and various superficial gas velocities.

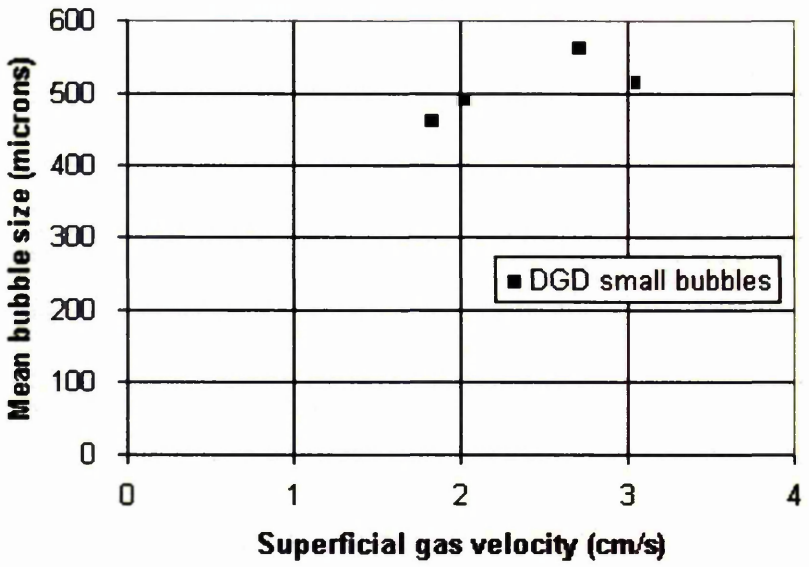

Figure 5-47: Buchi R1 geometry. Boiling aniline, small bubbles sizes from DGD analysis at 1300 rpm and various superficial gas velocities.

5.8.7 Gas Hold-up

Gas hold-up results for the various fluids tested are shown in previous Figure 5-20 to Figure 5-25 and following Figure 5-48 to Figure 5-51. Comments worth noting are:

The percentage of small bubbles in the dense phase varies very significantly with the fluids. For sodium sulphate it is around 8% (Figure 5-20); for water (Figure 5-48) and boiling glacial acetic acid (Figure 5-51) it is around 10%, whilst the 20 ppm PPG solution has a dense phase of 30 to 48% (Figures 5.21 to 5.25). Boiling aniline at 33% hold-up appears to be still operating in the homogeneous regime (Figure 5.50). Note that, as seen earlier in Figure 5-24 and Figure 5-25, the dense phase fraction is also affected by agitation.

The gas hold-up fraction is therefore not just a function of bubble size and bubble rise velocity but also depends on the volume of gas in the dense phase.

Bubble Studies using the Buchi Rig

One might speculate that a balance between break-up and coalescence rates control the dense phase volume. In the heterogeneous regime the concept of non-coalescing fluids are meaningless as coalescence is clearly occurring.

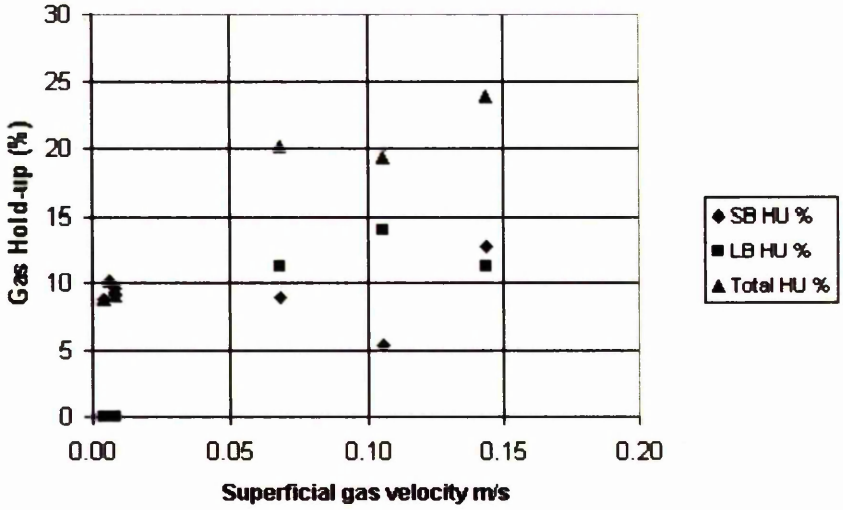

Figure 5-48: Gas hold-up for cold water in Buchi 1 geometry: *P/V* varied. Operation in homogeneous and heterogeneous regime/

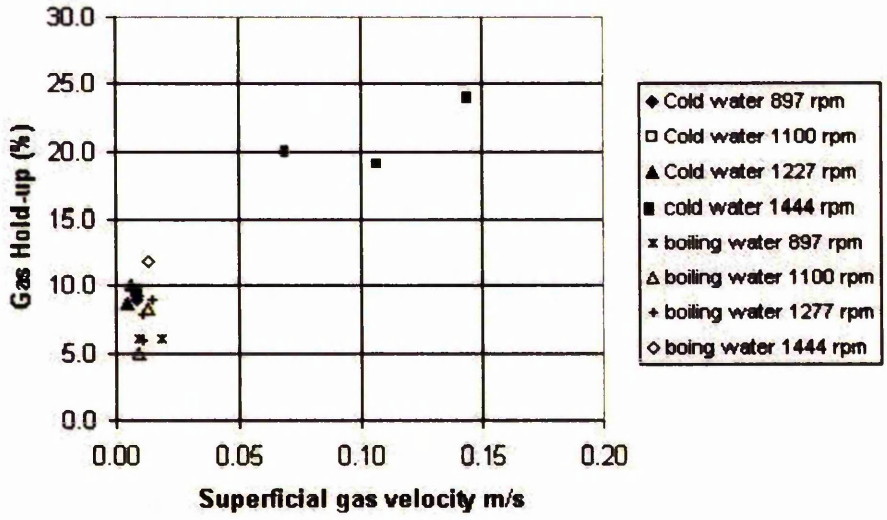

Figure 5-49: Total gas hold-up for cold and boiling demineralised water in Buchi 1 as a function of superficial gas velocity.

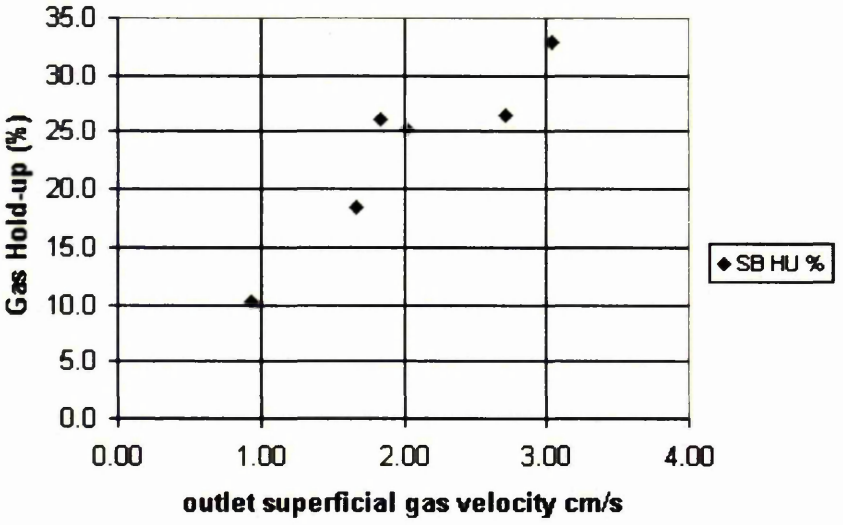

Figure 5-50: Gas hold-up for boiling aniline in Buchi 1 geometry. Operation is in the homogeneous regime. *P/V* varied.

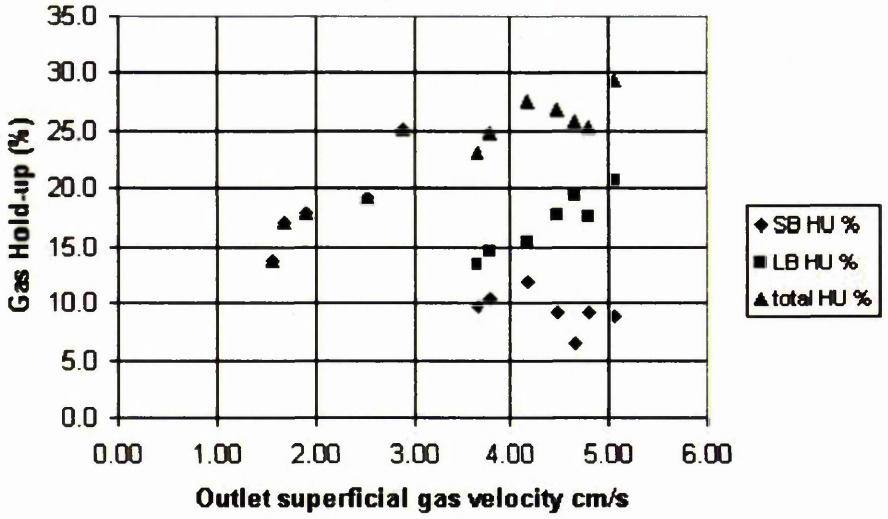

Figure 5-51: Gas hold-up for boiling acetic acid in the Buchi 1 geometry: Operation in homogeneous and heterogeneous regime. *P/V* varied.

5.7.9 Test of Equation (5.2) $v_S = \left(\frac{dh}{dt}\right)_I$

Bubble Studies using the Buchi Rig

Initial disengagement rate data is compared with the steady-state superficial gas velocity in Figure 5-52. Data is from the 2ft vessel, R2 geometry for a 0.2 molar sodium sulphate solution. The agreement between the initial disengagement rate and the steady-state superficial gas velocity confirms that the initial disengagement rate does indeed give a good indication of the vessel superficial gas velocity even when applied to a mechanically agitated vessel. This provides confirmation that the dynamic disengagement technique work can be extended to the mechanically stirred reactor area. It also provides a way of estimating the superficial gas velocity for the boiling case. It could be extended to provide boil up rates for heat transfer calculations.

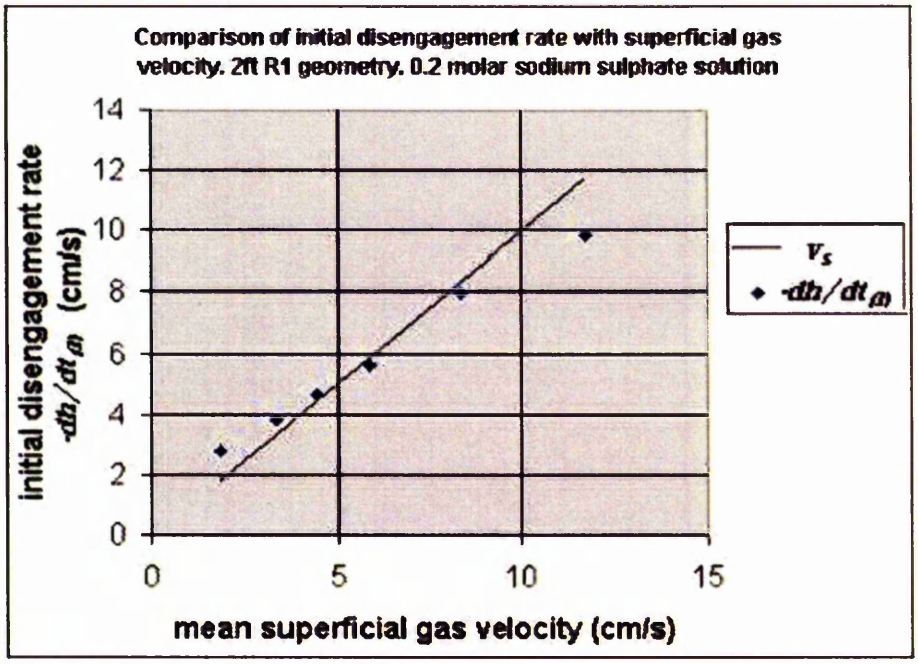

Figure 5-52: Test of equation (5.2) $(dh/dt)_{(0)} = v_S$ at steady state

5.7.10 Effect of Solids on the Small Bubble Fraction

De Swart and Krishna (1995) showed that solids supplant small bubbles in the dense phase in bubble column reactors operating in the heterogeneous regime.

This work shows the same effect occurs in mechanically stirred contactors as illustrated by Figure 5-53. The total volumetric hold-up of gas plus solid remained constant with increasing solids concentration, with the solids replacing the gas in the dense phase. Solids were 205 micron glass ballotini beads. The test fluid was a 20 ppm PPG solution that supports a large concentration of particles in the dense phase. It is interesting to speculate on the effect on other systems such as water or a 0.2 molar sodium sulphate solution where 10% by volume solids would completely supplant the gas in the dense phase, suggesting potentially a very large effect on gas-liquid mass transfer.

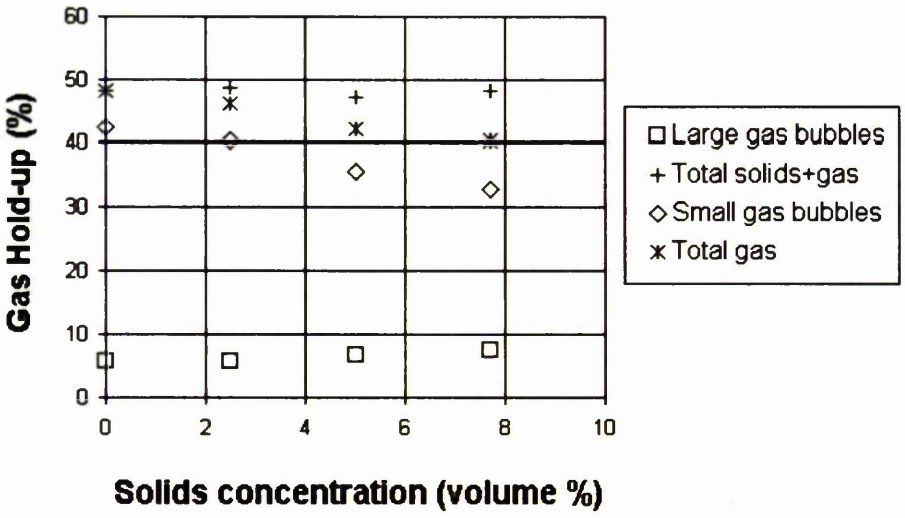

Figure 5-53: Effect of 205 micron glass ballotini solids on the dense phase gas hold-up. Data from the 0.61m vessel R2 geometry. Superficial gas velocity is constant at 0.07 m/s.

A selection of the work from this chapter was presented at Eurotherm 71, "VISUALIZATION, IMAGING AND DATA ANALYSIS IN CONVECTIVE HEAT AND MASS TRANSFER, October 28-30, 2002, REIMS, FRANCE by Cooke *et al.* (2002)

Acknowledgements

The author would like to acknowledge the contribution of Tom Phillips, Mona Rafi and Bill Merideth in ICI technology group who assisted in the experiments and bubble analysis

Also ICI Technology (ICI Research and Technology Centre, UK), Huntsman Polyurethanes (3078 Everburg, Belgium) and DuPont (UK) Limited (DuPont Polyester Technologies), who supported this work.

Chapter 6 : Single Phase Hydrodynamics
: Covering the Effects of Geometry and Scale on Flow, Mixing and Agitator Power In Mechanically Agitated Vessels under Fully Turbulent Conditions

6.1 Summary

This chapter describes power, mixing and hydrodynamics for single-phase fluids using novel agitators or agitator combinations with comparisons against conventional agitators such as the Rushton turbine. The mixing literature is reviewed and compared with the results of these studies. An equation is proposed for the effect of scale and blade geometry on the power number of concave hollow blade agitators.

Mixing, flow visualisation and power in single-phase turbulent flow are measured for five agitator types: two radial types - two different diameters of disc turbines and a 6SRGT - and three mixed flow or axial types; a 4MFD, 4FMU and a Lightnin A310 as illustrated in Figure 6-1 (a to f). These are all compared on a single scale (T = 0.288 m) as a function of agitation speed and aspect ratio H/T.

Further studies compared the use of a single agitator with triple disc turbines or triple A345 agitators for vessel geometries of $H = 2T$.

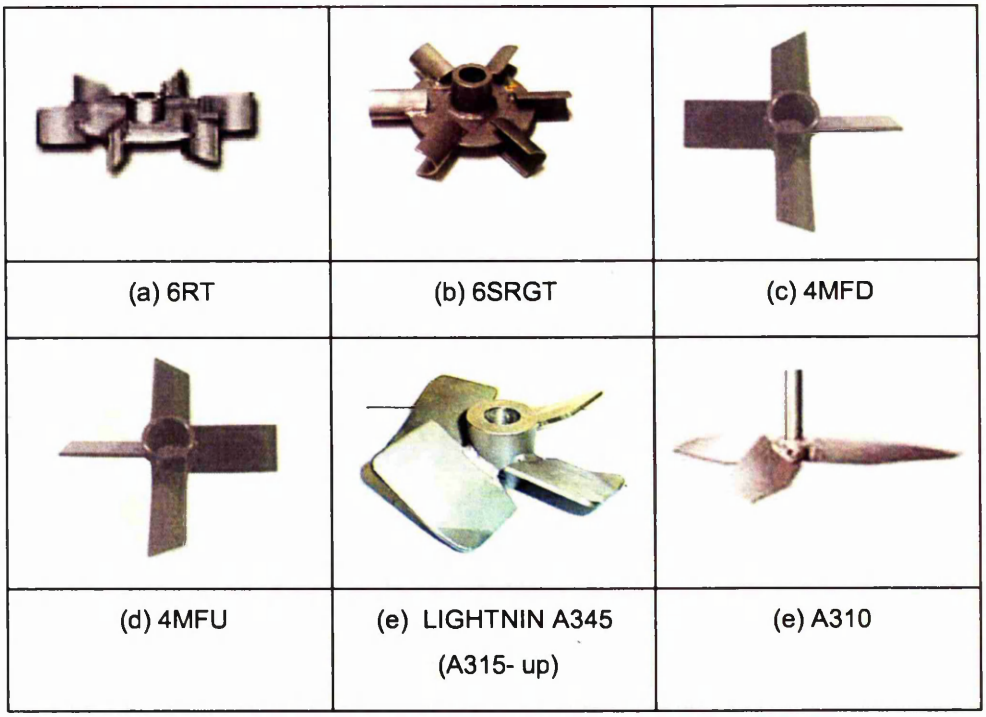

Figure 6-1: Types of agitators used in the mixing studies. Note A315 –up rotates in anti-clockwise direction. The remaining agitators are rotated clockwise.

Even for $H = T$ geometries it is found that all the mixing time data cannot be accurately described by a single correlation as claimed for example by Ruszkowski (1994). With the disc turbines, the larger D/T is more energetically efficient for mixing. This agrees with earlier published work of Cooke *et al.* (1988) and Ruszkowski (1994). The LIGHTNIN A310 and the 4MFU are the least energetically efficient for mixing at the $c = T/4$ clearance used in this work. This is consistent with the flow visualisation and it could be that optimising the clearance would improve the mixing which should be considered in further work. All the other agitators can be described by a single correlation.

The effect of H/T on mixing time was dependent on the flow patterns. However it is demonstrated that a single agitator at a clearance of $T/4$ was more energetically efficient than multiple disc turbines for mixing up to $H = 2T$. This is because the latter produces flow compartmentalization (see page

13). For single agitators the effect of aspect ratio on mixing is shown to approximate to a proportionality of $(D/H)^{2.0}$.

Mixing tests with multiple agitators confirm that the overall mixing depends upon the flow patterns and the degree of compartmentalization (see page 15). The triple A345 agitators with agitator and surface separations of $\leq 1D$ were found to have excellent mixing capabilities.

Work on larger scales indicates that the mixing time constant (as defined in section 2.5.5.5) has not scaled up. Results for the single 4MFD at $H = 1.25T$ and for the triple A345 show a larger Nt_{90} on scale-up, even accounting for any small differences in D/T ratios. This effect has been noted by other workers, for examples, Kipke (1983) and Raghav Rao and Joshi (1988) have both reported that for geometrically similar vessels, Nt_{mix} increases on scale-up at constant power per unit volume. This, nether the less, was a somewhat unexpected result and is worthy of further study. Kipke (1983) argues this may result from the larger turbulent eddies that exist on a larger scale that take longer to decay. It may also be due to a longer lag time on scale-up.

Finally the ITS 2000 ERT tomography sensors on the 0.61m diameter vessel are used to demonstrate the techniques for the study of mixing at selected pixels and inter-zone mixing between sensor planes. The mixing times found by tomography are favourably compared with those obtained using mixing probes.

6.2 Aims of the Study

This study is aimed at extending the work on the standard geometry to different aspect ratios and other agitator geometries including multiple agitators in order to produce some guidelines on the effect of geometry on flow and mixing. This means trying to link flow visualisation studies with power

measurements and mixing measurements in order to gain an insight into the mechanisms controlling the mixing process.

Much of the stirred tank literature is concerned with studies based on standard tank geometries as described in Chapter 2 (Figure 2-3). In the "real world" vessel geometries frequently deviate from this geometry, both with respect to the number, types and position of the agitators and also with respect to the aspect ratio (H/T).

Hollow blade agitators are finding increasing popularity due to their ability to handle gas without significant loss of power. However there are a number of designs on offer and not much in the way of power number data. Therefore these were studied to determine the effect of blade geometry and scale on the power number. A correlation to describe the power number in terms of geometry and scale is proposed.

6.3 Background to these Mixing Studies

An overview of mixing was given in Chapter 2, section 2.5. In earlier published work (Cooke *et al.* 1988) mixing at different scales was studied, comparing single agitators in vessels of aspect ratios $H = T$ with multiple agitators in tall vessels. It was shown that for single agitators in $H = T$ vessels, disc turbines and ICI Gasfoils, although widely differing in power numbers, could correlated together using a common constant by an equation of the form,

$$N\theta . Po^{1/3} (D/T)^{\beta} = \text{constant} \qquad (6.1)$$

where N is agitation speed, θ a specified degree of mixing, Po is agitator power number (either ungassed or gassed providing operation was above the flooding point); D is the agitator diameter and T the tank diameter. In that work for 90% mixing the power law index (β) was found to be 2.2 and the constant 3.9.

More recently Ruszkowski (1994) reported that equation (6.1) could be equally applied to a range of pitch blade impellers, a disc turbine and a propeller

agitator. For 95% mixing the quoted power law index (β) was 2.0 and the constant 5.3. When compared at the same degree of mixing, Cooke *et al* (1988) and Ruszkowski (1994) predict very similar mixing times (see Chapter 2, section 2.5.5) suggesting that specific power input (rather than circulation) may be the dominant factor for mixing, in agreement with turbulence theory (see Chapter 2, section 2.4).

In terms of energy input equation 6.1 can be rearranged (chapter 2, Eq. (2.59)) to give

$$\theta = k\left(\frac{4}{\pi}\right)^{1/3} \varepsilon_T^{-1/3}\left(\frac{D}{T}\right)^{5/3}\left(\frac{D}{T}\right)^{-\beta} \qquad (6.2)$$

Not all workers agree that all impellers are equally energetically efficient. The correlations of Khang and Levenspiel (1976) are similar to the Ruszkowsi (1994) correlation, but do not contain a power number term. However, the power number is introduced into the constant for calculation purposes. Their correlations are based on circulation time theory and imply that the propeller is more energy efficient for mixing than a disc turbine by a factor of around 4, when used with their power numbers of 5 for the disc turbine and 0.6 for the propeller. Shiue and Wong (1984), using a thermal response technique to measure t_{95} for a range of agitators at a clearance of $T/2$ in a 0.4 m diameter vessel, found that axial agitators were more efficient for mixing than radial agitators. Raghav Rao and Joshi (1988) measuring close to complete mixing, using a graphical conductivity tracer technique, found that pitch blade turbines (PBTs) were more energy efficient than disc turbines, with down-pumping the most efficient mode. The PBT down (4MFD) at $D = T/3$ was the most efficient of all. Their correlation for the 4MFD was given as,

$$N\theta \propto (T/D)^{1.83} \qquad (6.3)$$

If the power numbers were constant with D/T, then from equation (6.2) this would lead to, $\theta \propto (D/T)^{-0.16}$, that is the mixing time would decrease with increasing D/T at constant specific power input. The result that the smaller

D/T gave the smallest mixing time at constant P/V is therefore surprising and results from the fact that smaller D/T agitator has the lowest power number, probably due to this producing the most axial flow. However, the differences were small and could be within the error bands.

In Chapter 2 (section 2.5.5.7) it was demonstrated using equation (2.59) or (6.2) that the power law indices (β) found to fit equation (6.1) implies that large (D/T) agitators are more energetically efficient for mixing. When (β) =2, then $\theta \propto (D/T)^{-1/3}$ and for (β) =2.2, then $\theta \propto (D/T)^{-0.533}$, assuming Po is constant with changes in D/T.

However, increasing D/T increases torque for a given power and that means heavier shafts and bigger gearboxes resulting in increased installation costs. With mixed flow agitators, the power number can also be function of diameter. Hence the optimum agitators for mixing are not obvious. The hydrofoil hollow blade radial agitators such as the Scaba 6SRGT have power numbers relatively independent of D/T within normal limits. These are attractive for mixing since their relatively low power numbers minimise the torque at the larger (D/T) for a given power input compared to the Rushton turbine.

For gas-liquid duties, radial hollow blade turbines (HBTs) and up-pumping impellers are often preferred for the dispersion duty. Therefore one of the aims of this study was to extend the agitator mixing comparisons to include up-pumping impellers and another type of commonly used HBT; namely the Scaba 6SRGT.

Equation (6.1) relates to $H = T$ geometries. It is quite common to see single agitators in higher aspect ratio vessels. A common configuration using a 2:1 elliptical base is to site the agitator at the bottom tan-line (clearance $c = T/4$) and to operate at a liquid level equal to T above it, giving an overall H/T = 1.25. One might reasonably expect that the effect on the mixing time of the increased head above the agitator would be different depending on whether or not the main circulation loop reaches the surface and this may well be agitator

dependent. If the level is increased further the chances of the main circulation loop reaching the surface will decrease.

Cooke *et al.* (1988) found that mixing took considerably longer in tall vessels agitated with multiple disc turbines when compared at equal specific energy inputs. In order to fit data for a triple impeller agitated $H = 2T$ vessel with the data for the $H = T$ vessel the equation proposed was,

$$\mathrm{Nt}_{90} \cdot \mathrm{Po}_{\mathrm{total}}^{1/3} (D/H)^{2.43} = \text{constant} \qquad (6.4)$$

where H is the height of the gas-liquid dispersion above the bottom of the base, and $\mathrm{Po}_{\mathrm{total}}$ is the sum of the power numbers based on a common diameter. If agitators of different diameters are used it is common to base the total power on the larger diameter. To correct the Po of agitator 1 (A_1) to the different diameter of agitator 2 (A_2) then since for the same power,

$$\mathrm{Po}_1 \rho N^3 D_1^5 = \mathrm{Po}_2 \rho N^3 D_2^5. \text{ Therefore } \mathrm{Po}_2 = \mathrm{Po}_1 \left(\frac{D_1}{D_2} \right)^5$$

The constant in equation (6.4) was found to be 3.3 for three Rushton turbines and approximately half that number when the two top impellers were replaced by down-pumping axial impellers (either Plenty hydrofoils or 6MFDs). The increase of mixing time with multiple agitators is believed to be due to compartmentalization especially when radial agitators are used. Colour change mixing experiments on triple radial agitators showed that mixing occurred rapidly in the stage where the tracer addition was made and this is then mixed rapidly in the second agitator stage followed by the third. In each stage this mixing was essentially complete before the colour change started in the next stage. Using axial-radial agitator combinations reduced the staging effect. Other workers have reported similar staging effects using multiple radial impellers for example Cronin *et al.* (1994) for Rushton turbines. Manikowski *et al.* (1994) and Otomo *et al.* (1995) confirmed that the overall mixing time reduced by about 50%, when the two upper turbine agitators were replaced with axial flow

agitators. Note that feeding simultaneously to each agitator should eliminate this staging effect and this is worthy of further study.

There is a paucity of information for mixing with single agitators at aspect ratios greater than one, even though this is quite a common processing configuration. Therefore tests were included in this study with single agitators at a clearance of $T/4$ with aspect ratios up to 2:1 for a range of agitators. Power measurements and flow visualisation studies were also carried out. The mixing results reported by Cooke *et al* (1988) were weighted towards the Rushton turbine data obtained in the large 1.79 m vessel. This vessel had a flat base that meant that the volume is greater than for a dished vessel operated at the same total depth of liquid. The flat bottom may also give "dead zones" in the corners. For this earlier work the raw data were analysed graphically to obtain t_{90}-mixing times and operation in some cases was above the onset of surface aeration giving noisy data. Also it is not clear whether $N\theta$ is scale independent. Kipke (1983) reviewed scale-up anomalies and noted that the expression $N\theta$ = constant, for geometrically similar vessels, does not necessarily scale-up. He argued that this was because the macro-scale of turbulence scales with impeller size. Thus larger eddies are found in large vessels that result in larger variations and therefore the final state of mixing is achieved later in larger vessels. Raghav Rao and Joshi (1988) reported that for geometrically similar vessels, $N\theta$ increased on scale-up at equal specific energy input (P/V). For these reasons it was therefore deemed wise for these comparisons to include disc turbines in the present study and to limit operations before the onset of surface aeration so that a good comparative set of mixing data could be obtained at the same scale.

The decision to do all the work at a single clearance requires justification. It may well be that there is an optimum position of an agitator for mixing purposes and this may also depend upon the type of agitator and D/T. Indeed, this is what some experimenters have found. Raghav Rao and Joshi (1988) tested clearances of $T/3$, $T/4$ and $T/6$ and found that for Rushton turbines and MFU agitators the mixing time decreased with decreasing clearance,

whereas it increased with decreasing clearance for MFD agitators. For the pitched blade agitators (MFD or MFU) this effect decreased with increasing diameter as the component of axial flow decreased. These authors linked their findings to the observed flow patterns.

The main circulation loop for up-flow agitators is known to turn over just above the agitator with much poorer agitation above as shown for example by Bujalski *et al.* (1988) and Hari-Prajitno *et al.* (1998). This might suggest that the optimum position for mixing with up-pumping agitators may well be very much higher up the vessel, as demonstrated by the videos shown by Nienow (2003). However for processing purposes, a low clearance is often preferred since this limits surface aeration and batch processes are often run at different levels including quite low levels. Thus for these comparisons all this work was done at a clearance of $T/4$.

For gassed vessels Chapter 2 (section 2.2.2.4.2) recommends multiple up-pumping impellers or up-pumping impellers above a radial impeller to provide stable flows. Mixing data are also reported for these combinations, along with comments about agitator positions and flow.

6.4 Details of Tests and Geometries

Chapter 3 gives details of the three Perspex vessels of diameters 0.286 m, 0.61 m and 0.914 m and the techniques for flow visualisation, shaft power measurement, mixing, and ERT measurements that have been used in these studies. Also available to this study (courtesy of ICI Technology) was a 1.79 m diameter polypropylene vessel with a flat bottom and Perspex portholes in the side and base for flow visualisation. This vessel was instrumented in the same way as the UMIST - Dept. Chemical Engineering, vessels with a torque strain gauge on the shaft to measure shaft power, as previously described by Cooke *et al.* (1988). It is used in this study for scale-up work.

6.4.1 Comparative Mixing Tests

For these tests the start fluids were water at conductivities (Σ) of about 100 μS/cm and finished at around 1000 μS/cm after some 10 additions before the water was changed. Data were collected in LABVIEW in a program that allowed up to 4 probes to be sampled at a hundred times per second.

For overall mixing with a single agitator a single conductivity probe (see Figure 3-7 for probe details) was used. This was sited in the base towards the back of the vessel. The tracer was added on the surface at the front of the vessel, approximately midway between the baffles and midway between the wall and shaft.

The procedure adopted for a single operator doing the tests was as follows.

- Set vessel conditions – agitator, levels, and agitation speed.
- Simultaneously start the data acquisition at 100/s and the stopwatch.
- Add tracer to surface and simultaneously stop the stopwatch.
- Monitor data acquisition to equilibrium value and at least 10s at equilibrium (typically 40s for small tank work)
- Save file
- Repeat process at least 7 times for each mixing time.
- Transfer data to MS excel files for analysis. These excel are attached in the accompanying CD in the folder "Mixing". The spreadsheet names reflect the data. For example 1DT360HTS.xls are the worksheets for a single disc turbine agitated at 360 rpm in an $H = 2T$ geometry.

The time from starting the data acquisition to adding tracer to the surface is typically 7 seconds. Therefore the base-line data are around 700 points for each probe that is more than sufficient to establish the base-line properties. Equilibrium values were collected for a similar length of time. These data traces were then normalised 0 to 1 before analysing by the method described in Chapter 2, section 2.5.5.3.

Tracer concentrations of 200 g/l occasionally proved problematic for tomography measurements and concentrations as low as 50 g/l were sometimes used with proportionally higher addition volumes. Checks found no significant difference to the 95% confidence limits according to a Students t-test between results for 50 g/l and 200 g/l when the final change in concentration was kept constant.

6.4.2 Notes on Flow Visualisation

The aim was to establish major flow patterns, secondary flow and areas that are comparatively poorly mixed. Decolouration experiments described in Chapter 3 are useful for determining regions of relatively poor mixing. To look more closely at flow patterns tracers were used, either gas and/or polystyrene beads to highlight flows whilst lighting the tank through a slit light at the side to highlight a vertical slice.

6.4.3 Geometries of the Vessels and Agitators

The geometries of the vessels and agitators are detailed in Table 6-1 and Table 6-2.

Vessel Diameter	(T)	0.286 m
Material of construction		Clear Perspex
Type of base		2:1 elliptical
Depth of dish		$T/4$
Clearance of agitator	(c)	$T/4$
Type of baffles	(b)	Wall
Number of baffles	(nb)	4
Width of baffles	(Wb)	$T/10$
Position of mixing probe		Upwards at base
Position of tracer addition		Surface
Liquid level	H	Varied from $H/T = 0.75$ to 2

Table 6-1: Details of 0.286 m vessel geometry

Agitator Type	Number blades	Diameter D mm	Blade length mm	Actual blade width mm	Disc diameter mm	Angle of attack degrees	Blade thickness mm	Disc thickness mm	Power No Po total
6RT	6	143.5	36.0	27.8	108	90	2.5	2.5	4.70
6RT	6	95.7	24.8	19.5	72	90	1.0	1.5	5.11
6SRGT	6	149	37.5	19.0	90	90	2.0	2.0	1.63
4MFD	4	145		28.6		45 down	1.0		1.35
4MFU	4	145		28.6		45 up	1.0		1.08
A310	3	150				?	1.0		0.3
3 x 6RT	6	144	36.0	27.8	108	90	2.5	2.5	11.98
3XA345	4	143				38 up			2.4

Table 6-2: Details of agitators used in the 0.286 m diameter vessel. Agitators are shown in Figure 6.1.

6.5 Results

6.5.1 Results for Comparative Tests on the 0.286 m Vessel

6.5.1.1 Agitator Power Numbers in Fully Turbulent Flow

Agitator Power Numbers for fully turbulent flow are listed in Table 6-2 and Table 6-4. The results for various individual agitators as a function of Reynolds number are shown in are in Figures 6-2 to 6-6. Note that the operating level makes no significant difference to the power number when no surface aeration occurs.

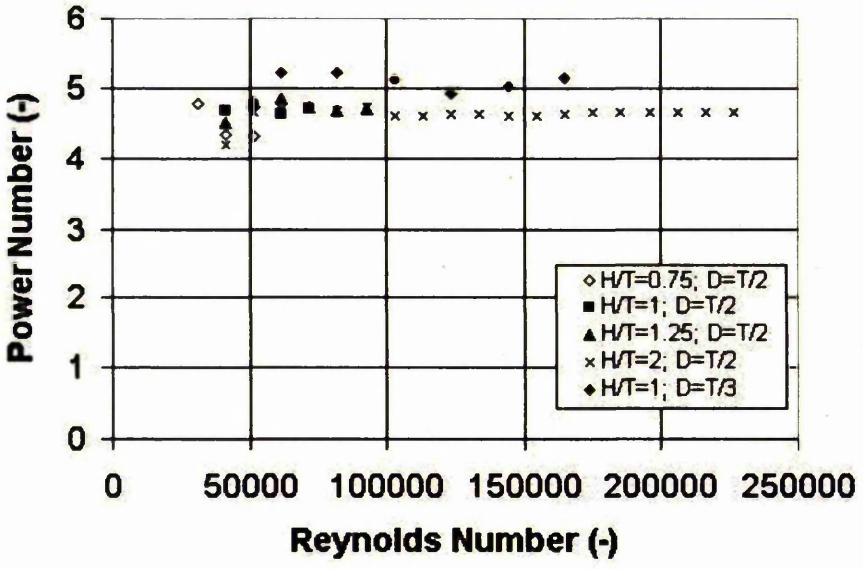

Figure 6-2: Power numbers for the Rushton turbines used in the mixing work on the 0.286 m diameter tank.

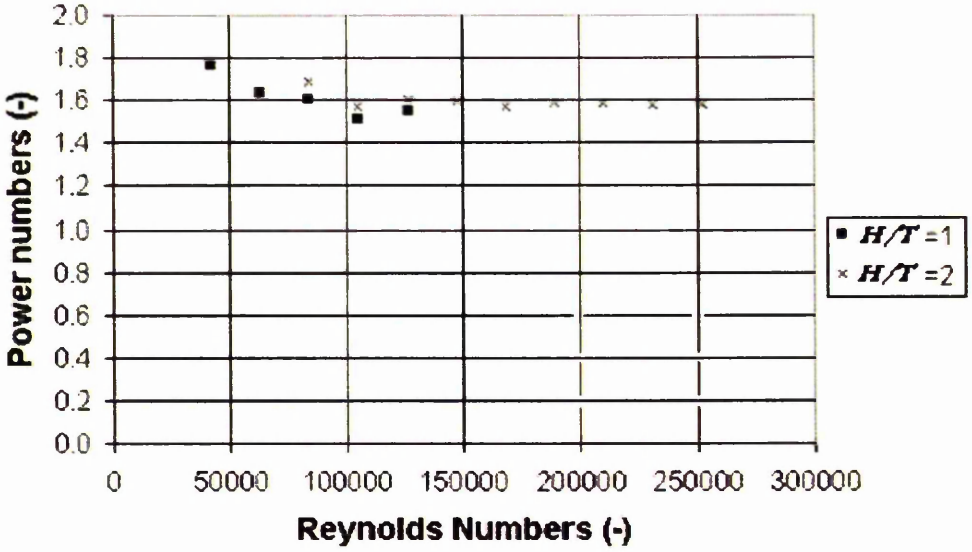

Figure 6-3: Power numbers for the D = T/2, SCABA 6SRGT obtained in water in the 0.286 m diameter tank

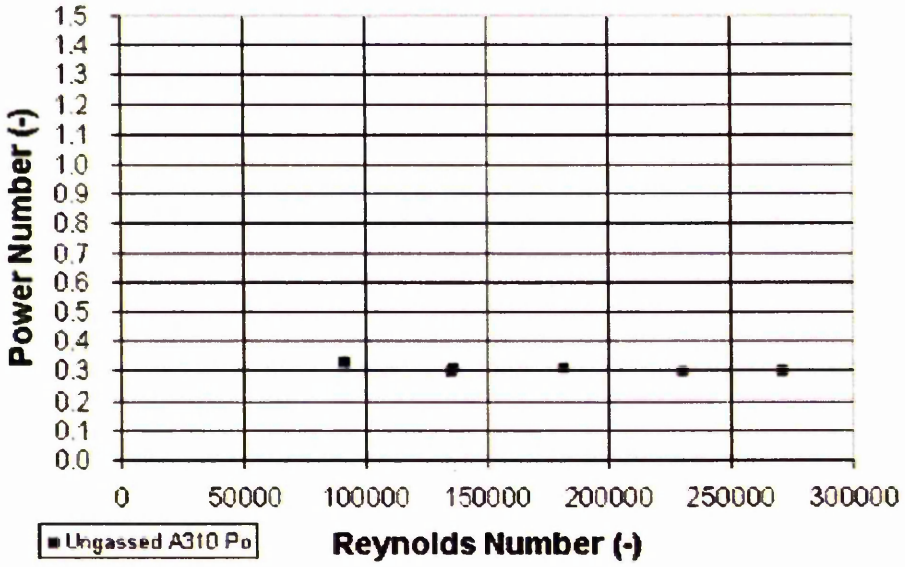

Figure 6-4: Power numbers for the 0.15 m diameter LIGHTNIN A310 agitator in water in the 0.286 m diameter tank for $H=T$.

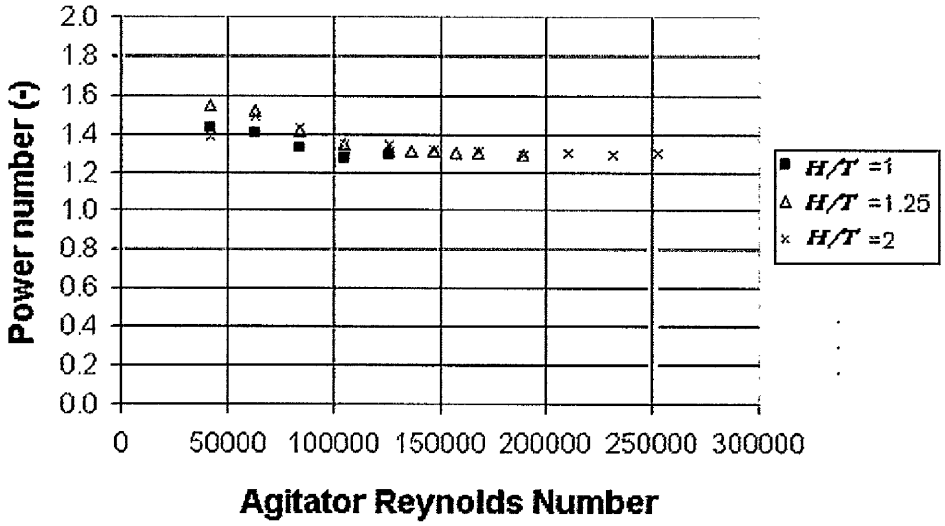

Figure 6-5: Power numbers for the 0.145 m diameter 4MFD agitator in water in the 0.286 m diameter tank

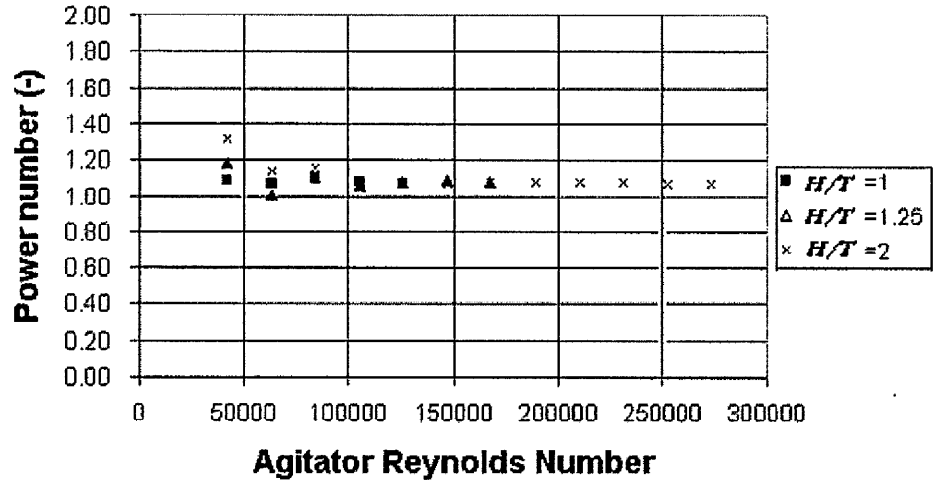

Figure 6-6: Power numbers for the 4MFU agitator in water in the 0.286 m diameter tank

6.5.1.2 Flow Visualisation for Various Agitator Configurations in Fully Turbulent Flow

Flow-fields in mechanically stirred tanks are very complicated. The sketches in Figures 6-7 (a), (b) and (c) and 6-8 (a), (b) and (c) are an attempt to capture a 2-

dimensional picture of a vertical slice of flow between the baffles, for operation in fully turbulent flow.

Primary flow is that derived directly from the impeller. Secondary flow is flow induced by the primary flow (in an opposing direction). Compartmentalization often exists when multiple agitators are used. This compartmentalization consists as boundaries between primary flow-fields where interchange rates between the primary flow loops are much lower the mixing rates that exist within the primary flow loops.

However, even when secondary flow is dominant in much of the upper reaches of the vessels (as it inevitably is when a single agitator located towards the base is used to agitate a tall vessel) the baffles still play a major role in the axial transport of fluid. This is particularly important with radial turbines where upward flow occurs before the baffles and down-flow behind the baffles viewed from the perspective of the radial flow.

The single agitator sketches in Figures 6-7 illustrate that for $H=T$ geometries the disc turbine and 4MFD agitators are both fully agitated by primary flow. Therefore, these should mix better than the 4MFU agitator 6-6(c) that relies on secondary flow to mix the top of the vessel.

When the liquid level is raised to $H = 2T$ all the agitators tested relied on secondary flow to mix the op of the vessel.

The series of sketches (a) (b) and (c) in Figures 6.8 represent some possible ways of configuring a tall reactor with multiple agitators.

Even when 3 axial flow agitators are used at separations of $\leq 1.2\ D$ some flow instabilities are present due to opposing flow at the interchange [Figure 6-8a (right)]. If the separation is increased to $> 1.2\ D$, then zoning and compartmentalization is likely (Figure 6-8b).

Secondary flow is responsible for some of the mixing when the agitator is $> 1.2\ D$ from the surface.

The geometry in Figure 6-8 c shows good interchange between the agitators with flow reinforcement at the interchange.

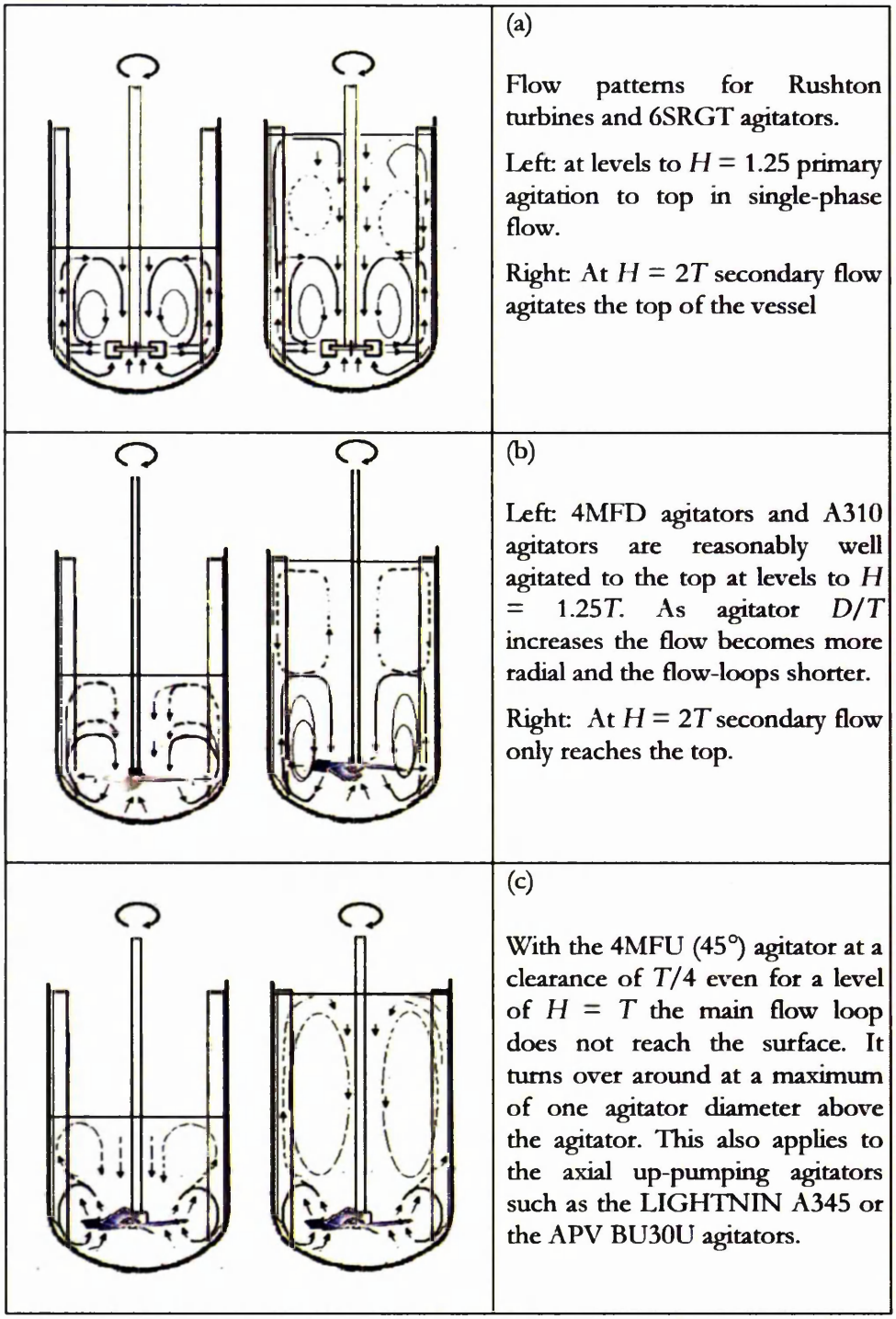

(a)

Flow patterns for Rushton turbines and 6SRGT agitators.

Left: at levels to $H = 1.25$ primary agitation to top in single-phase flow.

Right: At $H = 2T$ secondary flow agitates the top of the vessel

(b)

Left: 4MFD agitators and A310 agitators are reasonably well agitated to the top at levels to $H = 1.25T$. As agitator D/T increases the flow becomes more radial and the flow-loops shorter.

Right: At $H = 2T$ secondary flow only reaches the top.

(c)

With the 4MFU (45°) agitator at a clearance of $T/4$ even for a level of $H = T$ the main flow loop does not reach the surface. It turns over around at a maximum of one agitator diameter above the agitator. This also applies to the axial up-pumping agitators such as the LIGHTNIN A345 or the APV BU30U agitators.

Figure 6-7: Flow patterns for single agitators at a clearance of $T/4$, illustrating the effects of agitator choice and H/T on the flow patterns.

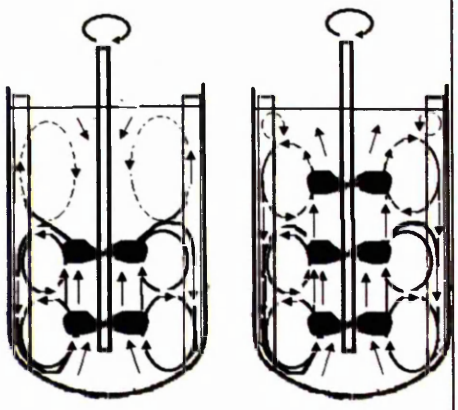

(a)

Multiple LIGHTNIN A345 agitators at a separation of 1*D*. The flows loops work together with some internal recirculation.

Left: A dual A345 with separation between top Agitator and surface ≅ 2*D*. Strong flows in bottom section, much weaker flows above.

Right: Strong flows to surface if surface separation < 1.2*D*.

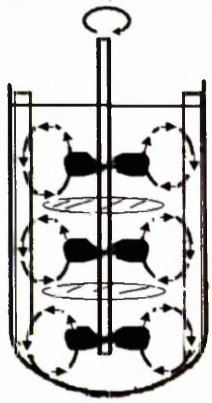

(b)

Multiple A345 (up-pumping) in single-phase turbulent flow. If separation ≥ 1.2*D* then zoning and compartmentalization occurs.

Note that on gassing the up-flow of gas destroys the zoning.

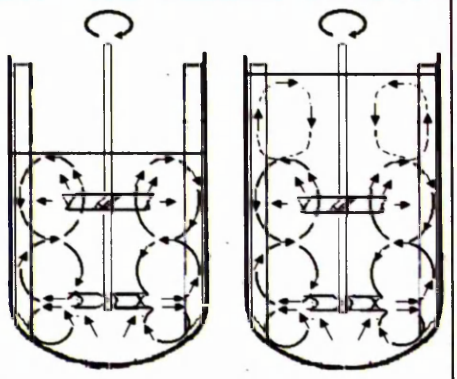

(c)

Left: A combination of a lower radial turbine (shown here as a hollow blade turbine) and an upper 6MFU (or other up-flow impeller) produces a well-agitated vessel with positive flow reinforcement at the interchange.

Right: If top agitator > 1.2*D* from the surface there is an extra flow loop and radial type flow at the top. This gives a higher Po and longer mixing time. At a large D/T this effect occurs at $s/D < 1.2$.

Figure 6-8: Flow patterns for multiple agitators: Effect of agitator separation and the clearance of top agitator on the flow patterns.

: Single Phase Hydrodynamics

With the dual agitator system shown in Figure 6-8(a) (sketch on left) there is some compartmentalization as shown in colour change experiment depicted in Figure 6-9. A degree of compartmentalization also occurs for the hollow blade arrangement shown in Figure 6-8(c), even for a 6MFU surface clearance of one agitator diameter, as illustrated by the video clip shown in Figure 6-10. Although there is a good interchange of flow between the hollow blade upper agitator flow loop and the 6MFU main flow loop, the portion of the vessel agitated by the hollow blade agitator is essentially mixed before significant transfer to the 6MFU agitated section occurs.

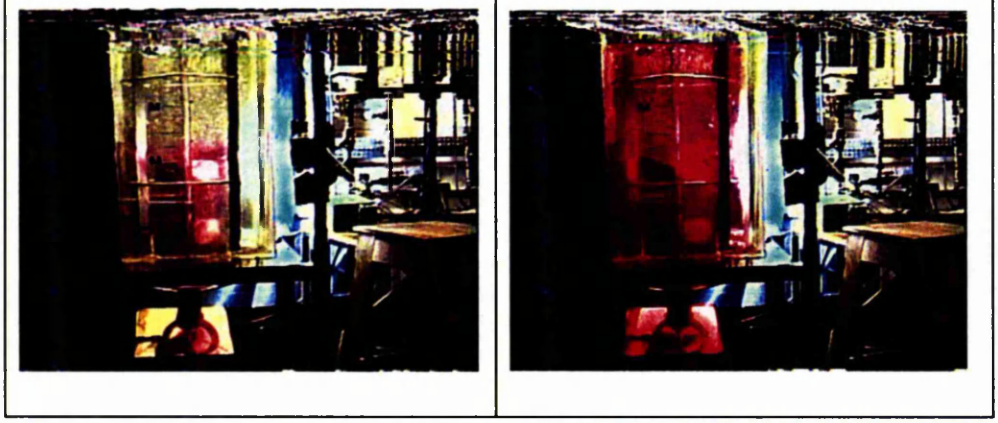

Figure 6-9: Dual A345 agitators. Caustic injected into the bottom zone:

(left) bottom zone pink **(right) whole tank pink.**

Figure 6-10: A 6HBT below a 6MFU as per Figure 6-7(c). The 6MFU is one agitator diameter from the free surface. Video clip from a colour change experiment obtained by adding caustic at the side of the bottom 6HBT.

Bottom zone well mixed before significant transfer to top zone

6.5.1.3 Mixing Times in Fully Turbulent Flow

A typical summary sheet for a given test is illustrated by Table 6-3. The comparative mixing results on the 0.286 m diameter tank are listed in Table 6-4. Mixing time constants are quoted for both 90% and 95% mixing. For any given agitator at a clearance of $T/4$ up to operating levels of $H/T = 1.25$, $N\theta \cong$ constant with no significant different between the results for different agitation speeds. However for the Rushton turbines at $H = 2T$, with the single agitator, $N\theta \neq$ constant and the result at the lower speed is distinctly second order. All the other results exhibit reasonable first order behaviour including the triple Rushton turbine results with the 95% mixing being reasonably predicted by the 90% result. Assuming first order there should be a factor of 1.3 between the two mixing times. On average the experimental factor was 1.27.

Run	*N*	t_{90}	t_{95}	Nt_{90}	Nt_{95}
1	180	2.37	3.46	7.11	10.38
2	180	4.28	4.37	12.84	13.11
3	180	3.85	4.13	11.55	12.39
4	180	3.01	4.75	9.03	14.25
5	180	3.31	6.12	9.93	18.36
6	180	3.69	4.24	11.07	12.72
7	180	3.15	3.31	9.45	9.93
8	180	2.67	3.76	8.01	11.28
9	180	2.4	4.54	7.2	13.62
10	180	3.93	4.05	11.79	12.15
	Predicted t_{95} (s)	4.246			
	Average	3.266	4.273	9.798	12.819
	Std	0.665	0.7692	1.995	2.375
	%std	20.36	18.53	20.36	18.53

Table 6-3: Results for mixing with 6SRGT at 180 rpm and $H = T$.

No tests n	Agitator Type	N rpm	T m	D m	H m	D/T	ε_T W/kg	H/T	Po	Nt_{90}	Nt_{95}
7	6RT	240	0.286	0.096	0.286	0.335	0.159	1	5.11	17.01	23.21
7	6RT	420	0.286	0.096	0.286	0.335	0.821	1	5.11	16.41	21.51
7	6RT	120	0.286	0.144	0.215	0.502	0.173	0.75	4.48	5.91	7.46
7	6RT	120	0.286	0.144	0.286	0.502	0.135	1	4.69	7.30	8.50
7	6RT	150	0.286	0.144	0.286	0.502	0.269	1	4.69	6.31	8.76
7	6RT	180	0.286	0.144	0.286	0.502	0.452	1	4.69	6.55	8.39
7	6RT	240	0.286	0.144	0.286	0.502	1.085	1	4.69	7.50	9.39
7	6RT	120	0.286	0.144	0.358	0.502	0.103	1.25	4.71	8.16	9.61
5	6RT	120	0.286	0.144	0.572	0.502	0.058	2	4.63	15.40	28.45
5	6RT	360	0.286	0.144	0.572	0.502	1.727	2	4.69	29.98	35.38
7	6SRGT	180	0.286	0.149	0.286	0.521	0.192	1	1.63	8.42	9.30
10	6SRGT	180	0.286	0.149	0.286	0.521	0.192	1	1.63	9.80	12.82
10	6SRGT	240	0.286	0.149	0.286	0.521	0.448	1	1.61	9.41	10.50
7	6SRGT	180	0.286	0.149	0.572	0.521	0.092	2	1.6	49.43	58.78
14	4MFD	180	0.286	0.145	0.286	0.507	0.145	1	1.35	11.52	13.91
8	4MFD	240	0.286	0.145	0.286	0.507	0.324	1	1.33	11.60	14.29
6	4MFD	300	0.286	0.145	0.286	0.507	0.606	1	1.27	10.57	14.53
7	4MFD	180	0.286	0.145	0.358	0.507	0.123	1.25	1.35	14.62	18.65
9	4MFD	300	0.286	0.138	0.409	0.483	0.329	1.43	1.32	29.27	
7	4MFD	180	0.286	0.145	0.572	0.507	0.073	2	1.35	71.84	93.87
9	4MFU	180	0.286	0.145	0.286	0.507	0.110	1	1.08	15.80	20.30
11	4MFU	300	0.286	0.145	0.286	0.507	0.513	1	1.08	17.30	20.66
7	4MFU	180	0.286	0.145	0.358	0.507	0.081	1.25	1.08	16.59	20.40
7	4MFU	180	0.286	0.145	0.572	0.507	0.056	2	1.11	47.30	64.58
7	A310	180	0.286	0.150	0.286	0.524	0.037	1	0.3	20.10	25.08
7	A310	300	0.286	0.150	0.286	0.524	0.167	1	0.3	23.43	27.67
7	A310	420	0.286	0.150	0.286	0.524	0.446	1	0.29	21.78	27.74
7	3 x 6RT	90	0.286	0.144	0.572	0.503	0.071	2	11.98	45.31	55.01
8	3XA315 up	300	0.286	0.143	0.486	0.500	0.604	1.7	2.4	16.65	
8	3XA315 up	450	0.286	0.143	0.486	0.500	2.037	1.7	2.4	16.76	
8	3XA315 up	600	0.286	0.143	0.486	0.500	4.828	1.7	2.4	16.73	

Table 6-4: Mixing results for tests on the 0.286 m diameter vessel. Note that n is number of tests comprising each mixing time. Other symbols take their usual meaning.

6.5.1.3.1 Mixing Times in Fully Turbulent Flow for $H = T$ aspect ratio

6.5.1.3.1.1 Effect of Specific Power Input on Mixing

The mixing time data for $H = T$ geometries are shown on log-log plots of mixing times versus specific power input in Figures 6-11 and 6-12. These data show approximately constant slopes of –1/3, indicating that:

$\theta\varepsilon_T^{1/3}$ is approximately constant.

The slopes for t_{90} vary from -0.273 to - 0.414 with a mean of -0.330 and a standard deviation of 0.0506

The slopes for t_{95} vary from -0.292 to - 0.387 with a mean of -0.332 and a standard deviation of 0.0386.

The same result would be achieved by a plot of log (N.θ) versus log (Po) since on a single scale for a given agitator diameter ε_T is proportional to $N.Po^{1/3}$

Therefore for a given agitator type and diameter,

$$N\theta.Po^{1/3} = \text{constant} \qquad (6.5)$$

This is in agreement with equation (6.1). The group $N\theta.Po^{1/3}$ may be considered as a mixing power number.

The mixing versus energy input data divide into two main bands. The most energy efficient band comprises the $D = T/2$ Rushton turbine, 6SRGT and the 4MFD. The least energy efficient band comprises the $D = T/3$ Rushton turbine and the $D = T/2$ A310 and 4MFU.

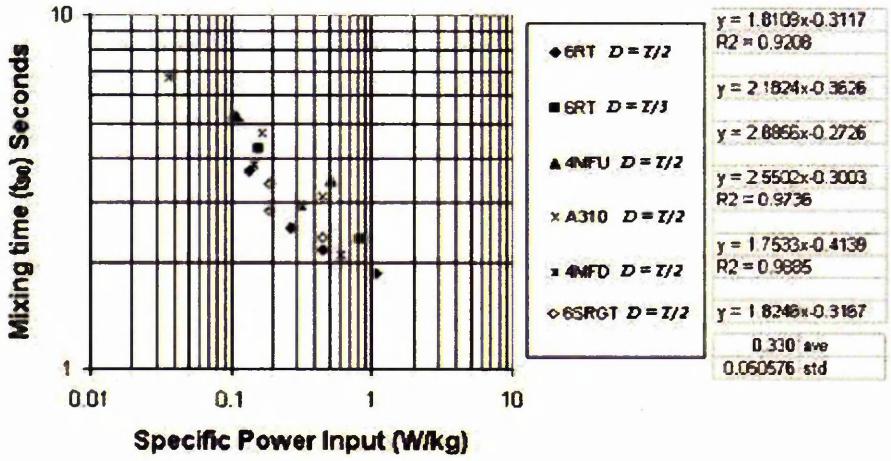

Figure 6-11: Effect of specific power input on mixing to 90% in water for various agitators in the 0.286 m vessel. Note that in all cases the D/T on the figure is approximate. For example the actual *D* of the A310 is 0.524*T*. The actual *D/T* is used in all calculations. See Table 6-4 for precise *D/T* information.

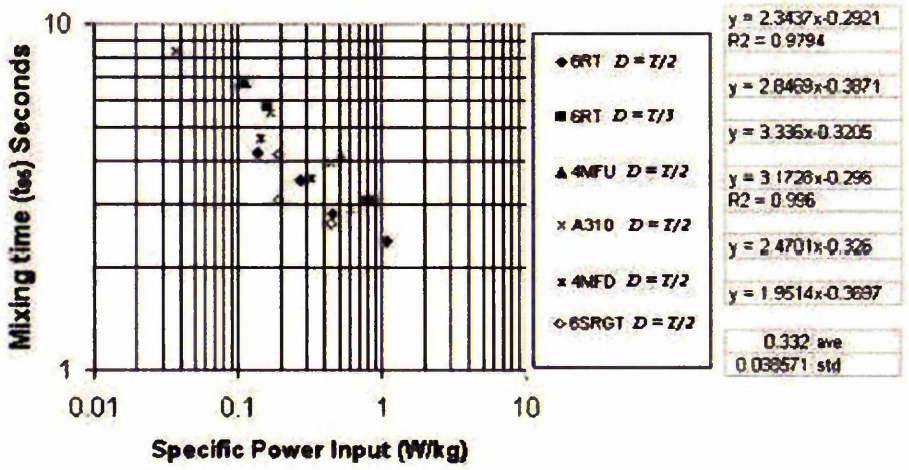

Figure 6-12: Effect of specific power input on mixing to 95% in water for various agitators in the 0.286 m vessel.

6.5.1.3.1.2 Effect of *D/T* on the Rate of Mixing

The effect of the D/T ratio on the rate of mixing could only checked to any degree of accuracy with the Rushton turbines where the D/T ratio was varied

between $T/3$ and $T/2$. This was for 90 and 95% mixing as shown in Figure 6-13. The results correlated according to:

$$Nt_{90}Po^{1/3}(D/T)^{2.25} = \text{constant}\ .\ R^2 = 0.981 \qquad (6.6)$$

$$Nt_{95}Po^{1/3}(D/T)^{2.38} = \text{constant}\ \ R^2 = 0.992 \qquad (6.7)$$

The mean exponent on D/T is 2.3 which is identical to that found by Khang and Levenspiel (1976) for Rushton turbines and also compares favourably with the exponent of 2.4 found by Shiue and Wong (1984) and the exponent of 2.2 found by Cooke *et al.* (1988).

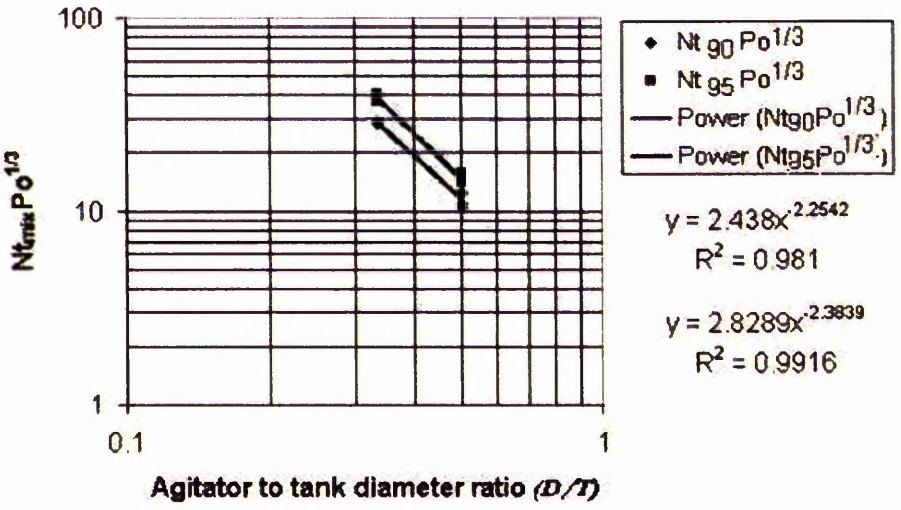

Figure 6-13: Determination of the effect of agitator diameter on mixing for Rushton turbines in water in the 0.286 m diameter tank. Power law fit.

6.5.1.3.1.3 Comparisons with Earlier Work for *H= T* Geometries

The t_{90} data for $H = T$ geometries were tested against predictions from the Cooke *et al.* (1988) correlation which for $H = T$ geometries reduces to,

$Nt_{90}Po^{1/3}(D/T)^{2.2} = 3.9$ (equation 2.54)

These comparisons are illustrated in Figure 6-14. This is interesting since the only the data for the Lightnin A310 and the 4MFU correspond to the predicted line. The data for the other four agitators line on a roughly parallel line below

the 1988 prediction, that is, with a lower multiplication factor (more energy efficient mixing). A similar pattern emerges by a comparison of the data with the Ruszkowski (1994) correlation given by equation 2.55 and depicted in Figure 6-15). The lower multiplicity factor, compared to the earlier work, could be due to the combinations of the low noise data achieved by operating below the onset of surface aeration, the data smoothing (working with a 32 point moving average) and the small scale. The increase in the multiplication factor for the 4MFU agitator is believed to be due to the flow patterns since the primary flow patterns do not reach the surface, see Figure 6-7. The reason for the A310 result is not quite as clear-cut although there is not a lot of surface movement until the onset of surface aeration at 600 rpm and the large diameter (D =0.524T) means that the axial flow component is compromised.

All the $H = T$ data for the two disc turbines, the Scaba 6SRGT and 4MFD could be well correlated according to,

$$Nt_{90}Po^{1/3}(D/T)^{2.3} = 2.4 \qquad (6.8)$$

with a standard deviation of 0.178 and correlation coefficient R2 = 0.955

and,

$$Nt_{95}Po^{1/3}(D/T)^{2.3} = 3.1 \qquad (6.9)$$

with a standard deviation of 0.255 and correlation coefficient R2 = 0.954

Note that the power law index of (2.3) has only been confirmed for disc turbines in this work. Also the difference in the constants between 90% and 95% mixing agrees with a first-order mixing model.

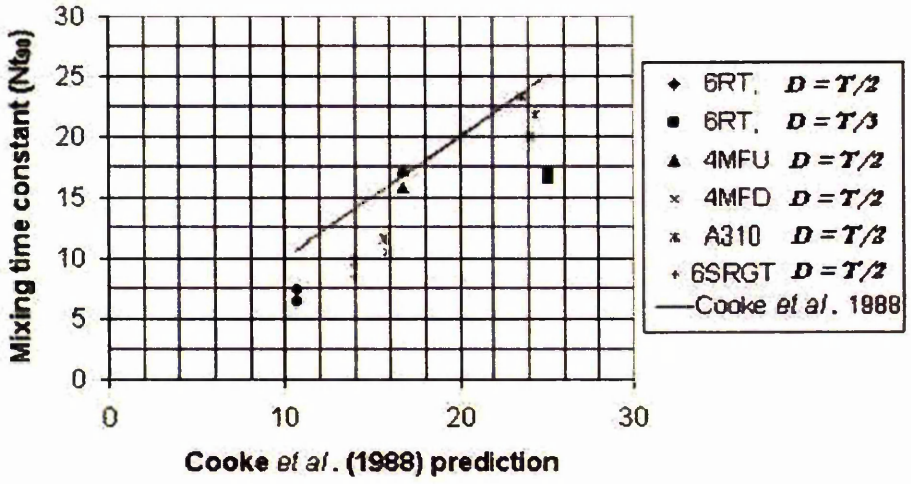

Figure 6-14: Data for $H = T$ geometries plotted against the Cooke *et al* (1988) correlation (equation 2.54).

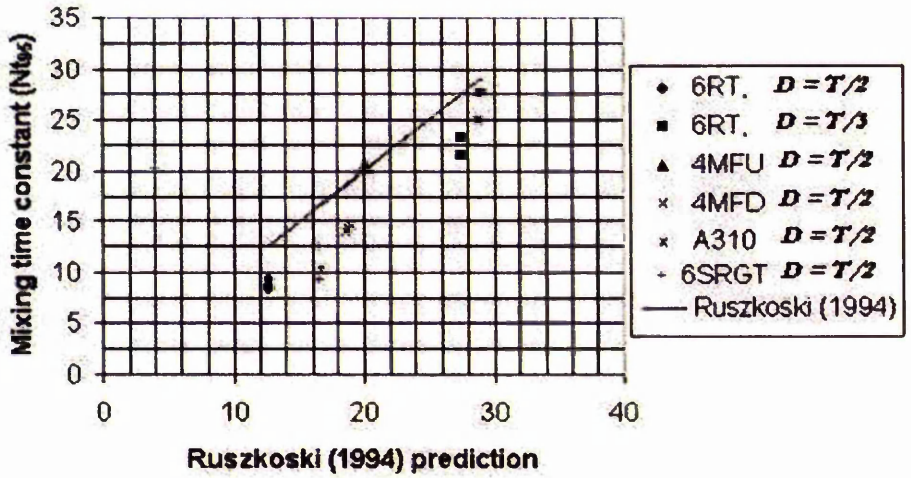

Figure 6-15: Data for $H = T$ geometries against the Ruszkowski (1994) correlation (equation 2.55).

6.5.1.3.2 Mixing Times in Fully Turbulent Flow for all Aspect Ratios in the 0.286 m Diameter Vessel

The mixing data (for cases where H/T was altered) are plotted on log axes as values of the mixing power numbers ($Nt_{95}Po^{1/3}$) against the H/T (liquid

height/vessel diameter) in Figure 6-16. Each of the agitator types was subjected to a power law fit and the equations of the lines and R^2 correlation coefficients are all included on the graph. Finally the data for all the agitators was fitted to a single power law fit.

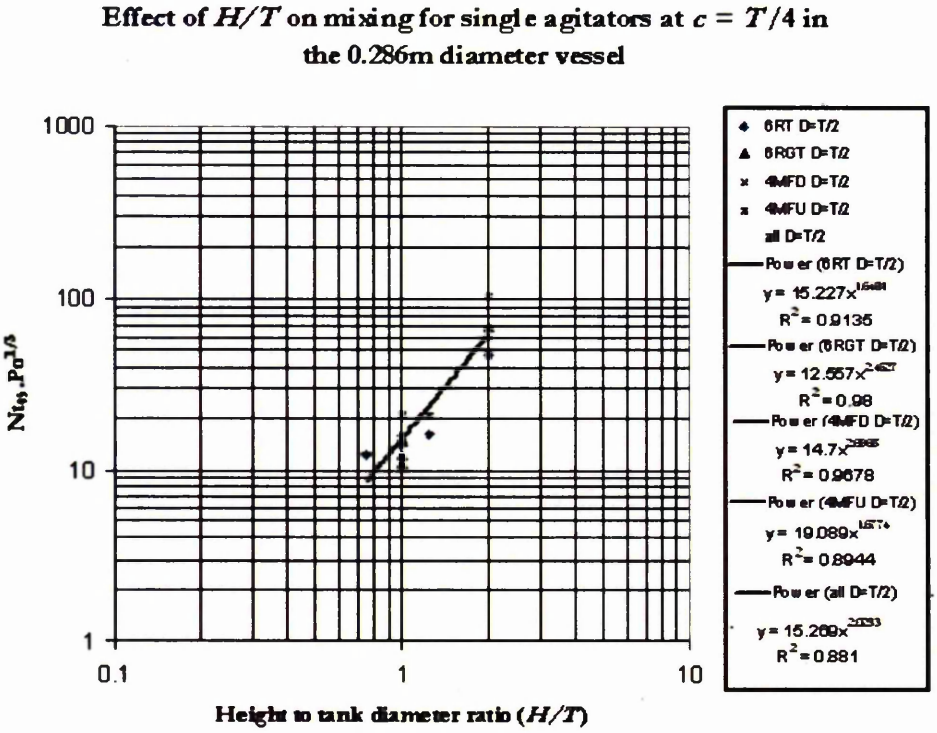

Figure 6-16: The effect of H/T on the mixing power number ($Nt_{95}Po^{1/3}$) for single agitators at $c = T/4$ in the 0.286 m diameter vessel.

The data does not fit particularly well but there is a clear message that increasing H/T has a strongly detrimental affect on mixing. The overall fit for all these data is:

$$Nt_{95}Po^{1/3}(T/H)^{2.0} = 15.3 \qquad (6.10)$$

If you could mix a vessel using a single circulation loop you would expect the bulk mixing to be directly proportional to H. The exponent on H/T is therefore an indication of how well the mixing approaches this ideal.

Note that the exponents on D/T and T/H in the mixing equations are similar (approximately 2.0) as found previously by Cooke *et al.* (1988) using multiple agitators. This means that the effects of D/T and H/T on mixing can be reduced to an effect of D/H. Following this earlier work, the data for the single agitators were plotted as values of the mixing power number ($Nt_{95}Po^{1/3}$) against the D/H (agitator diameter/liquid height) in Figure 6-17. The A310 and the small RT agitators are included in these data sets as D/H ratios are altered by the change in D.

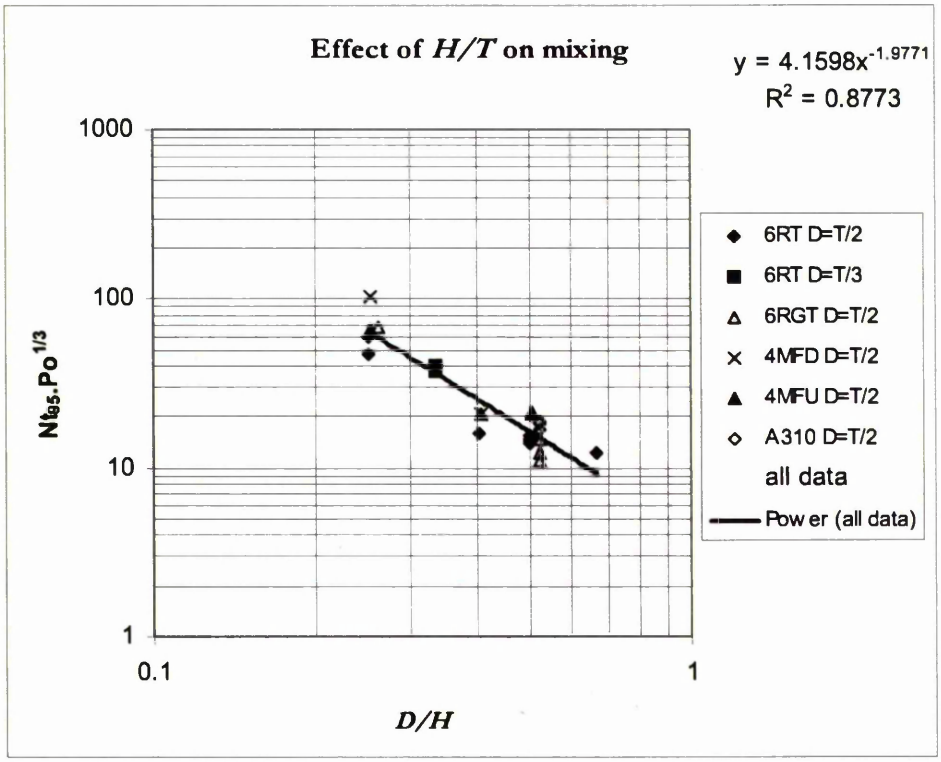

Figure 6-17: The effect of the liquid height on the mixing power number ($Nt_{95}Po^{1/3}$) for single agitators at $c = T/4$ in the 0.286 m diameter vessel.

There is a strong effect of height on mixing and this is roughly proportional to $(D/H)^{-2}$. At a value of H/T= 2 (D/H = 0.25) the 4MFD is the least efficient at mixing. The flow visualization shows that secondary recirculation is responsible for mixing the top of the vessel at this height (Figure 6-7).

Note that the correlation R^2 coefficient is quite low indicating that this type of "catch-all" correlation has quite wide error bars. Setting the exponent at –2.0 the correlation is rounded up to,

$$N.t_{95}Po^{1/3}(D/H)^{2.0} = 4.2 \qquad (6.11)$$

with a standard deviation of 0.914 and correlation coefficient $R^2 = 0.877$

In spite of the crudeness of this correlation (low R^2 value) it is useful to focus the mind on the important variables on scale-up. It may be, in some cases where mixing is particularly important, that vessel diameter is increased at constant H so that D/H can be maintained.

In order to see whether single or multiple agitators are the most efficient for mixing, the effect of the operating height on the mixing time constant Nt_{90} for single agitators is compared against the prediction for three Rushton turbines due to Cooke *et al.* (1988) in Figure 6-18.

The mixing time constants for the single agitators at aspect ratios are lower for all cases above the aspect ratio of 1, than those predicted by Cooke *et al.* (1988). Note also that the recent check data point for three radial impellers (Table 6-4) is in good agreement with the earlier work. The earlier work on the 3 turbines at the 3:1 aspect ratio was also done on the 0.286 m mixing-rig.

The fact that a single agitator is more energy efficient for mixing than multiple radial turbines is interesting given that for the single agitator, the upper reaches are mixed mainly by secondary recirculation. The use of multiple radial flow impellers is not recommended in high aspect ratio vessels where overall mixing rates are important, in spite of the fact that this is a commonly used geometry.

Triple A345 agitators are particularly efficient at mixing with a measured Nt_{90}, approximately 1/3 of that predicted for the triple Rushton turbines at the same H/T.

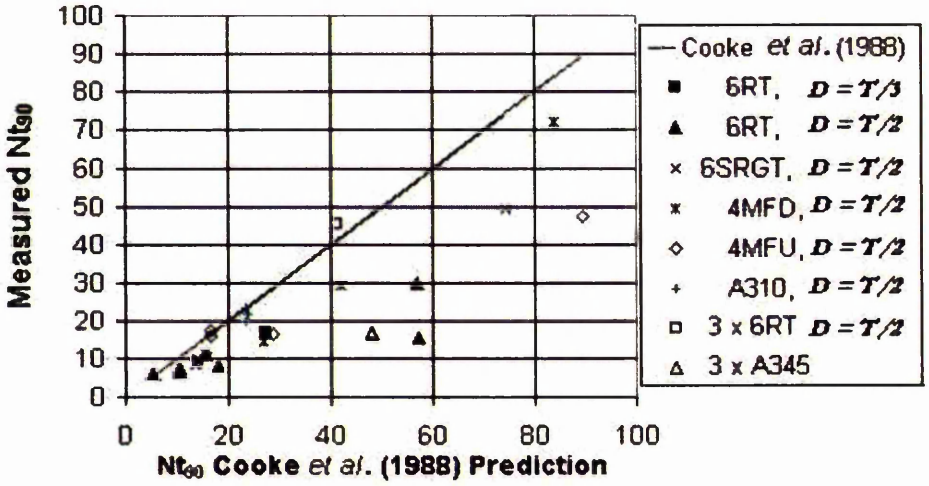

Figure 6-18: Comparisons of mixing constants at different aspect ratios (H/T) for single agitators in 0.286 m diameter vessel with the Cooke *et al.* (1988) prediction given by equation (6.2)

6.5.2 Results of Comparative Tests on the 0.61m Diameter Vessel

The geometrically similar 0.61 m diameter vessel is used in conjunction with the 2:1 elliptical base of depth $T/4$. Agitator geometries considered here are single and multiple agitators in water under fully turbulent flow conditions:

- Single 4MFD-45°. At H/T=1.25 to compare against the 0.286 m diameter vessel work, Similar to 0.286 vessel design).
- Hollow blade radial agitator (6HBT) below a 6MFU-45°(Figure 6-19)
- Dual LIGHNIN A345 (Figure 2-27)
- Triple LIGHNIN A345.

(a) curved parabolic blade agitator (6HBT)

b) 6 blade 45⁰ Pitched blade turbine pumping up (6MFU)

Figure 6-19: dual agitators, a parabolic blade 6HBT below a 6MFU-45°.

The geometries are listed in Table 6-5 and a summary of the mixing results is given in Table 6-6. For the multiple agitators the Power number given is the combined power number based on the diameter of the lowest agitator as described in Section 6.3). Geometry 5 is used for a comparison with ERT results with tracer at the bottom agitator and measurement in the base. For all the other experiments the tracer is added at the surface.

Note that some of the geometries reported here were used for parts of research projects carried out under the terms of confidentiality agreements that prohibit detailed explanation of why these particular geometries were used.

Geometry	Agitator Types	*c* (m)	*D* (m)	*D/T* (-)	*H/T* (-)	*S/D* (-)	Vol. (m^3)	Po (-)
1	4MFD-45°	0.164	0.322	0.53	1.25	1.89	0.208	1.22
2	6HBT	0.174	0.291	0.48	1.03	0.71	0.168	1.13
	6MFU-45°	0.422	0.272	0.45				1.83
3	6HBT	0.122	0.305	0.50	1.03	0.64	0.168	1.14
	6MFU-45°	0.432	0.272	0.45				1.83
4	6HBT	0.220	0.321	0.53	1.4	1.17	0.234	1.21
	6MFU-45°	0.525	0.272	0.45				1.83
5	6HBT	0.220	0.305	0.50	1.38	0.74	0.230	1.12
	6MFU-45°	0.525	0.366	0.6				2.69
6	A345	0.248	0.295	0.48	1.63	1.67	0.276	0.76
	A345	0.501	0.295	0.48				0.76
7	A345	0.248	0.295	0.48	1.63	0.81	0.276	0.76
	A345	0.501	0.295	0.48				0.76
	A345	0.755	0.295	0.48				0.77

Table 6-5: Geometries used in the 0.61 m diameter vessel single-phase mixing tests in fully turbulent conditions. *S* is the agitator separation from the surface.

n	Agitator Type	Geometry	N RPM	T m	D m	H m	D/T	P/V W/kg	H/T	Po	Nt_{90}
7	4MFD	1	100	0.61	0.322	0.762	0.53	0.09	1.25	1.22	23.2
6	4MFD	1	179	0.61	0.322	0.762	0.53	0.54	1.25	1.22	23.9
7	4MFD	1	250	0.61	0.322	0.762	0.53	1.47	1.25	1.22	26.4
6	6HBT			0.61	0.291		0.48				
	+ 6MFU	2	240	0.61	0.272	0.628	0.45	1.79	1.03	1.96	24.8
7	6HBT			0.61	0.305		0.50				
	+ 6MFU	3	240	0.61	0.272	0.628	0.45	1.97	1.03	2.25	22.1
8	6HBT			0.61	0.321		0.53				
	+ 6MFU	4	210	0.61	0.272	0.854	0.45	1.26	1.4	2.02	39.6
2	6HBT			0.61	0.305		0.50				
	+ 6MFU	5	120	0.61	0.366	0.841	0.6	0.72	1.38	7.84	11.8
6	2 x A345	6	274	0.61	0.295	0.994	0.48	1.18	1.63	1.52	29.9
6	3 x A345	7	180	0.61	0.295	0.994	0.48	0.51	1.63	2.34	21.6
6	3 x A345	7	274	0.61	0.295	1.013	0.48	1.76	1.66	2.27	20.2

Table 6-6: Summary of single-phase mixing results for the 0.61 m diameter vessel.

6.5.2.1 Discussion of the Results of the Mixing Tests from the 0.61 m Vessel.

Comparing the results in Table 6-6 with the earlier results printed in Table 6-4 it is apparent that:

- The mixing time constant has not scaled up. Results for the single 4MFD at H=1.25T and for the triple A345 show a longer mixing time constant (Nt_{90}) on scale-up, even accounting for any small differences in D/T ratios. Other workers have noted this effect; Kipke (1983) and Raghav Rao and Joshi (1988) both reported that for geometrically similar vessels, Nθ increased on scale-up. See section 6.2.
- The dependency of mixing on H/T is confirmed for the dual agitator (6HBT below a 6MFU) results. The difference between the mixing times for H/T=1.03 and H/T=1.4 is reasonably well predicted by the

form of equation (6.11) - $Nt_{90}Po^{1/3}(D/H)^{2.0}$ = constant .

- Assuming first order mixing, the constant in equation (6.11) is 3.22 for the 90% mixed case. Using this constant and the power number and agitator diameter based on the 6HBT diameter predicts a mixing time constant, Nt_{90} of 12.4 for the geometry 5, compared with the measured value of 11.8, which is well within the accuracy of the experimentation.
- The triple A345 agitators with agitator and surface separations of < 1D exhibit excellent mixing characteristics. There is no zoning seen in the colour change experiments and the mixing time constant is the lowest for these comparative tests in spite of operating at the highest H/T. Therefore if mixing is a primary objective this configuration is highly recommended. Note that for single-phase work it might not matter whether these were up or down pumping (similar flow patterns would be expected resulting in similar mixing times). However, for gas-liquid multi-phase operations pumping upwards is the most stable mode as gas up-flow reinforces the mechanically agitated liquid flow (see also Chapter 2, section 2.2.2.4).

6.5.3 Mixing Studies using the ERT Tomography Sensors in the 0.61m Diameter Vessel

The electrical resistance tomography baffle cage with 8 rows of 16 electrodes described in Chapter 3, section 3.2.6 and in detail in Chapter 9 was used to look at the mixing details for a tracer added close to the side of the hollow blade turbine for the geometry 5 set-up shown in Table 6-5. This was a dual agitator arrangement of a 6MFU above a 6 hollow blade turbine.

The tomography data were analysed two ways:

I. **4-pixel time history.** This monitors the conductivity at 4 selected (any chosen) pixels. These are averaged and compared graphically. See for example Exp13pixelHis.xls in the attached CD. This sort of

information could be used for example to study a take-off position with a tracer injected at a feed position to look at possible by-pass. A graphical example for this is shown as Figure 6-20. The threshold values are at 90 and 110% of the step change and are added to illustrate the 90% mixed point.

II. **Mutual bulk resistance (MBR) for all planes.** This is calculated from the voltage measurements and injection current and is an inverse measure of the mean conductivity time-history in each plane. An example for geometry 5 is depicted graphically in Figure 6-21 and the analysis of these curves to give inter-zone mixing data is listed in Table 6-7.

The estimation of the mixing times from the 4 pixel time-history and the MBR results is done in an Excel spread sheet by normalizing the resistance data from 0 to 1 and determining the 90% mixing point graphically. This is reproduced as Table 6-7. The MBR data are quite interesting as they provide information on zonal mixing. They might yield very useful information on exchange rates between multiple agitators and this would be a worthy topic for future work.

The 4-pixel data were for a point at the top of the vessel with the injection in the feed. These gave an Nt_{90} mixing time constant of 19.4. This compares with a mean value of 13.8 from the MBR data. However the MBR plane at the top of the vessel had a mixing time constant of 18.0 and that is comparable to the 4-pixel data. The MBR data close to the mixing point have a mixing time constant of 11.9 that is comparable to the result obtained by the bottom-mixing probe for the injection at the bottom agitator.

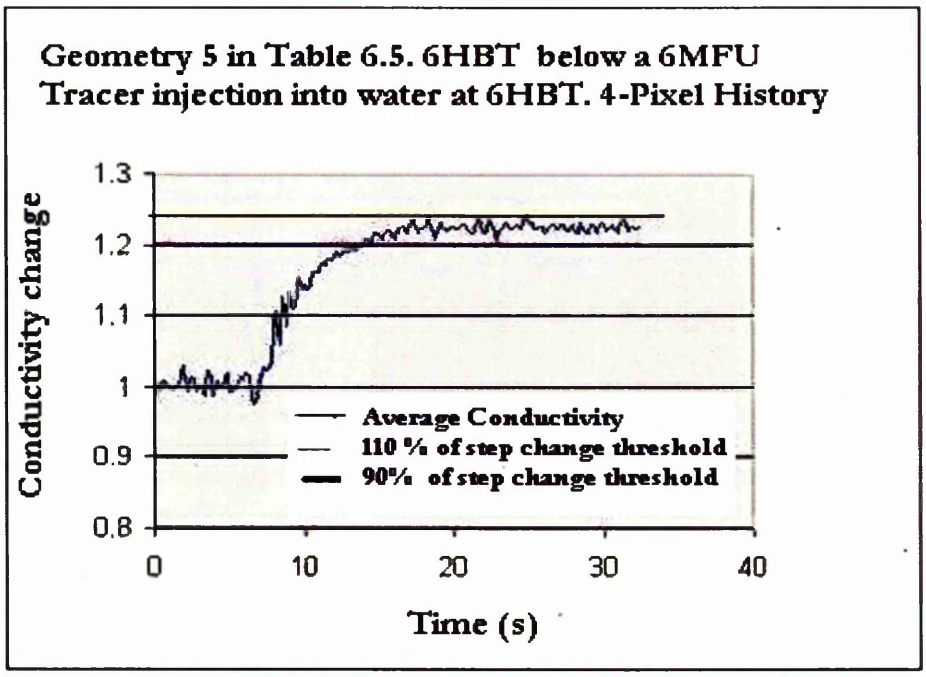

Figure 6-20: Typical average 4-pixel conductivity-time history. From the measurement file the injection first appeared at frame 21 and 150 data points were collected in 33.0 s. From this data 90% mixing is achieved at frame 65. Thus: t_{90} = (65-21) x 33/150 = 9.68 s

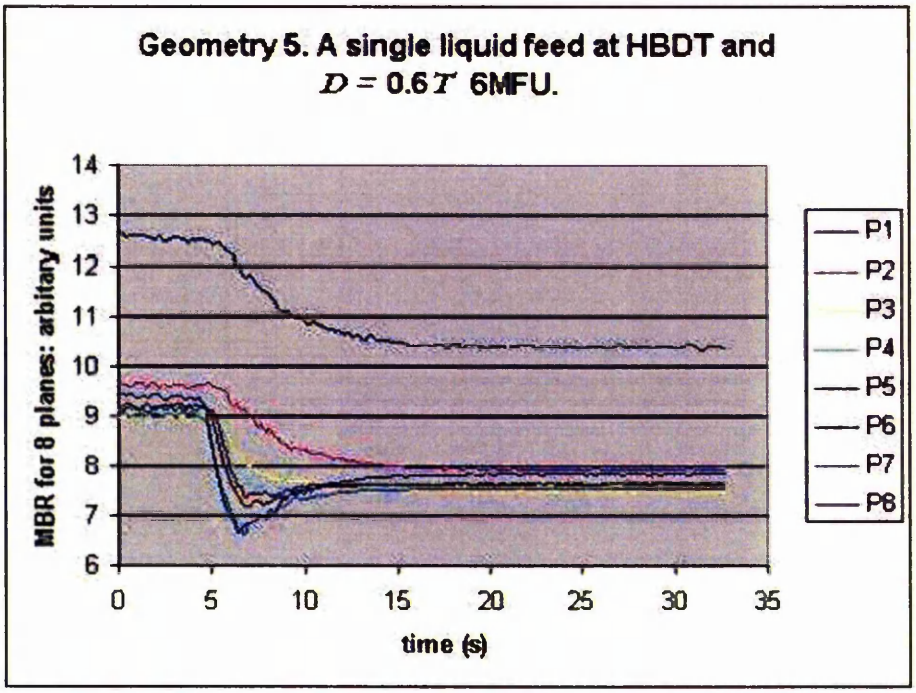

Figure 6-21: Typical mutual bulk resistance time history. P1 to P8 are the tomography plane numbers, with 16 electrodes in each plane.

Data from ITS excel files analysed to give t_{90} mixing time												
plane	N	zero	Equil.	span	0.1span	1.1span	0.9span	start	end time	90%	Ave t_{90}	ave Nt_{90}
	rpm							time s	S	time t90		
1	120	12.51	10.39	2.12	0.212	10.602	10.178	3.96	12.98	9.02	6.88	13.75
2	120	9.6	7.94	1.66	0.166	8.106	7.774	3.96	12.32	8.36		
3	120	8.95	7.47	1.48	0.148	7.618	7.322	3.96	12.1	8.14		
4	120	9.05	7.57	1.48	0.148	7.718	7.422	3.96	6.82	2.86		
5	120	9.19	7.64	1.55	0.155	7.795	7.485	3.96	9.46	5.5		
6	120	9.27	7.64	1.63	0.163	7.803	7.477	3.96	9.9	5.94		
7	120	9.04	7.55	1.49	0.149	7.699	7.401	3.96	11	7.04		
8	120	9.4	7.84	1.56	0.156	7.996	7.684	3.96	12.1	8.14		

Table 6-7: Analysis of MBR data for geometry 5 for data shown in Figure 6-21

6.6 Power Numbers for Hollow Blade Turbines

The studies on the power numbers of the hollow (concave) 6-blade agitators were prompted by the fact that these are finding increasing favour especially for multi-phase work where their ability to deliver power and disperse gas efficiently for a wide range of gassing rates makes them a obvious choice. The shape of these blades varies considerably from simple pipe sections to sophisticated streamlined curves as shown in Figure 6-22. The effect of these changes on power number is studied.

Bujalski *et al.* (1988), found that the power numbers of disc turbines was a power law function of scale ($Po \propto T^{0.065}$) and directly proportional to the ratio of blade height to the swept diameter (a/D_S). This appears to be a reasonable starting point for any attempted correlation of hollow blade turbines. The power number data for a number of types of disc and arm-mounted turbines are tabulated as Table 6-8. From this table, the average (a/D_S) in this work was 0.168 or approximately $D_S/6$. The normalized power numbers (Po_N) are therefore obtained as follows,

$$Po_N = \frac{Po}{6.0.(T)^{0.065}(a/D_S)} \qquad (6.12)$$

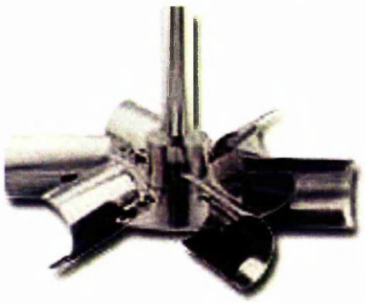

(a) Chemineer CD-6

Similar to that described by Van't Riet *et al.* (1976)

(b) Scaba 6SRGT

Curvature of blade ends in fold or spline. See

Figure 6-23 section through "Y – Y" for blade details.

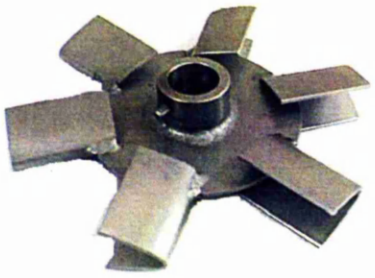

(c) Parabolic blade mounted on disc

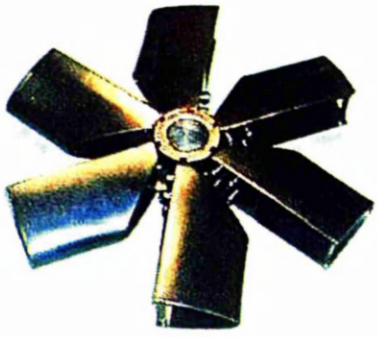

(d) Parabolic blade – arm mounted

Figure 6-22: Various hollow blade shapes and mountings. Shown as clockwise rotation so concave to flow direction.

The dimensions thought to affect the power number are identified in Figure 6-23.

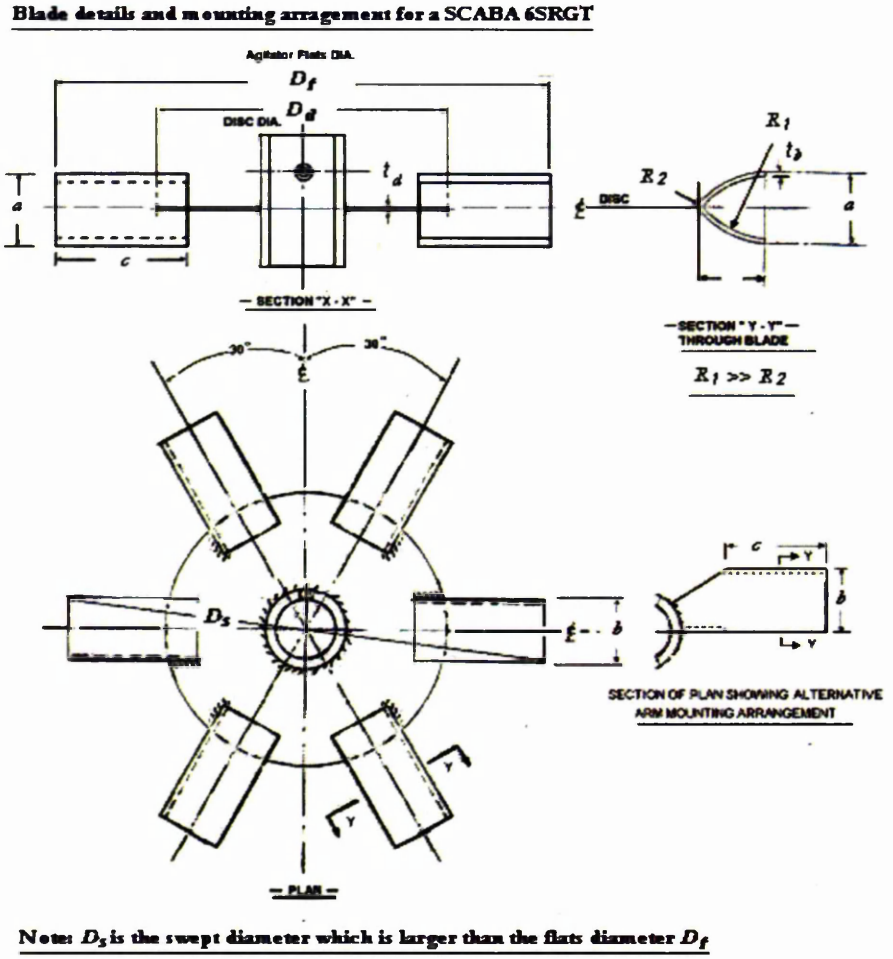

Figure 6-23: Concave hollow blade details referred to in Table 6-8.

The normalized power number (Po_N) increases as the ratio of the blade depth *(b)* to blade height (*a*) decreases, that is as the blade becomes less streamlined. This is illustrated graphically in Figure 6-24. Regression analysis established that a power law could adequately describe the affect of the blade aspect ratio on the power number as indicated by the R^2 correlation coefficient values.

6HBT Type	vessel Diam.	Agitator swept Diam.	Blade thickness	Disc thickness	Overall blade Height	Overall blade depth			Aspect ratio		Normalized
	T	D	t_b	t_d	a	b	D_s/T	a/D_s	b/a	Po	Po_N
	(m)	(m)	(m)	(m)	(m)	(m)	(-)	(-)	(-)	(-)	(-)
* Data from Kovacs (2001) – Po normalized to swept diameter ** Data from Saito *et al* (1992) – assumed that Po was given for swept diameter *** Data from Van't Riet (1976) - Po normalized to swept diameter											
6SRGT	0.286	0.149	0.002	0.002	0.022	0.018	0.521	0.148	0.795	1.60	1.96
6SRGT*	0.800	0.292			0.045	0.037	0.365	0.155	0.826	1.77	1.93
6SRGT**	0.610	0.200			0.030	0.025	0.328	0.150	0.833	1.5	1.72
Spined	0.286	0.151	0.002	0.002	0.028	0.020	0.528	0.185	0.714	1.97	1.92
Parabolic	0.305	0.144	0.002	0.002	0.022	0.020	0.472	0.152	0.913	1.44	1.70
Parabolic	0.610	0.248	0.0025	0.003	0.037	0.050	0.407	0.149	1.351	1.28	1.48
Van't Riet***	0.440	0.176	0.002		0.036	0.012	0.400	0.205	0.333	3.95	3.39
Van't Riet	1.790	0.5842	0.007	0.007	0.125	0.042	0.326	0.214	0.336	4.1	3.08
Spined	0.286	0.15	0.002	arm-mount	0.024	0.029	0.524	0.158	1.202	1.21	1.38
Parabolic	0.286	0.145	0.002	arm-mount	0.022	0.024	0.507	0.150	1.083	1.28	1.54
Parabolic	0.286	0.145	0.002	arm-mount	0.022	0.028	0.507	0.153	1.279	1.14	1.35
Parabolic	0.610	0.3048	0.003	arm-mount	0.045	0.060	0.500	0.147	1.337	1.17	1.37
Parabolic	0.914	0.4148	0.002	arm-mount	0.088	0.074	0.454	0.213	0.843	2.43	1.91
							ave	0.168			

Table 6-8: Power Numbers and geometries of various types of 6-blade concave hollow blade turbines (6HBT)

There are two types of mountings: disc and arm-mounted (where the blades are attached directly to the hubs) and three types of blade shapes: spined (like the 6SRGT where the blade profile ends on a fold) parabolic blades (where the blade section is described by a parabolic curve) and the Smith type (where the blade section is a section of circular pipe). The data for the disc-mounted types were considered separately from the total data set. The arm-mounted data were not considered separately, due to the limited data. Figure 6-24 (a) illustrates the fit for the disc-mounted types of 6-hollow blade turbines.

The equation of the line is,

$$Po_N = 1.6746\left(\frac{b}{a}\right)^{-0.586} \qquad (6.13)$$

Therefore, all the 6-hollow blade disc turbines listed here can be described by the equation,

$$\mathrm{Po} = 10.05(T)^{0.065}(a/D_S)(b/a)^{-0.59} \qquad (6.14)$$

The R^2 correlation coefficient is 0.972

All the data, including the disc and arm-mounted types can be described by the equation,

$$\mathrm{Po_N} = 1.6406\left(\frac{b}{a}\right)^{-0.6193} \qquad (6.15)$$

or,

$$\mathrm{Po} = 9.84(T)^{0.065}(a/D_S)(b/a)^{-0.62} \qquad (6.16)$$

with an R^2 correlation coefficient is 0.973.

The fit to all the data is no worse than for the disc types alone. Omitting the scale term ($T^{0.065}$) does however result in a worse fit. The constants are rounded-up without significant loss of accuracy to give,

$$\mathrm{P}o = 9.89(T)^{0.065}(a/D_S)(b/a)^{-0.6} \qquad (6.15)$$

The standard deviation on the proportionality constant is 0.477, which means it fits all the power number data to within ± 10%. This is accurate enough for design purposes.

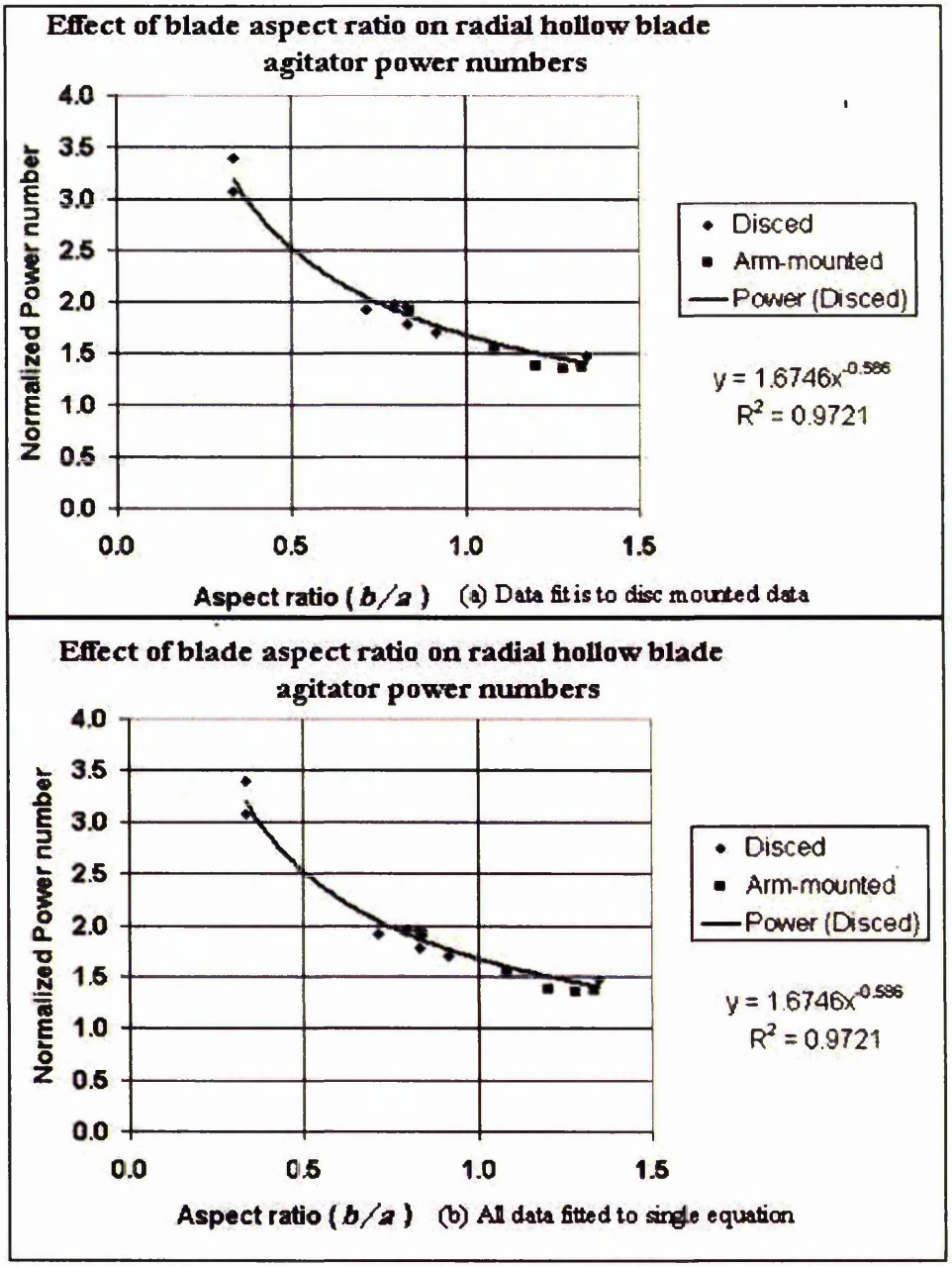

Figure 6-24: Fitting the normalized Power numbers of hollow 6-blade turbines to the aspect ratio of the impeller; (a) - best fit for disc type hollow blade turbines; below – (b) fit for all types of concave hollow blade turbine

Chapter 7 Multi-phase Hydrodynamics

This chapter covers high gas fractions, high superficial gas velocities and specific agitator power inputs from zero (bubble column) up to ~10 W/kg. Mixing in two-phase (gas-solid and gas-liquid) and three-phase (gas-solid-liquid) is measured and discussed. A solid-liquid interface is found to dramatically increase overall mixing time. When gas is introduced to this system, it destroys the interface and reduces the mixing time to the liquid only value.

Gas-liquid mass transfer, gas-hold-up and hydrodynamics are studied and correlations proposed. These are compared with the literature.

The "flooding-loading" transition is studied for a number of types of hollow blade agitators. These compare favourably with the Rushton turbine particularly as their low power numbers mean that they achieve the minimum Froude number for dispersion at a lower energy input than a similarly sized Rushton and the gassed power factor stays close to unity, resulting in minimal loss of power and pumping efficiency on gassing. However, no evidence was found to support the literature claims that they are more energetically efficient for dispersion above the minimum Froude number. A simple method, resulting from these studies, is proposed to avoid "flooding" for radial turbines, including the hollow-blade types, under gassed conditions.

A method for assessing the effect of changes in process conditions (agitation rates, gassing rates, and pressure on mass transfer using experimental data is proposed.

Rules for avoiding foam out at high phase fractions are developed.

Solid suspension with novel agitators for two and three phase systems are tested and relationships developed. The curved hollow blade agitator is shown to be more energetically efficient for solid suspension than most common alternatives, especially under gassed conditions.

Multi-phase Hydrodynamics

7.1 Scope

The chapter compares hollow blade turbines; agitator combinations of hollow blade turbines with up flow agitators and multiple up flow agitators with more traditional choices such as the Rushton turbine, particularly at extreme conditions of high phases fractions and specific power.

Phases of interest in this work are:

- Gas-liquid
- Solid-liquid
- Gas-liquid-solid.

Areas of study are:

- Gassed power measurement and hydrodynamics.
- Gas-liquid hold-up - both local and overall.
- Mixing in 2 and 3-phase systems with comparisons against single-phase mixing.
- Solid suspension in 2 and 3-phase systems.
- Gas-liquid mass transfer
- Use of experimental data to assess the effect of changes in the overall mass transfer coefficient, driving force and liquid volume on the overall mass transfer rate.

7.2 Gas-Liquid Power and Hydrodynamics

For gas-liquid dispersions the Rushton turbine (RT) traditionally has been used as the main gas disperser due to its cost effective ability to disperse gas. Latterly the hollow blade turbine (HBT) designs which apply varying degrees of streamlining behind the blades, are finding increasing favour especially under intense operating conditions with aeration numbers above 0.1 and, or high solids loadings. A number of these designs are now commercially available (Figure 7-1) for examples the CHEMINEER CD-6 and BT-6, the SCABA

6SRGT and the ICI Gasfoil designs disclosed in US patent 5,198,156. It is claimed that at high aeration numbers the HBTs are able to handle more gas than the RTs, without the power loss associated with the latter, see for example Saito *et al.* (1992). The data of Frijlink *et al.* 1990 suggest that the HBT design is the most energy efficient impeller for solid suspension at aeration numbers above 0.08. Hjorth (1994) found the suspension characteristics of the 6SRGT to be dependent on diameter and position relative to the base, but when these parameters were optimised it could suspend 65% magnetite very economically compared with other impellers and the agitation speed required to just suspend the solids is virtually independent of gassing rates.

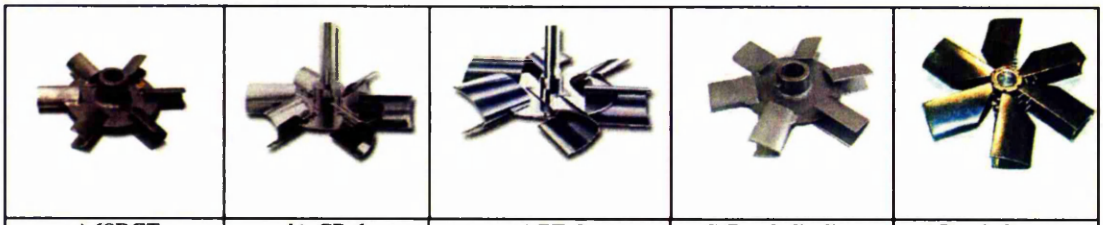

a) 6SRGT	b) CD-6	c) BT-6	d) Parabolic disc-type 6HBDT	e) Parabolic arm-mounted 6HBT

Figure 7-1: Selection of hollow blade agitators

The up-pumping high solidity hydrofoil agitators have been shown to be very effective at dispersing large quantities of gas without the instabilities that are associated with down-flow agitators, where the up flow of gas opposes the agitator flow as reported for instance by Chapman *et al.* (1983), Cooke (1989) and Nienow *et al.* (1994). Hence these have been studied along with combinations of hollow blade radial agitators (6HBT) below an up-pumping pitched blade turbine (6MFU) – a combination which gives stable operation at $H/T > 1$ where a single agitator is often undesirable.

Comparisons are made as the ratio of gassed to ungassed power as a function of gas flow number both with a fixed agitation rate and variable gas rates and also at fixed gas rates and variable agitation rate.

Multi-phase Hydrodynamics

From the flow visualisation work, using air-water, the gas-loading point (flooding – loading transition) and the complete dispersion (loading – complete dispersion transition) are identified and compared with literature predictions for Rushton turbines and hollow blade agitators and the literature claims made for the improved gas handling abilities of the latter are critically examined.

7.2.1 Cavity Structure of Radial Turbines under Aerated Conditions

The literature review in Chapter 2 (Section 2.3.1) showed the relationship between the gas cavities behind the blades and the reduction in power on gassing. The cavity structures for disc turbines and their affect on gassed power are described, for example, by Nienow *et al.* (1985). The hollow blade agitators have also been shown to have a cavity structure under aerated conditions. However because of the streamlined shape of these blades, the attached gas bubble does not affect the drag in the same way as it does with a flat blade and hence the power loss is much less. For the SCABA 6SRGT (Figure 7-1a) Saito *et al.* (1992) describe these cavities as vortex cavities in air-water changing to vortex-clinging cavities at high gas rates or in CMC solutions. These authors claim that the gas-liquid flow spills out from the inside of the hollow blades at all gas rates and this gives rise to the trailing vortex cavities in aerated water. This description is not easy to accept, since it might be assumed that the high-pressure area inside the blades would naturally exclude gas, which is more likely to be entrained into the vortex from the lower pressure region behind the blades in a similar manner to the Rushton turbine.

Cavity formation for hollow blade agitators was studied by the author, whilst at ICI, in the late 1980's. The stills shown in Figure 7-2 and Figure 7-3 are from a digital copy of a video made of the 0.286 m vessel fitted with a 0.144 m diameter Scaba 6SRGT. Date of the original video is 27/11/87. The agitator clearances were $T/3$ and $H = T$ and the fluid was 0.4% CMC (grade Hercules powder grade 7H4C). The CMC solution was used because it proved very difficult to film the cavities in air-water with this equipment. The main problem

being that at realistic agitation and gas rates, it was like trying to film through a fog.

Air was introduced through the bottom bearing (similar to a central point pipe sparge). The original film was made on a high-speed video and the time shown is real time. The first part of film is shot through the base at agitation speeds of 120, 240, 360, 480 and 600 rpm with gas at 5, 10, 20 and 40 litres per minute of air. The last part of film is shot through the side at 480 rpm and 5, 10 and 20 litres per minute of air. Note that even with CMC it proved difficult to get good pictures at high gas and agitation rates.

The apparent viscosity of the 0.4% CMC is described by the law,

$$\mu_a = 0.5\dot{\gamma}^{-0.4} \tag{7.1}$$

where the average shear rate ($\dot{\gamma}$) is approximately equal to $10N$ (see Chapter 2, section 2.6.2 and Chapter 4. Table 4-1. The relevant flow conditions for this work are listed in Table 7-1.

The stills from the video shown in Figure 7-2 are shot from below and cover the full range of agitation rates chosen. Vortex-clinging cavities can be clearly seen at all agitation speeds used and when viewed from below it does indeed look as if the agitator is pumping a gas-liquid mixture. Gas cavities can also be seen behind the blade. In picture (f) there appears to be a large wedge shaped gas-filled cavity behind a blade.

The stills shown in Figure 7-3 are viewed from the side and show what happens in the first four seconds after 5 litres per minute of gas is introduced at an agitation speed of 480 RPM. There is no evidence from these pictures to support a gas core inside the blades, although gas can clearly be seen going over the blades. Looking clockwise from the open view of the blade to the view behind the preceding blade it appears that cavities are developing behind the blades. Observations from these pictures do not support the proposal of a gas core inside the blades, although gas can clearly be seen going over the blades. Looking clockwise from the open view of the blade to the view behind

the preceding blade, it appears that cavities are developing behind the blades. It is concluded that even in highly gassed liquids the hollow blade agitator pumps essentially liquid and that the gas is entrained and broken up by the liquid jet. Similar cavities behind the blades have been seen for other hollow blade turbines, in particular for the ICI Gasfoil described by Cooke *et al.* (1988) and the arm-mounted parabolic blade design. .

Gas flow rate Q m^3/s	Agitation rates N (rps)	Apparent viscosity $\cong 0.5(10N)^{-0.4}$ Pa. s	Re	Fl Q/ND^3	*VVM*	Fr N^2D/g
0.000333	2	0.151	275	0.0558	1	0.059
0.0005	2	0.151	275	0.0837	1.5	0.059
0.000167	4	0.114	726	0.0140	0.5	0.236
0.0005	4	0.114	726	0.0419	1.5	0.236
0.000333	8	0.087	1915	0.0140	1	0.942
8.33E-05	8	0.087	1915	0.0035	0.25	0.942
8.33E-05	10	0.079	2617	0.0028	0.25	1.472

Table 7-1: Conditions used in the flow visualization work with the Scaba 6SRGT agitator in 0.4% CMC.

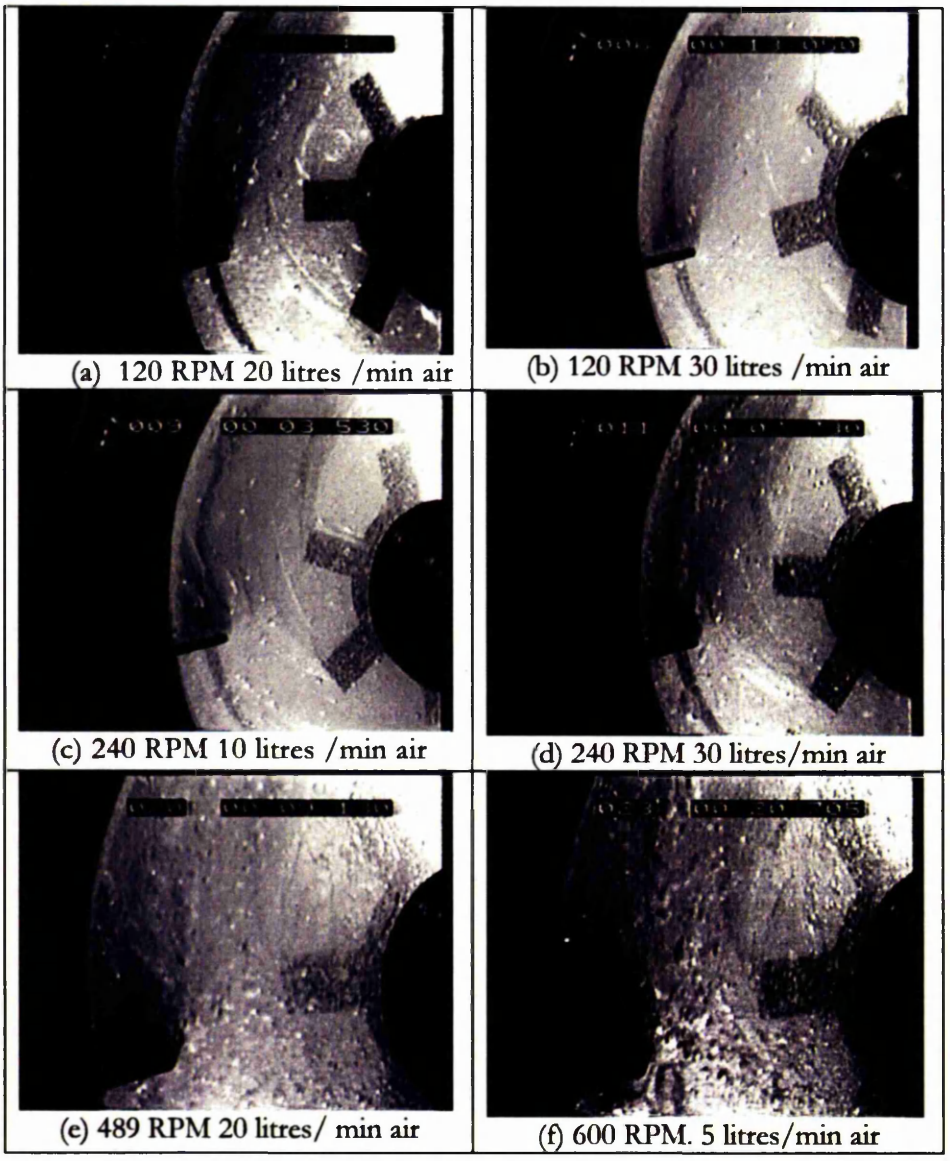

Figure 7-2: Pictures of flow from a $D = T/2$ SCABA 6SRGT in aerated 0.4% CMC, viewed from below. $T = 0.286$ m. Agitator clearance was $T/3$. For flow conditions see Table 7-1.

Figure 7-3: Same as Figure 7.1 but viewed from the side. Agitation rate is 480 RPM. Still (a) is as the gas is introduced. Subsequent pictures are shown in real time as shown on the video clock. Flow conditions are given in Table 7-1.

7.2.2 Hydrodynamics of Radial Turbines – Literature and Discussion

When considering the hydrodynamics of Rushton turbines, the flow visualizations attributed to Wisdom (1973) are frequently used to define the various operating regimes as described in Chapter 2, section 2.3. The first sequence of Wisdom's drawings, which are now taken as representing

operation under "flooded" conditions, with the original annotations, are reproduced as Figure 7-4, (a), (b) and (c).

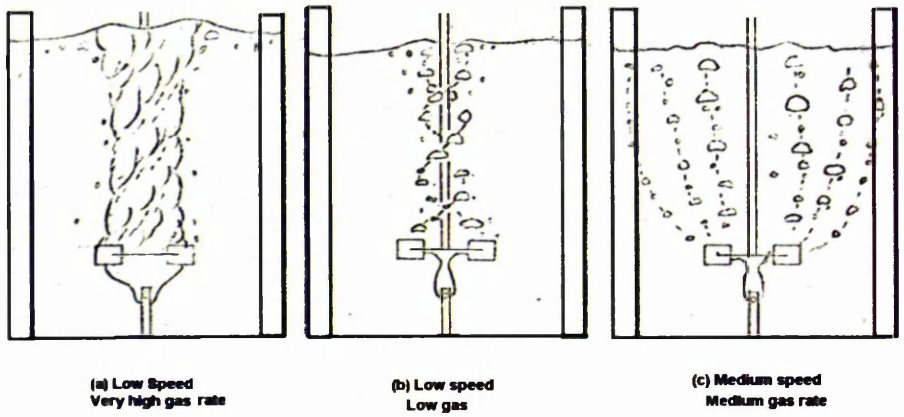

Figure 7-4: From Wisdom (1973), depicting the effect of agitation and air rate on gas distribution using a Rushton Agitator under "flooded" conditions

Figure 7-5 (a), (b), (c) and (d) is a commonly used representation of the effect of agitation speed (N) and the gassing rate (Q_G) on the transitions between "flooding" to "loading" and "loading" to "complete dispersion".

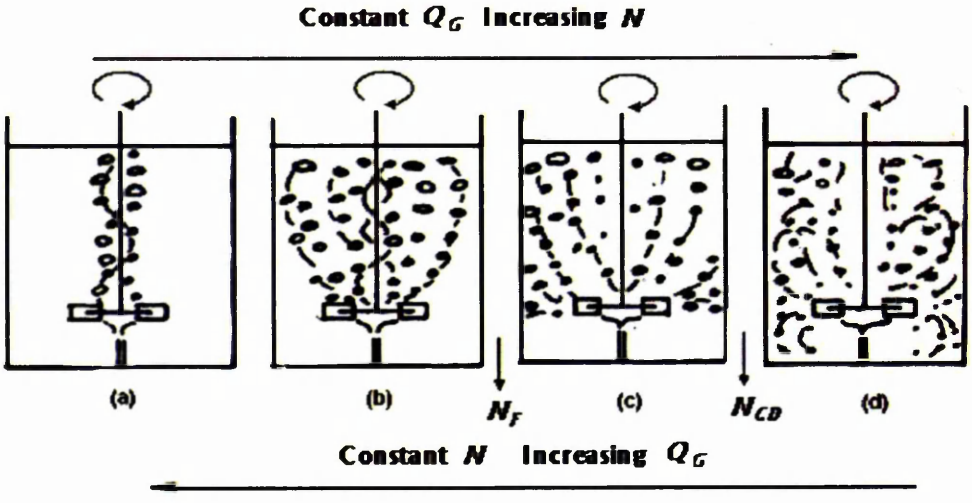

Figure 7-5: Showing the transition between "flooding" and "loading" (N_F) and "loading" to "complete dispersion" (N_{CD}) for radial turbines

Whilst accepting that these pictures represent conditions found for air-water in small laboratory type vessels at modest power inputs and aeration rates up to 1 or 2 *VVM*, they are not representative of conditions applicable on large-scale plant that often operate superficial gas velocities in access of 0.1 m/s. In Chapter 2, equation (2.113) the gas buoyancy power due to potential energy in a cylindrical vessel was shown to equal,

$$P_Q = Q_G(\rho_L - \rho_G)g(H_L - c_S)$$

where c_S was the height of the sparger. Note that considerable energy can be expended at the sparger in terms of kinetic energy. However, this energy is not usefully employed due to the compressible nature of gases (Middleton *et al.* (1994)).

Thus for a cylindrical vessel when the gas input is at the base and the gas density can be ignored, the specific gas power input is,

$$\frac{P_Q}{\rho_L V_L} = \frac{4Q_G\rho_L g H_L}{\rho_L \pi T^2 H_L} \text{ (W/kg)} \qquad (7.2)$$

As superficial gas velocity is,

$$v_S = \frac{4Q_G}{\pi T^2} \text{ (m/s)} \qquad (7.3)$$

It follows that specific gas power is approximately,

$$\frac{P_Q}{\rho_L V_L} = v_S g \text{ (W/kg)} \qquad (7.4)$$

Therefore, the specific power input (W/kg) due to the air rising through the vessel is approximately ten times (g) the superficial gas velocity, which means the power input at a superficial gas velocity of 0.1 m/s is approximately 1 W/kg. This energy is sufficient without any mechanical agitation at all to produce flow more like that shown in Figure 7-5 (c) than Figure 7-5 (a). Therefore under intense operating conditions Figure 7-5 can no longer be used to define "flooded" or "loaded" conditions. By comparison 2 *VVM* gas on an

Multi-phase Hydrodynamics

$H = T$, 30 cm laboratory scale cylindrical vessel (very high gas rate by Wisdom (1976) definition) has a superficial gas velocity of 0.01 m/s or a gas specific energy input of 0.1 W/kg.

Also, when small bubbles are present due to the presence of surfactants or salts, the transition from loaded to complete dispersion cannot be distinguished even at low superficial gas velocities as the tiny bubbles are always dispersed.

How then can the "flooding" – "loading" point be recognized at these high superficial gas velocities?

In Chapter 2, section 2.3.1 it was claimed the flooded regime could still be recognized from observation of the surface where the flooded regime is distinguished by gas bypass with gas spouting up near the centre. However, this gas spouting could also be attributable to a transition from homogeneous to heterogeneous flow, hence great care must be taken in the interpretation of the flow visualization. The literature is reconsidered in the following sections.

7.2.2.2.1 Literature studies on Flooding of Rushton turbines

The prediction of the point at which gas is adequately dispersed in mechanically agitated vessels is a paramount design parameter and one that has attracted considerable academic study. The flooding-loading (F-L) transition for disc turbines has been linked to transitions in cavity types. Below the loading point only ragged or clinging cavities are found. Warmeoskerken and Smith (1985) claim that large cavities cannot exist below a Froude number (Fr) of about 0.045 and below this value the agitator is always flooded. This makes some kind of physical sense since gravity has to be overcome in order to capture the gas cavity.

$$\mathrm{Fr} = N^2 D/g \qquad (7.5)$$

Fr represents an agitator "g" force.

The actual "g" force, at the rotating agitator tip is,

$$"g" = \frac{(2\pi N)^2 D}{2g} \qquad (7.6)$$

Therefore by comparison of equations (7.5) and (7.6), 19.74 "g" = Fr and therefore 1.0 "g" ≅ 0.05 Fr (close to the 0.045 Fr proposed for stable cavities).

Warmoeskerken and Smith (1985) defined flooding, as a regime in which there is an axial flush of gas through the impeller plane up to the liquid surface. The loading point occurs when the agitator starts to act as a pump and disperses gas to the impeller wall. This was measured using a small propeller flow meter. There is a significant step in the rate of radial outflow at the F-L transition. This $N_{F\text{-}L}$ transition was also marked by a significant positive step in the gassed power curve related to a change in cavity formation.

Warmoeskerken and Smith (1985) gave an extensive literature review of the flooding of Rushton type disc turbines. They compared the merits of theories based on a minimum tip speed (agitator shear rate) required for dispersion and those based on agitator pumping rates. From an energy balance between gas buoyancy driven flows and agitator driven flows, it was shown that (providing the disc turbine gassing factor could be assumed to be constant at the F-L point for a range of gassing rates) the variables could be arranged to give an equation of the type,

$$\mathrm{Fl_F} = A\,\mathrm{Fr_F} \qquad (7.7)$$

Where $\mathrm{Fl_F}$ is the gas flow number (aeration number) at the flooding point ($Q_G/N_F D^3$), $\mathrm{Fr_F}$ is the Froude number at the flooding point ($N_F^2 D/g$) and A is an agitator specific proportionality constant.

The data obtained for the $D = 0.4T$ disc turbines on 3 scales were fitted by equation (7.7) and the specific proportionality constant was found to be 1.2. Thus,

$$\mathrm{Fl_F} = 1.2\,\mathrm{Fr_F} \qquad (7.8)$$

Multi-phase Hydrodynamics

Other workers had previously shown that F-L data could be adequately fitted in the form of equation (7.7).

Analysis of the data of Warmoeskerken and Smith (1985) for Rushton turbines of $D = 0.4T$ in vessels from 0.44 m to 1.2 m diameter reveals the maxima in the values of N_F and Q_{GF} listed in Table 7-2. If it is assumed (sensible estimate) that the gassed power number of a Rushton turbine is 3.0 at the flooding point for modest power inputs, the maximum specific agitation power and gas power at the (F-L) transition is of the order of 0.52 W/kg. The equality of the gas and agitation powers is plausible since in order to disperse the gas it could be argued that the agitator power must at least equal the gas power.

Tank diameter	Agitator Diameter	Liquid Volume	$Fr_{(F-L)}$ Max.	$Fl_{(F-L)}$ Max.	$Nmax_{(F-L)}$ Maximum	$Qmax_{(F-L)}$	Superficial Gas vel.	Specific Gas power	Est Pg using $P_U/P_G = 0.6$	*Specific shaft Power* $Pg/\rho_L V$ gassed
M	m	litres	(-)	(-)	s^{-1}	m^3s^{-1}	ms^{-1}	W/kg	W	W/kg
0.44	0.176	66.90	0.3	0.36	4.09	0.00803	0.053	0.52	34.64	0.52
0.64	0.256	205.89	0.2	0.24	2.77	0.01115	0.035	0.34	69.99	0.34
1.2	0.48	1357.17	0.17	0.204	1.86	0.04205	0.037	0.36	495.04	0.36

Table 7-2: Maximum Froude and Gas flow numbers extracted from the data of Warmoeskerken and Smith (1985) and used to calculate N and Q and to estimate the specific power inputs by the agitator and by the gas.

The precise equality of the gas and agitation powers at the flooding loading point (Table 7-2) found by Warmoeskerken and Smith (1985) is not coincidental. The form of the equation was derived from an energy balance between the gas buoyancy driven circulation and agitator driven circulation. The specific gas buoyancy is approximately $v_S g$ (equation 7.4). The specific agitator power $\varepsilon_T = P_S/\rho_L V_L$. Therefore equation (8) can be derived from $\varepsilon_T = v_S g$ to give,

$$\varepsilon_T = v_S g = \frac{4\,\mathrm{Po}\,\rho_L N^3 D^5}{\rho_L \pi T^3} = \frac{4Q_G}{\pi T^2} g \qquad (7.9)$$

The equation can be reduced further by cancelling the common denominators and substituting $T = 2.5D$ to provide the following expression:

$$\frac{Q_G}{ND^3} = \frac{\text{Po}}{2.5}\frac{N^2 D}{g} \qquad (7.10)$$

The substitution of the gassed power number = 3.0 at the flooding condition into equation (7.10) reproduces equation (7.8).

Nienow *et al.* (1985) obtained F-L data for a range of Rushton turbine D/Ts from 0.22 to 0.5. They found that the increase in gassing rate, which caused a transition from loading to flooding, is accompanied by a change from 3 large plus three small clinging cavities to 6 ragged cavities for D/T of $\leq$ 0.4. At the same time there is a step increase in the power drawn. When D/T = 0.5, the transition was from clinging to ragged cavities, accompanied by a step decrease in the power drawn. However, in this case the F-L transition is reported to occur below Fr = 0.045. The step decrease in power at the flooding point does not appear to be a general rule for $D = T/2$ disc turbines. In earlier work, Nienow *et al.* (1977) and Smith *et al.* (1977) stated that flooding was marked by a minimum in the gassing factor when plotted against Fl at constant N (Q_G varied). Similar observations were obtained for their $D = T/2$ data (power increased on flooding). However, in these cases the Fr was greater than 0.045. It is notoriously difficult to determine the F-L transition by eye on a small vessel with a large $D = T/2$ turbine. From the reasoning given in the development of equation (7.6), it is wise to assume that all cases below Fr = 0.05 (1 "*g*") are in fact flooded. Note that not all workers agree that the minimum in the gassing factor curve marks the F-L transition. Westerterp (1963) states that, "the minima in the curves occur in the neighborhood of the minimum agitation rate" (for dispersion) "but do not coincide".

The F-L data for Nienow *et al.* (1985) were fitted by the form of equation (7.7) and the constant A in this equation was found to be a function of D/T. From a double log plot of A versus D/T, which included the Warmoeskerken and Smith (1985) constant, they determined an overall equation as follows:

$$Fl_F = 30\left(\frac{D}{T}\right)^{3.5} Fr \qquad (7.11)$$

The Nienow *et al.* (1985) analysis of this equation showed that at constant scale, equation (7.11) infers that to disperse a given amount of gas, then the grouping $N_F D^{2.5}$ is constant, They argued that is close enough to ND^3, which is constant for pumping rate and so one can presume that agitator pumping rate is a controlling variable.

No error analysis is provided on equation (7.11) in the Nienow *et al.* (1985) paper. A back calculation of equation (7.11) to predict of A for comparison with the original values indicates a poor fit, especially for $D = T/2$ turbines. For these, equation (7.11) predicts a value of A of 2.65 compared with an original value of 4.7. However, as earlier stated, it is difficult to judge accurately the F-L point with large turbines and it may well be that some sort of weighting was used in the original analysis, but a simple un-weighted analysis of the original (A) versus D/T results in a better fit for,

$$Fl_F = 54\left(\frac{D}{T}\right)^{4.0} Fr \qquad (7.12)$$

with an R^2 correlation coefficient of 0.9634 (see Table 7-3 and Figure 7-6).

Analysis of equation (7.12) results in $N_F D^{2.67}$ required to disperse a given amount of gas at a single scale (even closer to the constant pumping rate case).

Rushton turbine D/T	Experimental constant "A"	Nienow *et al.* (1985) (eq 7.11) predicted constant "A"	This work eq. (7.12) predicted constant "A"
0.22	0.13	0.15	0.13
0.22	0.17	0.15	0.13
0.3333	0.48	0.64	0.67
0.4	1.2	1.21	1.38
0.5	4.7	2.65	3.38

Table 7-3: Data from Nienow *et al.* (1985) showing measured and predicted constants in eq. 7.8. Fit very poor for $D/T = 0.5$. See graphical fit in Figure 7-6.

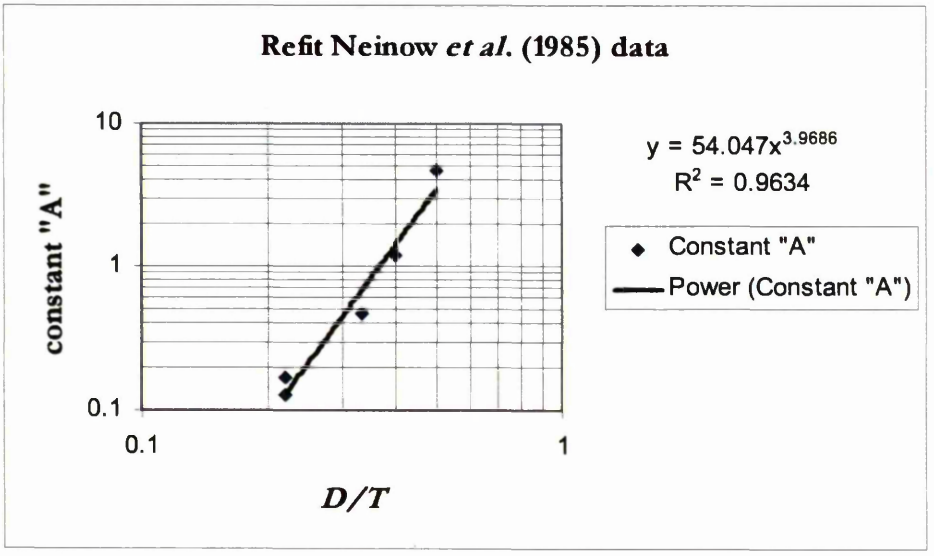

Figure 7-6: Refit of for D/T in equation 7.5 from Nienow *et al.* (1985)

Nienow *et al.* (1985) also found no effect of liquid height on the F-L transition, which they explained is contrary to the original theory, which was based on an energy balance. The specific gas energy is independent of height whilst the agitator specific energy decreases in proportion to the liquid height.

7.2.2.2 Flooding of Hollow Blade Turbines

It is claimed that the hollow blade turbines are capable of handling much more gas than the Rushton turbine. CHEMINEER claim on their website (www.chemineer.com) that the CD-6 can handle about 2.4 times the maximum gas capacity of the D-6 (Rushton turbine) impeller and that the DT-6 can disperse nearly six times the gas handling capability of the D-6.

Saito *et.al.* (1992) showed that a 6SRGT will handle around 3 times the gas as a similar diameter Rushton turbine when compared at the same ungassed power. However because of the disparity in gassing factors, the actual operational power is much higher with the 6SRGT. These authors also claim that the disparity in ungassed power numbers between a RT and HBT allows a bigger

HBT to be retrofitted with an added benefit to the pumping rate, which is higher at the same power input for the larger agitator. From Bakker (2004) it appears that the CHEMINEER claims of improved gas dispersion with their HBT's are also based on retrofits from Rushton turbines to larger diameter HBT's operating at the same ungassed power but with a significantly higher gassed power input.

Saito *et al.* (1992) compared $D = T/3$ Rushton and SCABA 6SRGT turbines in air-water and air-CMC systems. They reported that with the 6SRGT in an air-water system, the F-L transition was accompanied by a considerably enhanced up-ward step in power and a hysteresis loop. This hysteresis occurs because once cavities are formed, at a given agitation speed, they persist even when the gas rate is reduced. They did not find an up-ward step for the 6SRGT with the air-CMC system and this they argue [citing Machon *et al.* (1980)] is due to the binomial bubble distribution with a fraction of very tiny bubbles which are dispersed at all agitation speeds, making the concept of "flooding" difficult to apply. However, it could be argued that this applies also to air-water systems at high superficial gas velocities. When they used a slightly different constant in equation (7.11) they claimed the upper transition line for the 6SRGT followed the same trend as the RT (though this is not clearly apparent from their Figure 9 (reproduced here as Figure 7-7) that represents their data).

Gezork *et al.* (2000) compared a 0.15 m diameter RT with a 0.161 m diameter 6SRGT in an air-acetic acid solution and illustrated on a plot of N versus superficial gas velocity that the F-L data for both agitators fitted on a line predicted for the 0.15 m diameter RT from equation (7.11).

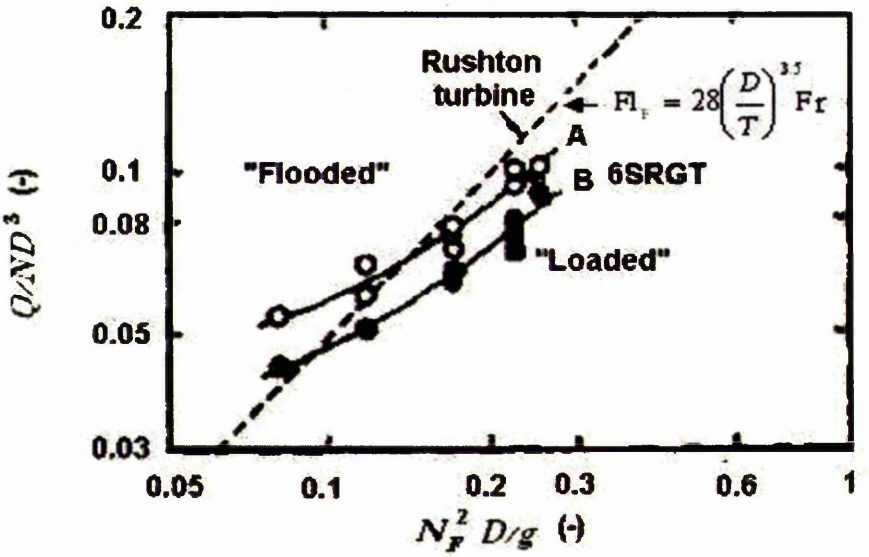

Figure 7-7: Data of Saito *et al.* (1992) relating Gas flow number and Froude number for D=T/3 Rushton and 6SRGT turbines in air-water.

Curve A is loading to flooding. Curve B is flooding to loading.

7.2.3 Experimental Studies of the "Flooding-Loading" and "Loading-Compete Dispersion" Transitions with Rushton and Hollow Blade Turbines.

In this section the hydrodynamic regimes of the Rushton turbine are confirmed by visual observations on the 0.9144 m and the 1.79 m diameter vessels and the results of studies on the "flooding-loading" point for various hollow blade turbines are compared. For the hollow blade turbines, the "flooding-loading" point is determined both by analysis of the gassed power curve looking for the enhanced up-ward step in power and hysteresis loop in air-water as reported by Saito *et al.* (1992) for Scaba 6SRGT turbines. In the experiments reported here, these have been found at low specific power inputs for hollow blade designs tested of the types (b), (c) and (d) in Figure 6-22. By inference the behaviour of type (a) - not tested here - would be expected to be similar. The "flooding-

loading" point is also estimated from visual observations. The "agreement" between these two methods is discussed.

7.2.3.1 Experimental Studies using Rushton Turbines

The "flooding-loadings" and "loading-complete dispersion points are estimated from visual inspection with reference to Figure 7-5. It is much easier to discern the "flooding-loading" transition in larger vessels, fitted with agitators of D ≤ $0.4T$ than in small vessels especially when these are fitted with $D = T/2$ turbines. Therefore the data included for the 0.9144 m and 1.79 m vessel are considered the most accurate – this in spite of the fact that the 1.79m vessel is constructed from spun polypropylene with viewing through strategically sited Perspex port holes in the walls and base. The experimental data show reasonable correspondence to the transition equations proposed by Nienow *et al.* (1985), equations (2.25) and (2.26). The comparisons are shown in Figure 7-8. Hence these equations appear to give a reasonable prediction of N_F and N_{CD} in air-water at scales up to 1.79 m. Note that flooding point at 240 RPM on the 0.9144 m vessel was determined by observation of the surface looking for evidence of gross gas bypass. The superficial gas velocity at which it occurred is around the transition from homogeneous to heterogeneous flow and may be due to this transition. It is also very difficult to gauge the transition points at high superficial gas velocities so by observation it is really only possible to judge the transitions at modest gas rates.

It was not possible to confirm loading at Froude numbers below 0.045, which Smith and Smit (1988) identify as the minimum for the retention of stable cavities. This Froude number equates to a "g" force at the agitator tips of 0.9. Realistically loading is not expected to occur at agitation speeds below a "g" of 1 or Fr = 0.05. As a general rule applicable to all agitators it is expected that gas dispersion will depend on the following operating parameters:

- Agitator pumping rates (which depends on agitator type, N and D).

Multi-phase Hydrodynamics

- The ratio of agitator power to gas buoyancy power.
- The "g" forces on blade tip.
- The bubble size, slip velocity and the ratio of the bubble rise velocity to agitator induced liquid velocities.

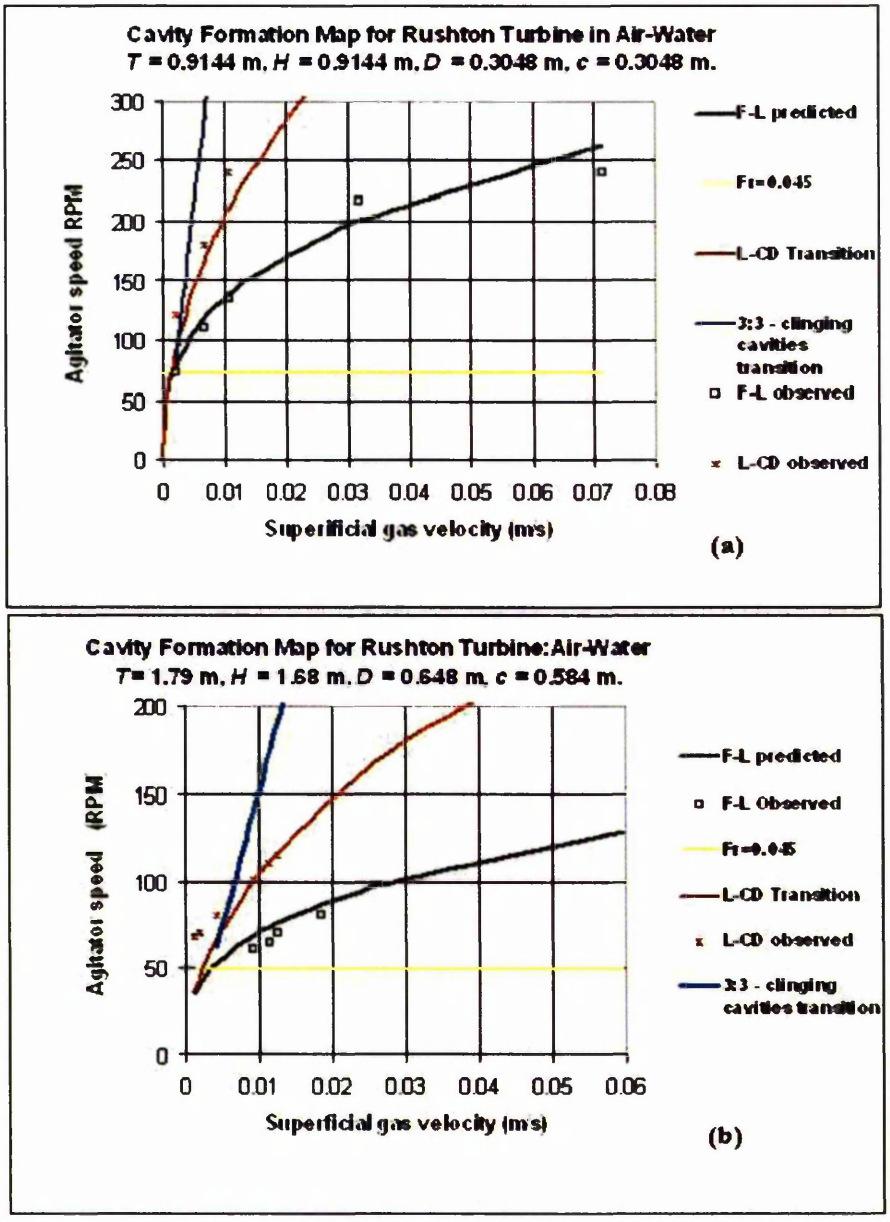

Figure 7-8: Observed "flooding-loading" and "loading-complete dispersion" transition: comparison with theory of Nienow *et al.* (1985). Top (a) is for the 0.9144 m vessel and bottom (b) is for the 1.79 m diameter vessel.

7.2.3.2 Experimental Studies on the Flooding of Hollow Blade Turbines.

The agitator and vessel geometries for these studies are listed in Table 7-4. The agitator types are depicted in Figure 6-22. Where possible the flooding-loading transition was checked by visual inspection. This visual method is not reliable at high superficial gas velocities as the gas energy itself gives dispersion.

Key to Agitator Type	6HBT Type	Vessel diam.	Agitator swept diam.	Blade thickness	Disc thickness	Overall blade Height	Overall blade depth			Aspect ratio	
		T	D	tb	Td	a	B	Ds/T	a/Ds	b/a	Po
		(m)	(m)	(m)	(m)	(m)	(m)	(-)	(-)	(-)	(-)
A	6SRGT	0.286	0.149	0.002	0.002	0.022	0.018	0.521	0.148	0.795	1.60
B	Parabolic	0.610	0.248	0.0025	0.003	0.037	0.050	0.407	0.149	1.351	1.28
C	Parabolic	0.286	0.145	0.002	arm-mount	0.022	0.028	0.507	0.153	1.279	1.14
D	Parabolic	0.914	0.4148	0.002	arm-mount	0.088	0.074	0.454	0.213	0.843	2.43

Table 7-4: Power Numbers and geometries of the types of 6-blade concave hollow blade turbines tested to determine the Flooding-Loading transition. Note that for all cases the liquid height equalled the vessel diameter. Type A and B were operated at an agitator clearance $c = T/4$. Type C and D were operated at $c = T/3$.

For all four hollow blade agitator types (A, B, C and D as listed in Table 7-4 and depicted in Figure 6-22); plots of gassing factors (P_G/P_U = the ratio of gassed to un-gassed power or power numbers) against agitation speed at fixed gas rates produce very similar sets of data for all four agitators tested, in spite of the difference in blade shapes (spined versus parabolic) and mounting arrangements (arm-mounted versus disc mounted). These are illustrated in Figure 7-9 to Figure 7-12.

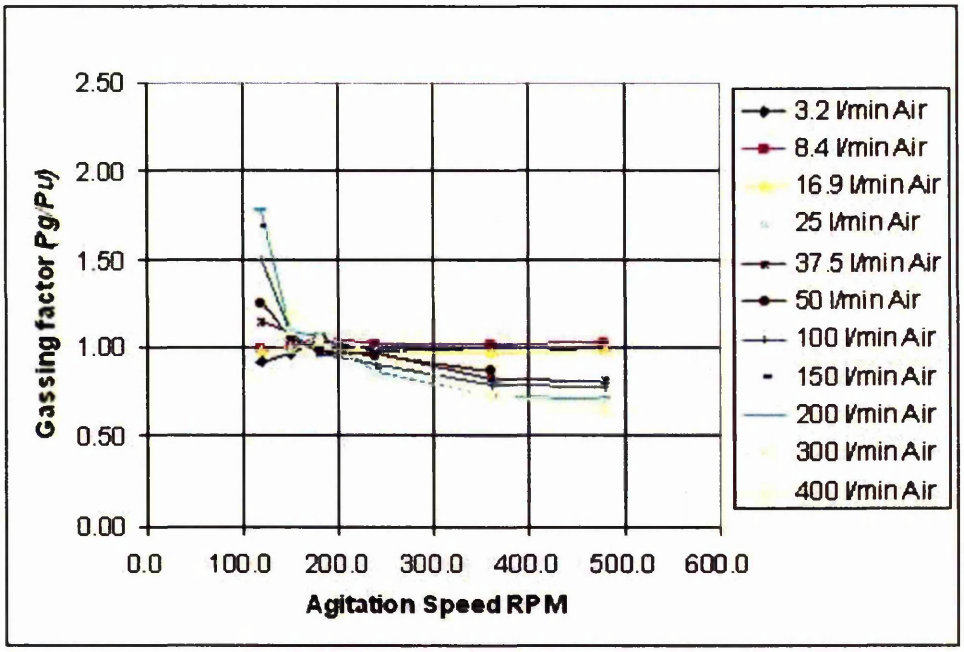

Figure 7-9: Type A: Gassing factors versus agitation speed for the 0.149 m diameter 6SRGT agitator in the 0.286 m diameter vessel for air-water. (Note that in these figures the gassing rates are given at outlet conditions).

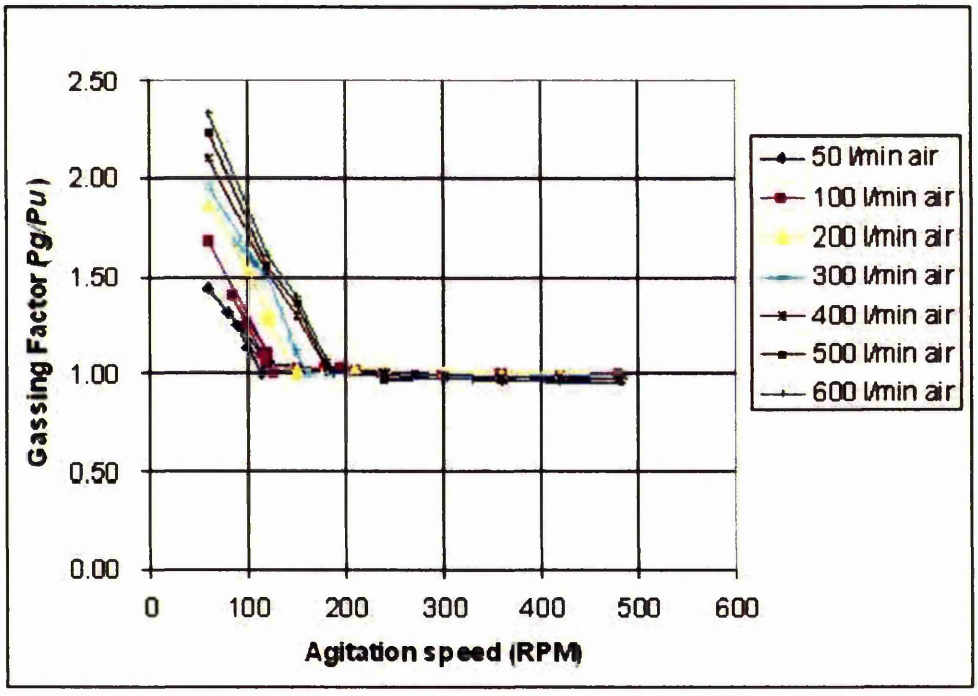

Figure 7-10: Type B: Gassing factors versus agitation speed for the 0.248 m diameter parabolic 6HBDT agitator in the 0.61 m diameter vessel for air-water.

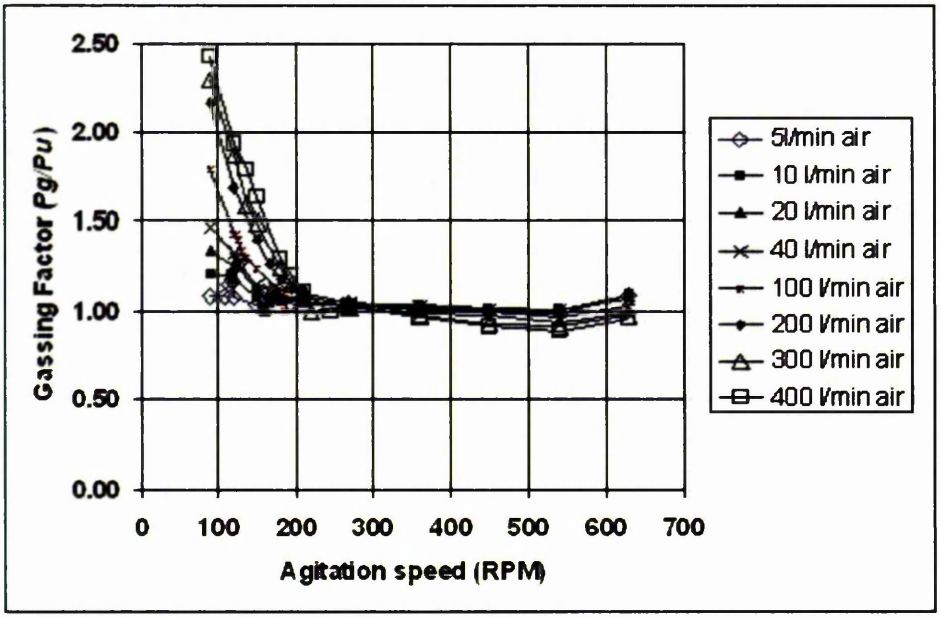

Figure 7-11: Type C: Gassing factors versus agitation speed for the 0.145 m diameter parabolic 6HBT agitator in the 0.286 m diameter vessel for air-water.

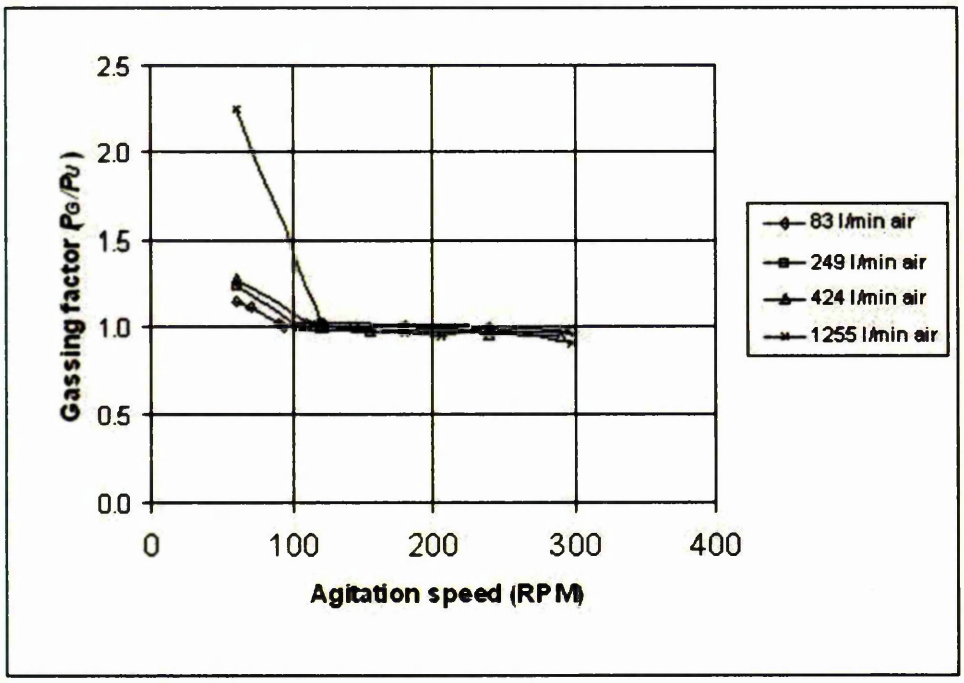

Figure 7-12: Type D: Gassing factors versus agitation speed for the 0.4148 m diameter parabolic 6HBT agitator in the 0.914 m diameter vessel for air-water.

Characteristics of these data sets are:

- The gassing factor exceeds 1.0 at low agitation speeds (low specific power).
- The enhancement in the gassing factor can be as high as 2.5 times the ungassed power at high gas rates.
- The enhancement of the gassing factor at low speeds increases with increasing gas rates.
- The gassing factor curve is very flat for air-water at agitation above the loading point (assuming this coincides with the lowest agitation speed coincident with a gassing factor of 1.0).
- The parabolic blades give improved performance (higher gassing factor at high agitation speeds and high gas rates) than the spined-back blades of the 6SRGT, which may suggest that the parabolic blades are more streamlined.
- It is noted that the enhancement of the gas factor occurs at low specific shaft-power inputs. This is illustrated in Figure 7-13 by a plot of the gassing factor data (shown in Figure 7-10) for the 0.248 m disc type parabolic hollow blade agitator against specific power. The highest specific shaft power coincident with the transition is 0.2 W/kg, which is much lower than one would normally design a system for gas-liquid agitation.

Why does an enhancement of the gassing factor occur under flooded conditions and why does it increase with increasing gas-rate? A plausible explanation is that the energetic gas flow, rising in the close proximity of the agitator blades, offers an extra resistance to radial flow, which has to be overcome by developing a higher pumping head. This resistance is removed when the gas is fully dispersed. This explanation tallies with the Warmoeskerken and Smith (1985) findings that in gassed conditions a critical minimum agitation speed must be exceeded before the radial flow can be

detected and this corresponds to the "flooding-loading" transition.

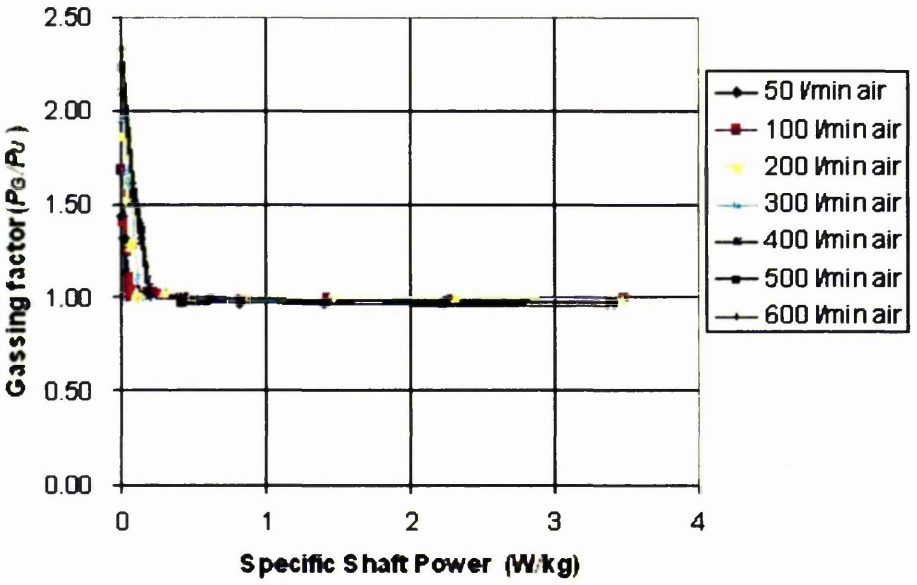

Figure 7-13: Type B: Gassing factors versus specific shaft power for the 0.248 m diameter parabolic 6HBDT agitator in the 0.61 m diameter vessel for air-water.

Agitator key Refer to Table 7-4	Agitator type	Vessel diameter	Agitator diameter	Mean Gasrate Q	N (F-L) Nienow *et al.* (1985).	N (F-L) Observed	N (F-L) Graph
Type		T (m)	D (m)	litres/min	RPM	RPM	RPM
A	6SRGT	0.286	0.149	8.3 16.7 24.7	57.9 73.1 83.3	102 102 108	79 112 110
B	Parabolic	0.610	0.248	48.6 97.2 194.4 291.6 388.9 486.1 583.3	70.7 89.1 112.2 128.4 141.4 152.3 161.8	100 115.1 149.7 150.1 180 180.2 180.	115.5 127 149 160 180 180 187
C	Parabolic	0.286	0.145	4.9 9.9 19.3 39.5	52.1 65.7 82.7 104.3	117 117 123 126	120 155 160 180
D	Parabolic	0.914	0.4148	83.1 379.5 424.2 1255.2	37.5 54 64.5 92.6	91 106 116 121	94 106 120 123

Table 7-5: Comparison of observed "flooding – loading" speeds with those observed from the power curve transitions and those predicted using the disc turbine equation [eq. (7.11)] proposed by Nienow *et al.* (1985).

The transition points were extracted from Figure 7-9 to Figure 7-12 and compared with visual interpretations of the loading points in Table 7-5. The transitions were obtained from an expanded view of the transition region as revealed for example in Figure 7-14.

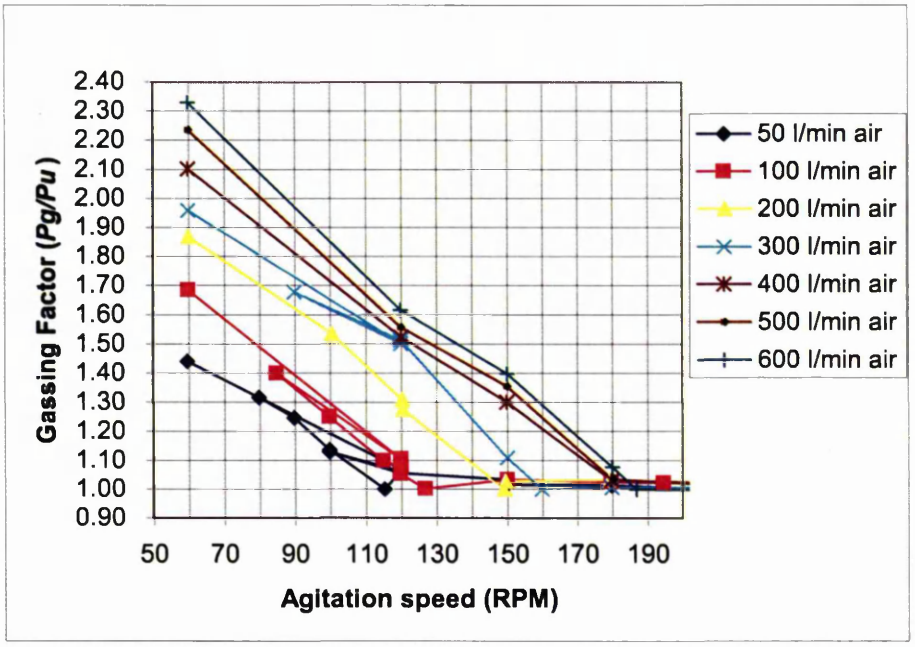

Figure 7-14: An expanded view of the "flooding- loading" transition for data from Figure 7-8 - Type B: Gassing factors versus agitation speed for the 0.248 m diameter parabolic 6HBDT agitator in the 0.61 m diameter vessel for air-water.

It is concluded, considering Table 7-5, that there is a strong correlation between the observed "flooding-loading" point and the transition in the gassed power data where there is a sharp rise above unity in the gassing factor even though these points are not always coincident. This maybe due to experimental error as the error bars on power measurement is larger when low powers are measured and the precise flooding point by observation is difficult to evaluate and is subject to operator interpretation. Also hysteresis (described by Saito *et al.*, (1992)) occurs and this blurs the transition. However, the equation proposed by Nienow *et al.* (1985), for disc turbines, consistently underestimates the flooding-loading point. In many cases the more serious underestimations using this equation resulted in Froude numbers below 0.045, considered by

Smith and Smit (1988) as the minimum for the retention of stable cavities and below which it is suggested that loading does not occur. However, eliminating predictions below Froude of 0.045, a clear trend of underestimation of the "flooding-loading" point emerges, using the disc turbine equation (7.11) when compared to experimental data for the hollow blade agitators.

Clearly then, in the loaded and dispersed state they produce a much flatter power versus gassing relationship than the Rushton turbine. Also because of their low power they exceed the minimum Froude number required to produce dispersion at a lower power

In Table 7-2, for D = 0.4T Rushton turbines the equality of gas buoyancy power and agitator power at the "flooding-loading" transition was apparent. It is pointed out in the discussion that agitator pumping-rates also plays an important role in the dispersion role and that large agitators are more energy efficient at dispersion than smaller agitators of the same type. However, it is interesting to compare the specific gas buoyancy power with the specific shaft power at the "flooding-loading" transition for all the hollow blade agitators tested here and this is done in Figure 7-15.

Note that for very low gas rates (very low gas buoyancy power) it may be necessary for the shaft power to be considerably greater than the gas power in order to overcome gravitational forces (minimum Froude number for dispersion). However, for the most part, as one might reasonably expect, there is a strong correlation between the shaft power and the gas buoyancy power. Generally the amount of specific agitator power (ε_T) to just disperse the gas is slightly less than the specific gas buoyancy power (ε_Q). For the data plotted in Figure 7-15 a regression analysis of the transition gives,

$$\varepsilon_{T(F-L)} = 0.82\varepsilon_{Q(F-L)} \qquad (7.13)$$

with a regression coefficient, $R^2 = 0.856$.

The low value of the regression coefficient reflects the reality of a fairly poor fit, which might be expected since the D/T ratios vary between 0.4 and 0.52

between the four agitators tested and it is known the pumping rate depends upon D/T. However, there is more to it than this, since the type D with a D/T of 0.45 appears to perform worse than the type B with a D/T of 0.4. The main difference between these two blade types is the degree of streamlining, reflected in the ungassed power numbers (see Table 7-4). However, the differences are small, considering the errors in the estimations, and an assumption that in all these cases that the gas and agitator powers are equal at the F-L point (above a Froude number of 0.05) would not be far from reality.

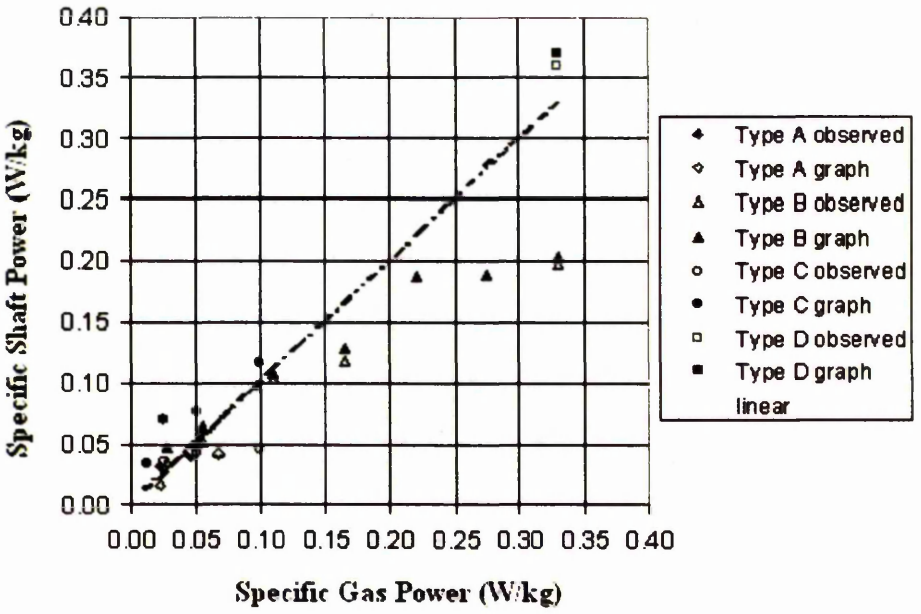

Figure 7-15: Comparison of the specific gas buoyancy power with the specific shaft power at the "flooding-loading" transition for the various hollow blade agitators described in Table 7-4. The dotted line represents equal gas and shaft power at the transition. Data for both graphically and visually determined transitions are included.

The behaviour of the hollow blade turbines, at the D/T ratios tested here, is similar to that found by Warmoeskerken and Smith (1985). That is an approximate equality of gas and agitator specific power at the F-L transition. This suggests that the Rushton and HBTs of like diameters require a similar amount of power to overcome flooding. It was earlier shown that equal diameter RT and 6SRGT agitators compared at equal D and ε_T had very similar

pumping rates (see Chapter 2, section 2.2.4 Agitator Pumping Rates). This may be taken as confirmation that at a given scale, equal pumping rates are required to disperse a given amount of gas. Consequently when the agitators are compared on a gassed power basis and similar diameters, no real evidence was found to support the literature claims [for example Saito *et al.* (1992)] that the hollow blade agitators will handle a lot more gas than a Rushton turbine before unloading (flooding).

How do the Saito *et al.* (1992) and the Gezork *et al* (2000) RT and 6SRT comparisons fit with the above conclusion?

The Saito *et al.* (1992) data are quite difficult to compare because the plot is Fl versus Fr and the curves for the RT and the 6SRGT have different slopes (Figure 7-7). Their agitators were of a diameter 0.2 m in a 0.61 m diameter vessel. The highest Fr for the *Saito et al.* (1992) 6SRGT experimental data using the upper curve A (of their Figure 9) is around 0.28, which is equivalent to $N =$ 3.67 and a specific energy input of 0.15 W/kg. The corresponding flow number is 0.1. The back calculation of the gas rate gives a superficial gas velocity of 0.01 m/s and a gas power input of 0.1 W/kg. This cannot be compared directly with a disc turbine, because the power numbers and gassing factors are different. However when the equation of the line given on the graph is used, then for the same size disc turbine with a gassed power number of 3 (assumption made earlier) a Froude number of 0.21 would give an N of 3.2 and a specific power input of 0.18 W/kg. A back calculation using the equation of the line results in a gas flow number of 0.119 that equates to a superficial gas velocity of 0.01 m/s and a specific gas power input of 0.1 W/g. Thus, although claimed to handle more gas than a conventional Rushton turbine, when compared at (confidently measurable) approximately equal gassed power they appear to be similar.

The Gezork data were presented as a plot of N_F versus v_s in their Figure 5. The data for both the RT and 6SRGT correspond closely to the line predicted for the RT from equation (7.11).

Multi-phase Hydrodynamics

- Taking a typical v_S of 0.06 m/s, their Figure 5 reveals that both the 6SRGT and the 6RT require an agitation speed of 177 rpm to overcome flooding (the data are on the line predicted using equation (7.11) and 177 rpm is the back-calculated value that agrees with the estimate from the axes).
- Ungassed power numbers (given) are 1.58 for the 6SRGT and 5.15 for the 6RT.
- At 177 rpm and a v_S of 0.06 m/s the gassing factors (estimated from Figures 10 and 11 of Gezork *et al.* (2000) are 6SRGT = 0.9 and 6RT = 0.4.
- Diameters (given) are 6SRGT = 0.161 m and for the 6RT = 0.15 m.
- Liquid density is approximately 1000 kg/m^3.

6SRGT Power = $1.58 \times 0.9 \times 1000 \times (177/60)^3 \times 0.161^5 = 3.95$ W

6RT Power= $5.15 \times 0.4 \times 1000 \times (177/60)^3 \times 0.15^5 = 4.02$ W

Hence the estimated power draws for the 2 agitators, at this flooding – loading condition, are very similar. Note also that the 6SRGT is a slightly bigger diameter than the 6RT and this means that it will have a bigger pumping rate than it would have at an equal diameter (equation (7.11)).

Therefore the literature data are not in conflict with the findings here.

The parabolic blade agitators generally have a lower Po than the 6SRGT, which perhaps explains why equation (7.11) does not fit these data. With the 6SRGT and 6RT, the ungassed power number times the gassing factor can be approximately equal for equal diameter agitators under some conditions explaining why equation (7.11) approximately fits both agitators. A fit based on equation (7.7) could undoubtedly be found to account for all the agitators tested here. It does not appear logical to do this as the theory on which it is based is shown by Nienow *et al.* (1985) to be flawed. These authors argue that

at a given scale, equal pumping rates to handle a given amount of gas appears to be consistent with their data.

7.3 Recommendations for the Design of Radial Turbines for Dispersion.

The important features for gas dispersion by an agitator based on this and earlier work suggest that a simple design procedure for avoiding flooding with radial agitators (including hollow blade agitators) would be:

Agitator "g" force = $\omega^2 D/2g \geq 1$ or $Fr_{(F\text{-}L)} \geq 0.05$. (7.14)

Since in order to disperse gas in horizontal plane gravity must be overcome.

$$\varepsilon_{T(F-L)} \geq \varepsilon_{Q(F-L)} \quad (7.15)$$

Specific agitator power equals or exceeds specific gas buoyancy power. This is important to ensure that the system is not gas dominated.

As this condition is also shown to be loaded, for turbines of diameters $\geq 0.4\ T$ in an $H = T$ geometry, this is all that needs to be ensured for any of the radial turbines considered here.

7.3.1 Consideration of H/T, D/T, Impeller Clearance and Multiple Impellers for Gas Dispersion

Nienow et al. (1985) show no effect of impeller clearance or liquid height on the F-L transition. Therefore for $H < T$, the assumption that $H = T$ in calculations based on equation (7.15) will suffice.

For $H > T$, equation (7.15) is still recommended if there is a single agitator to ensure the system is not gas dominated. For multiple agitators it is recommended that the calculations be based on the main gas dispersion agitator and an assumed $H = T$.

For smaller D/T agitators it is suggested that the agitation energy needs to be increased in accordance with a constant pumping case, in a ratio to the $D = 0.4T$ case.

7.4 Conclusions Regarding F-L with HBT agitators

The findings of this work is that at very low gassing rates the HBT are more energetically efficient at dispersing gas than a RT of the same diameter because it achieves the minimum Froude number needed to disperse gas at a lower power. Above the minimum Froude condition, when compared at equal diameters and gassed agitation powers, the HBT and RT require a similar gassed power to overcome flooding. This is believed to be because under these conditions the pumping rates are equal.

When comparisons of the hollow blade turbines with the Rushton turbines are made on an "ungassed" power basis, as is the usual literature case, then the HBT designs are more efficient because of their ability to disperse gas without significant loss of power.

7.5 Gassed Power

The reduction of power under gassed conditions is an important design consideration. Often 2-speed gearboxes are used to maximise the gassed power and as this can lead to problems if the power losses on gassing are less than predicted and will lead to motor overload trips. Also it is known that the specific power input effects mass, heat and momentum transfer rates. The loss of power on gassing is attributed to a number of parameters, which includes:

- Type and position of agitators.
- Types and positions of gas inputs.
- Amount of gas input/output.
- Amount of gas local to the agitators.
- Geometrical considerations such as D/T, H/T, agitator clearances, baffles and agitator separation.

Multi-phase Hydrodynamics

- Physical properties of the fluid that influences bubble size, gas recirculation, bubble break-up and coalescence rates, gas recirculation and gas hold-up and distribution.

This latter point is often neglected and often designs done on the basis of air-water literature correlations are wide of the mark when applied to "real" industrial fluids.

In this section the reduction in power on gassing is examined for a number of different agitators using air-water at different levels of agitation defined by the specific energy input. The effect of physical properties is then explored on a selection of the above by adding a surfactant to the water (polypropylene glycol [MW 2025] which inhibits coalescence and gives a very large reduction in bubble size with a correspondingly large increase in gas hold-up.

Agitators and vessel details tested for the air-water work are listed in Table 7-6. The gassing data for the 6 cases listed are plotted at two (ungassed) agitation levels approximating to 0.5 and 3 W/kg in Figure 7-16 and Figure 7-17 respectively.

Figure 7-18 is a plot of the gassing factor for a hollow blade turbine (6HBT) for air-water and an air-20ppm PPG solution.

Figure 7-19 is a plot of the gassing factor for two Rushton turbines (6RT) at two different scales, at constant ungassed power against the superficial gas velocity.

The types of agitator affect the gassing factor, the scale and the specific energy input levels as follows:

- Gassing factors depend on the gassing rate and decrease as the gas rate increases
- Gassing factors depend on the agitation rate and decrease with increasing agitation. This is because the gas recirculation increases with increasing agitation.

Multi-phase Hydrodynamics

- Gassing factors depend on agitator type. The 6RT agitators show a big drop of power on gassing. The gassing factors for the 6HBT type of agitators remain close to unity even under highly aerated conditions with up to 25% gas hold-up in air-water.

- The gassing factors depend on scale and are higher on the larger scale when compared at the same gas flow number and energy input level. This is very noticeable for the 6RT agitators that suffer the largest loss of power on gassing (see Figure 7-16), making scale-up of these agitators more problematic.

- The fluid system also affects the gassing factor, which is significantly lowered when surfactant is added (see Figure 7-18). However, using a parabolic hollow blade turbine the gassing factor does not drop below 0.7 even for an overall gas hold-up of 50% and a gas flow number of 0.3. On a similar scale the disc turbine-gassing factor dropped to 0.3 in air-water with an overall gas hold-up of 20%. For an air - acetic acid solution Gezork *et al* (2000) found a RT gassing factor to drop as low as 0.2.

- The data for the Rushton turbine gassing factors do not merge when re-plotted at constant ungassed power, against superficial gas velocity (see Figure 7-19). The difference between the curves is judged to be due to the decrease in alpha factor (ratio of recalculated to spared gas at the agitator) on scale-up) as described by van's Rite (1976).

Agitator Types	Vessel Diam. T (m)	Agitator Diam. D (m)	Agitator clearance c	Vessel bottom type	Height to diameter ratio H/T	Total ungassed Power number Po	Agitation speed N (RPM)	Data source MS Excel Spreadsheet (see attached CD)
parabolic 6HBT	0.286	0.145	T/3	flat	1	1.14	300	12KGFHU.xls
6RGT (HBDT)	0.286	0.149	T/4	dish	1	1.6	240	6RGTPOW1.xls
Parabolic 6HBDT	0.61	0.248	T/4	flat	1	1.28	240	KAGFPHU1.xls
ICI Gasfoil 6HBDT	1.79	0.9144	T/4	flat	0.94	2.2	70	GF-Power.xls
6RT Rushton	0.61	0.305	T/3	dish	1	4.88	121	Gassedpow2.xls
6RT + 6MFU	0.61	0.305 0.305	T/3 1.25T	dish	2	8.65	120	Gassedpow2.xls

Table 7-6: Agitation details for the air-water gassing factor comparisons

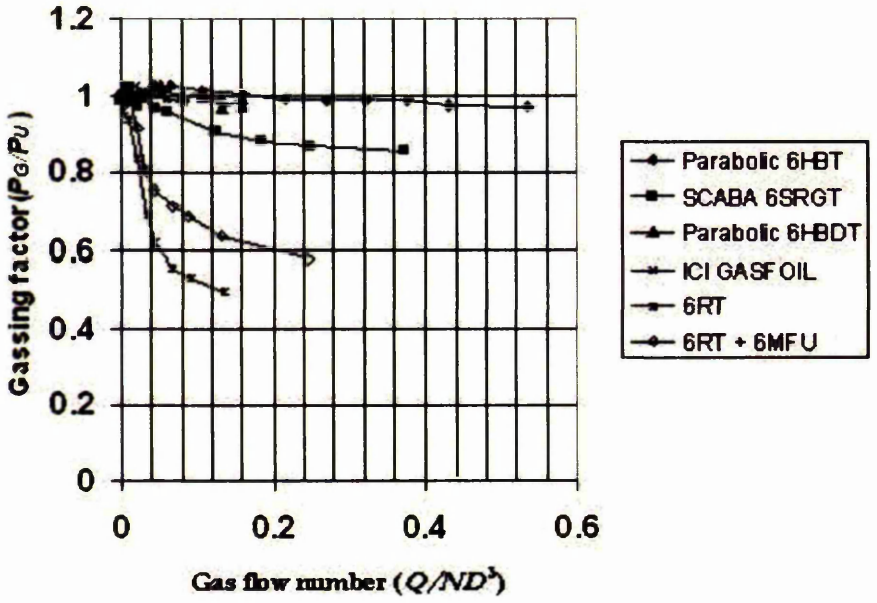

Figure 7-16: Gassing factors as a function of gas flow number for various agitator types and scales at an ungassed specific power input of approximately 0.5W/kg in air -water

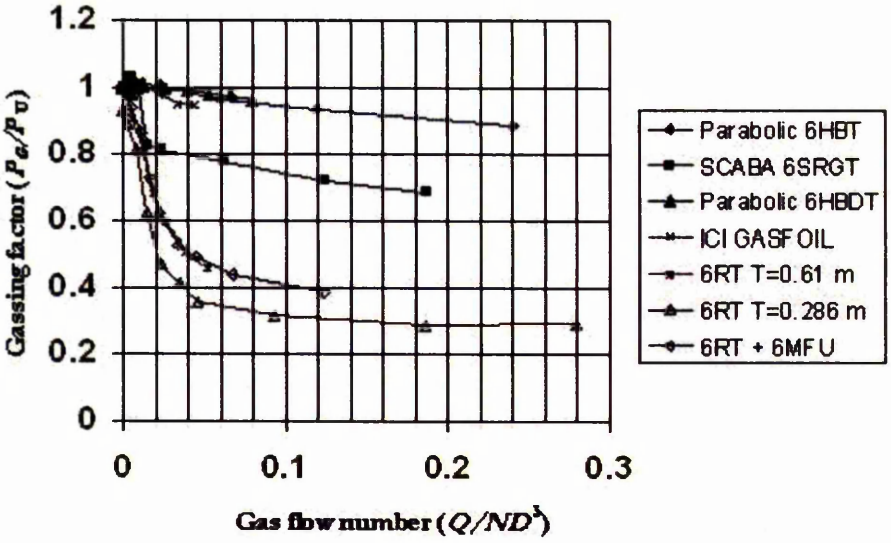

Figure 7-17: Gassing factors as a function of gas flow number for various agitator types and scales at an ungassed specific power input of approximately 3 W/kg in air –water.

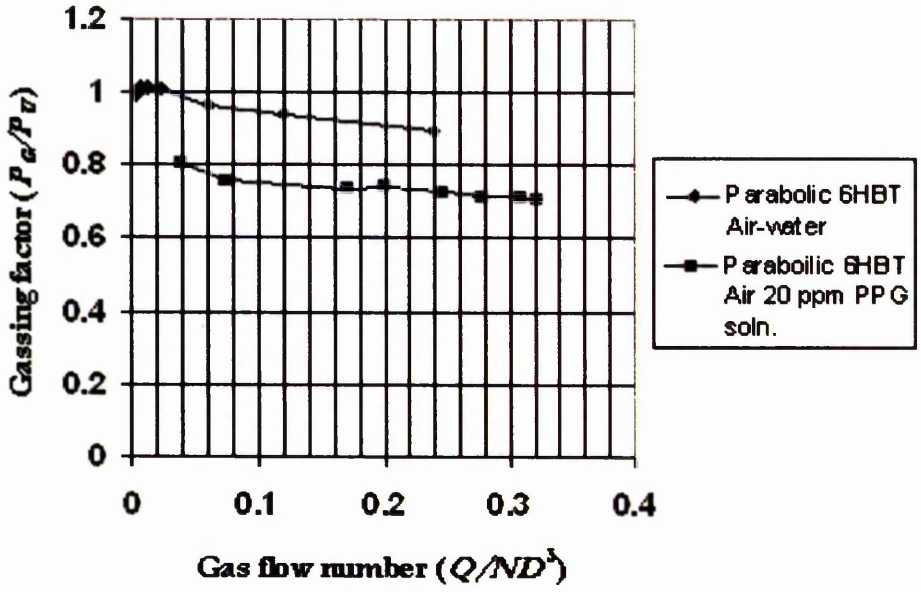

Figure 7-18: The effect of adding surfactant to the water on the gassing factor for the same hollow blade turbine (6HBT), at a specific energy input of approximately 3W/kg

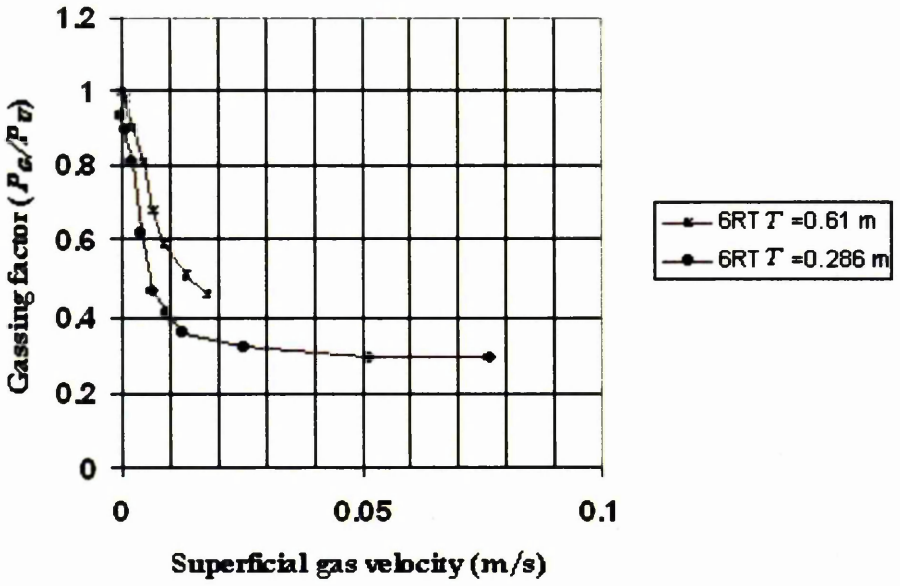

Figure 7-19: Gassed power data for Rushton turbines on two scales plotted against the superficial gas velocity, at an ungassed specific power input of approximately 3 W/kg.

7.6 Gas Hold-up

The gas-liquid hold-up is an important design parameter for gas-liquid contactors. Since the ullage is generally fixed, the gas hold-up determines the liquid volume and for steady-state operation the liquid residence time, both of which are important considerations for mass transfer and reaction engineering.

Providing the operating regime is known, simple performance criteria can be used to judge the effects of process changes such as agitation (types or speeds), gassing rates and operating pressure on the gas hold-up.

Knowledge of the operating regime is very important, because in Chapter 5 the gas hold-up behaviour was shown to follow different trends in the bubble regime and the homogeneous regime. If the bubble size and rise velocity of the bubbles pertaining to the "dense phase" (homogeneous regime) bubbles are

known then a simple performance criteria is that if the gas superficial velocity exceeds the rise velocity of the homogeneous bubble class then operation must be in the heterogeneous regime. Here, as was noted in Chapter 5, the effect of agitation and gas rates on the gas-liquid hold-up is small, since any extra gas goes into to large bubble diameter formation.

In Section 7.2 it became clear that in order to distribute the gas properly the agitation power should at least be equal to the potential power input of the gas. Thus if gas input power is large, it may be arguable whether a mechanical agitator is necessary or whether a bubble column design might be more appropriate.

Air-water bubbles in agitated vessels are generally between 1 mm to 6 mm in diameter in the bubble regime and these all rise at a velocity of around 0.25 m/s, as illustrated by the Hagerman and Morton, (1956) plot of terminal bubble rise velocities for air-water reproduced in Figure 2-43. Thus, under most normal operating conditions, operation is likely to be in the homogeneous regime for air-water.

In the following section therefore air-water is used as an example to show how the overall air-water hold-up can be simply correlated to represent the effects of gassing rates and agitation rates (in terms of specific energy input).

Similar correlations can be applied to other systems providing the operating envelope is fully understood or the correlations are not extrapolated beyond the experimental conditions.

Finally, the axial distribution of local gas hold-ups are compared for two different agitator combinations for an air – 20 pip PPG solution using measurements obtained from the local hold-up probe described in Chapter 3, section 3.2.4.

7.6.1 Overall Gas Hold-up

In this work gas hold-up is measured by level rise which is estimated from either time averaged calibrated video records or using a time averaged signal from an Enders and Hauser (UK) Ltd., DU13 ultrasonic level probe as described in Chapter 3, section 3.2.3. Only data pertaining to conditions above the loading point are considered. The data collection analysed in this work includes data from other sources as indicated in Table 7-7. These cover scales from 20 litres to 20 m^3, superficial gas velocities from 0.0017 to 0.127 m/s and specific power inputs from 0.1 to 6.7 W/kg.

Agitator types include Rushton turbines, hollow blade turbines (disc and arm-mounted types) and 4MFD's at bottom agitator clearances at $T/4$ and $T/3$.

Series	Agitator types	Vessel Diam. T (m)	Agitator Diam. D (m)	Agitator clearance c	Vessel bottom type	Height to diameter ratio H/T	Agitation Speed range N (RPM)	Data source MS Excel Spreadsheet (see attached CD)
1	6RT 4MFD 4MFD	2.1	0.762 0.915 0.915		dish	3	124 to162	TOTHUAW.WK4
2	6RT	1.79	0.149	T/4	flat	0.94	60 to 100	TOTHUAW.WK4
3	ICI Gasfoil 6HBDT	1.79	0.9144	T/4	flat	0.94	70-130	TOTHUAW.WK4
4	6RT	0.914	0.457	T/4	flat	1	100-220	Davies (1986)
5	6RT	0.61	0.305	T/4	flat	1	150-300	Davies (1986)
6	6RT	0.303	0.144	T/4	flat	1	200-503	Davies (1986)
7	6RT with various gas distributors	1.79	0.648	T/3	flat	0.94	58-160	TOTHUAW.WK4
8	Parabolic 6HBT	0.286	0.145	T/3	flat	1	180-630	12KGFHU.xls
9	Parabolic 6HBDT	0.61	0.248	T/4	flat	1	100-482	KAGFPHU1.xls

Table 7-7: Details of agitators and vessel geometries included in the overall gas hold-up correlation

Multi-phase Hydrodynamics

Gas distribution range from a central pipe, off centre-pipe, multiple sparge pipes at the impeller centre-line, to a sparge ring below the bottom agitator. Tank aspect ratio (H/T) is from 0.94 to 3.0. Data sources are published work or analysed from data obtained in this study, recorded in spreadsheet form in Lotus 123 (.wk4) or MS excel format (see attachment CD).

Smith *et.al.* (1977), Davies (1986) and Middleton, Chapter 15, in Harnby *et al.* (1997) among other workers, indicate that air-water gas hold-up can be simply correlated with specific power input and superficial gas velocity in the form;

$$\varepsilon_G = a\varepsilon_T^b v_S^c \qquad (7.16)$$

where ε_G is the gas hold-up as defined by equation (3.3), ε_T is the total specific energy input from the shaft and buoyancy power in W/kg and a, b and c are the multiplicity factor and the exponents for ε_T and v_S respectively.

The collection of 388 data sets was subjected to a multi-linear least squares regression to determine the best fit for the constants. The data was made linear by taking logs. The results are tabulated as Table 7-8. This yields the expression,

$$\varepsilon_G = 76.6\varepsilon_T^{0.39} v_S^{0.56} \ (\%) \qquad (7.17)$$

with a correlation coefficient of 0.971.

The standard deviation on the proportionality constant for the data is 9.6 or 12.5%.

This is similar to the correlation proposed by Middleton, Chapter 15, in Harnby *et al.* (1997) for a much smaller data set.

Constant		76.64
Std Err of Y Est		0.1288
R Squared		0.9708
No. of Observations		388
Degrees of Freedom		385
X Coefficient(s)	0.3882	0.5563
Std Err of Coef.	0.006499	0.008272

Table 7-8: Correlation of air-water gas hold-up data

These data are plotted against eq. (7.17) in Figure 7-20. Equation (7.17) fits the data well, although there are some deviations at the highest values, possibly due to the onset of heterogeneous flow.

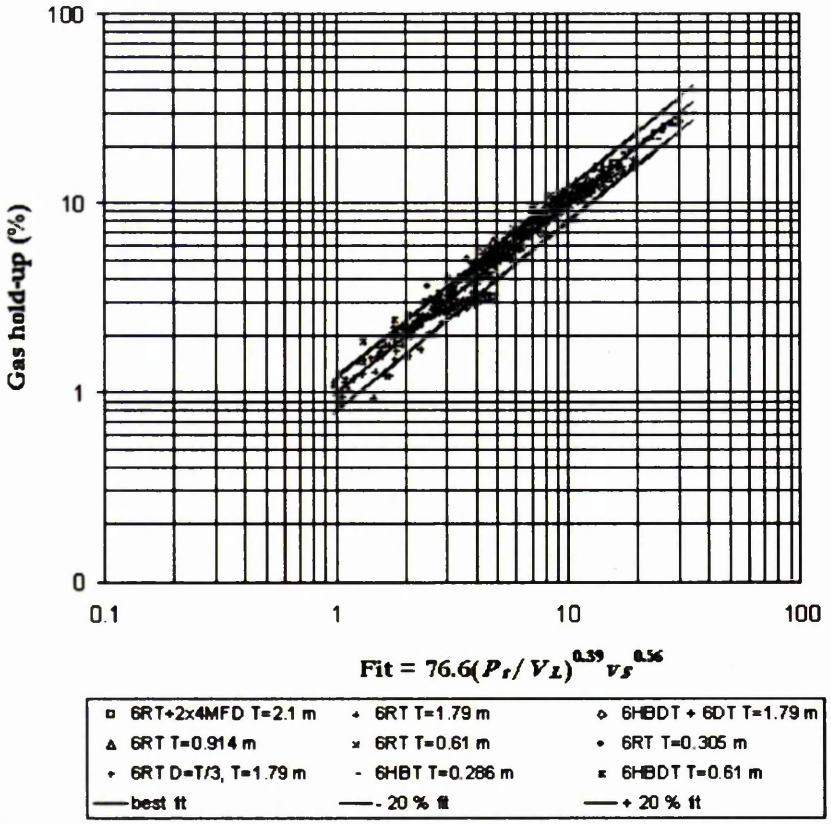

Figure 7-20: Illustrating the fit of the air-water hold-up data for various agitators and vessel geometries to eq. (7.13).

7.6.2 Local Gas Hold-up

Knowledge of the distribution of gas hold-up is important for modelling purposes. In this work the axial distribution of gas hold-up for a bubble column is compared with different two multi-impellor systems using the local hold-up probe described in Chapter 3, section 3.2.4. The local hold-up probe is supported from two parallel rails above the top of the vessel by a vertical 0.5-inch diameter stainless steel tube that carries the conductivity cables. The

vertical tube is marked in centimetre divisions to enable the probe to be located in known vertical positions. The probe was connected to a WPA CM35 conductivity meter and the output was collected as a digital data file in LABVIEW. The system used in these tests was an aerated 20-ppm PPG solution, which produces small bubbles, high gas phase fractions and which tends to foam. The geometries compared are listed in Table 7-9

The results are compared graphically in Figure 7-21 to Figure 7-23 respectively.

Series	Agitator Types	Vessel Diam. T (m)	Agitator Diam. D (m)	Agitator clearance c (m)	Vessel bottom type	Height to diameter ratio H/T	Agitation Speed range N (RPM)	Data source MS Excel Spreadsheet (see attached CD)
1	none	0.61	none		dish	2.5	-	bubcollhu.xls
2	3 x A345	0.61	0.295	0.25 0.51 0.76	dish	1.65	275	A345lhu.xls
3	6HBT 6MFU	0.61	0.305 0.305	0.172 0.67	dish	1.7	300	GF6MFUlhu.wk4

Table 7-9: Geometries compared for the axial hold-up scans

These graphs illustrate some interesting features:

- The bubble column data (Figure 7-21) have the highest mean gas hold-up around 60% (due in part to the foamy nature of the medium), and the local axial profile shows the gas hold-up fraction to increase linearly up the column.
- The profile for the three up-pumping LIGHTNIN A345 agitators (Figure 7-22) is much flatter especially in the region encompassed by the agitators. There is a peak above the top agitator (recirculation), above which the gas hold-up follows a bubble column type profile. The lower overall hold-up is attributable in part to the operating temperature that was 18°C (this was deliberate to match the model overall hold-up to a known plant hold-up as part of a modelling study), compared with 13°C for the bubble column work (again the latter was

part of a commissioned modelling study). As previously mentioned the gas hold-up in PPG solutions is very temperature sensitive (see Figure 4-3)

- The gas-hold-up profile for the hollow blade turbine below a 6MFU (Figure 7-23) is also flat in the agitated region, but there are two distinct hold-up peaks above the tips of both agitators, again due to recirculation. These illustrate a compartmentalization of the flow, which is not seen with the triple up-pumping impellers where the gas and liquid flows are acting in unison to produce a single circulation loop. Above the top impeller the gas-hold-up increases steeply showing bubble column type behaviour. The gas hold-up peaks above the agitators indicate strong recirculation patterns where bubble coalescence rates are likely to be high.

From these experiments it is concluded that mechanical agitation strongly influences the gas distribution and hence gas break-up and coalescence rates. For mass transfer purposes these facts have significance beyond the gas hold-up fraction that may be as high as or higher in a bubble column than a mechanically agitated vessel at the same gassing rates. Since gas-liquid mass transfer is seen to increase with increasing agitation, the interfacial area (linked to gas hold-up) is not the all-controlling factor; surface renewal rates (bubble break-up and coalescence) also play a big role.

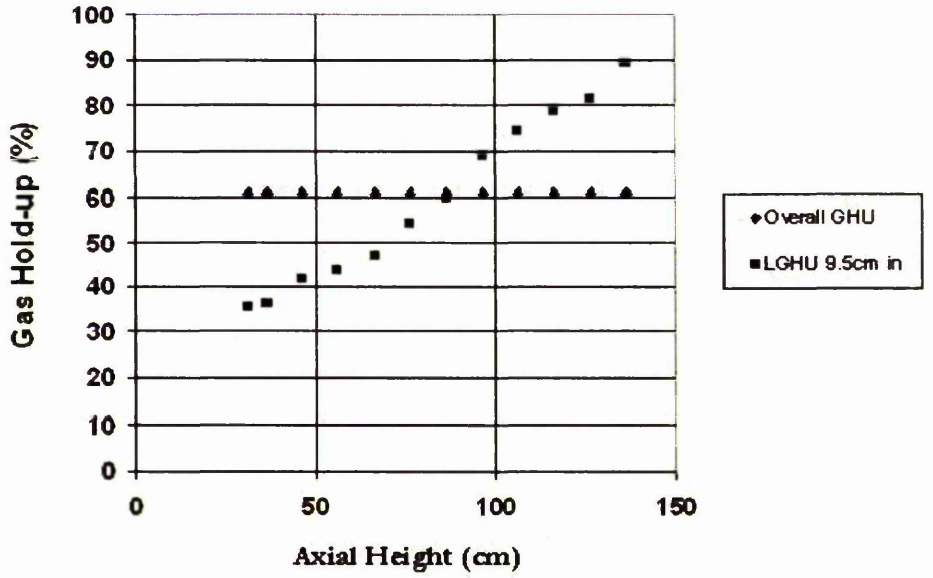

Figure 7-21: Comparison of overall gas hold-up with local axial values for a 0.61 m diameter bubble column. Local hold-up probe is 9.5 cm from the vessel wall. Fluids are air-20 ppm PPG. The superficial gas velocity is 0.06 m/s

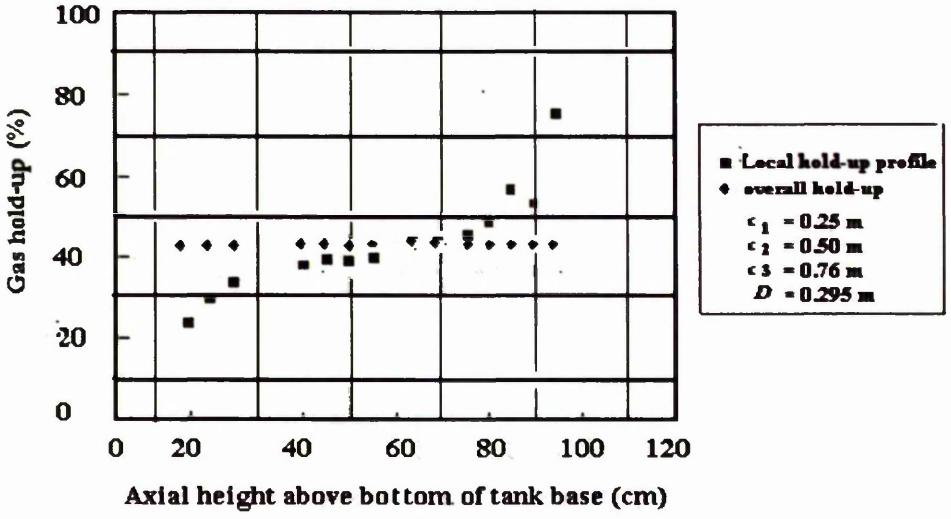

Figure 7-22: Comparison of overall gas hold-up with local axial values in the 0.61 m diameter vessel agitated with three LIGHTNIN A345 up-pumping agitators at 274 RPM and a superficial gas velocity of 0.05 m/s in aerated 20 ppm PPG solution. Axial profile is taken 7 cm from the vessel wall, midway between the baffles.

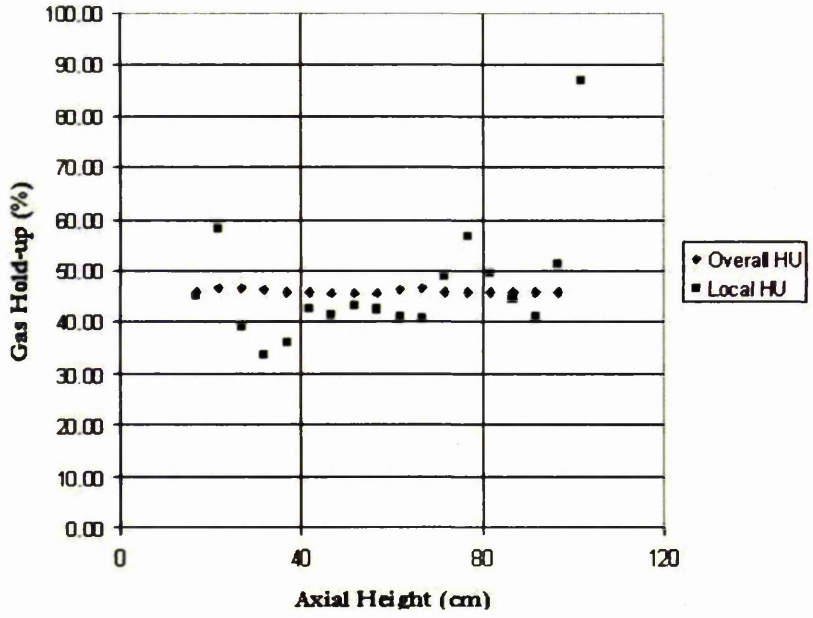

Figure 7-23: Comparison of overall gas hold-up with local axial values in the 0.61 m diameter vessel agitated with a 6HBT below a 6MFU agitator at 300 RPM and a v_S of 0.07 m/s in aerated 20 ppm PPG solution. Axial profile is taken 7 cm from the vessel wall, midway between the baffles.

7.6.3 Foam

Foaming is covered in greater detail in Chapter 8.

Foam is defined as an "agglomeration of gas bubbles separated from each other by thin liquid films" (Bikerman, 1953). Foaming occurs when gas bubbles separated by a thin lamella of liquid do not coalesce and therefore accumulate at the surface of the liquid.

Foam is (an often) undesirable consequence of operation in "real" fluids since pure liquids do not foam. In order for foaming to occur, gas must be introduced into liquid containing surface-active agents (surfactants), which lower the surface tension. The gas may be from surface entrainment, boiling, chemical reaction or physical sparging. Surfactants reduce bubbles size and bubble coalescence rate (Deshpande and Barigou, (1999)). High surface viscosity [defined by Bikerman (1953) as the viscosity of thin liquid layers

adjacent to gas phase] also favours foaming since it delays the drainage of the liquid film between bubbles and thus prevents the foam from collapsing.

The physical problems caused by foam include (Vardar-Sukan, (1998) and Ditl *et al.* (1997))

- Lower mass and heat transfer rates
- Reduction of liquid volume due to increased gas hold-up
- Reduction in apparent viscosity
- Decreased circulation rate leading to longer mixing times
- Errors in monitoring and control
- Reduction in aeration (necessary to prevent foam-out)
- Blockages of gas filters.
- Carry-over of product in the gas lines
- Pump cavitation which in severe cases leads to loss of pumping
- Loss of solid suspension

The two main methods of foam control are:

- Chemical using antifoam agents.
- Mechanical foam breakers – such as breaker bars and specially designed, high shear agitators operated at the liquid surface.

In Chapter 8 spinning cones are evaluated for foam control.

The results of the experiments carried out for this thesis lead to the conclusion that conventional agitators can control foam providing they are sited close to the dispersion surface. A separation of 0.6-to1.0 agitator diameters (0.6 to 1D) is optimum for foam control. Above a separation of 1.2D the agitator influence is too remote to break-up the foam and in foamy solutions, the foam level builds-up. Optimally positioned high solidity up-pumping agitators appear to be particularly suitable for foam control as they directly influence the flow at

the liquid surface, re-entraining the foam layer into the agitator region where coalesce can occur.

7.7 Gas-liquid Mass Transfer

Mechanically agitated vessels and bubble columns are frequently used for gas-liquid mass transfer operations. In many cases the rate of mass transfer between the gas and liquid phases is the rate-limiting step. Muller (1993) quotes the example of an aerobic fermentation where parameters such as micro biological growth rate, production rate, product composition and maximum available biomass are all strongly dependent on the oxygen transfer rate. In this thesis the overall gas mass transfer factor k_La, that is the product of the mass transfer coefficient (k_l) and the interfacial area of the gas per unit volume of liquid (a), is used.

7.7.1 Experimental Gas-liquid Mass Transfer Measurements

The peroxide technique employing Catalase is used to measure k_La, as described in Chapter 3, section 3.3.7. This technique is used to compare overall mass transfer factors for three different agitation systems in the same vessel operated at the same level in an aerated solution of 20 ppm PPG. The geometries chosen are listed in Table 7-10. Note that the gas sparger arrangement is not optimised for this work. In other work (not detailed here) the measured mass transfer coefficient improved when the gas sparger arrangement was optimised.

Two dissolved oxygen probes were used to measure the liquid phase oxygen concentration. Both were introduced through the analysis block (see Chapter 3), one opposite the bottom agitator; the other was at the centreline of the top agitator. Note that the measured liquid phase concentrations are different for

the two probes leading to different $k_L a$ values being measured (see results). This is not an unexpected result, as the overall system cannot be considered well mixed with respect to mass transfer as the mixing and mass transfer time constants are of the same order (see discussion in Chapter 2, section 2.8.3.3.3 and Figure 2-54). However, it does mean that the results must be considered with a degree of caution, since the analysis assumes a well-mixed liquid phase. The calculated mass transfer is consistently higher for the probe in the top zone. This is consistent with the higher gas hold-up in this region (see Figure 7-22). In the graphical representation of the results (Figure 7-24), the average of the 2-probe results are shown. Gas-liquid mass transfer data for aerated PPG solution in the small 0.286 m diameter vessel operated at an $H = T$ aspect ratio (well mixed liquid phase) has been found to fit (Cooke *et al* (1991)):

$$k_L a = \text{factor x } \varepsilon_T^{0.6} v_S^{02} \qquad (7.18)$$

where the multiplicity factor for 25 ppm PPG solution was found to be 0.153. In spite of the increase in surface area, the presence of surfactants at the gas-liquid interface can hinder mass transfer giving a rigid interface and an extra barrier (Van de Donk *et al.* (1979), although for some systems the increase in "a" produces an overall improvement in $k_L a$ as reported for example by Cooke *et al.* (1988) and Muller and Davidson (1993).

Series	Agitator types	Vessel Diam. T (m)	Agitator Diam. D (m)	Agitator clearance c (m)	Superficial Gas velocity (m/s)	Sparge Pipes	Dispersion Height (m)
1	6HBT 6MFU	0.61	0.311 0.310	0.26 0.83	0.07	2 side	1.35
2	3 x A345 + 30° cone	0.61	0.344 0.344 0.344 0.305	0.203 0.623 1.043 1.35 (top)	0.13	2 under	1.35
3	3 x A345 no cone	0.61	0.344 0.344 0.344	0.203 0.623 1.043	0.06	2 under	1.35
4	3 x A345 no cone	0.61	0.344 0.344 0.344	0.203 0.623 1.043	0.19	2 under	1.35

Table 7-10: Geometries used in gas-liquid mass transfer work.

For this work in a solution of 20 ppm PPG, the hollow blade turbine below a 6MFU agitator combination fitted equation (7.18) with a multiplicity factor of 0.188. Therefore all the mass transfer results were plotted against this result for comparative purposes in Figure 7-24. From an inspection of this figure there is nothing to suggest that there is any real difference in the mass transfer performance of the three options tested.

There is also no evidence to suggest that the spinning cone fitted above the three up-pumping LIGHTNIN A345 impellors enhanced (or otherwise) the gas-liquid mass transfer performance.

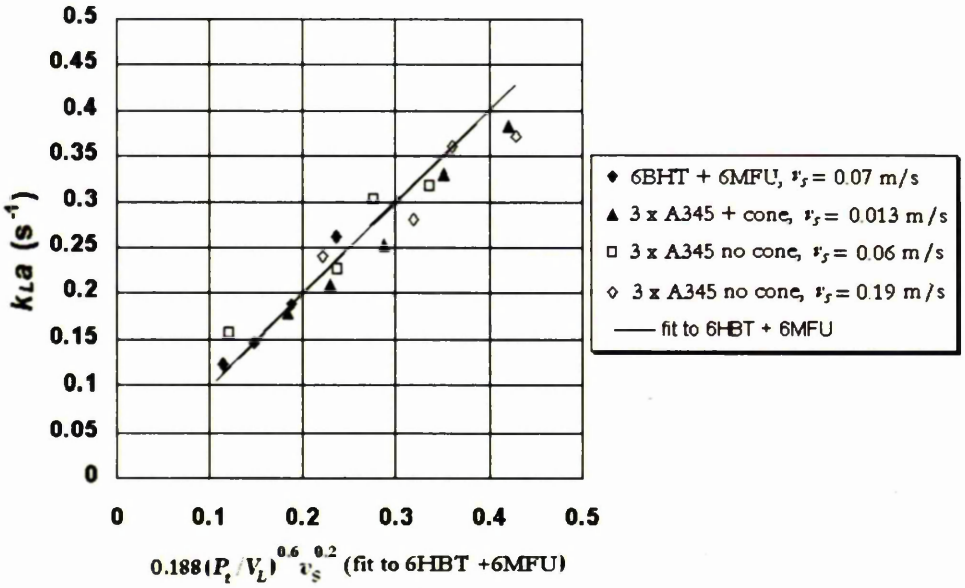

Figure 7-24: Comparison of mean k_La values in the 0.61 m diameter vessel, in aerated 20 ppm PPG solution, for three different agitator configuration at various agitation and gas rates.

Series	Stirrer rate (RPM)	Superficial gas velocity v_S (mid pt) (m/s)	liquid volume [m³]	P/V_L Shaft W/kg	P/V_L Gas W/kg	P/V_L Total W/kg	Plug flow k_La [1/s]
1	150	0.068	0.186	0.480	0.667	1.147	0.108
1	150	0.068	0.186	0.480	0.667	1.147	0.138
1	200	0.068	0.186	1.080	0.667	1.747	0.133
1	200	0.068	0.186	1.080	0.667	1.747	0.161
1	250	0.068	0.186	1.980	0.667	2.647	0.178
1	250	0.068	0.186	1.980	0.667	2.647	0.199
1	300	0.068	0.186	3.200	0.667	3.867	0.236
1	300	0.068	0.186	3.200	0.667	3.867	0.291
2	180	0.133	0.187	0.725	1.303	2.028	0.172
2	180	0.133	0.187	0.725	1.303	2.028	0.186
2	240	0.133	0.185	1.622	1.303	2.926	0.198
2	240	0.133	0.185	1.622	1.303	2.926	0.222
2	300	0.133	0.182	2.984	1.304	4.288	0.241
2	300	0.133	0.182	2.984	1.304	4.288	0.268
2	360	0.133	0.180	4.654	1.304	5.958	0.319
2	360	0.133	0.180	4.654	1.304	5.958	0.344
2	420	0.133	0.179	6.779	1.305	8.083	0.370
2	420	0.133	0.179	6.779	1.305	8.083	0.396
3	160	0.064	0.187	0.666	0.624	1.291	0.120
3	160	0.064	0.187	0.666	0.624	1.291	0.194
4	160	0.191	0.187	0.584	1.876	2.460	0.210
4	160	0.191	0.187	0.584	1.876	2.460	0.273
3	300	0.077	0.187	2.974	0.754	3.728	0.200
3	300	0.077	0.187	2.974	0.754	3.728	0.253
4	300	0.191	0.186	2.647	1.877	4.524	0.244
4	300	0.191	0.186	2.647	1.877	4.524	0.318
3	360	0.064	0.186	4.477	0.625	5.102	0.252
3	360	0.064	0.186	4.477	0.625	5.102	0.354
4	360	0.177	0.186	3.935	1.733	5.667	0.302
4	360	0.177	0.186	3.935	1.733	5.667	0.423
3	420	0.064	0.186	6.482	0.625	7.107	0.267
3	420	0.064	0.186	6.482	0.625	7.107	0.370
4	420	0.184	0.185	5.685	1.802	7.487	0.310
4	420	0.184	0.185	5.685	1.802	7.487	0.440

Table 7-11: Mass transfer results. For key to series see Table 7-9

7.7.2 Performance Equations for Mass Transfer Operations.

It was shown in Chapter 2 that for liquid film controlled processes the molar rate of mass transfer (r) is given by (eq. 2.98),

$$r = k_L a \Delta C V_L$$

where k_L is the overall liquid film mass transfer coefficient (m/s), "a" is the specific gas-liquid interfacial area (m^2/m^3), ΔC is the concentration driving force (mol/m^3) and V_L is the liquid volume (m^3).

Taking, for example, an air oxidation system that behaves as air-water, it is expected that the overall mass transfer factor will follow the relationship (Cooke *et al.* (1991)),

$$k_L a = 0.2 \varepsilon_T^{0.7} v_S^{0.3} \qquad (7.19)$$

Hence, if the total specific power input were doubled, the overall mass transfer factor would be expected to increase by a factor of $2^{0.7} = 1.62$. In many instances this is as far as consideration of the mass transfer equation goes and it is sometimes claimed (erroneously) that by such a change, the mass transfer rate can be increased by a factor of 1.62. However, examination of equation (2.98) clearly shows it is more complicated than that.

The effect of this change on the driving force (ΔC) depends upon the control strategy, the oxidation kinetics and the gas phase mixing. Assuming that the liquid phase oxygen level C_L is controlled at a set value, then an appropriate model for the gas-phase mixing is required. A fully back-mixed gas phase model can never be justified except for operation at very high specific power inputs on a small scale (Davies *et al.* (1985)). The gas phase can however be reasonably modelled (for example) as a plug flow gas with recycle. In this model, the presence of inerts (with air supplying the oxygen) means that the (mixed) inlet gas will depend on the recycle ratio (α); that is the volumetric

ratio of recirculated to freshly supplied gas (van't Riet (1976), Nienow *et al.* (1979 and Middleton (1997)).

Assuming the oxygen concentration of the recirculated gas equals the exit concentration and fresh gas and recirculated gases are fully mixed at the dispersion agitator, then - to the first approximation - an oxygen mass balance over the impeller gives,

In = out

$$Q_F C_{GI} K_{IMP} + Q_R C_{GO} K_{IMP} = (Q_F + Q_R) C_{G(IMP)} K_{IMP} \qquad (7.20)$$

where Q is the volumetric flow rate of gas m^3/second at the impeller pressure, C_G is the mol fraction of oxygen, and K_{IMP} is a factor, determined using the ideal gas law, to convert mol fractions to mol/m^3:

$$K_{IMP} = \frac{P_{IMP}}{RT} \qquad (7.21)$$

with P_{IMP} equal to the pressure at the impeller in *Pa*, this is the sum of the head at the impeller plus atmospheric pressure plus the over-pressure.

R is the gas constant = 8.314 $J.mol^{-1}.K^{-1}$.

T is the absolute temperature in °*K*.

The subscripts F refers to fresh gas, R to recycle gas, I, O and IMP to inlet, outlet and impeller out-flow conditions.

As $\alpha = Q_R/Q_F$ it follows that the impeller oxygen concentration C_{Gimp} is,

$$C_{Gimp} = \frac{\alpha C_{GO} + C_{GI}}{1 + \alpha} \qquad (7.22)$$

For air-water, the alpha factors can be estimated from Middleton (1997), (see p.345 of that reference). This indicates that the alpha factor approximately trebles when the specific agitator power is doubled. For air-water α unlikely to rise above 3, hence in most cases the effect on the oxygen driving force is likely to be small unless the outlet oxygen concentration is very low or a high liquid-

phase concentration is desired. . For example if the inlet concentration is 0.21 mol fraction O_2 and the outlet is 0.05 mol fraction O_2, the alpha factor is 0.36 (for $T.P/V = 1$ from Middleton 1997) and the estimated mol fraction of the mixed gas at the impeller is 0.168.

If the power input is doubled, alpha increases to 1.1 and the impeller mixed gas oxygen mol fraction falls to 0.126, which represents a considerable decrease in oxygen driving force. These values would need to be substituted into a log mean driving force equation, with an appropriate liquid phase concentration to determine how just how significant such a change to the driving force would be.

Thus, it is plain that increasing agitator power will increase gas phase mixing which will in turn decrease the concentration driving force, when gaseous inerts are present.

The effect on the liquid volume can also be estimated by means of an appropriate hold-up equation. For example using eq. (7.17) would predict that doubling the total specific power input would result in an increase the gas hold-up fraction by a factor of $2^{0.39} = 1.31$. For a constant dispersion volume, the resultant affect on the liquid volume depends on the start value of the gas hold-up. For example if the starting gas phase hold-up was 10% then the liquid volume for this example would reduce by a factor of (1-0.131)/(1-0.1) = 0.965. Hence the combined effect of mass transfer factor and liquid volume change on the overall transfer rate for the above example would be a factor of 1.62 x 0.965 = 1.56. As specific energy input and liquid volume are linked parameters these performance equations need to be solved iteratively and base-line conditions need to be defined to allow a full mass balance to be effected. However, when base-line conditions are known it is possible to use experimentally determined lumped parameter equations for k_La, gas hold-up and alpha factors to determine the likely effect of process changes on the overall mass transfer rate using simple iterative spreadsheet programs.

7.8 Solid Suspension

In this work the suspension of particles heavier than the liquid is considered.

Much has already been published on this subject as described in Chapter 2, section 2.7. When considering the suspension of solids the Zwietering "just suspension" (N_{JS}) criteria is usually used, Zwietering, (1958), Nienow, (1968) Chapman *et al.* (1983), Bujalski, (1986), Frijlink *et al.* (1990), Mak *et al.* (1997).

Zwietering defined the just suspension criterion, from observations through a transparent base, as the point when no particles remain stationary on the bottom of the vessel for longer than one to two seconds. This is defined as off-bottom suspension and is not necessarily a homogeneous suspension. The homogeneity of the suspension at N_{JS} depends upon particle size (settling velocity) and whether the vessel agitation system is designed to ensure primary circulation to all parts of the vessel. For a high aspect ratio vessel with a single agitator set close to the bottom this may well not be the case even for small particles with settling velocities around 1 to 2 cm/second.

From dimensional analysis Zwietering (1958) proposed the following empirical correlation to fit his extensive experimental data: Eq. (2.76),

$$N_{JS} = \frac{s d_p^{0.2} X^{0.13} \mu_L^{0.1} [g(\rho_S - \rho_L)]^{0.45}}{\rho_L^{0.55} D^{0.85}}$$

where s is an agitator dependent shape factor, which also depends on the geometric ratios c/T and D/T, d_p is the mean particle diameter and X is the weight of solids per weight of liquid expressed as a percentage.

A great deal of work on solid suspension has been done since Zwietering. However, the general consensus from the references quoted at the beginning of this section is that Zwietering got it just about right and the Zwietering equation is widely used with appropriate "s" factors to design for solid suspension.

Multi-phase Hydrodynamics

Although much is already published in this area, the published data for hollow blade agitators is sparse; therefore an appropriate contribution in this work is to study the characteristics of the hollow blade agitators for solid suspension duties and to compare these with other agitators (see Table 7-12).

7.8.1 Experimental Measurements of N_{JS} for Various Agitators

These were determined by observation of the base as the point when no particles were stationary on the bottom for more than 1 to 2 seconds (The Zwietering (1958) just suspension criteria).

For the work on the 0.286 m vessel these measurements were confirmed by video and camera. This technique involved top lighting the vessel and recording the suspension viewed from the side and the base (viewed through an angled mirror see Figure 7-26 and Figure 7-27). Figure 7-25 contains views of the agitators used in the investigation.

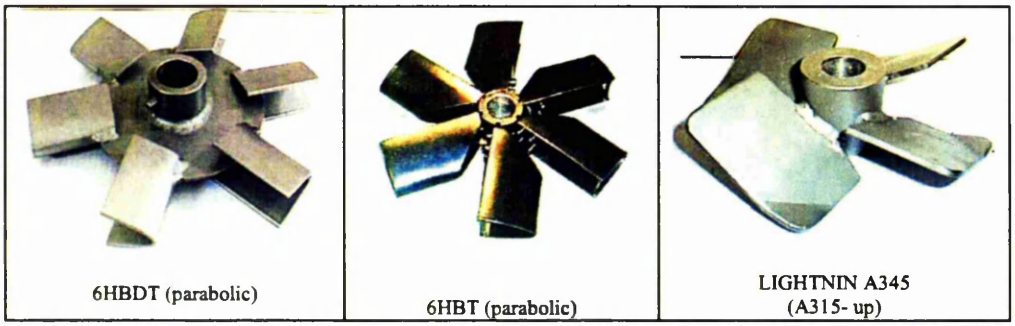

Figure 7-25: Agitators tested *for* solid suspension on the 0.286 m vessel

Table 7-12 lists the conditions used and the experimentally determined Zwietering factors on both vessels.

The agitators tested were all nominally $D = T/2$. Zwietering's factor is dependent on D/T and large agitators are known to be more energetically efficient for solid suspension (see for example Chapman (1981)). Also, it was found in Chapter 2, section 2.4.4.1 that larger D/T agitators are more

energetically efficient for mixing and pumping (Chapter 2, section 2.2.5.7) therefore there is a need to consider the D/T ratio.. In Chapter 2, section 2.7.1 it was concluded that there is a strong body of evidence that scale-up for solid suspension should be at constant specific energy input W/kg (for example, Mak *et al.* (1997)) whereas the Zwietering equation implies that for constant physical properties scales N_{JS} scales with $sD^{0.85}$.

Vessel diameter *T* (m)	0.286			0.61		
Geometry key	1	2	3	4	5	6
Operating *H* = *T*	0.286	0.286	0.286	0.61	0.61	0.61
Levels (m) *H* = 1.34*T*	0.384	0.384	0.384			
Base type	Dish	Dish	dish	dish	dish	Dish
Agitator type	6HBDT	6HBT	A345	6HBT	4MFD (45°)	A315
Agitator Diameter (m)	0.145	0.15	0.143	0.344	0.322	0.343
Agitator Clearances	T/4	T/4	T/4	T/4	T/4	T/4
Agitator Power No Po	1.42	1.40	0.71	1.14	1.22	0.75
%Mass fraction solids *X* (*H* = *T*) (Wt solids/wt water)100	54 to 80.6			25 to 37.5		
Density of particles Kg/m^3	2550	2550	2550	2550	2550	2550
Mean particle size d_p (microns)	206	206	206	206	206	206
Zwietering shape factor for *H* = *T* (*s*)	2.97	3.17	5.02	3.94	5.02	5.95

Table 7-12: Geometric details for the experimentally determined Zwietering factors for solids suspension.

If constant properties and geometric similarity are maintained on scale-up, then the specific energy on scale-up in the fully turbulent region (assuming a constant power number) is proportional to $N^3D^5/D^3 = N^3D^2$ as D is proportional to T for constant D/T.

$$\text{At } N = N_{JS} = sD^{0.85} \tag{7.23}$$

according to Zwietering. Thus, if s is constant with scale ε_{JS} is proportional $T^{0.55}$.

On a single scale s can be adjusted for small changes in D/T assuming ε_{JS} remains constant according to

$$N_{JS1}{}^{3}D_1{}^{5} = N_{JS2}{}^{3}D_2{}^{5} \tag{7.24}$$

Substituting $N_{JS} = sD^{0.85}$ in 7.24,

$$s_2 = s_1\left(\frac{D_1}{D_2}\right)^{\left(\frac{2.45}{3}\right)} \tag{7.25}$$

If however ε_{JS} is constant (as proposed) with geometric scale-up then s must vary with scale according to

$$s_2 = s_1\left(\frac{D_2}{D_1}\right)^{\left(\frac{0.55}{3}\right)} \tag{7.26}$$

This implies an increase in the value of s on scale-up.

To aid comparison, equations (7.25) and (7.26) were used firstly to adjust all the s values to a common $D = T/2$ value and then to a common $T = 0.61$ m scale value. These corrections are listed in Table 7-13.

For constant physical properties, scale and geometric similarity, the specific energy input is proportional to:

$$\varepsilon_{JS} \propto s^3 Po \tag{7.27}$$

Equation (7.27) is used to rank the energy efficiency of the suspension process in the last two rows in Table 7-13. The results in this table indicate that the hollow blade agitator to be the most energy efficient for solids suspension of those tested. A similar conclusion can be drawn from the work of Frijlink *et al.* (1990) who investigated the suspension of solid particles with gassed impellers.

Note also that the experimental Zwietering factors for the hollow blade agitators are consistently lower than those of the other agitators tested suggesting that at the geometry chosen for these tests they are excellent agitators for solids suspension.

Vessel diameter T(m)	0.286			0.61		
Geometry key	1	2	3	4	5	6
Agitator type	6HBDT	6HBT	A345	6HBT	4MFD (45°)	A315
Agitator Diameter (m)	0.145	0.15	0.143	0.344	0.322	0.343
Zwietering shape factor (s)for $H = T$	2.97	3.17	5.02	3.94	5.02	5.95
Agitator Power No Po	1.42	1.40	0.71	1.14	1.22	0.75
Zwietering shape factor (s) for $H = T$ is corrected to $D = T/2$, eq. (7.25)	3.00	3.30	5.02	4.35	5.25	6.55
Zwietering shape factor s*for $H = T$ and $D = T/2$ corrected to $T = 0.61$ m, eq. (7.26)	3.45	3.79	5.77	4.35	5.25	6.55
S^{*5}Po relative specific power at N_{JS}	58.4	76	136.2	93.6	176.3	210
Relative to large 6HBT Power	0.62	0.81	1.46	1.00	1.88	2.25

Table 7-13: Relative efficiency of various agitators tested compared at the same scale and the same ($D=T/2$) D/T ratio

7.8.2 Affect of Increasing the Liquid Level at Constant Solids for Various Agitators

When the $H = T$ ratio was changed in the 0.286 m diameter vessel without change to the solids in the vessel it was noted that:

N_{JS} remained the same in spite of the corresponding decrease in the solid fraction.

The solid liquid interface level at various operating speeds remained the same. This means that a design for N_{JS} at aspect ratios different from $H = T$, is simply achieved by taking the Zwietering factor for $H = T$ and calculating the solids fraction based on the weight of solids in the operating volume with the

weight of liquid that would have been present had a $H = T$ design been chosen.

The Figures 7-23, (i), (ii), (iii) and (iv), illustrate how solids collect under the agitator below the just suspension speed. These piles of solids shrink in size up to N_{JS} when all solids are mobile.

(i) 210 rpm < N_{JS}

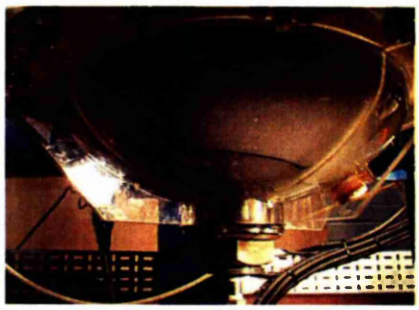

(ii) 240 rpm < N_{JS}

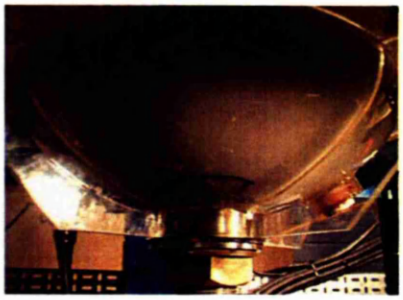

(iii) 255 rpm < N_{JS}

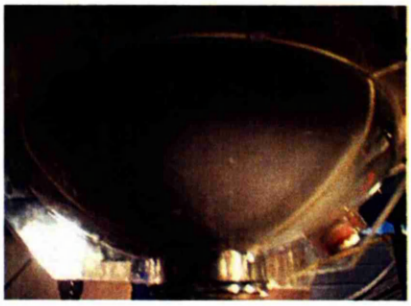

(iv) 264 rpm N_{JS}

Figure 7-26: A 0.15 m diameter 6HBDT agitator in the 0.286 m diameter tank for a 0.54 wt fraction of glass ballotini in water. Illustrating the progression of solids pick-up, from the vessel base, with increasing agitation speed up to N_{JS}.

For glass ballotini solids a clear interface between suspended solids and clear liquid is seen until the agitation speed is approximately twice N_{JS} when the total liquid H/T was raised to 1.34T. This is illustrated by the following sequence of photographs, Figures 7-24 (a) to (i).

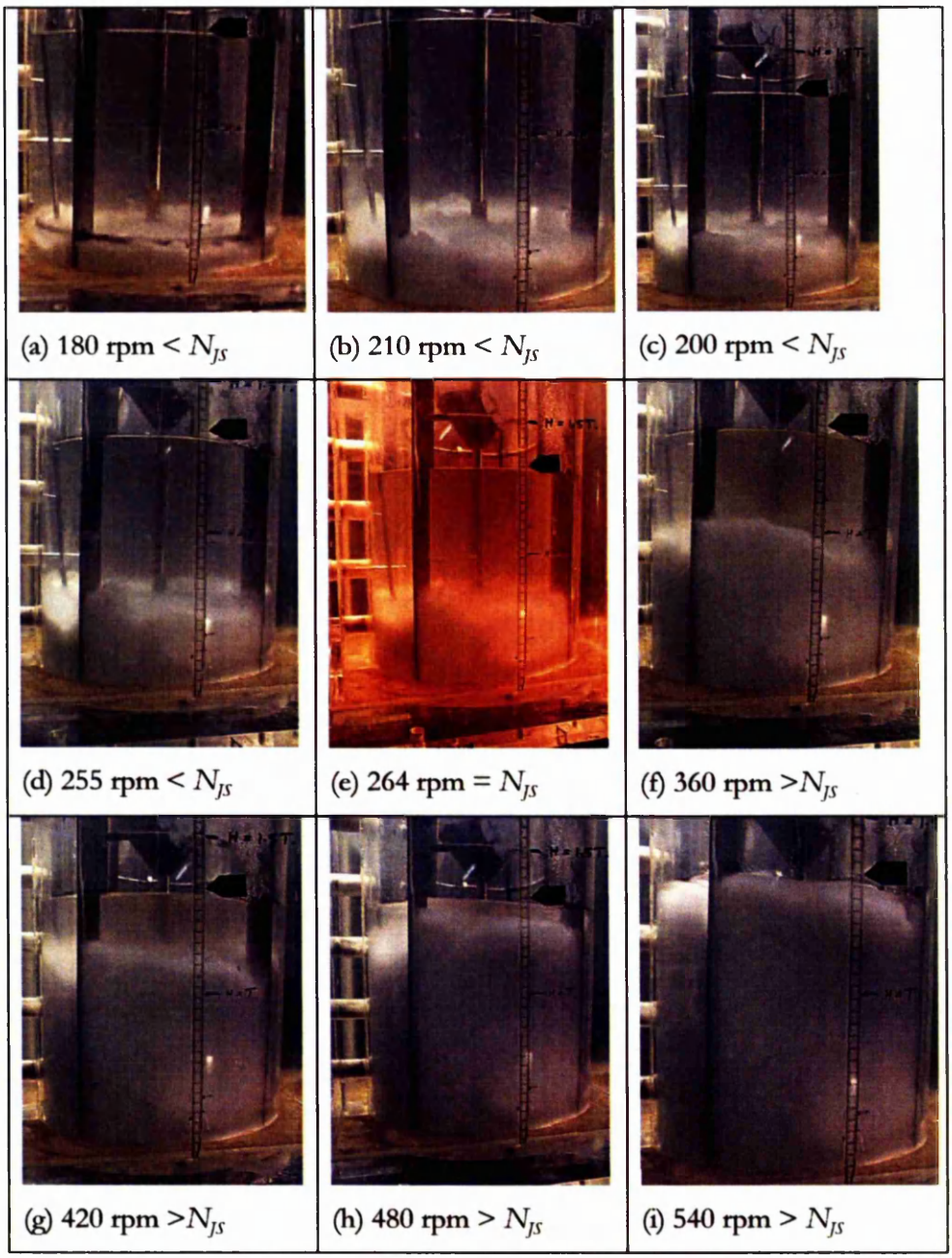

Figure 7-27: The above pictures are of the 0.286 m vessel containing 0.54 wt fraction of 206 micron glass ballotini beads. Agitation is by the 0.15 m diameter 6HBDT. They illustrate the progressive expansion of solids bed as agitation speed is increased. For glass Ballotini solids it requires approximately twice the just suspension speed to obtain a bed expansion to the surface, when no gas is introduced.

Multi-phase Hydrodynamics

The solid-liquid interface that exists when "heavy" solids are suspended at N_{JS} (Figure 7-27e), have implications for design and operation. Some of these implications are:

- Different residence times for solid and liquid phases in steady-state operation can affect product quality.
- Solids removal. If the solids take-off point is at a solids lean point, too high in the vessel then the mean solid concentration increases and "sand-in" of the agitator can occur as solids accumulate lower in the vessel.
- The power draw in batch systems can be higher than design when the concentration of solids in the vicinity of the agitator is much higher than the vessel mean.
- The presence of a "solid-liquid" - liquid interface can lead to compartmentalization and very long overall mixing times (see Chapter 2, section 2.5.5.2). This is investigated experimentally in section 7.9.

7.8.3 Experimental Determination of the Effect of Gas on Solid Suspension for Hollow Blade and Up-pumping LIGHTNIN A345 Agitators.

It is known that the presence of gas can adversely affect solid suspension for many agitators due to the reduction in specific power input and liquid pumping rates caused by the change to the agitator hydrodynamics on gassing. The literature on this area is covered in some detail in Chapter 2, section 2.7.3.

Chapman *et al.* (1983) and other workers have shown that up-pumping impellers perform very well for solid suspension under gassed conditions since the flow of gas and liquid is complementary. As the hollow blade design loses very little power on gassing one might expect these to be "good" agitators for gas-liquid-solid mixing. Indeed the work of Frijlink *et al.* (1990) indicated that

the "Smith type" (Figure 6-22a) hollow blade agitator was the most energetically efficient agitator (of those they tested) for gassed solid suspension.

The solid suspension characteristics of the hollow blade and LIGHTNIN A345 agitators depicted in Figure 7-25 are compared with no gas and gas introduced to the agitator at a superficial gas velocity of up to 0.023 m/s.

The results are listed in Table 7-14.

Note that the (% susp.) column labeled in this table, is obtained by dividing the height of solid-liquid suspension interface by the dispersion height, measured from the bottom of the tank base and expressed as a percentage. For (100% susp.) the solids are suspended to the free liquid surface.

Agitator Type	Agitator Diam. (m)	Aspect ratio (H/T)	Volume Fraction Solids	%Wt solids/ Wt water (X)	N_{JS} RPM	ε_{JS} W/kg	% *susp.*	P/P_U	v_S m/s
6HBDT	0.145	1.34 1.0 1.0	0.175 0.240 0.240	54 80.6 80.6	255 255 252	0.47 0.60 0.54	51.8 70.3 66.6	1.22 1.04 0.98	0 0 0.023
6HBT	0.150	1.34 1.0 1.0	0.175 0.24 0.24	54 80.6 80.6	264 264 264	0.58 0.81 (-)	56.8 78 (-)	1.16 1.09 (-)	0 0 0.023
A345	0.143	1.0 1.0	0.24 0.24	80.6 80.6	414 414	1.23 1.07	90.2 100	1.08 0.94	0 0.017

Table 7-14: The suspension characteristics of 3 types of agitators for the suspension of 10.13 kg of 206 micron glass Ballotini beads of density 2550 kg/m³ in water and aerated water in the 0.286 m diameter tank

Comments regarding the above results:

- **For the 0.145 m diameter 6HBDT:** With air introduced at a superficial gas velocity of 0.023 m/s to the water-solid system the just suspension speed reduced slightly to 252 rpm. At 300 rpm the action of the air took the solids to the top and destroyed the solid-liquid

interface. With air-water-solids the gas-liquid hold-up was low around 4%.

- **With the 0.15 m diameter 6HBT:** This was similar to the above but with air introduced at the same superficial gas velocity to the water - solid system the just suspension speed remained at 264 rpm. At an agitation speed of 270 rpm the action of the air took the solids to the top and destroyed the solid-liquid interface. At N_{JS} the suspension is more homogeneous than the former case probably because of the higher total specific energy ε_{JS}.

- **For the 0.143 m diameter A345 agitator:** Again, no increase in agitation speed was required above the unaerated N_{JS} when gas was introduced, although this was only tested up to a superficial gas velocity of 0.017 m/s (about 3 *VVM*). The energy requirement of this agitator to achieve N_{JS} is approximately twice that of the hollow blade agitators although this is offset by the observation that the suspension is more homogeneous at the just suspended condition.

- The quality of the suspension at N_{JS} is reflected in the power factor (ratio of measured power number to the power number in water at the same speed). The measured power number uses a slurry density based on a homogeneous suspension density. For a bottom heavy suspension the power factor will therefore be above unity. The affect of agitation speed on the power factor is explored in Figure 7-28.

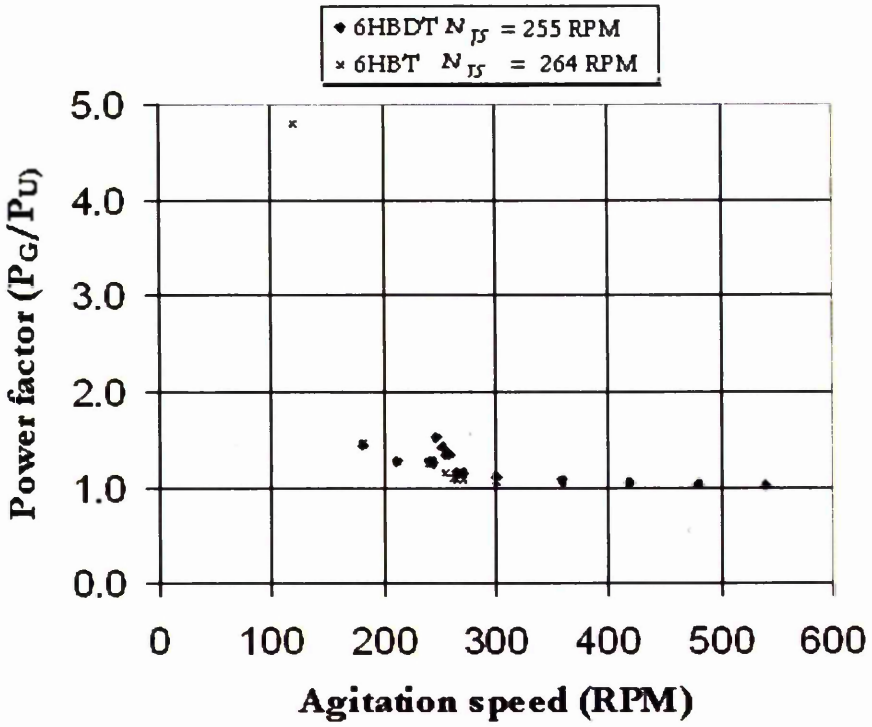

Figure 7-28: Illustration of the increase in power factor below N_{JS} for hollow blade agitators suspending 206 micron glass ballotini in water, in the 0.286 m tank.

This sort of approach could be used to determine the just suspension and the homogeneous suspension point when high solids loadings are used for solid-liquid systems.

The conclusions from this investigation is that the $D = T/2$ hollow blade agitators are very energetically efficient for solid suspension duties both in gassed and ungassed conditions. The LIGHTNIN A345 is also a useful agitator for solid suspension especially under gassed conditions.

Comparisons of the Zwietering s values with literature values are difficult since the just suspension speed is very dependent of vessel base geometry. In this work the vessels have dished bases and the shaft extends down into a bottom bearing which eliminates a point at which solids are known to accumulate. Therefore it is expected that the s values determined here to be lower than

values obtained in flat-bottomed vessels where much of the literature values have been obtained.

7.9 Multi-phase Mixing

This section looks at liquid phase mixing when solids, gas or gas plus solids are present.

Earlier published work by the author (Cooke *et al.* (1988)) concluded that the mixing time constant (Nt_m where t_m is the mixing time for a specified degree of mixing) is proportional to $Po^{-1/3}$, where Po is the power number and that under gassed conditions the gassed power number can be used in the prediction equation, providing the mixing in the vessel is agitator dominated (agitation power >> gas buoyancy power)

Where gas and liquid flow patterns positively reinforce each other such as with an up-pumping LIGHNIN A345 agitator (or other similar agitators) the mixing efficiency can actually improve with gassing but generally the former work has stood the test of time.

In this thesis the effect of the solid phase on mixing is studied both in gassed and ungassed conditions.

Three series of mixing tests were measured by the method described previously, for liquid, solid-liquid and gas-liquid-solid using the 0.15 m diameter 6HBT in the 0.286 m diameter tank. The results summarized in Table 7-15 are average values for several repeated tests.

Note the big increase in mixing time when a solid-liquid interface was present. Similar results have been reported in the literature: Harrop *et al.* (1997) found that solids can increase the liquid mixing time by a factor of 6 for a LIGHTNIN A315 impeller when operated with a solid-liquid interface (generally below N_{JS} in their experiments) at sand concentrations between 10

and 20% by mass, due to a zoning effect when a solid-liquid interface is present.

Agitators	Vessel Diameter T (m)	Operating Height H (m)	N RPM	System	Mean t_{90} (s)	Mean Nt_{90} (-)	Stdev Nt_{90} (-)
6HBT D=0.15m C=0.0715m	0.286 Dished base	0.384	270 > N_{JS}	Water	5.8	25.9	5.98
				Water + 10.31 kg Ballotini	31.4	141.3	46.3
				Water + 10.31 kg Ballotini+ air at v_S = 0.023 m/s	5.7	25.8	7.30

Table 7-15: Mixing time results for tracer added to surface, measured in the base.

In these experiments, when air is introduced at a superficial gas velocity of 0.023 m/s to the water-solid system the solids–liquid interface disappears and solids are observed throughout the vessel. The liquid mixing time then improves to the single-phase value.

This effect has been reported in the literature: Takenaka *et al.* (2001) studied a 3-phase liquid-gas-solid system at solids concentrations up to 40% by weight and gas flow rates up to 2 *VVM*. They used two different radial flow impellers, a Scaba 6SRGT and a Rushton turbine plus a six-bladed mixed flow impeller with pitch angle of 45° that was operated in both downward and upward pumping modes. They confirmed the Harrop *et al.* (1997) trend of increased mixing time for the solid-liquid case compared with the liquid only case. However, for the three-phase case the increase in mixing time was relatively small, especially with the Scaba and 6MFU impellers. It appears the gas-phase prevents a stable solid-liquid interface forming.

Chapter 8 : Spinning Cones as Pumps and Degassers.

8.1 Summary

The literature on spinning cones as pumps and degassers is reviewed. Experiments on a spinning cone rig designed to measure spinning cone-pumping rates are described. A large number of experiments were carried out, measuring pumping rates as a function of cone angle and immersion depth. Cone half angles were from 15 to 60 degrees. Most of the tests were done with water but a number of runs were carried out with 75% by volume glycerol solution. This changed the viscosity and fluid density. An equation is proposed to predict the volumetric pumping rate (Q) of a cone in terms of its geometry and the physical properties of the fluids.

Experiments with gassed fluids indicate that the liquid pumping rate of a spinning cone is independent of any gas present. It was also found that both outside and inside surfaces of the cone contribute equally to the fluid pumping process.

The effectiveness of spinning cones as a degasser and/or level controller have been tested in mechanically agitated baffled vessels using cones mounted on the agitator shaft at the liquid surface. Under gassed conditions and with surfactants added to the liquid, the spinning cone was shown to be effective in controlling the level and reducing the gas voidage over a wide range of operating conditions. The effectiveness of the cone as a defoamer appears to scale at equal tip speed suggesting that shear rate is the dominant mechanism. Tests were done on 2ft (0.61 m) and 3ft (0.914 m) diameter stirred tanks.

Following the reporting of this work at Bradford by Cooke *et al.*, 2002, published as Cooke *et al.* (2004), tests were carried out at NOVOZYMES A/S in Copenhagen, Denmark using a 45° cone to control foam in bacterial fermentations and it was found antifoam additions can be completely eliminated using a spinning cone, achieving similar titres and final fillings to

the antifoam controlled control experiments carried out in identical fermenters inoculated with the same seed.

8.2 Introduction

Many industrial processes involve the introduction of gases to liquid systems or result in gaseous products through reaction, heat input or pressure reduction. Examples are oxidations, fermentations and hydrogenations. Equipment is used that is designed to maximise mass transfer and ease the separation of the component phases. The physical characteristics of these systems often result in the formation of foam, which can be problematic in terms of control and subsequent processing. Proprietary equipment, in the form of multiple spinning cones, is used in the food and related industries, for degassing foaming products. Other rotating mechanical devices, such as breaker bars, impellers and spinning discs, are also widely used for degassing foams in a wide range of industries. This work evaluates the effectiveness of a spinning cone as a degasser and potentially as a level control device in stirred tanks and hence it's potential for adaptation in a wide range of industrial processes.

A hollow spinning cone fitted to the shaft of a stirred vessel, close to the operating level of the tank can act as a pump and reduce the gas hold-up. The cone picks up liquid from a pool at the inlet, accelerates it as a thin film up the walls and ejects it as a radial sheet at the top. Previous laboratory work using a foaming system indicated that the foam could be eliminated using a cone, with the foam level controlled at the cone outlet level. Under the same conditions without a spinning cone the contents foamed over the top. This suggested that the spinning cone might be a usefully employed to control level and foaming in industrial gas-liquid stirred tank applications. Also, since spinning cones have been used to intensify gas-liquid mass transfer (for example Middleton, 1997) it is argued that the reduction in gas voidage could be done without detriment to the mass transfer operation.

A literature search indicates that foam reduction occurs mainly through the application of shear stress (Goldberg and Rubin (1967), and Gutwald and Mersmann, (1997)). With a spinning cone this occurs at the wetted surfaces and from the radial sheet of liquid discharged from the top lip of the cone. The centrifuging action on the surface of the cone must also be a factor. Although many workers have studied the films on spinning cones, these were closed at the apex; therefore the film thickness measured was associated with a flow of liquid supplied to the cone surface by a separate pump. Hence the literature indicated a knowledge gap regarding the spinning cone as a self-priming pump and could not tell us how to predict the pumping rates from the physical and geometric properties.

A major aim of this work is to collect sufficient data to be able to fit it to an empirical model to represent the operation of the cone in terms of physical properties (cone speed; cone tip velocity; density, surface tension and viscosity of the pumped liquid and the geometrical properties of the cone).

8.3 Literature Review

Literature examples of the commercial uses of spinning cones to intensify mass and heat transfer operations, for atomisation and for shear spinning are given in Table 8-1.

Commercial Uses of Spinning Cones	Reference source
Intensify mass and heat transfer operations	Prince *et al.* (1997) Zivdar *et al.* (2001) Sykes and Prince (1992) Middleton (1997) Wright and Pyle (1995) Badcock *et al* (1994) Vallet, L. (1980) Vira and Fan, Dah Nien. (1981)
Atomisation	Hinze and Milborn, (1950) Dombrowski and Lloyd (1974) Dombrowski and Lloyd (1973) Alcock and Froelich (1986) Hashem (1991) Eisner and Martonen (1988)
Shear spinning	Semka *et al.* (1969) Straub and Hailey (1966), Rose and Watervliet (1966),

Table 8-1: Literature examples of uses of spinning cones

When this work was started, no papers that used of spinning cones as degassers were found, although they are used commercially for de-foaming vessel outlets, for example FUNDAFOM produced by CHEMAP AG of Switzerland. A recent paper by Takesono *et al.* (2002) compared six rotating defoamers fitted to a different shaft from the agitator: a six-blade vaned-disc, a six-blade turbine, a two-blade paddle, a conical rotor, a fluid-impact dispersion apparatus (FIDA) and a rotating disc. These authors discuss the effect of gas flow rate on critical speed (minimum speed to prevent foam from rising above the foam breaker level), shaft power consumption and liquid hold up in foam. They found that the critical speed N_{cri} is an increasing linear function of gas flow rate Q_G. They also found that the gas-liquid hold-up is an increasing function of Q_G. Therefore when Q_G increases, the foam formed is wetter and more stable and the rotational speed required to disrupt the foam is greater. They found that their cone was not efficient at controlling

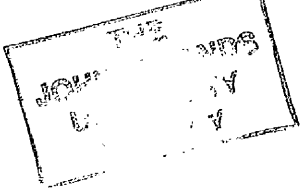

foam for superficial gas velocities greater than 0.38 cm/s. They operated with a shallow cone (half angle of 70°).

A number of papers have been published concerning the use of spinning "cups" as atomisers for agricultural sprays, slurries and molten metals. These generally focus on the form of the liquid film moving up the inside of the cups and the state of the fluid thrown from the cup periphery. As such there are some interesting results that are helpful from the viewpoint of understanding the experimental data.

The mechanism of foam break-up was explored by Goldberg and Rubin (1967), who concluded that most mechanical processes for foam reduction consist basically of the application of shear stress. Tests were performed with foam discharged vertically onto a spinning disc and their results were compared with other methods of foam reduction such as liquid sprays, centrifugal, mechanical agitation or blowing through nozzles.

Hinze and Milborn, (1950), describe three basic processes that influence the form of a liquid film thrown from the rim of a spinning cone. For a cone rotating at a fixed angular velocity, these processes can be summarised as follows:

Disintegration by direct drop formation: At low pumping rates a liquid torus is formed close to the edge of the cone. The diameter of the torus is determined by the liquid properties (density, viscosity and surface tension). External disturbances cause the torus to become varicosely deformed. Droplets are formed at the various bulges on the torus and are flung off by centripetal force.

Disintegration by ligament formation: At intermediate pumping rates, the bulges in the torus become more pronounced and the liquid leaves the cone in the form of thin jets or ligaments. If the pumping rate is gradually increased, the number of ligaments increases until a critical value is reached. If the pumping rate is increased further, the thickness of the ligaments increases but the number of ligaments remains constant. The ligaments flung from the cone are unstable and break up into drops some distance away from the edge of the cone.

Disintegration by film formation: The torus disappears at high pumping rates and a continuous sheet of liquid is flung from the edge of the cone. This sheet extends a small distance from the edge and then breaks chaotically into ligaments that in turn break into drops. Dombrowski and Lloyd (1974), divide this mode of disintegration into two separate categories that they call "aerodynamic wave disintegration" and "turbulent disintegration". In the former the sheets break up into drops within a narrow radial band whereas in the latter disintegration takes place over a relatively large distance. From their experiments it appears that, for a given pumping rate, the break up category, either aerodynamic or turbulent, depends solely on the speed of the cone periphery.

The transition from disintegration by film formation to disintegration by ligament formation occurs when the following inequality is true.

$$\left(\frac{Q}{D_C}\right)\left(\frac{\rho}{\sigma D_C}\right)^{0.5}\left[ND_C\left(\frac{\rho D_C}{\sigma}\right)^{0.5}\right]^{0.6}\left[\frac{\mu}{(\rho\sigma D_C)^{0.5}}\right]^{0.167} < 0.442 \qquad (8.1)$$

Similarly, the transition from disintegration by ligament formation to that by drop formation occurs when the following inequality is true

$$\left(\frac{Q}{D_C}\right)\left(\frac{\rho}{\sigma D_C}\right)^{0.5}\left[ND_C\left(\frac{\rho D_C}{\sigma}\right)^{0.5}\right]^{0.25}\left[\frac{\mu}{(\rho\sigma D_C)^{0.5}}\right]^{0.167} < 2.88x10^{-3} \qquad (8.2)$$

where Q is the pumping rate, DC is the cone outlet diameter, ρ is the fluid density, μ is the fluid viscosity, σ is the surface tension and N is the rotational speed of the spinning cone (rev/s).

The authors correlated the drop sizes measured in the various regimes. In the "aerodynamic wave regime" they obtained the following expression:

$$d_{32} = 0.742 Q^{1/3} \sigma^{1/3} \mu^{0.192} (v_S \rho^{1/6}) \tag{8.3}$$

where d_{32} is the volume-surface mean diameter and v_S is the velocity with which the liquid leaves the spinning cone. v_S is effectively equal to the velocity of the cone periphery ($2\pi N r_o$) except for liquids of low viscosity.

In the turbulent regime the data for oil and water were correlated separately:

$$d_{32} = 0.664 \left(\frac{Q^{0.303}}{N^{1.36} D_C^{1.18}} \right) \textbf{ (for water)} \tag{8.4}$$

$$d_{32} = 0.132 \left(\frac{Q^{0.392}}{N^{1.27} D_C^{0.819}} \right) \textbf{ (for oil)} \tag{8.5}$$

For ligament disintegration the following equation was recommended for drop size:

$$d_{32} = 0.0397 \left(\frac{Q^{0.334}}{N^{1.32} D_C^{1.22} \mu^{0.1}} \right) \tag{8.6}$$

The impact of fluid viscosity on the drop size is an interesting feature of the above correlations. The effect of viscosity seems to depend on the mechanism of drop formation. For example, viscous liquids seem to give a smaller drop size than less viscous ones when disintegration follows the route of ligament formation, but produces a larger drop size when a sheet is formed.

Hinze and Milborn (1950), calculate the fluid flow within the cone using the following assumptions:

The liquid layer thickness is small compared with the cone dimensions.

The flow within the layer is viscous.

The flow within the cone is rotationally symmetric.

The static pressure across the liquid layer is constant

The components of velocity normal to the surface of the cone and circumferentially around the cone are negligible compared with the component parallel to, and vertically up the cone surface. This implies that the path described by any liquid element with respect to the cone is practically straight and radial.

For the pumping rate (Q), the result is:

$$Q = (2\pi / 3\mu)\rho\omega^2 r_o{}^2 \delta^3 \sin\phi_C \qquad (8.7)$$

where ω = angular velocity (rad/s); r_o =outlet radius of cone; δ = film thickness; ϕ_C = cone half angle. This expression cannot be evaluated as δ is unknown.

An alternative expression for the cone pumping rate was suggested by Jones (1996):

$$Q = 2\pi r_o^2 \sqrt{\frac{\omega\mu \sin\phi_C}{\rho}} \qquad (8.8)$$

where r_o is the larger radius of the cone.

Hinze and Milborn (1950) suggested that the mean radial velocity (v_{av}) can be predicted by the following expression:

$$v_{av} = \left(\frac{Q^2 \rho \omega^2 \sin \phi_C}{12\pi^2 \mu r_o} \right)^{1/3} \tag{8.9}$$

A more recent paper by Makarytchev *et al.*, (2001), gives an equation for the film thickness modelled as a wavy layer on top of a laminar sub-layer attached to the disc surface. In their work liquid is supplied via a pump to the inner surface of a closed cone. For this case they found that the thickness of the film can be described by an additive modification of the Nusselt model thickness $\delta^+ = \delta_N^+ + \delta_{wave}^+ = 0.91\eta^{2/3} + 1.95\eta^3$, where η is a normalized radial distance. In the dimensional form, the proposed models express the film thickness and radial velocity as functions of cone geometrical and operating parameters. The authors maintain that the validity of the models is consistent with independent velocity measurements on a rotating cone and film thickness measurements on rotating disks. The definition of η contains Q and so cannot be resolved without knowledge of the flow rate.

Alcock and Froelich (1986) calculate the energy balance for a spinning cone based on a unit mass flow Bernoulli equation and use this to predict the discharge velocity. The basic assumptions used are that:

The change in internal energy of the fluid is negligible.

The thermal energy input is zero.

The potential energy change of the fluid on passing through the cone is negligible

The change in specific volume of the fluid is zero.

These give:

$$\frac{\mu P_i}{\rho}+\frac{v_i^2}{2}+W_S=\frac{\mu P_o}{\rho}+\frac{v_o^2}{2} \tag{8.10}$$

where v is the fluid velocity, W_S is the work input per unit mass and P is the pressure. The subscript i refer to the entrance to the cone and o the exit at the outer edge of the cone. Using this, the exit velocity is:

$$v_o=\sqrt{2(\mu/\rho)(P_i-P_o)+v_i^2+2W_S} \tag{8.11}$$

The specific power W_S (= $P_C/Q\rho$, where P_C is the power requirement and Q is the volumetric pumping rate) can be related to the theoretical power requirement (P_i) by expressing the torque (M) in terms of the momentum change ($M = m\Delta v$).

Thus, the theoretical power requirement is:

$$P_i=Q\omega^2\rho\frac{(r_o^2-r_i^2)}{2} \tag{8.12}$$

and the specific power becomes:

$$W_S=\omega^2\frac{(r_o^2-r_i^2)}{2} \tag{8.13}$$

Substituting this in the previous equation for v_o and assuming that the first two terms are negligible, that is $v_i << v_o$; $r_i << r_o$ and $2(\mu/\rho)(P_i-P_o)$ is small – for example for water $(\mu/\rho) = 1 \times 10^{-6}$ m^{2}s^{-1} and $(P_i - P_o)$ is typically of order 1-2 kPa) gives:

$$v_2=\omega r_o \tag{8.14}$$

Therefore the tangential velocity reasonably approximates the fluid velocity at the exit of the cone.

The drop trajectories were calculated by Hashem (1991), by assuming that the initial velocity of the drops is the same as the rim of the cone and that the drops are produced at the cone rim. The equations of motion used are:

$$a_z = -g - (3\rho_a C_d / 4\rho d)|v|v_z \quad (8.15)$$

$$a_x = -(3\rho_a C_d / 4\rho d)|v|v_x \quad (8.16)$$

where a = acceleration,

C_d = drag coefficient = $(24/\mathrm{Re})(1 + 0.1875\mathrm{Re} + 0.00026\mathrm{Re}^2)$,

Re = drop Reynolds number = $vd\rho/\mu$, $v = (v_x + v_z)^{1/2}$ and d = drop diameter. The subscript z refers to the vertical direction, x to the horizontal, a refers to air and l to the liquid phase.

Given that the initial velocity of the drops is equal to the speed of the rim of the cone (that is $v_{x,0} = \omega r_o = \pi N D_c$) then, for a specified drop diameter, the equations of motion can be numerically integrated: once to give the drop velocity and twice to give the horizontal distance travelled for a given fall.

8.4 Experimental Details

Experiments were carried out in mechanically agitated vessels and on a purpose built spinning cone rig designed to measure pumping rates.

8.4.1 The Stirred Tank Rigs

A schematic of the experimental rigs is shown in Figure 8-1.

These consist of two similar cylindrical mechanically agitated vessels each fitted with a quarter dish base. One is 0.61m mm inside diameter the other 0.91m. They are described in detail in Chapter 3.

The vessel and agitator geometries are listed in Table 8-2.

		Vessel		
Vessel diameter	T (m)	0.61	0.61	0.914
Geometry key		1	2	2
Operating levels	H (m)	1.0	1.0	1.5
Agitator type	Bottom	A345	Radial turbine	Radial turbine
	Mid	A345	-	-
	Top	A345	PTB 6-blade 45° up	PTB 6-blade 45° up
Agitator diameters	D (all) (m)	0.292	0.305	0.305/0.457
Agitator clearances	Bottom (m)	0.25	0.305	0.305
	Mid	0.5	-	-
	Top	0.75	0.5	1.143
Operating volume	V (dispersion) m3	0.28	0.28	0.94

Table 8-2: Vessel and agitator geometries

The cones used were approximately $Dc = T/2$ with cones half angles of 30and 15° on the 0.61m scale and 30° on the 0.914 m scale.

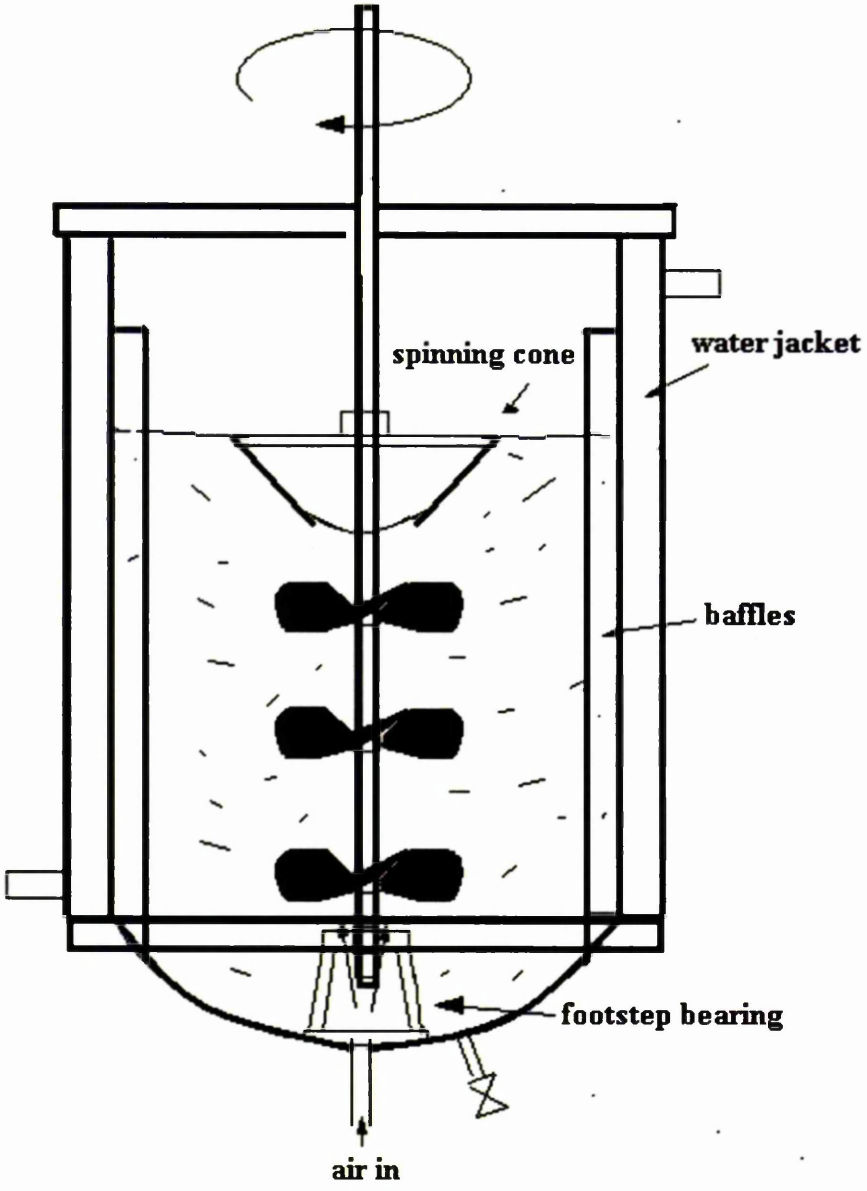

Figure 8-1: Schematic of the stirred tank rigs using a spinning cone with three LIGHTNIN A345 agitators.

8.4.2 The Spinning Cone Rig to Measure Pumping Rates

Figure 8-2 is a schematic representation of the apparatus that was put together to measure cone pumping rates. The cones used in the tests are

listed in Table 8-3. The data and analysis is Excel spreadsheet mccones.xls in the attached CD.

Cone half angle	Cone material of construction	Outlet diameter of cone D_C (m)	Inlet diameter of cone Di (m)	Tested with inside blocked up?
15°	PVC	0.138	0.075	No
30°	Stainless Steel	0.180	0.050	No
30°	Stainless Steel	0.305	0.064	No
30°	PVC	0.142	0.025	Yes
45°	PVC	0.139	0.025	Yes
60°	PVC	0.144	0.025	Yes

Table 8-3: Cones used in pumping rate tests

The operating procedure was as follows: -.

The motor rotated the shaft, onto which the hollow spinning cone was firmly affixed. Liquid was pumped into the trough (into which the cone was operating) from the reservoir. When the liquid started to immerse the cone, centripetal forces pumped a film of liquid up the cone's surfaces to the top rim where it was discharged as a radial sheet of liquid over the sides of the trough. This liquid entered the reservoir to be recirculated. Eventually a steady state was reached where the rate at which liquid entered the trough from the reservoir equalled the rate at which the cone ejected liquid back into the reservoir. At that point the liquid flow rate shown on the rotameter equalled the pumping rate of the cone. At this equilibrium point, the height of the liquid and the liquid flow rate was noted.

Liquid heights and pumping rates were measured for a range of angular velocities, cone immersion depths and cone geometries. The effect of viscosity on pumping was tested using a glycerol solution. The effect of gas on pumping was tested by pumping the same fluid under gassed and ungassed conditions using the same geometry. In order to find the contribution of the inside and outside surfaces to the pumping rate, experiments were repeated with the inlet blocked allowing only material on the outside to be pumped.

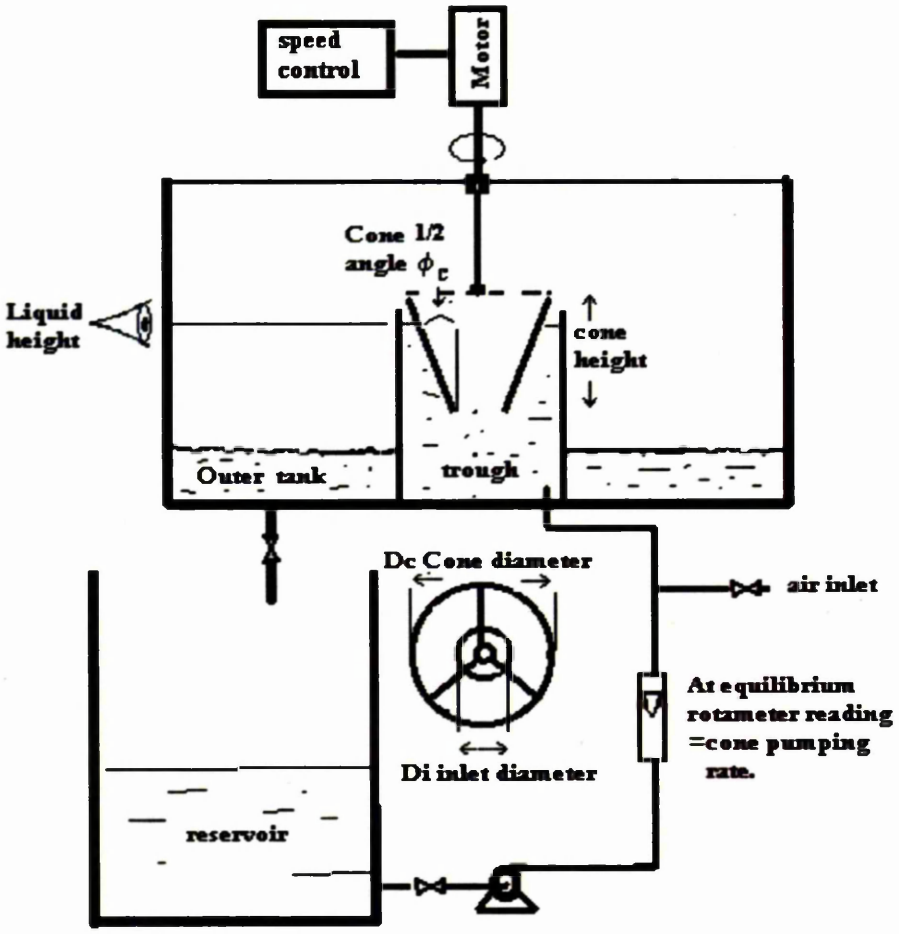

Figure 8-2: Cone pumping-rate measuring rig

8.4.3 Scouting Experiments on Reactor 2 Geometry (Table 8-2)

An Imperial standard 12 inch diameter stainless steel funnel (Figure 8-3) with a half angle of 30°, was adapted to fit the 0.61 m reactor 2 apparatus. The gassing rate used in the test gave a superficial gas velocity of 0.11 m/s. A few ml of ASDA ULTRA washing up liquid had been added to the solution to cause severe foaming, so that without mechanical agitation, this gas rate caused the liquid to foam over the top of the cone. The level rapidly came under control when the agitator and cone was switched on. The foam was

dispelled with the level controlled at the top of the cone. This sequence of events was captured on camera.

*

Figure 8-3: Cones used in scouting experiments in the 0.61m diameter vessel

Inspection of the flow visualisation reveals that the cone picks up liquid from a pool at the inlet, accelerates it as a thin film up the walls and ejects it as a radial sheet at the top. This action destroys the foam and provides a dramatic reduction in gas hold-up.

Several questions that arose concerning the mechanisms that caused the foam to be destroyed and at the same time creating the dramatic fall in gas hold-up included:

Were the effects due to: "g" force (= $\omega^2 r/g$)? Shear force? Do both inside and outside surfaces contribute? What is the optimum cone angle? Does it scale up and how?

8.4.3.1 Effect of Cone Angle - Tests with a 15° Cone

To test whether "g" forces are the dominant parameter, a 15° cone (shown in Figure 8-3) was tested on the 0.61 m diameter reactor geometry 2. This was not as effective as a degasser compared with the 30° cone at the same operating conditions. Compared with the no cone case, at a superficial gas velocity of 0.11 m/s and 10 "g" the 15° cone allowed an increase of the liquid volume by 15% compared with a 20% increase in liquid volume when the 30° cone was used.

8.4.4 Cone Pumping Rate Measurements

: Spinning Cones as Pumps and Degassers.

Consider sketch in Figure 8.4: Cone of ½ angle ϕ_C, inlet radius r_i and outlet radius r_o immersed in pool of liquid to a depth of Z. When it is spun at speed N it is apparent that:

- To spin liquid up from r then *"g"* $(= \omega^2 r/g)$ must be >1 at r
- To pump liquid down to r_i on inside of cone then *"g"* must be >1 at r_i.
- The velocity increases up the cone. Therefore, the film must thin up the cone or form rivulets (ligaments).
- To exit the cone, the liquid rises through the height h along length l.
- "h" and "l" are related via cos ϕ_c.
- "l" is related to (r_o-r) via sin ϕ_c.

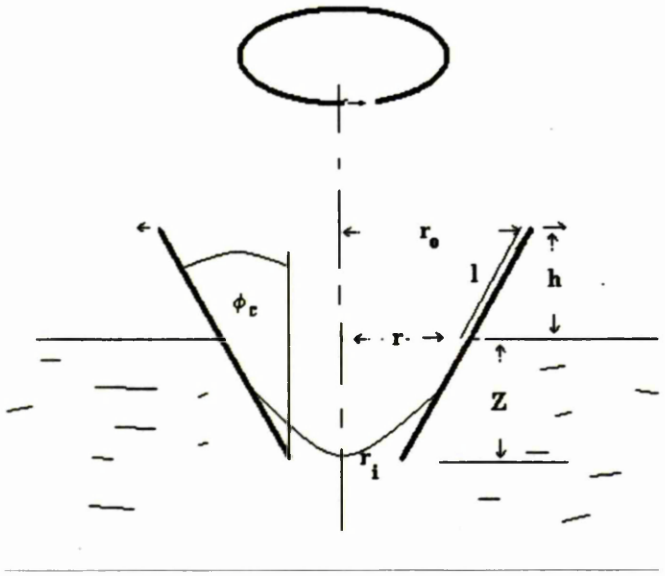

Figure 8-4: Cone pumping considerations

8.4.5 Experiments with Cones with an Half Angle of 30°

: Spinning Cones as Pumps and Degassers.

Two 30° cones with outlet diameters of 0.18 m and 0.142 m respectively and inlet diameters of 0.05 m and 0.025 m respectively were tested for a range of rotational speeds in water. The steady state immersion depths (Z) at different liquid supply rates (Q) were noted. Q was found to vary with the square of the agitation speed (N^2). By multiple regressions it was found the data for the two sizes of cones could all be correlated as:

$$Q = 21.8" g_r "r^{1.37} (l/\min) \qquad (8.17)$$

where "g" = $\omega^2 r/g$ and "g_r" is "g" force at r

Correlation coefficient for the expression (8.17) is $R^2 = 0.91$

Equation 8.17 implies that the volumetric pumping rate is directly proportional to the applied "g" forces. The fit to the correlation is illustrated in Figure 8-5.

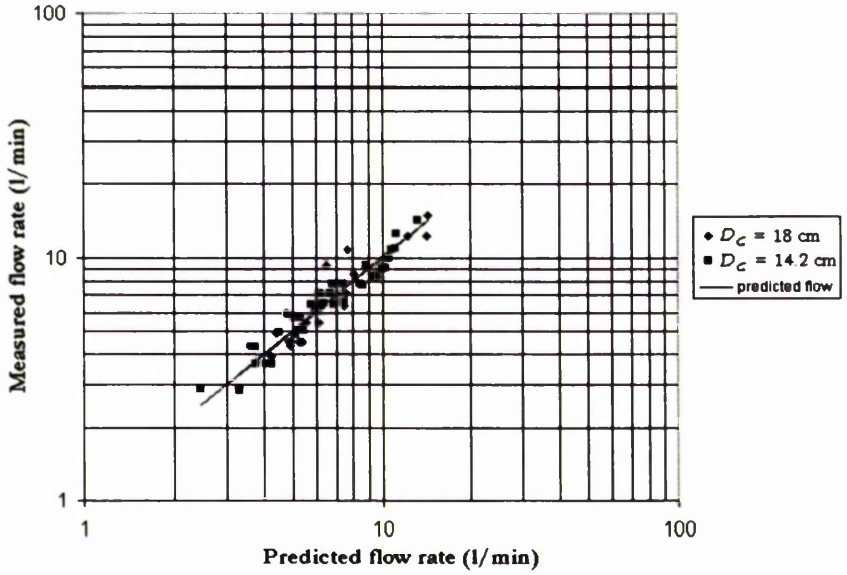

Figure 8-5: Data fit for 30°cones to: $Q = 21.8" g_r "r^{1.37} (l/\min)$

8.4.6 Effects of Cone Angle, Geometry and Physical Properties

: Spinning Cones as Pumps and Degassers.

A large number of experiments were carried out with a range of cone half angles from 15 to 60 degrees. Measurement of the immersion height was estimated to be accurate to 2 mm. Most of the tests were done with water but a number of runs were carried out with a 75% by volume glycerol solution. This increased the viscosity from 1mPa s to 56.5 mPa s and fluid density from 1000 to 1193 kg/m^3.

The results were analysed by the following dimensionless parameters:

Dimensionless flow rate as:

Q/NV, where Q = volumetric pumping rate, N = rotational speed and V = submerged volume of cone

Q/NV$_C$ as (a) but V_C = total volume of cone

Cone half angle as the sin, cos and tan of ϕ_C.

Ratio of centripetal forces to gravitational forces *"g"* = $(\omega^2 r/g)$ with radius at r and r_o both tested.

Ratio of inertial to viscous forces as Tay number (cone Reynolds number) = $\rho\omega r^2/\mu$ with radius at r and r_o both tested.

(r/r_o) ratio of cone radius at submergence level to cone radius at the top

(r_o/r_i) ratio of cone outlet radius to inlet radius.

Viscosity ratio as μ/μ_w, where μ is the fluid viscosity and μ_w is the viscosity of water at ambient temperature (20^{0}C).

After carrying out a large range of multiple regressions, it was found both *"g"* and the Tay number gave better correlations when outlet values were used. Similarly cone volume V_C gave an improved fit to the submerged volume. It was also found that correlations could be obtained with similar correlation coefficients involving both the sin and tan of ϕ_C. When sin ϕ_C was used, then the ratio r_o/r_i dropped out of the correlation without any significant change in the regression correlation coefficient. Examination of the fits showed that

although tan ϕ_C gave a good fit for 30° and 45° cones it gave a very poor prediction for 60° cones and over predicted some flow rates quite considerably. This did not show up on the correlation coefficient, as there are only a few data points for 60° cones. Inclusion of the viscosity ratio improved the data fit.

The best overall fit with correlation coefficient R^2=0.951 was:

$$\frac{Q}{"g"V_C N} = 155.6(\sin\phi_C)^{1.75} Tay^{-0.8} (r/r_o)^{2.5} (\mu/\mu_W)^{-0.5} \qquad (8.18)$$

where *"g"* and Tay are based on r_o and V_C is the total volume of the cone. The fit is illustrated in Figure 8-6.

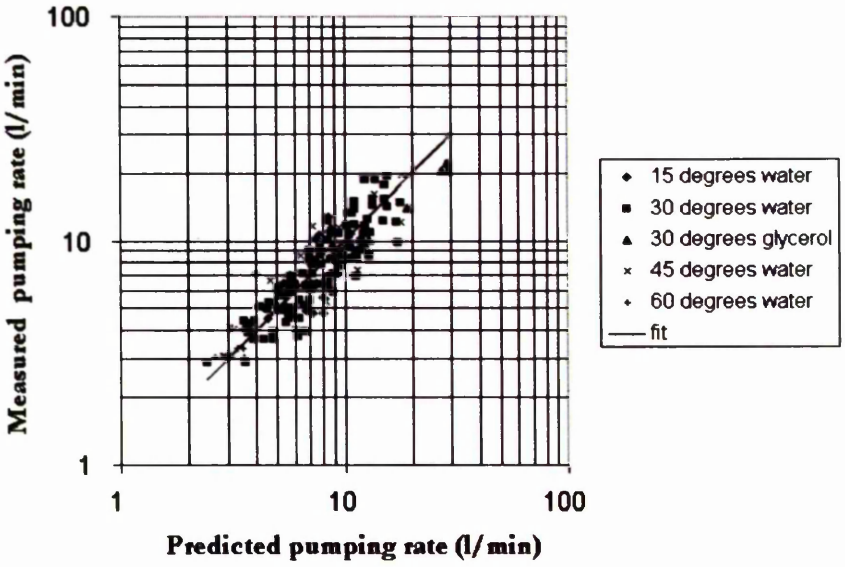

Figure 8-6: Data fit for all cones to:

$$\frac{Q}{"g"V_C N} = 155.6(\sin\phi_C)^{1.75} Tay^{-0.8} (r/r_o)^{2.5} (\mu/\mu_W)^{-0.5}$$

For SI units Q is in m³/s. To obtain the graph this has been multiplied by 60,000.

To test for hydrodynamic effects on the data correlation, the data were split into separate sets obeying the literature criteria for transition to break-up

from film to ligament formation as defined by equations (8.1) and (8.2). The majority of our data 119 points fell into the break-up from film disintegration. The fits to this data alone were worse (best correlation coefficient $R^2 = 0.93$) than for the entire data taken as one set. The smaller data set of 35 points all fell into the break-up from ligament formation. This correlated better with an R^2 coefficient of 0.97. There was nothing to suggest however, that the 2 sets obeyed different scaling rules.

8.4.7 Test of Literature Equation

Equation (8.8), proposed by Jones (1996), was tested against the experimental data. When r was taken as the large radius of the cone the equation did not fit. However, if r is taken as the radius of the cone at the submerged level it does give the right order of magnitude to the flow prediction and follows the trends, although the fit is poor as illustrated in Figure 8-7.

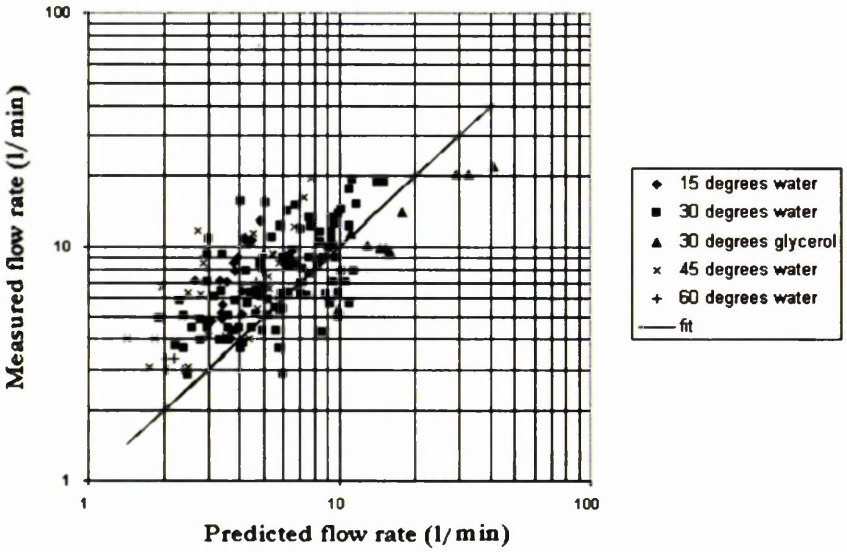

Figure 8-7: Pumping rate data fit to: $Q = 2\pi r^2 \sqrt{\frac{\omega\mu \sin\phi_c}{\rho}}$

8.4.8 Optimum Cone Angle

Equation (8.18) was used to predict pumping rates for a hypothetical range of cone ½ angles assuming a large diameter of cone (D_C) of 15 cm with an inlet diameter (D_i) of 5 cm, spinning in water with immersion to D_C. This of course gives very long depths of immersion for low ½ angles. The predicted pumping rates for cones of various angles rotated at 600 rpm are plotted against cone ½ angle in Figure 8-8. The curve shows a maximum pumping rate around a cone ½ angle of 40°, though the pumping rate is relatively insensitive to angles between 30° and 50°.

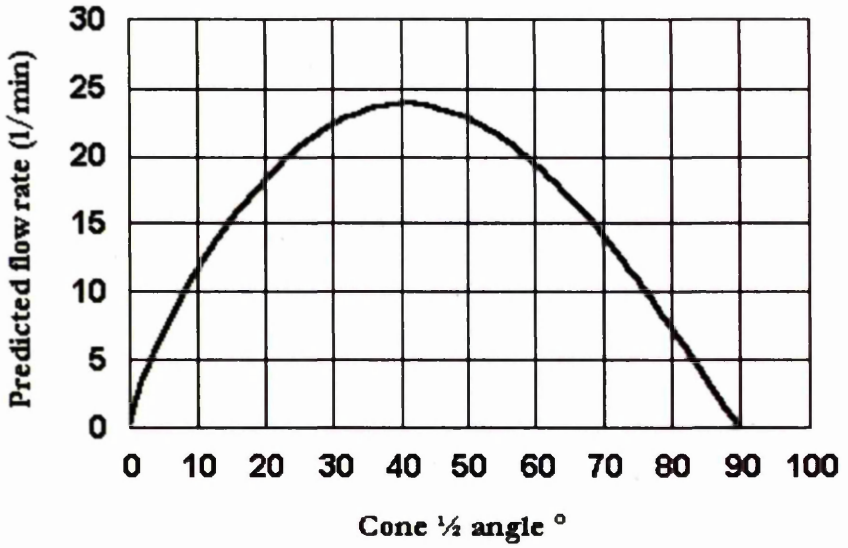

Figure 8-8: Optimum cone angle for pumping with fixed cone inlet and outlet diameters. Predicted using equation (8.18) for water with conditions N = 600 RPM, r_o = 7.5 cm and r_i = 2.5 cm. Indicates maxima at around 40°.

8.4.9 Effect of Aeration on Pumping

Polypropylene glycol (PPG) (mol wt 2025) was used as a surfactant and ASDA ULTRA washing up liquid was used to induce foaming at levels of 10 parts per million (ppm). Back to back experiments were carried out with the

same cone mounted in precisely the same position with water, water/PPG/soap and air-water/PPG/soap solution.

The visual comparisons of water results with those of water/PPG/soap solution indicated that the change in surface tension did not unduly affect the pumping rate, in spite of the large reduction in surface tension caused by the addition of the surfactants. ½°

When the solution was aerated to give approximately 20% gas hold-up, the pumping rate of the cone did not change significantly. This is confirmed by a plot of ($Q/"g"$) against radius of immersion for the aerated soap solution and the ungassed water in Figure 8-9. Observations of the film suggested that only liquid was being pumped and that gas-liquid disengagement is very rapid. Note however, that examination of the data set showed that all this data have been obtained at high *"g"* (>20 based on outlet flow). No similar comparisons have been made at *"g"* forces more realistic to large vessel operation.

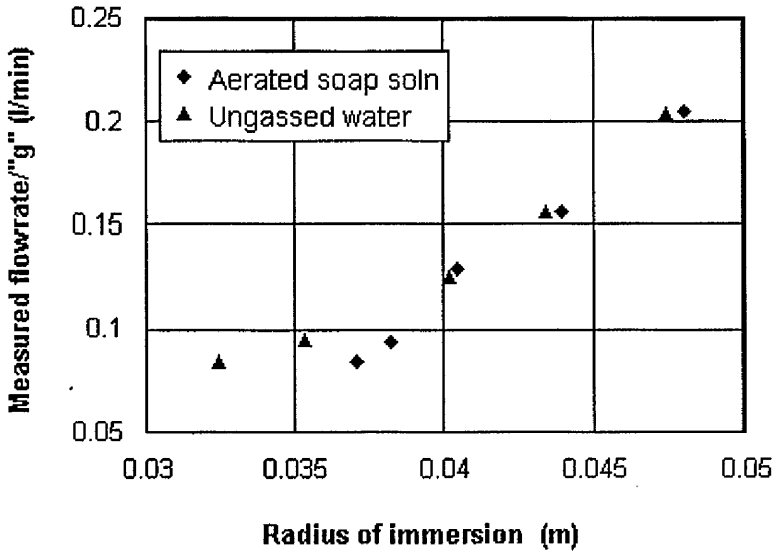

Figure 8-9: Affect of aeration and surfactants on the pumping rates of cones, for 30° plastic cones. Gas hold-up approximately 20% under aerated conditions.

8.4.10 Contribution of the Internal and External Cone Surfaces to Pumping

In the cases where the inside of the cone was blocked up to ensure that all flow was up the outside of the cones, the pumping rate was approximately halved. In fact, as the external diameter is greater than the internal, slightly more than a half was pumped. The pumping was found to be almost equally dependent upon the outside and the inside surface of the cones. Visually, this was a feasible conclusion to draw from examination of the rig when it was pumping with the inside blocked up. An example showing the 30° cone comparisons is given in Figure 8-10.

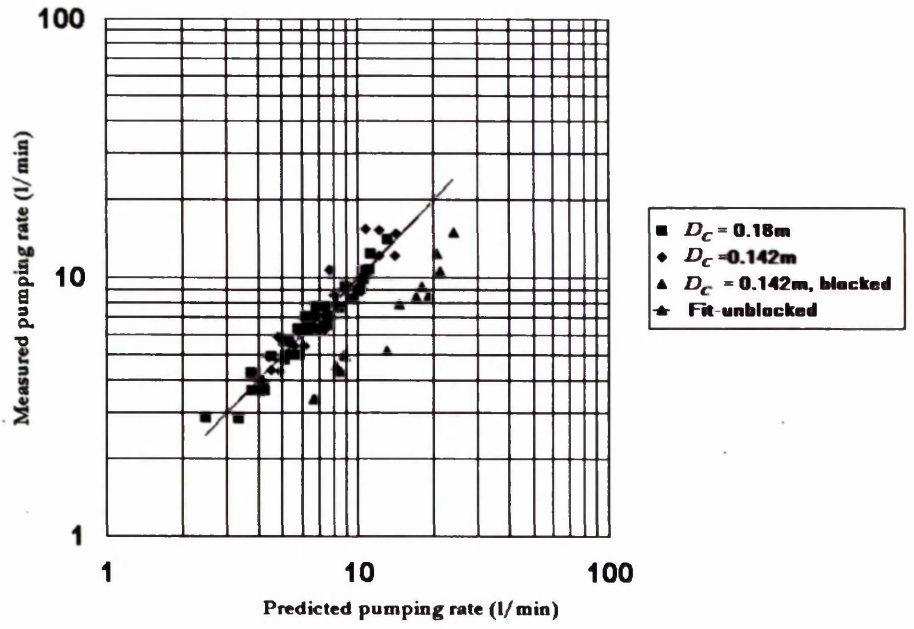

Figure 8-10: Showing the effect of blocking-up the inside of a 30° cone on pumping. Flow rate is approximately halved Solid line is prediction from equation (8.17)

8.4.11 Stirred Tank Experiments

Tests were run on reactor geometry 2 (Table 8-2) using 20 ppm polypropylene glycol as a surfactant. With this geometry the reactor foamed

quite badly when gassed without a cone. The 30° cone illustrated in Figure 8-3 was used in the tests. A gassing rate of 1980 l/min free air delivered was used for the tests, giving a superficial gas velocity of 0.11 m/s. Agitation rates were increased from 160 rpm to 300 rpm in steps of 20. The experimental data are plotted in Figure 8-11, in terms of gas hold-up against *"g"* force on the cone. When operated at the normal liquid level, the cone gave a significant reduction in gas hold-up compared to operation without a cone. The effectiveness levels off above approximately 10 *"g"* or a cone peripheral velocity around 4 m/s.

When similar tests were done with reactor geometry 1 (Table 8-2), the tendency to foam was not as great. This is due to the proximity to the surface of the top agitator. Tests proved that much of the foam could be eliminated by operating with an agitator at 0.6 to 1.2 agitator diameters from the dispersion surface, especially at high specific power inputs (>2W/kg). Even so typical reductions in gas hold-up of 10% were found for tests with a 20-ppm PPG solution when the 30°, ½ angle cone was used. This cone was tested at operations up to a gas rate giving a superficial gas velocity of 0.87 m/s without flooding.

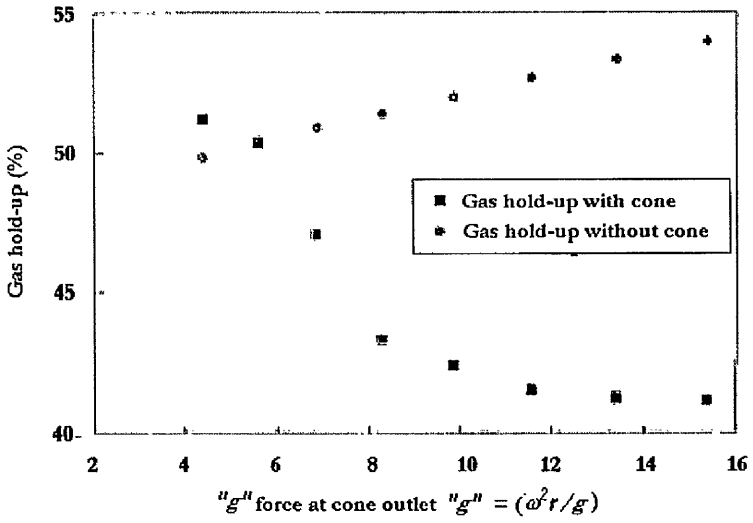

Figure 8-11: Reduction in gas hold-up using a 30° cone on reactor geometry 2. System is air-water with 20-ppm polypropylene glycol added as a surfactant.

8.4.12 Scale-up

A solution of 8 ppm PPG and 10 ppm ASDA ULTRA washing up liquid was used for the tests. On the 0.61 m and 0.914 m diameter vessels tests showed that this solution foamed over when the cone was not fitted at the test gas superficial gas velocities of 0.07 m/s. Foam out on our 0.61 m vessel is depicted in Figure 8-12.

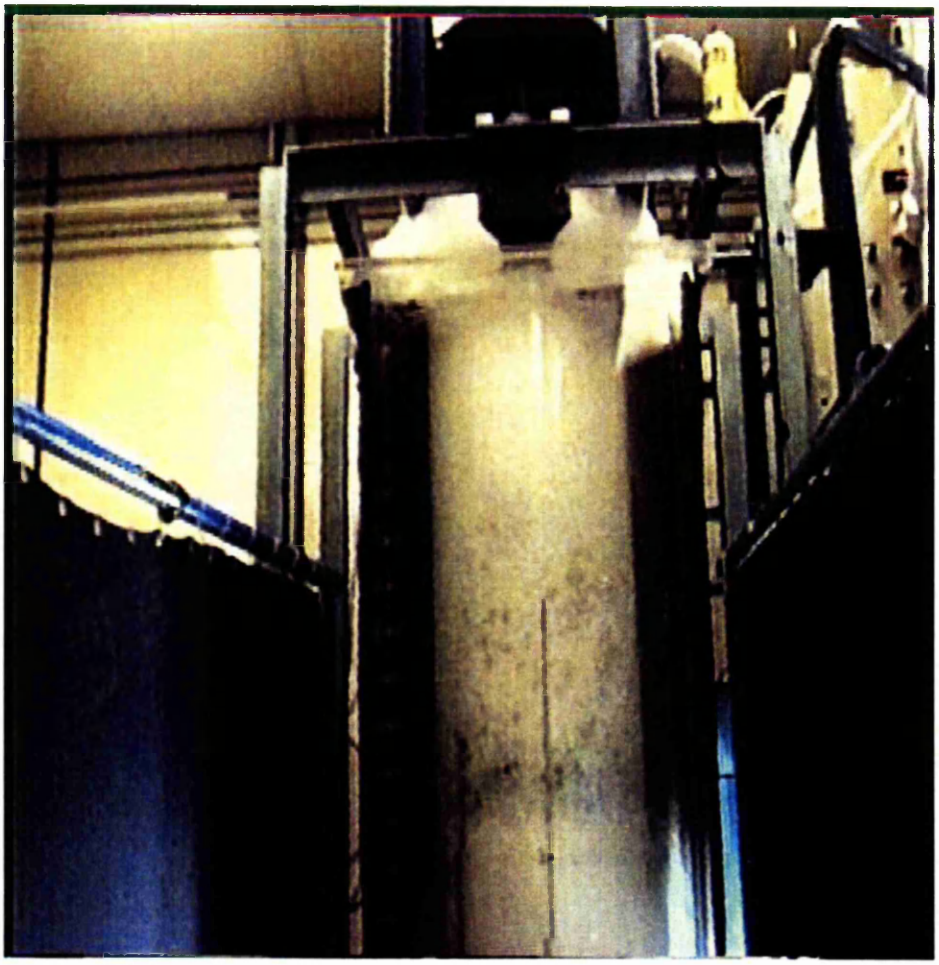

Figure 8-12: Foam out on the 0.61 m vessel due to aerated 10 ppm soap.

Figure 8-13: Dual A345 agitators with a 30°cone in the 0.61 m diameter vessel.

8.4.12.1 Studies with the 0.61 m Vessel

A 12-inch diameter, 30° to the vertical cone pictured in Figure 8-3 was used in the 0.61m diameter tank for this work. Agitator geometry was that of reactor 1; see Table 8-2 and Figure 8-13. The cone was demonstrated to be

effective between 240 rpm and 330 rpm for controlling foam due to a 10 ppm soap solution. Figures 8-14 to 8-16 illustrate the reduction in foam when the cone is switched on at 274 rpm. When the soap level of the solution was increased to 16 ppm, the cone was flooded at 274 rpm (Figure 8-17). The performance improved with increasing agitation speed. For controlling the foam due to 16 ppm soap solution, it was needed to operate at 390 rpm to match the 240 rpm performance for 10 ppm soap solutions. The *"g"* forces were varied from 10 to 26 with tip speeds between 3.8 to 6.2 m/s. At 274 rpm the tip speed was 4.4 m/s with a *"g"* of 12.8.

Figure 8-14:. 0.61 m vessel. Cone flooded, agitator switched on to bring foam under control for a 10 ppm soap solution.

Figure 8-15: Level coming under control in the 0.61 m vessel at 274 rpm for a 10 ppm soap solution.

Figure 8-16: Level completely under control for the 0.61 m vessel at 274 rpm for a 10 ppm soap solution.

Figure 8-17: The cone is flooded in the 0.61m diameter vessel at 274 rpm for a soap solution increased to 16 ppm.

8.4.12.2 Studies with the 0.914 m vessel

On the 0.914 m vessel, the tests were done on a cone of 18-inch diameter and a half angle of 45° depicted in Figure 8-18. Geometry was that of No 2 reactor (Table 8-2). The cone was effective for foam control between 150 rpm and 208 rpm for a 10 ppm soap solution. Starting at 40 rpm the cone was completely flooded at the operational gas rate. Increasing agitation to 180 rpm quickly brought the level under control. Figure 8-19 captures a picture of the foam layer being reduced shortly after the agitation rate was increased. Conditions quickly stabilised at this speed with no splashing and the level reduced so that only an inch or so of foam was visible on the inside of the cone (Figure 8-20). By reducing the speed in stages, the cone could just control this foam down to speeds of 140 rpm. At 150 rpm it was quite stable (Figure 8-21) with a foam layer about 1/3 of the way up the cone. At a speed of 140 rpm it appeared that operation was verging on the edge of instability

with foam occasionally spilling back into the cone (Figure 8.22). Below 140 rpm it started to flood. Increasing speed to 208 rpm did not cause any surface instability and the foam was well under control.

For the range of speeds from 150 to 208 rpm the *"g"* forces varied from 5.7 to 11 with tip speeds between 3.6 to 5.0 m/s. At 180 rpm (equivalent to operation at 274 rpm on the 0.61 m vessel scale) the tip speed was 4.3 m/s with *"g"* = 8.3.

8.5 Conclusions

The use of a spinning cone for foam control and as a level control device is shown to work effectively up to the largest scale tested which was on a 0.914 m diameter vessel. Scaling at constant tip speed gave a very slight improvement with scale-up. This is certainly not due to the agitator geometry change, which had been shown to be detrimental on the 0.61 m vessel work. It was probably due to the cone geometry change. Figure 8-8 indicates that a ½ angle cone of 45° is more efficient at pumping than one of 30°.

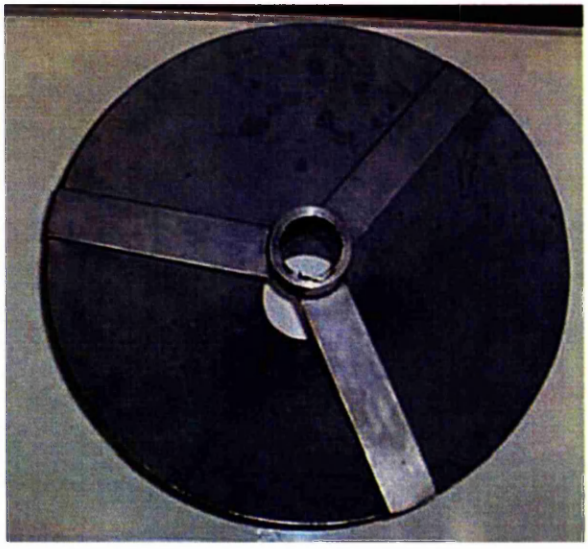

Figure 8-18: picture of cone used in the 0.914m vessel work

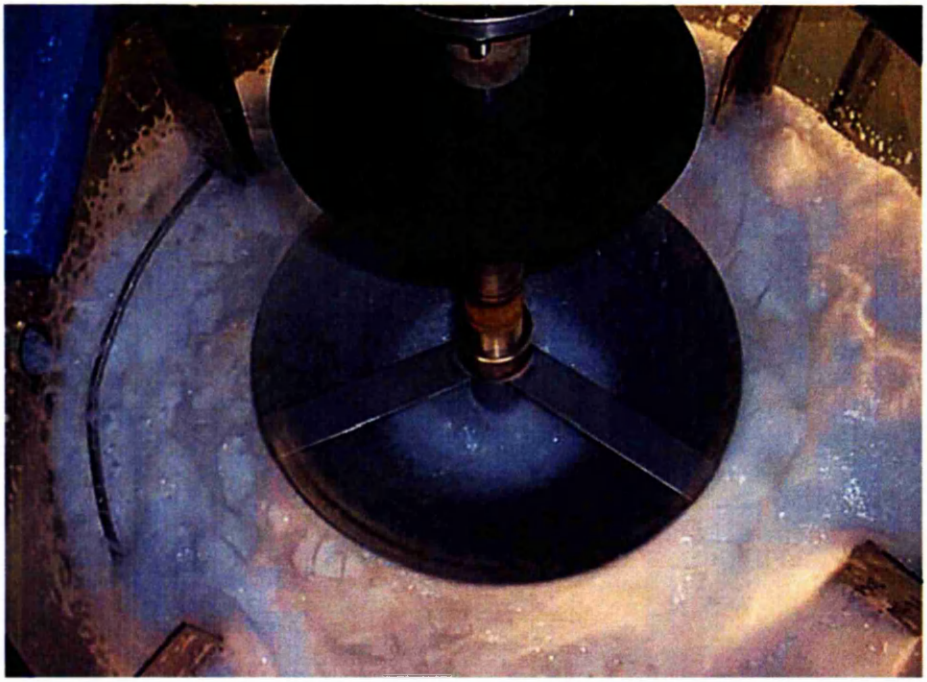

Figure 8-19: The reduction of the foam at 180 rpm after complete foam-out at 40 rpm in the 0.914 m tank for a 10 ppm soap solution.

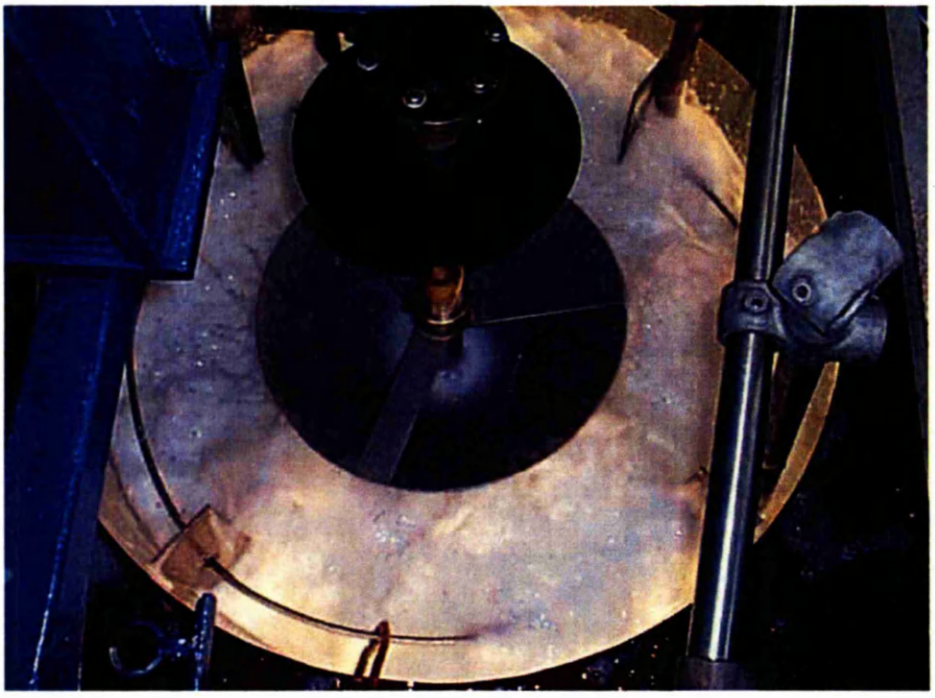

Figure 8-20: Equilibrium foam at 180 rpm in the 0.914 m tank for a 10 ppm soap solution.

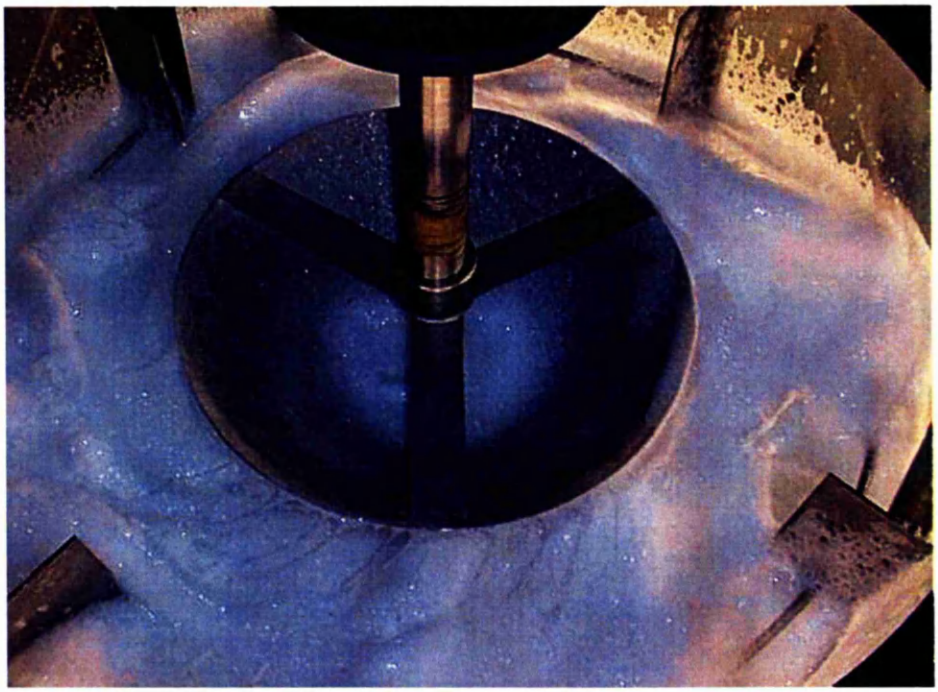

Figure 8-21: Stable operation at 150 rpm in the 914 m tank for a 10 ppm soap solution.

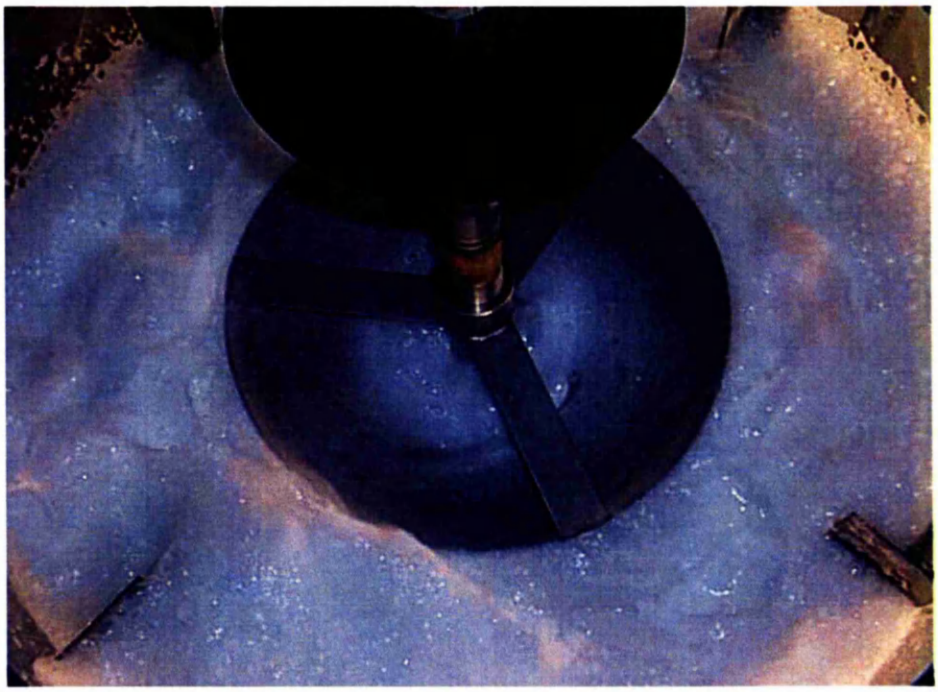

Figure 8-22: Just coping with foam at 140 rpm in the 0.914 m tank for a 10 ppm soap solution.

8.6 Power Draw for Spinning Cones

The theoretical cone power P_t can be predicted from the Adcock and Frolic (1986), equation (8.12).

$P_t = Q\omega^2\rho(r_o^2-r_i^2)/2$ (Watts)

Q is estimated from equation (8.18). Reasonable experimental agreement with equation (8.12) was obtained when the cone was operating with the liquid level at the height of the top of the cone. For lower levels the power draw was lower. Measured power numbers for the cone varied from 0.2 when fully submerged down to 0.03 when the level is low. The error bands were quite large for these results due to the predominance of the agitator contribution to the total power. More recent work, Perdriau (2003), with a fully baffled 45° cone fitted without other agitators gave a maximum power number based on the outlet diameter of the cone of 0.08 when fully flooded in water. This power number was constant with speed, which means that the power number is proportional to N^3 (similar to a conventional agitator).

8.7 Further Work

Further experimentation has been carried out at Novozymes A/S in Denmark, on their pilot plant fermenters and at UMIST, department of chemical engineering.

8.7.1 Pilot Fermenter Work

The cone used in these experiments (Figure 8-23) was designed at UMIST on the basis of the work reported above. The following is a summary of the experiments from Stocks *et.al.* (2004) of Novozymes..

The purpose of the work was to test the effectiveness of an inverted hollow

spinning cone (IHSC) in pilot scale equipment in currently commercially exploited recombinant *Bacillus* fermentation with the characteristically challenging foaming and hold up issues of this genus; in this case the *Bacillus* produced an extra cellular enzyme with technical applications.

Method

A total of nine *Bacillus* fermentations, in 550L reactors were conducted. The reactors were configured in sets of three so that three identically equipped and instrumented reactors were inoculated by one seed reactor, also of equal geometry. Vessels were 0.688 m internal diameter and were equipped with two Rushton Turbines 0.235 m in diameter. Agitation speeds were in the range 450-475 rpm. Aeration speed was 400 l/min (STP) at a steady 1bar head space pressure. The cone was of stainless steel construction, had an inlet opening of 90 mm a half angle of 45° and an exit of 344 mm (half a tank diameter). A sight glass in the top of the vessel permitted sufficient view of cone for the collection of video footage and some indication of the foam/hold-up status of the contents. Initial fill was 220kg of a complex, proprietary, production medium. As is typical in maximising batch productivity in commercial fermentations, the vessel ran in fed batch mode using a concentrated carbohydrate feed substrate. For the first and second set of fermentations, no foam control additive (FCA) addition was permitted in the first reactor, FCA was added on demand in the second, and the third reactor ran without FCA addition, only the cone was used to combat foam or hold up development. After running the first two sets, it was decided that it was economically intolerable to run without FCA addition in the first tank due to foam in the exit and so FCA addition was permitted for the third run.

Results

Reactor weights and product activity in the fermentations are depicted in figure 8-24. The tanks where no FCA was added lost 52 ± 15kg (at 95% confidence), compared to the reference batches where FCA was allowed on demand, which ended at 308 ± 6kg. The tanks containing the cone did not

loose any contents ending on a statistically indistinguishable filling of 319 ± 13kg (p=0.18, T-Test or ANOVA). The enzyme activity in all tanks was not statistically distinguishable (p=0.84, ANOVA).

Conclusion

The use of the cone successfully controlled foaming and hold-up at pilot scale in a commercially relevant *Bacillus* fermentation, with a performance at least equal to that of the conventional FCA addition. Such encouraging results indicate great potential savings in both fermentation and recovery costs since FCA addition can be completely avoided under fermentation. A full-scale production evaluation is justified and is currently under consideration.

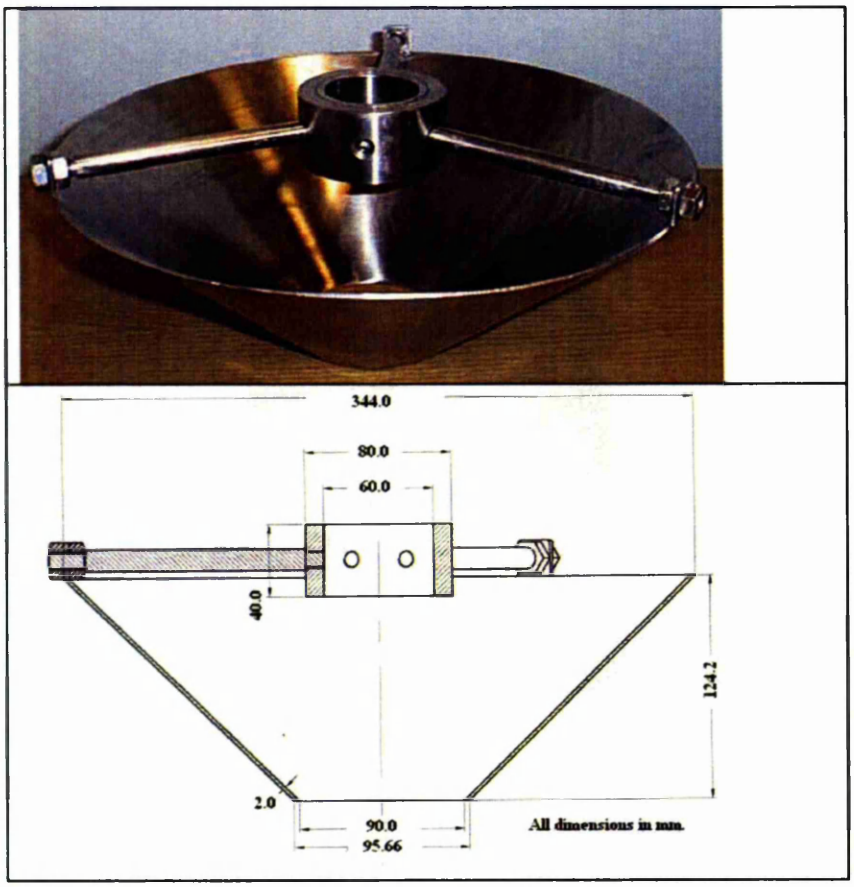

Figure 8-23: Cone used in the Novozymes fermenter tests

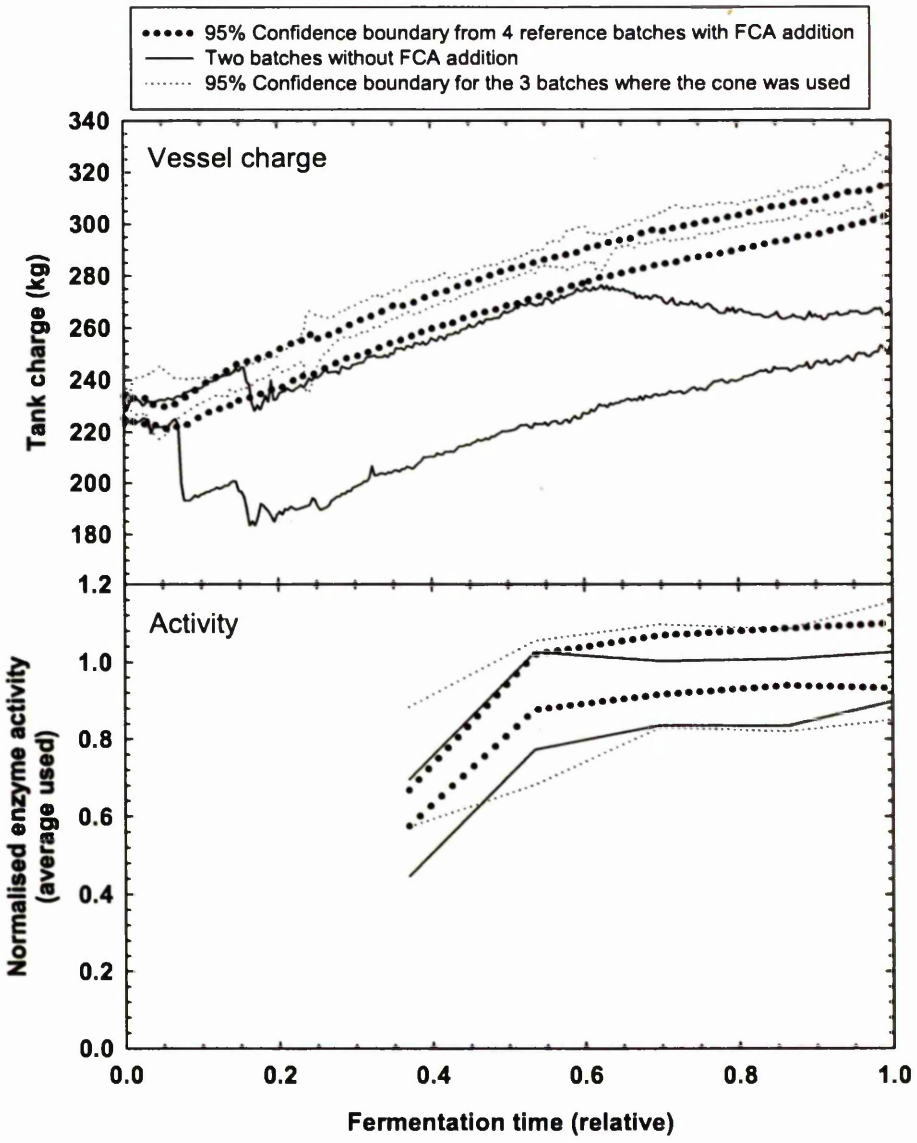

Figure 8-24: Comparison of pilot plant runs with and without the spinning cone.

8.7.2 Further Work at UMIST

Three 45°, ½ angle cones of diameters, 0.4T, 0.5T and 0.6T were constructed to fit the 0.61 m diameter vessel. These were used to determine the effect of D_C/T on foam suppression. This work was the subject of an MSc sponsored by ICI by Perdriau (2003).

Chapter 9 : An Electrical Resistance Tomography (ERT) System as a Diagnostic Tool

9.1 Aims of the Study

This work is in two parts:

- To determine whether a commercial ERT tomography package can be applied to the study of intense multi-phase reactors using an 8-plane ERT sensor arrangement fitted to a stirred tank.
- To determine the radial sensitivity and any 3-D effects in the above arrangement.

9.2 Summary of the Work

An 8 plane by 16 electrode Electrical Resistance Tomography (ERT) sensor is employed as a measurement and visualisation tool for the investigation of mixing processes in the 0.61 m diameter Perspex vessel described in Chapter 3. The ERT system used during these studies is an Industrial Tomography Systems (www.itoms.com) P2000 instrument. This system utilises image reconstruction algorithms based on two-dimensional (2*D*) electric field simulation to represent the planar data. Three-dimensional (3*D*) representations of the conductivity distribution are obtained by stacking together the reconstructed images from each plane with a linear interpolation performed between adjacent planes.

Part 1 of this study comprised modifying the existing 0.61 m diameter stirred tank facility in order to demonstrate that an 8 plane by 16 electrodes ERT can be successfully applied to the study of gas-liquid reactors operated at intense conditions. Mechanical agitation for these tests is by dual $T/2$ diameter impellers operated at energy dissipation rates (ε_T) of up to ~ 10 kW/m^3 liquid

and superficial gas velocities of up to 0.1 m/s. Gas hold-ups up to 50% are achieved by the addition of a surfactant.

Because of the design of the existing 0.61 m model vessel, the tomography set-up requires to be an add-on unit that fits inside the vessel with minimum interference with flow visualisation and with no interference to analysis ports and existing instrumentation. To facilitate this end, the tomography sensors are designed to form an integral part of a specially designed baffle cage. Some commissioning problems caused by the large size of the metal agitators and the metal support rings are solved by replacing the metal rings with plastic and by powder coating the agitators. The unit is then successfully demonstrated and these results are presented.

Part 2 of this work is aimed at determining the extent to which the reconstructed images are affected by the $3D$ distribution of the actual electric field within each electrode ring and also to establish the limits of detection. Tests are carried out using a selection of highly conducting and non-conducting spheres.

Spheres, varying in size from one to three inches in diameter, are suspended on a thin thread from a support bar placed across the top of the vessel. The shaft and agitators are removed from the vessel. The spheres are moved in stages across the diameter of the vessel at the centre of plane 5 and equidistant between planes 4 and 5. Data are collected from all 8 planes for each sphere in each position.

It is found that the ERT system can detect an object with a minimum diameter between 4% and 7% of the vessel diameter depending on the conductivity difference between the sphere and the fluid background. The distance between the sphere and the sensors also affects the limits of detection. The response of the system to the sphere is greatest when the object is closer to the sensor. When a highly conducting object is close to a sensor some "ghosting" is apparent due to distortion of the electrical fields.

: An Electrical Resistance Tomography (ERT) System as a Diagnostic Tool

9.3 Part 1: Demonstration of a Novel Retrofit Tomography Baffle Cage, for Gas-liquid Mixing Studies under Intense Operating Conditions

9.3.1 Background to ERT Retrofit

Following a one day meeting on process tomography for fluid mixing at UMIST, Manchester (15 March 2000), sponsored by the IChemE Fluid Mixing Processes, Subject Group, two of our industrial sponsors, DuPont (UK) Limited and Huntsman Polyurethanes expressed an interest in seeing electrical resistance tomography (ERT) demonstrated on a model akin to some of their high intensity industrial reactors. Although tomography is clearly out of its infancy as far as a process tool is concerned, the mixing literature has mostly concentrated on modelling single agitators typically $D = T/3$ operated at modest power inputs and relatively low gas hold-ups. Both the above sponsors have reactors with multiple large ($D = T/2$) agitators operated at high intensities with unaerated energy dissipation rates of up to $\sim 10\ kW/m^3$, superficial gas velocities ≥ 0.1 m/s and gas hold-ups up to 50%.

Under these intense operating conditions operation is in the heterogeneous regime. Recent studies: Ellenberger and Krishna, (1999) for bubble columns and Gezork *et. al.* (2000) for stirred vessels, show that as superficial gas velocities are increased, a transition from the homogeneous (bubble regime) to the heterogeneous regime occurs. For a bubble column this happens when the superficial gas velocity exceeds the rise velocity of the bubbles in the bubble regime. In mechanically agitated vessels internal circulation causes an earlier transition. Gezork et. al. (2000) showed that this occurred at a superficial gas velocity of around 0.04 m/s for the coalescing air-water system in mechanically agitated vessels and at a lower superficial gas velocity in non-coalescing systems, which have smaller bubbles. In the heterogeneous regime there is a mixture of large and small bubbles and the interchange between

these bubble populations has a pronounced effect on the gas-liquid mass transfer process.

ERT is seen as a tool, which could provide the means to probe some of these interactions by yielding data on local population densities and may be to "see" liquid feed distributions through the gas fog. Our industrial sponsors agreed to finance a retrofit to the UMIST - Dept. Chemical Engineering 0.61 m diameter mixing rig to include an ERT package. The aim was to demonstrate the ability to obtain meaningful data at high ε_T and gas-liquid hold-ups. In particular to be able to assess gas phase distributions and fluctuations and to follow rapid mixing processes even at high gas phase fractions.

9.3.2 Electrical Resistance Tomography System

The ERT system used during this study was an Industrial Tomography Systems P2000 instrument. This instrument is a further development of the P1000 as reported by Primrose and Qiu (1999). The main advances being an increase in injection current range from 0.1-30 mA to 0.1-75 mA, an increase in the maximum number of electrodes from 64 to 128 and a reduction in the time of acquisition for one frame from 40 ms to 20 ms.

The P2000 instrument is driven by a Microsoft Windows based software package that can be used for both measurement and data analysis. Image reconstruction was performed by linear back projection. Further data and statistical analysis features include pixel history which allows image pixels of specific interested to be monitored, for example, the region close to a feed point, bulk properties which clearly show when complete mixing has been achieved.

9.3.3 Previous Applications of ERT to Mixing Processes

Mixing processes are arguably the most reported application area of electrical and other tomographic measurement techniques as demonstrated at the 1st

World Congress by Wang *et al.* (2000) and Buchmann and Mewes (1999). These techniques offer new opportunities for quantifying the degree of mixing and efficiency of mixing processes containing many types of process materials. The most critical operating parameter in a stirred tank is the agitation speed. Since the type, number and size of impeller can vary, the most appropriate method for reporting the power input into a stirred tank is by the power per volume ratio (P/V). In the majority of previous applications of ERT to mixing processes, the P/V ratio has been low. Specific examples include the measurement of:

Solid-liquid mixing at agitation rates between 75 and 105 rpm: Mann *et al.* (2000).

Gas-liquid mixing for low and high viscous liquids: Wang *et al.* (1999).

The effect of altering the feed location while agitating at 150 rpm: Holden *et al.* (1999).

The behaviour of different impellers at agitation speeds of 75 rpm: Holden *et al.* (1998).

'Just suspension speed' for solid-liquid mixtures: McKee *et al.* (1995).

In all these cases a single impeller was used at specific power inputs in the range 0.1 to 1 kW/m^3.

9.3.4 Experimental Details

9.3.4.1 Retrofit of the 0.61 m Stirred Tank Facility to Include an ERT Capability

The 0.61 m stirred tank rig is described in detail in Chapter 3. The ERT assembly (designed to fit into this vessel) consisted of 8 rows of 16 electrodes (128) terminating in 8 centronic connectors, wired to UMIST - Dept. Chemical Engineering instructions, to plug into an Industrial Tomography Systems, P2000 instrument. The rows were 8 cm apart designed to span an

H=T cylindrical section. Because of the special design of the model vessel, the tomography set-up needed to be an add-on unit that fitted inside the vessel with minimum interference with flow visualisation and with no interference to analysis ports and existing instrumentation. To achieve this, the tomography sensors were made to form an integral part of a specially designed baffle cage. All electrical connections were sealed internally and were made water and chemical proof. All exposed metal was minimised and was stainless steel to avoid stray emf's generated by dissimilar metals. The baffles and electrode/wire carriers were made from plastic. Three expansion rings held the baffle cage in position. A picture of the tomography baffle cage is shown in Figure 9-1.

The tomography planes were numbered from the top. The top agitator was located at plane 4 and the bottom agitator was level with plane 8.

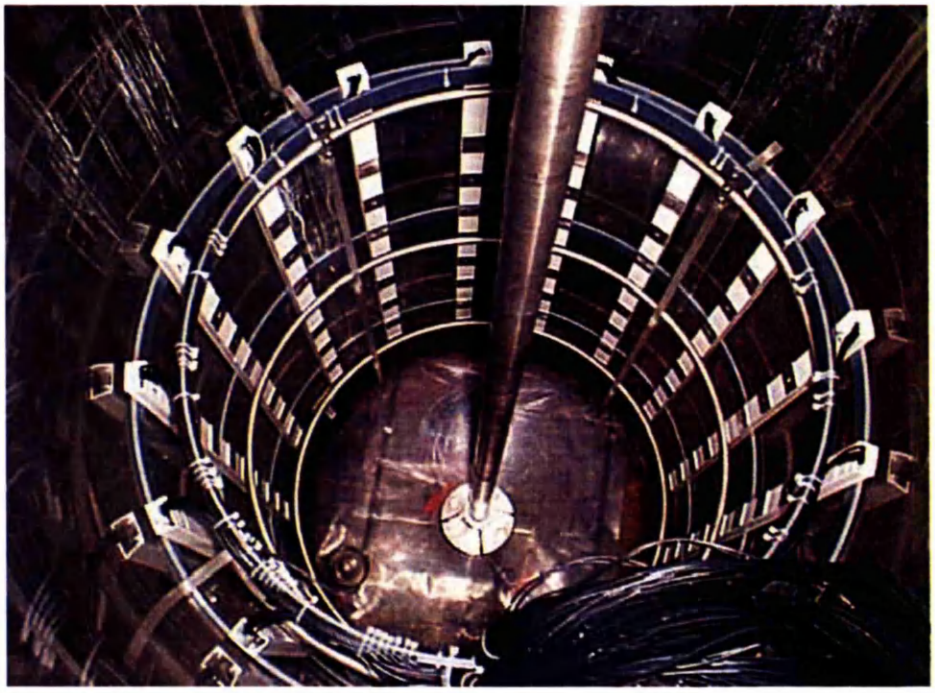

Figure 9-1: View looking inside the vessel at the tomography cage

: An Electrical Resistance Tomography (ERT) System as a Diagnostic Tool

9.3.4.2 Geometric Details

Two agitator arrangements in the 0.61 m vessel were investigated:

A dual radial/axial agitator combination. The bottom agitator was a hollow parabolic shape blade design (Figure 9-2a) and the top one was a 6MFU (Figure 9-2b). Both agitators had a diameter of 0.5*T*. They were located at clearances of 0.22 m and 0.525 m above the bottom of the base. H/T was constant at 1.36.

(a) curved parabolic blade agitator,

b) 6 blade 45⁰ Pitched blade turbine pumping up (6MFU)

Figure 9-2: Agitator used in tests

A single 4MFD, D=0.48T, c=T/4, Po =1.31, H/T =1.44 operating in water at 234 rpm.

In order to look at gas distribution for case (i) two types of air spargers were investigated.

A 4-airsparge arrangement of pipes with exit horizontal at the centre-line of the parabolic agitator, tangential in the direction of flow located at 5, 95, 185, 275 degrees

A single air sparge centrally in the base, pointing vertically upwards.

: An Electrical Resistance Tomography (ERT) System as a Diagnostic Tool

There were 4 x 90-degree wall baffles of width $T/10$ located at 10, 100, 190 and 280 degrees. These were tapered flush into the dished base.

A liquid feed input was located horizontally at the centreline of the parabolic agitator at a position of 330 degrees through which a conductivity pulse could be injected. The injection loop held 7.5 ml of conducting tracer.

In order to obtain gas hold-ups of up to 50%, the water was dosed with surfactant (PPG).

9.3.5 Commissioning Trials

9.3.5.1 Tribulations

The vessel was filled with tap water ($\sigma \approx 100$ μS/cm) and each measurement plane was tested individually beginning with plane 1, the lowest plane. For plane 1 the injection current was altered between 5 and 75 mA and the optimum current was found to be 30 mA which gave stable voltage readings in the range 17.4 to 913.1 mV with a mean of 182.8 mV with maximum relative change from frame to frame of ± 1%. Planes 2 to 8 were tested individually with an injection current of 30 mA. Planes 2, 5 & 6 performed similarly to plane 1, however, planes 3, 4, 7 & 8 produced nonsensical voltage measurements due to the presence of many negative values. Having run a series of tests and seeking advice from experts in UMIST and ITS, it became clear that there were three main contributors to the problem.

Wiring faults. The wiring was not fully consistent with the ITS specification, providing insufficient grounding and shielding. This had an adverse effect on the signal to noise (SN) ratio. This omission was a result of poor communication early in the project.

The three expansion rings holding the baffle cage to the wall were stainless steel. These were close to the wall and were shown to be interfering with the

electrical measurements in the planes closest to them by acting as current sinks, resulting in the electric field not penetrating the process volume.

The large metal agitators also acted as a current sink distorting measurements and affecting the SN ratio. This was particularly true for the parabolic agitator due to its bulky design.

9.3.5.2 The Fix

The connectors were rewired to ITS specifications and all planes were grounded into the process fluid. The metal support rings were replaced with plastic and the agitators were powder coated with a hard plastic insulated finish as shown in Figure 9-2. On completing these modifications the unit was successfully commissioned with excellent stability and low SN ratio in all planes.

9.3.6 Demonstration Trials

Following the successful commissioning of the electrical tomography sensor, a demonstration to the supporting industrial companies was arranged for 14th Dec. 2000 with subsequent tests on Dec. 21st.

For the dual agitator set-up, eight tests were performed as detailed in Table 9-1.

Test	Description
Test 1	No agitation. Air injected into water through sparge ring with 4 gas injection points at increasing gas flow rates and then injected through central sparge pipe at maximum flow rate ($v_S \approx 0.1$ m/s)
Test 2	High conductivity tracer($\sigma \approx 0.1$ S/cm) added at liquid surface while agitating at 90 rpm. $P/V \approx 0.1$ kW/m^3.
Test 3	High conductivity tracer($\sigma \approx 0.1$ S/cm) added at feed pipe close to lower impeller while agitating at 90 rpm.
Test 4	Air injected at 150 l/min into surfactant/water, while agitating at 300 rpm. Average gas hold-up = 23.4 %; $P/V \approx 5$ kW/m^3; $v_S \approx 0.01$ m/s, i.e. operation in the bubble regime.
Test 5	High conductivity tracer ($\sigma \approx 0.1$ S/cm) added to gas-liquid mixture (average gas hold-up = 23.4 %) at liquid surface while agitating at 300 rpm. Hydrodynamics as for test 4.
Test 6	High conductivity tracer added to gas-liquid mixture (average gas hold-up 40 %) at feed pipe close to lower impeller while agitating at 300 rpm and 1m^3/minute gas injection rate. $P/V \approx 5$ kW/m^3; $v_S \approx 0.07$ m/s, i.e. operation in the heterogeneous regime.
Test 7	Gas injection through central sparge at maximum ($v_S \approx 0.1$ m/s) whilst agitating at 360 rpm. Measured steady-state hold-up by tomography in 8 planes. Average gas hold-up $\approx$ 50 %, $P/V \approx 8.5$ kW/m^3. Operation in the heterogeneous regime
Test 8	High conductivity tracer ($\sigma \approx 0.1$ S/cm) added at feed pipe close to lower impeller while injecting through central sparge at 1 m^3/minute ($v_S \approx 0.07$ m/s) and agitating at 360 rpm. Tomography trace for bottom plane 8 only. Average gas hold-up $\approx$ 40 %, $P/V \approx 8.5$ kW/m^3. Operation in the heterogeneous regime

Table 9-1: Test schedule for demonstration

9.3.7 Results

Results from all the tests were promising with some qualifications. Initially as the gas flow rate was increased in test 1, regions of gas were identified above each of the four-sparge pipes. When the gas was switched to a central injection point a large central column of high gas hold-up was measured throughout the vessel. Figure 9.3 is two tomographic images from plane 5: the first when the air was sparging through the ring distributor with 4 outlets and the second when the gas inlet was switched over to a central injection point.

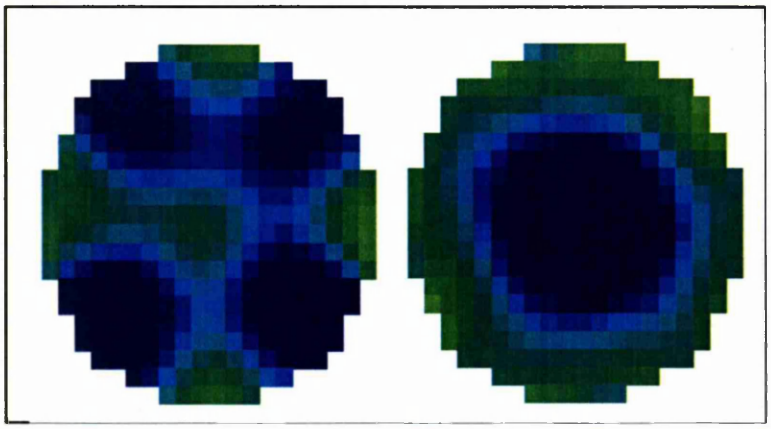

Figure 9-3: Gas sparging with no agitation

Test 2 and test 3 was carried out at the maximum sampling rate of 15 frames per second for a single 16-sensor plane, for the settings used. The results indicated that this rate was unlikely to be fast enough to follow a fast mixing process using all 8 planes. For 8 planes the whole system was sampled every 0.53 seconds. Hence the initial mixing process was completed in about four measurement cycles. Figure 9-4 depicts a sequence of two measurement sets following the addition of high conductivity tracer near lower impeller for test 3. Rates of 20 ms per plane are claimed, so clearly the system was not fully optimised. Note that although the tracer was added at the side of a radial impeller, the radial mixing is surprising poor. The mixing in the axial plane is much faster.

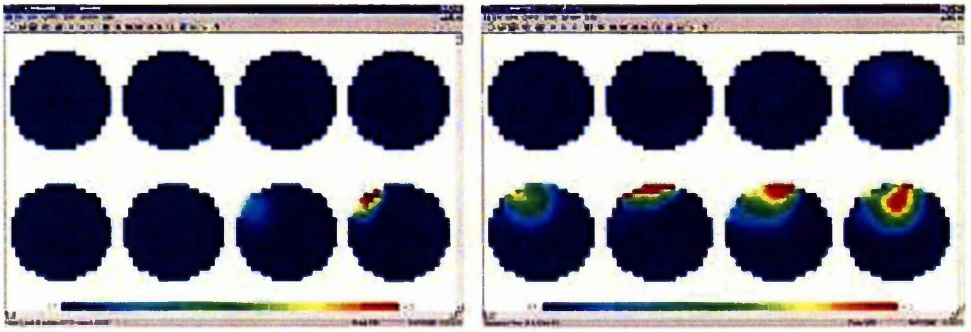

Figure 9-4: Sequence of two measurement sets following the addition of a high conductivity trace near the lower impeller (time interval approximately 0.5 s).

Figure 9-5 illustrates some of the measurements from test 4. The first window is a tomogram of liquid being agitated at 300 rpm with no gas injection. The presence of an air vortex is being detected in planes 1, 2 and 3 due to surface entrainment. The second window shows the distribution of gas in the liquid at the same agitation rate. As expected there is a gas lean area in the centre of the tank base (the gas was being injected through the ring sparger with 4 injection points). Interestingly there is also gas lean region in the centre of the vessel at planes 3 and 4. This is just above the top impeller.

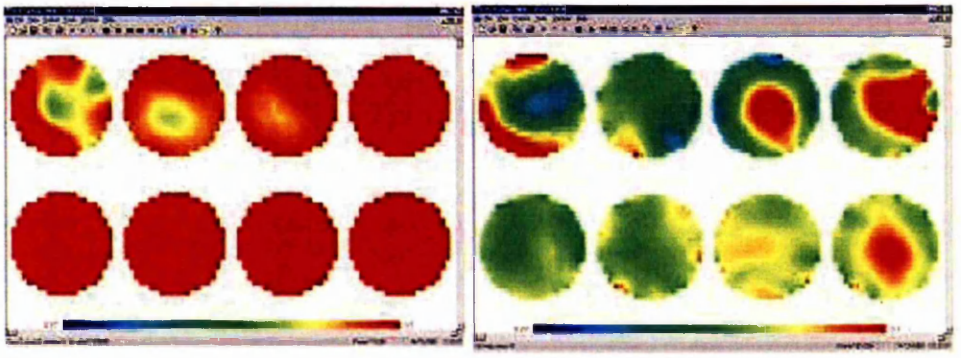

Figure 9-5: Tomographical images of (left) liquid and (right) gas-liquid mixing at 300 rpm. Overall gas-liquid hold-up for the gas-liquid case was 23.4%. Operation was in the bubble regime.

Tests 5 and 6 yielded a similar picture to Tests 2 and 3. They reveal some interesting data regarding the axial/radial mixing patterns, but the mixing is too fast for a complete picture. In order to yield information for very fast mixing processes with this system, the sample rate needs to be optimised to the maximum, or sample fewer sensors either by decreasing number of planes or the number of sensors in a plane.

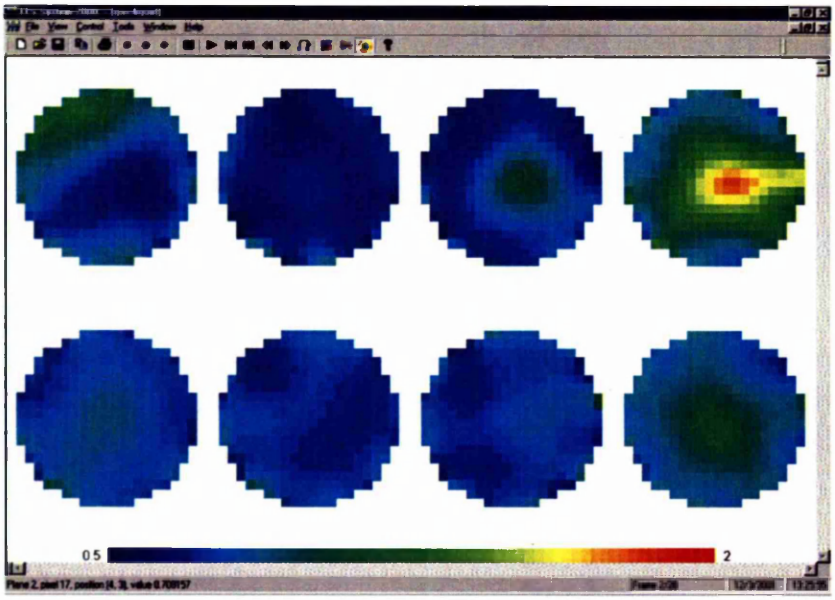

Figure 9-6: Tomographic images for mixing at 360 rpm. Overall gas hold-up 50%. v_S = 0.1m/s

Results for test 7 are shown in Figure 9-6. These are for steady-state operation at high power inputs (approaching 10 kW/m^3) and high gas hold-up (50 %) in the heterogeneous regime. Gassing patterns are similar to the gassing picture in Figure 9-5 for operation in the homogeneous regime but the range of electrical resistivities is much larger.

Test 8, following the mixing at the bottom plane for intense operating conditions, is depicted in Figure 9-7. The 6 images are at intervals of 0.33 seconds after addition of tracer at bottom plane. This mixing is almost complete after 2 seconds

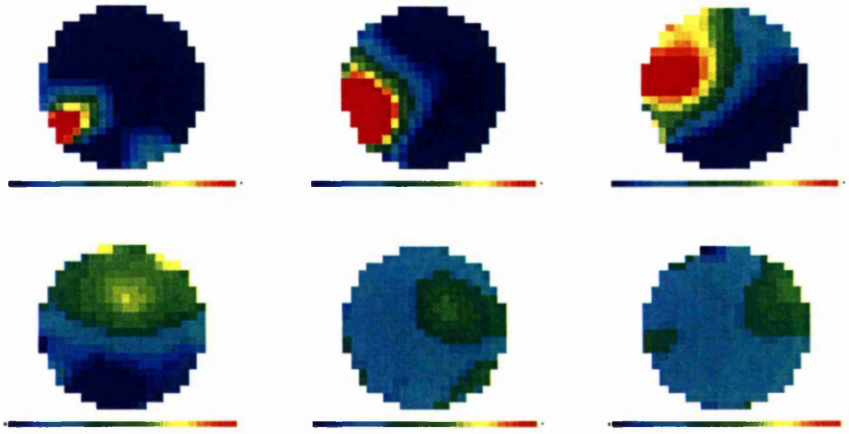

Figure 9-7: Sequential mixing of tracer in the bottom plane. Addition is top left. There is a 0.33 s time interval between images.

For a single agitator in a high aspect ratio vessel (case ii), the overall mixing rate is much slower and can be followed by the full array of sensors. The tests done provided an interesting comparison of injection points; on the liquid surface far from the impeller or below the surface close to the impeller. Figure 9-8 compares the two cases. The plots show the mean conductivity values (calculated from the reconstructed images) for all 8 planes during the two tests. It can be seen that the injection point close to the impeller ensured a quicker mixing time than injection on the liquid surface as well as smaller peak values. Mixing times can be estimated from these plots.

9.3.8 Conclusions and Further Work

The technique is clearly demonstrated to be applicable at high specific power inputs and phase fractions. Some optimisation is required for monitoring very fast mixing events either by optimising the sampling time and/or by selection of sampling planes. It is planned to use the system to aid the optimisation sparge and feed systems on specific reactor system.

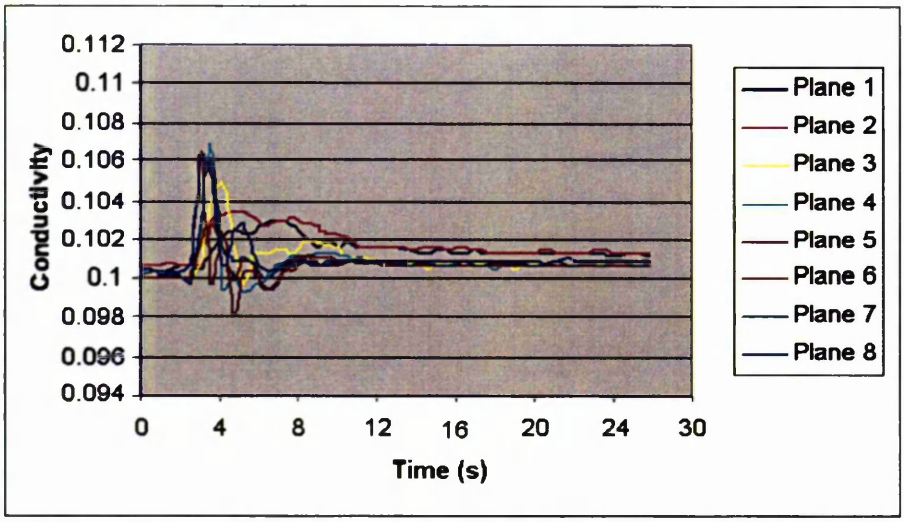

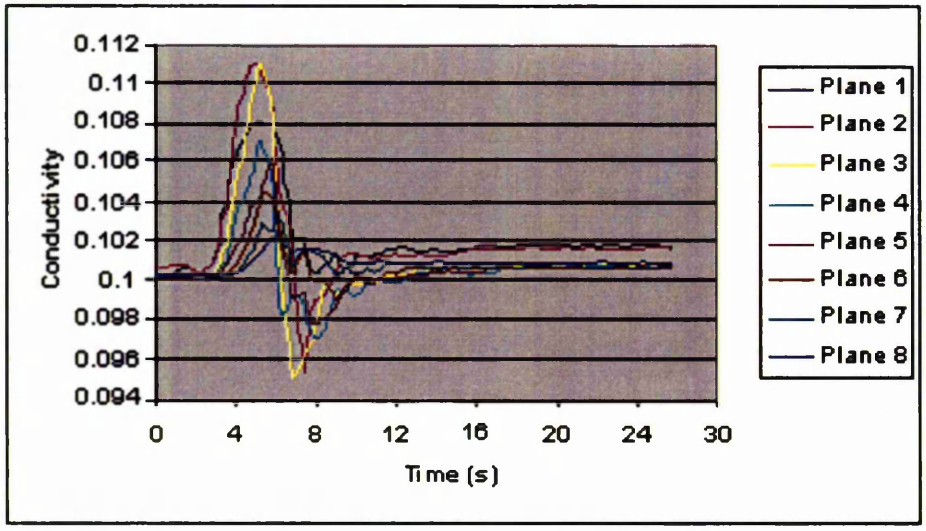

Figure 9-8: Mean conductivity values at each measurement following addition of high conductivity pulse (top) addition near impeller, (bottom) on liquid surface

: An Electrical Resistance Tomography (ERT) System as a Diagnostic Tool

9.4: Determination of the Radial Sensitivity and 3*D* Effect in an 8-plane ERT Sensor Arrangement Fitted to a Stirred Tank

The previous section was concerned with demonstrating that the technique is applicable to investigation of intense mixing. This section is concerned with the determination of the spatial resolution and radial sensitivity of the reconstructed images. The main aims here are to determine the extent to which the reconstructed images are affected by the 3*D* distribution of the actual electric field within each electrode ring and also to establish the limits of detection.

9.4.1 Introduction

Electrical Resistance Tomography (ERT) has been employed as a measurement and visualisation tool for the investigation of mixing processes. The sensor commonly comprises up to eight electrode rings each with 16 electrodes. In most applications, measurements are made between electrodes within each ring and no measurements are made between electrodes in different rings. Image reconstruction algorithms based on two-dimensional (2D) electric field simulations are adopted. In order to obtain three-dimensional (3D) representations of the conductivity distribution (and hence, for example, gas hold-up distribution) reconstructed images from each measurement plane are stacked together and a linear interpolation performed between adjacent planes.

The reconstructed 2D images are affected by the 3D distribution of the actual electric field within each electrode ring. This experimental programme investigates the extent of these 3D effects when using an image reconstruction scheme based on 2D electric field simulation and the sensitivity within a measurement plane. It has been reported by Wang (1999) that ERT sensors

are more sensitive to changes in conductivity the nearer these changes are to the electrodes

9.4.2 Experimental Equipment

A photograph of the internal of the stirred tank fitted with the ERT sensor is shown in Figure 9-1. The sensors were connected to an ITS P2000 ERT instrument and a laptop computer. During these experiments the impeller shaft was removed. The vessel had an internal diameter of 0.61 m.

Four spherical objects were used during these tests although one of these was found to be below the detection level of this sensor. The objects and their characteristics are listed in Table 9-2.

Object No.	Material	Diameter, mm	Conducting/ Non-conducting	Comments
1	Stainless steel	76 (3 inch)	Conducting	
2	Stainless steel	25 (1 inch)	Conducting	
3	Golf Ball	42.7	Non-conducting	
4	Ceramic	25 (1 inch)	Non-conducting	Below detection level

Table 9-2: Spherical object details

Photographs of the spherical objects are shown in Figures 9-9 and 9-10.

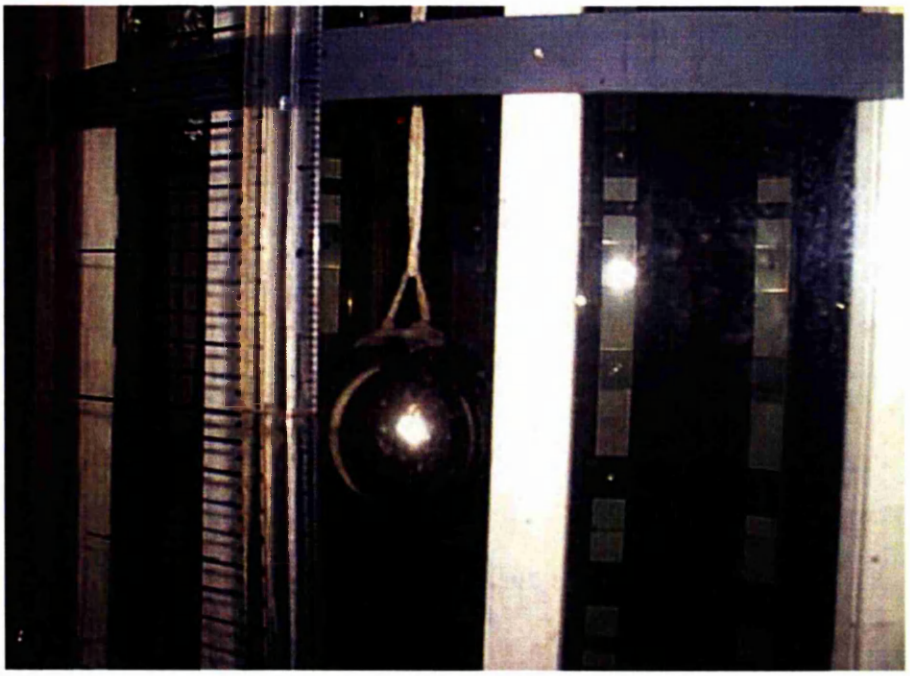

Figure 9-9: Large ball suspended in vessel

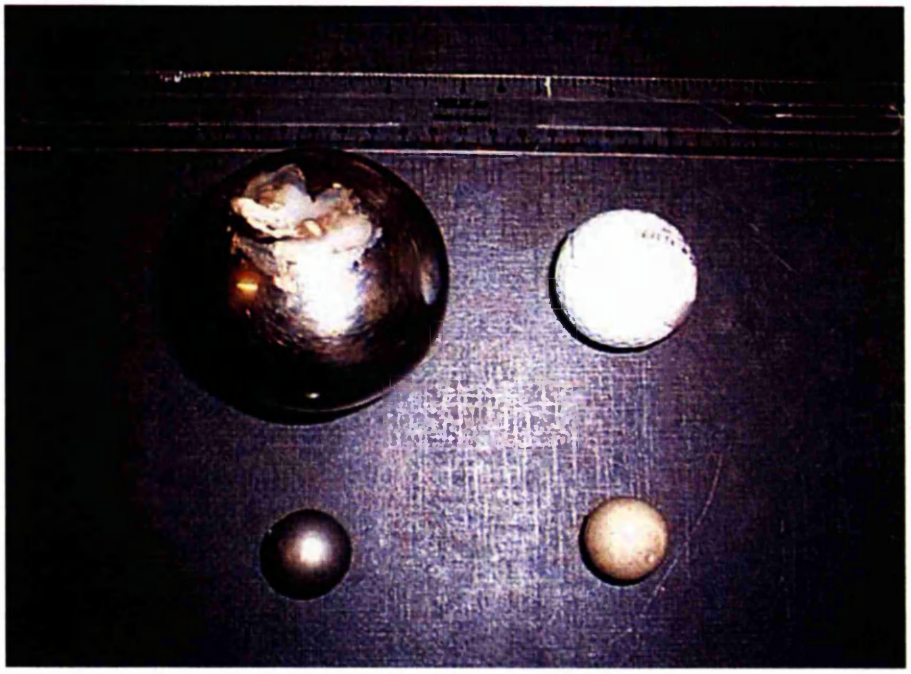

Figure 9-10: Balls used in test

9.4.3 Procedure

Each sphere was suspended by thin thread from a support bar placed across the top of the stirred tank. Figure 9-11 is a schematic of the experimental set up. Two data sets were collected for each object; one for the object located in measurement plane 5 and one for the object located mid-way between measurement planes 4 and 5. For each data set 5 measurements were taken for each of the eleven radial positions along a diameter of the vessel as indicated on Figure 9-13. These were 6. 10, 15, 20, 25, 30, 35, 40, 45, 50 and 54 cm from the edge of the tank adjacent to electrode 5 along a virtual diameter joining electrodes 5 and 13. It can be seen that the eleven positions are not quite symmetrical about the centre of the vessel, for example the position nearest to electrode 5 is 3.7 cm from the electrode whereas the position nearest to electrode 13 is 4.7 cm from the electrode. The electrodes are offset from the wall of the tank by 2.3 cm as shown in Figure 9-12.

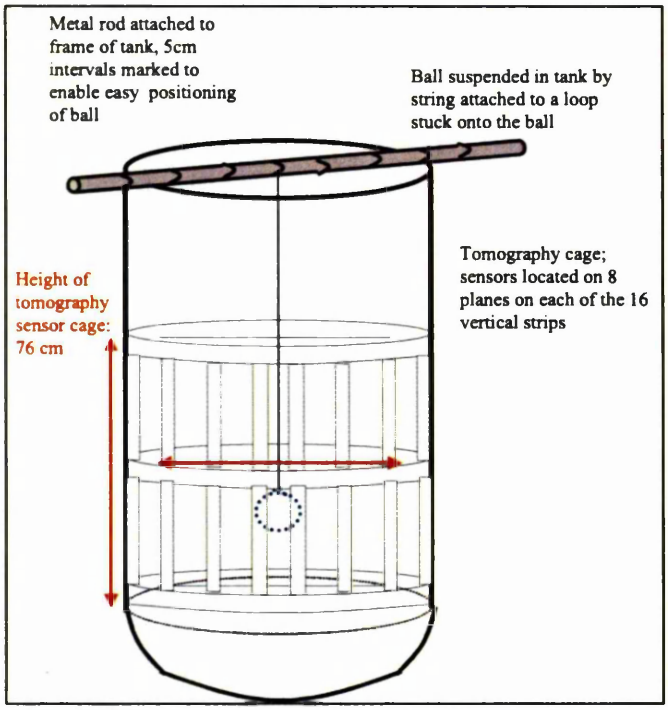

Figure 9-11: Experimental Set Up

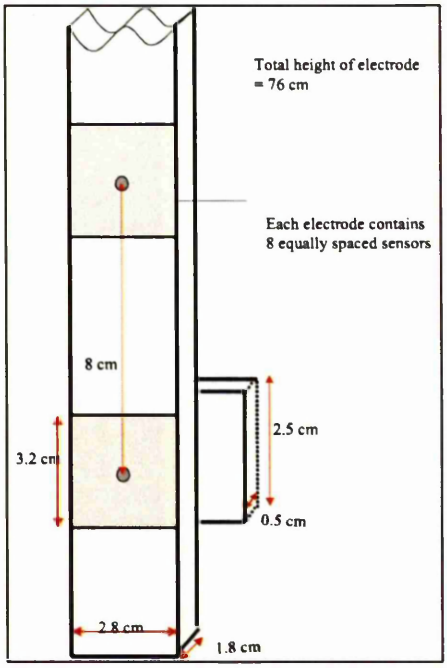

Figure 9-12: Schematic of electrode strip

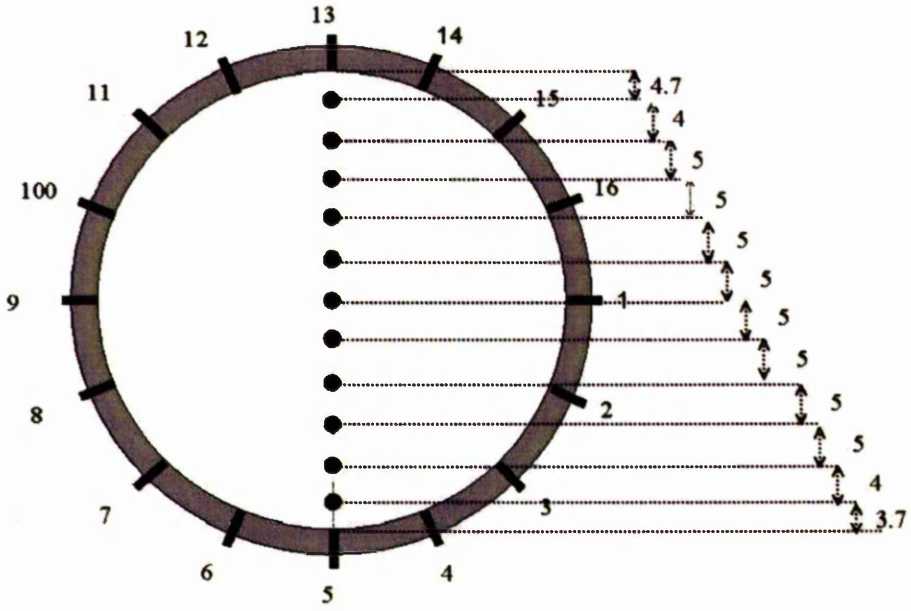

Figure 9-13: Radial positions of object within sensor

The positions of the spheres (with respect to the wall of the tank) against measurement set frame number are shown in Table 9-2. These were the same for all measurement sets.

Frames	1-5	6-10	11-15	16-20	21-25	26-30	31-35	36-40	41-45	46-50	51-55	56-60
Position		6	10	15	20	25	30	35	40	45	50	54

Table 9-2: Spherical object details: Position of spheres with measurement frame number

9 .4.4 Results

The presence of a highly conducting (or non-conducting) sphere will create a region of high (or low) conductivity on the reconstructed conductivity image. The maximum (or minimum) pixel conductivity value is likely to correspond to the pixel that represents the location of the conducting (or non-conducting) object. Therefore plots of maximum pixel conductivity for the stainless steel spheres and minimum pixel conductivity for the non-conducting sphere have been generated. The background water conductivity is defaulted to the reference value of 0.1.

9.4.4.1: 76 mm Diameter Stainless Steel Ball

Data were collected from all 8-measurement planes with the ball located in measurement plane 5 (3-inch-ss-p5, where ss signifies stainless steel and p5 is plane 5) and mid-way between planes 4 and 5 (3-inch-ss-p4-5). In both cases the quality of the data was good. The first 5 frames of 3-inch-ss-p5 (without

the ball) had maximum deviations of ± 3% with most data falling within ± 1%.

Figure-9-14 represents a time series of tomographic images from plane 5 of 3-inches-p5 as the stainless steel sphere is moved across the sensor. The colour scale represents the electrical conductivity with blue indicating low conductivity and red indicating high conductivity. The scale has been set so that the background liquid – tap water – gives a green image. The first image was taken before the object was placed in the sensor. The presence of a stainless steel sphere would be expected to result in a region of high conductivity. This occurs for all positions except when the ball is close to an electrode as observed in the second image where the region of red is surrounded by blue colouring.

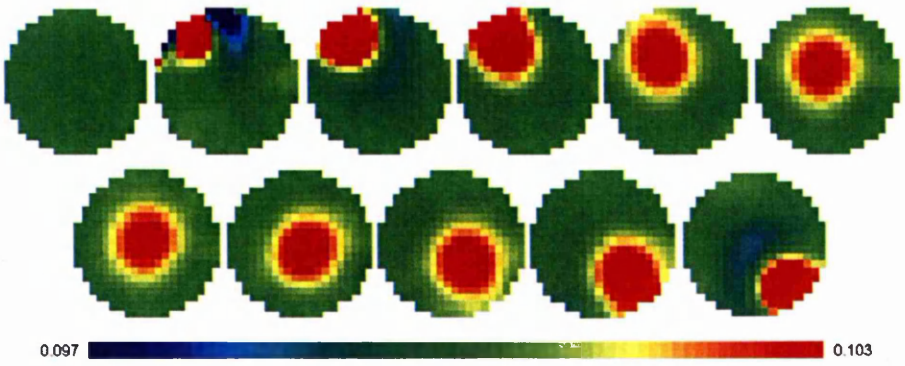

Figure-9-14: Time series of tomographic images from plane 5 as the 3 inch stainless steel ball is moved across the measurement plane

The presence of the stainless steel ball was also strongly detected by the tomographic images for planes 4 and 6 and to lesser extent planes 3 and 7.

: An Electrical Resistance Tomography (ERT) System as a Diagnostic Tool

Figure 9-15(a) is a plot of the maximum pixel conductivity for all eight of the measurement planes against measurement frame number for the 76 mm diameter stainless sphere located in measurement plane 5. The introduction of the stainless steel ball close to electrode 5 is clearly detected within measurement planes 4, 5 and 6 at frames 6-10. The maximum pixel values drops significantly at frame 11 as the sphere is moved away from electrode 5. It drops significantly again at frame 16 but remains fairly constant (and detectable) as the sphere is moved along the virtual diameter from 15 to 45 cm. Figure 9-15(b) is the same information for planes 4, 5 and 6 only. The non-symmetrical positioning of the object along the diameter between electrodes 5 and 13 is detected with higher readings for the 2 positions next to electrode 5 compared to the corresponding positions at electrode 13.

Although the ball was detected in planes 3 and 7 from the tomographic images these plots of maximum conductivity are not of a sufficient scale to show the object in these planes.

Figure 9-16(a) illustrates the maximum pixel conductivity for all eight of the measurement planes plotted against measurement frame number for the 76 mm diameter stainless sphere located mid-way between measurement planes 4 and 5. The introduction of the stainless steel ball close to the axis of electrode 5 is clearly detected within measurement planes 4 and 5 and to a much lesser extent plane 3 at frames 6-10. The maximum pixel values drops significantly at frame 11 as the sphere is moved away from electrode 5. It drops significantly again at frame 16 but remains faitly constant (and detectable) as the sphere is moved along the virtual diameter from 15 to 45 cm. Figure 9-16(b) shows the same information for planes 4 and 5 only. The presence of the ball was detected strongly in planes 3 and 6 and to lesser extent in planes 2 and 7 from the tomographic images.

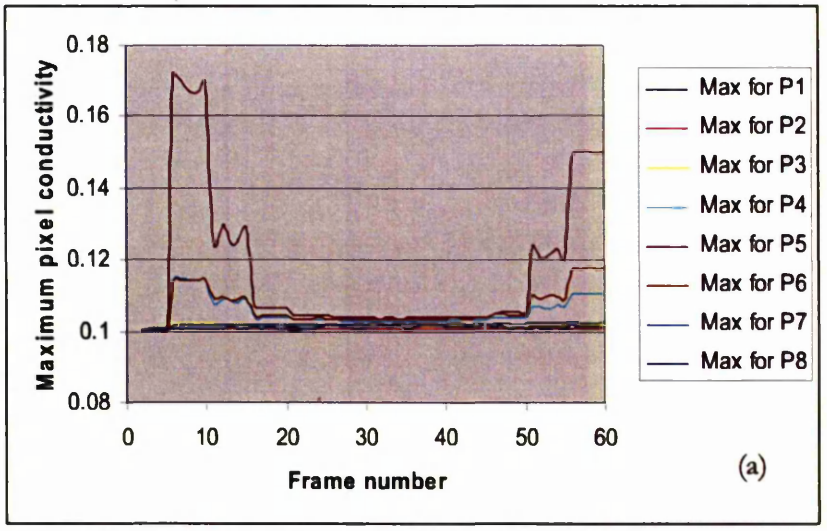

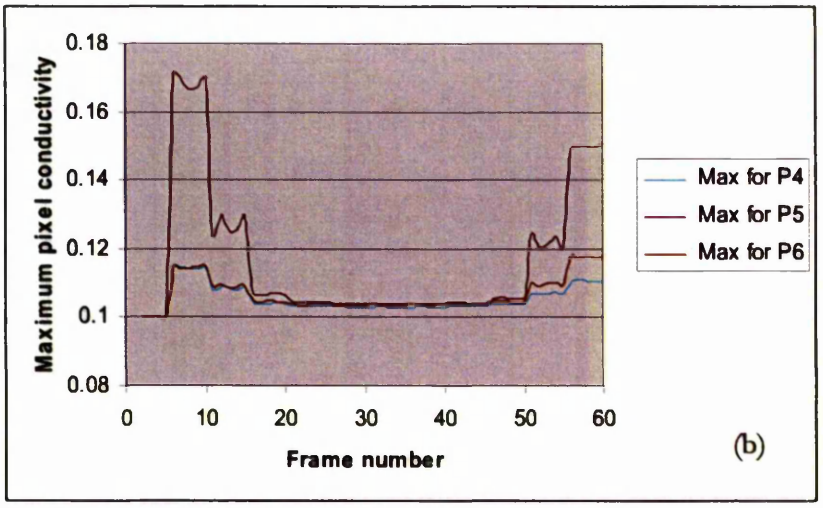

Figure 9-15: Maximum pixel conductivities with 76 mm stainless steel sphere suspended in measurement plane 5 for (a) all measurement planes and (b) measurement planes 4, 5 & 6

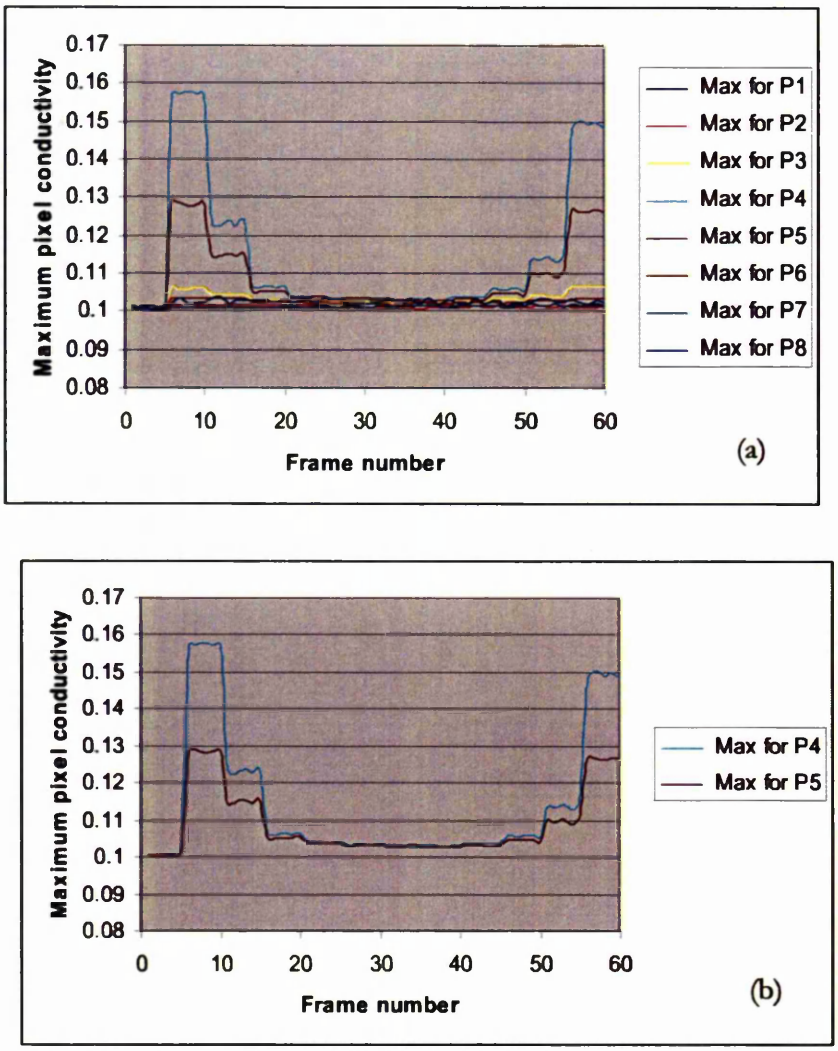

Figure 9-16: Maximum pixel conductivities with 76 mm stainless steel sphere suspended between measurement planes 4 & 5 for (a) all measurement planes and (b) measurement planes 4 & 5

Figure 9-17 is a 3D representation of the ball within the 8-plane sensor, obtained by stacking the 8 image 'slices' together and performing a linear interpolation between adjacent images to correct for the geometry of the sensor. An iso-surface has been defined which joins together all pixel conductivity values of a certain value and above.

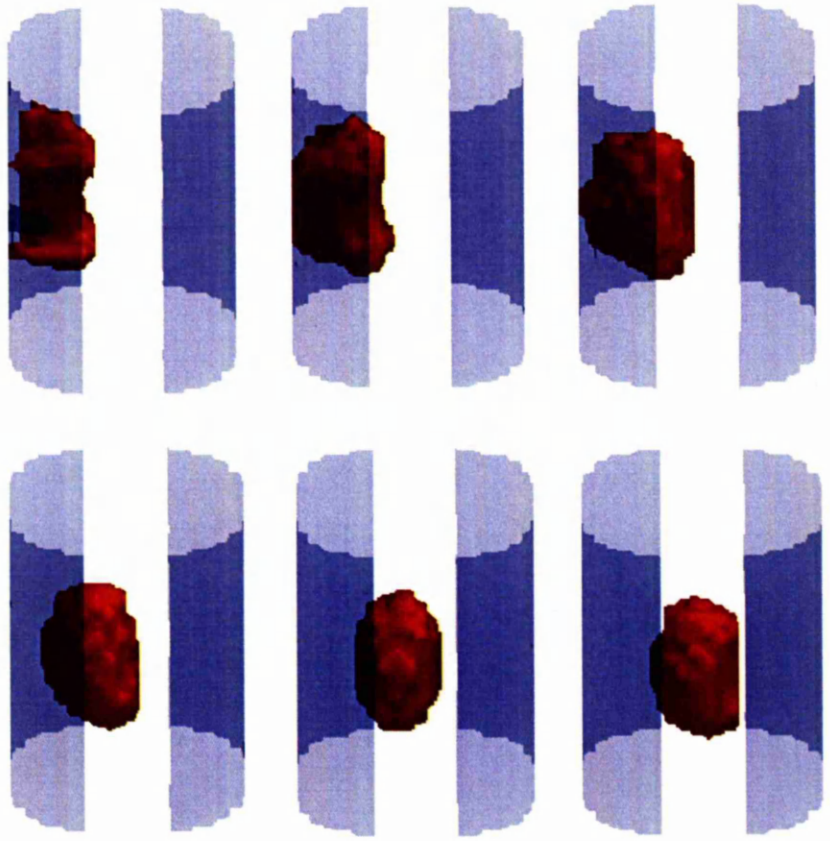

Figure 9-17: 3-*D* images of the sensor showing the ball in the first six positions

9.4.4.2: 25 mm Diameter Stainless Steel Ball

Data were collected from all 8-measurement planes with the ball located in measurement plane 5 (1-inch-ss-p5) and mid-way between planes 4 and 5 (1-inch-ss-p4-5). In both cases the quality of the data was good. The first 5 frames of each measurement set (without the ball) showed maximum deviations of ±2% with most data falling within ±1%.

Figure 9-18(a) is a plot of the maximum pixel conductivity for all eight of the measurement planes against measurement frame number for the 25 mm

diameter stainless sphere located in measurement plane 5. The introduction of the stainless steel ball close to electrode 5 is clearly detected within measurement planes 4, 5 and 6 at frames 6-10. The maximum pixel values in plane 5 drops significantly at frame 11 as the sphere is moved away from electrode 5. It drops significantly again at frame 16 but remains fairly constant and just above the detection threshold of the instrument as the sphere is moved along the virtual diameter towards electrode 13. Figure 9-18(b) depicts the same information for planes 4, 5 and 6 only.

The tomographic images from this measurement set start with the ball located next to electrode 5 in planes 4, 5 and 6. However, when it is first moved at frame 11 it is barely detected in planes 4 and 6 but remains detectable in plane 5. After this the ball is not detected from the images.

Figure 9-19(a) shows the maximum pixel conductivity for all eight of the measurement planes plotted against measurement frame number for the 25 mm diameter stainless sphere located mid-way between measurement planes 4 and 5. The introduction of the stainless steel ball close to the axis of electrode 5 is detected within measurement planes 4 and 5 at frames 6-10. The maximum pixel values drops significantly at frame 11 as the sphere is moved away from electrode 5 and is no longer detectable from this data until it is near to electrode 13. Figure 9-19(b) shows the same information for planes 4 and 5 only.

There is significant noise on this data. Taking a running average could smooth this.

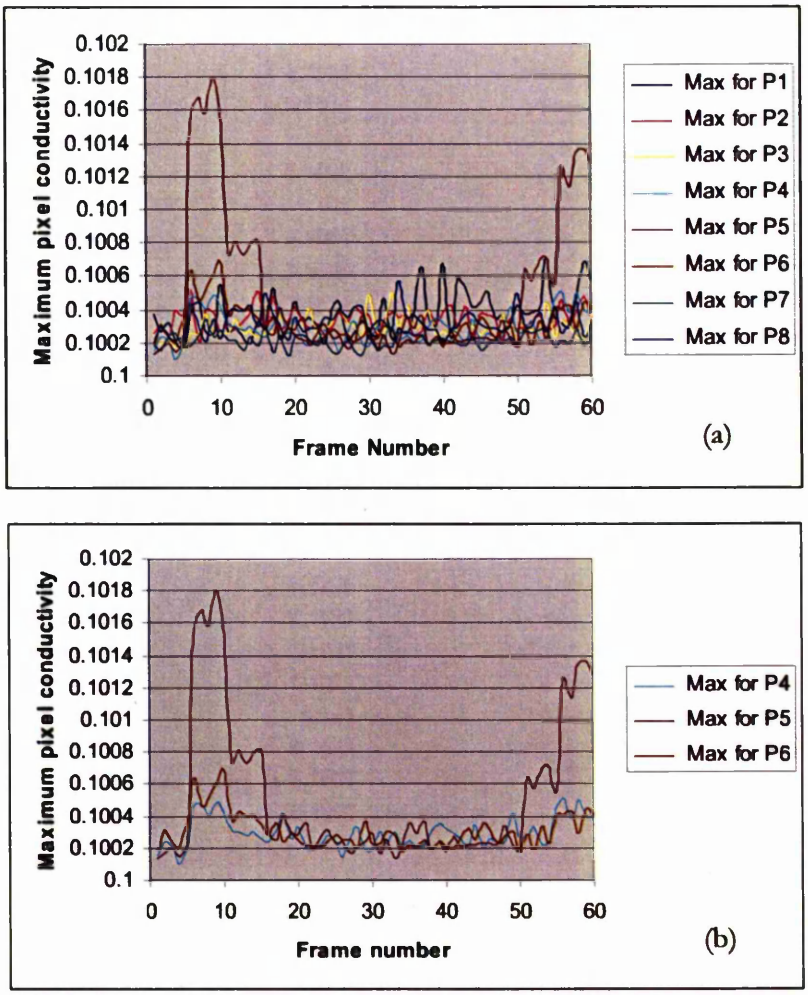

Figure 9-18: Maximum pixel conductivities with 25 mm stainless steel sphere suspended in measurement plane 5 for (a) all measurement planes and (b) measurement planes 4, 5 & 6

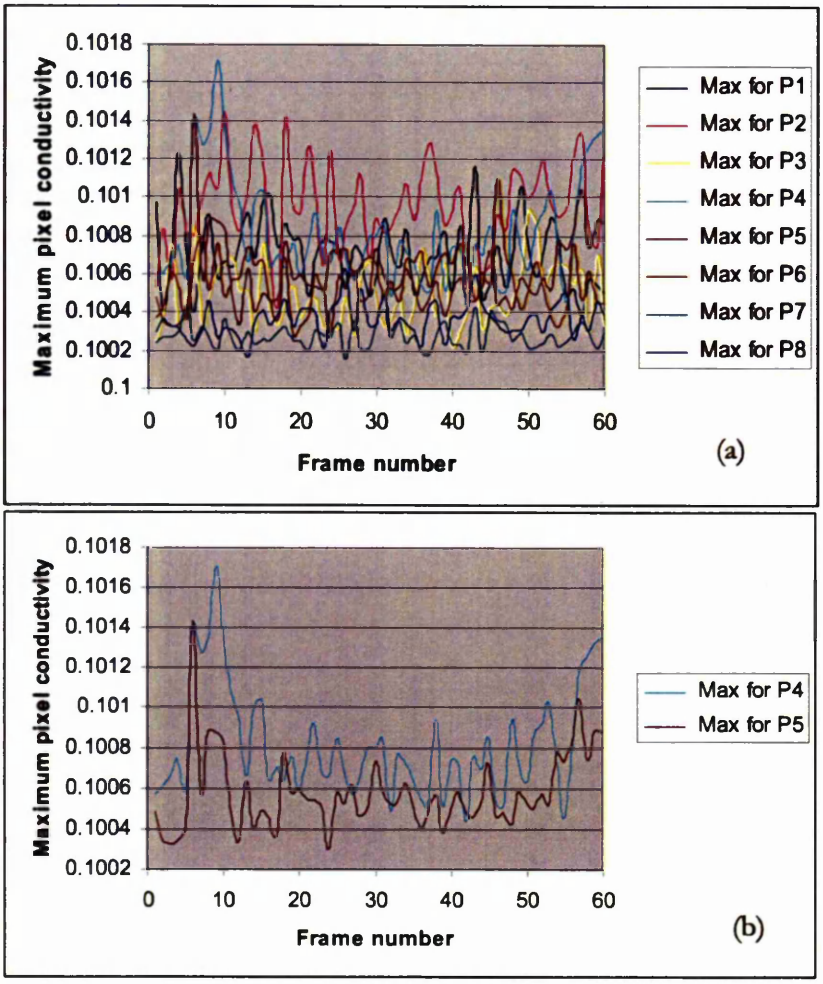

Figure 9-19: Maximum pixel conductivities with 25 mm stainless steel sphere suspended between measurement planes 4 & 5 for (a) all measurement planes and (b) measurement planes 4 & 5

9.4.4.3: 42.7 mm Diameter Golf Ball

Figure 9-20(a) is a plot of the minimum pixel conductivity for all eight of the measurement planes against measurement frame number for the golf ball located in measurement plane 5. The introduction of the golf ball close to electrode 5 is clearly detected within measurement planes 4, 5 and 6 at frames 6-10. The minimum pixel values increases significantly at frame 11 as the sphere is moved away from electrode 5. It increases significantly again at

frame 16 but remains fairly constant (and detectable) as the ball is moved along the virtual diameter from 15 to 45 cm. Figure 9-20(b) shows the same information for planes 4, 5 and 6 only.

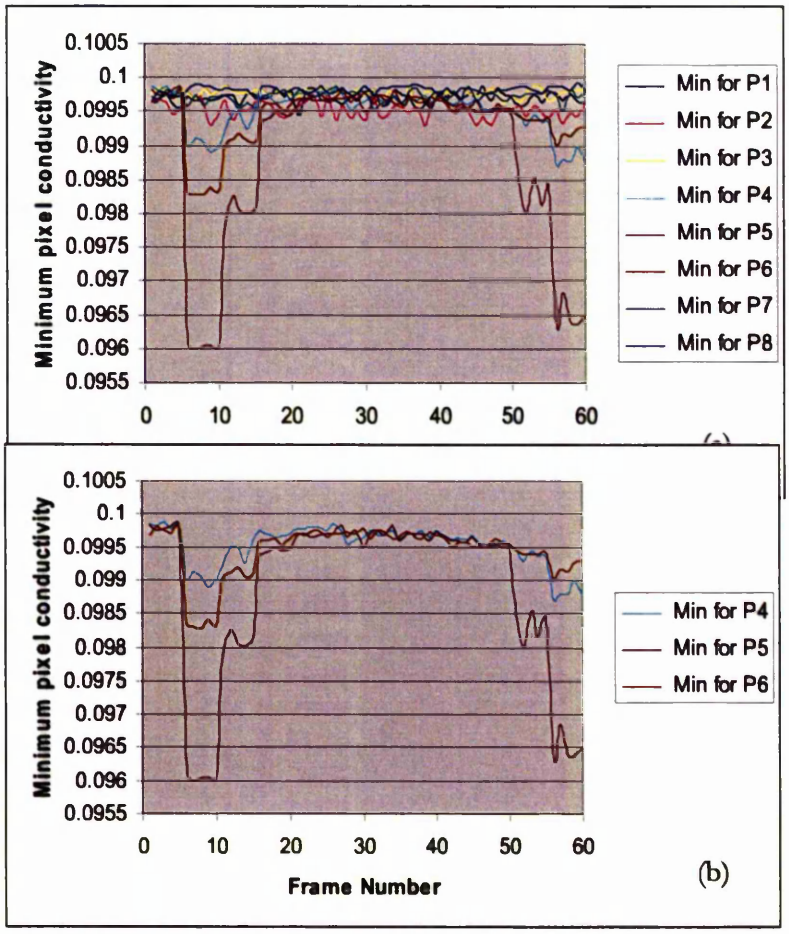

Figure 9-20: Minimum pixel conductivities with golf ball suspended in measurement plane 5 for (a) all measurement planes and (b) measurement planes 4, 5 & 6

Figure 9-21(a) depicts the minimum pixel conductivity for all eight of the measurement planes plotted against measurement frame number for the golf

ball located mid-way between measurement planes 4 and 5. The introduction of the golf ball close to the axis of electrode 5 is clearly detected within measurement planes 4 and 5 at frames 6-10. The minimum pixel values increases significantly at frame 11 as the ball is moved away from electrode 5. It increases significantly again at frame 16 and is no longer detectable from this data as the sphere is moved along the virtual diameter from 15 to 45 cm.

Figure 9-21(b) shows the same information for planes 4 and 5 only.

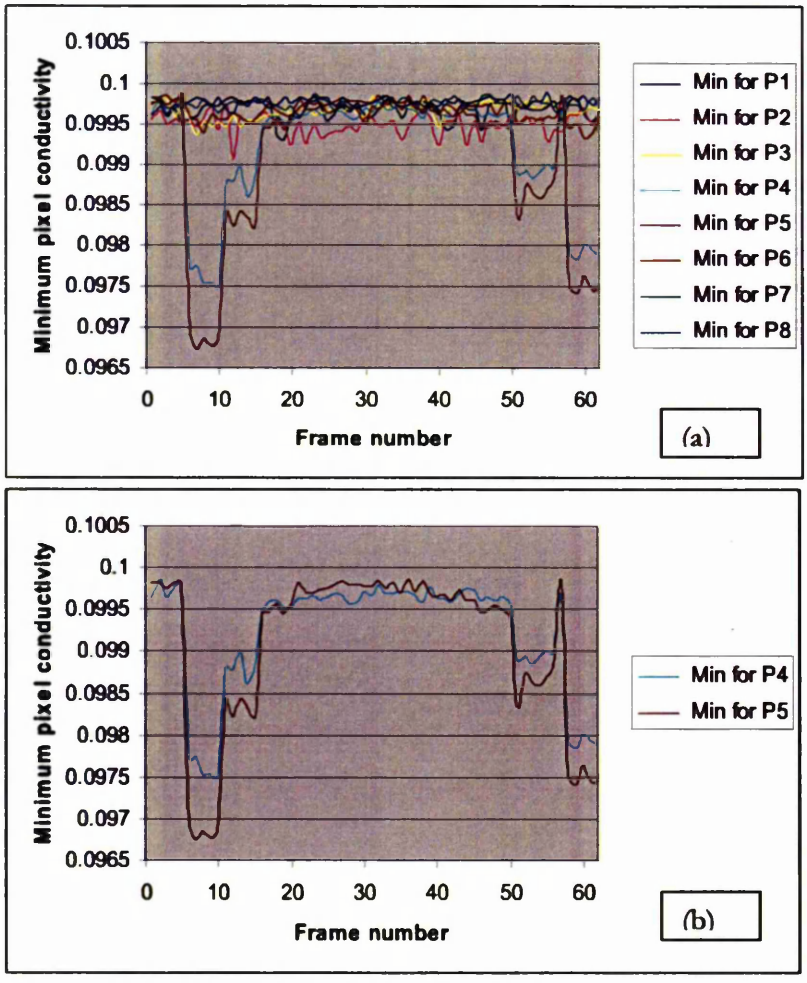

Figure 9-21: Minimum pixel conductivities with golf ball suspended between measurement planes 4 & 5 for (a) all measurement planes and (b) measurement planes 4 & 5

9.4.5 Conclusions

The 25 mm diameter highly conducting sphere was clearly detectable in the location plane at all positions across the vessel. This represents a detection limit down to at least 4.2% of the vessel diameter. The maximum conductivity is highest close to the sensor and drops (though still detectable) towards the centre.

The 42.7 mm diameter non-conducting sphere (golf ball) was also clearly detectable in the location plane at all positions across the vessel. This represents a detection limit down to at least 7% of the vessel diameter. The minimum conductivity is detected close to the sensor.

The 25 mm diameter (4.2% of the vessel diameter) non-conducting sphere (ceramic) was below the limit of detection. Therefore the limit of detection for a non-conducting sphere is in the range 4.2 to 7%.

From the above it can be seen that the limits of detection are influenced by the conductivity contrast between the background and the object, and the distance of the object from the sensor.

Some blurring of the images, due to 3-*D* effects, is apparent. Even the smallest object tested was detectable in the adjacent planes. However this appears to be fairly constant across the vessel diameter and the size of the image is approximately constant across the diameter of the vessel.

The size of an object that can be resolved by a 8 x 16-electrode array depends on the scale of operation. In sizing the electrodes, care was taken to scale-up the area of the sensors with the vessel size. Assuming a 5 % of the vessel diameter resolution, a similar scaled array on a 5 m diameter vessel would only resolve individual objects or clumps to 0.25 m. In order to "see" very small "clumps" requires work on a very small scale or an increase in the number of sensors. Increasing the number of electrodes would mean the electrode size

has to be reduced which may make it difficult to resolve the electric fields. The inability to "see" to the centre of the vessel could be improved by utilising sensors in the centre either by using the shaft as an electrode or by mounting electrodes on a sleeve surrounding the shaft.

Chapter 10 : Summary, Main Conclusions and Suggestions for Further Work

10.1: Summary

The thesis was introduced by a description of the authors 24 years experience in industry working on mixing and multi-phase reactor design problems. Its theme is the design of contactors and reactors with "Attitude". The general aim of that work was to identify where and how fluid flow phenomena such as mixing, multi-phase dispersions and separations were influencing chemical reactions or other process requirements and optimise those to the benefit of process performance, safety and cost.

The thesis itself builds on that experience through commercially sensitive work carried at UMIST. This makes the thesis somewhat different from typical sponsored research theses. The work going into this thesis comprises a number of discrete research programmes in the area of experimental fluid dynamics that were fully defined by discussion and agreement between the companies and UMIST before commencement. Although confidentially agreements prevent the discussion of commercial sensitive information some overall description of the type of processes worked on and how these problems were tackled and in particular to how they relate to the material in this thesis are helpful to put the work in perspective.

The work pertains to the design of large-scale plant, in particular to the reactors that are at the core of the processes. More than one process is involved. These are multi-phase, boiling gas-liquid-solid reactions and involve corrosive and/or toxic chemicals. Gas rates are high, typically with mean superficial gas velocities in the order of 0.15 m/s. The reactions are known to be sensitive to local concentrations of species transferred from the gaseous

phase. The reactor product distributions are also known to be mixing sensitive such that local concentrations of reaction species affect the yield.

The information required is how best to configure such reactors so that:

- Gas-liquid mass transfer rates are optimised
- Liquid phase mixing time is minimised
- Feed and take-off positions are optimised to minimise local concentration gradients whilst avoiding bypass.

Other information typically required is:

- The number of feed pipes required to achieve a good approach to homogeneity
- The power-draw for all agitators under 3-phase conditions at plant operating conditions
- Overall gas hold-up under a range of operating conditions
- The distribution of gas under a range of operating conditions as a function of agitator types and sparge pipe geometry.

The starting point for any such study is data about the reacting system. Hence the Buchi rig, Chapter 5 is a key part of the investigation. In the studies reported here, results for pure solvents are described. However, this work can be (and was) extended to look at reactor mother liquors. These data are not included for commercial reasons. The work yields valuable data about dense phase bubble sizes, dense-phase bubble hold-up, bubble rise velocities and the superficial gas velocity at the homogeneous to heterogeneous transition. These investigations also revealed that some of these systems tended to foam and this prompted work on looking at agitator types and positions to minimise foam (Chapter 7, section 7.4.3) and spinning cones as a foam and level control device (Chapter 8).

: Summary, Main Conclusions and Suggestions for Further Work

Gas hold-up for the reacting system was high (from information gleaned from the Buchi work and confirmed by reactor radio-active scans), typically 50% overall. Therefore, to investigate how this affected agitator power draw, cold model analogue fluids were required. Polypropylene glycol (Molecular weight =2025) had been previously used by the author as antifoam and this agent had been noted to increase gas-hold-up (Cooke *et al.* 1988). The temperature dependency of gas hold-up behaviour for this surfactant makes it a useful choice for cold modelling of different boiling reaction mixtures producing a range of gas hold-ups, when scaled at constant Fl and agitator ε_T (Chapter 4, section 4.4).

It was clear from the Buchi work that at typical reactor superficial gas velocities, the systems of interest are heterogeneous. Much of the literature on mechanically agitated vessels deals with air-water systems at superficial gas velocities below the transition (in the bubble regime) so the studies reported in Chapter 5 on the hold-up behaviour under heterogeneous conditions are new and original work.

Similarly, the need to suspend solids and disperse gas whilst mixing rapidly at high phase fractions called for the exploration of new agitator configurations such as the HBT and 6MFU combinations and the multiple Lightnin A345 for these extreme duties (see Chapters 6 and 7). Again, in these chapters, techniques and results pertinent to these measurements are described and the results are presented for power, hold-up gas-liquid mass transfer and mixing times.

The use of ERT to study mixing and gas-phase distributions (Chapter 6, section and Chapter 9) had never previously been reported for these extreme conditions of heterogeneous operation at high ε_T and phase fractions.

In all cases the work commenced with the assembly of as much relevant data as possible and agreed programme of work with clear objectives and milestones.

: Summary, Main Conclusions and Suggestions for Further Work

The thesis contains a lot of information. To be useful this has to be retrievable. The literature review is extensive and mostly confined in a single chapter. This thesis deals with the design of multiphase contactors and reactors with "Attitude" so is concerned with exploring "difficult" designs: large scale, high phase fractions, rheologically complex, high superficial gas velocities and specific agitator power input. A lot of the information is the form of working spreadsheets and data. These may well be of value of the reader and are included in the attachment CD in folders that are self-explanatory. A list of these folders is given in Appendix 9.

This thesis is probably best summarised as a practical man's guide to multi-phase reactor design and mixing area, and by that I would wish the reader to infer it to be written by a person who would be happier described as an experimentalist than a true theoretician. Because of the broad scope of this work and the need to protect commercially sensitive information, many facets are covered as snapshots rather than highly detailed studies and in that respect there is probably scope for several research projects to add flesh and fundamental understanding to many of the areas covered in this work and some of these are detailed in the following discussions.

10.2: Some Successes.

Major successes include the following:

- The development of cold model fluids for boiling systems allowed data on accurate gassing factors for plant design to be obtained on the models at the same gas flow number, gas hold-up and ε_T as the operational plant reactors even at the high phase fractions.
- Understanding how solids affect the dense-phase gas hold-up (and thereby the total gas hold-up) allows the operating gassing factor to be adjusted for solids loadings.

- The effect of scale and blade-geometry on power numbers was evaluated for the hollow blade turbines (equation 6.14) giving increased confidence on scale-up.
- A number of major manufacturing plants have agitator designs based on this work and are operating successfully. The work contributed to a patent, [Bickham *et al.* 2003, USA patent number 10/443542] for large-scale reactor technology that is successfully licenced worldwide.
- Spinning cones for foam control, were successfully trailed at pilot plant level by Novozymes. (Stocks *et al.* 2005).

10.3 General Conclusions and Design Recommendations

The design of multiphase reactors operating at high specific power inputs up to 10 W/kg and superficial gas velocities >0.1 m/s offer a special challenge. For gas dispersion the shortcomings of the Rushton turbine have long been recognized since the gassing factor drops significantly upon gassing to values as low as 0.2 in these intense systems (Gezork *et al.* 2000). Under these conditions solids suspension, gas dispersion, agitator pumping rates, mixing and interfacial mass transfer are all compromised.

If radial flow agitators are required it is much better to use hollow blade designs. Even at extreme conditions the gassing factors only drop to around 0.7, and the effect of minor geometry and scale on the ungassed power number are predictable (eq. 6.15). These offer similar pumping rates to the Rushton turbine when compared at the same diameter, reactor geometry and ε_T and are shown to be excellent agitators for solid suspension especially under gassed conditions.

Designs should be configured to "go with the flow". This means that liquid and gas inlets should be oriented with the direction of agitator flow. This avoids flow instabilities, wasted energy and should improve the mixing

efficiency. Where multiple agitators are used they should be chosen to give positive flow reinforcements at the interchanges. Multiple radial flow turbines should be avoided if overall liquid mixing times need to be minimized as they suffer from flow compartmentalization. The HBT turbine below a 6MFU (or another high solidity up-pumping hydrofoil) has been shown to be a good design in terms of stability, mixing, gas dispersion and solid suspension, see Chapters 6 and 7. The use of a lower radial HBT turbine is also a good design for gas-liquid mass transfer due to the excellent gas handling capabilities of these agitators (see chapter 7 section 7.5.1). Multiple high solidity up-pumping hydrofoils (for example multiple LIGHTNIN A345s) have been shown to be a good design for gas-liquid and gas-liquid-solid dispersion in terms of flow stability, (figure 6.8) solid suspension (chapter 7, section 7.6.1) and gas-liquid mass transfer (Chapter 7, section 7.5.1). They also offer significantly shorter overall mixing times than other multiple agitator designs (Chapter 6, section 6.5.1.3.2).

A high solidity up-pumping agitator operated 0.6 to 1.2 D helps to control foam by acting as a foam breaker (chapter 8, section 8.4.11).

Where minimizing overall liquid-mixing times is a required design parameter the vessel/agitator aspect ratio is shown to be important. In chapter 6, mixing times are shown to be approximately proportional to $(H/T)^2$ and $(T/D)^2$ giving an overall dependence of $(H/D)^2$. This tells the designer to consider minimizing H and maximizing D in order to minimize the mixing time. The relationships have only been tested in the ranges of $0.75T \geq H \leq 2T$ and $0.33T \geq D \leq 0.6T$.

By consideration of the agitator power equation for fully baffled turbulent flow (equation 2.11) and a dependency of mixing on $(H/D)^2$, it can be easily shown that if agitator D/T, ε_T and operating volume is maintained then changing the geometry from $H = 2T$ to $H = T$ can be expected to reduce the overall mixing time by a factor of >3. Using a bigger agitator D/T ratio at the

same ε_T is also advantageous for mixing and these also have a greater pumping capacity and therefore are better for gas and solid dispersion.

Knowledge is a key parameter in a successful reactor design. In order to understand the process you need as much information as possible. If it is an existing process, knowledge already exists. Plant managers tend to be transient and are often changed (every 3 years or so). If you are not careful you can finish up "reinventing the wheel". Often the process memory resides with an old cynical foreman "been there, bought the tee-shirt". This person has seen all the changes, knows what worked and what didn't and will have their own ideas why. Find that person and talk to them.

Knowledge is a powerful tool. It isn't gained easily; it comes from experience, experimentation, reading, listening, and learning. Experience can be a painful tutor. If you are presented a problem to solve, it is usually because there is a real need for a solution. Therefore if you present a plausible solution there is a good chance that it will be tested. In my own experience the ideas suggested that work in practice are usually accepted without fanfare. It is the ones that don't work that you hear about and those experiences can be a hard lesson. There is an old adage; "a person who never made a mistake, never did anything". However, to avoid getting caught out too many times it is necessary to think very carefully about recommendations and here knowledge and experience are critical parameters. This certainly does not mean, "sit on a fence" and avoid decisions, rather making clear judgements and recommendations in the light of carefully thought out experimentation designed on sound principles, carried out and documented meticulously.

10.4: Comments on the Experiments and Suggestions for Further Work.

10.4.1: The Hard Bits

Not all of the work went smoothly. From the study of the literature to the experiments themselves it was impossible to avoid being judgemental. Much of the literature is contradictory. The shear rates that are responsible for drop and bubble break-up is one such example. Drop and bubble beak-up depend on shear. Van't Riet (1975a) claims that the maximum shear rate, responsible for bubble break-up, occurs in the vortices behind the blades of rotating turbines and this scales with *N*. Oldshue (1983) reports the maximum shear is at the blade tips and this scales with *ND*. Shear rates at the Kolmogov scale (1946, 1949) are very high and this theory would predict the drop-size should scale at equal ε_T. However, nobody (to my knowledge) has yet produced a picture of a drop being broken by a turbulent eddy and scale-up at geometric similarity and constant ε_T results in smaller drops on scale-up. The intermittency theory (intermittent bursts of intense energy) has been introduced to explain these anomalies but a close look at the literature indicates that this theory isn't truly predictive (see Chapter 2, Sections 2.2.4.1 and 2.4.1). The experimental evidence points to the relevant scale-up relationship being geometric similarity and constant tip speed and that then is my judgement until someone comes up with a better predictive relationship.

Being judgemental is not always easy or comfortable. The Fl versus Fr relationships to describe the flooding-loading transitions has an excellent pedigree "Smith, Warmoeskerken and Nienow". The extension of the Rushton turbine equation to describe the flooding-loading transition (equation 7.5) to include the hollow blade agitators indicated that these were capable of handling a lot more gas than a Rushton turbine before flooding. This view is supported by the work of Saito *et al.* (1992) and Gezork *et al.* (2000) for the

6SRGT. The Chemineer literature claims the BT-6 will handle up to 6 times the gas of a Rushton turbine before flooding. These claims are powerfully supported by the likes of A. W. Nienow and A. Bakker.

The data in this thesis do not support that view. Equation 7.5 seriously underestimates the N required to overcome flooding (Table 7-5) for the hollow blade turbines tested here. What is found is that compared at equal D and gassing the Rushton turbine and all the various types of hollow blade agitator (including the 6SRGT) require very similar amounts of power to overcome flooding. Re-analysis of the Saito *et al.* (1992) and Gezork *et al.* (2000) data reveals that this is true for their data also.

For the work of Saito *et al.* (1992) the Rushton turbine and 6SRGT lines clearly are not coincident, though the authors assume they are. For the Gezork *et al.* (2000) data, the lines are almost coincident but the 6SRGT is a larger diameter than the 6RT. In both cases consideration of the ungassed power number, gassing factor and diameter show they draw the same power as the Rushton turbine at the flooding-loading point.

Re-examination of the Nienow (1985) data indicates that the effect of D/T on the F-L transition is closer to the view that at a constant scale of operation a given pumping rate is required to disperse a given amount of gas (first proposed by Nienow *et al.* 1985). It was shown in Chapter 2 (using published agitator flow numbers) that compared at equal D and agitation power the Rushton turbine the Scaba 6SRGT have similar pumping rates and this supports the arguments above.

It was considered whether it was worthwhile correlating all of the HBT data in the form of Fl versus Fr relationships. However the Fl versus Fr relationship can be transposed directly to a specific agitator power versus specific gas power relationship (see Chapter 7, section 7.2.2) and this fact suggests that an energy balance may be a simpler and more meaningful way of dealing with this transition. The $0.4T$ diameter Rushton turbine data of Warmoeskerken and Smith (1985), (Table 7-2) indicates an equality of gas and agitator power at the

F-L transition. A similar correspondence is found for the hollow blade agitators tested herein. To propose that for a mechanically agitated vessel at least as much energy should be input by the agitator as the gas, in order to ensure the system is not gas dominated appears self-apparent. For radial agitators of diameters < 04*T* the effect of D/T on the agitator pumping rate needs to be considered.

10.4.2: Comments on the Buchi Rig Work and Suggestions for Further Work

Chapter 5 covers an often-neglected area: the behaviour of "real" fluids under reaction conditions. Often the information available to the designer, modeller or researcher is sparse, especially if it involves corrosive and toxic chemicals at high temperature and / or pressure. A recommended first step for a gas-liquid system is to shake up some of the reactor mother liquor in a volumetric flask (providing it is safe to do so). For a boiling reaction, boiling some of the material in a glass flask in a fume cupboard can also be enlightening. Among things to note would be:

- How big are the bubbles?
- How quickly do they disengage?
- Is it frothy,
- Does it foam?

The latter can be very important, since if the high gas-phase fraction is due primarily to foaming then the residence time and productivity can be effected greatly by controlling the foaming by techniques described for example in Chapters 7 and 8.

The beauty of the Buchi rig is that it allows the study of real systems at not only reaction conditions but at scale hydrodynamic conditions which allows a step-change in perception of important design parameters such as bubble size,

bubble rise velocities gas-liquid hold-up and bubble fractions. There is a lot of mileage in this approach.

Areas worthy of further study should include the affect of solids on the gas bubble distribution and the link between the steady-state gas hold-up and the initial dynamic gas disengagement work. These areas are discussed below.

10.4.2.1: Effect of solids on the gas bubble distribution.

De Swart and Krishna (1995) showed that solids supplant small bubbles in the dense phase in bubble column reactors operating in the heterogeneous regime. This work shows the same effect occurs in mechanically stirred contactors as illustrated by Figure 5-53. The total volumetric hold-up of gas plus solid remained constant with increasing solids concentration, with the solids replacing the gas in the dense phase. The solids were 205-micron glass ballotini beads. The test fluid was a 20-ppm PPG solution that supports a large concentration of particles in the dense phase. It is interesting to speculate on the effect on other systems such as water or a 0.2 molar sodium sulphate solution where 10% by volume solids would completely supplant the gas in the dense phase, suggesting potentially a very large effect on gas-liquid mass transfer.

When the solid volume fraction is equal or greater than the saturation dense phase fraction there can be no small gas-bubbles. One might presume the fraction of solids in the dense could strongly influence gas-liquid mass transfer. At solids concentrations below the transition they may or may not influence gas-liquid mass transfer rates dependent upon bubble break-up and coalescence rates. Does this result in a gradual diminishment in mass transfer rates as the transition is approached? Is there a catastrophic fall in gas-liquid mass transfer when the dense phase is saturated with solids? Further work is highly recommended.

10.4.2.2 : Implication of Equation (5.2) $v_S = \left(\frac{dh}{dt}\right)_I$

Initial disengagement rate data is compared with the steady-state superficial gas velocity in Figure 5-52. The agreement between the initial disengagement rate and the steady-state superficial gas velocity confirms that the initial disengagement rate provides a good indication of the vessel superficial gas velocity even when applied to a mechanically agitated vessel. This provides confirmation that the dynamic disengagement technique work can be extended to the mechanically stirred reactor area. It also provides a have a way of estimating the superficial gas velocity for the boiling case. It could be extended to provide boil up rates for heat transfer calculations. This should be considered for further work.

10.4.3: Regarding Chapter 6: Single Phase Hydrodynamics

In Chapter 6 it was the mixing work that produced the most surprises and opened many potentially fruitful avenues for further work.

10.4.3.1: Effect of clearance on mixing

Even for $H = T$ geometries it is found that all the mixing time data could not be accurately described by a single correlation as claimed for example by Ruszkowski (1994). With the disc turbines, the larger D/T is the more energetically efficient for mixing. This agrees with earlier published work. The LIGHTNIN A310 and the 4MFU are the least energetically efficient for mixing at the $c = T/4$ clearance used in this work. This is consistent with the flow visualisation and it could be that optimising the clearance would improve the mixing which should be considered in further work. This should be linked to flow visualisation.

ERT and CFD studies should also be considered for this work.

10.4.3.2: Effect of Agitator Choice on Mixing in Tall Vessels.

When rapid top-to-bottom mixing is required in tall vessels multiple up-pumping high solidity hydrofoils such as the LIGHNIN A345 are recommended. When the top agitator is positioned 0.5 to 1.2 agitator diameters from the dispersion surface these are useful for controlling foaming. The optimisation of agitator configurations for a particular process is generally a balancing act in the art of compromise since often the agitation system has to cope with conflicting demands – liquid mixing, gas and/or solid dispersion, heat, mass and momentum transfer, residence time etc. It would be foolish to pretend that all is now known in these areas, thus there will always be areas worthy of further study.

Cooke *et al.* (1988) Manikowski *et al.* (1994) and Otomo *et al.* (1995), report that the overall mixing time reduced by about 50%, when the two upper turbine agitators were replaced with axial flow agitators. This work finds that when triple A345 agitators are used the mixing time is reduced by a factor of three compared with triple radial turbines at the same specific power input. A single disc turbine a clearance of $T/4$ is more energetically efficient than equal diameter triple disc turbines in a $H = 2T$ vessel. One presumes the long overall mixing times associated with the triple disc turbines is due to the flow fields preventing direct axial transport of fluid via the baffles resulting in compartmentalization of the mixing zones.

Feeding simultaneously to each disc turbine should eliminate this staging effect and eliminate/reduce local concentration variations. ERT tomography is a useful tool to study inter-zonal mixing and exchange rates (see Chapter 6, section 6.5.3). This area is worthy of further study.

10.4.3.3: The Effect of Scale-up on Mixing.

It was noted that in this work the mixing time constant has not scaled up. Results for the single 4MFD at H=1.25T and for the triple A345 show a longer mixing time constant (Nt_{90}) on scale-up, even accounting for any small differences in D/T ratios. Kipke (1983) suggests this effect maybe due to the larger turbulent eddies found on a large scale taking longer to decay. Another explanation (for the work reported in this thesis) may be that adding tracer to the surface in order to measure the overall mixing time results in longer lags in larger vessels. Here, a mixing time is defined as a time to reach a specified degree of homogeneity from the time of tracer addition.

The scale-up of the mixing time constant requires further study. To determine whether lag-time alone accounts for this anomaly, the tracer injection needs to be studied. Injection of tracer at the main agitator should eliminate lags. The tracer injection point and addition time needs to be standardized to eliminate the influence of these. It may be possible to use frequency analysis to study the affects of eddy sizes on the mixing process.

10.4.3.4: Regarding Chapter 7: Multi Phase Hydrodynamics

On my wish list for work reported in Chapter 7 is a complete re-appraisal of the flooding loading transition criterion. The main shortcoming in much of the work reported is consistently good data. At high superficial gas velocities and high D/T visual appraisal can be misleading. There is no certain proof the inflections in the power curve mark the exact transitions. The data of Warmoeskerken and Smith (1985) obtained with the turbine flow meter appear to be the most consistent. Data for a range of turbines types and diameters obtained in a self consistent manner for a large range of gassing

rates should determine conclusively whether "g" forces (Fr) or pumping rates determine the transition and settle the argument whether one type of blade is more energetically efficient at dispersing gas when compared at equal diameter and gassed power.

10.4.5: Inverted Hollow Spinning Cones

Inverted hollow spinning cones, rettofitted to mechanically stirred reactors, are shown to offer an attractive economic method of foam control in Chapter 8. However, it would be naive to say that the mechanisms involved are fully understood and further mechanistic work in this area could be very rewarding. The area of scale-up needs further work. It is my own ambition to see inverted spinning cones successfully trailed on a large scale for level reduction and foam control.

10.4.6 Tomography

With the rapid advances in computational speed and memory-size, multi-phase computational fluid dynamics is an area that can now be generally realised. However, CFD demands good experimental data and techniques to allow model verification and optimisation. Tomographic techniques described in Chapters 6 and 9 are one such tool that shows great promise and these tools can also be used for process diagnostics and control.

Areas that could be usefully developed via further work include:

- **The use of ERT to evaluate exchange rates between agitators.** This may be possible using the mutual bulk resistance (MBR) for all planes facility on the ITS system see Chapter 6, section 6.5.3.
- **Use of ERT in 3-Phase studies.** 2 possible methods come to mind. (I) Use a solid with a higher conductivity than the liquid. This would

allow the higher conductivity solids and the non-conducting gas to be imaged. (II) Use a range of frequencies to identify differences in impedance between the non-conducting solid and gas.

- **Measurement of rate processes.** ERT is admirably suitable for studying rate processes and because of the 3-D characteristics of the measuring technique could be used to measure differing rates occurring in different parts of the vessel. It could be usefully employed measuring bubble build up and destruction rates. Starting from a clear liquid, the gas is introduced at time zero. As bubbles form the hold-up increases. Periodically interrupting the gas flow allows large bubbles to escape (10s - 15s) so the yielding information on large and small bubble formation and destruction rates. Muller (1993) and Muller and Davidson (1992) show how these bubble formation curves can be analysed to yield these rates and how the analysis can be extended to different bubble classes (small and tiny bubbles). It may also be possible to use spectrum analysis techniques to deconvolute the rate data to identify different bubble size classes.

Appendices

Appendix 1: Shaft Torque and Power.

Shaft torque is measured using calibrated strain gauges bonded to the shafts and protected by waterproof covering: Chatwin and Nienow (1985). They work on the principle that the elastic resistance of metal varies in proportion to the strain put upon it – in this case torque. The strain gauges are provided in the form of chevrons, designed to cancel out any bending moments. The strain gauge forms one-arm of a Wheatstone bridge allowing the un-balance caused by torque to be accurately measured.

Each strain gauge is wired to an ASTECH strain gauge bridge fitted with telemetry readout. The torque (M) data is acquired during one to two minutes whenever experiment conditions were changed, the value of the torque being recorded every second.

Under operating conditions a zero reading needs first to be acquired. Most of the experiments were conducted with the impeller shaft running in a Teflon bottom steady bearing. This means there is some danger of the shaft sticking in a position such that when stationary there is a torsional strain on the shaft. In that case a static zero is not accurate. A more accurate zero is obtained by either running the motor at the operating speed with only the bottom bearing covered (the agitator running in air) or obtaining a running zero at such a low speed that the mean shaft torque is essentially zero. As power is proportional to N^3, operation at 3 rpm generally satisfies the latter condition. Checks show that there is no significant difference in power readings with the zero determined by the two methods and for simplicity the latter method is generally used. Hence data treatment is as follows:

Calculate the arithmetic mean and the standard deviation of the torque at $N =$ 3 rpm to work out the zero value and at each experimental speed.

Appendices

Subtracting the zero to the torque mean value at each speed to get the torque value M in volts.

Converting he acquired torque in volt in Nm using the appropriate calibration factor.

The shaft power is calculated as follow:

$$P = 2\pi(N/60)M \qquad \text{(A.1)}$$

where the agitation speed N is measured in rpm.

A1.1 Calibration of Strain Gauges

The strain gauges are calibrated by mounting the shaft horizontally on a torque table as shown in Figures A1.1 and A1.2.

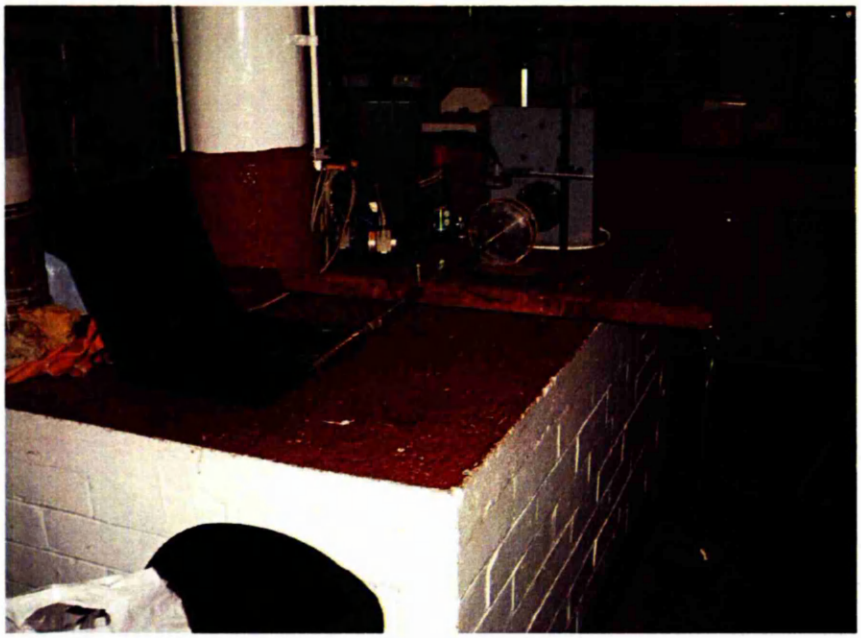

Figure A1. 1: Strain gauge calibration table.

Appendices

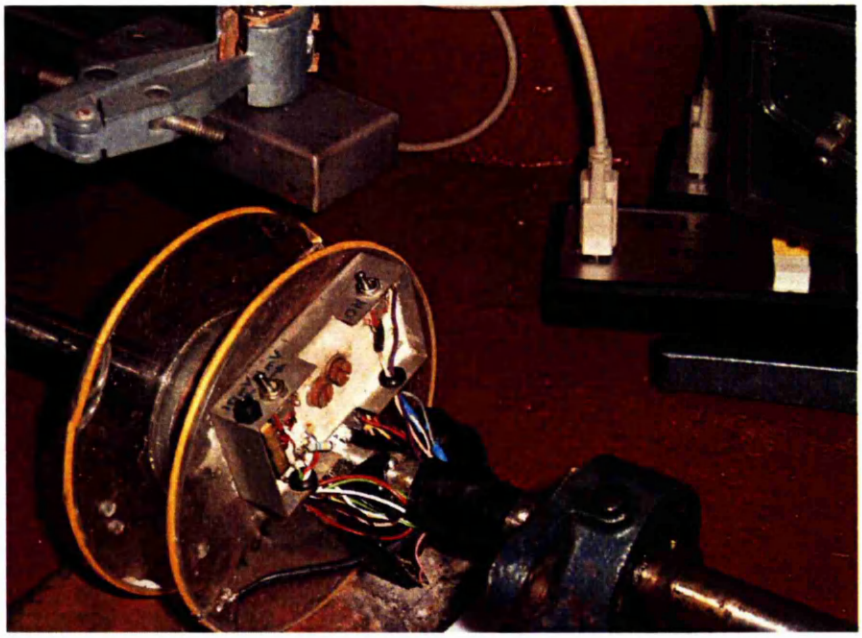

Figure A1. 2: Strain gauge calibration, close-up of telemetry transmitter, aerials and receiver.

The torque arm is clamped to the shaft in a horizontal position and to this is hung a weighing arm at a fixed (0.5 m) distance from the centre of the shaft: Figure A1.1. Calibrated weights are added (weighed on a calibrated accurate balance) and the resulting voltage readings recorded on the Lab View data acquisition system at 1 Hz. For a torque arm length of 0.50 m, the applied torque at each applied weight is:

mass (kg) x 0.5 g (N m) (A1.1)

where g is the gravitational constant = 9.81 m/s.

A typical calibration is shown in Table A1.1. This is for the 0.61 m diameter tank shaft mid strain gauge, on the low sensitivity setting for clock-wise torque recorded on No 3 receiver. The strain gauge constant was found to be 20.26 Nm/V with an R^2 correlation coefficient of 0.99997.

Appendices

2FTCAL00.WK4 23/2/00

Mid Strain Gauge.
No3 Rec. LABTECH NOTEBOOK clockwise torque
Low Sensitivity

Data from 2ftsgcal.WK4

weight kg	weight Newton	Length of torque arm m	Power Difference (V)	Torque (Nm)
0.02009	0.1971	0.5	0.0099	0.0985
0.52426	5.1430	0.5	0.1301	2.5715
1.02748	10.0796	0.5	0.2505	5.0398
1.51842	14.8957	0.5	0.3665	7.4479
2.02164	19.8323	0.5	0.4863	9.9161
2.53021	24.8214	0.5	0.6092	12.4107
3.03343	29.7579	0.5	0.7307	14.8790
4.02759	39.5107	0.5	0.9704	19.7553
5.03433	49.3868	0.5	1.2133	24.6934
7.04098	69.0720	0.5	1.7021	34.5360
8.04828	78.9536	0.5	1.9471	39.4768
9.04244	88.7063	0.5	2.1989	44.3532

Regression Output:		
Constant		0
Std Err of Y Est		0.08543605
R Squared		0.99996808
No. of Observations		14
Degrees of Freedom		13
X Coefficient(s)	20.2635613	
Std Err of Coef.	0.02184708	

Table A1. 1: A typical strain gauge calibration

Appendices

Appendix 2: Overall Gas Hold-up

Gas hold-up is estimated from the level, which is determined either from the vessel wall scale (measured by video) or by use of a calibrated ultra sonic hold-up probe.

A2.1 Overall Gas Hold-up by Video

A calibration scale on the vessel wall allows the level to be measured to 1 mm, accurate to approximately ± 1 mm. The liquid level can be estimated from this during gas-liquid agitation. However, at high agitation rates this is very unsteady and errors in readings are potentially high. Recording the level on video, then playing the video back frame by frame to allow a good average level to be determined, can reduce the errors. Prior to this, the camera is set-up in a known 3-demensional position with the viewing lens axis horizontal and calibrating the "as seen by camera" level against the "as seen by eye". This is done using water at different fill levels and no agitation. An equation is fitted to these data to allow corrections to be made.

For a flat base cylindrical tank, the volumes are simply calculated from the heights. If the unaerated height is H_L m and the gassed height is H_G m, then if the volumes of the internals are ignored, (considering equation (3.3)):

$$\varepsilon_G = 100 \times \left(\frac{H_G - H_L}{H_G} \right) (\%) \qquad \text{(A1.2)}$$

For other vessel or base shapes the volumes have to be calculated taking the geometry into account.

A2.2 Overall Gas Hold-up by Ultra Sonic Level Probe

This is measured using an Endress and Hauser (UK) Ltd Ultrasonic level probe type Nivosonic 27580 DU 213. Technical data, accuracy and operating instructions as follows:

Appendices

Application

The ultrasonic ECHO unit NIVOSONIC FMU 2780 is used for continuous non-contact level measurement in tanks containing liquids when connected to SENSOR DU 212, and also for non-contact flow measurement in open channels when connected to SENSOR DU 213.

The characteristic of the liquid surface (wave formation) does not affect measurement. The sound waves penetrate light foam up to 2 cm thick. Where the foam is thick and dense, the NIVOSONIC FMU 2780 detects the surface of the foam.

Measuring system

This comprises the NIVOSONIC FMU 2780 and the ultrasonic sensor DU 213 or DU 212.

As optional extras we can supply adapter pipes and sensor clamps. Indicating meter, electronic limit controllers, linearisers for flow measurement, etc. can be connected to the current and voltage output of the NIVOSONIC FMU 2780.

Operating principle

A sensor emits ultrasonic pulses at a frequency of approx. 46 kHz. The inaudible sound waves are reflected by the liquid surface and are received by the sensor. The round-trip time (i.e. the time elapsed between transmitting and receiving the echo) is measured electronically in the FMU 2780 and appears as an output signal proportional to level.

If the sensor does not receive an echo, a safety circuit of the FMU 2780 is initiated which causes the output signal to drive up scale over 100%, or down below 0%, according to choice.

The built-in temperature probe in the ultrasonic sensor automatically compensates round-trip time errors which are caused by the temperature coefficient of the speed of sound in air.

For open channel flow measurement, the level proportional signal is modified by a lineariser programmed with the Q/h characteristic of the channel.

Installation

Sensor:

See Technichal Information sheet for ultrasonic sensor DU 213/DU 212.

Electronic module:

The NIVOSONIC FMU 2780 is a plug-in unit (Minocyst). For installation and cabling only the base plate with the terminal block is needed. The electronics module is then merely plugged in and secured with two retaining screws.

See figure 1 for dimensions and drilling template.
When fitted individually or at least 10 mm apart, max ambient temperature in the switch cabinet during operation is 60 °C.

Connection

See figure 2 for electrical connections of NIVOSONIC FMU 2780. Note voltage on label.

By re-soldering a bridge on the printed circuit board (see figure 3), the instrument can be adapted for another voltage. Change voltage on label.

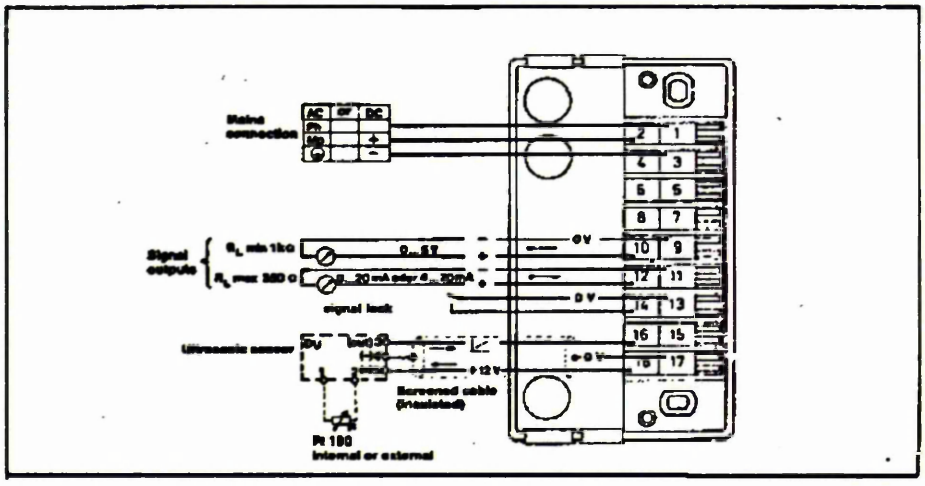

Appendices

Connection

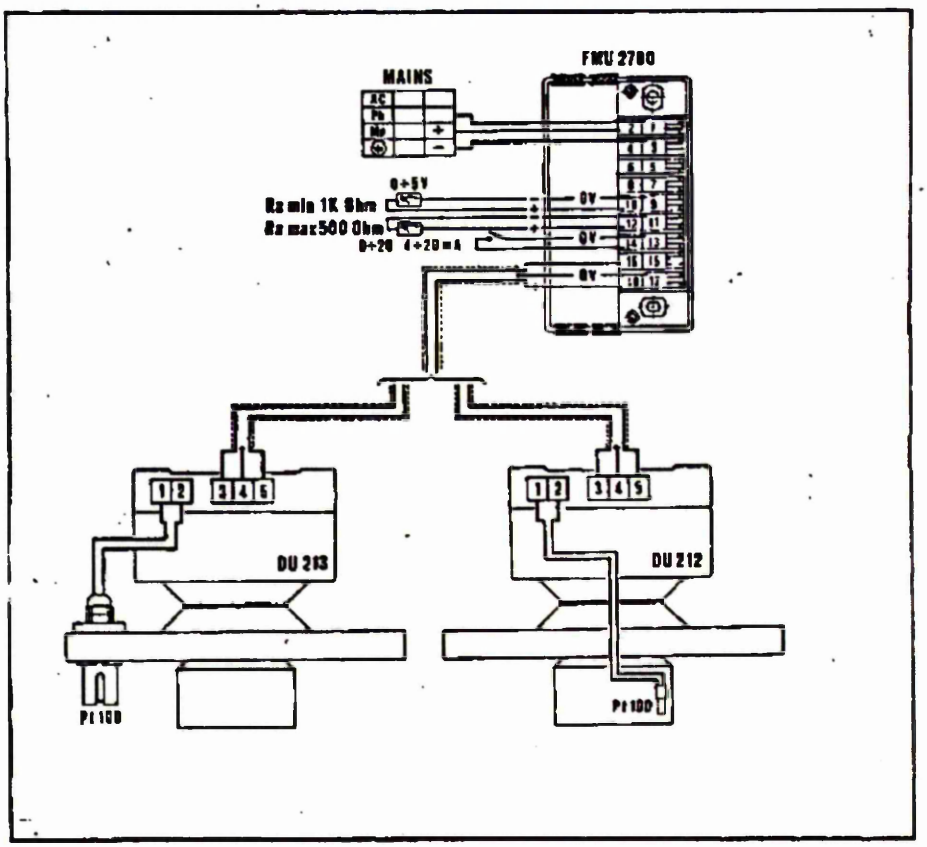

Appendices

Endress+Hauser (U.K.) Ltd.
Ledson Road, Manchester M 23 9PH
Tel. 061-9980321
Telex 668501

Technical Information
E 01.82.02/01

ULTRASONIC SENSORS
DU 213/DU 212

Technical Data

DU 213/DU 212

Housing:	Protective system IP 65
Dimensions:	see figure 1
Max ambient temperature:	— 20 °C to + 60 °C
Supply:	from FMU 2780
Accuracy:	see FMU 2780 and below
Minimum blocking distance	
DU 213:	45 cm
DU 212:	70 cm
	see FMU 2780
Sensor cable:	2-core screened cable, max 20 Ohm per core, max 50 nF between core and screen.
Temperature compensation gauge	
DU 213:	external feeler
DU 212:	built-in

Mounting

General remark: E/F-value should be kept as small as possible to achieve the highest possible accuracy: It is therefore useful not to mount the sensor higher than necessary above the 100%-level, but also not lower than the minimum allowed blocking distance.

For standard applications the mounting heights (distance between the underside of the sensor flange and the 100%-level) are:

- DU 213: 45 cm
- DU 212: 70 cm.

For non-standard applications (presence of strong ripples, foam or agitators in vessels) the mounting distance must be increased to allow the use of a larger blocking distance than standard.

When an extension tube is used to lift the sensor above the roof of the vessel (this applies mainly for DU 212), the free end of the pipe must be cut at 45 °C (to avoid spurious echos) and the blocking distance must not be shorter than the pipe length plus 15 cm.

Avoid the measurement in guide-tubes because of the high working frequency (46 kHz): small droplets of liquid or solid deposits left by the process liquid will cause spurious reflections.

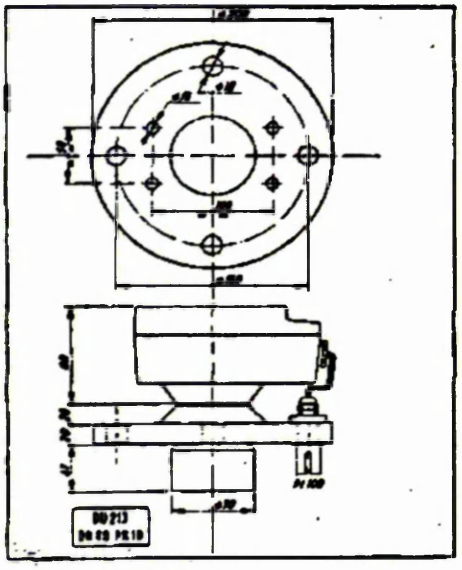

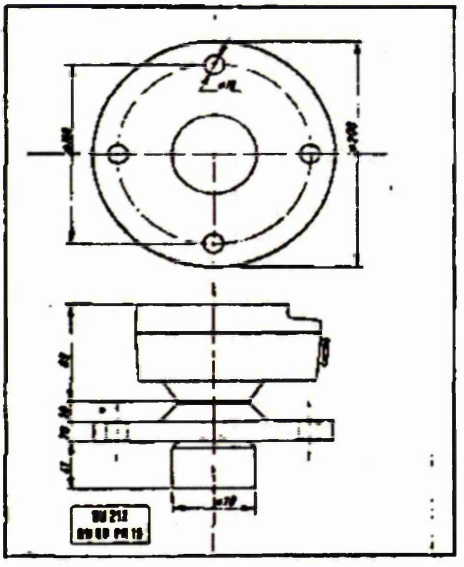

Appendices

Calibration

The pins, switches and potentiometers needed for calibration are on the programme board behind the front plate on the FMU 2780. The front plate can be removed by turning both retaining screws 90° (Slit vertical) Figure 5 shows the components.

A. Current Output

Plug in pin for required range
0 ... 20 mA or 4 ... 20 mA

B. Minimum/Maximum Fail-safe mode

There are three possibilities:

1. Signal storage: Plug in lead to the pin "Lock".
   If no echo is received by the sensor, the last measured value is stored for some time.
2. Minimum fail-safe: Pin Min connection.
   If no echo is received by the sensor, the indication will fall to below 0% after max one minute. This will also occur when switching on after mains failure.
3. Maximum fail-safe: Pin Max connection.
   If no echo is received by the sensor, indication will rise to above 100% after max one minute. This will also occur when switching on after mains failure.

   The fail-safe facility allows connected alarm and control units to operate as they would in a normal case of exceeding or falling below the required level. When the fail-safe facility is in operation, a safety lamp lights up.

C. Integration Time

The integration time is that period which elapses after a rapid change in level from 0 to 100% before the output signal catches up 63% of the new value (response time)

In the MIN position, this is approx. 10 seconds;
in the MAX position, this is approx. 90 seconds.

We recommend normally a mid position (arrow on the potentiometer pointing upwards).

D. Blocking Distance

Normal positions:

- with DU 213: arrow of the potentiometer on "DU 213"
- with DU 212: arrow of the potentiometer on "DU 212".

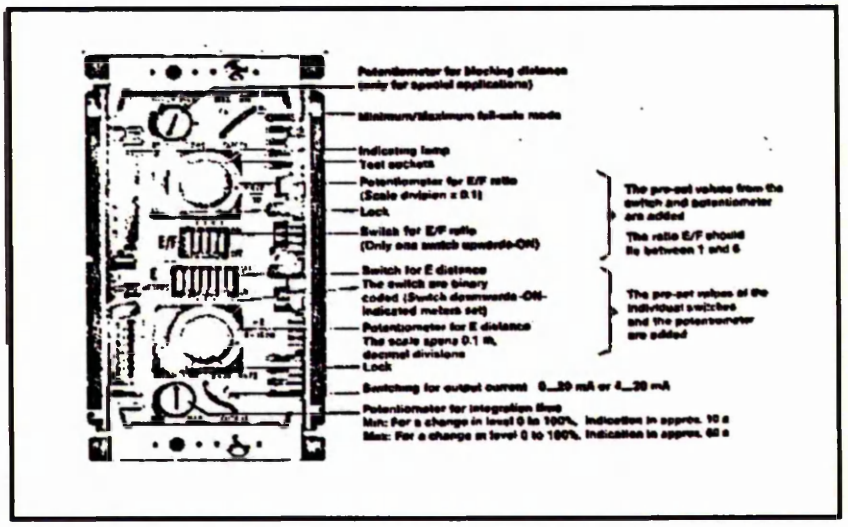

Appendices

E. Calibration

A big feature of the instrument is that calibration can be achieved by calculation without the need to change levels. To facilitate calculations, certain definitions are explained below (see also figure 8).

Reference line: Also called virtual zero.
This is the line from which the measurement of the distance is based.

Z: Distance between the underside of the flange and the reference line, which is always above the underside of the flange. Z is determined by the physical and electronic delay of the measuring system. Z is constant for the particular ultrasonic DU sensor and is shown on the label (typically 20 ... 30 mm).

Range = distance between the reference line and 0% (minimum level).

F: Measuring Span = difference between 0% and 100% level.
Make the liquid surface at 100% level must not be closer to the underside of the flange than the minimum blocking distance for the particular sensor.

M: Blocking Distance = the equivalent time for which the receiver is desensitized after a burst has been transmitted. The minimum permissible distances are:
- 45 cm for DU 213
- 70 cm for DU 212.

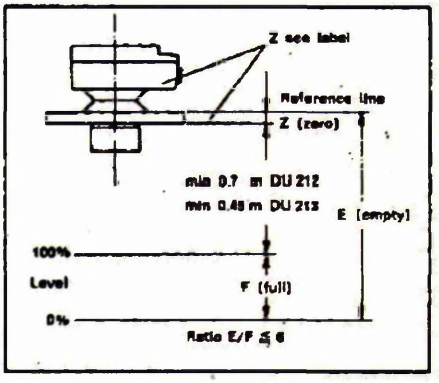

F. Calibration by Calculation

The following must be known or calculated:

1. Installation height of the underside of the sensor flange above 0% level
2. Z of the sensor (refer to label)
3. F
4. Calculate E
5. Calculate E/F.

Then the following must be adjusted:

1. All switches to "OFF". Loosen potentiometer locking
2. Adjust distance E with incremental switches and potentiometer
3. Adjust E/F with one switch and potentiometer
4. Lock both potentiometers.

Calibration example for DU 213

Given:

1. Installed height of the underside of the sensor flange above zero = 0.93 m
2. Z of the sensor = 23 mm
3. Difference in level between 0% and 100% = 0.53 m

Calculate:

4. E = 0.93 m + 0.023 m = 0.953 m
5. E/F = 0.953 m / 0.53 m = 1.80

Adjust:

6. E = 0.953 m, set the following switches to "ON":

4 =	0.800 m
1 =	0.100 m
	0.900 m

and adjust for the balance on the potentiometer:

	0.053 m
	0.953 m

(since the total scale of 10 major divisions of the potentiometer is equivalent to 0.1 m (10 cm), set the potentiometer to 5.3 on the scale).

Adjust:

7. E/F = 1.80
Push switch 1 upwards to "ON" = 1.000

and adjust for the balance on the potentiometer:

	0.800
	1.800

(since the total scale of 10 major divisions of the potentiometer represents 0.1 E/F, set the potentiometer to 8.0 on the scale).

Calibration example for DU 212

Given:

1. Installed height of the underside of the sensor flange above zero = 2.343 m
2. Z of the sensor is 26 mm
3. Difference in level between 0% and 100% = 1.30 m

Appendices

Calculate:

4. E = 2.345 m + 0.026 m = 2.371 m
5. E/F = 2.371 m/1.58 m = 1.58

Adjust:

6. E = 2.371 m, set the following switches to "ON":

5 =	1.600 m
3 =	0.400 m
2 =	0.200 m
1 =	0.100 m
=	2.300 m

and adjust for the balance on the potentiometer:

0.071 m
2.371 m

(since the total scale of 10 major divisions of the potentiometers is equivalent to 0.1 m (10 cm), set the potentiometer to 7.1 on the scale).

Adjust:

7. E/F = 1.58
Push switch 1 upwards to "ON" = 1.000

and adjust for the balance on the potentiometer:

0.58
1.58

(since the total scale of 10 major divisions of the potentiometer represents 0.1 E/F, set the potentiometer to 5.8 on the scale).

G. Calibration by changing level without calculation

1. Calibration with an empty tank or empty channel (Level 0%).

If it is not possible to bring the level to 0% dismantle the sensor and position it exactly perpendicular to a smooth wall or board at the correct 0% distance.

1.1 Only E/F switch 1 (left) to "ON".
$\frac{E/F}{10}$ Potentiometer to 0

1.2 All E switches to "ON". E potentiometer to 10

1.3 The green lamp should flash. Indicated output should be below 100%

1.4 E switches release to "OFF" from right to left (i.e. switch 7 is the first = 0.4 m)

— Check whether indicated output reduces.

— If indication remains unchanged or sinks below 0, switch the previous E switch to "ON".

— Switch the next switch for E with the smaller value to OFF until the indicated value is less than 20%.

— E/F switch 1 to "OFF" and switch E/F 2 to "ON" (i.e. the previously indicated value becomes 5 times greater).

— Switch next E switch to "OFF" etc. until switch 1 (left = 0.1 m).

— Calibrate to exactly 0 with the E potentiometer. Lock potentiometer.

— Empty calibration is then completed.

2. Calibration on full tank or channel (Level 100%)

If necessary simulate 100% level.
The indicated value is usually above 100%.

2.1 E/F switch 5 to "OFF"
E/F switch 4 to "ON"
E/F switch 3 to "OFF"
E/F switch 2 to "ON"

Continue until indicated value reduces to below 100%.

2.2 Calibrate exactly to 100% with the $\frac{E/F}{10}$ potentiometer

Lock potentiometer

– Full calibration is now completed.

Orientate slits on the screws on the front plate vertically.

Operation

Switch on power supply:

The green lamp lights up. Depending on fail-safe mode, indication either drops below 0%, exceeds 120% or show a value appropriate to the level in the tank or channel. Only when the lamp flashes is the indicated value exactly that of the level.

If the reflecting surface exceeds the distance for which the gauge is calibrated (distance E), the measurement is ignored, i.e. the incoming echo signals are not evaluated (protection against double reflections).

As far as possible, the calculated and calibrated values for E and E/F can be checked on either an empty or full tank, and if necessary, correction made by the use of the appropriate potentiometer.

Maintenance

The NIVOSONIC FMU 2780 requires no maintenance.

Appendices

Accuracy

The actual accuracy of the measurement depends firstly on the measuring conditions (waves, ripples, foam, sudden variations of temperature which cannot be followed fast enough by the temperature compensation) and secondly on the mounting conditions, that is on the factor E/F.
The sum of these two effects, measure accuracy plus inherent accuracy, gives the overall accuracy.
As the manufacturer cannot influence the measuring conditions only the inherent accuracy can be defined in advance.

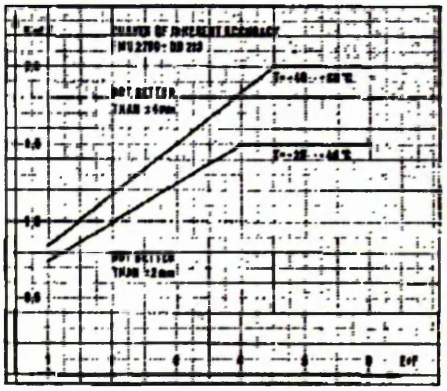

Inherent accuracy

The inherent accuracy of the equipment is defined as the accuracy achieved when the measurement is performed against a flat, well reflecting surface (wooden board, steady water mirror or similar). In these conditions, the following overall accuracies can be achieved:

DU 213

1) - for temperature range: — 20 °C ... + 40 °C and E/F = 6
± 1.5% of F, but not better than ± 2 mm

2) - for temperature range: + 40 °C ... + 80 °C and E/F = 6
± 2% of F, but not better than ± 4 mm.

If mounting conditions allow a smaller E/F than 6, the inherent inaccuracy will decrease by the same factor, plus a constant equal to 0.5% of F.
For example, if E/F = 2 (3 times smaller than max allowed) the inherent accuracy (referred to F) will be (1.5% : 3) + 0.5% = 1% (of F).

The general formula for the temperature range — 20 °C ... + 40 °C, which applies for E/F < 4 (because of the fix term) is:

$$\text{Error. } \varepsilon = \left(1.5 : \frac{6}{E/F}\right) + 0.5\% \text{ of F}$$

but not better than ± 2 mm.

For the temperature range + 40 °C ... + 80 °C the formula, which applies for E/F < 4.5, is:

$$\varepsilon = \left(2 : \frac{6}{E/F}\right) + 0.5\% \text{ of F}$$

but not better than ± 4 mm.

Some examples referred to the temperature range — 20 °C ... + 40 °C.

1) Mounting height: 450 mm
Measure span: 80 mm
Z of sensor: 21 mm

E = 351 mm F = 80 mm E/F = 8.88
Measurement not possible because E/F > 6

2) Mounting height: 450 mm
Measure span: 118 mm
Z of sensor: 23 mm
E = 391 mm F = 118 mm E/F = 3.8

From figure 2
$\varepsilon_r = \pm 1.5\%$ of F → $\varepsilon = \pm 1.77$ mm
± 1.77 mm being smaller than ± 2 mm, the latter applies. Therefore, the inherent accuracy of this particular application will be:
$\varepsilon = \pm 2$ mm → $\varepsilon_r = 1.7\%$ of F

3) Mounting height: 450 mm
Measure span: 360 mm
Z of sensor: 20 mm
E = 830 mm F = 320 mm E/F = 2.31
From figure 2
$\varepsilon_r = \pm 1.08\%$ of F → $\varepsilon = \pm 3.8$ mm
From the formula

$$\varepsilon_r = \left(0.5 + 1.5 : \frac{6}{2.31}\right) \% \text{ of F} = 1.08\% \text{ of F}$$

4) Mounting height: 850 mm
Measure span: 430 mm
Z of sensor: 15 mm
E = 1095 mm F = 430 mm E/F = 2.55
From figure 2
$\varepsilon_r = 1.15\%$ of F → $\varepsilon = \pm 5$ mm

DU 212

— for temperature range: — 20 °C ... + 80 °C and E/F < 2
± 1.5% of F, but not better than ± 1.5 cm

Under normal operating conditions the probe was set-up mid way between the baffles and mid way between the vessel wall and the shaft and the integration time set at the mid point. This gives an average level over one quadrant of the vessel. The span was chosen to gives the highest inherent accuracy, consistent with covering the desired level change due to gassing. Calibration is as described in the operational instructions.

Appendices

Appendix 3: Local Gas Hold-up

See Chapter 3, section 3.2.4: Local Gas-Liquid Hold-up. A typical calculation work sheet is in accompanying CD as bubcolLHU.xls.

Appendix 4: Comparative Mixing Times Data Analysis

A typical data analysis is included in the accompanying CD titled IDT150HT1.xls. This is a eight-page spreadsheet. The original data for the seven repeat runs that constitute the average mixing time and data summary are in the sheet entitled datasum. The analyses of each run as described in Chapter 3, section 3.2.5 (Overall Liquid Mixing Times), are in the sheets Run1, run2, and run3 to run7.

Appendix 5: An Example k_La Calculation Using the Peroxide Method

In this work the equilibrium oxygen concentrations are taken from final average steady-state readings rather than predicted as described by Gezork *et al.* (2001). It is difficult to control the temperature exactly especially at high specific power inputs, so the effect of temperature on the equilibrium oxygen due to air is first determined to enable equivalent 100% air saturation values, as a function of temperature, to be estimated for all the runs. The peroxide mass flow rate is determined by placing the hydrogen peroxide container on an accurate balance and determining the flow from weight differences over time measured by an accurate (1/100 s) stopwatch.

The calculation sheet, that also includes the theory, is attached as 3A345KLA.xls. Note that gas phase oxygen concentrations are calculated from the ideal gas-law,

Appendices

$$PV = nRT \qquad \text{(A5.1)}$$

where P is the pressure and 1 atmosphere is 1.013×10^5 Pa, T is absolute temperature = (temperature in Celsius + 273.13) and R is gas constant = 8.314 $J.mol.K^{-1}$.

Thus, for air containing 21% oxygen at one atmosphere and 20°C, the oxygen concentration in mol/m^3 is,

$$\frac{0.21 \times 1.013 \times 10^5}{8.314 \times (273.13 + 20)} = 8.729 \ mols\ O_2/m^3 \text{ air} \qquad \text{(A5.2)}$$

The Henry's law constant H for oxygen in water varies with temperature according to,

$$H = ((1.316 \times 10^4 \times T°C) + (4.573 \times 10^5)) \qquad \text{(A5.3)}$$

Fitted to data taken from International Critical Tables (1933).

Therefore at 20 °C, RT/H is,

$$\frac{8.314 \times (273.13 + 20)}{((1.316 \times 10^4 \times 20) + (4.573 \times 10^5))} = 0.03382 \qquad \text{(A5.4)}$$

and the equilibrium liquid phase concentration is

$$8.729 \times 0.03382 = 0.2953 \text{ mol } O_2/m^3 \text{ water.} \qquad \text{(A5.5)}$$

The liquid phase equilibrium oxygen concentration is assumed to apply at a (mid point) liquid head of half the liquid height between the inlet and outlet. For air in at the base and a liquid height of water H_L the factor increase in oxygen pressure is,

$$(1 + (0.5 \times H_L \times 0.09678)) \qquad \text{(A5.6)}$$

Hence the equilibrium mol O_2/m^3 water = eq. (A5.5) x eq. (A5.6) (A5.7)

The hydrogen peroxide equilibrium oxygen concentration is the product of the value calculated in equation (A5.7) and the factor increase in oxygen

output reading at equilibrium, when running at constant peroxide addition rate.

Appendix 6: Measurement of Viscosity.

Viscosity is measured as described in 3.2.8 and in accordance to the manufactures instructions.

A typical calibration and result is illustrated in viscosity eg.xls

Appendix 7: Analysis of Dynamic Gas Disengagement Curves

Refer to Chapter 5

For a bimodal bubble distribution obtained for operation in the heterogeneous regime the disengagement curves are analysed according to Scumpe and Grund (1986)

During disengagement, the local liquid superficial velocity equals gas flow in the opposite direction (i.e. $U^*_L = -U^*_G$). Hence the initial fall $(dh/dt)_I$ is equal to the superficial gas velocity at steady state (U_G).

For a homogeneous bubble distribution (single slope on the disengagement curve) then:

$$v_S = -(dh/dt) \qquad \text{(A7.1)}$$

$$U_B = v_S / \varepsilon_G \qquad \text{(A7.2)}$$

Appendices

Bubble size from rise velocities

In this work, the relationship between small bubble rise velocity, relative to a stationary liquid, and the terminal rise velocity of a small bubble in an infinite medium, proposed by Marrucci (1965) is used to correct for this effect:

$$u_t = \frac{U_{B,s}(1-\varepsilon_{G,s}^{5/3})}{(1-\varepsilon_{G,s})^2} \qquad \text{(A7.3)}$$

No corrections have been made for the rise velocity of larger bubbles. Krishna *et al.* (1999) claim that a large bubble swarm can rise faster than a single spherical cap bubble because of the interactions with the wake of the previous bubbles.

From the corrected value of the rise velocity, the bubble diameters are calculated using one of two methods:

For Reynolds number (Re) $\leq$ 2, Stoke's law is used to estimate bubble diameters as follows,

$$d_{b,s} = \left(\frac{18\mu_l u_t}{g(\rho_l - \rho_g)} \right)^{1/2}$$

Where inertial terms (Re>2) are important a drag coefficient (C_d) is used to fit the experimental data. From Valentin (1967), this is given by the following relationship,

$$C_d = \frac{4}{3}\left(\frac{\rho_L - \rho_G}{\rho_L} \right)\left(\frac{d_b g}{u_t^2} \right) \qquad \text{(A7.4)}$$

where ρ_L is the liquid density, ρ_G is the bubble density, d_b is the bubble diameter, g is the acceleration due to gravity and u_t is the terminal bubble rise velocity.

Hill (1998) used two (empirical) curve fits to the drag coefficient versus Reynolds curve for pure water shown in

Appendices

Figure 5-6 for the drag coefficient as a function of bubble Reynolds number. These are:

For ($Re_b < 450$),

$$\ln(C_d) = 2.699467-0.335816.\ln(Re_b)-0.07135617.[\ln(Re_b)]^2 \qquad (A7.5)$$

and for ($Re_b > 450$),

$$\ln(C_d) = -51.77171+13.16707.\ln(Re_b)-0.82356.[\ln(Re_b)]^2 \qquad (A7.6)$$

These equations are of the quadratic type; $f(x) = a(x)^2 + bx + c$

Whose roots can be found when arranged in the form of,

$0 = a(x)^2 + bx + c$ from,

$$x = \frac{-b \pm \sqrt{b^2 = 4ac}}{2a}$$

to yield bubble diameters from rise velocities as follows:

unknown in eq. (A7.4) is bubble diameter d_b

Let $c_1 = \frac{C_d}{d_b}$

Let $c_2 = c_1 \times \frac{d_b}{\mathrm{Re}_b} = \frac{C_d}{\mathrm{Re}_b}$

Then $C_d = \mathrm{Re}_b \times c_2$

$\log_e C_d = \log_e \mathrm{Re}_b + \log_e c_2$

$0 = a + b\log_e \mathrm{Re}_b + c\log e(\mathrm{Re}_b)^2 - \log e\,\mathrm{Re}_b - \log_e c_2$

For the form $(0 = a(x)^2 + bx + c)$ then,

$a = c(quad)$, $(b-1) = b(quad)$ and $(c - \log_e c_2) = a(quad)$

Thus, the bubble Re_b can be evaluated from the roots of the equation and from this the bubble size estimated from the bubble rise velocity. A typical work sheet illustrating how this is evaluated from the disengagement trace is attached as (cfdis2.xls).

Appendix 8: Examples of Frequency Counts from Bubble Size Measurements

Examples of bubble frequency results from the bubble size measurements both semi-automatic and manually sized are attached in kclfreq.xls.

Appendix 9: List of Folders in Accompanying CD

- Buchi work
- Calibrate
- Cones
- Documents
- Hydrodynamics
- K_La
- Local HU
- Mixing
- Overall HU
- Pictures
- Tomography

Bibliography

Alcock, R. and Froelich, D. (1986), "Analysis of rotaery atomisers".Trans. ASAE, Vol. 29(6) pp.1514-1519.

Alper, E., Wichtendahl, B. and Deckwer, W.D. (1980) "Gas adsorption mechanism in catalytic slurry reactors" Chem.Eng. Sci. Vol. 35, pp. 217-222.

Armenante, P. M. and Li, Tong. (1993) "Minimum agitation speed for off-bottom suspension of solids in agitated vessels provided with multiple flat-blade impellers". AIChE Symposium Series (1993), 293(Process Mixing), pp. 105-11.

Armenante, P. M. and Uehara-Nagamine, E. (1997) "Solid suspension and power dissipation in stirred tanks agitated by one or two impellers at low off-bottom impeller clearances". Recents Progres en Genie des Procedes 11(52, Mixing 97: Multi-phase Systems), pp. 73-80.

Armenante, P. M., Huang, Yu Tsang and Li, Tong. (1992) "Determination of the minimum agitation speed to attain the just dispersed state in solid-liquid and liquid-liquid reactors provided with multiple impellers". Chem. Eng. Sci. Vol 47(9-11), pp. 2865-70.

Badcock, R.J., Benwell, R. A. and Gray, C. (1994). "An evaluation of spinning cone column technology for low alcohol beer production". Proc. Conv. - Inst. Brew. (Asia Pac. Sect.) 23rd pp.170-175.

Bailey, J. E. and Ollis, D. F. (1986), "Biochemical Engineering Fundamentals" 2nd Edition. McGraw-Hill Book company, New York.

Bakker, A. (2004). Comments at the poster session when this data was presented at the ISMIP5 Congress, Seville, Spain.

Bakker, A. and van den Akker, H.E.A. (1991), "A computational study of dispersing gas in a stirred reactor" , Proc of 7th European Mixing Conf., Brugge, Belgium: pp 199-207.

Baldi, G. Conti, R. and Alaria, E. (1977) "Complete suspension of particles in mechanically agitated vessels" Chem. Eng. Sci. 33, pp. 21-25.

Baldyga, J. Bourne, J.R., Pacek, A.W. Manullah, A. and Nienow, A.W. (2001), "Effect of agitation and scale-up on drop size in turbulent dispersion, allowance for intermittency". Chem. Eng. Sci. Vol. 56, pp. 3377-3385.

Bates, R.L., Fondy, P.L. and Corpstein, R.R. (1963), "An examination of some geometric parameters of impeller power", Industrial and Engineering Chemistry, Vol. 2(4), pp. 310-314.

Bickham, D.R., Housley, S.D., McDonnell, F.G., Cooke, M. and Davis, M.R.D. (2003) "Apparatus for and method of producing aromatic carboxylic acids" USA patent application No. 10/443542.

Bongenaar, J.J.T.M., Kossen, N.W.F., Metz, B. and Miejboom, F.W. (1973), "A method for characterizing the rheological properties of viscous fermentation broths". Biotechnol. Bioeng. Vol. 15, 201.

Bourne, J.R. (1982), "The characterization of micromixing using fast multiple reactions". Chem. Eng. Commun. Vol. 16, pp. 79-90.

Bourne, J.R. (1997) "Mixing in single phase chemical reactors". Chapter 10 in Harnby, N, Edwards, M.F. and Nienow, A.W , editors (1997) "Mixing in the process industries" 2nd edit. Butterworth/Heinman (paperback).

Bourne, J.R., Kozicki, F., and Rys, P. (1981), "Mixing and Fast Chemical Reaction I". Chem. Eng. Sci. Vol. 36(10), pp. 1643-1648.

Bibliography

Bowers, R.H. (1965), "An investigation of flow phenomena in stirred liquids". A.I.Chem.E. symposium series No 10, pp.8-13.

Brooks, G. and Su, G. J., (1959) Chem. Eng. Progr., Vol. 55(10), p 54. taken from Uhl, V.W. and Gray, J.B. (1966) "Mixing: Theory and practice", Volume 1, published by Academic Press.

Bruggeman, D.A.G. (1935) "Calculation of different physical constants of heterogeneous substances". Annln. Phys., Vol. 24, pp. 636-679.

Bruijn, W., van't Riet,K. and Smith, J.M. (1974), "Power consumption with aerated Rushton turbines". Trans I Chem E 1974, Vol. 54, pp. 88-104.

Bruining, W. J., Joosten, G. E. H., Beenackers, A. A. C. M. and Hofman, H. (1986), "Enhancement of gas-liquid mass transfer by a dispersed second liquid phase". Chem. Eng. Sci., 41(7), pp. 1873-1877.

Bryant, J. and Sadeghzadeh, S. (1979), "Circulation rates in stirred and aerated tanks". Proc. 3rd Eur. Conf. Mixing (Vol. 1), York, UK pp. 325-336.

Buchmann, M. and Mewes, D. (1999), "Tomographic Measurements of Micro- and Macromixing Using the Dual Wavelength Photometry". Proceedings 1st World Congress on Industrial Process Tomography, Buxton, UK, pp. 281-288.

Buchmann, M., Kling, K. and Mewes, D. (2000), "Spatially resolved measurements and calculations of micro- and macromixing in stirred vessels". Proceedings of the 10th European Conference on Mixing, Delft, Netherlands, pp. 25-34.

Buckland, B.C., Gbewonyo, K, Jain, D., Glazomitsky, K., Hunt, G., and Drew, S.W. (1988), "Oxygen transfer efficiency of hydrofoil impellers in both 800L and 19000L fermentors". Proc 2nd Int Conf Bioreactors, BHRA, Cambridge, pp. 2-16.

Bujalski, W. (1986) "Three Phase Mixing" PhD thesis, Birmingham University UK.

Bujalski, W., Konno, M. and Nienow, A.W. (1988), "Scale-up of 45°pitched blade turbine agitators for gas dispersion and solid suspension", 6th Euro. Conf. on Mixing, Pavia, Italy, pp. 389-398.

Bujalski, W., Nienow, A.W., Chatwin, S. and Cooke, M. (1987) "The dependency of scale on power numbers of Rushton disc turbines". Chem. Eng. Sci. Vol. 42, pp. 317-326.

Bujalski, W., Nienow, A.W. and Huoxing, L. (1990), "The use of upward pumping 45°pitched blade turbine impellers in three phase reactors". Chem. Eng. Sci., Vol. 45, pp. 415-421.

Bujalski, W., Sanchez, A., Torres, G. L. E. and Nienow A.W. (1993) "Hydrodynamics of an Independently-Driven, Dual Impeller Bioreactor for Very Large Scale Fermentations". Proc. 1st Industrial Chemical Engineering Technology Topical Conference, St. Louis, U.S.A., 1993; A.I.Ch.E., New York, pp 25-30.

Buurman, C., Resoort, G. and Plaschkes, A. (1986) "Scaling-up rules for solids suspension in stirred vessels". Chem. Eng. Sci. Vol. 41(11), pp. 2865-2871.

Buurman, C., Resoort, G. and Plaschkes, A., (1985), "Scaling-up rules for solids suspension in stirred vessels". Proc. 5th Eur. Conf. Mixing . pp. 15-26.

Calabrese, R.V. Pacek, A.W. and Nienow, A.W. (1993) "Coalescence of Viscous Drops in Stirred Dispersions". I.Chem.E. Res.Event, The University of Birmingham, U.K., Jan.1993; I.Chem.E., Rugby, U.K., pp 642-644.

Calderbank, P.H (1958) "Physical rate processes in Industrial Fermentation, Part 1: The Interfacial area in gas-liquid contacting with mechanical agitation". TransIChemE, Vol 36, pp 443-463.

Bibliography

Calderbank, P.H. and Moo-Young, M.B. (1961) "The continous phase heat and mass transfer properties of dispersions". Chem. Eng. Sci. Vol. 16, pp. 39-54.

Chapman, C.M. (1981) "Studies on gas-liquid-particle mixing in stirred vessels". PhD thesis, University College London. UK.

Chapman, C.M. Gibilaro, L.G. and Nienow, A.W. (1982) " A dynamic response technique for the estimation of gas-liquid mass transfer coefficients in a stirred vessel" Chem.Eng.Sci., Vol. 36, pp. 891-896.

Chapman, C.M., Nienow, A.W. and Middleton, J.C., and Cooke, M. (1983) Particle-gas-liquid mixing in stirred vessels, Trans IChemE ., Vol. 61, pp.71-81, 82-95, 167-181, 182-185.

Chatwin, S. and Nienow, A.W. (1985) "Successful power measurement in agitated vessels" Lab. Sc. Tech., Vol. 1, p. 69. (1 page)

Clayton, T.M. and Slater N.K.H. (1995) "Mixing and Oxygen Transfer in a Large Scale Animal Cell Bioreactor", Proc. 3rd Int.Symp.Biochem.Eng., Stuttgart, Germany. E. Kurz and Co., Stuttgart, Germany, pp 162-164.

Clift, R., Grace, J. R. and Weber, M.E. (1978) "Bubbles, drops and particles" Academic Press, New York, p.172.

Colenbrander, G. W. (2000), "Experimental findings on the scale-up behavior of the drop size distribution of liquid/liquid dispersions in stirred vessels". Proceedings of the 10th European Conference on Mixing, , Delft, Netherlands, pp. 173-180.

Cooke, M., Heggs, P.J., Eaglesham, A. and Housley, D. (2002) "Spinning cones as pumps, degassers and level controllers". Paper presented at IChemE Fluid Mixing Subject Group, Fluid Mixing 7, Bradford Univ., 10-11 July 2002.

Cooke, M., Heggs, P.J., Eaglesham, A. and Housley, D. (2004) "Spinning cones as pumps, degassers and level controllers in mechanically stirred tanks" Trans IChemE Part A, Chemical Engineering Research and Design. 82(A6) pp. 719-729.

Cooke, M., Heggs, P.J., Eaglesham, A. and Housley, D. (2002), "Bubble studies under cold and boiling conditions using dynamic gas disengagement coupled with videoand photographic techniques". Proceedings of Eurotherm 71, University of Reims, France, October 2002. pp.95-101.

Cooke, M., Bolton, G., Jones, D.H. and Housley, D. (2001) "Demonstration of a novel retrofit tomography baffle cage, for gas- liquid mixing studies under intense operating conditions". 2nd World Congress on Industrial Process Tomography, Hannover, Germany August 2001, pp. 652-660

Cooke, M., Bolton, G., Jones D.H. and Housley, D. (2003) "Demonstration of a novel retrofit tomography baffle cage, for gas- liquid mixing studies under intense operating conditions". Reprinted in June edition of Chemical Technology, published by Crown publications South Africa. www.crown.co.za pp.19-22.

Cooke, M and Middleton, J.C. (1997) "Behaviour of gas-liquid stirred vessels at high void fraction". Mixing XVI Conference, NAMF, Williamsburg, 1997.

Cooke, M., Dawson, M.K., Nienow, A.W., Moody, G.W. and Whitton, M.J. (1991) "Mass transfer in aerated agitated vessels: Assessment of the NEL/Hickman steady state method". Proc. 7th Europ. Conf. on Mixing, Royal Flemish Society of Engineers, Brugge, Belgium,pp. 409-418.

Cooke, M. (1989) "Reflection in a Bioreactor" The Chemical Engineer, p. 39, Jan. 1989.

Cooke, M., Middleton, J.C. and Bush, J.R. (1988) "Mixing and mass transfer in filamentous fermentations". Proc 2nd Int Conf Bioreactors, BHRA, Cambridge, pp.37-64

Bibliography

Cooper, R.G. and Wolf, D. (1968) "Velocity profiles and pumping capacities for turbine type impellers". Can. J. of Chem. Eng., Vol. 46, pp. 94-100.

Costes, J. and Couderc, J.P. (1982) "Pumping capacity and turbulence intensity in baffled stirred tanks; Influence of the size of the pilot unit." Proc. 4th Erop. Conf. On Mixing, Noordwijkerhout, Netherlands, Sponsored by BHRA fluid engineering, pp.25-33.

Craig, V. S. J., Ninham, B. W. and Pashley, R. M. (1993) "The effect of electrolytes on bubble coalescence in water". J. Phys. Chem., 97: 10192-10197.

Cronin, D.G., Nienow, A.W., Moody, G.W. (1994) "Mixing studies in a large laboratory proto-fermenter: Rushton turbines". Food and Bioproducts Processing, Trans. Institution of Chemical Engineers, Part C, Vol. 72, pp 35-40.

Cutter, L.A. (1966) "Flow and turbulence in a stirred tank". A.I.Chem.E. Journal, Vol.12, pp.35-45.

Dang, N.D.P., Karrer, D.A. and Dunn, I.J. (1977) "Oxygen Transfer Coefficients by Model Moment Analysis". Biotech. and Bioeng.,Vol 22. pp. 853-865.

Dankwerts, P.V. (1951), "Significance of Liquid Film Coefficient in Gas Absorption." Ind. Eng. Chem., Vol. 4 p. 1460.

Dankwerts, P.V. (1970) "Gas-liquid reactions" McGraw-Hill, New York.

Davies, S.N. (1986) "The evaluation of overall gas-liquid mass transfer coefficients in gas sparged agitated vessels". PhD thesis, University College London. UK.

Davies, S.N., Gibilaro, L.G., Middleton, J.C., Cooke, M. and Lynch, P.M. (1985) "The application of two novel techniques for mass transfer coefficient determination to the ccale-up of gas sparged agitated vessels". Proc. 5th Europ. Conf. on Mixing, Wurzburg, pp. 27-34.

Dawson, M.K. (1991) "The influence of agitator type on fluid dynamics and oxygen mass transfer in a pilot scale mixing vessel". PhD Thesis, The University of Birmingham, UK.

Dawson, M.K., Nienow, A.W. and Moody, G.W., (1993) "Comparison of Intermig and Rushton Turbine Gas-Liquid Mass Transfer in a Pilot Scale Mixing Vessel". The I.Chem.E. Res.Event, The University of Birmingham, U.K., Jan.1993; I.Chem.E., Rugby, U.K., pp 645-647.

De Swart, J. W. A and Krishna, R. (1995) "Influence of particle concentration on the hydrodynamics of bubble column slurry reactors" 2nd Int. Conf. on Gas-Liquid-Solid Reactor Engineering, Cambridge, pp.308-313.

De Swart, J. W. A., Van Vliet, R. E. and Krishna, R. (1996) "Size, structure and dynamics of "large" bubbles in a two-dimensional slurry bubble column". Chem. Eng. Sci., 51: 4619-4629.

Deshpande, N.S. and Barigou, M. (1999) "Performance characteristics of novel mechanical foam breakers in a satirred tank reactor" J.Chem. Tech. and Biotechnology, Vol. 74, pp. 797-987.

Deshpande, N. S. and Barigou, M.(2000) "Mechanical suppression of the dynamic foam head in bubble column reactors". Chemical Engineering and Processing Vol. 39(3), pp. 207-217.

Distelhoff, M.F.W. and Maquis, A.J. (1999) "Scaler mixing measurements in a continously operated stirred tank agitated with a Rushton turbine using a LIF line scan technique". Fluid Mixing 6, IchemE symposium series No. 146, pp. 147-158.

Ditl, P., Rieger, F. and Novac, V. (1997) "Undesirable air entrainment in agitated baffled vessels". Recents Prog. Genie Procedes (Vol. 11, 52, Mixing 97: Multi-phase Systems), pp. 131-136.

Bibliography

Dombrowski, N. and Lloyd, T.L. (1974) "Atomisation of liquids by means of a spinning cup". Chem. Eng. Journal, Vol. 8 p. 63.

Dombrowski, N. and Lloyd, T. L. (1973), "Air drag on ligaments produced from rotating cups". J. Chem. Eng. Jap. Vol. 6(4), pp. 363-365.

Dunlap, I.R. and Rushton, J.H. (1953) "Heat transfer coefficients in liquid mixing using vertical tube baffles". Chem. Eng. Progr. Vol. 49, Heat transfer symposium series No. 5, pp. 137-151.

Dunn, I.J. and Einsele A.J. (1975) "Oxygen transfer coefficients by the dynamic method". J. of Applied Chemistry and Biotechnology, Vol. 25, pp. 707-720.

Dyster, K.N., Koutsakos, E., Nienow A.W. and Jaworski, Z. (1993) "An LDA study of the radial discharge velocities generated by a Rushton turbine : Newtonian fluids, Re > 5". Chem.Eng.Res.Des., 71, pp.11-23.

Eckenfelder, W.W. and Ford, D.L. (1968) "New concepts in oxygen transfer" in "Advances in water quality improvement" Gloyna, E.F. and Eckenfelder, W.W., editors, p. 216, Univ. of Texas press, Austin.

Edwards, M.F. and Wilkinson, W.L. (1972) "Heat transfer in agitated vessels Part I – Newtonian fluids". The Chemical Engineer, August, pp. 310-319.

Eisner, A. D. and Martonen, T. B. (1988), "Simultaneous production of two monodisperse aerosols using a spinning-top aerosol generator". Aerosol Sci. Technol. Vol. 9(2), pp. 105-113.

Ellenberger, J. and Krishna, R., (1994), "A unified approach to the scale-up of gas-solid fluidized bed and gas-liquid bubble column reactor", Chem. Eng. Sci., 49: pp. 5391-5411.

Elson, T.P., Cheeseman , D.J. and Nienow, A.W. (1986) "X-Ray studies of cavern sizes and mixing performance with fluids possessing a yield stress". Chem. Eng. Sci. Vol. 41(10), pp. 2555-2562.

Fascano, J.B., Bakker, A. and Penney, R.W. (1994) "Advanced impeller geometry boosts liquid agitation" Chem. Eng., Aug. 1994. pp.110-116.

Fort, I and Mala, J. (1982) "Hydraulic characteristics of turbine impeller" Collection Czeechoslovak Chem. Commun. Vol 47, pp. 421-429.

Frijlink, J. J., Bakker, A. and Smith, J. M. (1990) "Suspension of solid particles with gassed impellers". Chem. Eng. Sci., 45(7), pp. 1703-1718.

Frish, U. and Parisi, G. (1985) "On the singularity structure of fully develped turbulence" in M Ghil, R. Benzi and G.Parisi (eds) Turbulence and predictictability in geophysical fluid dynamics and climate dynamics, pp. 84-88, Amsterdam, Netherlands.

Galindo, E. and Nienow A.W. (1993) "The performance of the 6SRGT agitator in the mixing of simulated xanthan gum broths". Chem.Eng.Technol., pp.16102-108.

Galindo, E. and Nienow A.W. (1992) "Mixing of highly viscous simulated xanthan fermentation broths with the Lightnin' A315 impeller". Biotech. Prog., 8, pp. 233-239.

Gezork, K.M., Bujalski, W., Cooke, M. and Nienow, A.W., (2000) "The transition from homogeneous to heterogeneous flow in a gassed, stirred vessel". Trans ChemE, Vol. 78, Part A, pp. 363-370.

Gezork, K.M., Bujalski, W., Cooke, M. and Nienow, A.W., (2001) "Mass transfer and hold-up characteristics in a gassed, stirred vessel at intensified operating conditions". TransIChemE, Vol 79A, pp. 965-972

Gibilaro, L.G., Davies, S.N., Cooke, M, Lynch, P.M. and Middleton, J.C. (1985) "Initial response analysis to mass transfer in a gas-sparged stirred vessel". Chem.Eng.Sci., Vol.40 (10), pp.1811-1816.

Bibliography

Goldberg M, and Rubin, E. (1967) "Mechanical foam breaking". Ind. Eng. Chem. Process. Des. Dev., Vol. 6 pp. 195-199.

Gutwald, S. and Mersmann A. (1997) "Mechanical foam breaking – A physical model for impact effect with high speed rotors." Chem. Eng. Technol., Vol. 20, pp 76-84.

Haberman, W.L. and Morton, R.K (1956) "An experimental study of bubbles rising in liquids" Trans. Amer. Soc. Civil. Engrs., 121, Paper No 2799, pp. 257-252.

Hall, K.R. and Godfrey, J.C. (1970) "Power consumption by helical ribbon impellers," Trans.I.Chem.E., Vol 48, paper T201.

Hall, P., Sedney, R. and Gerber, N. (1990), "Dynamics of the fluid in a spinning coning cylinder". AIAA J Vol. 28(5), pp. 828-835.

Harnby, N., Edwards, M.F. and Nienow, A.W., (Eds), "Mixing in the Process Industries", 2nd Edition (in paperback), Butterworth Heinemann, London, 1997, 414 pages

Hari-Prajitno, D. Mishra, V.P. Takenaka, K Bujalksi, W. Nienow, A.W and McKemmie, J. (1998) "Gas-liquid studies with multiple up- and down-pumping hydrofoil impellers: Power characteristics and mixing time". Can. J. of Chem. Eng.,Vol. 76, pp. 1056-1068.

Hari-Prajitno, D. (1997) " A study of unaerated and aerated mixing with single and dual hydrofoil impellers: Power characteristics and mixing time". P.hD thesis, The University of Birmingham, U.K

Harrop, K.L., Spanfelner, W.H., Jahoda, M, Otomo, N., Etchells, A.W., Bujalski, W. and Nienow A.W. (1997), "Impact of suspended solids on the homogenisation of the liquid phase under turbulent conditions", Recents Prog. Genie Procedes 11(52, Mixing 97: Multi-phase Systems), pp.41-48.

Hashem, A. (1991), "Determining the spray drop size spectrum from a spinning cup atomizer". Appl. Eng. in Agric., Vol.7(3), pp.305-310.

Heggs, P. J. and Linn, L. M. (1988), "Induction heating of the impeller in agitated vessels". UK Natl. Conf. Heat Transfer, 2nd Vol. 1, pp. 241-58.

Heggs, P. J. and Hills, P. D. (1994), "The design of heat exchangers for batch reactors". From: Heat Exchange Engineering, Volume 4, " Advances in design and operation" pp. 219-235. Editors Foumeny, E.A and Heggs, P.J. Published by Honeysuckle International Puplications.

Heggs, P. J.(2000) "Overview of extended surface heat transfer fins". Developments in Heat Transfer (2000), 5(Recent advances in analysis of heat transfer for fin type surfaces), pp. 1-13.

Heijnen, J.J., Van't Riet, K. and Wolthuis, A.J. (1980) "Influence of very small bubbles on the dynamic K_La measurement in viscous gas-liquid systems" Biotech and Bioeng, Vol. 22, pp. 1945-1956.

Herringe, R.A. (1979)"The behaviour of mono sized particle slurries in a fully baffled turbulent mixer." Proc. of 3rd European Conf. On Mixing, York, England. Paper D1, pp.199-216.

Hickman, A.D. (1985) "Agitation, mixing and mass transfer in simulated high viscosity fermentation broths." PhD thesis. Chem. Eng. Dept. University of Birmingham, UK.

Hickman, A.D. (1988), Gas-liquid mass transfer and scale-up. A novel experimental technique with results for mass transfer in aerated agitated vessels, 6th European Conf. on Mixing, (BHRA), pp369-374, Pavia, Italy.

Hill, D. P. (1998) "The computer simulation of dispersed two phase flow" Ph.D Thesis, Imperial College of Science, Technology and Medicine, Dept. of Mechanical Engineering, London, July 1998.

Bibliography

Hinze, J.O. (1955) "Fundamentals of the hydrodynamics mechanisms of splitting in dispersion processes" AIChemE.J., Vol. 1, pp.289-295.

Hinze, J.O. and Milborn, H, (1950) "Atomisation of liquids by means of a rotating cup". J. App. Mech., Vol.17, pp. 145-153.

Hjorth, S. (1994) "Agitation in gassed magnetite suspensions". 8th Eur. Conf. on Mixing, I Chem E, Cambridge, UK., pp. 293-300.

Hirata,Y., Nienow, A.W. and Moore, I.P.T. (1994) "Estimation of cavern sizes in a shear-thinning plastic fluid agitated by a Rushton turbine based on LDA measurements"> J.Chem.Eng., Japan, Vol. 27, pp. 235-237.

Holden, P.J., Wang, M, Mann., R., Dickin, F.J. and Edwards, R.B. (1999) "On detecting mixing pathologies inside a stirred vessel using electrical resistance tomography". Trans IChemE, Vol. 77, Part A, Nov. 1999, pp 709-712.

Holden, PJ., Wang, M., Mann, R., Dickin, F.J. and Edwards, R.B. (1998) "Imaging stirred-vessel macromixing using electrical resistance Tomography". A.I.Ch.E. J., Vol. 44,(4), pp. 780-790.

Ibrahim, S.B., Nienow A.W. and Chatwin, S. (1992) "Solid suspension studies with traditional and novel impellers". The 1992 I.Chem.E. Res.Event, UMIST; I.Chem.E., Rugby, pp 122-124.

Ibrahim, S.B. and Nienow, A.W. (1994) "The effect of viscosity on mixing pattern and solid suspension in stirred vessels". Inst. Chem. Eng. Symp. Series No 136 (Eighth European Conference on Mining, pp 25-32.

Ibrahim, S.B. and Nienow, A.W. (1995) "Power curves and flow patterns for a range of impellers in Newtonian fluids : 40 < Re < 5 x 105". Chem.Eng.Res.Des., (Trans.I.Chem.E., Part A), 73, pp. 485-491.

Internation Critical Tables (1933), Vol.5, p.17.

Jackson, M.L. and Shen, C.C. (1978) "Aeration and mixing in deep tank fermentation systems", AIChEJ, Vol. 24, pp.63-70.

Jaworski, Z. and Nienow A.W. (1994) "LDA measurements of flow fields with hydrofoil impellers in fluids with different rheological properties". Proc. 8th European Mixing Conf., Cambridge, Sept. 1994: I.Chem.E., Rugby, pp 105-112.

John, A.H.(1997) "A novel eeactor with independently driven dual impellers for gas-liquid processing". PhD thesis, University of Birmgham, UK.

John, A.H., Bujalski, W. and Nienow, A.W. (1997) "A novel reactor with independently driven dual impellers for gas-liquid processing". Mixing IX, Recents Progres en Genie des Precedes, Vol 2, number 52, pp 169-176.

Jones, A. F. (1996) Manchester University Maths Dept. Private Communication.

Joosten, G. E. H., Schilder, J. G. M. and Janssen, J. J. (1977) "The influence of suspended solid material on the gas-liquid mass transfer in stirred gas-liquid contactors". Chem. Eng. Sci., Vol. 32(5), pp. 563-566.

Joshi, J.B., Pandit, A.B. and Sharma, M.M. (1982) "Mechanically agitated gas-liquid reactors" Chem. Eng. Sci., Vol. 39, pp.813-844.

Karcz, J. and Kaminska-Brzoska, J. (1994) "Heat transfer in a jacketed stirred tank equiped wirh baffles and concave disc impeller" 8th Eur Conf on Mixing, I Chem E, Cambridge, UK. pp. 449-456.

Kars, R.L., Best, R.S. and Drinkenburg, A.A.H. (1979) "Sorption of propane in slurries of active carbon in water" Chem. Eng. J. Vol. 17,pp. 201-207.

Bibliography

Keitel, G. and Onken, U. (1981), "Errors in the determination of mass transfer in gas-liquid dispersions" Chem, Eng. Sci., Vol. 36,12, pp.1927-1932.

Khang, S.J. and Levenspiel, O. (1976), "New scale-up and design methods for stirrer agitated batch mixing vessels". Chem. Eng. Sci., Vol. 31, pp. 569-577.

Kipke, H. (1977) in Bioreaktoren, BMFT-statusseminar "Bioverfahrenstechnik" p, 187.

Kipke, H. (1983), Ger. Chem. Eng. Vol. 6, p 119.

Kolmogov, A. N. (1941) "The local structure of turbulence in compressible viscous flow for very large Reynolds numbers" Doklady Akademii Nauk SSSR, Vol. 30, pp. 301-305.

Kolmogov, A. N. (1949) "Disentegration of drops in turbulent flow" Doklady Akademii Nauk SSSR,Vol. 66, pp. 825-828.

Konno, M., Muto, T. and Saito, S. (1988) "Coalescence of dispersed drops in an agitated tank". J.Chem. Eng. Of Japan, Vol. 21, pp.335-338.

Kovács, T, Tragardh, T and Fuchs, L. (2001) " Flow and turbulence in the discharge of radial pumping turbines: influence of the turbine type". Chem. Eng. Technol. 24(10), pp. 1035-1044.

Krisha, R, Urseanu, M.I., van Baten, J.M. and Ellenberger, J. (1999) "Rise velocity of a swarm of large bubbles in liquids". Chem. Eng. Sci., Vol 54, pp 171-183.

Krishna, R. and Ellenberger, J. (1995) "A Unified approach to the scale-up of "fluidized" multi-phase reactors". Tran I Chem E, Vol 73, Part A , pp 217,221,April 1995.

Langrish. T. A. G., Prince, R. G. H., Messner, S., Sykes, S. and Meldrum, A. L. (1993) "The flow of liquid in spinning cone columns". Off. Proc. Comb. Conf., 6th Conf. Asia Pac. Confed. Chem. Eng., 21st Australas. Chem. Eng. Conf., 2 pp. 13/2-17/2.

Lee, J.C. and Meyrick, D.L. (1970) "Gas-liquid interfacial area in salts solutions in an agitated tank". Vol. 48, pp 37-45.

Lee, K.C. and Yianneskis, M. (1997) "A liquid crystal thermographic technique for the measurement of mixing characteristics in stirred vessels". Trans.IChemE, Vol. 75, Part A, pp. 746-754.

Lessard, R. R. and Zieminski, S. A. (1971) Bubble coalescence and gas transfer in aqueous electrolytic solutions, Ind. Eng. Chem. Fundam., Vol.10(2), pp. 260-269.

Levenspiel, O. (1972), "Chemical Reaction Engineering". 2nd ed, Wiley (W I E) publication.

Linek, V. and Vaclav, V. (1971) "Oxidation of aqueous sulfite solutions". Chem. Eng. Sci., Vol. 26(3), pp. 491-494.

Linek, V. Benes, P. Vacek, V. and Hovorka, P. (1982) "Analysis of differences in k_La values determined by steady-state and dynamic methods in stirred tanks". The Chem. Eng. J. Vol. 25, pp. 77-88.

Linek, V., Benes, P. and Vacek, V. (1989) "Measurement of aeration capacity of fermenters". Chem. Eng. Technol. Vol. 12(3), pp. 213-217.

Linek, V., Moucha, T., Dousova, M. and Sinkule, J. (1994) "Measurement of k_La by dynamic pressure method in pilot-plant fermentor". Biotechnology and Bioengineering, Vol. 43(6), pp. 477-82.

Linek, V., Sinkule, J. and Benes, P. (1991) "Critical assessment of gassing-in methods for measuring k_La in fermentors". Biotechnology and Bioengineering, Vol. 38(4), pp. 323-330.

Linek, V., Sinkule, J. (1993) "State of art in measuring volumetric oxygen transfer coefficients in fermentors". Scientific papers of the University of Chemical Technology Prague Vol. 1, pp. 35-49.

Bibliography

Linek, V., Vacek, V. and Benes, P. (1987) "A critical review and experimental verification of the correct use of the dynamic method for the determination of oxygen transfer in aerated agitated vessels to water, electrolyte solutions and viscous liquids". Chemical Engineering Journal (Amsterdam, Netherlands), Vol. 34(1), pp. 11-34.

Linn, L. M. (1989), "Heat transfer in mixing vessels using induction heated impellers" PhD thesis, Bradford University, UK.

Lopes de Figueiredo, M. M. and Calderbank, P. H. (1979) "The scale up of aerated mixing vessels for specified oxygen dissolution rates". Chem. Eng. Sci., Vol. 34(11), pp. 1333-1338.

Lu, W.M., Wu, H.Z. and Chou, C.Y. (2002) "Gas recirculation rate and its influence on mass transfer in multiple impeller systems with various impeller combinations". Can.J.ChemE., Vol. 80, pp. 51-62.

Machon, V., Vlcek, J., Nienow, A.W. and Solomon, J. (1980), "Some effects of pseudoplasticity on hold-up in aerated agitated vessels". Chem. Eng. J. Vol. 19, pp. 67-74.

Machon, V. and Linek, V. (1974) "Effect of salts on the rate of mass transfer across a plane interface between a gas and mechanically agitated aqueous solutions of inorganic electrolytes". Chemical Engineering Journal, Vol. 8(1), pp. 53-61.

Machon, V., Pacek, A.W. and Nienow, A.W. (1997) "Bubble sizes in electrolyte and alcohol solutions in a turbulent stirred vessel., Trans IChemE, 75A: pp. 339-348.

MacTaggart, R. S., Nasr-El-Din, H. A. and Masliyah, J. H. (1993) "Sample withdrawal from a slurry mixing tank". Chem. Eng. Sci. Vol. 48 (5), pp. 921-931.

Mak, A.; Yang, S.; Ozcan-Taskin, N. G (1997), "The effect of scale on the suspension and distribution of solids in stiffed vessels". Recents Prog. Genie Procedes 11(52, Mixing 97: Multi-phase Systems), pp. 97-104.

Makarytchev, S. V.; Langrish, T. A. G.; Prince, R. G. H. (2001) "Thickness and velocity of wavy liquid films on rotating conical surfaces". Chem. Eng. Sci., Vol. 56(1), pp.77-87.

Manikowski, M., Bodemeier, S., Lübbert, A., Bujalski,W. and Nienow, A.W. (1994) "Measurement of Gas and Liquid Flows in Stirred Tank Reactors with Multiple Agitators". Can.J.Chem.Eng., Vol. 72, , 769-781.

Mann, R, Stanley, SJ, Vlaev, D, Wabo, E. and Primrose, K (2000) "Augmented-reality visualisation of fluid mixing in stirred chemical reactors using electrical resistance tomography". Proceedings of SPIE Vol. 4188, 5-6th November 2000, Process Imaging for Automatic Control.

Mann, R., Knysh, P. E .A. Rasekoala, E.A. and Didari, M. (1987) "Mixing of a tracer in a closed stirred vessel: A network-of zones analysis of mixing curves acquired by fibre-optic photometry". I.Chem.E.Symposium Series 108(55), pp. 49-62.

Mann, R., Mavros, P. P. and Middleton, J.C. (1981) "Mixing in a gas-liquid stirred vessel from observations of dynamic gas disengagement2. I.Chem.E. Symposium Series No 64, Fluid Mixing 1, G1-G14.

Mann, R., Middleton, J.C. and Parker I.B. (1977) "Deteriorating mixing quality and yield losses on scaling up gas-liquid reactors: A theoretical analysis". Proc. 2nd Euro. Conf. on Mixing, BHRA Fluid Engineering, Cranfield, pp. F3, pp. 35-50.

Marrucci, G. (1965) "Rising Velocity of a Swarm of Spherical Bubbles". Ind. Engng. Chem. Funam. Vol 4, pp. 224-225, May 1965.

Martin, T. (1996) "Gas dispersion with radial and hydrofoil impellers in fluids with different coalescence characteristics". PhD Thesis, ISBN 3/89675/104/2, (The University of Birmingham, UK).

Bibliography

McKee, SL, Williams, RA and Boxman, A (1995) "Development of solid-liquid mixing models using tomographic techniques". The Chemical Engineering Journal, Vol. 56, pp. 101-107.

Martin, T., McFarlane C.M. and Nienow A.W. (1993) "Effect of Coalescence Inhibition on Impeller Performance in Gas-Liquid Systems". I.Chem.E. Res.Event, The University of Birmingham, U.K., Jan.1993; I.Chem.E., Rugby, U.K., pp 648-650.

Martin, T., McFarlane C.M. and Nienow A.W. (1994) "The influence of liquid properties and impeller type on bubble coalescence behaviour and mass transfer in sparged, agitated bioreactors". Proc. 8th European Mixing Conf., Cambridge, Sept. 1994: I.Chem.E., Rugby, pp 57-64.

Maxwell J.C. (1881) "A treatise on Electricity and Magnetism". Claredon Press, Oxford.

McKee, S.L., Williams, R.A. and Boxman, A .(1995) "Development of solid-liquid mixing models using tomographic techniques". The Chemical Engineering Journal, Vol. 56, pp. 101-107.

Metha, V. D. and Sharma, M. M. (1971) "Mass transfer in mechanically agitated gas-liquid contactors". Chem. Eng. Sci., Vol. 26, pp. 461-479.

Metzner, A.B. and Otto R.E. (1957) "Agitation of non-Newtonian fluids". A.I.Ch.E.J., Vol.3, pp. 3-11.

Middleton, J. C. (1979) "Measurement of circulation within large mixing vessels". Proc. 3rd Eur. Conf. Mixing, Vol. 1, pp. 15-36. York UK.

Middleton, J. C. Pierce, F and Lynch, P.M. (1986) "Computations of flow fields and complex reaction yield in turbulent stirred reactors, and comparison with experimental data". Trans IChemE ., Vol. 64, pp. 18-22.

Middleton, J.C. (1997) "Gas-liquid dispersion and mixing" Chapter 15 in Harnby, N, Edwards, M.F. and Nienow, A.W , editors (1997) "Mixing in the process industries" 2nd edit. Butterworth/Heinman (paperback).

Middleton, J.C. (2002), Private communication on Lewis Richardson poem.

Middleton, J.C., Cooke, M. and Litherland, L. (1994) "The role of kinetic energy in gas-liquid dispersion: do * need an agitator?". I Chem E Symposium Series No 136, paper 75, 8th Eur Conf on Mixing, I Chem E, Cambridge, pp.595-602.

Midoux, N. and Charpentier, J.C. (1984) "Mechanically agitated gas-liquid reactors" Int. Chem. Eng., Vol. 24, No 2, pp. 249-265.

Mitchel,B.J. and Miller, S.A. (1962) "Power requirements of gas-liquid agitated sytems" AIChemEJ, Vol.8, 262-266.

Muller, F.L. and Davidson, J.F. (1992), "On the contribution of small bubbles to mass transfer in bubble columns containing highly viscous liquids". Chem. Eng. Sci., Vol. 47, pp. 3525-3532.

Muller, F.L. and Davidson, J.F. (1993), "On the effect of surfactants on mass transfer to viscous liquids in bubble columns ". Trans.IChem.E., Vol. 43, part A pp. 291-296.

Muller, F.L. (1993), "Mass transfer to viscous liquids in bubble columns ". PhD thesis, Cambridge University, UK. Jan. 1993.

Musgrove, M. and Ruszkowski, S. (2000) "Influence of impeller type and agitation conditions on the drop size of immiscible liquid dispersions". Proceedings of the 10th European Conference on Mixing, Delft, Netherlands, July 2-5, 2000, pp. 165-172.

Myers, K., Reeder, M., Bakker, A. and Rigden, M.(1996) "Agitating for success". Chemical engineering, issue 620, Oct 1996.

Bibliography

Nagata, S. (1975) "Mixing: Principles and Applications". Halsted press, Wiley, New York.

Nagata, S., Nishikawa, M., Kayama, T. and Aakajuna, M. (1972) "Heat transfer to cooling coil acting as rotating impeller in highly viscous liquids". J. Chem. Eng. Jap. (1972), Vol. 5(2), pp. 187-192.

Nienow, A. W. (1968) "Suspension of solid particles in turbine agitated baffled vessels" Chem. Eng. Sci. Vol. 23, pp. 1453-1459.

Nienow, A. W. and Miles, D (1978) "Effect of impeller/tank configurations on fluid-particle mass transfer" Chem. Eng. J. Vol. 15, pp. 13-24.

Nienow, A. W., Middleton, J.C. and Chapman,C.M. (1979) "Gas recirculation rate through impeller cavities and surface aeration in sparged agitated vessels". Chem. Eng. J. Vol. 17, pp. 111-118.

Nienow, A. W., Warmoeskerken, M.M.C.G.,Smith, J.M. and Konno, M. (1985) "Flooding/loading transition and the complete dispersal condition in aerated vessels agitated by a Rushton turbine". Proc. of 5th European Mixing Conf., Germany, BHRA Fluid Engineering , Cranfield, pp. 153-154.

Nienow, A.W. (1994) "Recent studies on stirred bioreactors at the SERC centre for biochemical engineering at Birmingham". From, "Advances in Bioprocess Engineering", (E. Galindo and O.T. Ramirez, Eds.), Kluwer, Netherlands, pp 141-148.

Nienow, A.W., (2003) "The versatility of up-pumping hydrofoil agitators" Invited lecture for Research Colloquia, UMIST - Dept. Chemical Engineering, 27 Feb 2003.

Nienow, A.W. (1998) "Hydrodynamics of stirred bioreactors". Appl. Mech. Rev., Vol. 51, pp. 3-32.

Nienow, A.W., Buckland B.C. and Hunt, G. (1994) "A fluid dynamic study of the retrofitting of large bioreactors: Turbulent flow". Biotech. Bioeng., Vol.44, pp. 1177-1186.

Nienow, A.W., Weetman, R.J., Hunt, G. and Buckland, B.C. (1993) "A fluid dynamic study of the retrofitting of a large pilot ccale agitated bioreactor". Proc. 3rd International Conf. on Bioreactor and Bioprocess Fluid Dynamics, (Ed. A.W. Nienow), Cambridge 1993, BHR Group/MEP, London, pp. 505-519.

Nikiforaka, K.C., Lee, K.C., Yianneskis, M. (1999) "Circulation time measurements with minature radio frequency identication devices". Fluid Mixing 6, IChemE symposium series 146, Edited by Hadj Benkreira, pp. 47-57.

Nocentini, M., Fajjner, D., Pasquali, G. and Magnelli, F. (1993) "Mass transfer in multiple-Rushton turbines: Water and water-glycrol solutions". Ind.Eng.Chem.Res. Vol. 32, pp. 19-26.

Oldshue, J.Y. (1983) "Fluid Mixing Technology" Chemical Engineering McGraw Hill publication.

Oldshue, J.Y. (1989) "Fluid Mixing in 1989" Chemical Engineering Progress, Vol 5, pp 33-42.

Otomo, N., Bujalski, W. and Nienow, A. W., (1995) "An Application of a Compartment Model to a Vessel Stirred with Either Dual Radial or Dual Axial Flow Impellers", The 1995 IChemE Research Event, pp. 829-831.

Oyevaar, M.H., Bos, R. and Westerterp, K.R. (1991) "Interfacial areas and gas hold-ups in gas-liquid contactors at elevated pressures from 0.1 to 8.0 Mpa". Chem. Eng. Sci., Vol. 46, p. 1217.

Pandit, A. B., Gogate, P. R. and Dindore, V. Y. (2000) "Effect of tracer properties (volume, density and viscosity) on mixing time in mechanically agitated contactors". 10th European

Bibliography

Conference on Mixing, Proceedings of the European Conference, Delft, Netherlands, July 2-5, pp. 385-393.

Pantula, P. R. K., Ahmed, N. (1997), "The impeller speed required for complete solids suspension in aerated vessels: a simple correlation" Recents Prog. Genie Procedes 11(52), Mixing 97: Multi-phase Systems, pp. 11-18.

Patel, S.A., Daly, J.G. and Bukur, D.B. (1989) "Hold-up and interfacial area measurements using dynamic gas disengagement". AICHE J, Vol. 35, pp. 931 –941..

Patterson, G.K. (1991) "Measurements and modelling of in gas sparged agitated vessels". Proc of 7th European Mixing Conf., Brugge, Belgium: pp. 209-216.

Pearce, B.A. and Thomas, N.H. (1990) "Structure and force transits of bubbles shedding from rotating stirrers". Trans. IChemE. Vol. 68, part A. pp. 57-62.

Perdriau, A. (2003) "Gas –liquid mixing and mechanical foam breaking in a mechanically agited vessel". MSc thesis, UMIST, Department of chemical engineering, Manchester, UK.

Perry, R.H. and Chilton, C.H. editors, "Chemical Engineering Handbook" 5th Edit. (3-324) McGraw Hill.

Plichon, B., Decq, A. and Guillaume J. B. (1976) "Influence of air enriched with oxygen injection on the bacterial yield during the fermentation and correction of the anti-foam effect". **(author's transl)**. ANNALES DE MICROBIOLOGIE, Vol. 127(4), pp. 521-528.

Podgorska, W., Baldyga, J. (2001) "Scale-up effects on the drop size distribution of liquid-liquid dispersions in agitated vessels". Chem. Eng. Sci., Vol. 56(3), pp. 741-746.

Primrose, K. and Qiu, C. (1999) "Performance and application studies of an electrical resistance tomography system". In Proc: 1st World Congress on Industrial Process Tomography, Buxton, UK, pp. 133-139.

Prince, R. G. H., Desho, S. and Langrish, T. A. G. (1997) "Spinning cone column capacity and mass transfer performance". Inst. Chem. Eng. Symp. Series 142 (Distillation and Absorption '97, Vol. 2), pp. 769-781.

Raghav Rao, K. S. M. S. and Joshi, J. B. (1988) "Liquid phase mixing in mechanically agitated vessels". Chemical Engineering Communications. Vol. 74 pp. 1-25.

Revill, B.K. (1982) "Pumping capacities of disc turbine agitators – A literature review". Proc. 4th Erop. Conf. On Mixing, Noordwijkerhout, Netherlands, Sponsored by BHRA fluid engineering, pp. 11-24.

Richardson, J.F. and Zaki, W.N. (1954) "Sedimentation and fluidization". Trans. Inst. Chem. Eng., Vol. 22, pp.35-53.

Rieger, F. and Ditl, P. (2000) "Mixing equipment for particle suspension - generalized approach to designing". 10th European Conference on Mixing, Proceedings of the European Conference, Delft, Netherlands, July 2-5, pp. 415-422.

Rieth, T and Beek, W.J. (1970) "Bubble coalecence rates in a stirred tank contactor" TransIChemE., Vol. 48, pp. T63-T68.

Rose, C. H. and Watervliet A. (1966) "Application of shear-spinning techniques in forming molybdenum missile components". U. S. C. F. S. T. I., AD Rep. 1966, (AD 631423), 29 pp. From: U.S. Govt. Res. Develop. Rept. 41(11), 53.

Rousar, I. and van den Akker, H.E.A. (1994) "LDA measurments of liquid velocities in sparged agitated tanks with single and multiple Rushton turbines". 8th Eur Conf on Mixing, I Chem E, Cambridge, UK. pp. 89-96.

Bibliography

Ruszkowski, S. (1994) "A rational method of measuring blending performance and comparison of different impeller types". 8th Eur. Conf. on Mixing, I Chem E, Cambridge, UK. pp. 283-292.

Sachs, J.P. and Rushton, J.H. (1954) "Discharge flow from turbine-type mixing impellers" Chem. Eng. Prog., Vol. 50, pp. 597-603.

Saito, F., Nienow, A.W., Chatwin, S. and Moore, I.P.T. (1992) "Power, gas dispersion and homogenisation characteristics of Scaba SRGT and Rushton turbine impellers". J.Chem.Eng., Japan, Vol. 25, pp.281-287.

Schumpe, A. and Grund, G. (1986) "The gas disengagement technique for studying gas hold-up structure in bubble columns". Can. J. Chem. Eng., Vol. 64, pp. 891-896.

Seichter. P., Pesl, L. and Mazoch, J. (1997) "Agitation effects of axial mixers in highly concentrated suspensions of fine particles". Recents Prog. Genie Procedes (Vol. 11, 52, Mixing 97: Multi-phase Systems), pp. 27-32.

Semka, R. P. and Ledman, J. L. (1969) "Development of shear spinning technology for beryllium". U. S. At. Energy Comm. (SC-R-69-1233), 34 pp. From: Nucl. Sci. Abstr. 1969, 23(15), 29985.

Shamlou, P.A. and Edwards, M.F. (1985) "Power consumption of helical ribbons in viscous Newtonian and non-Newtonian fluids". Chem.Eng.Sci., Vol 40, pp. 1773-1781.

Sharma, M.M. and Danckwerts, P.V. (1970) "Chemical methods of measuring interfacial area and mass transfer coefficients in two fluid systems". Brit. Chem. Eng. Vol. 15, pp. 522-528.

Shiue, S. J. and Wong, C. W. (1984) "Studies on homogenization efficiency of various agitators in liquid blending". Canadian Journal of Chemical Engineering. Vol. 62(5), pp. 602-609.

Sideman, S., Hortacsu, O. and Fulton, J.W. (1966) "Mass transfer in gas-liquid contacting systems". Ind, and Eng. Chem., Vol. 58(7), pp. 32-47.

Sieder, E N. and Tate, G. E. (1936) "Heat transfer and pressure drop of liquids in tubes". Indust. Eng. Chem. 28, pp. 1429-1434.

Singh, V., Hessler, W., Fuchs, R. and Constantinides, A. (1986) "On-line determination of mixing parameters in fermenters using pH transients". Proc 1st Int. Conf. Bioreactors, sponsored by BHRA, Cambridge UK. pp. 231-256.

Smit, L. (1994) "An alternative scale procedure for stirred vessels". 8th Eur Conf on Mixing, I Chem E, Cambridge, UK., pp. 309-316.

Smith, J.M. (1994) Agitator power draw in sparged boiling reactors". 8th Eur Conf on Mixing, I Chem E, Cambridge, UK. pp.179-186.

Smith, J.M. and Smit, L. (1988) "Impeller Hydrodynamics in Boiling Reactors". 6th Euro.Conf. on Mixing, Pavia, Italy, pp. 297-304, May 1988.

Smith, J.M. and Warmoeskerken,M.M.C.G. (1985) "The dispersion of gases in a liquid with a turbine". 5th Euro. Conf. on Mixing, Wuzburg, West Germany, pp115-126, June 1985.

Smith, J.M. van't Riet, K and Middleton, J.C.M. (1977) "Scale up of agitated gas-liquid reactors for mass transfer". 2nd Euro. Conf. on Mixing, Cambridge UK, paper F4 –51 to 66, March 1977.

Sobotka, M., Prokop, A., Dunn, I. J. and Einsele, A. (1982) "Annual reports of fermentation processes". Vol. 5, pp. 127-210.

Solomon, J., Elson, T.P., Nienow, A.W. and Pace G.W. (1981) "Cavern sizes in agitated fluids with a yield stress". Chem. Eng. Commun. Vol. 11, pp. 143-164.

Bibliography

Spriet, J.A. and Botterman, J.H. (1984) "Correction factors for the dynamic measurement of the volumetric mass transfer coefficient". J.Chem.Tech.Biotechnol. Vol. 34A. pp. 137-153.

Sridharan, K. and Sharma, R.R. (1976), "New systems and methods for the measurement of effective interfacial area and mass transfer coefficients in gas-liquid contactors" Chem. Eng. Sci., Vol. 31, pp. 767-774.

Sriram, K and Mann, R (1976) "Dynamic gas disengagement: A new technique for assessing the behaviour of bubble columns". Chem Eng. Sci., Vol 32 pp. 571-580.

Stocks, S.M., Cooke, M. and Heggs P. J. (2004) "Inverted hollow spinning cone as a device for controlling foam and hold up in pilot scale gassed agitated fermentation vessels. ISMIP5. Serville.

Stokes, G.G. (1880) "Mathematical and physical papers", Vol 1, Cambridge University Press.

Straub, C. and Hailey, R. W. (1966), "Spinning of refractory metals". Metall. Soc. Conf. [Proc.] Vol. 30, pp. 423-431.

Strek, F. and Karcz, J. (1997) "Heat to Newtonian fluid in a stirred tank – A comparative experimental study for vertical tubalar coil and a jacket". Recents Prog. Genie Procedes 11(51, Mixing 97: Multi-phase Systems). pp 105-112.

Sunden, B. and Heggs, P. J. (Editors). (2000) Recent advances in analysis of heat transfer for fin type surfaces. [In: Dev. Heat Transfer, 2000; 5], p.293.

Sykes, S. J. and Prince, R. G. H. (1992), "The design of spinning cone distillation columns". Inst. Chem. Eng. Symp. Ser. 128 (Distillation and Absorption '92, Vol. 1), pp. A167-A179.

Takenaka, K., Ciervo, G., Monti, D., Bujalski, W., Etchells, A. W. and Nienow, A.W. (2001) "Mixing of three-phase systems at high solids content (up to 40% w/w) using radial and mixed flow impellers". Journal of Chemical Engineering of Japan, Vol. 34 (5), pp. 606-612.

Takesono S., Onodera M., Yoshida M., Yamagiwa K. and Ohkawa A. (2002). "Performance characteristics of mechanical foam-breakers fitted to a stirred-tank reactor". J. Chem. Technol. Biotechnol., Vol. 78, pp.48-55.

Tatterson, G. B. (1991) "Fluid mixing and gas dispersion in agitated tanks". McGraw-Hill inc. New York.

Tragardh, Ch. (1988) "A hydrodynamic model for the simulation of an aerated agitated fed-batch fermenter". Proc. 2nd Int. Conf. Bioreactors, sponsored by BHRA, Cambridge UK., pp. 117-134.

Treybal, R.E. (1968) "Mass transfer operations". Second edition. International students edition, published by McGraw Hill Kogakusha, LTD.

Uhl, V.W. (1966) "Mechanically aided heat transfer". Chapter 5 in "Mixing: Theory and practice", Volume I, edited by Uhl, V.W., published by Academic Press.

Uhl, V.W. and Gray, J.B. (1966) "Mixing: Theory and practice". Volume 1, published by Academic Press.

Uhl, V.W. and Gray, J.B. (1967) "Mixing: Theory and practice". Volume 2, published by Academic Press.

Valentin, F.H.H. (1967) "Absorption in gas-liquid dispersions". Spon Chemical Engineering Series.

Vallet, L. (1980) "Thin film evaporation for the removal of solvents". Engl. Editor(s): Curling, John M., Methods Plasma Protein Fractionation pp. 211-22. Publisher: Academic, London, UK.

Bibliography

Van de Donk, J. A. C., Van der Lans, R. G. J. M. and Smith, J. M. (1979) "The effect of contaminants on the oxygen transfer rate achieved with a plunging jet contactor". Proc. Eur. Conf. Mixing (3rd(Vol. 1), pp. 289-302.

Van der Molan, K. and van Maanen H.R.E. (1975) "Laser Doppler measurements of the turbulent flow in stirred tanks to establish scaling rules". Chem. Eng. Sci. Vol 33, pp.1161-1168.

Van't Riet, K. and Smith, J.M. (1973), "The behaviour of gas-liquid mixtures near Rushton turbine blades". Chem. Eng. Sci., Vol. 28, pp. 1031-1037.

Van't Riet, K. and Smith, J.M. (1975b) "The trailing vortex system produced by Rushton turbine agitators".Chem. Eng. Sci., Vol. 30, pp. 1093-1105.

Van't Riet, K. (1975a) "Turbine agitator hydrodynamics and dispersion performance". Ph.D. Thesis , Univ. of Delft, Netherlands.

Van't Riet, K. (1979) "Review of measuring methods and results in non-viscous gas-liquid mass transfer in stirred vessels". Ind.Eng.Chem. (Proc. Res.Des.), Vol. 18, pp. 357-364.

Van't Riet, K., Boom, J.M. and Smith, J.M. (1976) "Power consumption, impeller coalescence and recirculation, in aerated vessels.". Trans. ICHEME, Vol. 54, pp.124-131.

Vasconcelos, J.M.T., Nienow, A.W., Martin, T., Alves, S.S. and McFarlane, C.M. (1997) "Alternative ways of applying the hydogen peroxide steady state method of k_La measurement", Trans IChemE, 75A, pp.467-472.

Vira, N. R., and Fan, Dah Nien. (1981), "Heat transfer from a cone spinning in a corotating fluid". J. Heat Transfer Vol.103(4), pp. 815-817.

Vogel, A.I. (1961) " A textbook of quantitative inorganic analysis, 3RD edition". London, Longmans, Green and Co LTD, pp. 295-296.

Votruba, J. and Sobotra, M. (1976) "Measurement of fermenter aeration capacity by fast-response oxygen electrode" Biotechnology and Bioengineering, Vol. 18, pp. 1815-1819.

Votruba, J. and Sobotra, M. and Prokop, A. (1977) "The effect of air hold-up on readings of dissolved oxygen probes" Biotechnology and Bioengineering, Vol. 19, pp. 435-438.

Votruba, J. and Sobotra, M. and Prokop, A. (1978) "The effect of air hold-up on readings of dissolved oxygen probes II" Biotechnology and Bioengineering, Vol. 20, pp. 913-916.

Wang, M. (1999) "Three-dimensional effects in electrical impedance tomography". Proceedings 1st World Congress on Industrial Process Tomography, Buxton, UK, pp. 410-416.

Wang, M., Dorward, A., Vlaev, D. and Mann R. (1999) "Measurements of gas-liquid mixing in a stirred vessel using electrical resistance tomography". Proceedings 1st World Congress on Industrial Process Tomography, Buxton, UK, pp. 78-83.

Wang, M., Jia, X. and Williams, R.A. (2000) "Electrical tomographic imaging for bubble column measurement and control". Proceedings of SPIE Vol. 4188, 5-6th November 2000, Process Imaging for Automatic Control.

Warmoeskerken, M. M. C. G. and Smith, J. M. (1978) "Surface contamination effects in stirred tank reactors". C. R. - Int. Symp. Mixing Mons, Paper C13, 16 pp. Publisher: Fac. Polytech. Mons, Dep. Chem. Eng., Mons, Belg

Warmoeskerken, M.M.C.G. and Smith, J.M. (1985), "Flooding of disc-turbines in gas-liquid dispersions: A new description of the phenomenon". Chem. Eng. Sci., Vol. 40, pp. 2063-2071.

Warmoeskerken, M.M.C.G., Speur, J.and Smith, J.M. (1984a) "Gas-liquid dispersion with pitched blade turbines". Chem. Eng.Commun. Vol 25, pp. 11-29. Jan. 1984.

Bibliography

Warmoeskerken, M.M.C.G., van Houwelingen, M.C., Frijlink, J.J..and Smith, J.M. (1984b) "Role of cavity formation in stirred gas-liquid-solid reactors". Trans IChemE ., Vol. 62, pp.197-200.

Weetman, R.J. and Olshue, J.Y. (1988) "Power, flow and shear characteristics of mixing impellers". 6th Euro.Conf. on Mixing, Pavia, Italy, pp. 43-50, May 1988.

Westerterp, K.R. (1963) "Design of agitators for gas-liquid contacting". Chem. Eng. Sci. Vol. 18, pp 495 -502.

Whitton, M.J. and Nienow, A.W. (1993) "Scale-up orrelations for gas hold-up and mass transfer coefficients in stirred tank reactors". Proc. 3rd International Conf. on Bioreactor and Bioprocess Fluid Dynamics, (Ed. A.W. Nienow), Cambridge 1993, BHR Group/MEP, London, pp 135-145.

Wichterle, K and Wein, O. (1981) Threshold of mixing of non-Newtonian liquids". Int. Chem. Engng. Vol. 21, pp.166-120.

Wilkinson P.M. and Van. Dierendonck L.l. (1990) "Pressure and gas density effects on bubble break-up and gas hold-up in bubble columns". Chem.Eng.Sci., Vol 45(8), pp. 2309-2315.

Wilkinson, P. M., Spek, A. P. and Van Dierendonck, L. L. (1992) "Design parameters estimation for scale-up of high-pressure bubble columns". AIChE 38(4), pp 544-554.

Williams, J.W. (1961) "Studies in aeration and agitation". pp 143-172, from "Progress in Industrial microbiology" edited by Hockenhull, D.J.D. puplished by Heywood & Company LTD, London.

Wisdom. D.J. (1973) "Fundamental studies of disc turbines in aerated vessels". PhD thesis, University College London. UK.

Wright, A. J. and Pyle, D. L. "Extractive fermentation and the spinning cone column: preliminary studies". IChemE Res. Event--Eur. Conf. Young Res. Chem. Eng., 1st (1995), 2, pp. 998-1000.

Zhou, G. and Kresta, S. M. (1998) "Correlation of mean drop size and minimum drop size with the turbulence energy dissipation and the flow in an agitated tank". Chem. Eng. Sci., Vol. 53(11), pp. 2063-2079,

Zivdar, M., Langrish, T. A. G. and Prince, R. G. H. (2001) "Comparison of mass-transfer efficiencies of SCC and structured packing". Int. J. Eng. Vol.14(1), pp. 1-8.

Zwietering T.H.N, (1958) "Suspending of solid particles in liquid by agitators". Chem. Eng. Sci., vol. 8, pp. 244-253.